# Organic geochemical analysis and comparison of oils, condensates and bitumens from the SW Barents Sea

*Maturity, organic facies, biodegradation and migration assessment*

Lars Jonas Jørgensen Narvhus

Master Thesis in Geosciences
Petroleum Geology and Petroleum Geophysics
30 credits

## Department of Geosciences
## The Faculty of Mathematics and Natural Sciences

UNIVERSITY OF OSLO

June / 2016

# Organic geochemical analysis and comparison of oils, condensates and bitumens from the SW Barents Sea

*Maturity, organic facies, biodegradation and migration assessment*

Lars Jonas Jørgensen Narvhus

Master Thesis in Geosciences
Petroleum Geology and Petroleum Geophysics
30 credits

**Department of Geosciences**
**The Faculty of Mathematics and Natural Sciences**

UNIVERSITY OF OSLO

June / 2016

© Lars Jonas Jørgensen Narvhus

Tutor(s): Assoc. Prof. Dag A. Karlsen

2016

Organic geochemical analysis and comparison of oils, condensates and bitumens from the SW Barents Sea

Lars Jonas Jørgensen Narvhus

http://www.duo.uio.no/

Trykk: Reprosentralen, Universitetet i Oslo

# Abstract

The SW Barents Sea is a relatively unexplored area compared to the Northern North Sea and the Norwegian Sea. The area has undergone several events of upliftment and erosion making it very complex, with numerous source rocks capable of expelling petroleum. The upliftments are believed to have pushed the larger quantities of oil to basin margins and structural highs. In order to get a better understanding of the region nine oils and two condensates have been geochemically analyzed from the area. In addition, 15 shallow core samples from the Finnmark Platform and Norkapp Basin have also been extracted and analyzed. The geochemical analyzation methods used are TLC-FID, GC-FID and GC-MS. The derived information from these analyses was mainly focused on maturity and organic facies parameters, level of biodegradation and migration pathways.

The core samples contain almost exclusively polar compounds, indicating severe biodegradation of the bitumen. Henceforth, elevated isoprenoid values relative to n-alkanes can be found in the shallower oil discoveries, where the lighter n-alkane fraction seems to be microbial degraded. Some of the deeper wells express elevated UCM “humps” but no other clear evidence of biodegradation. This could be related to an older biodegraded petroleum charge and a new charge masking the biodegradation. Mixing of hydrocarbon fractions can be seen in some of the oils based on the bimodal n-alkane signatures found in the GC-FID chromatograms. Moreover, conflicting maturity signatures based on the n-alkane distribution for some of the oils and condensates give a strong indication of mixed petroleums. This is in accordance with the conflicting maturity parameters for the saturated and aromatic biomarkers, and the medium-range biomarkers seen in many of the oils. Thus, suggesting a mixture of petroleums, where the former estimates maturities in the early oil window and the latter peak oil production maturities. All of the oils in the sample set appear to be influenced by two hydrocarbon charges, one lighter fraction ($C_{15-}$) and a heavier black oil fraction ($C_{15+}$).

Two oil/condensate families can be discerned based on the ETR, $C_{24}$-tetracyclic terpanes and bisnorhopane. The first family seems to originate from Jurassic and the second form a pre-Jurassic source. The pre-Jurassic discoveries are found on the Loppa High in Permian rocks and in the margins between the Hammerfest Basin and the Finnmark Platform, and are possibly of Paleozoic age. The Jurassic sourced discoveries can be found in the whole study area, with a lighter fraction in the center of the Hammerfest Basin and heavier remigrated oil in the margins and structural highs. The light fraction is believed to be live. The oil has probably remigrated due to Cenozoic upliftment. Profoundly geochemical similarities with the remigrated paleo-oil in the Hammerfest Basin and the discoveries in Johan Castberg could suggest a remigration of oil into the field.

# Acknowledgements

I would like to thank my supervisor Dag Arild Karlsen for great educational skills in the petroleum system course earlier in the master degree. This triggered me for further work with petroleum geochemistry. He has also been an excellent supervisor, giving me helpful guidance and for being a really colorful discussion partner.

I would also thank Kristian Backer-Owe for helpful discussions and guidance related to practical laboratory work and IKU for providing the shallow cores used in this thesis. Furthermore, I would like to thank Tesfamariam Berhane Abay for laboratory guidance and assistance. Morover, I would like to thank Zagros Matapour for laboratory assistance and Benedict Lerch for providing templates used in the discussion chapter of this thesis.

Lastly, I would also like to thank my fellow student Fredrik Wesenlund for valuable discussions and great ideas. Also I would like to thank Anders Rønning for answering a lot of question I had regarding organic geochemistry.  Finally, I have to thank the fellow students at UiO for making the writing of this thesis a great time.

Oslo, June 2016

Lars Jonas Jørgensen Narvhus

# Table of content

Abstract ........ I

Acknowledgements ........ II

1. Introduction ........ 1

  1.1 Introduction to the SW Barents Sea ........ 1

  1.2 Introduction to the Loppa High, the Hammerfest Basin, the Nordkapp Basin and the Finnmark Platform........ 2

  1.3 Thesis objectives ........ 3

2. Geological Setting ........ 5

  2.1 Introduction to the Barents Sea ........ 6

  2.2 Structural evolution of the SW Barents Sea ........ 7

  2.3 Stratigraphy of the SW Barents Sea ........ 9

    2.3.1 Paleozoic Succession: ........ 10

    2.3.2 Mesozoic Succession ........ 11

    2.3.3 Cenozoic Succession ........ 12

  2.4 Key structures in the SW Barents Sea ........ 12

    2.4.1 Loppa High ........ 12

    2.4.2 Hammerfest Basin ........ 13

    2.4.3 Finnmark Platform ........ 13

    2.4.4 Nordkapp Basin ........ 13

  2.5 Petroleum system in the SW Barents Sea ........ 15

    2.5.1 Source Rocks ........ 15

    2.5.2 Maturity history ........ 15

    2.5.3 Overview of petroleum plays in the SW Barents Sea ........ 17

3. Sample set and well description ........ 19

  3.1 Study area ........ 19

  3.2 Description of selected oils and condensates from wells in the SW Barents Sea ........ 22

  3.3 Description of selected core samples with extracts from the Finnmark Platform and the Nordkapp Basin ........ 25

  3.4 Sample List ........ 30

4. Analytical methods ........ 33

  4.1 Introduction ........ 33

  4.2 Preparation and extraction of samples ........ 34

4.3 TLC-FID ........ 34
4.4 GC-FID – GAS chromatography ........ 36
4.4 Molecular sieving........ 37
4.5 GC-MS ........ 38
5. Petroleum geochemical interpretation parameters ........ 41
5.1 Interpretation parameters based on the TLC-FID ........ 42
5.1.1 Saturated and aromatic hydrocarbons and polar compounds ........ 42
5.2 Interpretation parameters based on the GC-FID ........ 43
5.2.1 N-alkane distribution ........ 43
5.2.2 Pristane/phytane ratio ........ 44
5.2.3 Pristane/n-C17 and Phytane/n-C18 ratios........ 45
5.2.4 Odd/Even Predominance (OEP) and the Carbon Preference Index (CPI)........ 46
5.3 Interpretation parameters based on the GC-MS ........ 46
5.3.1 Terpanes........ 47
5.3.2 Steranes........ 48
5.3.3 Triaromatic steroids ........ 50
5.3.4 Monoaromatic steroids ........ 51
5.3.5 Phenanthrene, methylphenanthrene and methyldibenzothiophene........ 52
5.3.6 The standard parameters for maturity and organic facies based on the GC-MS ........ 54
5.4 Other parameters based on the GC-MS ........ 61
5.3.1 Extended tricyclic terpane ratio ........ 61
6. Results ........ 63
6.1 Iatroscan results ........ 63
6.1.1 Summary of oils and condensates from SW Barents Sea ........ 64
6.1.2 Summary of bitumens from FP and NB ........ 64
6.2 Results based on the GC-FID........ 67
6.2.1 Summary of the GC-FID parameters for the oils and condensates ........ 67
6.2.2 N-alkane distribution of the oils and condensates ........ 67
6.2.3 Summary of the GC-FID parameters for the extracted core samples........ 69
6.2.4 N-alkane distribution of the Oils and Condensates ........ 70
6.3 Results based on the GC-MS ........ 72
6.3.1 Summary of the GC-MS results ........ 73
6.5 Downscaled TLC-FID, GC-FID and GC-MS chromatograms ........ 76
7. Discussion ........ 105
7.1 Gross sample evaluation based on the Iatroscan TLC-FID........ 107

7.1.1 Gross sample evaluation based on the Iatroscan TLC-FID of the core extracts from the Finnmark Platform and the Nordkapp Basin ........ 107

7.1.2 Oil/Condensate evaluation based on the Iatroscan ........ 109

7.2 Medium range maturity parameters ........ 111

7.2.1 Qualitative approach to the n-alkane distribution of the GC-FID chromatogram ........ 111

7.3 Maturity of the oils, condensates and core extracts ........ 114

7.3.1 Maturity estimation based on the biomarkers ........ 114

7.3.2 Maturity assessment based on medium ranged maturity parameters ........ 121

7.3.3 Summary of the maturity parameters ........ 127

7.4 Organic Facies ........ 127

7.4.1 Organic Facies Tables ........ 128

7.4.2 Summary of organic facies ........ 137

7.5 Biodegradation ........ 137

7.5.1 Biodegradation based on temperatures at present day ........ 137

7.5.2 In-situ temperature for oils and condensates ........ 138

7.6 Oil/condensate families and mixing of sources ........ 139

7.6.1 The LH samples ........ 142

7.6.2 The JC samples ........ 143

7.6.3 The Heilo prospect (H1) sample ........ 145

7.6.4 The S samples ........ 145

7.6.5 The Alke structure (A1) sample ........ 145

7.6.6 The FP and NB samples ........ 146

7.7 Migration pathways ........ 146

8. Conclusions and future work ........ 151

8.1 Conclusions ........ 151

8.2 Suggestions for future work ........ 152

References ........ 155

Appendix A ........ 161

Appendix B ........ 176

Appendix C ........ 190

Appendix D ........ 272

# 1. Introduction

## 1.1 Introduction to the SW Barents Sea

The Barents Sea is located off the coast of Norway and Russia (see Figure 1.1). The surface area of the sea is 1,400,000 km$^2$ (Halland et al., 2014). The Barents Sea comprises vast unexplored territories, and exploration activities have hitherto mostly been confined to the SW part of the Norwegian sector.

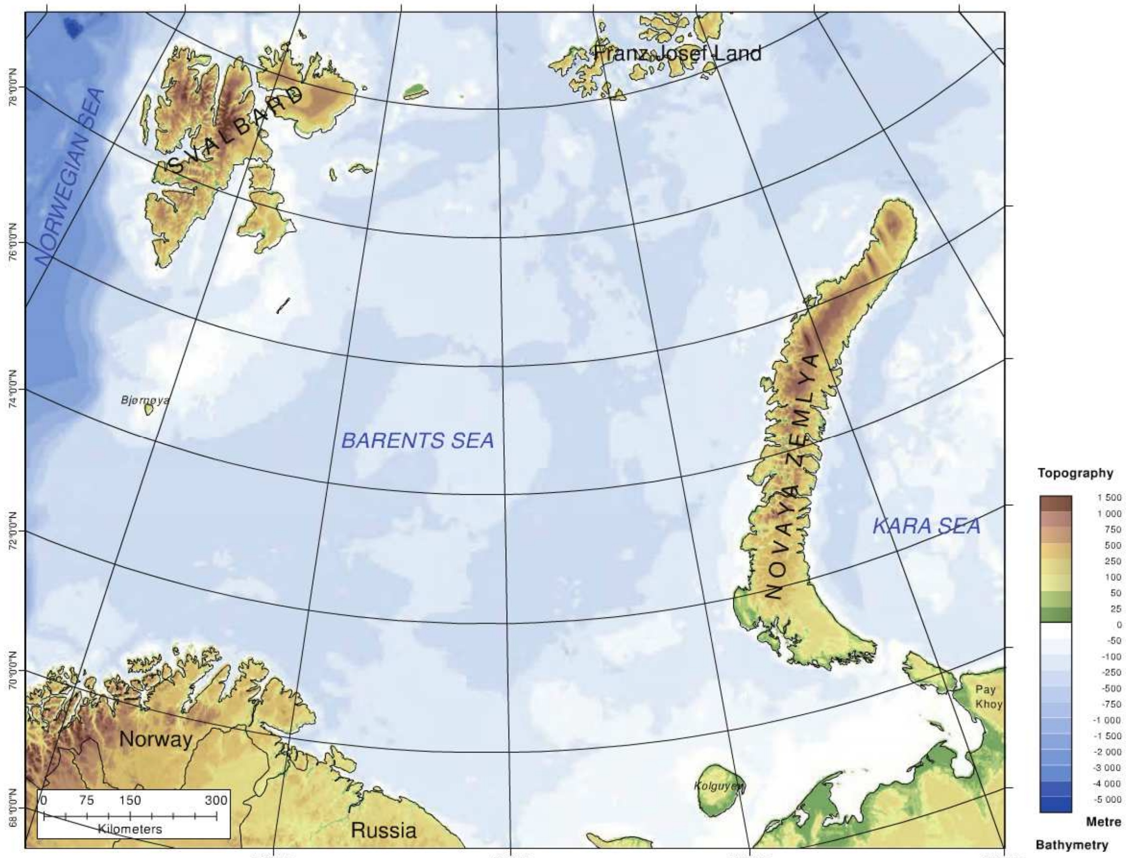
Franz Josef Land
SVALBARD
NORWEGIAN SEA
Bjørnøya
BARENTS SEA
NOVAYA ZEMLYA
KARA SEA
Pay Khoy
Norway
Russia
Kolguyev
0 75 150 300
Kilometers
78°0'0"N
76°0'0"N
74°0'0"N
72°0'0"N
70°0'0"N
68°0'0"N
30°0'0"E
40°0'0"E
50°0'0"E
60°0'0"E
Topography
1 500
1 000
750
500
250
100
50
25
0
-50
-100
-250
-500
-750
-1 000
-1 500
-2 000
-3 000
-4 000
-5 000
Metre
Bathymetry

**Figure 1.1: The Barents Sea is situated outside the coast of Norway and Russia, covering an area of 1.4 million km$^2$. The topography and bathymetry are visualized with colors (modified from Halland et al., 2014).**

The first geophysical investigations began during the early 1970s, and the first offshore drilling in the beginning of the 1980s in the Norwegian sector (Dore., 1995). Early explorations lead to the first commercial discovery of the Snøhvit gas field in 1984 located within the Hammerfest Basin (Berglund et al., 1986). Moreover, the discovery of dry traps containing residual black paleo-oil with columns up to 200 m (Knutsen et al., 2000), indicates previous generation and migration of petroleum, which later have remigrated from the reservoirs, due to Cenozoic upliftment (Henriksen et al., 2011a). The upliftment resulted in expansion of the gas column as a cause of changes in pressure, forcing the oil below the spill point (England and Mackenzie, 1989, Henriksen et al., 2011a). Ohm et al. (2008) also believed remigration of the paleo-oil is a result of fault reactivation leading to cap-rock failure. Consequently, the Norwegian sector of the Barents Sea was considered a gas-prone area for many years. The more recent oil discoveries, Goliat field in 2000, the Nucula field in 2007, Johan Castberg oil field in 2011, Havis discovery in 2012 and the novel Gotha discovery in 2013 (Lerch et al., 2016a, NPD, 2013), disproved this assumption. The aforementioned discoveries revived the interest in the area as a promising place for commercial quantities of oil. The remigration of the oil has lead exploration to the uplifted margins of the basins, assuming oil to migrate up-dip (Lerch et al., 2016a). Oil discoveries with profoundly contradistinctive signatures can be found in and around the Hammerfest Basin, and on the Loppa High (Ohm et al., 2008, Lerch et al., 2016b, Bjorøy et al., 2010), suggesting oil and condensate discoveries to originate from several source rocks and possible mixing of sources.

## 1.2 Introduction to the Loppa High, the Hammerfest Basin, the Nordkapp Basin and the Finnmark Platform

Larger quantities of oil have recently been discovered on the Loppa High (7120/1-3), situated in carstified Permian rocks (NPD, 2013). Oil shows have also been discovered on the Loppa High in Late Jurassic – Cretaceous rocks in well 7120/1-2 (NPD., 2014). On the western part of the Loppa High oil remnants in Late Carboniferous to Early Permian Formations have also been found in well 7220/6-1 (NPD., 2014). Most of the discoveries of petroleum have been done in and at the margins of the Hammerfest Basin, e.g. Snøhvit, Goliat and Nucula. Discoveries in the middle part of the basin tend to be condensate/gas while discoveries in the margins contain oil (Lerch et al., 2016b). The reservoirs in the Hammerfest Basin are mostly of Jurassic age, e.g. Snøhvit (7120/6-1) and Tornerose (7122/6-1), while the Goliat field is of Triassic age. The Hammerfest Basin is also believed to be a kitchen for the surrounding structural highs and fault complexes (Ohm et al., 2008). Much less exploration activity has been done in the Nordkapp Basin and on the Finnmark Platform. Nonetheless, well 7228/7-1 has showed remnants of oil in the Late Triassic Snadd Formation (NPD., 2016b). Moreover, well 7128/4-1 on the Finnmark Platform found remnants of oil and gas in Late Permian Formations (NPD., 2016b).

## 1.3 Thesis objectives

The main emphasis in this thesis is on the petroleum geochemical signatures of the Loppa High sample from 7120/2-1. However, to attain a broader perspective of the complex area, adjacent wells on the Loppa High and the surrounding areas as the Bjørnøyrenna Fault Complex and the Hammerfest Basin are also investigated. The addition of samples gives valid information on source rock relations to one another and source rock origin of the respective discoveries. As most of the discoveries in the Hammerfest Basin seem to have been sourced by the Jurassic Hekkingen Formation (Ohm et al., 2008), it is interesting to investigate if the discoveries on the Loppa High and the Bjørnøyrenna Fault Complex (Johan Castberg) discoveries reflect the same geochemical signatures. In addition, shallow core samples from the Finnmark Platform and the Nordkapp Basin have also been extracted and geochemically analyzed. The shallow cores situated on the Finnmark Platform are within Carboniferous to Permian rocks reflecting the same depositional environment and geological era as the 7120/2-1 discovery. Therefore, it is relevant to compare the extracted bitumen from the Finnmark Platform with the Permian oil from the Loppa High, to investigate if they can be related to the same source. Subsequently, the shallow core from the Nordkapp Basin within Early Jurassic Formation can be compared to the Jurassic oil discoveries.

The main objectives in this MSc thesis are as follows:

- To investigate if the Loppa High sample is related to a pre-Jurassic source, in other words, source rock determination of well 7120/2-1 DST 4. Determination of source rock origins will also be done for the rest of the sample set. The maturity and organic facies parameters will be the main tools to answer these questions.
- To address the quality of the source rocks for the sample set.
- To evaluate geochemical similarities and discrepancies of the respective oils/condensates. To later use this information to determine if they originate from the same source or not.
- To investigate the level of biodegradation of the sample set.
- Discuss what effects upliftment have had on the region.
- To address if the discoveries contain a mix of petroleums.
- Assess migration pathways in the area.

- Finally, to compare the bitumen samples from the Finnmark Platform with the depositional analog from the Loppa High and the Nordkapp Basin core with related Jurassic discoveries.

# 2. Geological Setting

Chapter two gives an overview of the geological framework in the Barents Sea with special emphasis on the SW part. The source rock potential, maturity history and geological plays will also be briefly introduced.

The chapter is structured as follows:

2.1 Introduction to the Barents Sea

2.2 Structural elements and evolution of the SW Barents Sea

2.3 Stratigraphy of the SW Barents Sea

- 2.3.1 Paleozoic Succession:
- 2.3.2 Mesozoic Succession
- 2.3.3 Cenozoic Succession

2.4 Key structures in the SW Barents Sea

- 2.4.1 Loppa High
- 2.4.2 Hammerfest Basin
- 2.4.3 Finnmark Platform
- 2.4.4 Nordkapp Basin

2.5 Petroleum system in the SW Barents Sea

- 2.5.1 Source Rocks
- 2.5.2 Maturity history
- 2.5.3 Overview of petroleum plays in the SW Barents Sea

## 2.1 Introduction to the Barents Sea

The Barents Sea is a large pericontinental sea covering the continental shelf of NW Eurasia, bounded in the West and North by Cenozoic passive margins (Figure 1). A relatively complete strata ranging from Late Paleozoic to Quartenary with vertical thickness up to 15 km can be found (Gudlaugsson et al., 1998). The region is described as very complex, with basins, platforms, structural highs, fault zones, and diapiric provinces (Johansen et al., 1993, Worsley, 2008). The sea was formed by two major continental collisions and later ripped apart by a continental separation. The first compressional event started 400 Ma ago as the Caledones developed; this resulted in the closing of the Iapetus Sea. The eastern margins of the Barents Sea were further developed by the orogeny of the Urals approximately 250 Ma ago. This finalized the closing of the continents and Pangea were formed (Scotese, 1987) During Late Paleozoic and Mesozoic the Barents Sea was dominated by extensional forces. The tensile forces resulted in an area dominated by major rift basins with platforms and structural highs (Dore., 1995).

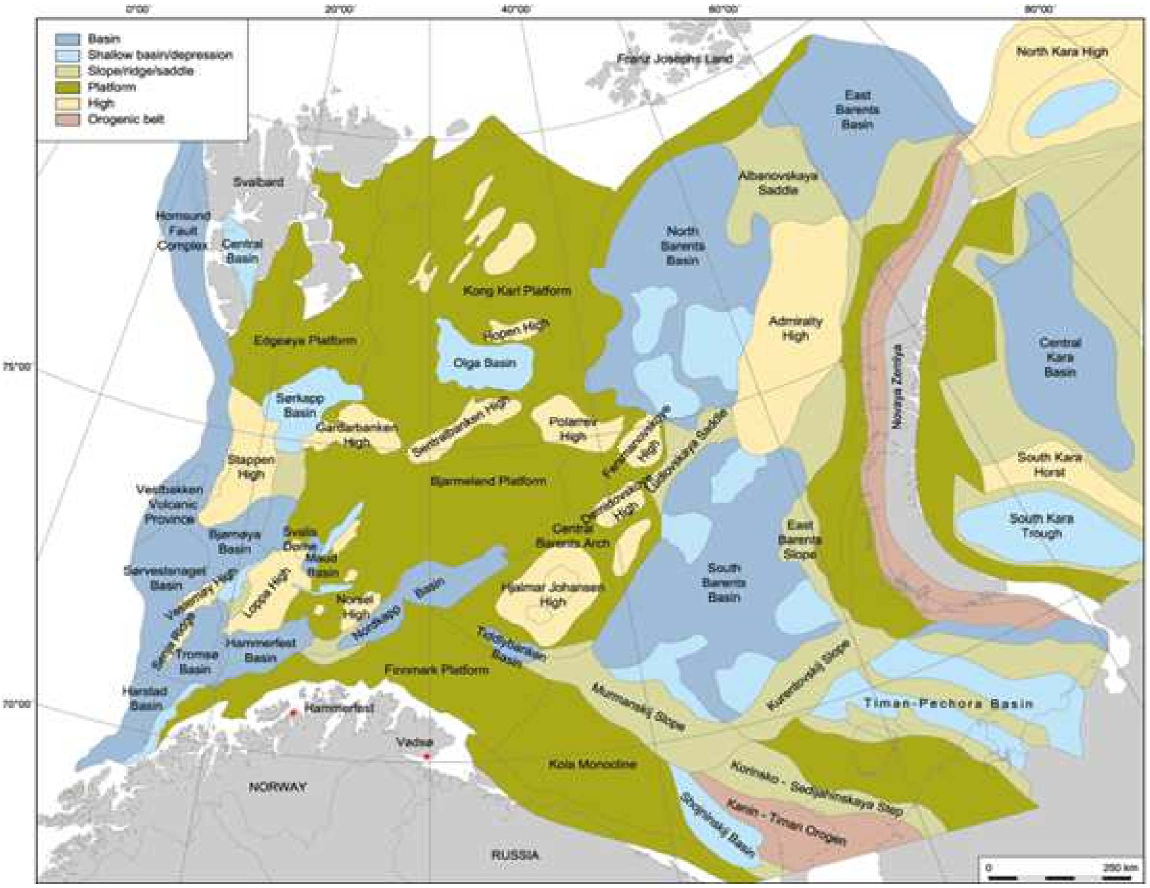
0°00'
20°00'
40°00'
60°00'
80°00'
75°00'
70°00'
Basin
Shallow basin/depression
Slope/ridge/saddle
Platform
High
Orogenic belt
Franz Josephs Land
North Kara High
East Barents Basin
Svalbard
Hornsund Fault Complex
Central Basin
Albanovskaya Saddle
North Barents Basin
Kong Karl Platform
Admiralty High
Hopen High
Edgeøya Platform
Olga Basin
Novaya Zemlya
Central Kara Basin
Sørkapp Basin
Gardarbanken High
Sentralbanken High
Polarrev High
Stappen High
South Kara Horst
Bjarmeland Platform
Vestbakken Volcanic Province
Central Barents Arch
South Kara Trough
Bjørnøya Basin
Svalis Dome
Maud Basin
East Barents Slope
Sørvestsnaget Basin
Loppa High
Hjalmar Johansen High
South Barents Basin
Nordsel High
Nordkapp Basin
Tromsø Basin
Hammerfest Basin
Finnmark Platform
Harstad Basin
Hammerfest
Murmanskij Slope
Timan-Pechora Basin
Vadsø
Kola Monocline
NORWAY
Kanin - Timan Orogen
RUSSIA
0
250 km

**Figure 2.1: Structures of the greater Barents Sea (Both Russian and Norwegian sector) (Henriksen et al., 2011b)**

## 2.2 Structural evolution of the SW Barents Sea

The western Barents Sea can be divided into three geological provinces: 1) a basinal province with an EW trend which is located from the coast of Norway to 74°; 2) to the North an elevated platform area towards Svalbard; and 3) the continental margin to the west (Faleide. et al., 1984). The development of several fault bounded basins and structural highs in the western Barents Sea reflects a high tectonic activivity in the area.

The western Barents Sea sediments are situated above a Late Silurian to Early Devonian Crystaline metamorphic basement. This basement was consolidated during the Calodian Orogeny (Faleide. et al., 1984, Smelror. et al., 2009)

The main structures in the SW Barents were developed due to three Post-Caledonian extensional tectonic events:

1) Sediments from Devonian were compressively deformed during the Late Devonian and are referred to as the Svalbardian movements where the compressional regime from the Svalbardian movements changed the compressional regime to a sinestral shear regime with large scale strike slip movements (Faleide. et al., 1984).

2) In mid Jurassic to Early Cretaceous the mid and Late Kimmeriane phase, where subsidence between Greenland and Norway took place at a rapid pace.

3) The last phase occurred in the Cenozoic and was related to the opening of the Norwegian-Greenland Sea. This break-up phase is associated with Cenozoic upliftment and erosion (Johansen et al., 1992). The upliftment is estimated by Vorren et al. (1991) to be between 500-3000m in the area. The Barents Sea continental shelf was dominated by ENE-WSE to NE-SW and NNE-SSW to NNW-SSE structural trends (Gabrielsen et al., 1990). The extensional force during Late Paleozoic times resulted in a westward migration of the rifting, and well defined pull-apart basins were formed in the SW. Subsidence due to Jurassic-Cretaceous rifting resulted in the development of several sedimentary basins from the Rockall Trough and northwards.

The Barents Sea was situated in a rift shear interaction having relations to both the North Atlantic and Arctic region (Faleide. et al., 1984). In the Late Paleozoic a NE 600km extending rift zone was formed. The rift zone was 300km wide. Subsidence due to Jurassic-Cretaceous rifting resulted in the development of several sedimentary basins from the Rockall Trough and northwards. The rift zone was an extension of the north Atlantic rift between Norway and Greenland. The development of the rift zone created a series of fan shaped arrays and highs, and the orientation was NE in the main rift zone and north at the continental margin to the West (see Figure 2.2). Evaporates were deposited during Late Devonian-Carboniferous and in the Early to Mid Mesozoic the main graben formation and salt tectonic development took place in the SW Barents Sea (Smelror et al., 2009) (see Figure 2.2). Subsidence due to Jurassic-Cretaceous rifting resulted in the development of several sedimentary basins from the Rockall Trough and northwards.

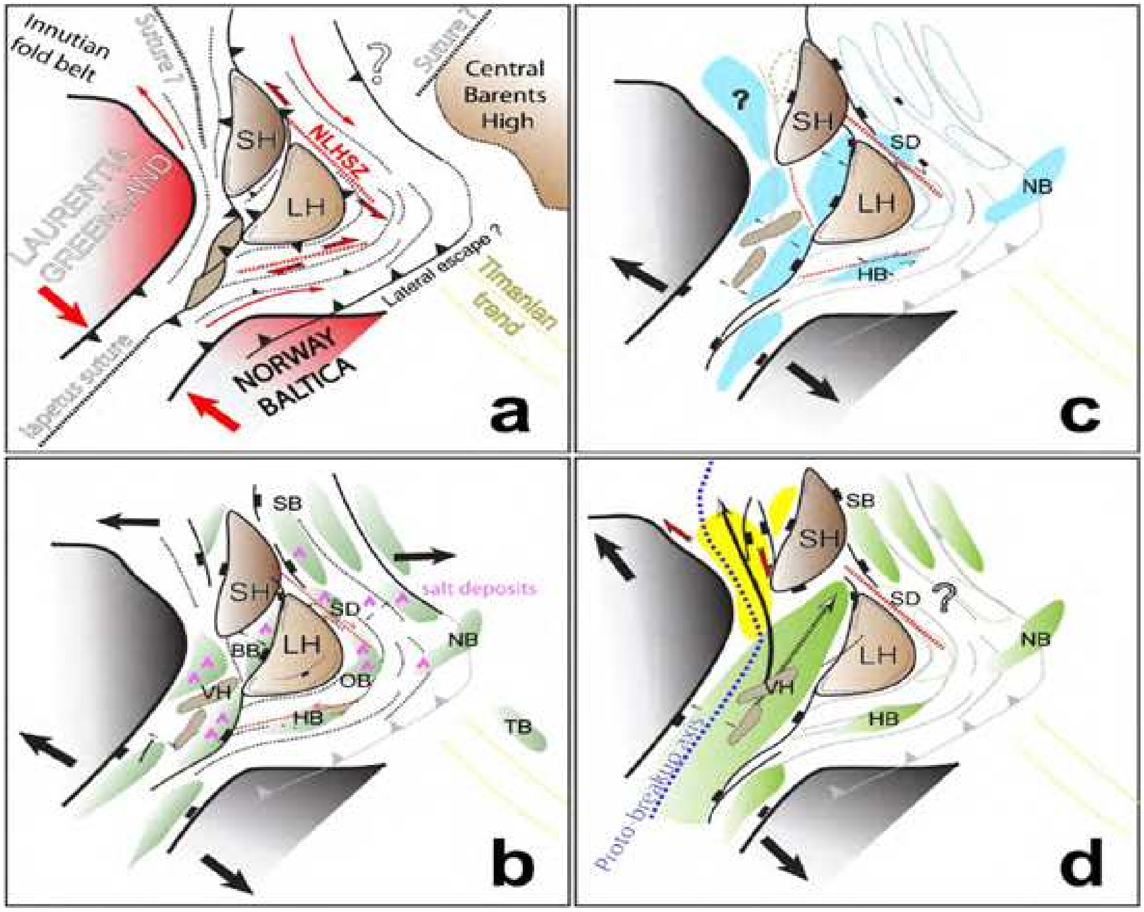
Innutian fold belt
Suture ?
?
Suture ?
Central Barents High
SH
NLHSZ
LH
LAURENTIA GREENLAND
Lateral escape ?
Timanian trend
NORWAY BALTICA
Iapetus suture
a
?
SH
SD
NB
LH
HB
c
SB
SH
salt deposits
SD
NB
BB
LH
OB
VH
HB
TB
b
SB
SH
SD
?
NB
LH
VH
HB
Proto breakup axis
d

**Figure 2.2: Structural evolution of the SW Barents Sea; a) Late Devonian time the area escaped laterally from the compressional regime ; b) Reactivation of main features and graben development from the Palezoic in Late Devonian to Carboniferous ; c) The main stage of graben development and salt tectonics from Early to Mid Mesozoic; d) In the Late Mesozoic the extensive thinning of the crust resulted in the break up between the Laurentia and Baltica plate in early Cenozoic (Gernigon and Brönner, 2012).**

## 2.3 Stratigraphy of the SW Barents Sea

The stratigraphy of the SW Barents Sea ranges mainly from Late Carboniferous to Early cretaceous (see Figure 2.3). However, younger strata from the Cenozoic can also be found in the region. The Groups are more thoroughly explained below:

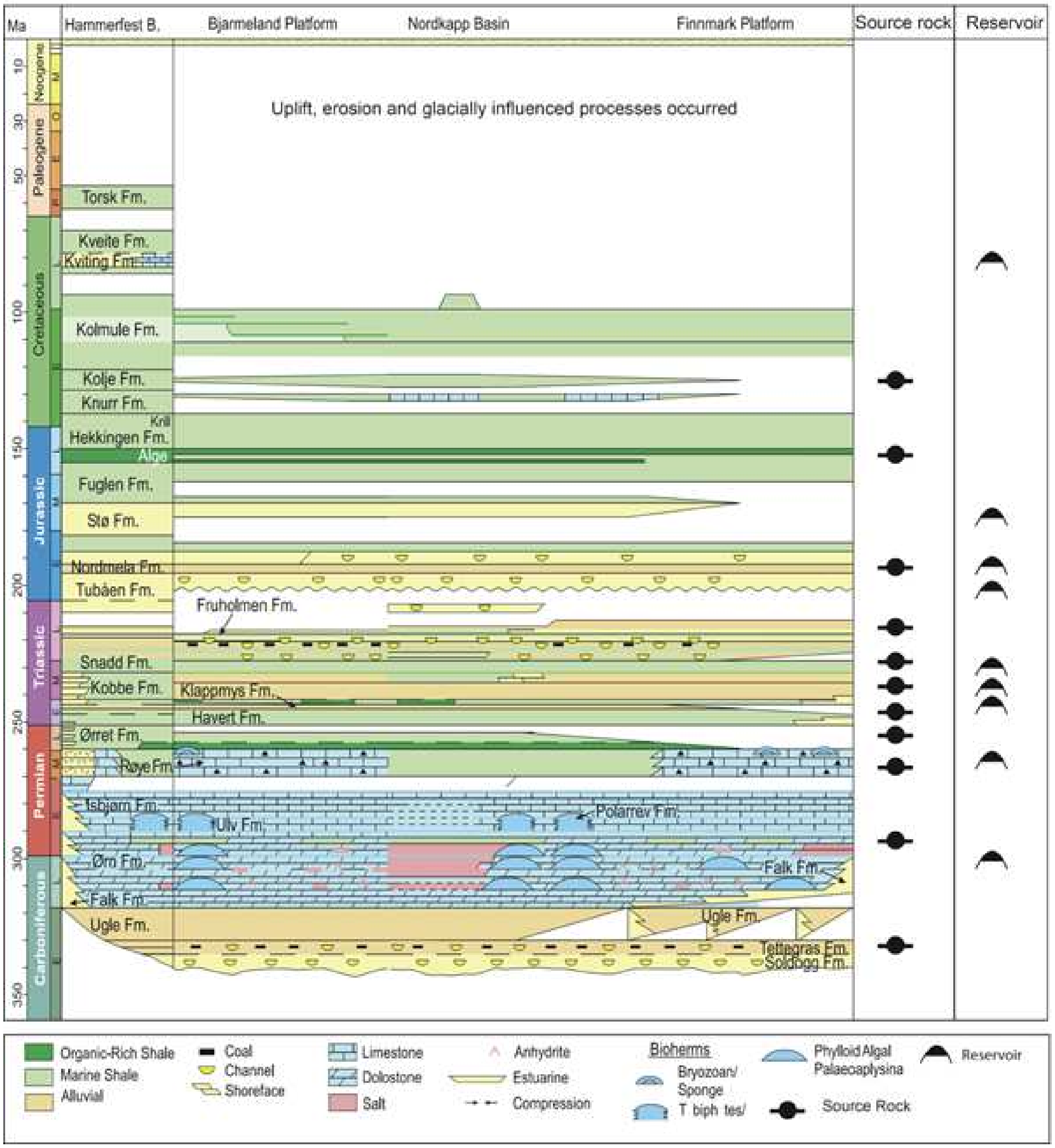

**Figure 2.3: The lithostratigraphy from Carboniferous to Neogene is displayed for the areas in the SW Barents Sea: the Hammerfest Basin, the Bjarmland Platform, the Nordkapp basin and the Finnmark Platform. The Formations related source rocks and reservoirs are also illustrated in the Figure 2.3. The picture is modified by Lerch et al. (2016b) taken from (Ohm et al., 2008).**

## 2.3.1 Paleozoic Succession:

***The Billefjorden Group***

The sediments were deposited in Late Devonian to Early Carboniferous and are dominated by fluvial deposits in the lower part of the Group transitioning into shallow marine siliclastics (Larssen et al., 2002). Some coal can also be found in this Group. The Group is subdivided into three Formations; Soldogg, Tettegras and Blærerot (NPD., 1988) (see Figure 2.3).

***The Gipsdalen Group***

The Group was deposited Mid Carboniferous to Early Permian and consists of red colored warm-water siliclastics and dolomized carbonates. The basal area has significant amounts of evaporates indicating an arid climate. A significant presence of evaporates and diapirs appear in the Nordkapp Basin (Larssen et al., 2002). Three Formations are assigned to the Gipsdalen Group; the Ugle Formation, Falk Formation and Ørn Formation (NPD., 1988) (see Figure 2.3).

***The Bjarmland Group***

The Group is dated by Ehrenberg et al. (2001) to be of Early Permian age. It is dominated by light bioclastic limestone from a cool-water fauna, with crinoids, bryozoans, brachiopods and siliceous sponges (Larssen et al., 2002). The presence of siliclastic material is rare in the Formation except on the Polheim Subplatform. The thickest succession of the Group can be found on the Bjarmland Platform and at the Loppa High. The Bjarmland Group is built up by three Formations Polarrev, Ulv and Isbjørn respectively (see Figure 2.3).

***The Tempelfjorden Group***

From Middle to Late Permian the Tempelfjorden Group was deposited. The unit is characterized by dark to light grey spiculites and silicified skeletal carbonates. It contains more coarse siliclastics in the Hammerfest Basin (Larssen et al., 2002). The Group is divided into two Formations, the Røye Formation and the Ørret Formation (NPD., 1988) (see Figure 2.3).

## 2.3.2 Mesozoic Succession

***The Ingøydjupet Group***

The lowermost Ingøydjupet Group in the Mesozoic succession in the SW Barents Sea is from Early-Mid Triassic. The Group is built up by the Havert, Klappmys, Kobbe and Snadd Formations. The Group is approximately 1700m thick and consists of a siliclastic and carbonate sequence in the lower part. The upper part is marked by a shale interval (Halland et al., 2014). Thin silt and sand beds are also present, especially in the upper part. Some carbonate and coal are also present (NPD., 1988) (see Figure 2.3).

***The Realgrunnen Group***

The Realgrunnen Group above the Ingøydjupet Group ranges from Late-Triassic to Mid Jurassic. The Group is divided into the Fruholmen,Tubåen, Nordmela and the Stø Formations. The thickness of the Group is around 430m. The lower part of the Group has some shale and coal intervals (Halland et al., 2014). The Group is dominated by pale grey sandstone especially in the middle and upper parts (NPD., 1988) (see Figure 2.3).

***The Teitengrunnen Group***

A truncation marks the boundary between the underlying Realgrunnen Group and the overlying Teistengrunnen Group. The Group is subdivided into Fuglen Formation and Hekkingen Formation. The vertical thickness varies from 300m north of the Finnmark Fault complex to 60m on the structural highs in the center of the Hammerfest Basin. The Group is dominated by shales and claystones, with some thin beds of dolomitic limestone. A few silt and sandstone beds are also present (NPD., 1988) (see Figure 2.3).

***The Nordvestbanken Group***

The Group consists of Dark grey to grey brown shales and claystone. Some thin interbeds of grey to grey brown siltstone, limestone and dolomite are also present. The Group was deposited from Early to Mid Cretaceous. Three Formation is assigned to this Group; Knurr, Kolje and Kolmule (NPD., 1988) (see Figure 2.3).

***The Nygrunnen Group***

It comprises greenish grey to grey claystone, with thin intervals of limestone in some parts. The Group is of Mid to Late Cretaceous age and is divided into the Kviting and Kveite Formation (NPD., 1988) (see Figure 2.3).

### 2.3.3 Cenozoic Succession

***The Sotbakken Group***

The Group is dominated by claystones with some siltstone, tuffaceous and carbonate horzions. The basal contact of the Group represents an unconformity between the Late Cretaceous and Early Paleocene in the Tromsøflaket area. Age is of Late Paleocene to Early-Middle Eocene. The Torsk Formations is within the Sotbakken Group (NPD., 1988) (see Figure 2.3).

***The Nordland Group***

The Group is dominated by sands and clay in the lower part, which grade into sandstones and claystone. The Group is coarsening upwards. Cobbles and boulders of quartzite, granite appear in the upper part of the Group (NPD., 1988). The age of the Group in the Hammerfest Basin is Late Pliocene to Pleistocene/Holocene (Eidvin et al., 1998).

## 2.4 Key structures in the SW Barents Sea

### 2.4.1 Loppa High

The Loppa High was formed due to Early Cretaceous tectonism and Late Createaceous to Early Tertiary tectonism (Gabrielsen et al., 1990). The Loppa High is an N-S trending feature (see Figure 2.4A). The structural feature has a history of several phases of tilting and erosion due to uplift and subsidence. Subsequently, rifting topography from Late Carboniferous was filled in by Upper Paleozoic siliclastics, evaporites and carbonate. In Late Paleozoic to Early Mezosoic Loppa High was uplifted and tilted, and a Triassic succession was deposited on top of this (Snadd Formation). On the southern part of the Loppa High remnants of Paleogene shale from the Sotbakken Group are overlying Middle Triassic claystones (Halland et al., 2014).

## 2.4.2 Hammerfest Basin

The Hammerfest Basin was probably established during Late Carboniferous, and is a fault-controlled basin extending E-W to WNW-ESE (Gabrielsen et al., 1990, Halland et al., 2014) (see Figure 2.4A). The basin was established by Early to Late Carboniferous rifting. The main subsidence occurred during the Triassic and Lower Cretaceous, although the basin development reached its peak in the Mid Cretaceous (Larssen et al., 2002). The basin is dominated internally by E-W trending faulted dome-structures developed during Late Jurassic tectonism (Halland et al., 2014).

## 2.4.3 Finnmark Platform

The Finnmark Platform has been sTable since Upper Paleozoic (Gabrielsen et al., 1990), the Platform is following the outside of the Norwegian mainland (see Figure 2,4A). The deeper part of the Finnmark platform consists of silliclastic sediments from the Early Carboniferous. These sediments are heavily faulted, with rotated fault blocks (Larssen et al., 2002). A Late Carbonifoures succession consisting mostly of carbonates is overlying the faulted blocks. A transgression during the Late Permian resulted in a thick succession of mixed silliclastic and carbonate deposits. The Finnmark Platform has a dipping trend towards North, due to several phases of upliftment, with the latest event during Tertiary (Larssen et al., 2002) (see Figure 2.4C).

## 2.4.4 Nordkapp Basin

The Nordkapp Basin is a Paleozoic rift basin. In Late Carboniferous – Early Permian significantly amounts of salt were deposited in the basin. Subsequently, the salt has been mobilized several times (Gabrielsen et al., 1990). Upper Paleozoic and Mesozoic sediments have been uplifted due to formation of salt diapirs during Early - Middle Triassic, Late Jurassic, Late Cretaceous and Tertiary (Bugge et al., 2002). The aforementioned sediments can be found at shallow depths around the salt diapirs.

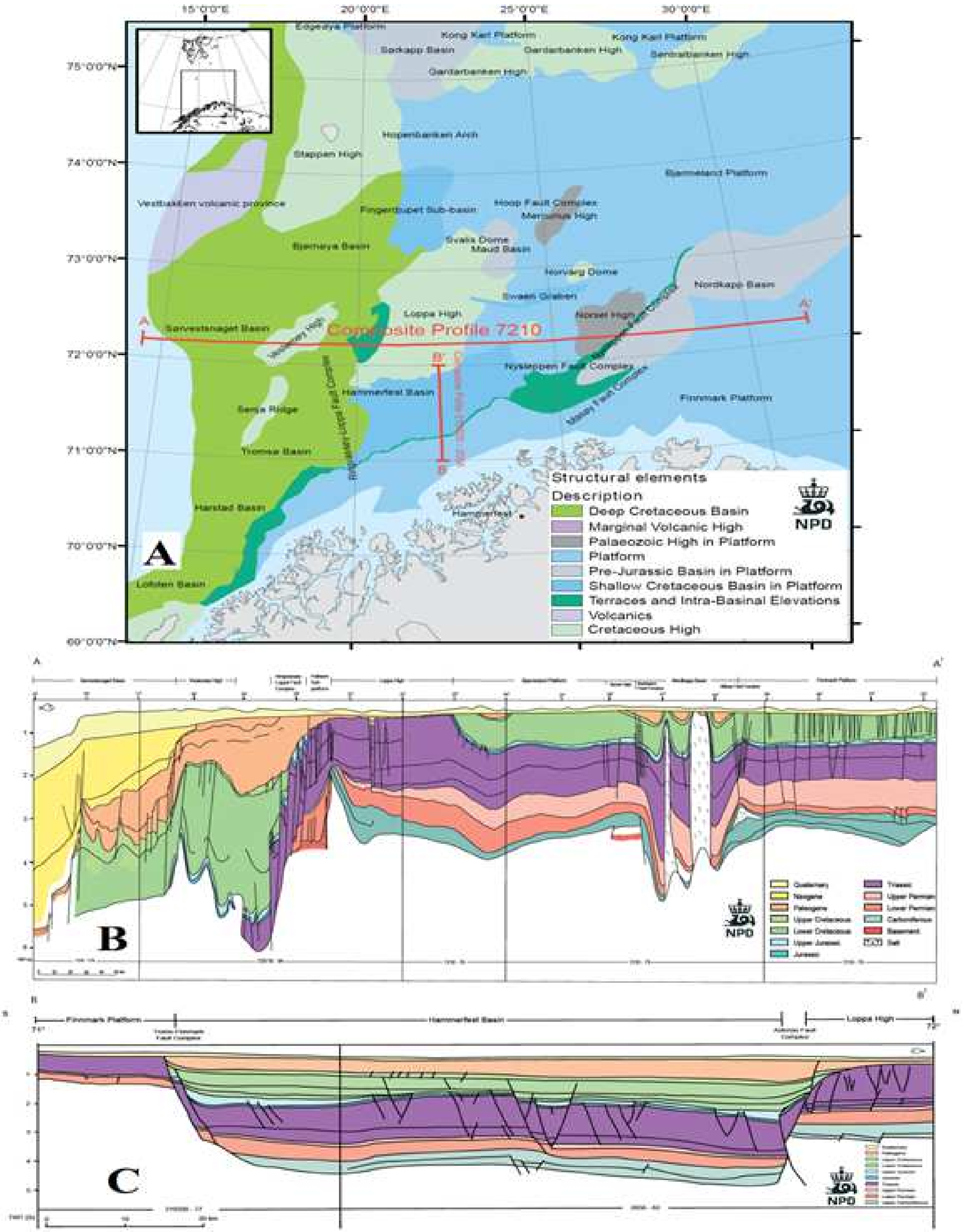
15°0'0"E
20°0'0"E
25°0'0"E
30°0'0"E
75°0'0"N
74°0'0"N
73°0'0"N
72°0'0"N
71°0'0"N
70°0'0"N
69°0'0"N
Edgeøya Platform
Kong Karl Platform
Sørkapp Basin
Gardarbanken High
Sentralbanken High
Stappen High
Hopenbanken Arch
Bjarmeland Platform
Vestbakken volcanic province
Fingerdjupet Sub-basin
Hoop Fault Complex
Mercurius High
Bjørnøya Basin
Svalis Dome
Maud Basin
Norvarg Dome
Nordkapp Basin
Swaen Graben
Loppa High
Nordsel High
Sørvestsnaget Basin
Veslemøy High
Composite Profile 7210
A
A'
B'
B
Nysleppen Fault Complex
Hammerfest Basin
Finnmark Platform
Senja Ridge
Ringvassøy-Loppa Fault Complex
Måsøy Fault Complex
Tromsø Basin
Harstad Basin
Hammerfest
Lofoten Basin
Structural elements
Description
🟩 Deep Cretaceous Basin
🟪 Marginal Volcanic High
⬛ Palaeozoic High in Platform
🟦 Platform
⬜ Pre-Jurassic Basin in Platform
🟦 Shallow Cretaceous Basin in Platform
🟩 Terraces and Intra-Basinal Elevations
🟪 Volcanics
🟩 Cretaceous High
NPD
A
B
C
Finnmark Platform
Hammerfest Basin
Loppa High
NPD

**Figure 2.4: The main areas of interest are shown in Figure 2,1A, Hammerfest Basin, Loppa High, Finnmark Platform and Nordkapp Basin respectively. Figure 2.1A also shows the transect of the geosection from western part of the Sørvestnsnaget Basin to the eastern part of the Finnmark Platform (A-A`) (Figure 2.1B). And the transect from the Finnmark Platform to the Loppa High (B-B`) (Figure 2.1C). The pictures are modified by Halland et al. (2014) made (Gabrielsen et al., 1990).**

## 2.5 Petroleum system in the SW Barents Sea

### 2.5.1 Source Rocks

The SW Barents Sea is proven to be a location for multiple source rocks, from Upper Carboniferous to Upper Jurassic (see Table 2.1 and Figure 2.3). The Cretaceous Kolje Formation has been suggested to be mature in the western part of the SW Barents Sea (see Figure 2.4) (Johansen et al., 1992). The source rock with the biggest potential for generation of hydrocarbons in the area is the Hekking Formation, but other Middle and Lower Jurassic source rocks have also shown potential to generate hydrocarbons (Ohm et al., 2008). Upper Triassic shales of the Snadd and Furuholm Formations have proven as prolific source rocks (Johansen et al., 1992). Lower to Middle Triassic Formations are also rich in organic matter (Lundschien et al., 2014). In the eastern part of the study area the Middle Permian Røye Formation and the Upper Permian Ørret Formation have potential for gas and oil generation (Johansen et al., 1992) (see Table 2.1 and Figure 2.4). The Tettegras Formation consists of coal and has the potential to generate liquid hydrocarbons (Van Koeverden et al., 2010). Moreover, Carboniferous shale with promising source rock potential has been reported on the Finnmark Platform (Johansen et al., 1992).

### 2.5.2 Maturity history

According to Vobes (1998) the SW Barents Sea has a geothermal gradient in the center of the Hammerfest Basin of about 35ºC/km and the uplfifted margins and surrounding highs 5ºC lower (30ºC/km). Due to rapid Cenozoic upliftment the Hammerfest Basin and surrounding uplifted regions are believed to be in thermal disequilibrium (Cavanagh et al., 2006). As a consequence of the upliftment the source rocks are assumed to have been exposed to higher maturities than at present day. Figure 2.5 shows where the Upper Jurassic Hekkignen Formation, the Triassic Snadd, Kobbe, Klappmys and Havert Formations and Permian/Carbonifereous source rocks are within the oil generation window.

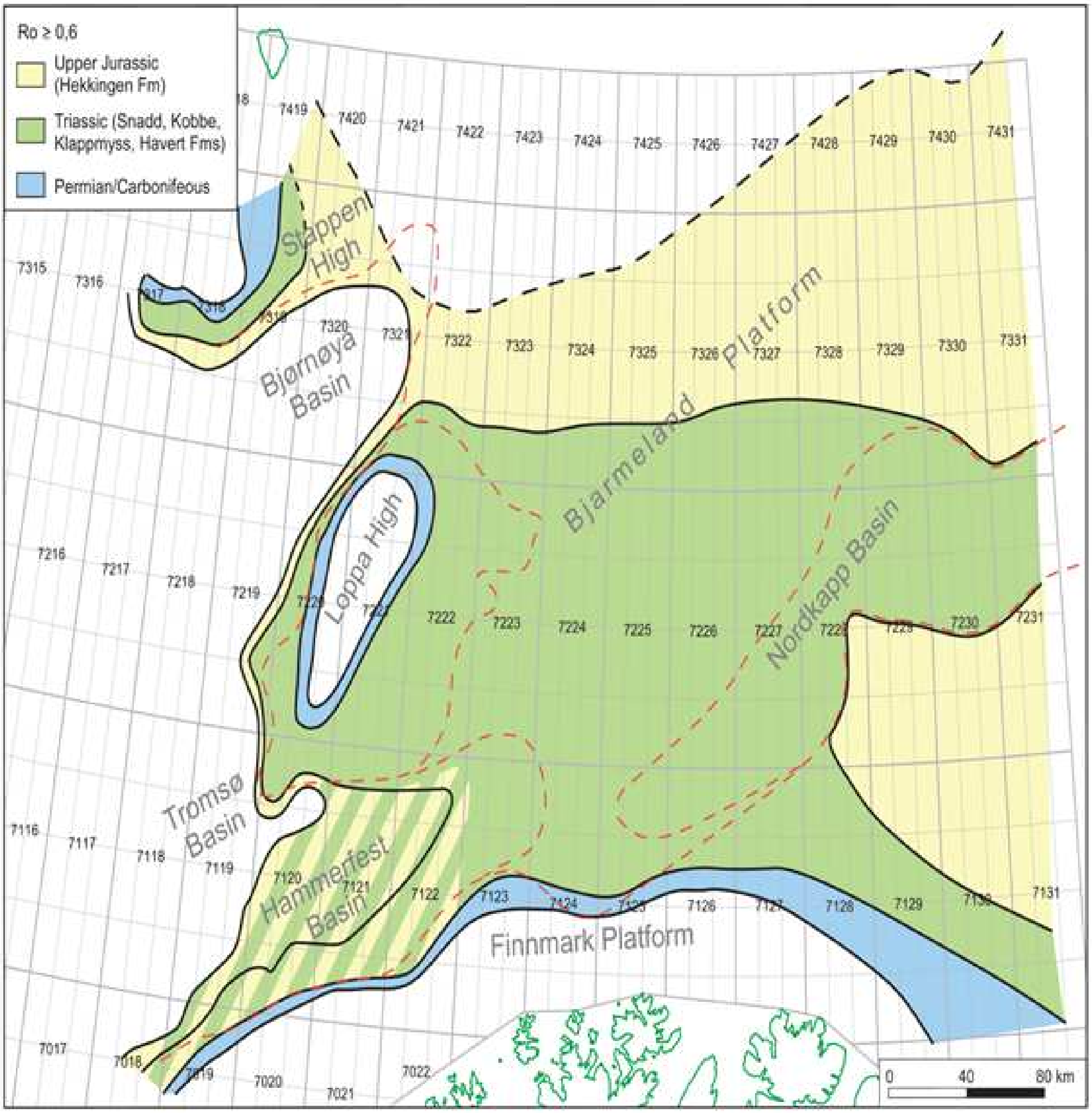
Ro ≥ 0,6
Upper Jurassic (Hekkingen Fm)
Triassic (Snadd, Kobbe, Klappmyss, Havert Fms)
Permian/Carbonifeous
Stappen High
Bjørnøya Basin
Bjarmeland Platform
Loppa High
Nordkapp Basin
Tromsø Basin
Hammerfest Basin
Finnmark Platform
7419
7420
7421
7422
7423
7424
7425
7426
7427
7428
7429
7430
7431
7315
7316
7317
7318
7319
7320
7321
7322
7323
7324
7325
7326
7327
7328
7329
7330
7331
7216
7217
7218
7219
7220
7221
7222
7223
7224
7225
7226
7227
7228
7229
7230
7231
7116
7117
7118
7119
7120
7121
7122
7123
7124
7125
7126
7127
7128
7129
7130
7131
7017
7018
7019
7020
7021
7022
0
40
80 km

**Figure 2.5: The map suggests where Permian, Triassic and Jurassic strata are oil mature. Based on maturity data from wells, semiregional maturity trends and depth maps (Ohm et al., 2008).**

## 2.5.3 Overview of petroleum plays in the SW Barents Sea

The SW Barents Sea has petroleum plays from a wide range of geological eras, ranging from Carboniferous to Jurassic. Table 2.1 summarizes the geological plays in the region.

**Table 2.1: Petroleum plays of the Southern Barents Sea modified from (NPD., 2014). [1]TFFC = Troms-Finnmark-Fault-Complex; [2] RLFC = Ringvassøy-Loppa-Fault-Complex**

| **Age** | Area | Reservoir Rock | Trap | Source Rock |
|---|---|---|---|---|
| Upper Jurassic - Lower Cretaceous | TFFC[1], Bjørnøya Basin, RLFC[2] | Sandstones in the Knur and Kolje Fms. | Stratigraphic pinch-out and some traps are also fault dependent | Late Jurassic shale (Hekkingen Formation) |
| Barents Sea - Lower to Middle Jurassic | Hammerfest Basin, TFFC[1] ,Bjarmeland Platform, Nordkapp Basin and Tromsø Basin | Kapp Toscana Group with Tubåen, Nordmela, Stø and Fruholmen Fms | Rotated fault blocks and some horst structures | Upper Jurassic shale (Hekkingen Formation), with possible contribution from older source rocks |
| Triassic | Bjørnøya Basin, Loppa High, Bjarmeland and Finnmark Platforms | Havert, Klappmyss and Kobbe Formations | Mainly stratigraphic, but also srotated fault blocks and halokinetic | Lower Carboniferous, Lower Permian, Upper Permian, Middle Triassic, Upper Triassic |
| Middle to Upper Permian | Finnmark Platform, Lopap High | Limestones and dolomites | Stratigraphic and a combination of Stratigraphic/structural | Lower Carboniferous, Upper Permian and Middle Triasic |
| Carboniferous to Permian | Finnmark Platform, Loppa High and Polheim Sub-Platform | Limestones, dolostones and sandstones in the Gipsdalen Group | Stratigraphic | Upper Devonian-Lower Carboniferous (Billefjorden Group), Lower Carboniferous , Upper Permian shales (Tempelfjorden Group), Middle Triassic (Steinkobbe Formation) |
| Lower Carboniferous | Finnmark Platform | Sandstone and conglomerates | Structural and stratigraphic | Upper Devonian - Lower Carboniferous (Billefjorden Group) |

# 3. Sample set and well description

In this chapter the oils and condensates will be presented, as well as the extracted core samples.

This chapter is structured as follows:

3.1 Study area

3.2 Description of selected oils and condensates from wells in the SW Barents Sea

3.3 Description of selected core samples and extracts from the Finnmark Platform and the Nordkapp Basin

3.4 Sample List

## 3.1 Study area

The area of this study is located in the SW Barents close to the mainland of Norway (see Figure 3.1 and 3.2). The oils and condensates samples are taken from the Hammerfest Basin, the Loppa High, Måsøy Fault Complex and the Bjørnøyrenna Fault Complex (see Figure 3.1). The shallow cores are situated on the Finnmark Platform and in the Nordkapp Basin (see Figure 3.2).

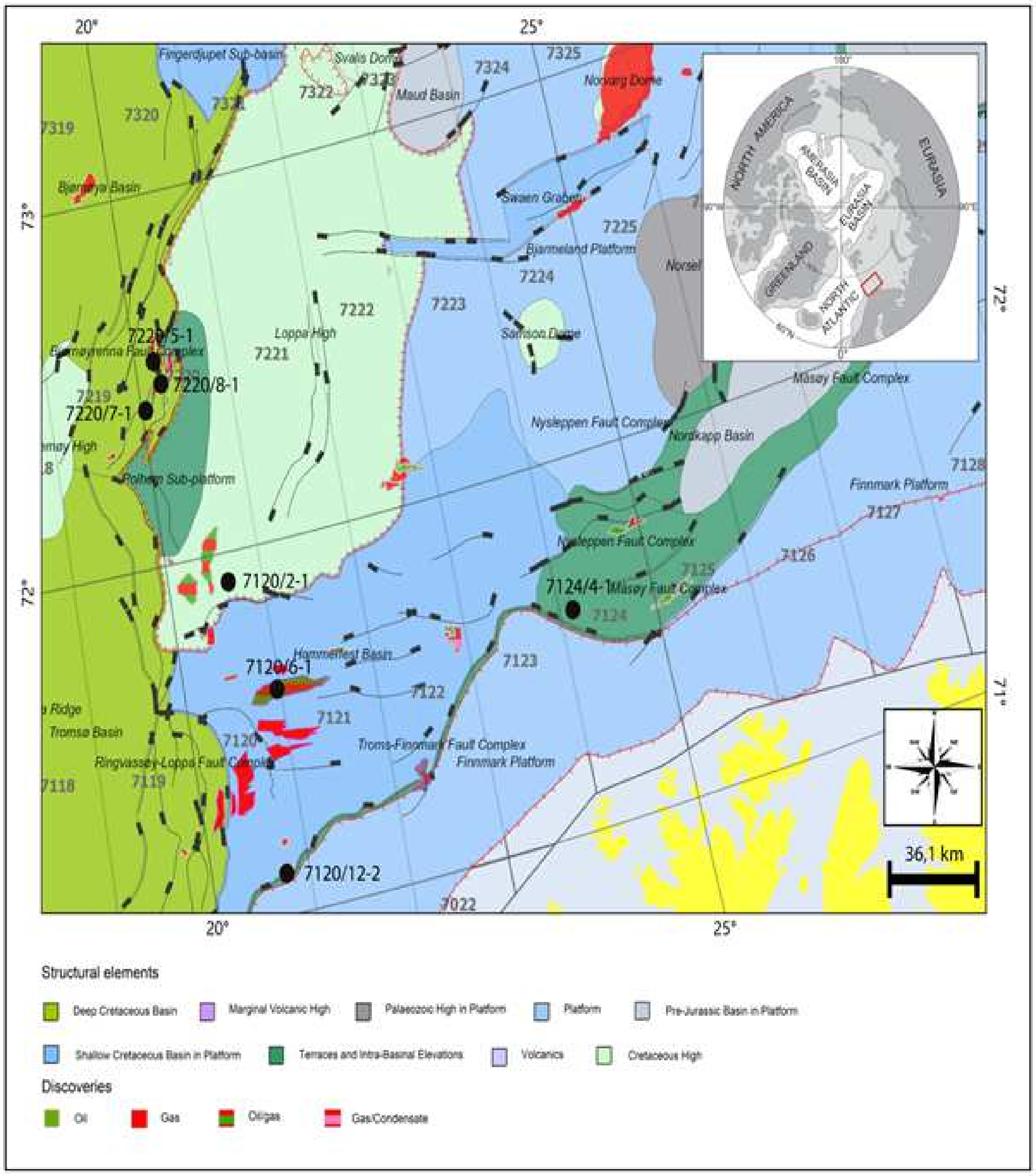
20°
25°
7220/5-1
7220/8-1
7220/7-1
7120/2-1
7120/6-1
7124/4-1
7120/12-2
Loppa High
Hammerfest Basin
Bjarmeland Platform
Nordkapp Basin
Finnmark Platform
Tromsø Basin
Ringvassøy-Loppa Fault Complex
Troms-Finnmark Fault Complex
Måsøy Fault Complex
Nysleppen Fault Complex
Polheim Sub-platform
Swaen Graben
Samson Dome
Norvarg Dome
Maud Basin
Svalis Dome
Fingerdjupet Sub-basin
Bjørnøya Basin
36,1 km
73°
72°
71°
NORTH AMERICA
EURASIA
AMERASIA BASIN
EURASIA BASIN
GREENLAND
NORTH ATLANTIC
Structural elements
Deep Cretaceous Basin
Marginal Volcanic High
Palaeozoic High in Platform
Platform
Pre-Jurassic Basin in Platform
Shallow Cretaceous Basin in Platform
Terraces and Intra-Basinal Elevations
Volcanics
Cretaceous High
Discoveries
Oil
Gas
Oil/gas
Gas/Condensate

**Figure 3.2: The area in the SW Barents Sea where the respective oils and condensates used in this thesis are taken from. The samples are marked with a black dot. The yellow area is the mainland of Norway. The picture is modified from NPD. (2016a)**

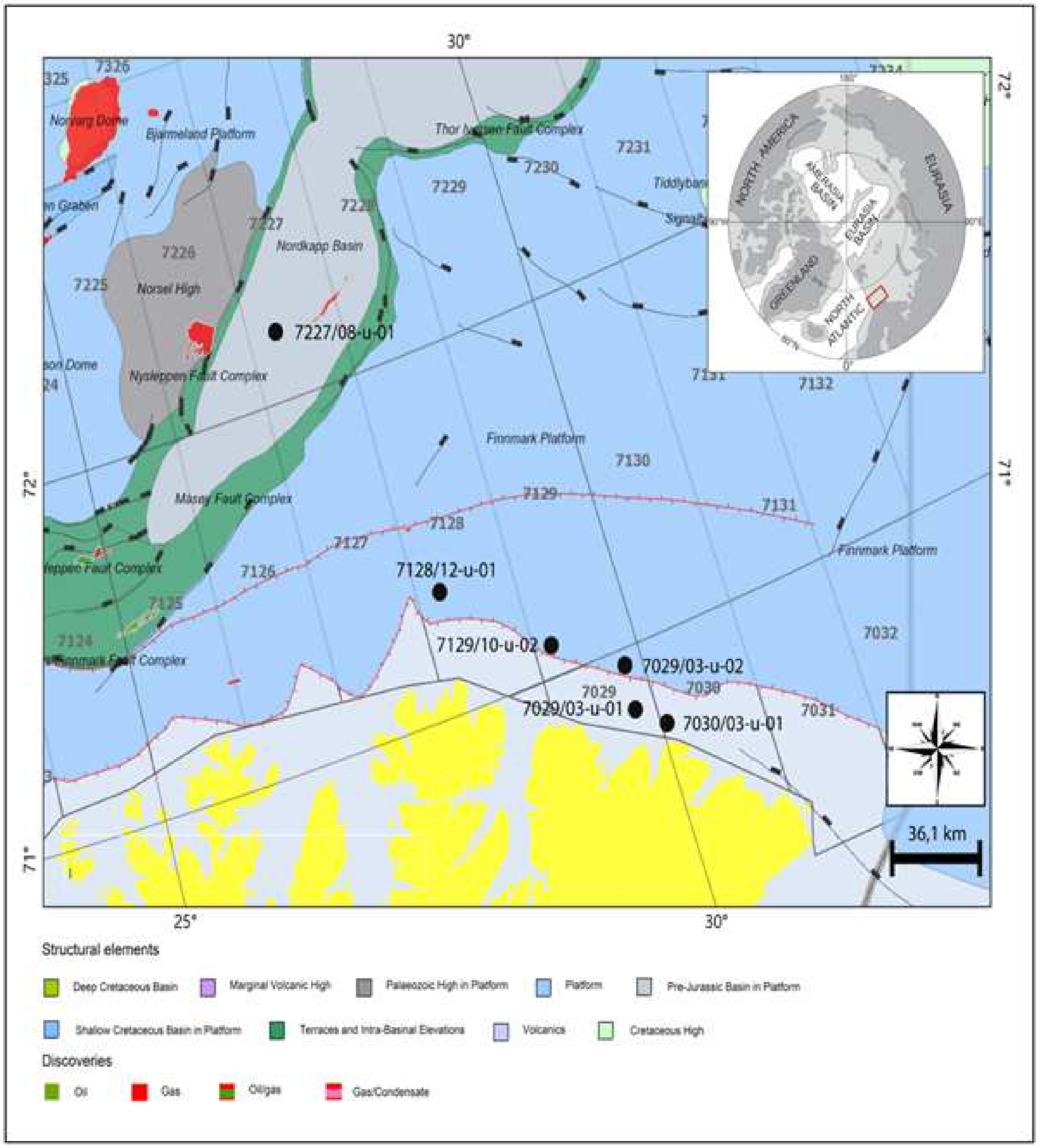
30°
72°
71°
25°
30°
7326
Norvarg Dome
Bjarmeland Platform
Thor Iversen Fault Complex
7231
7230
7229
7228
7227
7226
7225
Nordkapp Basin
Norsel High
Tiddlybanken
7227/08-u-01
Nysleppen Fault Complex
Finnmark Platform
7130
7131
7132
Måsøy Fault Complex
7129
7128
7127
7126
7125
7124
7128/12-u-01
7129/10-u-02
7029/03-u-02
7029/03-u-01
7030/03-u-01
7029
7030
7031
7032
Finnmark Platform
Troms-Finnmark Fault Complex
NORTH AMERICA
EURASIA
AMERASIA BASIN
EURASIA BASIN
GREENLAND
NORTH ATLANTIC
36,1 km
Structural elements
Deep Cretaceous Basin
Marginal Volcanic High
Palaeozoic High in Platform
Platform
Pre-Jurassic Basin in Platform
Shallow Cretaceous Basin in Platform
Terraces and Intra-Basinal Elevations
Volcanics
Cretaceous High
Discoveries
Oil
Gas
Oil/gas
Gas/Condensate

**Figure 3.3: The area in the SW Barents Sea where the respective shallow core samples used in this thesis are taken from. The cores from the Finnmark Platform are taken from Paleozoic strata. The sample form the Nordkapp Basin is within Early Jurassic strata. The samples are marked with a black dot. The yellow area is the mainland of Norway. (modified from NPD., 2016a).**

## 3.2 Description of selected oils and condensates from wells in the SW Barents Sea

### Well 7120/2-1 DST 4 – LH1

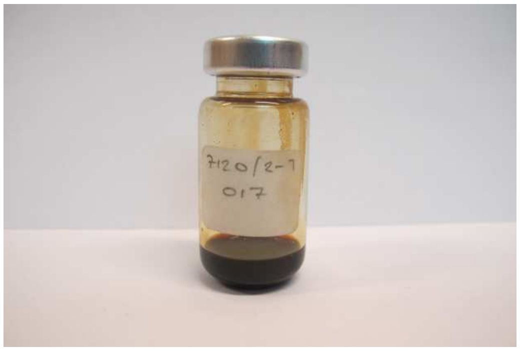

**Figure 3.3: Oil from the Loppa High well 7120/2-1 DST 4. The sample is from the interval 1944-2030m.**

The sample is named LH1 in this thesis. The drilling operator is Norsk Hydro Produksjon AS., The well was completed 29.10.1985 (NPD., 2016b). The well is located on the SW part of the Loppa High (see Figure 3.1). The sample is taken from 1944-2030m in the Ørn and Falk Formations from Late Carboniferous to Early Permian. The discovery is not characterized as a reservoir. Bottom Hole Temperature (BHT) at 3484 m is 97 °C (NPD., 2016b). The oil appears to have relatively high viscosity compared to the rest of the sample set (see Figure 3.3).

### Well 7220/5-1– Johan Castberg – JC1-JC3

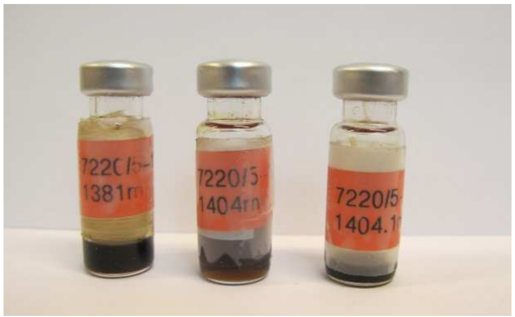

**Figure 3.4: Oil from the Johan Castberg field, well 7220/5-1. The samples are taken from 1381m, 1404m and 1404.1m. The sample taken from 1404m is diluted.**

The well was drilled by Statoil Petroleum AS and was completed the 24.03.2012 (NPD., 2016b). The well is located in the Bjørnøyrenna Fault Complex west of the Loppa High (see Figure 3.1). Oil samples from three different depths have been used in this thesis, 1381m (JC1), 1404m (JC2) and 1404.1m (JC3) respectively (see Figure 3.4). The shallowest sample seems to have slightly higher viscosity than the two others. From the well data at NPD. (2016b) the top reservoir is reported at 1337m, Gas Oil Contact (GOC) at 1365m and Oil Water Contact (OWC) at 1412m. The deepest remnants of oil are found at 1419m. Moreover, the gas column is 28m thick and the oil column is 47m thick. The BHT is 52 °C at 1740m. The three samples are found within the Stø and Top Nordmela Formations.

### Well 7220/7-1 – Johan Castberg – JC4-JC5

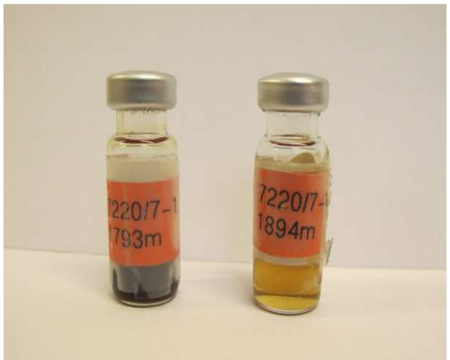

**Figure 3.5: Oil from the Johan Castberg field, well 7220/7-1. The samples are taken from 1793m and 1894m. Both samples are diluted with dichloromethane (DCM).**

The well is reported by NPD. (2016b) to have been completed the 24.01.2012 by Statoil Petroleum AS. The well was drilled in the Bjørnøyrenna Fault Complex southwest of the 7220/8-1 well (see Figure 3.1). The samples are taken from 1793m and 1894m, the former seems to have lower viscosity than the latter (see Figure 3.5). The reservoir top is at 1749m, the GOC at 1828m, OWC 1956m and the deepest remnants of oil discovered was reported to be at 2121m (NPD., 2016b). The discoveries are situated in the Stø Formation and Top Normela Formation. The BHT at 2229.0m is 72 °C.

### Well 7220/8-1 – Johan Castberg – JC6

7220/8-1
1380.5m

**Figure 3.6: Oil from the Johan Castberg field, well 7220/8-1. The sample is taken from 1389.5m.**

The well was drilled by Statoil Petroleum AS and was completed on the 02.02.2011 (NPD., 2016b). The discovery is located on the Bjørnøyrenna Fault Complex (see Figure 3.1). The oil sample depth is 1380.5m (see Figure 3.6), the reservoir top is at 1276m, GOC at 1312m, OWC 1395m and the deepest remnants of oil are at 1400m. The Gas column is 37m and the Oil column 83m (NPD., 2016b). The BHT temperature is not given. The sample originates from the Nordmela Formation.

### Well 7124/4-1 DST 3 – H1

7124/4-1
DST 3

**Figure 3.7: Oil from the well 7124/4-1. The depth of the sample is not given.**

The well was drilled by GDF SUEZ E&P Norge AS and completed 12.10.2011 (NPD., 2016b). The well is located in the transition zone between the Hammerfest Basin and the Norkapp Basin in the Måsøy Fault Complex (see Figure 3.1). The well which is found in the Heilo prospect is reported to be dry with a few oil remnants (see Figure 3.7). The depth is not given, however the lowest penetrating Formation is the Havert Formation (NPD., 2016b).

### Well 7120/6-1 – Snøhvit – S1-S2

The well was completed the 02.05.1985 by Norsk Hydro Produksjon AS (NPD., 2016b). The well was drilled in the middle of the Hammerfest Basin (see Figure 3.1). The 7120/6-1 DST 2 (S1) and 7120/6-1 DST 4 (S2) are found at the depths 2432.05-2436.02m and 2386.00-2401.00m respectively (see Figure 3.8). The former sample is an oil the latter is a condensate (see Figure 3.8). Both samples are found in the Nordmela Formation. The BHT of the well is 52 °C (NPD., 2016b).

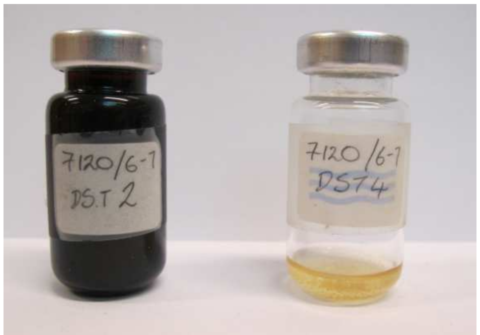

**Figure 3.8: Oil (S1) and condensate (S2) from the well 7120/6-1. The oil is taken from 2432.05-2436.02 m and the condensate is taken from 2386.00- 2401.00m.**

### Well 7120/12-2 DST 2 – A1

The drilling of this well was completed 11.09.1981, the operator was Norsk Hydro Produksjon AS. The sample is a condensate (see Figure 3.8) and is located in the southern margin of the Hammerfest Basin in the transition zone between the Finnmark Platform (see Figure 3.1). The condensate is found in the central part of the Alke structure. The depth of the DST is 1985-1991m and it is situated within the Stø Formation (NPD., 2016b).

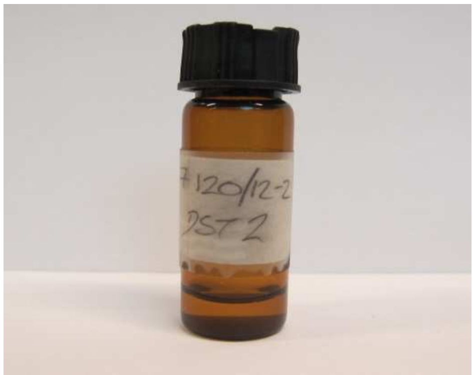

**Figure 3.8: Condensate (A1) from the well 7120/12-1. The condensate is taken 1985-1991m.**

## 3.3 Description of selected core samples with extracts from the Finnmark Platform and the Nordkapp Basin

### Well 7029/03-u-02

In 1987 well 7029/03-u-02 was drilled by IKU Petroleum Research on the Finnmark Platform (see Figure 3.2) (Bugge et al., 1995). Five cores from this well was used in this thesis 28.46 m (FP1), 30.93m (FP2), 31.00m (FP3), 44.45m (FP4) and 154.58m (FP5) below the sea bed (see Figure 3.9 and Figure 3.10A, 3.10B, 3.10C, 3.10D and 3.10E).The lowermost core at 154.58m is believed to be fan delta conglomerate from Middle - Upper Carboniferous, while the three shallower cores are from Late Carboniferous (Bugge et al., 1995).

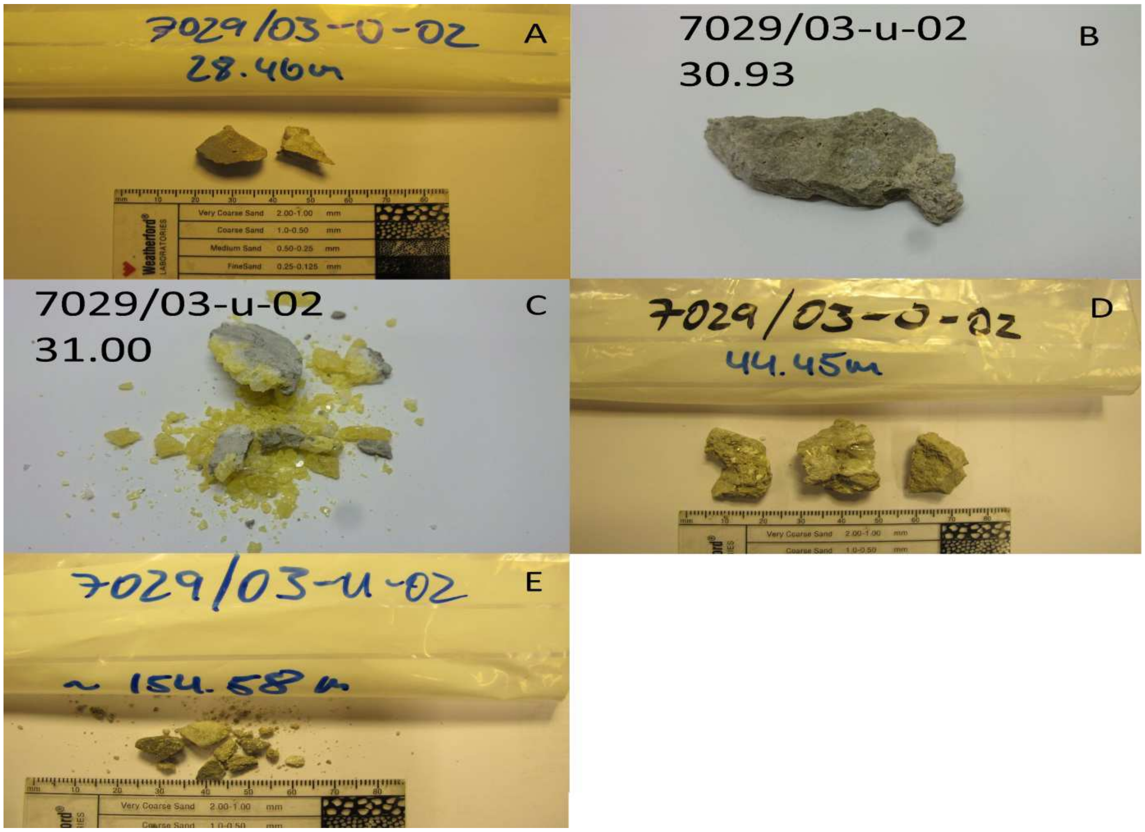

**Figure 3.10: The Figures are shallow cores from the Finnmark Platform. The core 3.9A is taken from 28.46m, 3.9B is taken from depth 30.93m, 3.9C are taken from 31.00m below the sea bed, the fourth core sample Figure 3.9D from depth 44.45m and the last sample (Figure 3.9E) is taken from 154.58m below the sea bed. The 3.9C sample has a very high amount of sulfur.**

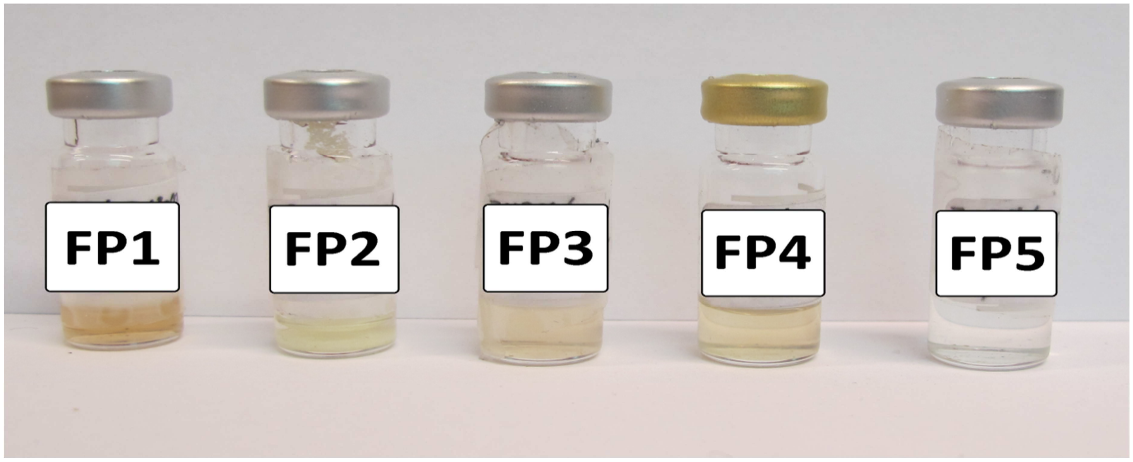

**Figure 3.9: Core extracts from well 7029/03-u-02. FP1 is the sample from 28.46m, FP2 is the core from depth 30.93m, the FP3 extract is taken from 31.00m below the sea bed, FP4 has the depth 44.45m and the FP5 is from the depth 154.58.**

### Well 7029/03-u-01

The well 7029/03-u-02 was drilled in 1987 by IKU Petroleum Research on the Finnmark Platform (see Figure 3.2) (Bugge et al., 1995). The core seen in picture 3.11 is taken from 85.51 (FP6) below the sea bed. The extracted bitumen can be seen in Figure 3.12. The core is from Middle-Late Carboniferous.

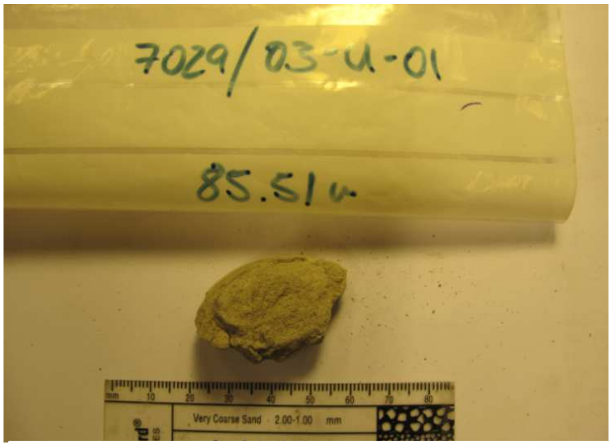

**Figure 3.11: The Figures are shallow cores from the Finnmark Platform. The depth of the core is 85.51m below the sea bed.**

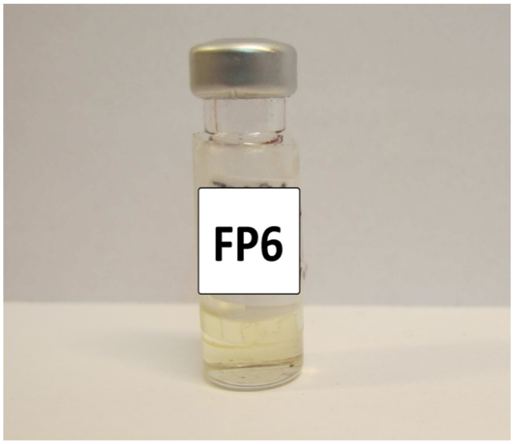

**Figure 3.12: The extracted bitumen from well 7029/03-u-01. FP6 is taken from 85.51m below the sea bed.**

### Well 7030/03-u-01

In 1987 well 7029/03-u-02 was drilled by IKU Petroleum Research on the Finnmark Platform (see Figure 3.2) (Bugge et al., 1995). The depths of sample FP7, FP8, FP9, FP10 are 57.08m, 78.53m, 83.18m and 132.05m respectively (see Figure 3.12a, 3.12b, 3.12c and 3.12d and

Figure 3.13). The deepest core originates from Late Carboniferous, the three remaining shallower cores are dated to be between Late Carboniferous and Early Permian.

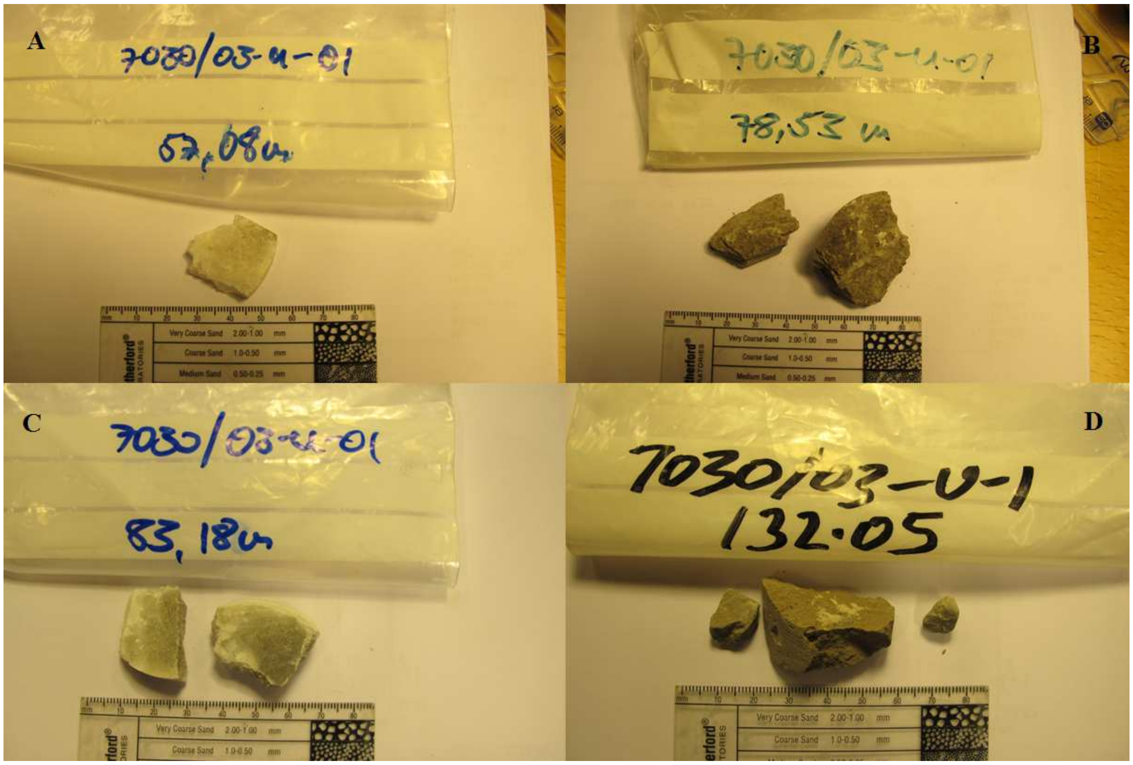
A
7030/03-u-01
57,08m
B
7030/03-u-01
78,53m
C
7030/03-u-01
83,18m
D
7030/03-u-1
132.05

**Figure 3.12: The samples are shallow cores from the Finnmark Platform. The depth of sample 3.12A is 57.08m, 3.12B is taken from depth 78.53m, 3.12C is taken from 83.18m below the sea bed and the deepest sample 3.12D from 132.05m.**

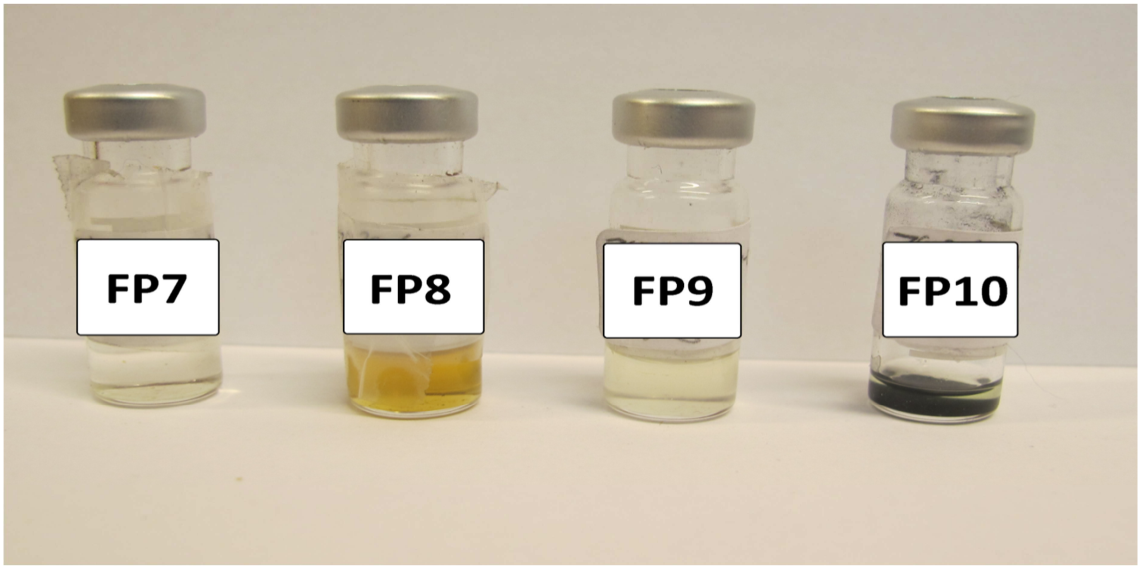
FP7
FP8
FP9
FP10

**Figure 3.13: The core extracts from well 7030/03-u-01. FP7 is the core taken from 57.08m, the core FP8 is from 78.53m below the sea bed. FP9 is from the depth 83.18m and the last sample FP10 is from the depth 132.05m.**

### Well 7128/12-u-01

Well 7128/12-u-01 (FP11) was drilled in 1988 by IKU Petroleum Research on the Finnmark Platform (see Figure 3.2) (Bugge et al., 1995). The core used in this thesis is from 156.50m below the sea bed, and is dated to be Upper Permian (Artinskian) (Bugge et al., 1995), and is grainstone from a shallow shore face environment. At 156.50m the core is within the Isbjørn Formation (see Figure 3.14 and Figure 3.15).

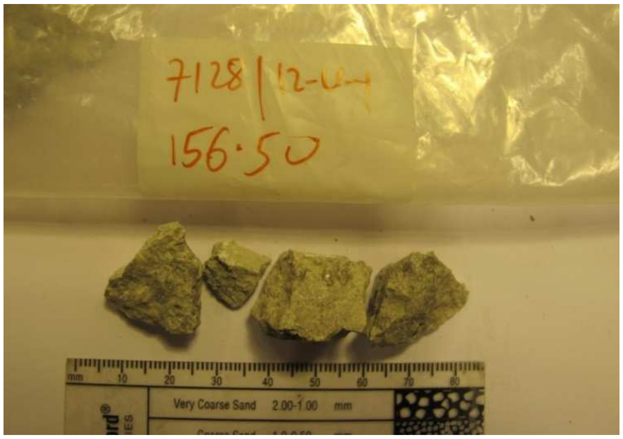

**Figure 3.14: The samples are shallow cores from the Finnmark Platform. The depth of the core is 156.50m below the sea bed.**

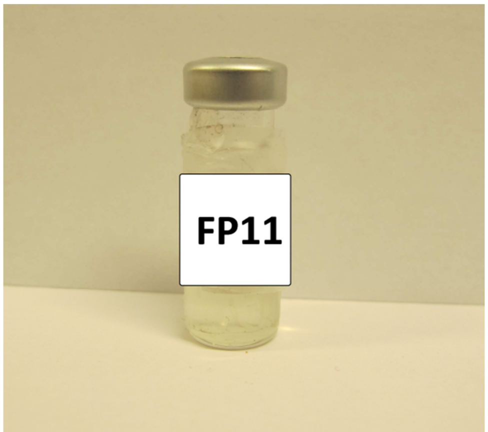

**Figure 3.15: Bitumen extract from well 7128/12-u-01.Sample FP11 is taken from 156.50m.**

### Well 7129/10-u-02

In 1987 well 7129/10-u-02 was drilled by IKU Petroleum Research on the Finnmark Platform (see Figure 3.2) (Bugge et al., 1995). Three cores from this well were used in this thesis, namely 30.40m (FP12), 48.85m (FP 13) and 85.74m below the sea bed (see Figure 3.16 and Figure 3.17). The lowermost core at 85,74m is of late Asselian age (Early Permian). At this depth the core is bioturbated wackestone (Bugge et al., 1995). At 48,85m the core is of Sakmarian age (Early Permian). The core consists of a high energy packstone, rich in crinoids (Bugge et al., 1995). The uppermost core at 30.4 m below sea bottom is from Upper Sakmarian age, and is bioturbated carbonates. All of the cores are within the Ørn Formation.

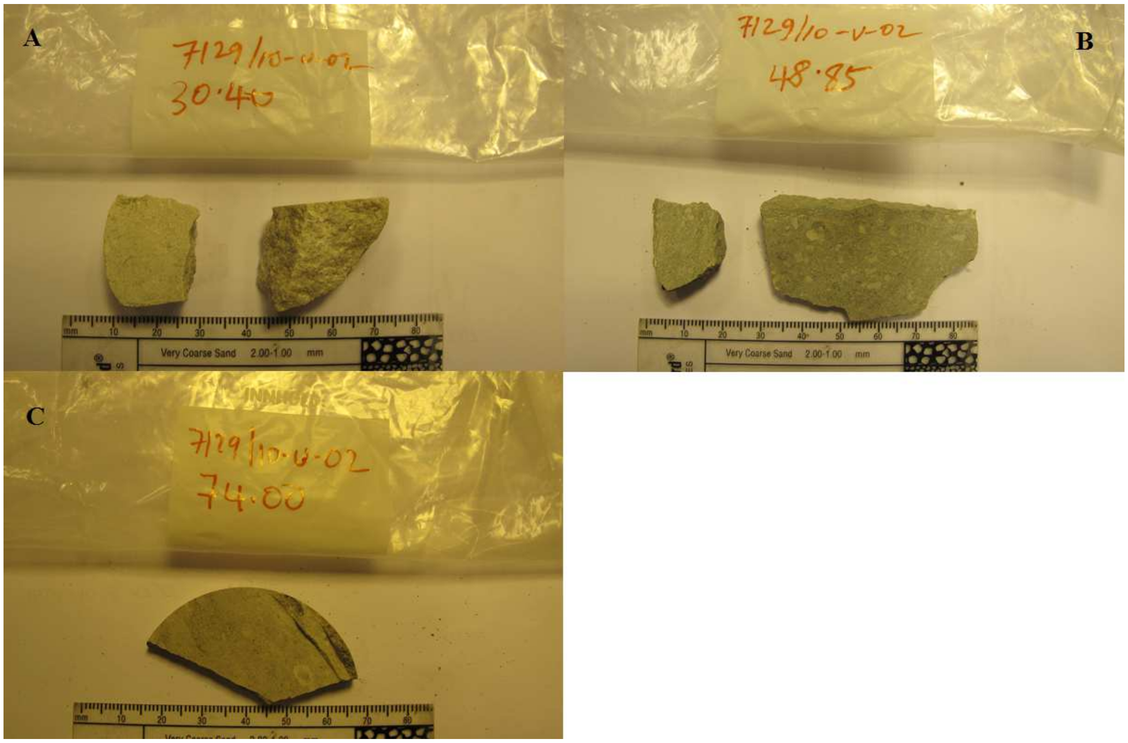
A
7129/10-u-02
30.40
B
7129/10-u-02
48.85
C
7129/10-u-02
74.00
Very Coarse Sand 2.00-1.00 mm

**Figure 3.16: The samples are shallow cores from the Finnmark Platform. The depth of sample 3.13A is 30.40m, 3.13B is taken from depth 48.85m, and 3.13Cis taken from 74.00m.**

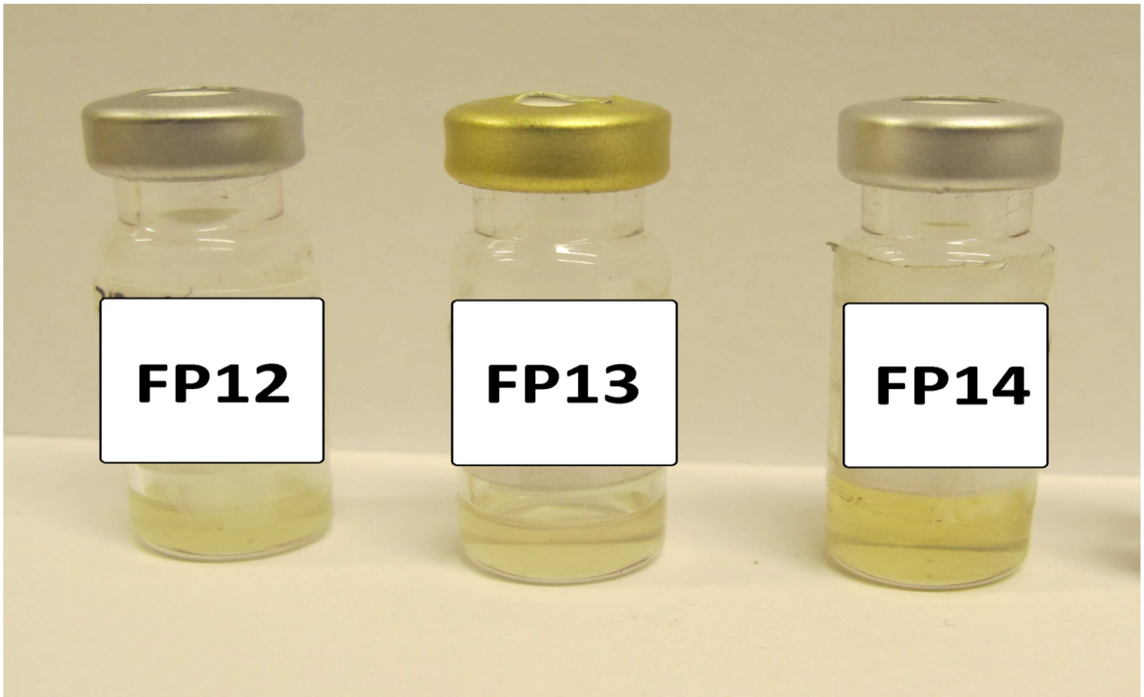
FP12
FP13
FP14

**Figure 3.17: The extracted core samples from well 7129/10-u-02. FP12, FP13 and FP14 are from depth 30.40m, 48.85m and 74.00m respectively.**

**Well 7227/8-u-1 31.96**

This well was drilled in 1986 by IKU Petroleum Research. The core is taken from the Nordkapp Basin (see Figure 3.2). The core sample is within Early Jurassic sediments at 31.96m depth, the sample ID is NB1 (see figure 3,18 and 3.19). The respective depth is within the Stø Formation (Virgan et al., 2014).

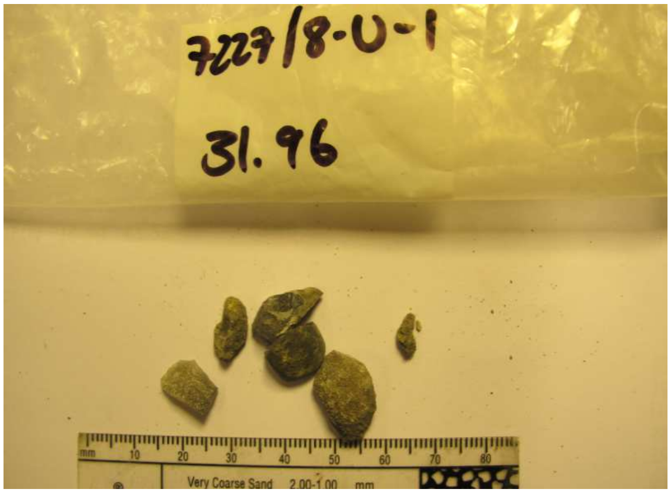

**Figure 3.18: The sample is a shallow core from the Nordkapp Basin. The depth of the core is 31.96m below the sea bed.**

**Figure 3.19: Bitumen from well 7227/8-u-1. The sample NB1 is from 31.96m.**

## 3.4 Sample List

The Table 3.1 gives an overview of the oils, condensates and core samples analyzed in this thesis.

**Table 3.1: The Table gives an overview of the Well name, Sample code, Depth of the sample, Sample type, Field name, Age of the sample, Area and Location given in coordinates. The information about the Oils and Condensate are given by NPD (2016b). The information about the cores was attained from Bugge et al. (1995). [1]O = Oils; C= Condensate; CE = Core Extracts: [2]JC = Johan Castberg; S = Snøhvit; O=Oseberg: [3]LH = Loppa High; BRF = Bjørnøyrenna Fault Complex; HB = Hammerfest Basin; FP = Finnmark Platform; NB = Nordkapp Basin; MFC = Måsøy Fault Complex**

| Sample name | Sample code | Depth(m) | Sample type[1] | Field name[2] | Age | Area[3] | Location (coordinates) |
|---|---|---|---|---|---|---|---|
| 7120/2-1 DST 4 | L1 | 1944-2030 | O | - | Late Carb-Early P. | LH | 71° 58' 57.94'' N<br>20° 28' 35.09'' E |
| 7220/5-1 | JC1 | 1338 m | O | JC | Early-Middle J. | BRF | 72° 31' 0.67'' N<br>20° 20' 29.15'' E |
| 7220/5-1 | JC2 | 1404 | O | JC | Early-Middle J. | BRF | 72° 31' 0.67'' N<br>20° 20' 29.15'' E |
| 7220/5-1 | JC3 | 1404,1 | O | JC | Early-Middle J. | BRF | 72° 31' 0.67'' N<br>20° 20' 29.15'' E |
| 7220/7-1 | JC4 | 1793 | O | JC | Early-Middle J. | BRF | 72° 27' 37.53'' N<br>20° 9' 8.59'' E |
| 7220/7-1 | JC5 | 1894 | O | JC | Early-Middle J. | BRF | 72° 27' 37.53'' N<br>20° 9' 8.59'' E |
| 7220/8-1 | JC6 | 1380.5 | O | JC | Early J. | BRF | 72° 29' 28.92'' N<br>20° 20' 2.25'' E |

| | | | | | | | |
|---|---|---|---|---|---|---|---|
| 7124/4-1 DST 3 | H1 | - | O | - | - | MFC | 71° 35' 16.14'' N<br>24° 5' 56.76'' E |
| 7120/6-1 DST 2 | S1 | 1985-1991 | O | S | Early J. | HB | 71° 37' 11.76'' N<br>20° 55' 59.72'' E |
| 7120/6-1 DST 4 | S2 | 2386-2401 | C | S | Early J. | HB | 71° 37' 11.76'' N<br>20° 55' 59.72'' E |
| 7120/12-2 DST 2 | A1 | 2432-2436 | C | - | Middle-Late J. | HB | 71° 7' 30.3'' N<br>20° 48' 19'' E |
| 30/6-1 | NSO-1 | 2320-2330 | O | O | Middle J. | | N60°33'15.1''<br>E2° 46''38.36'' |
| 7029/03-u-02 | FP1 | 28,46 | CE | - | Middle Carb | FP | 70° 56'07.O" N<br>29° 58'53.6" E |
| 7029/03-u-02 | FP2 | 30,93 | CE | - | Middle Carb | FP | 70° 56'07.O" N<br>29° 58'53.6" E |
| 7029/03-u-02 | FP3 | 31,00 | CE | - | Middle Carb | FP | 70° 56'07.O" N<br>29° 58'53.6" E |
| 7029/03-u-02 | FP4 | 44,45 | CE | - | Middle Carb | FP | 70° 56'07.O" N<br>29° 58'53.6" E |
| 7029/03-u-02 | FP5 | 154,58 | CE | - | Late-Middle Carb | FP | 70° 56'07.O" N<br>29° 58'53.6" E |
| 7029/03-u-01 | FP6 | 85,51 | CE | - | Middle-Upper Carb | FP | 70° 56'07.O" N<br>29° 58'53.6" E |
| 7030/03-u-01 | FP7 | 57,08 | CE | - | Late Carb – Early P. | FP | 70° 49' 36.2'' N<br>30° 44' 31.1'' E |
| 7030/03-u-01 | FP9 | 78,53 | CE | - | Late Carb – Early P. | FP | 70° 49' 36.2'' N<br>30° 44' 31.1'' E |
| 7030/03-u-01 | FP8 | 83,18 | CE | - | Late Carb – Early P. | FP | 70° 49' 36.2'' N<br>30° 44' 31.1'' E |
| 7030/03-u- 01 | FP10 | 132,05 | CE | - | Late Carb | FP | 70° 49' 36.2'' N<br>30° 44' 31.1'' E |
| 7128/12-u-01 | FP11 | 156,50 | CE | - | Late P. | FP | 71° 07'13.5" N<br>29° 13'23.1" E |
| 7129/10-u-02 | FP12 | 30,40 | CE | - | Early P. | FP | 71° 07'13.5" N<br>29° 13'23.1" E |
| 7129/10-u-02 | FP13 | 48,85 | CE | - | Early P. | FP | 71° 07'13.5" N<br>29° 13'23.1" E |
| 7129/10-u-02 | FP14 | 74,00 | CE | - | Late Carb – Early P. | FP | 71° 07'13.5" N<br>29° 13'23.1" E |
| 7227/8-u-01 | NB1 | 31.96 | CE | - | Early J. | NB | 72° 19'08.9" N<br>27° 33'21.3" E |

# 4. Analytical methods

This chapter presents the methods used to obtain the results in this master thesis.

The chapter is outlined as follows:

4.1 Introduction

4.2 Preparation and extraction of bitumen from rock samples

4.3 TLC-FID

4.4 GC-FID

4.5 Molecular sieving

4.6 GC-MS

## 4.1 Introduction

Geochemical analysis provides qualitative and quantitative information about bitumens, oils and gasses. The data acquired from the geochemical samples can be used to correlate source rock extracts with oils/gasses and between oils and gasses. Geochemical analyses give essential information about source rock/oil maturity and source rock facies (source rock quality). In situ reservoir alterations can also be addressed e.g. water washing and biodegradation.

Geochemical properties obtained by analytical methods can be divided into two main groups; bulk parameters and molecular parameters. The bulk parameters describe the compositional properties of an extract or petroleum sample; e.g. Thin Layer Chromatography – Flame Ionization Detector (TLC-FID) apparatus which quantify the amount of saturated, aromatic and asphaltenes/resins compounds. The chemical characteristic of a petroleum or source rock extract are represented by the molecular parameters. Gas Chromatography – Flame Ionisation detector (GC-FID) and Gas Chromatography – Mass Spectrogram (GC-MS) are accurate and rapid methods to acquire molecular parameters; e.g. biomarkers and n-alkanes. These methods identify specific molecules and determine the amount relative to others in a sample.

The GC-FID and GC-MS analyses are always performed with one run of the North Sea Standard Oil (NSO-1). The peak distribution in the chromatograms is well known; therefore it is a good indicator if the apparatus works correctly. The chromatogram peaks in the NSO-1 oil is identified and can therefore be used as a reference for peak identification in other samples.

## 4.2 Preparation and extraction of samples

The source rock sample is crushed by hand into fragments of 0.5 cubic meters and then grinded into fine powder in a sling mill before extraction of soluble bitumen.

The actual extraction process is done in a Soxtec System HT 1043 extraction unit from Tecator. Cellulose thimbles are pre-rinsed and boiled and filled with the crushed samples. Approximately 7.00 g of crushed rocks are filled in each sample. The thimble openings are covered with glass wool to prevent evaporation loss of the sample during the extraction process.

The extraction solvent is a mix between dichloromethane (DCM) and methanol (MeOH) with the ratio 93 vol% and 7 vol%, respectively (Karlsen and Larter, 1991). Approximately 50 ml of DCM is used for each sample. The presence of elemental sulphur in the samples is unwanted for further geochemical analysis. Removing the sulphur can be done by adding copper grains to the Solvent. The copper must be activated with Nitric acid ($HNO_3$) or Hydrochloric acid (HCL) (Weiss et al., 2000). Extraction from carbonate samples require approximately 30 minutes of boiling followed by 50 minutes of rinsing.

The extracted material is diluted in the DCM solvent. Consequently, further concentration of the extract is needed. This can either be done by evaporation of the DCM due to contact with air or by blowing nitrogen gas on the sample. The latter is faster, but some loss of the desired geochemical parameters may occur. When the DCM amount have been significantly reduces (solvent and extract is 2 ml or less) geochemically analysis can be performed.

## 4.3 TLC-FID

TLC-FID is a rapid way to quantify saturated and aromatic hydrocarbons, and asphaltenes/resins compounds, separating asphalthenes and resins are also possible (cf. Karlsen and Larter, 1991). The method is suiTable for solvent extracts of source rock, reservoir rocks and crude oils (Karlsen and Larter, 1991). The compound variations help us to distinguish the petroleum population in a reservoir, moreover, the method is also useful to select promising samples for further analysis with GC-FID and GC-MS (Bhullar et al., 2000).

Furthermore the TLC-FID is a effective method to distinguish in-situ generated hydrocarbons, migrated hydrocarbons and diesel-drilling fluid (Karlsen and Larter, 1991). The TLC-FID is a cheap and effective way to screen large sample volumes from a reservoir and select samples for high resolution analysis.

In order to perform the Iatroscan the samples are first applied to the base of silica rods (2-3µl), type Chromarods-S III (pore diameter 60 Å, particle size 5 µm). The rods are then soaked in solvents of increasing polarity to separate the fractions. To separate the saturated fraction from aromats and asphaltenes/resins the rods are soaked in n-hexane for 40 min (until the solvent covers 95% of the rod) and then dried for 3 minutes. When the n-hexane has dried out, the lower part of the silica rods are soaked in toluene for 8 minutes, until 50% of the rods are toluene wet. The aromatic fraction is soluble in the toluene and transported to the middle of the silica rods, while the asphaltenes and resin remains stationary (Karlsen and Larter, 1991). Consequently, the fractions are separated. 10 silica rods were used for each run, one of the rods is applied with NSO-1 oil and another with a DCM:MeOH solvent. The responses from these two applications are well known and are done to make sure the apparatus works perfectly.

The GC-FID burns the fractions with a flame fueled with hydrogen (180 ml/min) and air (2.1 l/min). A flame ionization detector records the response when the different fractions are combusted and stored in a computer. The scanning time of the chromarods are set to 30 sec/scan (see Figure 4.1).

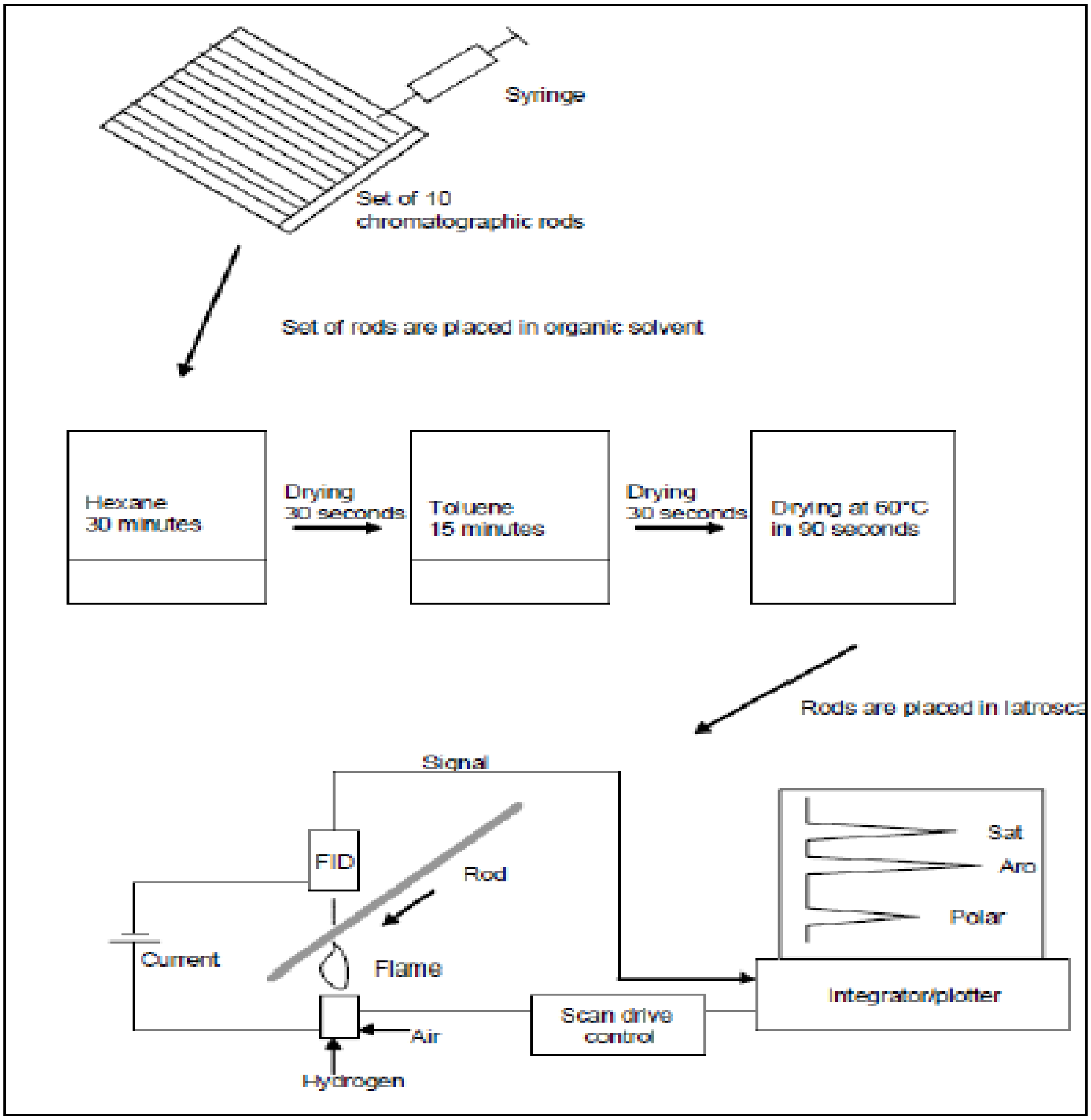
Syringe
Set of 10 chromatographic rods
Set of rods are placed in organic solvent
Hexane 30 minutes
Drying 30 seconds
Toluene 15 minutes
Drying 30 seconds
Drying at 60°C in 90 seconds
Rods are placed in Iatrosca
Signal
FID
Rod
Current
Flame
Air
Hydrogen
Scan drive control
Integrator/plotter
Sat
Aro
Polar

**Figure 4.1: The key steps in the TLC-FID analysis. The process separates and quantifies saturated hydrocarbons, aromatic hydrocarbons and asphaltenes/resins (modified from Pedersen 2002).**

## 4.4 GC-FID – GAS chromatography

GC-FID is a rapid and relatively cheap method to separate and obtain information about main components in petroleum or bitumen, e.g. n-alkanes, isoprenoids, toluene, xylen , benzene and hexane (Weiss et al., 2000). The quantification of these parameters can be done relative to each other (most common) and in absolute terms.

The sample is injected into the GC-FID and vaporized into a chromatographic column. A thin film layer on the inside of the column works as the stationary phase. An inert carrier gas e.g.

Nitrogen ($N_2$) Helium (H), are used to transport the vaporized sample through the column. Short-chained molecules with low boiling point and high vapor pressure travel with a fast pace throughout the column, while more complex molecules are transported slower by the carrier gas (see Figure 4.2). This results in a separation between molecules of different mass and structure.

The initial temperature of the chromatographic column is 80°C, this temperature is held for 1 minute. The column is heated to a temperature of 320°C with an increase in temperature of 4.5°C/min. When the maximum temperature is achieved, the instrument will run for 25 min at a constant temperature. The whole sequence takes about 79 min (can be adjusted). When the molecules exit the column a hydrogen flame burn the material, a FID will detect the combustion of molecules and a computer record the data (see Figure 4.2). The chromatogram is plotted in time (x axis) versus intensity (y axis).

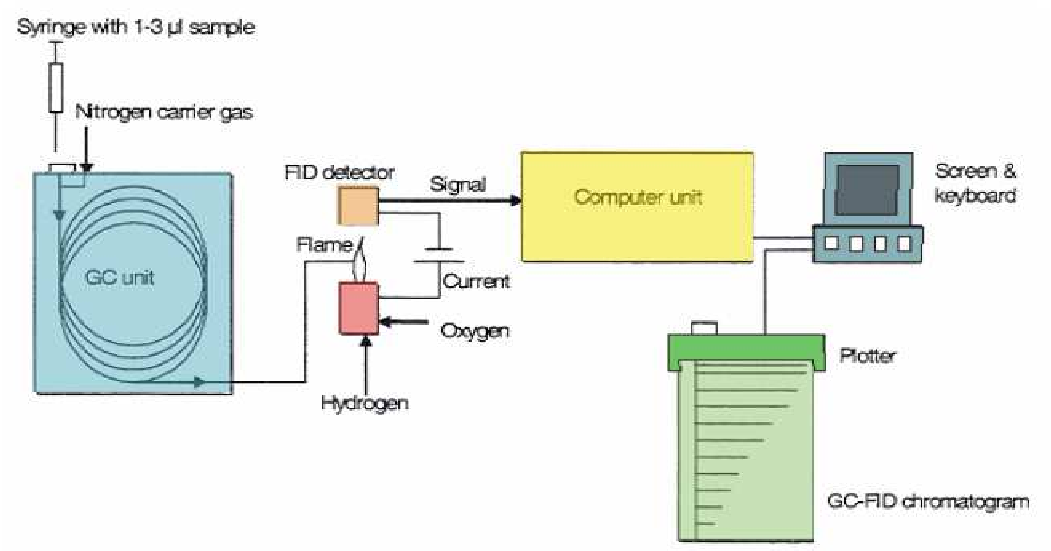
Syringe with 1-3 µl sample
Nitrogen carrier gas
GC unit
FID detector
Signal
Flame
Current
Oxygen
Hydrogen
Computer unit
Screen & keyboard
Plotter
GC-FID chromatogram

**Figure 4.2: The Figure illustrates the main components in a GC-FID analysis (Pedersen, 2002).**

## 4.4 Molecular sieving

The n-alkanes are usually higher concentrated in a sample relative to the biomarkers. The n-alkane footprints will override the biomarkers in a GC-MS analysis; therefore it is necessary to sieve out the n-alkanes before further analysis. Asphaltenes and resins are also removed during the sieving process (Pedersen et al., 2006). The thin long-chained n-alkanes have a much smaller radius than the larger and more complex biomarkers. By mixing the sample into a $SiO_2$ powder with open pores (about 5Å diameter), the n-alkanes, asphaltenes and resins are trapped in the powder. The solvent used for the sieving process is cyclohexane; the cyclohexane molecules are relatively small and will pass through the sieving powder with ease. A solvent like DCM will clog the pores and reduce the sieving powders ability to adsorb n-alkanes, asphaltenes and resins. The end result of the sieving process is that the sample is depleted of n-alkanes, asphaltenes and resins, and enriched in the biomarkers and aromatic fraction.

To perform the sieving a few drops of oil, condensate or extract are mixed with the sieving powder and 2-2.5 ml of cyclohexane with a pipette. The mixture is then centrifuged with a Heraeus Sepatech Labofuge H. apparatus for 2 minutes at 2000 rpm to separate the sieving powder from the remaining solvent/extract. This might have to be done several times if the first run is not satisfactory. After the sieving the sample must be concentrated and the redundant cyclohexane is evaporated (either by contact with air or pure nitrogen).

## 4.5 GC-MS

The GC-MS is the main principal tool for separation, identification and quantification of biomarkers (mainly medium range) (Peters et al., 2007). The apparatus works in the same manner as the GC-FID where the molecules travel with different velocity through the gas column. The mass spectrometer identifies compounds with different mass and ionization. Every molecule is broken and ionized by the MS, and are then identified from their mass (m) to charge (z) ratio (m/z) (Peters et al., 2005). The plotted chromatogram shows the relative intensity of ions with one specific m/z ratio (y axis) versus time (x axis). The biomarkers commonly have different m/z ratio and can therefore be distinguished and quantified.

The relative and absolute intensity of the different biomarkers can be measured in the chromatograms, providing information about the biomarker distribution. Biomarker intensity relative to each other provides essential information about maturity, source rock and facies. The identification of specific molecules can indicate specific facies and geological times

The GC-MS apparatus was set to an initial temperature of 40°, this temperature was held constant for 1 min. The temperature was increases with 20°C/min up to 180°C from there 1.7°C/min up to maximum temperature of 310°C. The maximum temperature was held for 40.53 min.

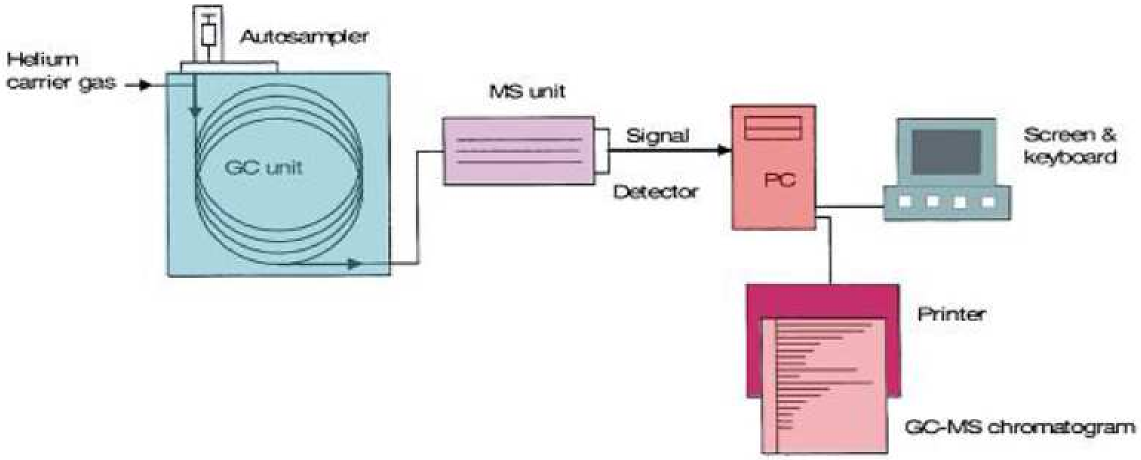
Autosampler
Helium carrier gas
GC unit
MS unit
Signal
Detector
PC
Screen & keyboard
Printer
GC-MS chromatogram

**Figure 4.3: A schematic overview of the main components in a GC-MS analysis (Pedersen, 2002).**

# 5. Petroleum geochemical interpretation parameters

The interpretation parameters are identified and generated from the results given by the TLC-FID, GC-FID and GC-MS.

These geochemical parameters provide information about:

- Source rock maturity
- Oil/Gas maturity at the time of expulsion from the source rocks
- Depositional environment and facies classification
- Determination of the time period petroleum/bitumen originate from
- In-situ alteration as biodegradation and water washing can also be addressed

Valuable qualitative information can also be gained from the chromatograms.

The chapter is outlined as follows:

5.1 Interpretation parameters based on the TLC-FID

- 5.1.1 Saturated and aromatic hydrocarbons and polar compounds

5.2 Interpretation parameters based on the GC-FID

- 5.2.1 N-alkane distribution
- 5.2.2 Pristane/Phytane ratio
- 5.2.3 Pristane/n-C17 and Phytane/n-C18 ratios
- 5.2.4 Carbon Preference Index (CPI) and the Odd/Even Predominance (OEP)

5.3 Interpretation parameters based on the GC-MS

- 5.3.1 Steranes
- 5.3.2 Terpanes
- 5.3.3 Triaromatic Steroids
- 5.3.4 Monoaromatic Steroids
- 5.3.5 Phenantrhene, metylphenanthrenes
- 5.3.6 Standard parameters for maturity and organic facies

5.4 Other parameters based on the GC-MS

- 5.3.1 Extended tricyclic terpane ratio

## 5.1 Interpretation parameters based on the TLC-FID

### 5.1.1 Saturated and aromatic hydrocarbons and polar compounds

The TLC-FID separates the main components in a rock extract or oil/condensate into saturated and aromatic hydrocarbon fractions and asphaltenes/resins.

The saturated and aromatic ratio (S/A) reflects thermal maturation, however phase fractioning can greatly alternate the ratio and must be considered (Larter and Mills, 1991). Moreover, quality of the source rock and Biodegradation also contributes to changes in the S/A ratio. The ratio is constant between 0-0.6 vitrine reflectance (%$R_o$), between 0.6-1%$R_o$ it increases significantly and peaks at 1%$R_o$. From 1-4 %$R_o$ the ratio decreases again. This is due to the higher stability of aromatic compounds at high temperatures (see Figure 5.1) (Clayton and Bostick, 1986). High amounts of polar compounds reflect low maturity as hydrocarbon generation has not yet begun. Low S/A ratios are usually associated with heavy oils, while light oil and condensates have a higher fraction of saturated hydrocarbons (Cornford et al., 1983). Biodegraded petroleum will usually show a low S/A ratio, since bacteria tend to attack saturated hydrocarbons (Clayton and Bostick, 1986). Migration distance also influences the S/A ratio for the gas fraction in phase fractioned petroleum. The ratio will increase with distance (Østensen, 2005).

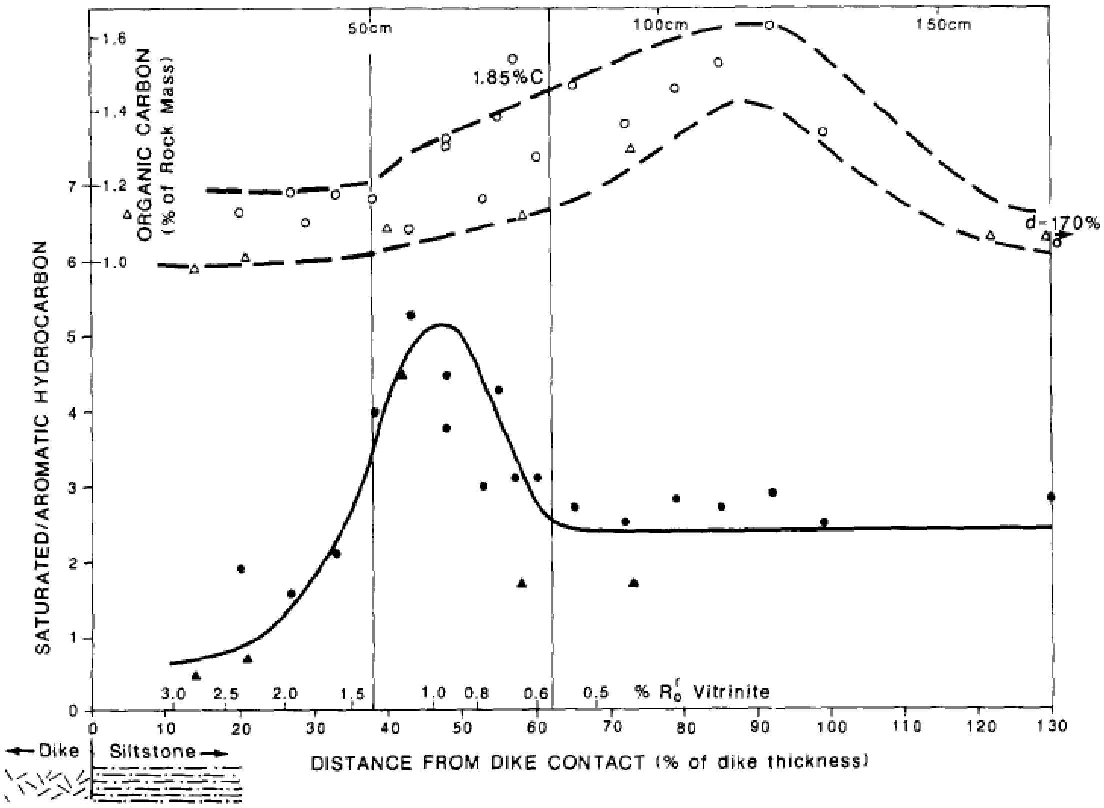

**Figure 5.1: Ratio of S/A for C15+, organic carbon and hydrocarbon are plotted with distance from dike (Clayton and Bostick, 1986).**

## 5.2 Interpretation parameters based on the GC-FID

The GC-FID main usage in this thesis is identification and distribution of n-alkanes and isoprenoids (pristane and phytane). The hydrocarbon C15+ fraction and its relationship with the isoprenoids are a helpful tool for facies identifications and maturity, and also biodegradation (Tissot and Welte, 1984).

### 5.2.1 N-alkane distribution

During the degradation of petroleum n-alkanes will be more depleted compared to isoprenoids, as the process is selective (Tissot and Welte, 1984). Bacteria tend to attack the n-alkanes in the ~C8–C12 range first. With severe biodegradation, n-alkanes will be attacked and disappear. When the n-alkanes are consumed the bacteria will move to the isoprenoids. The base line of the GC-FID chromatograms will be elevated due to Unresolved Complex Mixture (UCM), mostly caused by biodegradation. Therefore the amount of UCM can provide useful information about the level of biodegradation the sample has undergone. The GC-MS can distinguish between compounds which are resolved and have a specific mass spectra, UCM has a complexed organic structure and cannot be separated in the gas column (Sutton et al., 2005). Identification of n-alkanes are shown in Figure 5.2 in the NSO-1 reference oil from a GC-FID chromatogram.

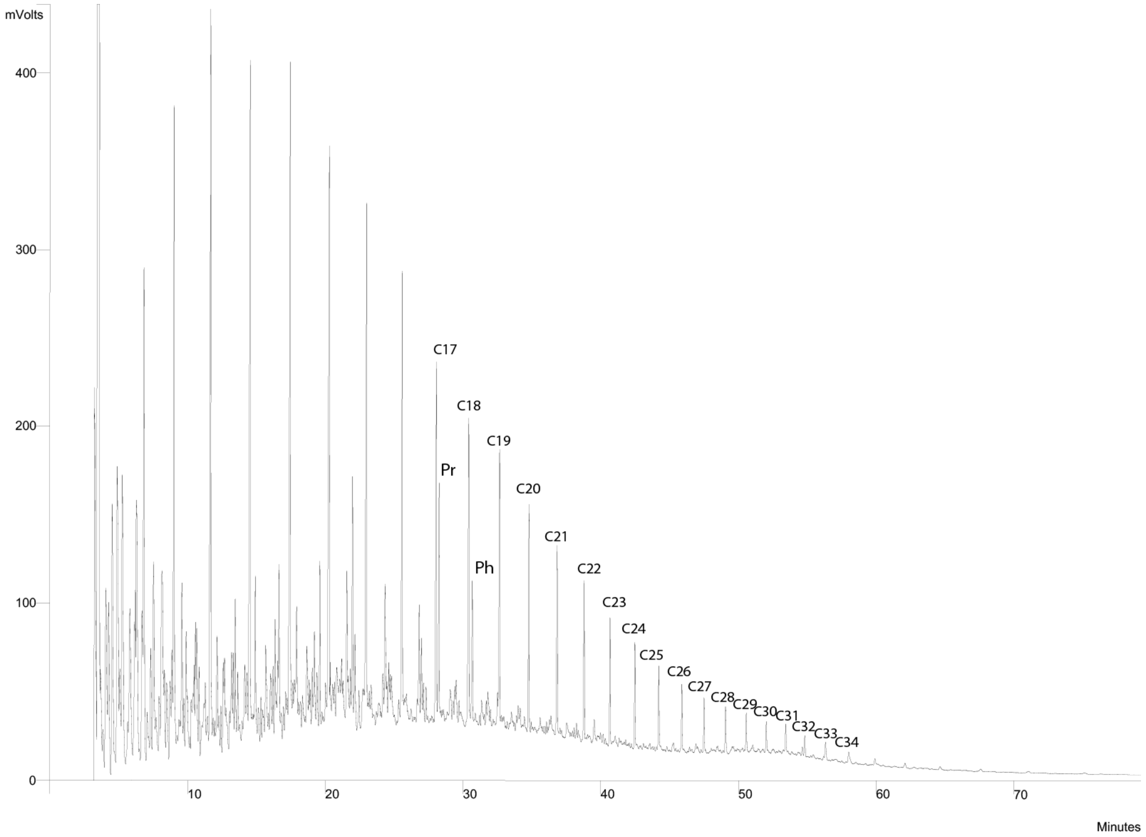

**Figure 5.2: The isprenoids (Pr and Ph) and C17-C34 n-alkanes peaks identified for the NSO-1 oil.**

### 5.2.2 Pristane/phytane ratio

Pristane (Pr) ($C_{19}$) and phytane (Ph) (C20) are isoprenoid isoalkanes biomarkers derived primarily from phytol, a side chain of the chlorophyll molecule and can be identified in the GC-FID (see Figure 5.3). The process happens during diagenesis. The depositional environment influences the pristane/phytane ratio. In an oxic environment phytol will oxidize to an acid which is later decarboxylated into C19-pristane. In a dys/an-oxic environment C20-acid will directly transform to phytane (Peters et al., 2005). Pristane/phytane ratios below 0.8 indicate a saline or hype saline environment, typical for carbonates and evaporate deposits.

Ratios above 3.0 indicate oxic conditions in a terrigenous setting. However, these values have a lot of uncertainties and must be correlated with other data. The pristane and phytane peaks are identified in Figure 5.3.

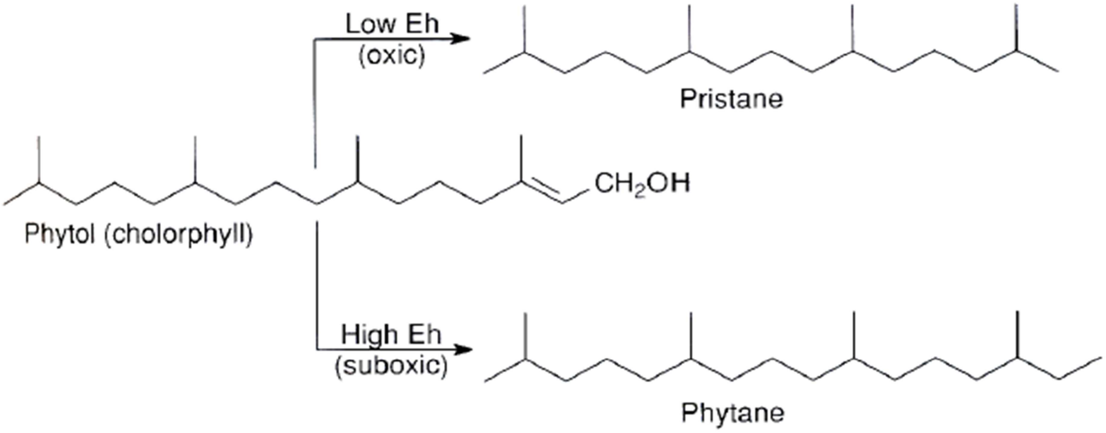

**Figure 5.3: The diagenetic origin of pristane and phytane (Peters et al., 2005)**

### 5.2.3 Pristane/n-C17 and Phytane/n-C18 ratios

Isoprenoids have slightly lower boiling points compared to n-alkanes. In a gas chromotagraphy pristane will arrive right after n-C17, and phytane will elute right after n-C18. To separate the pristane and phytane form their respective n-alkanes, high resolution chromatography is required. This became possible in the early 1980s after capillary GC-columns were developed (Tissot and Welte, 1984). During maturation of the kerogen in the oil window n-alkane will be generated (Tissot and Califet-Debyser, 1971). Thus the ratio between n-alkanes and isoprenoids will increase. Isoprenoids are less sTable during thermal maturation compared to n-alkanes; this will also contribute to increase the ratio. Hence the n-alkane/isoprenoids is a good maturity indicator. However, the ratios have limitations, the type of source input and biodegradation will alter the ratio (Peters and Moldowan, 1993). Thus the usage is limited to oils and bitumens that are related and not biodegraded.

### 5.2.4 Odd/Even Predominance (OEP) and the Carbon Preference Index (CPI)

The ratio between the abundance of odd-numbered and even-numbered n-alkanes is a maturation indicator, although, the ratio is also affected by the lithology. The Carbon Preference Index (CPI) was first introduced by Bray and Evans (1961) and a improved method Odd/Even Predominance (OEP) was presented by Scalan and Smith (1970). The latter can be calibrated for both shorter and longer n-alkanes. Ratio values significantly below or above 1.0 can be classified as immature, and furthermore used as a lithology indicator. Values below 1.0 indicate a carbonate or hypersaline depositional environment. Ratios above 1.0 are associated with a siliclastic source or lacustrine environment. The OEP variations are due to the fact bio-precursor molecule is an even numbered fatty acid. In a siliclastic environment the bio-precursor is mostly decarboxylated into odd-numbered n-alkanes by alpha-cleavage. Moreover, in carbonates and evaporates b-cleavage will dominate and maintain the even number, since two carbon atoms are lost (Tissot and Welte, 1984). With maturation OEP and CPI ratios will tend to approach 1.0, and is therefore a good maturity indicator. However, this ratio alone does not prove that the sample is mature and other calibration data should be taken into account (Peters et al., 2005)

Formulas used to calculate OEP and CPI:

$\mathrm{CPI} = 2(C_{23}+C_{25}+C_{27}+C_{29})/[C_{22}+2(C_{24}+C_{26}+C_{28})+C_{30}]$

$\mathrm{OEP}(1) = (C_{21}+6C_{23}+C_{25})/ (4C_{22}+4C_{24})$

$\mathrm{OEP}(2) = (C_{25} + 6C_{27} + C_{29})/(4C_{26} + 4C_{28})$

## 5.3 Interpretation parameters based on the GC-MS

The GC-MS is used to identify ions with a m/z ratio of 178, 191, 192, 198, 217, 218, 231, and 253. The geochemical parameters identified are further used as maturity and facies determination. The peak labelling is taken from the NIGOGA guide Weiss et al. (2000).

**Table 5.1: List of the m/z ratios and their belonging chemical compounds. SAT = saturated hydrocarbons, ARO= aromatic hydrocarbons and SARO.**

| Ion/mass ratio | Type | |
|---|---|---|
| **m/z = 191** | Terpanes | **SAT** |
| **m/z = 217** | Steranes | |
| **m/z = 218** | Steranes | |
| **m/z = 217** | Triaromatic steroids | **ARO** |
| **m/z = 253** | Monoaromatic Steroids | |
| **m/z = 178** | Phenantrene | |
| **m/z = 192** | Metylphenantrenes | |
| **m/z = 198** | Methyl-dibenzothiophenes | |

## 5.3.1 Terpanes

The terpanes are a part of the saturated hydrocarbon fraction, and can be identified in m/z = 191, the m/z= 191 chromatogram. Table 5.2 list the terpane peaks obtained from m/z = 191. The respective peaks listed in Table 5.2 are identified in Figure 5.4 for the NSO-1 oil.

**Table 5.2: List of the terpanes found in the m/z = 191 with their names and composition**

| Peak | Stereochemistry | Name | Composition |
|---|---|---|---|
| **23/3** | | Tricyclic terpane | $C_{23}H_{42}$ |
| **24/3** | | Tricyclic terpane | $C_{24}H_{44}$ |
| **25/3** | 17R + 17S | Tricyclic terpane | $C_{25}H_{46}$ |
| **24/4** | | Tetracyclic terpane | $C_{24}H_{42}$ |
| **26/3** | R+S | Tricyclic terpane | $C_{26}C_{48}$ |
| **28/3** | R+S | Tricyclic terpane | $C_{28}H_{52}$ |
| **29/3** | R+S | Tricyclic terpane | $C_{29}H_{54}$ |
| **27Ts** | | 18α (H) trisnorneohopane | $C_{27}$ |
| **27Tm** | | 17α (H) trisnorneohopane | $C_{27}$ |
| **27β** | | 17β (H) -22,29,30-trisnorhopane | |
| **28αβ** | | 17α (H), 21β (H)-28-30-bisnorhopane | $C_{28}H_{48}$ |
| **29αβ** | | 17α (H), 21β (H) norhopane | $C_{29}H_{50}$ |
| **29Ts** | | 18α (H) norneohopane | $C_{29}$ |
| **30d** | | 15α-methyl-17α (H) diahopane | $C_{30}H_{52}$ |
| **29βα** | | 17β (H), 21α (H) normoretane | $C_{29}H_{52}$ |
| **30αβ** | | 17α (H), 21β (H) hopane | $C_{30}H_{52}$ |
| **30βα** | | 17β (H), 21α (H) moretane | $C_{30}H_{52}$ |
| **30G** | | Gammacerane | |
| **31αβS** | | 17α (H), 21β (H) homohopane | $C_{31}H_{54}$ |
| **31αβR** | | 17α (H), 21β (H) homohopane | $C_{31}H_{54}$ |

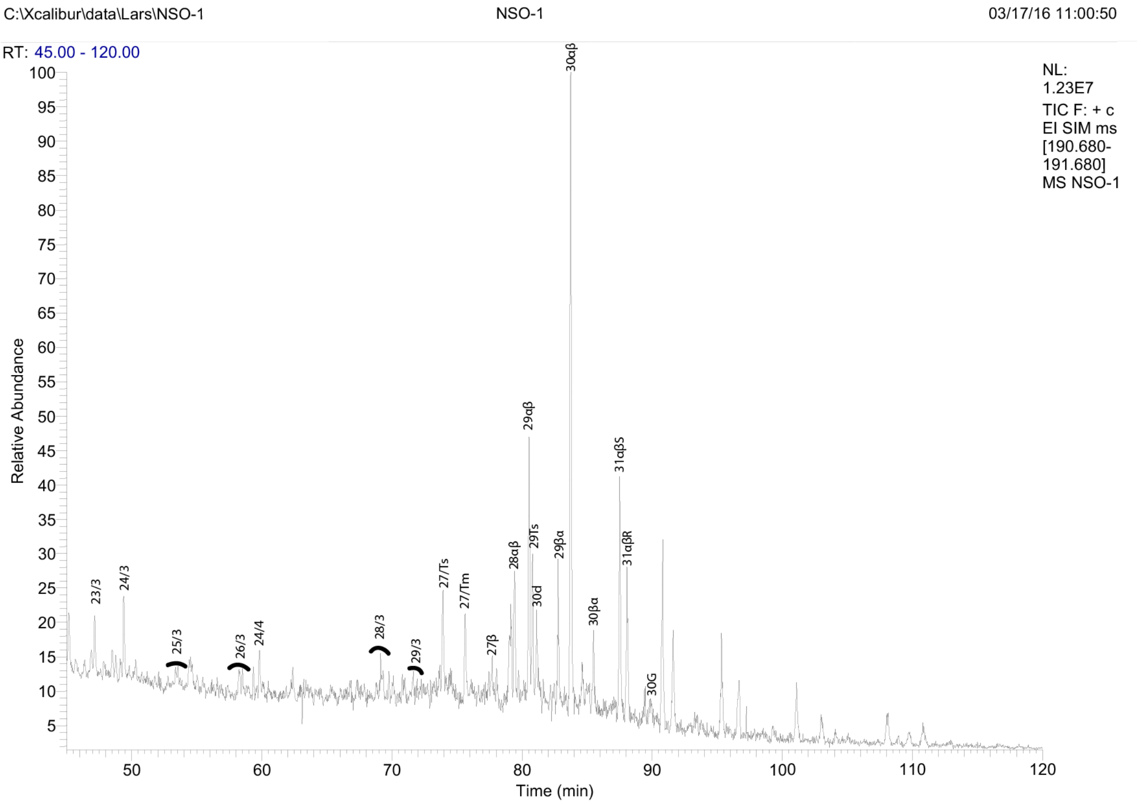

**Figure 5.4: Identification of the peaks corresponding to Table 5.2 (Terpanes) for the NSO-1 oils. The m/z = 191 for the chromatogram.**

## 5.3.2 Steranes

The steranes can be identified on the m/z chromatograms 217 and 218. The steranes are part of the tetracyclic saturated hydrocarbon fraction with one 5-chained aromatic ring and three 6-chained rings. Table 5.3 and 5.4 list the peaks identified in m/z = 217 and m/z = 218, respectively. Figure 5.5 display the peak labels for m/z = 217 for the NSO reference oil and Figure 5.6 for the m/z = 218.

**Table 5.3: The different peaks for m/z = 217 with their full name and composition.**

| Peak | Name | Composition |
|---|---|---|
| **27αβS** | 13β (H), 17α (H), 20 (S)-cholestane (diasterane) | $C_{27}H_{48}$ |
| **27αβR** | 13β (H), 17α (H), 20 (R)-cholestane (diasterane) | $C_{27}H_{48}$ |
| **29ααS** | 24-ethyl-5α (H), 14α (H), 17α (H), 20 (S)-cholestane | $C_{29}H_{52}$ |
| **29ββR** | 24-ethyl-5α (H), 14β (H), 17β (H), 20 (R)-cholestane | $C_{29}H_{52}$ |
| **29ββS** | 24-ethyl-5α (H), 14β (H), 17β (H), 20 (S)-cholestane | $C_{29}H_{52}$ |
| **29ααS** | 24-ethyl-5α (H), 14α (H), 17α (H), 20 (R)-cholestane | $C_{29}H_{52}$ |

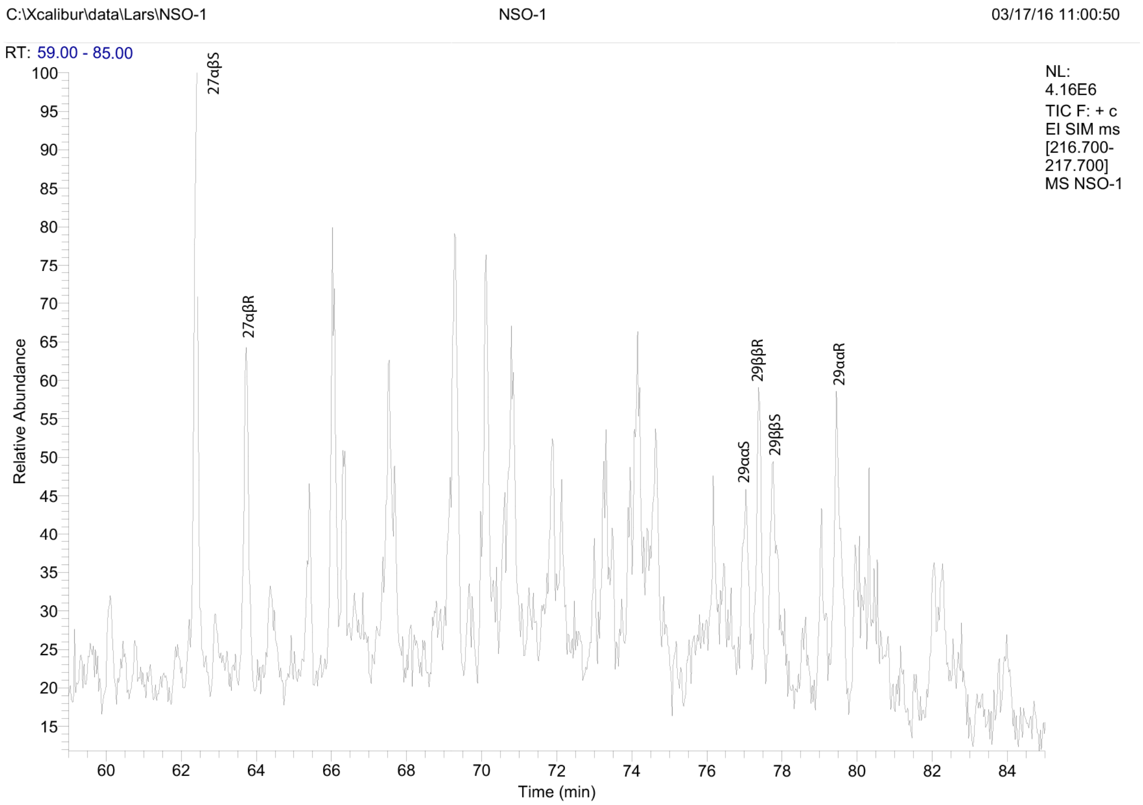

**Figure 5.5: Identification of the peaks corresponding to Table 5.3 (steranes) for the NSO-1 oils. The m/z = 217 for the chromatogram.**

**Table 5.4: The different peaks identified for m/z = 218 with their full names.**

| Peak | Name |
|---|---|
| **27ββR** | 5α (H), 14β (H), 17β (H), 20 (R)-cholestane |
| **27ββS** | 5α (H), 14β (H), 17β (H), 20 (S)-cholestane |
| **28ββR** | 24-methyl-5α (H), 14β (H), 17β (H), 20 (R)-cholestane |
| **28ββS** | 24-methyl-5α (H), 14β (H), 17β (H), 20 (S)-cholestane |
| **29ββR** | 24-ethyl-5α (H), 14β (H), 17β (H), 20 (R)-cholestane |
| **29ββS** | 24-ethyl-5α (H), 14β (H), 17β (H), 20 (S)-cholestane |

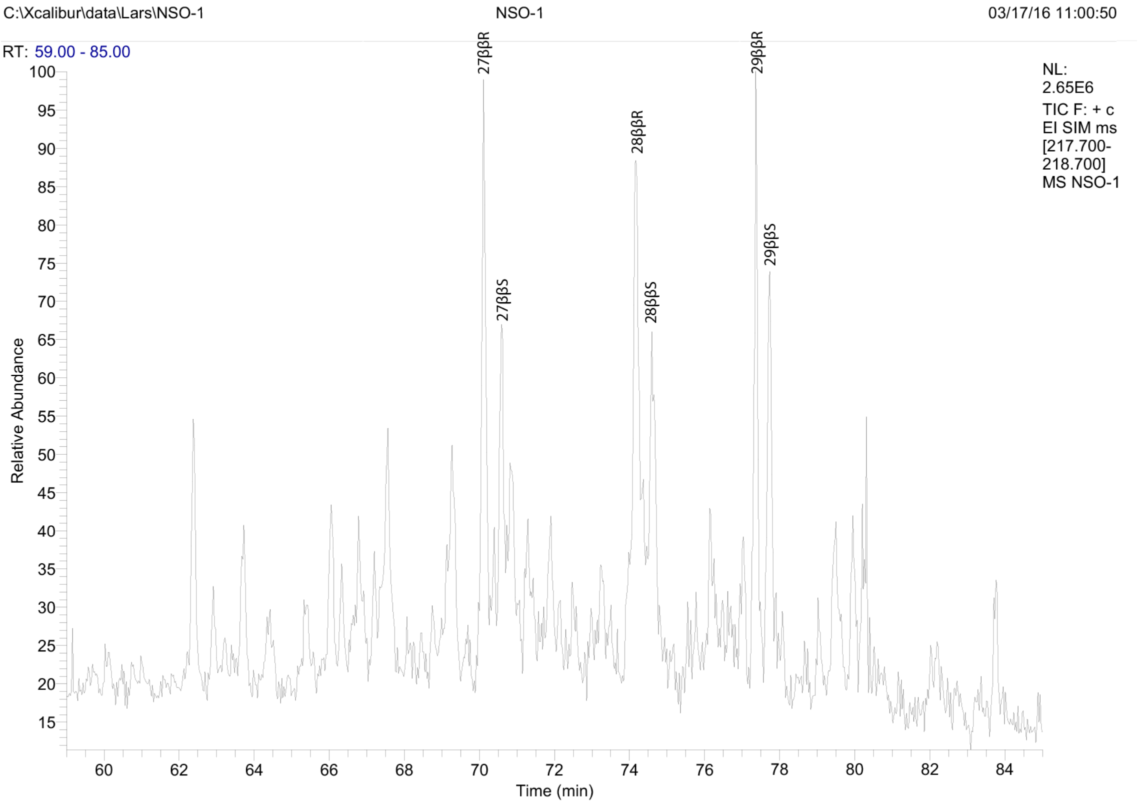

**Figure 5.6: Identification of the peaks corresponding to Table 5.4 (steranes) for the NSO-1 oils. The m/z = 218 for the chromatogram.**

## 5.3.3 Triaromatic steroids

Triaromatic steroids are a part of the aromatic fraction and can be identified at the m/z = 231.They are very useful for maturity assessment, due to the fact that short-chained aromatic steroids are more thermally sTable than those with longer chains (Beach et al., 1989). The most important peaks are listed in Table 5.5, with their respective substituents positions. The possible substituent positions are described in Figure 5.7. Figure 5.8 shows the identifications of the peaks from the reference NSO-1 oil.

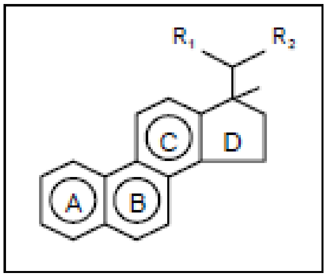

**Figure 5.7: Positions of substituents in triaromatic steroids (Weiss et al., 2000)**

**Table: 5.5: The most important peaks from the m/z = 231 chromatogram, with substituents for position $R_1$ and $R_2$.**

| Peak | $R_1$ | $R_2$ |
|---|---|---|
| **C20TA** | $CH_3$ | H |
| **C21TA** | $CH_3$ | $CH_3$ |
| **SC26TA** | $S(CH_3)$ | $C_6H_{13}$ |
| **RC26TA** | $R(CH_3)$ | $C_6H_{13}$ |
| **SC27TA** | $S(CH_3)$ | $C_7H_{15}$ |
| **SC28TA** | $S(CH_3)$ | $C_8H_{17}$ |
| **RC27TA** | $R(CH_3)$ | $C_7H_{15}$ |
| **RC28TA** | $R(CH_3)$ | $C_8H_{17}$ |

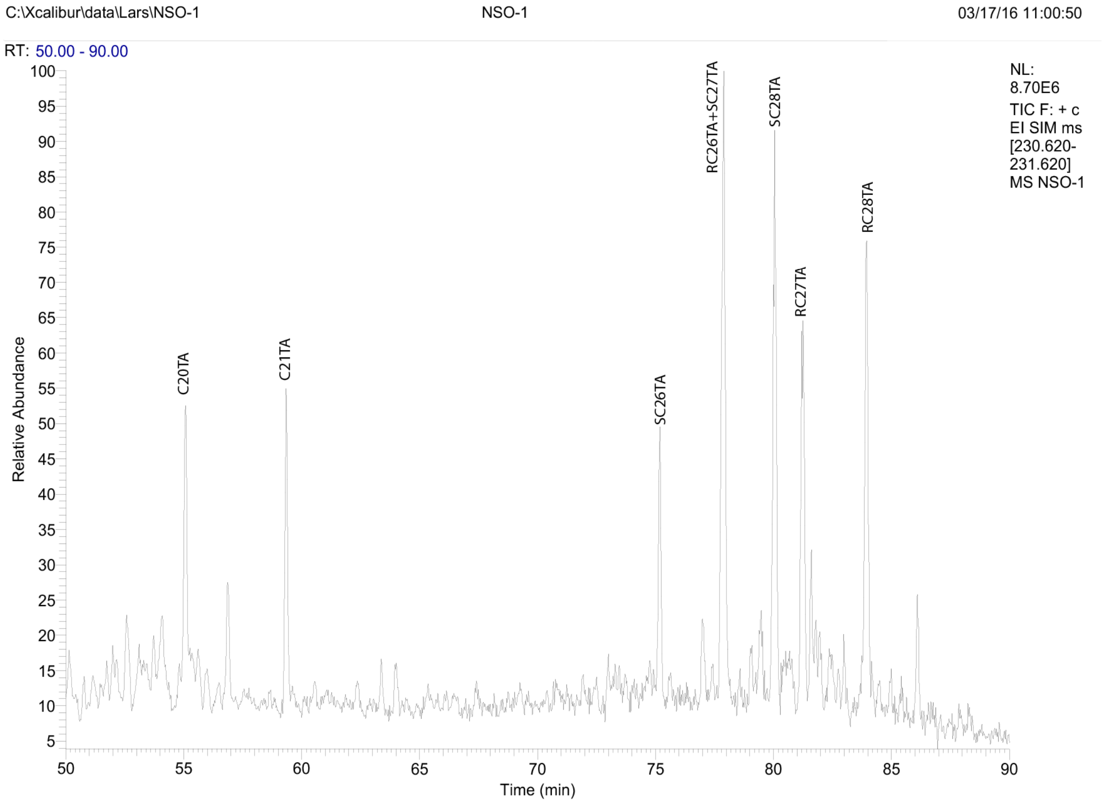

**Figure 5.8: Identification of the peaks corresponding to Table 5.5 (triaromatic steroids) for the NSO-1 oils. The m/z = 231 for the chromatogram.**

## 5.3.4 Monoaromatic steroids

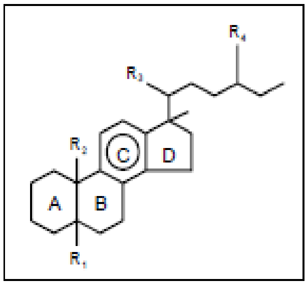

**Figure 5.9: Positions of substituents in monoaromatic steroids (Weiss et al., 2000)**

The monoaromatic steroids can be identified from the m/z = 253 chromatogram, and is a part of the hydrocarbon aromatic fraction. The most important peaks are listed in Table 5.7 with their substituents positions. The possible substituent positions are described in Figure 5.9. They are assumed to be precursor of the triaromatic steroids, the monoaromatic steroids form from regular steroids in the early stages of diageneses by aromatization (Tissot and Califet-Debyser, 1971). The relative abundance of monoaromatic steroids compared to triaromatic steroids is a maturity indicator, since more triarmotes will from during maturation (Peters et al., 2005).

**Table: 5.6: The most important peaks from the m/z = 253 chromatogram, with substituents for position $R_1$ and $R_2$.**

| Peak Group | R1 | R2 | R3 | R4 | Peak |
|---|---|---|---|---|---|
| H1 | α(H) | $CH_3$ | $S(CH_3)$ | $C_2H_5$ | αSC29MA |
| H1 | α(H) | $CH_3$ | $R(CH_3)$ | $CH_3$ | αRC28MA |
| H1 | β(H) | $CH_3$ | $R(CH_3)$ | $C_2H_5$ | βRC29MA |
| H1 | $bCH_3$ | H | $R(CH_3)$ | $C_2H_5$ | βRC29DMA |

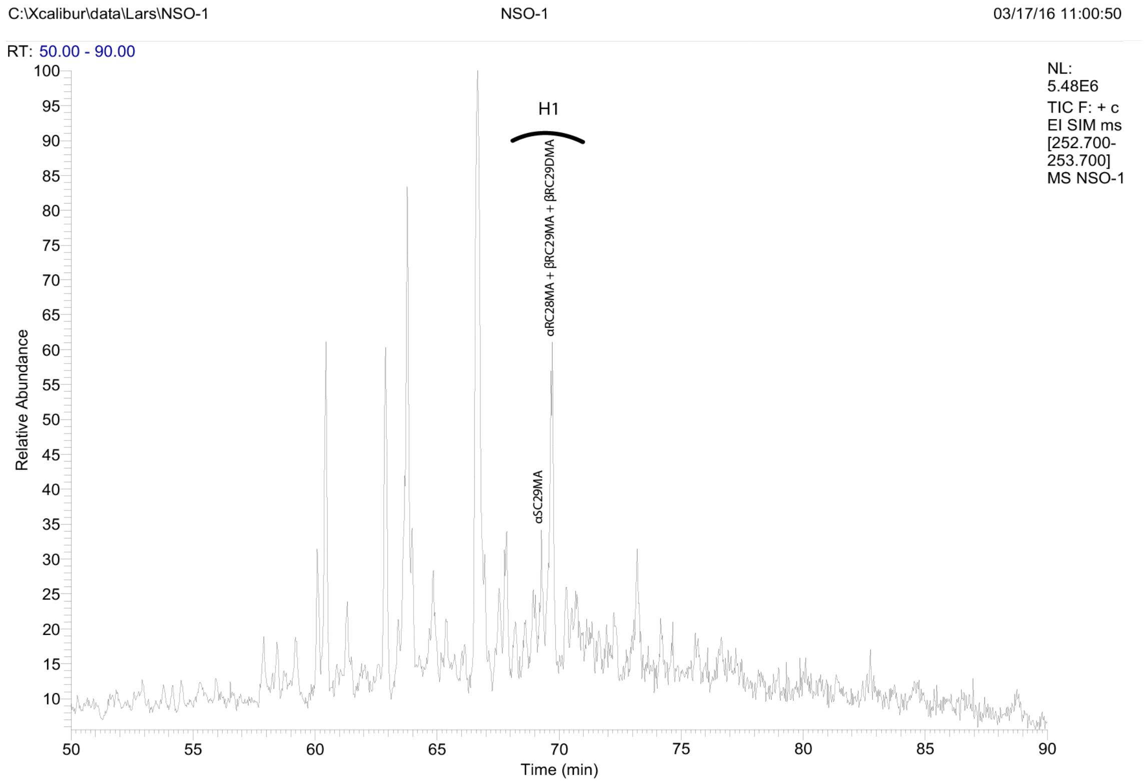

**Figure 5.10: Identification of the peaks corresponding to Table 5.6 (monoaromatic steroids) for the NSO-1 oils. The m/z = 253 for the chromatogram.**

### 5.3.5 Phenanthrene, methylphenanthrene and methyldibenzothiophene

The phenantrene can be identified at m/z = 178, methylphenantrene at m/z = 192 and methyldibenzothiophenes at m/z = 198. Figure 5.13 illustrates the respective peaks for chromatogram m/z = 178, m/ z= 192 and m/z = 198 for NSO-1 oil. The phenanthrene is a tri-aromatic with 14C atoms, the methylphenanthrene (C15) have a methyl situated in one of the positions showed in Figure 5.11. The most common places occupied are 1, 2, 3 and 9. The methyldibenzothiophene is a di-aromatic molecule with 13C and sulphur. The methyl group can be situated at 4 different positions as show in Figure 5.12. The phenatrene and some of the methyl positions are more sTable during thermal maturation, thus measuring the relative quantity of the phenathrene and the different isomers for methylphenanthrene and Methyldibenzothiophene this can give us valid maturity estimations.

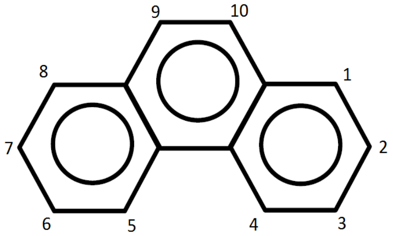

**Figure 5.11: Phenanthrene with possible isomers positions (Peters et al., 2005)**

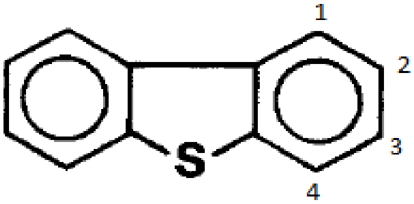

**Figure 5.12: Methyldibenzothiophene with the possible isomers positions (Peters et al., 2005).**

**Table 5.7: The most important peaks from the m/z = 178, m/z=192 and m/z=198 chromatogram**

| m/z | Peak | Name |
|---|---|---|
| **178** | P | Phenanthrene |
| **192** | 3-MP | 3-Methylphenanthrene |
| **192** | 2-MP | 2-Methylphenanthrene |
| **192** | 9-MP | 9-Methylphenanthrene |
| **192** | 1-MP | 1-Methylphenanthrene |
| **198** | 4-MDBT | 4-Methyldibenzothiophene |
| **198** | (3+2)-MDBT | 3+2-Methyldibenzothiophene |
| **198** | 1-MDBT | 1-Methyldibenzothiophene |

## 5.3.6 The standard parameters for maturity and organic facies based on the GC-MS

The standard 27 Parameters are listed in Table 5.8. The maturity range for some of the Parameters is listed in Table 5.15. A brief explanation of the Parameters follows after the Table.

**Table 5.8: Overview of the 27 parameters used in this thesis from the GC-MS. The parameters are used for maturity estimation and organic facies of the paleo-depositional environment.**

| No. | Parameter |
|---|---|
| 1 | Ts/(Ts + Tm), (Seifert and Moldowan, 1978) |
| 2 | Diahopane/(diahopane + normoretan), (Cornford et al., 1986) |
| 3 | 22S/(22S+22R) of C31 17a(H), 21ß(H)-hopanes (Mackenzie et al., 1980) |
| 4 | C30-hopane/(C30-hopane + C30-morethane), (Mackenzie et al., 1985) |
| 5 | 29Ts/(29Ts + norhopane) (Peters and Moldowan, 1991) |
| 6 | Bisnorhopane/(bisnorhopane + norhopane) (Wilhelms and Larter, 1993) |
| 7 | C23-C29 tricyclic terpanes/C30 aß-hopane (Mello et al., 1988) |
| 8 | C24 tetracyclic terpane/C30 aß-hopane (Mello et al., 1988) |
| 9 | Hopane/sterane (Mackenzie, 1984) |
| 10 | ßß/(ßß+aa) of C29 (20R+20S) sterane isomers (Mackenzie et al., 1985) |
| 11 | 20S/(20S+20R) of C29 5a(H),14a(H),17a(H) sterane isomers (Mackenzie, 1984) |
| 12 | Diasteranes/(diasteranes + regular steranes) (Seifert and Moldowan, 1978) |
| 13 | % C27 of C27+C28+C29 ßß-steranes (Moldowan et al., 1985) |
| 14 | % C28 of C27+C28+C29 ßß-steranes (Moldowan et al., 1985) |
| 15 | % C29 of C27+C28+C29 ßß-steranes (Moldowan et al., 1985) |
| 16 | C20/(C20+C28) triaromatic steroides (TA) (Mackenzie et al., 1985) |
| 17 | C28 TA/(C28 TA+C29 MA) (Mackenzie et al., 1985) |
| 18 | Methyl phenanthrene ratio, MPR (Radke et al., 1982b) |
| 19 | Methyl phenanthrene index 1, MPI1 (Radke et al., 1982a) |
| 20 | Methyl phenanthrene distribution fraction 1, MPDF (F1) (Kvalheim et al., 1987) |
| 21 | Methyl dibenzothiophene ratio, MDR (Radke, 1988) |
| 22 | Calculated vitrinite reflection, Rm = 1.1*log10 MPR + 0.95 (Radke, 1988) |
| 23 | Calculated vitrinite reflection, %Rc = 0.60*MPI1 + 0.40 (Radke, 1988) |
| 24 | Calculated vitrinite reflection, %Ro = 2.242*F1 - 0.166 (Kvalheim et al., 1987) |
| 25 | Calculated vitrinite reflection, Rm = 0.073*MDR + 0.51 (Radke, 1988) |
| 26 | 3-methyl phenanthrene/4-methyl dibenzothiophene (Hughes et al., 1995) |
| 27 | Methyl dibenzothiophenes/methyl phenanthrenes (Radke et al., 2001) |

### Parameter 1: Ts/(Ts + Tm)

Ts have higher stability during thermal maturation than Tm. Consequently the Ts/(Ts+Tm) ratio will increase. Therefore the ratio provides a good estimation of maturation and was first introduced by Seifert and Moldowan (1978). The ratio is valid for bitumen and oil samples >0.5%$R_0$ to about 1,4$R_0$%. Variation in the ratio is also influenced by source input. Carbonate derived oils will usually give a lower ratio than siliclastic sources (Peters et al., 2005). Hyper saline samples tend to make an over estimation of the maturity (ratio becomes too high) (Rullkötter and Marzi, 1988). To obtain the most certain estimation of maturation this ratio should be used for samples with the same organic facies.

**Paramter 2: Diahopane/(diahopane + normoretan)**

High ratios of parameter 2 indicate high maturity, influences by source input can also not be excluded (Peters and Moldowan, 1993)

**Parameter 3: 22S/(22S+22R)**

The 22S isomer is more sTable during thermal maturating than the 22R isomer. Therefore the ratio will indicate what stage of maturation a bitumen or oil is. The ratio reaches an equilibrium at around 0,6$R_0$% (Seifert and Moldowan, 1980). Thus the ratio will only give valid estimations for source rock samples and early oils.

**Parameter 4: C30-hopane/(C30-hopane + C30-morethane)**

The C30-hopane is more thermally sTable than the C30-morethane. Therefor the ratio is a maturation indicator (Mackenzie et al., 1985). The loss of C30-moretane occurs at low temperatures. Thus, the ratio is only useful for early oils samples and source rocks. Parameter 4 is also influences by source input (Rullkötter and Marzi, 1988).

**Parameter 5: 29Ts/(29Ts + norhopane)**

Norhopane is thermally less sTable than the 29Ts, and the ratio will indicate thermal maturation (Moldowan et al., 1991).

**Parameter 6: Bisnorhopane/(bisnorhopane + norhopane)**

Parameter 6 is mainly a facies indicator. Excessive amounts of bisnorhopane is assumed to indicate marine and anoxic conditions (Peters and Moldowan, 1993). However low concentrations of bisnorhopane doesn’t necessarily exclude an anoxic environment (Peters et al., 2005). However the ratio is also influences by maturity, the amount of bisnorhopane will decrease during thermal maturation. Hence immature samples tend to indicate a more anoxic environment than what is actually true. Samples of mainly the same maturity should be used for comparison.

**Parameter 7: C23-C29 tricyclic terpanes/C30 aß-hopane**

C23-C29 tricyclic terpanes and C30 hopane ratio are a good maturity indicator (Mello et al., 1988). This is due to the fact that the terpanes are more thermally sTable than the hopanes (Peters et al., 1990) and are released at a later stage of maturation from the kerogen. This results in a drastic jump of the ratio for samples above 0,75 $R_0$% (van Graas, 1990). The ratio is also influenced by phase- and evaporation fractioning (Karlsen et al., 1995, Karlsen and Skeie, 2006). Salinity variations in a sample influences the tricyclic terpanes abundance (Mello, 1988) and therefor, limits the usefulness of parameter 7 as facies indicator.

**Parameter 8: C24 tetracyclic terpane/C30 aß-hopane**

The amount of C24-tetracyclic terpanes will increase relatively to the amount of C30-hopane during thermal maturation (Peters and Moldowan, 1993). The ratio can also increase by biodegradation (Peters et al., 2005).

**Parameter 9: Hopane/Sterane**

Parameter 9 indicates depositional environment. Hopanes are derived mainly from bacteria while sterane comes from algae and higher land plants. High ratios tend to indicate a terrestrial environment while low ratios a planktonic source (Tissot and Welte, 1984). The ratio is also influenced by lithology, where high ratios is associated with Carbonate and low with shale (Peters et al., 2007). The inverted ratio (Sterane/Hopane) is also used in this thesis, as it is better suited to plot with the bisnorhopane/(bisnorhopane + norhopane) ratio.

**Parameter 10: ßß/(ßß+aa) of C29 (20R+20S) sterane isomers**

The ßß isomer are more thermally sTable during maturation than the aa isomer isomer (Mackenzie et al., 1985). The ratio equilibrates around peak oil production (0,9 $R_0$%). However the ratio may be influenced by minerology (Peters and Moldowan, 1993).

**Parameter 11: 20S/(20S+20R) of C29 5a(H),14a(H),17a(H) sterane isomers**

20R converts to 20S during maturation, the ratio equilibrates at 0.8-0.9$R_0$% (Moldowan et al., 1986). Parameter 11 may also be influenced by facies, weathering and biodegradation (Peters and Moldowan, 1993).

### Parameter 12: Diasteranes/(diasteranes + regular steranes)

Parameter 12 will increase with thermal maturity, due to diasterane is more thermally sTable than regular steranes (Seifert and Moldowan, 1978). The ratio will also be influenced by lithology variations, high ratios tend to indicate a silliclastic source while low ratios are usually a sign of carbonates (Mello et al., 1988). The ratio has also shown to be influenced by biodegradation (Seifert and Moldowan, 1979).

### Parameter 13,14 and 15: % C27, %C28 and %C29 ßß-steranes

C27%, C28%, C29% ßß-steranes relative percentage plotted in a ternary diagram, are helpful to distinguish different organic facies (Moldowan et al., 1985)

### Parameter 16: C20/(C20+C28) triaromatic steroides (TA)

The longer chained C28 triaromatic steroids are less thermally sTable than the C20 mono-aromatic steroid, hence variations in the ratio will indicate maturity (Beach et al., 1989). The parameter throughout the whole oil window (up to about 1,4$R_0$%) (see Figure 5.14). Phase fractioning will also have a strong influence on the ratio, and needs to be taken into consideration (Karlsen et al., 1995).

### Parameter 17: C28 TA/(C28 TA+C29 MA)

During thermal maturation mono-aromatic steroids are rearranged to tri-aromatic steroids. Thus the ratio can estimate the stage of maturation. The ratio is valid until peak oil generation (see Figure 5.15) (Peters et al., 2005).

### Parameter 18: Methyl phenanthrene ratio, MPR = 2-MP/1-MP

The MPR ratio is a maturity indicator for mature oils, the ratio is constant until $R_0$% of about 0,95 (Radke et al., 1982b).

### Parameter 19: Methyl phenanthrene index 1, MPI1 = 1, 5(3-MP + 2-MP)/ (P + 9-MP + 1-MP)

The 3-MP(α) and 2-MP (α) isomers are more sTable during thermal maturation compared to the 9-MP(β) and 1-MP(β). Thusly the MPI1 will increase during maturation (Radke et al., 1982a). However the phenanthrene has an even higher stability. When the α isomers begin to degrade in the late oil window. Only the phenanthrenes will remain (Radke et al., 1982a). Consequently, the MPI1 will decrease again at a late stage of the oil window. The MPI1 can be converted into vitrinite reflectivity and have a positive linear relationship between 0.65%R0 to 1.35%R0 and a negative linear relationship from 1.35%R0 to 2.00%R0 (see Figure 5.14). Later studies have shown that the ratio is less useful. This is due to the redox potential of the sedimentary rock which heavily influence the ratio (Szczerba and Rospondek, 2010).

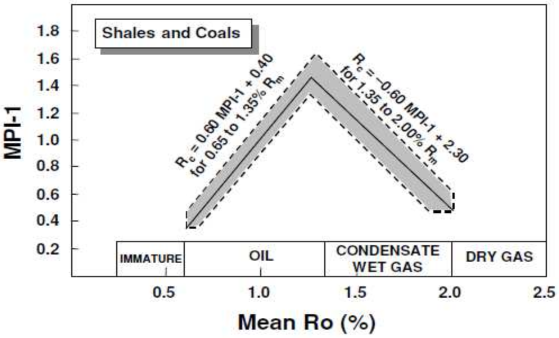

**Figure 5.14: The Figure illustrates how the MPI-1 ratio vary with maturation (Peters et al., 2007)**

### Parameter 20: Methyl phenanthrene distribution fraction 1, MPDF (F1) = (3-MP + 2-MP)/ (3-MP + 2-MP + 1-MP + 9-MP)

Parameter 20 presented by Kvalheim et al. (1987) is quite similar to parameter 19. The difference is that the phenanthrenes are not included. The result of this is that the ratio will only increase during maturation, the ratio will reach an equilibrium sooner than the MPI1 due to the lack of phenanthrenes in the equation.

### Parameter 21: Methyl dibenzothiophene ratio, MDR = 4-MDBT /1-MDBT

This parameter is based on the two isomers 4-MDBT and 1-MDBT, and is both a maturity and facies indicator. The MDR was introduced by Radke (1988). During maturation 4-MDBT is thermally more sTable than 1-MDBT and the ratio will increase. According to Radke et al. (1986) MDR samples between 0,4-0,7 vitrinite reflectivity will show significantly lower MDR for oil prone kerogen (type I-II) than gas prone kerogen (type III).

**Parameter 22: Calculated vitrinite reflectivity, Rm = 1.1*log10 MPR + 0.95**

Calculated vitrinite reflectivity calculated from the MPR parameter (Radke, 1988).

**Parameter 23: Calculated vitrinite reflectivity, %Rc = 0.60*MPI1 + 0.40**

Calculated vitrinite reflectivity calculated from the MPI1 parameter (Radke, 1988).

**Parameter 24: Calculated vitrinite reflectivity, %Ro = 2.242*F1 - 0.166**

Calculated vitrinite reflectivity calculated from the MPDF parameter (Kvalheim et al., 1987).

**Parameter 25: Calculated vitrinite reflection, Rm = 0.073*MDR + 0.51**

Calculated vitrinite reflectivity calculated from the MDR parameter (Radke, 1988).

**Parameter 26: 3-methyl phenanthrene/4-methyl dibenzothiophene**

Parameter 26 is a facies parameter, commonly plotted together with Pr/Ph ratios to indicate lithofacies (Hughes et al., 1995). The ratio can also provide information about the Sulphur content of the rock (Radke, 1988).

**Parameter 27: Methyl dibenzothiophenes/methyl phenanthrenes (Radke et al., 2001)**

The sum of the MDBT divided by the sum of the MP is a facies parameter. Values above one indicate carbonate facies, ratios below indicate shale (Hughes et al., 1995).

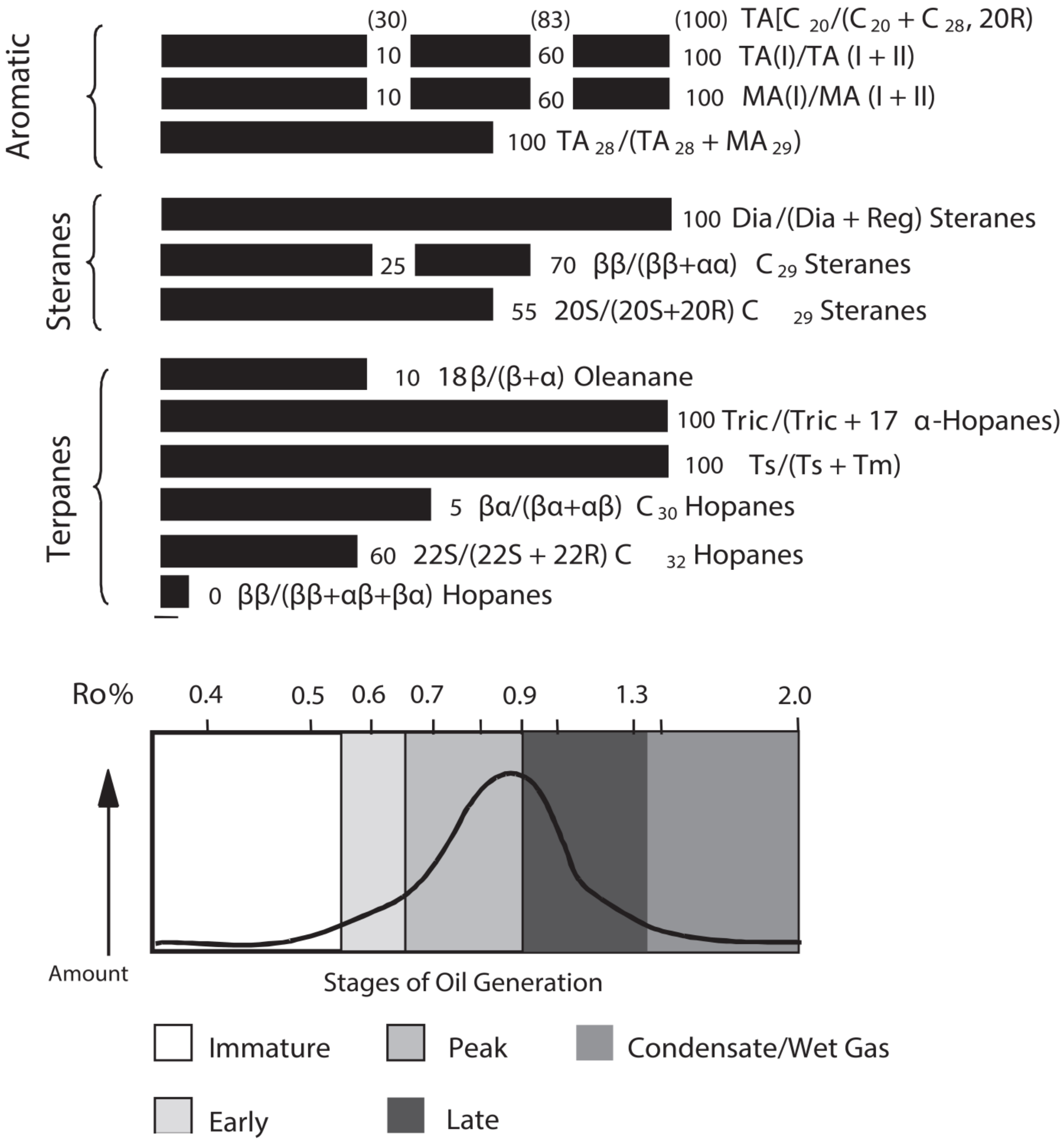

**Figure 5.15: The validity range of the biomarker parameters corresponding to the oil window (modified from Peters et al., 2007).**

## 5.4 Other parameters based on the GC-MS

### 5.3.1 Extended tricyclic terpane ratio

The extended tricyclic terpane ratio (ETR) (= (C28 + C29)/(C28 + C29 +Ts)) is mainly age related and are useful to distinguish Triassic from Jurassic oils samples (Holba et al., 2001). Pre-Triassic sources has also been attempted to be discerned based on the ETR (Ohm et al., 2008). The ratio is based on the m/z=191 chromotogram of the C28 and C29 tricyclic terpanes peaks and the 18α (H) trisnorneohopane peak.

# 6. Results

This chapter presents the interpretation parameters described in chapter 5 from the data provided by the analytical methods, described in chapter 4. Downscaled chromatograms of the respective samples are presented, and the full scale chromatograms can be found in appendix A, B and C.

The results are presented in the following order:

6.1 Iatroscan results

- 6.1.1 Summary of oils and condensates from SW Barents Sea
- 6.1.2 Summary of bitumens from FP and NB

6.2 Results based on the GC-FID

- 6.2.1 Summary of the GC-FID parameters for the oils and condensates
- 6.2.2 N-alkane distribution of the oils and condensates
- 6.2.3 Summary of the GC-FID parameters for the extracted core samples
- 6.2.4 N-alkane distribution of the Oils and Condensates

6.3 Results based on the GC-MS

- 6.3.1 Summary of the GC-MS results

6.4 Downscaled chromatograms for Iatroscan, GC-FID, GC-MS

## 6.1 Iatroscan results

The iatroscan results are based on the gross composition of the hydrocarbon fraction of saturates and aromatics and, of asphaltenes/resins. The results are based on the analytical method in section 4.3 and the parameters are described in section 5.1. The values can be viewed in Table 6.1 and downscaled TLC-FID chromatograms can be found in section 6.4. Full scale chromatograms are shown in appendix A.

### 6.1.1 Summary of oils and condensates from SW Barents Sea

The SAT (Saturated), ARO (Aromatic) and POL (Polar) composition for the oils/condensates ranges from 52.7-70.0%, 2.4-29.0% and 9.5-33.1% respectively (see Table 6.1 and Figure 6.1). The two condensates S2 and A1 have display the highest SAT values, the former has a SAT percentage of 62.0%. Henceforth, the lowest SAT value belongs to JC4 with 51.7%. Subsequently, the lowest ARO relative percentages belong to the S2 and A1 sample, 4.9% and 2.4% respectively. The highest SAT relative percentage is 29.0% estimated for the JC1 sample. The sample containing the most POL compounds is the S2 sample with 33.10%. Moreover, the SAT/ARO ratios range from 1.75727 to 29.1952. Furthermore, the SAT/ARO ratios range from 1.68 to 29.20, which is a vast spectrum (see Table 6.1). Again the condensate samples S2 and A1 have the highest ratios, where the former has a ratio of 12.62 and the latter a ratio of 29.20. The lowest ratio is assigned to the NSO-1 sample. For a better visualization of the SAT, ARO and POL distribution the reader should view Figure 6.1.

### 6.1.2 Summary of bitumens from FP and NB

The ranges of the SAT hydrocarbons and POL compounds for the extracted core samples are 0-48.6% and 51.4-100% respectively (see Table 6.1 and Figure 6.1). Sample FP3 and NB1 do not contain any saturated hydrocarbons, while FP6 has 48.6%, whereas the lowest amount of POL compound belongs to FP6. All the bitumen samples contain 0% ARO with the exception of FP9 which contains 9% ARO. The total extracTable organic matter is ranging from 0.0018 to 0.0030 (see Table 6.1). This is generally extremely low. The lowest value is assigned to FP9 and the highest value is assigned to FP6. To get a better idea of the distribution the reader is referred to Figure 6.1, the total extracTable organic matter for the core samples are also visualized in chapter 7, Figure 7.2.

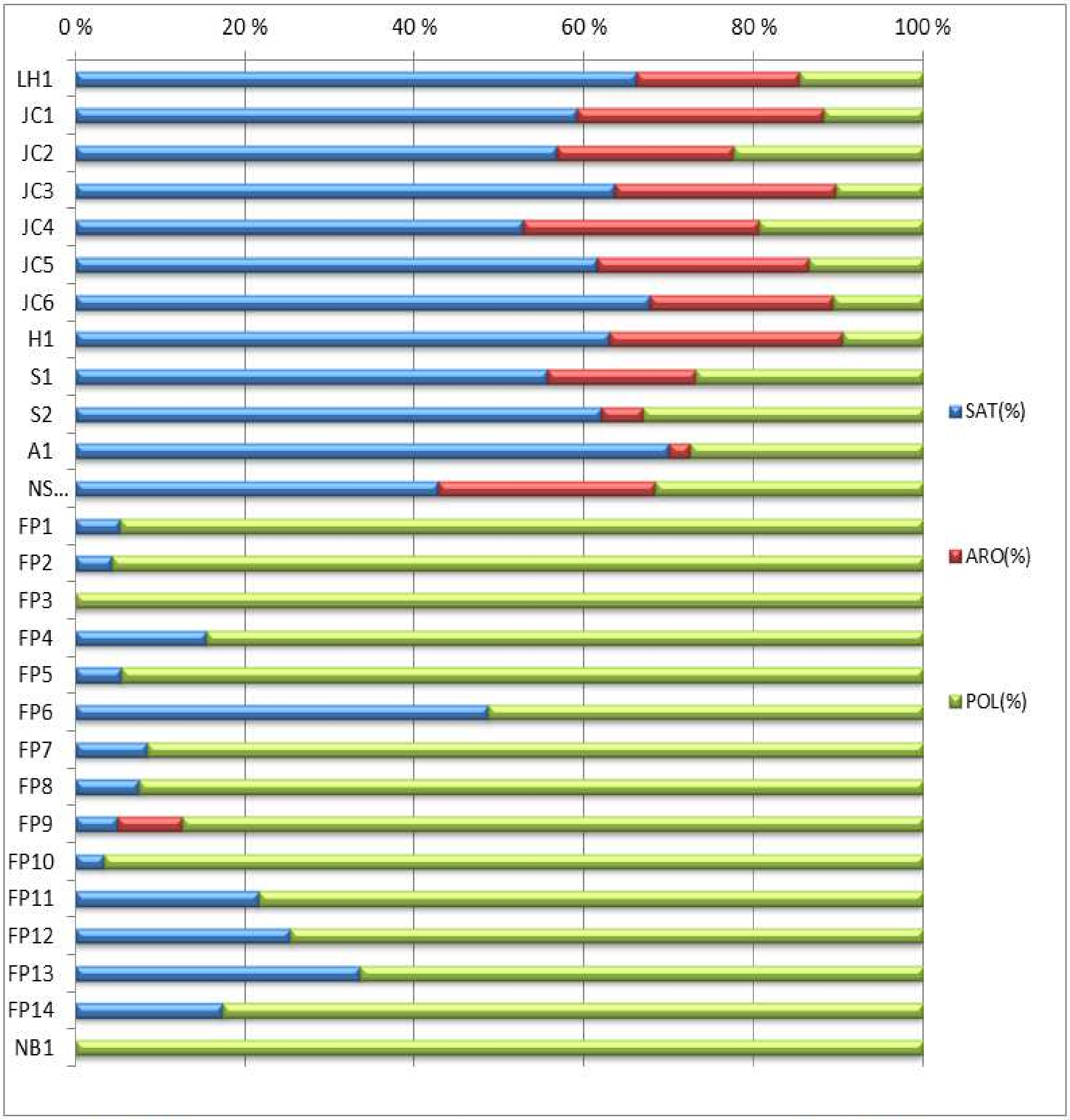

**Figure 6.1: The relative percentage amount of SAT (Saturated), ARO (Aromatic) and POL (Polar). FP9 is the only core sample containing an aromatic fraction.**

Table 6.1: Results from the IATROSCAN analysis. The organic matter are separated into three components Saturated (SAT) and Aromatic (ARO) hydrocarbons and non-petroleum fraction Polar (POL). The extract yield is also shown for the core samples in mg/g rock. SAT/ARO ratio for the oils, condensates and one of the extracts are also displayed. ND = Not Defined.

| | | | | Extract concentrations (%) | | | Extract yield (mg/g rock) | | | | |
|---|---|---|---|---|---|---|---|---|---|---|---|
| Samp-le ID | Sample weight (g) | Extract total volume (ml) | Sample volume (ul) | SAT | ARO | POL | SAT(mg/g rock) | ARO(mg/g rock) | POL(mg/g rock) | TOTAL | SAT/ARO |
| LH1 | ND | ND | 0.5 | 66.2 | 19.3 | 14.5 | ND | ND | ND | ND | 3.43 |
| JC1 | ND | ND | 0.5 | 59.2 | 29.0 | 11.8 | ND | ND | ND | ND | 2.05 |
| JC2 | ND | ND | 0.5 | 56.8 | 20.7 | 22.4 | ND | ND | ND | ND | 2.74 |
| JC3 | ND | ND | 3 | 63.6 | 26.0 | 10.4 | ND | ND | ND | ND | 2.45 |
| JC4 | ND | ND | 0.5 | 52.7 | 27.9 | 19.4 | ND | ND | ND | ND | 1.89 |
| JC5 | ND | ND | 0.5 | 61.5 | 24.9 | 13.6 | ND | ND | ND | ND | 2.47 |
| JC6 | ND | ND | 0.5 | 67.8 | 21.6 | 10.7 | ND | ND | ND | ND | 3.14 |
| H1 | ND | ND | 0.5 | 63.0 | 27.5 | 9.5 | ND | ND | ND | ND | 2.29 |
| S1 | ND | ND | 0.5 | 55.7 | 17.6 | 26.8 | ND | ND | ND | ND | 3.17 |
| S2 | ND | ND | 0.5 | 62.0 | 4.9 | 33.1 | ND | ND | ND | ND | 12.61 |
| A1 | ND | ND | 0.5 | 70.0 | 2.4 | 27.6 | ND | ND | ND | ND | 29.20 |
| NSO-1 | ND | ND | 3 | 42.8 | 25.6 | 31.6 | ND | ND | ND | ND | 1.68 |
| FP1 | 7 | 1.5 | 3 | 5.3 | 0.0 | 94.7 | 0.0001 | 0 | 0.0023 | 0.0024 | ND |
| FP2 | 4.7 | 1 | 3 | 4.3 | 0.0 | 95.7 | 0.0001 | 0 | 0.0023 | 0.0024 | ND |
| FP3 | 7.03 | 1.5 | 3 | 0.0 | 0.0 | 100.0 | 0.0000 | 0 | 0.0023 | 0.0023 | ND |
| FP4 | 7 | 1.5 | 3 | 15.5 | 0.0 | 84.5 | 0.0004 | 0 | 0.0021 | 0.0025 | ND |
| FP5 | 7 | 1.8 | 3 | 5.4 | 0.0 | 94.6 | 0.0002 | 0 | 0.0027 | 0.0029 | ND |
| FP6 | 7.01 | 1.5 | 3 | 48.6 | 0.0 | 51.4 | 0.0015 | 0 | 0.0016 | 0.0030 | ND |
| FP7 | 7.03 | 1 | 3 | 8.4 | 0.0 | 91.6 | 0.0001 | 0 | 0.0015 | 0.0016 | ND |
| FP8 | 7.01 | 1.5 | 3 | 7.5 | 0.0 | 92.5 | 0.0002 | 0 | 0.0022 | 0.0024 | ND |
| FP9 | 7 | 1.1 | 3 | 4.9 | 7.8 | 87.3 | 0.0001 | 0 | 0.0016 | 0.0018 | 0.63 |
| FP10 | 7.07 | 1.7 | 3 | 3.3 | 0.0 | 96.7 | 0.0001 | 0 | 0.0026 | 0.0027 | ND |
| FP11 | 7 | 1.5 | 3 | 21.6 | 0.0 | 78.4 | 0.0006 | 0 | 0.0020 | 0.0026 | ND |
| FP12 | 7.03 | 1.5 | 3 | 25.4 | 0.0 | 74.6 | 0.0007 | 0 | 0.0020 | 0.0026 | ND |
| FP13 | 7.01 | 1.5 | 3 | 33.5 | 0.0 | 66.5 | 0.0009 | 0 | 0.0018 | 0.0028 | ND |
| FP14 | 7.01 | 1.5 | 3 | 17.4 | 0.0 | 82.6 | 0.0004 | 0 | 0.0021 | 0.0025 | ND |
| NB1 | 7.02 | 1.5 | 3 | 0.0 | 0.0 | 100.0 | 0.0000 | 0 | 0.0023 | 0.0023 | ND |

## 6.2 Results based on the GC-FID

The results are based on the GC-FID analysis presented in section 4.3. The results are listed in Table 6.2. The ranges of the calculated parameters for the respective samples can be viewed in Figure 6.2. The calculated parameters are presented in section 5.2, the full scale GC-FID chromatograms for the respective samples can be found in appendix B and a downscaled version in section 6.5. The samples FP1, FP2, FP3, FP5, FP6, FP7, FP8 and FP14 have low Signal-to-Noise ratio, and the interpretation parameters from the GC-FID were not possible to gather. It is important to note that the remaining core samples have modest intensities, and the interpretation parameters are uncertain. Regardless, the results seem to have some value and are therefore presented in this section. Pr/n-C17 and Ph/nC18 ratios were not possible to calculate for any of the core extracts.

### 6.2.1 Summary of the GC-FID parameters for the oils and condensates

The Pr/n-C17 ratio calculated from the GC-FID ranges from 0.52 to 3.91, the lowest value is assigned to the NSO-1 sample (see Table 6.2 and Figure 6.2). Furthermore, JC1-3 and JC6 express high values, 3.22, 3.91, 3.13 and 3.79 respectively (see Table 6.2 and Figure 6.2). The Ph/n-C18 ratios express a narrower range than the above mentioned ratio, 0.38-1.88 respectively. As a contradiction to the Pr/n-c17 the NSO-1 sample does not express the lowest values, which are assigned to JC4. The highest samples on the other hand are still assigned to the JC1-3 and the JC6 samples (see Table 6.2). For the oils and condensates the Pr/Ph ratio ranges from 1.43-2.36 (see Table 6.2 and Figure 6.2). Furthermore, the CPI, OEP(1) and OEP(2) range from 0.84 to 1.08, 0.98 to 1.05 and 0.43 to 1.13 respectively (see Table 6.2 and Figure 6.2). As seen from Figure 6.2 the A1 and S2 samples express significantly lower OEP(2) values than the rest of the sample set. The former has the value of 0.50 and the latter 0.43.

### 6.2.2 N-alkane distribution of the oils and condensates

#### LH1

The chromatogram displays a slight bimodal distribution of the n-alkenes for sample LH1, with a slight slump in the n-C17 and n-C18 range. The n-C30+ amount is very low, and the distribution shows a linear increasing trend towards the lighter n-alkanes (see Figure 6.4 and appendix A).

**JC1**

The JC1 sample has a general n-alkane intensity which is quite low for the sample, while the Pr and Ph are very prominent. The light hydrocarbon fraction seems to be low. The sample shows moderate quantities of UCM as the baseline is elevated from min 10 to 60 (see Figure 6.5 and appendix B).

**JC2**

The sample has an n-alkane distribution very similar to JC1, with high Pr and Ph peaks relative to the n-alkanes. The baseline is elevated in the same matter (see Figure 6.6 and appendix B).

**JC3**

The JC3 sample expresses an n-alkane intensity which is relatively low to the Pr and Ph peaks. The sample also seems to have a moderate amount of UCM (see Figure 6.7 and appendix B).

**JC4**

The distribution of n-alkanes has a concave shape and the abundance is low for heavier n-Alkanes than C30+ for sample JC4. This sample contains a higher fraction of light saturated hydrocarbons. The baseline is slightly elevated however, and much lower than the previous JC samples (see Figure 6.8 and appendix B).

**JC5**

The n-alkane distribution has a convex shape, with low abundance of light saturated hydrocarbons. As for the JC4 sample the n-alkanes are dominating compared to the Pr and Ph. The baseline is slightly above zero mVolts (see Figure 6.9 and appendix B).

**JC6**

The JC6 sample show n-alkane distribution is similar to JC1, JC2 and JC3. The sample shows a moderate amount of UCM and high Pr and Ph values compared to n-alkanes (see Figure 6.10 and appendix B).

**H1**

The n-alkane distribution prospect sample in Heilo has a bimodal distribution, with curve peaks at C10 and C23. The baseline is slightly higher than 0 mVolts (see Figure 6.11 and appendix B).

**S1**

From qualitatively interoperating the n-alkane distribution for sample S1, a trimodal shape can be identified. The curve tops can be found at C11, C19 and C23. The baseline is slightly elevated between retention time 10 and 40 min, after 40 min the baseline is elevated further due to a big biomarker hump (see Figure 6.12 and appendix B).

**S2**

The S1 sample has a narrow n-alkane distribution (between 17 min and 50 min) and the shape is convex (see Figure 6.13 and appendix B).

**A1**

The chromatogram for the A sample has a strong skewness to the lightest hydrocarbons identified by the GC-FID method. C25+ saturated hydrocarbons are not possible to identify (see Figure 6.14 and appendix B).

**NSO-1**

N-alkenes can be identified to C35 and the distribution is convex for the NSO-1 oil (see Figure 6.15 and appendix B).

### 6.2.3 Summary of the GC-FID parameters for the extracted core samples

The bitumen Pr/Ph ratios range is between 0.40-1.28. The lowest ratio belongs to the NB1 sample and the highest to the FP13 sample. The Pr/Ph ratio was possible to calculate for sample FP4, FP9, FP10, FP11, FP12, FP13 and NB1. The CPI, OEP(1) and OEP(2) have the ranges 0.91-1.28, 0.92-1.12 and 0.90-1.19 respectively. The “odd-even” predominance parameters were only possible to calculate for sample FP4, FP9 and FP10.

## 6.2.4 N-alkane distribution of the Oils and Condensates

**FP4**

Sample FP4 has N-alkanes which are present from about 30 min retention time to 55 min retention time. The distribution is uneven and some other peaks seem to interfer (see Figure 6.19 and appendix B).

**FP9**

The measureable peaks in the GC-FID chromatogram are from 30 min to 50 min for sample FP9. The sample has a high UCM, the prominent UCM hump is also due to the low intensity of the peaks (about 7 mVolts) (see Figure 6.24 and appendix B).

**FP10**

The chromatogram has a high UCM hump for sample FP10, and as the previous core samples from the Finnmark Platform, the saturated hydrocarbons and isoprenoids can be found between 30 min and 50 min in the chromatogram (see Figure 6.25 and appendix B).

**FP11**

The peaks shown in the chromatogram for sample FP11 are short, and a big UCM hump transitioning into the biomarker hump can be seen (see Figure 6.26 and appendix B).

**FP12**

The sample FP12 shows more or less the same signature as the FP11 with a UCM hump transitioning into the biomarker hump (see Figure 6.18 and appendix B). CPI and OED values were not calculated, due to problems in distinguishing the respective n-alkenes.

**FP13**

The sample has a high UCM hump similar to FP12 and FP11 (see Figure 6.27 and appendix B). Neither CPI nor OED was possible to calculate.

**NB1**

This sample has a huge UCM hump, and n-alkanes in the range of 30 min and 60 min (see Figure 6.30 and appendix B).

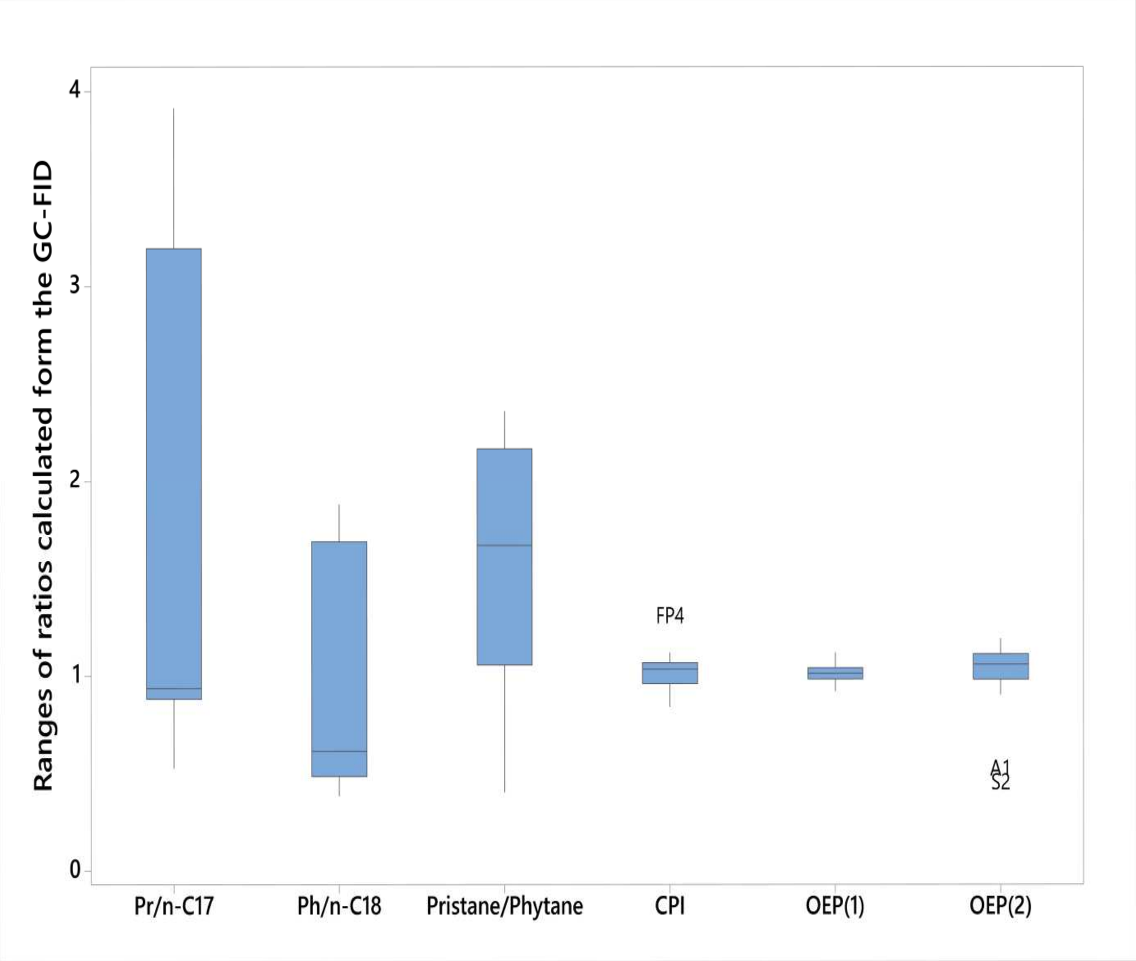

**Figure 6.2: The ranges of Pr/n-C17 ratio, Ph/n-C18 ratio, Pristane/Phytane ratio, CPI ratio, OEP(1) ratio and OEO(2) ratio for the sample set (Oils, condensates and Core samples). The interquartile box is the middle range of 50% of the data, the upper whisker is the 25% of the upper data and the lower whisker represents 25% of the lower data. The outliers are marked with their respective sample names. The two condensates seem to have significantly lower OEP(2) ratio than the rest of the sample set.**

**Table 6.2: The Table presents the Pr/n-C17 ratio, Ph/n-C18 ratio and the Pr/Ph ratio for the oils, condensates and core extracts. The CPI is calculated from the formula CPI = 2(C23+C25+C27+C29)/[C22+2(C24+C26+C28)+C30], and the OEP(1) and OEP(2) from the respective formulas OEP(1)= (C21+6C23+C25)/ (4C22+4C24) and OEP(2)= ($C_{25}$ + 6$C_{27}$ + $C_{29}$)/(4$C_{26}$ + 4$C_{28}$). ND = Not Defined. A summary of the Table values can be seen in Figure 6.3.**

| SAMPLE TYPE | Pr/n-C17 | Ph/n-C18 | Pristane/Phytane | CPI | OEP(1) | OEP(2) |
|---|---|---|---|---|---|---|
| **LH1** | 0.91 | 0.67 | 1.52 | 1.01 | 0.99 | 1.04 |
| **JC1** | 3.22 | 1.70 | 1.95 | 1.05 | 1.04 | 1.05 |
| **JC2** | 3.91 | 1.84 | 2.36 | 1.03 | 0.98 | 1.13 |
| **JC3** | 3.13 | 1.65 | 2.06 | 1.07 | 1.04 | 1.06 |
| **JC4** | 0.82 | 0.38 | 2.30 | 1.03 | 0.98 | 1.10 |
| **JC5** | 0.90 | 0.43 | 2.17 | 0.96 | 0.98 | 1.04 |
| **JC6** | 3.79 | 1.88 | 2.22 | 1.06 | 1.01 | 1.11 |
| **H1** | 0.91 | 0.59 | 1.67 | 1.06 | 1.01 | 1.07 |
| **S1** | 0.99 | 0.63 | 1.43 | 1.08 | 1.02 | 1.10 |
| **S2** | 0.88 | 0.56 | 2.09 | 0.84 | 1.02 | 0.43 |
| **A1** | 0.96 | 0.55 | 2.17 | 0.88 | 1.05 | 0.50 |
| **NSO-1** | 0.52 | 0.46 | 1.69 | 1.02 | 0.99 | 1.13 |
| **FP4** | ND | ND | 0.68 | 1.28 | 1.12 | 1.19 |
| **FP9** | ND | ND | 0.66 | 1.12 | 1.10 | 0.98 |
| **FP10** | ND | ND | 1.13 | 0.91 | 0.92 | 0.90 |
| **FP11** | ND | ND | 0.95 | ND | ND | ND |
| **FP12** | ND | ND | 1.06 | ND | ND | ND |
| **FP13** | ND | ND | 1.28 | ND | ND | ND |
| **NB1** | ND | ND | 0.40 | ND | ND | ND |

## 6.3 Results based on the GC-MS

The estimated parameters from the GC-MS analysis explained in section 4.5 are listed in Table 6.3, and Table 6.4. The ranges of the calculated parameters for the respective samples are listed as box-plots in Figure 6.4. The 27 respective parameters calculated are labeled in Table 5.9, and further explained in section 5.3.6. A full scale version of the GC-MS chromatograms can be found in Appendix C and a downscaled version in section 6.5. Parameter 3 and 4 are not included in the discussion. Most of the 27 parameters were not possible to calculate for the bitumen samples. However, parameter 10-15 and the parameters based on the methylphenanthrenes and methyldibenzothiophenes were possible estimate for some of the core samples (see Table 6.3 and Table 6.4).

### 6.3.1 Summary of the GC-MS results

All the ranges for Parameter 1-27 and the ETR are visualized in Figure 6.3 for the oils, condensates and core samples. The values are listed in Table 6.3 and Table 6.4, if the reader wishes to investigate specific values. For the majority of the parameters the range within the sample set is small (<0.5). The largest ranges of the calculated Parameters, are Parameter 7 (C23-C29 tricyclic terpanes/C30 aß-hopane), Parameter 21 (Methyl dibenzothiophene ratio), Paramameter 26 (3-methyl phenanthrene/4-methyl) and the ETR (see Figure 6.3). The biggest outliers are the LH1 sample for parameter 21 and the FP6 sample for parameter 26. The LH1 sample can be seen as an outlier in many of the parameters (see Figure 6.3). Moreover, the JC3, NB1 and the FP6 are the second most common outliers of the sample set. The LH1 and A1 are also outliers of the ETR value.

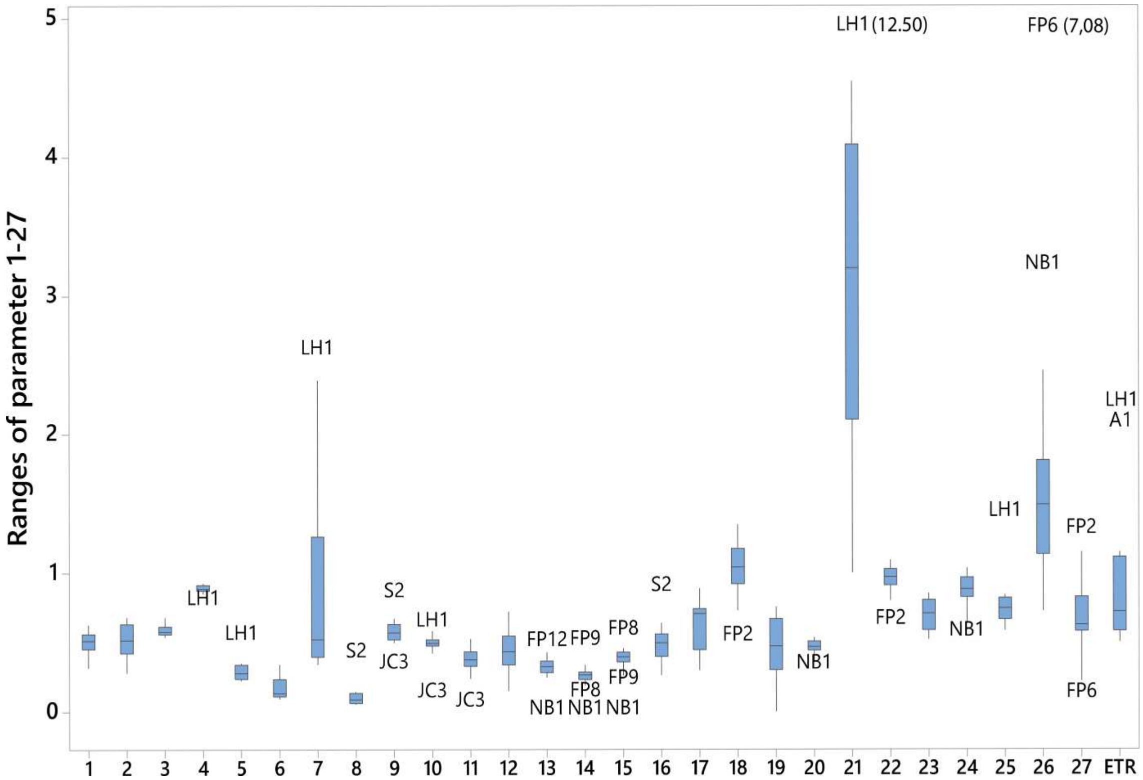

**Figure 6.3: The ranges of parameter 1-27 and the ETR. The interquartile box is the middle range of 50% of the data, the upper whisker is the 25% of the upper data and the lower whisker represent 25% of the lower data. The outliers are marked with labels of their respective sample names. The parameter 21 value for the LH1 sample are so high it's been extrapolated to fit into the plot same goes for the FP6 value for parameter 26.**

Table 6.3: The GC-MS parameters 1-14 for the sample set. The parameters are listed in Table 5.8 and described in section 5.2.6. A summary of the values can be seen in Figure 6.4. ND = No Data.

| SAMPLE TYPE | 1 | 2 | 3 | 4 | 5 | 6 | 7 | 8 | 9 | 10 | 11 | 12 | 13 | 14 |
|---|---|---|---|---|---|---|---|---|---|---|---|---|---|---|
| LH1 | 0.63 | 0.28 | 0.68 | 0.79 | 0.54 | 0.34 | 2.60 | 0.12 | 0.54 | 0.63 | 0.43 | 0.55 | 34.53 | 23.02 |
| JC1 | 0.43 | 0.64 | 0.54 | 0.91 | 0.25 | 0.11 | 0.34 | 0.05 | 0.64 | 0.49 | 0.44 | 0.34 | 24.70 | 33.91 |
| JC2 | 0.53 | 0.56 | 0.61 | 0.88 | 0.25 | 0.11 | 0.52 | 0.10 | 0.58 | 0.48 | 0.31 | 0.43 | 32.48 | 27.72 |
| JC3 | 0.44 | 0.55 | 0.57 | 0.87 | 0.26 | 0.13 | 0.57 | 0.11 | 0.33 | 0.12 | 0.06 | 0.15 | 36.63 | 23.81 |
| JC4 | 0.49 | 0.47 | 0.56 | 0.90 | 0.23 | 0.11 | 0.50 | 0.08 | 0.60 | 0.49 | 0.38 | 0.38 | 32.43 | 28.74 |
| JC5 | 0.50 | 0.43 | 0.59 | 0.88 | 0.30 | 0.15 | 0.75 | 0.14 | 0.50 | 0.52 | 0.36 | 0.46 | 36.28 | 22.56 |
| JC6 | 0.49 | 0.68 | 0.55 | 0.89 | 0.23 | 0.09 | 0.36 | 0.06 | 0.67 | 0.51 | 0.34 | 0.38 | 31.35 | 28.17 |
| H1 | 0.55 | 0.49 | 0.57 | 0.91 | 0.31 | 0.10 | 0.41 | 0.06 | 0.57 | 0.49 | 0.37 | 0.32 | 27.44 | 27.07 |
| S1 | 0.52 | 0.42 | 0.65 | 0.92 | 0.35 | 0.13 | 0.39 | 0.06 | 0.57 | 0.58 | 0.43 | 0.33 | 28.17 | 26.43 |
| S2 | 0.56 | 0.35 | 0.58 | 0.93 | 0.30 | 0.15 | 2.39 | 0.41 | 0.85 | 0.58 | 0.48 | 0.64 | 34.80 | 28.63 |
| A1 | 0.32 | 0.65 | 0.56 | 0.85 | 0.23 | 0.26 | 1.43 | 0.15 | 0.53 | 0.52 | 0.33 | 0.56 | 37.77 | 26.60 |
| NSO-1 | 0.57 | 0.61 | 0.62 | 0.88 | 0.35 | 0.34 | 0.52 | 0.07 | 0.52 | 0.51 | 0.38 | 0.49 | 28.25 | 28.62 |
| FP2 | ND | ND | ND | ND | ND | ND | ND | ND | ND | ND | ND | ND | ND | ND |
| FP3 | ND | ND | ND | ND | ND | ND | ND | ND | ND | ND | ND | ND | ND | ND |
| FP4 | ND | ND | ND | ND | ND | ND | ND | ND | ND | ND | ND | ND | 29.89 | 26.44 |
| FP5 | ND | ND | ND | ND | ND | ND | ND | ND | ND | ND | ND | ND | ND | ND |
| FP6 | ND | ND | ND | ND | ND | ND | ND | ND | ND | ND | ND | ND | ND | ND |
| FP8 | ND | ND | ND | ND | ND | ND | ND | ND | ND | 0.48 | 0.41 | 0.72 | 30.00 | 12.73 |
| FP9 | ND | ND | ND | ND | ND | ND | ND | ND | ND | ND | ND | ND | 28.26 | 50.00 |
| FP10 | ND | ND | ND | ND | ND | ND | ND | ND | ND | 0.43 | 0.24 | 0.37 | 40.84 | 23.56 |
| FP11 | ND | ND | ND | ND | ND | ND | ND | ND | ND | ND | ND | ND | 32.69 | 30.77 |
| FP12 | ND | ND | ND | ND | ND | ND | ND | ND | ND | ND | ND | ND | 49.23 | 24.62 |
| FP13 | ND | ND | ND | ND | ND | ND | ND | ND | ND | 0.42 | 0.53 | 0.43 | 42.98 | 19.01 |
| NB1 | ND | ND | ND | ND | ND | ND | ND | ND | ND | ND | ND | ND | ND | ND |

Table 6.4: The GC-MS parameters 15-27 and ETR for the sample set. The parameters are listed in Table 5.8 and described in section 5.2.6. A summary of the values can bee seen in Figure6.4. ND = No Data.

| SAMPLE TYPE | 15 | 16 | 17 | 18 | 19 | 20 | 21 | 22 | 23 | 24 | 25 | 26 | 27 | ETR |
|---|---|---|---|---|---|---|---|---|---|---|---|---|---|---|
| LH1 | 42.45 | 0.64 | 0.70 | 0.95 | 0.70 | 0.46 | 12.50 | 0.93 | 0.82 | 0.86 | 1.42 | 1.48 | 0.51 | 2,16 |
| JC1 | 41.39 | 0.26 | 0.74 | 1.13 | 0.75 | 0.48 | 4.27 | 1.01 | 0.85 | 0.90 | 0.82 | 1.46 | 0.64 | 0,57 |
| JC2 | 39.80 | 0.43 | 0.63 | 0.91 | 0.70 | 0.46 | 3.92 | 0.90 | 0.82 | 0.87 | 0.80 | 1.64 | 0.61 | 0,50 |
| JC3 | 39.56 | 0.45 | 0.30 | 0.97 | 0.69 | 0.46 | 3.57 | 0.94 | 0.81 | 0.86 | 0.77 | 1.64 | 0.58 | 0,71 |
| JC4 | 38.83 | 0.52 | 0.37 | 1.21 | 0,66 | 0.48 | 4.55 | 1.04 | 0.80 | 0.91 | 0.84 | 1.59 | 0.58 | 0,61 |
| JC5 | 41.17 | 0.55 | 0.66 | 1.02 | 0.63 | 0.45 | 4.50 | 0.96 | 0.78 | 0.85 | 0.84 | 1.49 | 0.60 | 0,83 |
| JC6 | 40.48 | 0.34 | 0.73 | 1.07 | 0.70 | 0.48 | 4.09 | 0.98 | 0.82 | 0.91 | 0.81 | 1.68 | 0.61 | 0,73 |
| H1 | 45.49 | 0.47 | 0.80 | 1.00 | 0.62 | 0.44 | 3.92 | 0.95 | 0.77 | 0.82 | 0.80 | 0.82 | 0.92 | 0,69 |
| S1 | 45.39 | 0.55 | 0.71 | 0.98 | 0.58 | 0.45 | 4.42 | 0.94 | 0.75 | 0.83 | 0.83 | 0.72 | 1.06 | 0,56 |
| S2 | 36.56 | 0.89 | 0.89 | 1.07 | 0.52 | 0.47 | 4.50 | 0.98 | 0.71 | 0.90 | 0.84 | 0.73 | 1.15 | 1,00 |
| A1 | 35.64 | 0.56 | 0.39 | 1.33 | 0.68 | 0.52 | 3.83 | 1.09 | 0.81 | 1.00 | 0.79 | 1.33 | 0.65 | 2,10 |
| NSO-1 | 43.12 | 0.39 | 0.71 | 0.79 | 0.57 | 0.42 | 2.62 | 0.84 | 0.74 | 0.77 | 0.70 | 1.39 | 0.64 | 1,15 |
| FP2 | ND | ND | ND | 0.53 | 0.42 | 0.36 | 1.00 | 0.65 | 0.65 | 0.63 | 0.58 | 0.90 | 1.30 | ND |
| FP3 | ND | ND | ND | 0.78 | 0.29 | 0.37 | 1.42 | 0.83 | 0.58 | 0.66 | 0.61 | 1.10 | 0.74 | ND |
| FP4 | 43.68 | ND | ND | 1.19 | 0.42 | 0.51 | 1.94 | 1.03 | 0.65 | 0.98 | 0.65 | 2.46 | 0.49 | ND |
| FP5 | ND | ND | ND | 1.18 | 0.24 | 0.53 | 2.63 | 1.03 | 0.55 | 1.01 | 0.70 | 2.17 | 0.59 | ND |
| FP6 | ND | ND | ND | 1.00 | 0.51 | 0.38 | 2.56 | 0.95 | 0.70 | 0.69 | 0.70 | 7.08 | 0.11 | ND |
| FP8 | 57.27 | ND | ND | 1.14 | 0.20 | 0.49 | 3.20 | 1.01 | 0.52 | 0.94 | 0.74 | 1.13 | 0.74 | ND |
| FP9 | 21.74 | ND | ND | 0.79 | 0.37 | 0.46 | 3.25 | 0.83 | 0.62 | 0.87 | 0.75 | 1.28 | 0.86 | ND |
| FP10 | 35.60 | ND | ND | 1.35 | 0.30 | 0.54 | 1.41 | 1.09 | 0.58 | 1.04 | 0.61 | 1.55 | 0.87 | ND |
| FP11 | 36.54 | ND | ND | 1.16 | 0.44 | 0.51 | 2.11 | 1.02 | 0.66 | 0.98 | 0.66 | 2.07 | 0.59 | ND |
| FP12 | 26.15 | ND | ND | 1.13 | 0.30 | 0.49 | 1.37 | 1.01 | 0.58 | 0.93 | 0.61 | 1.81 | 0.74 | ND |
| FP13 | 38.02 | ND | ND | 1.33 | 0.30 | 0.54 | 2.50 | 1.09 | 0.58 | 1.03 | 0.69 | 2.18 | 0.55 | ND |
| NB1 | ND | ND | ND | 0.73 | 0.33 | 0.32 | 2.16 | 0.80 | 0.60 | 0.56 | 0.67 | 3.20 | 0.22 | ND |

## 6.5 Downscaled TLC-FID, GC-FID and GC-MS chromatograms

The samples TLC-FID, GC-FID and GC-MS are presented in this sub-chapter. The m/z ratios from the GC-MS are 191, 217, 218, 231, 253 and 178-192-198 (on the same slide). A larger scale of the chromatograms are presented in Appendix A (TLC-FID), Appendix B (GC-FID) and Appendix C (GC-MS).

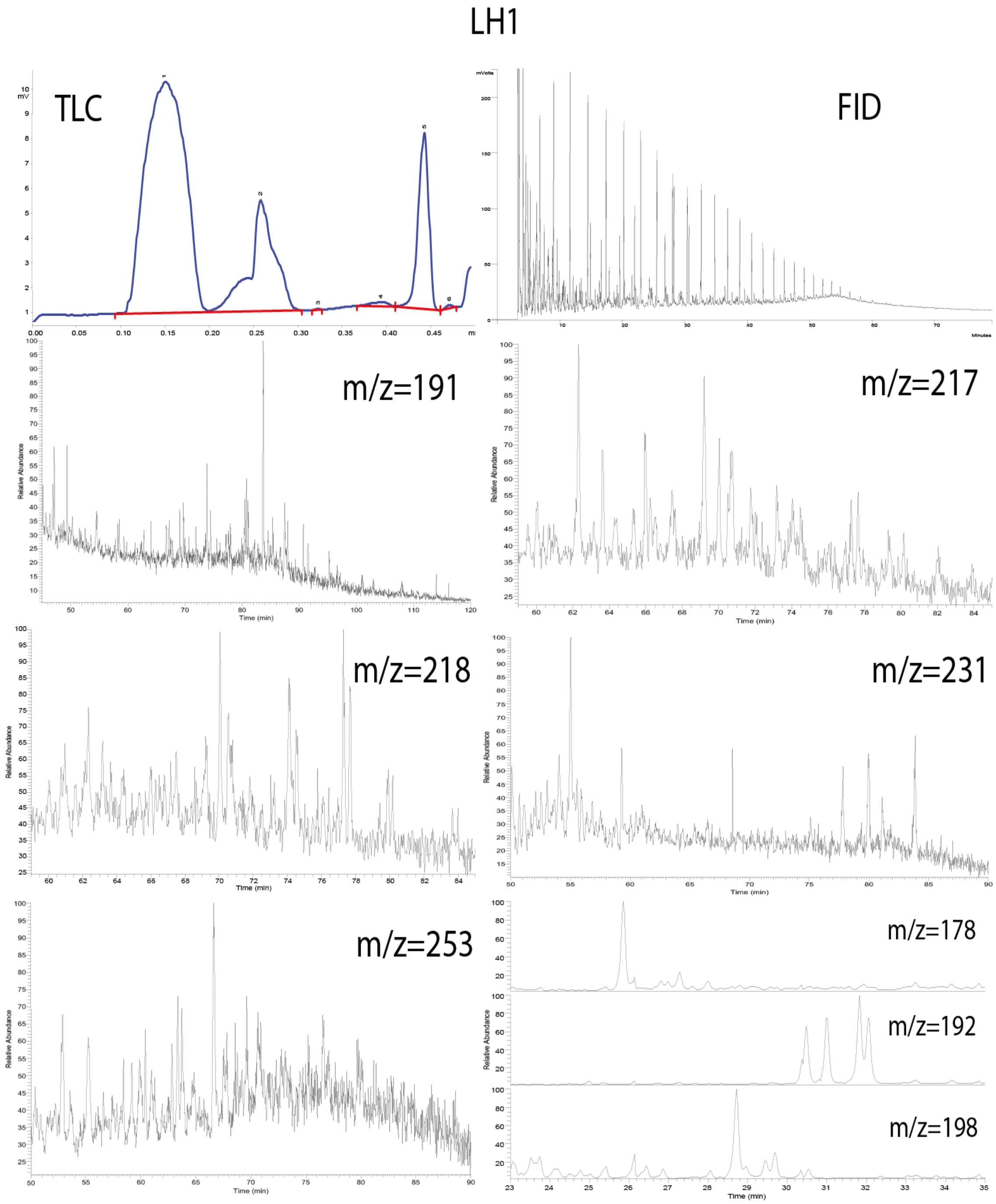

**Figure 6.4: Downscaled TLC-FID, GC-FID and GC-MS chromatograms for LH1.**

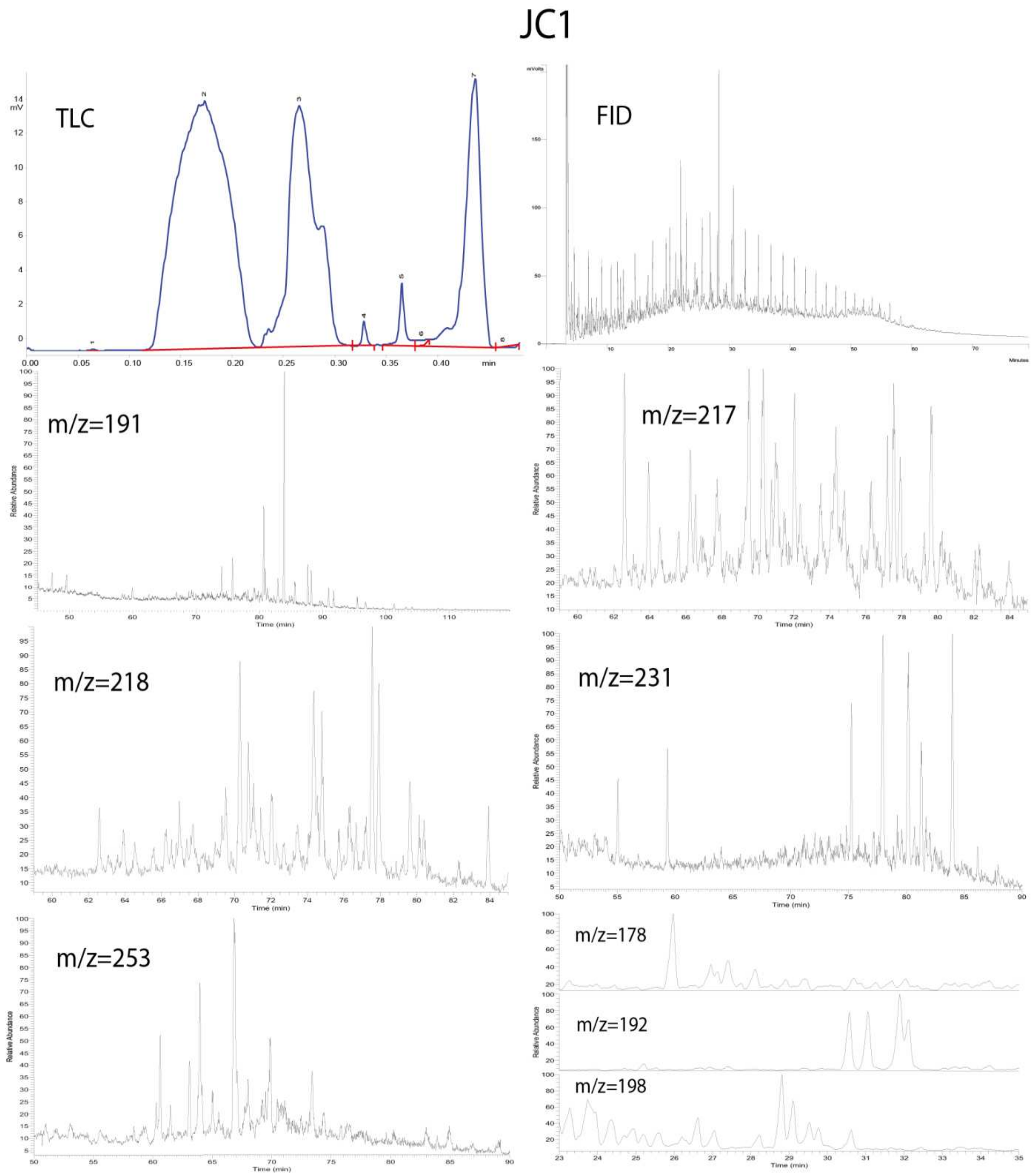

**Figure 6.5: Downscaled TLC-FID, GC-FID and GC-MS chromatograms for JC1.**

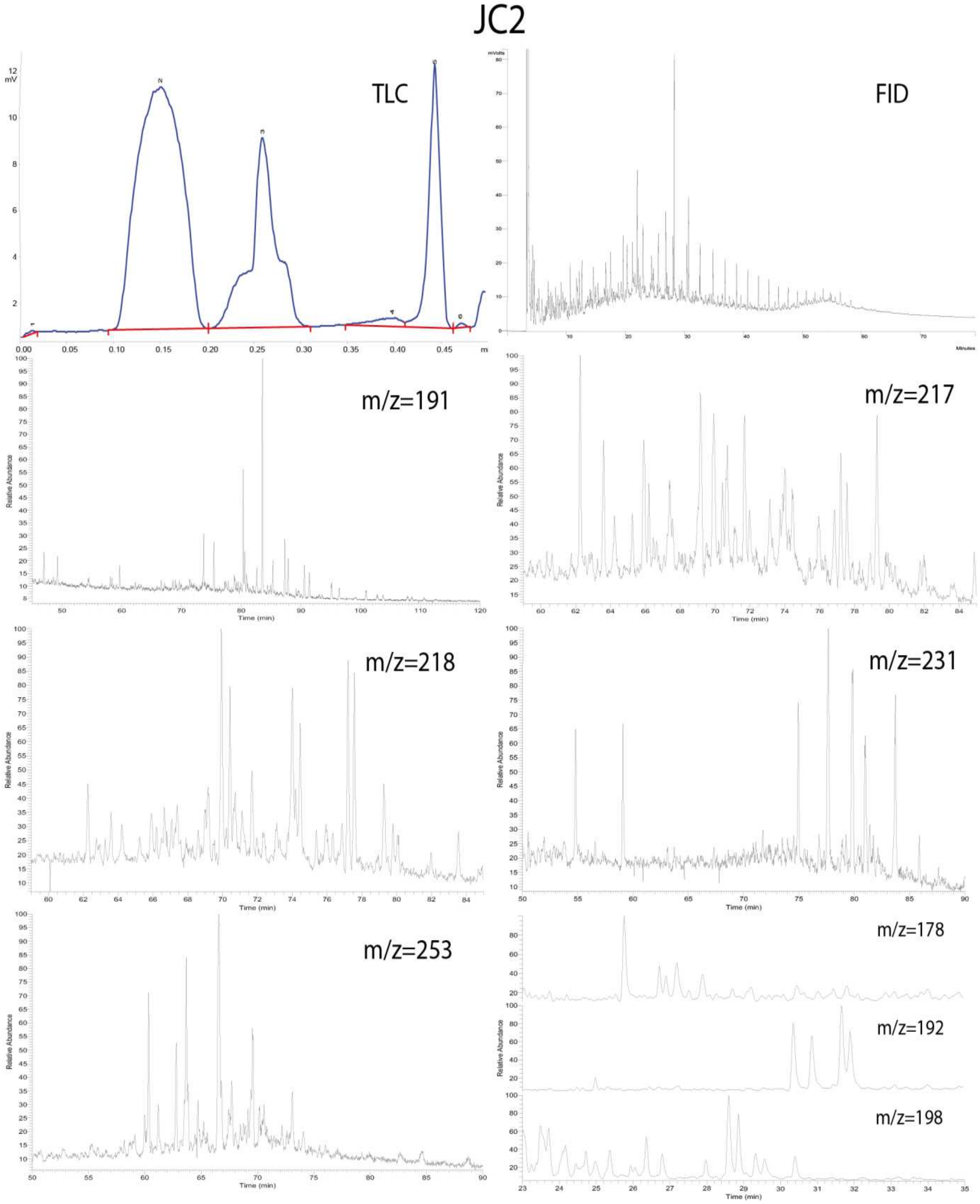

**Figure 6.6: Downscaled TLC-FID, GC-FID and GC-MS chromatograms for JC2.**

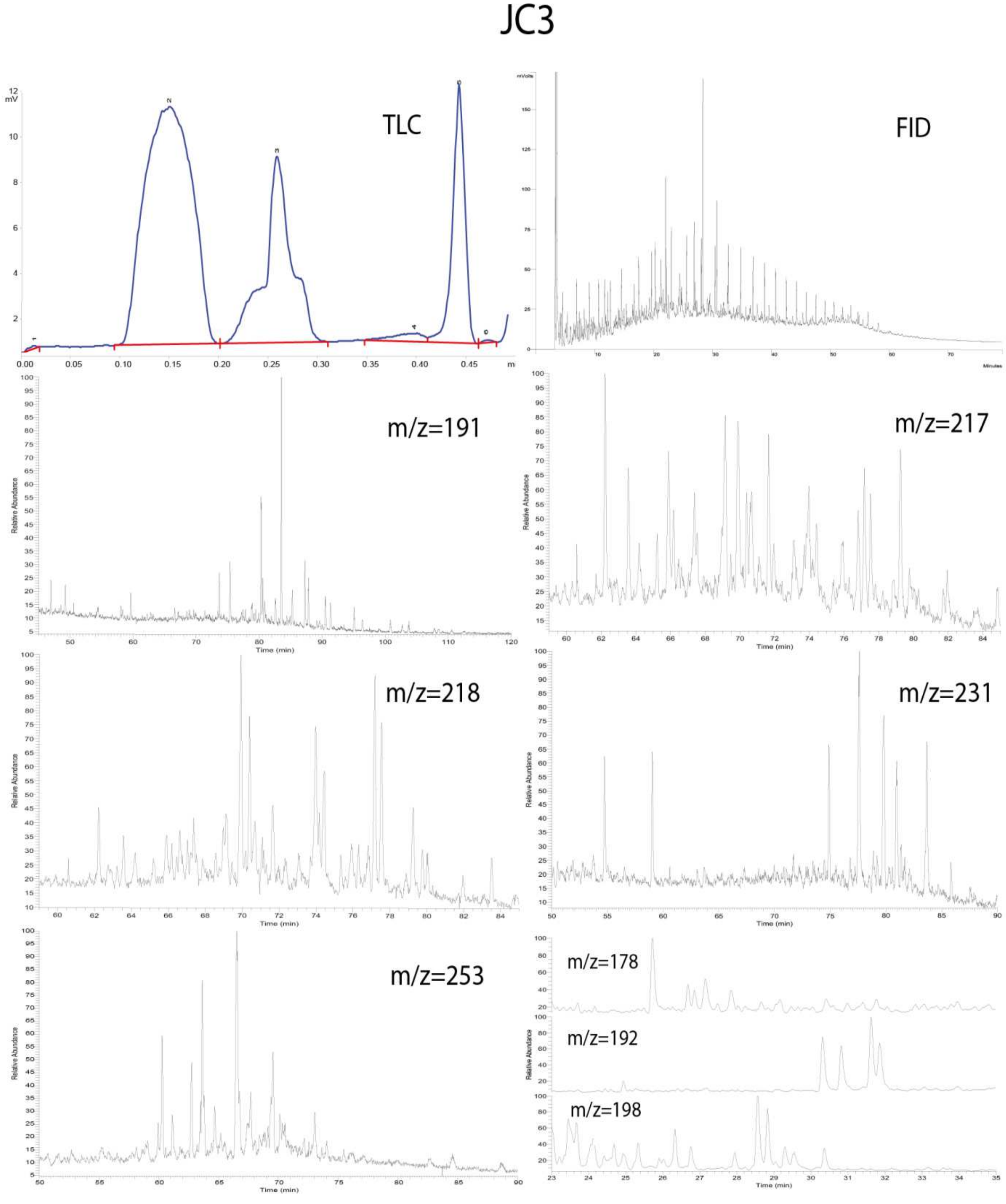

**Figure 6.7: Downscaled TLC-FID, GC-FID and GC-MS chromatograms for JC3.**

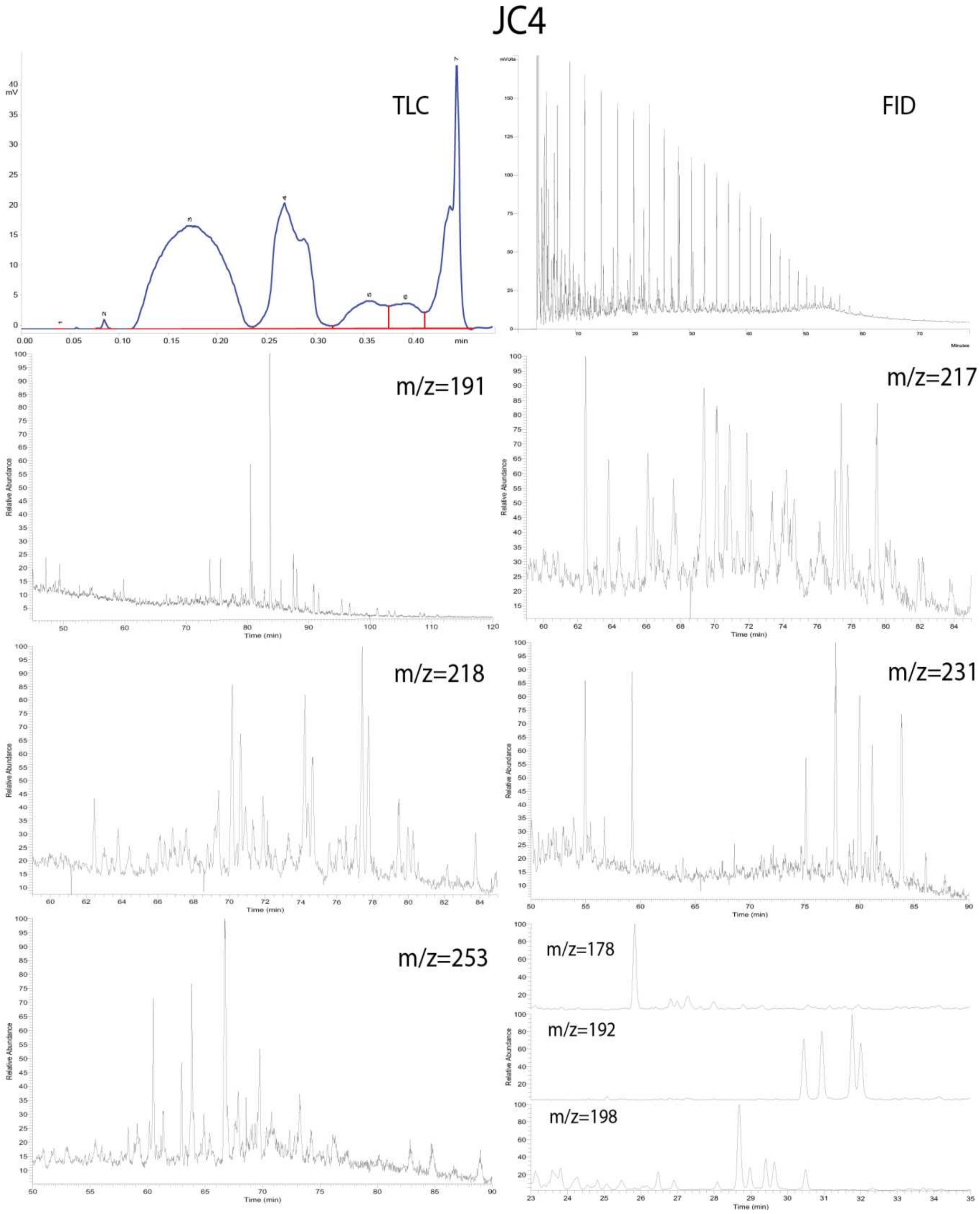

**Figure 6.8: Downscaled TLC-FID, GC-FID and GC-MS chromatograms for JC4.**

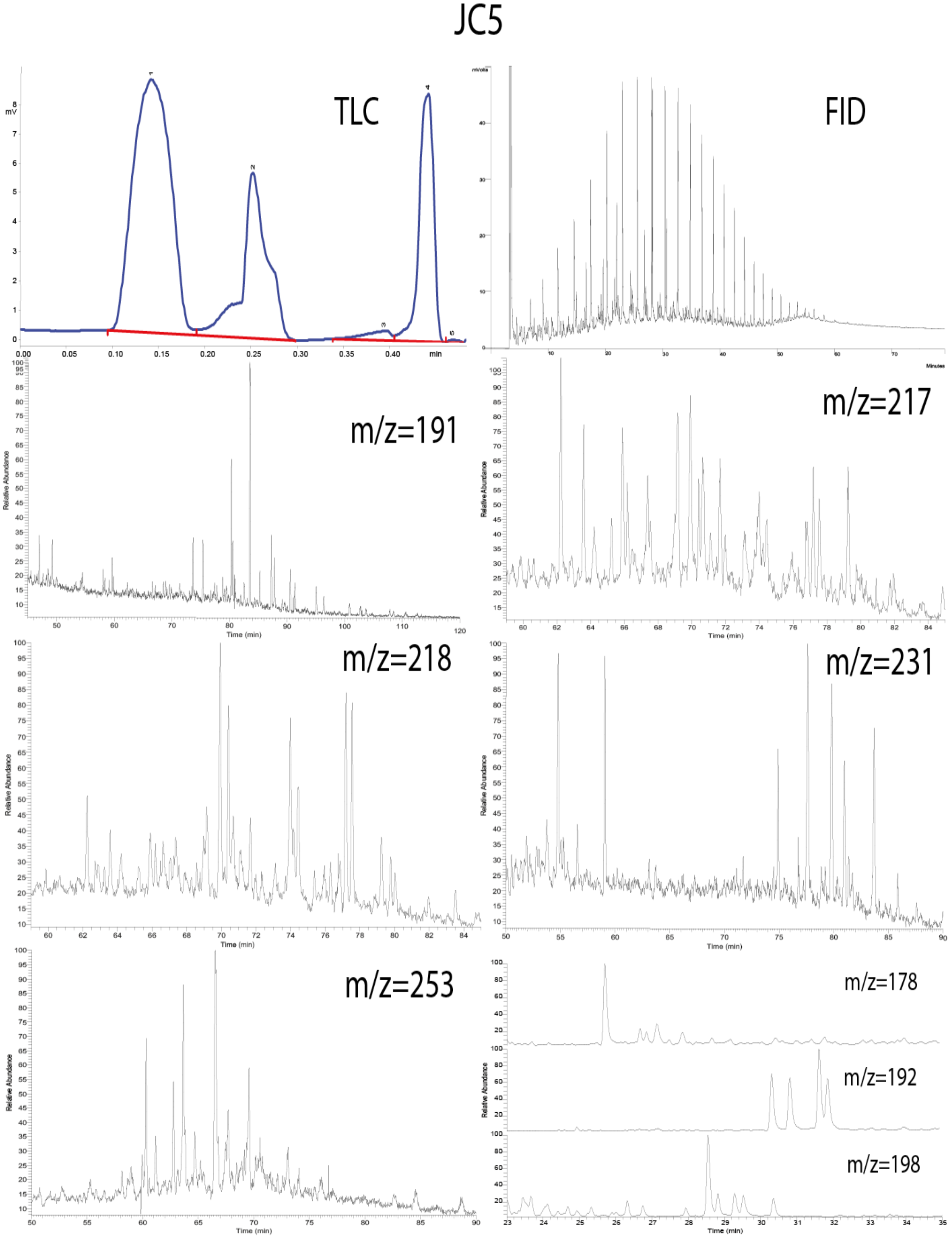

**Figure 6.9: Downscaled TLC-FID, GC-FID and GC-MS chromatograms for JC5.**

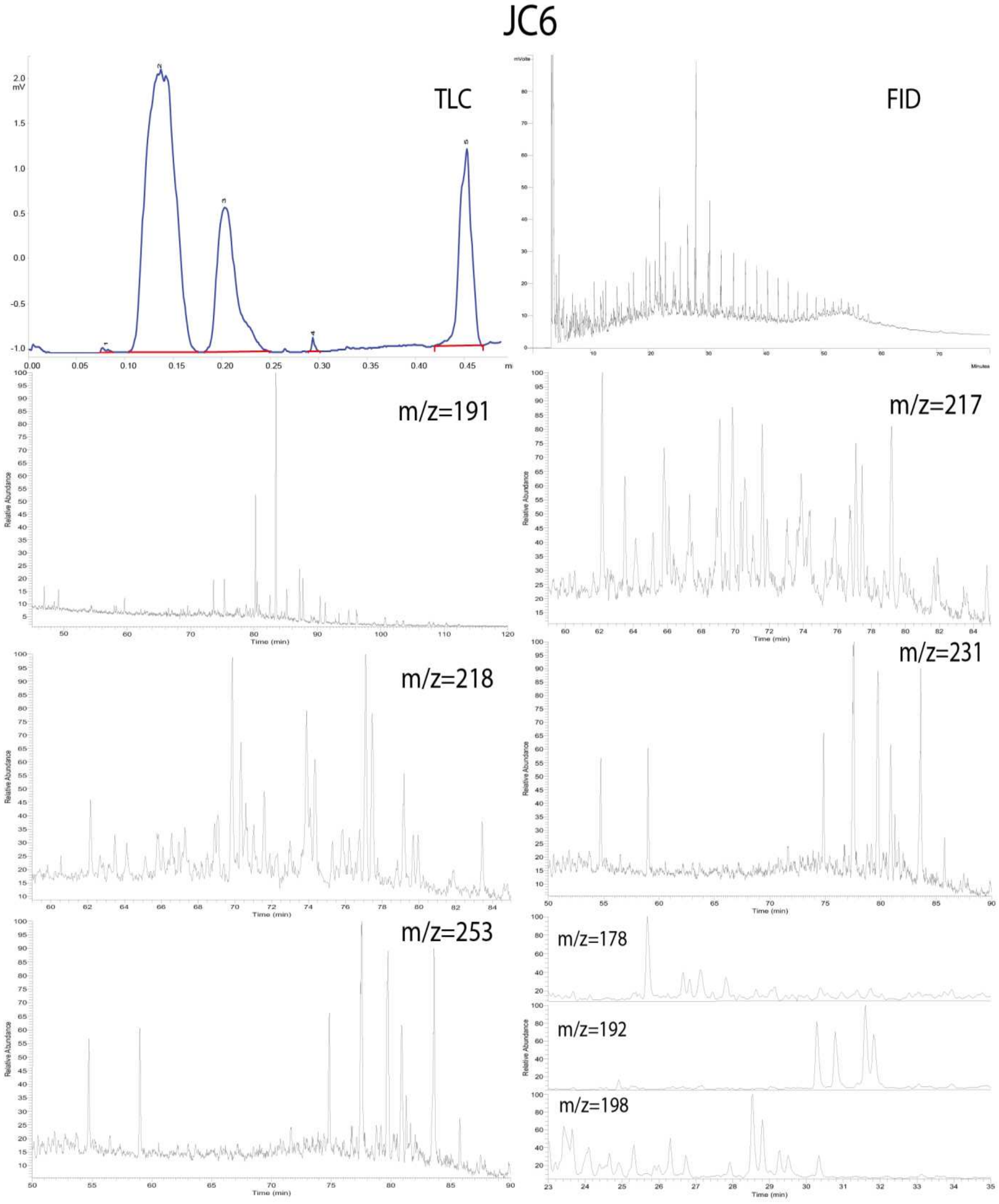

**Figure 6.10: Downscaled TLC-FID, GC-FID and GC-MS chromatograms for JC6.**

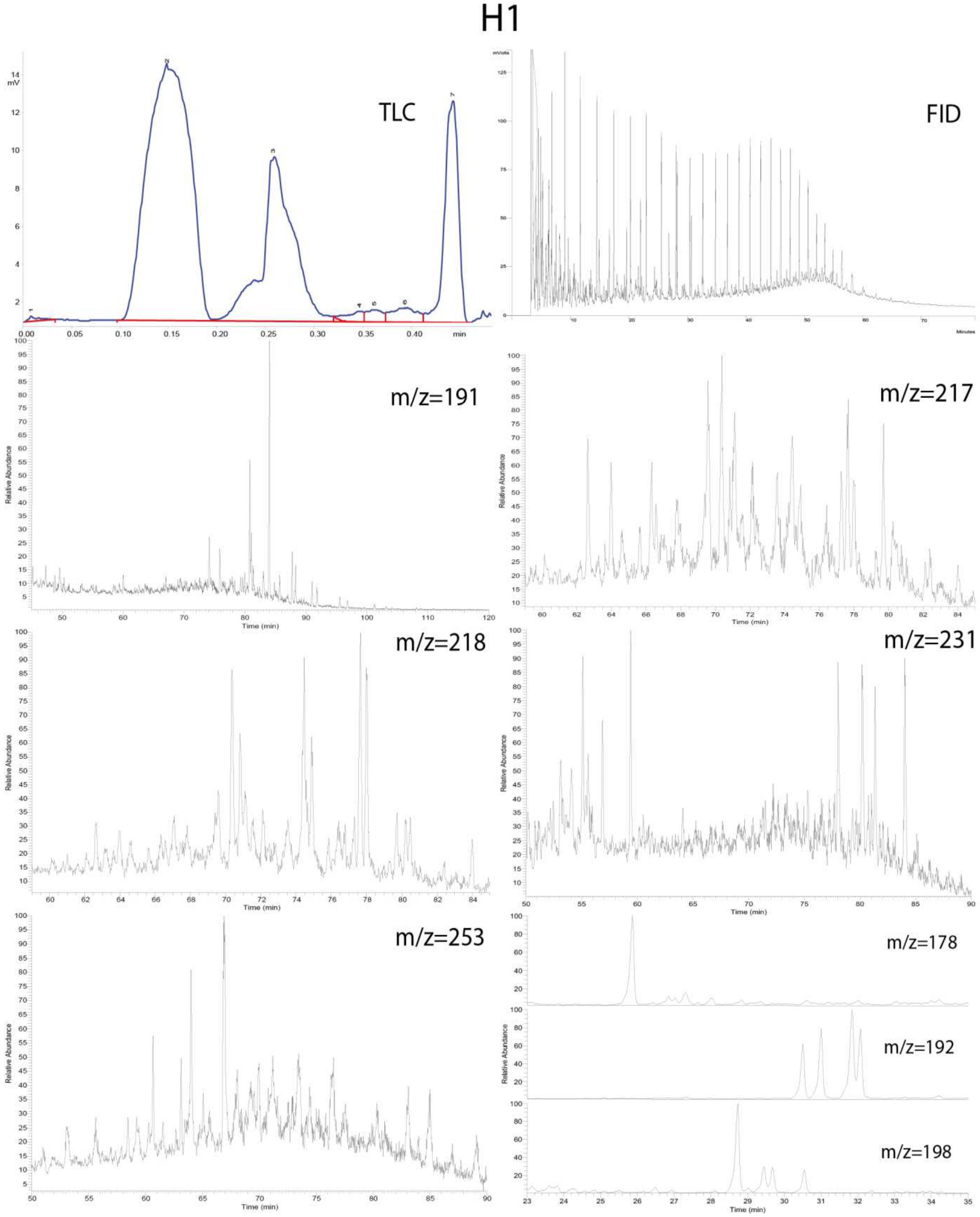

**Figure 6.11: Downscaled TLC-FID, GC-FID and GC-MS chromatograms for H1.**

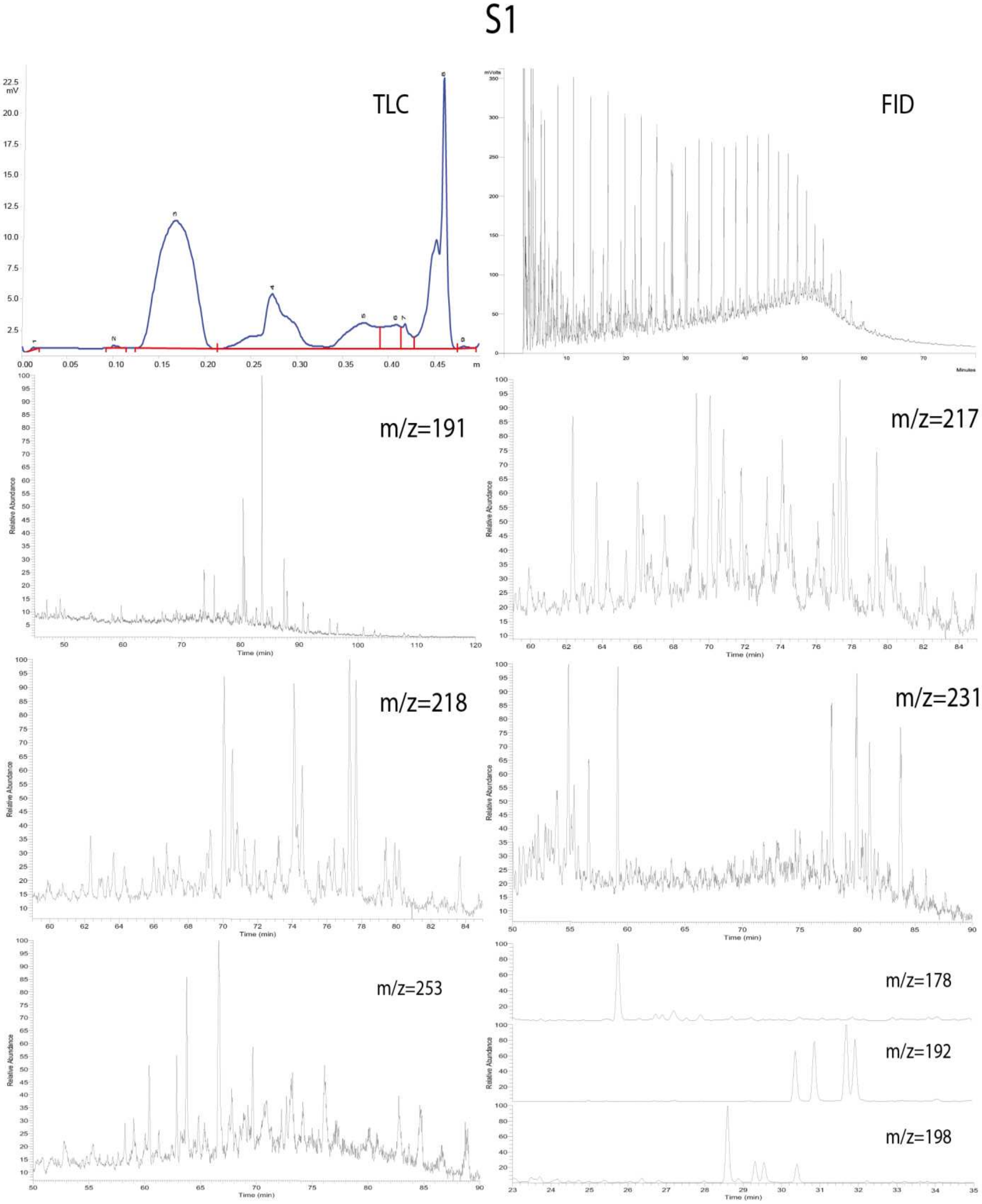

**Figure 6.12: Downscaled TLC-FID, GC-FID and GC-MS chromatograms for S1.**

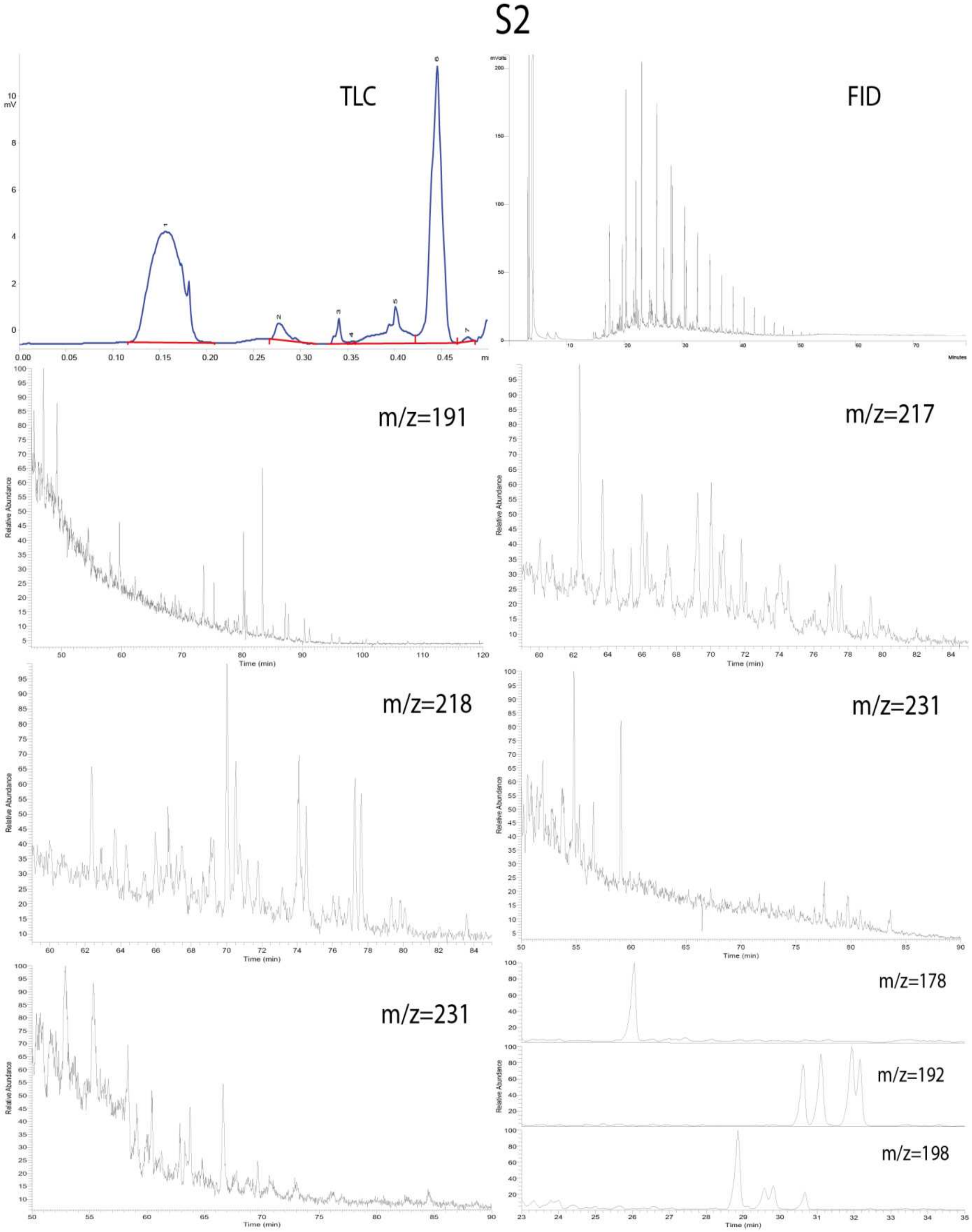

**Figure 6.13: Downscaled TLC-FID, GC-FID and GC-MS chromatograms for S2.**

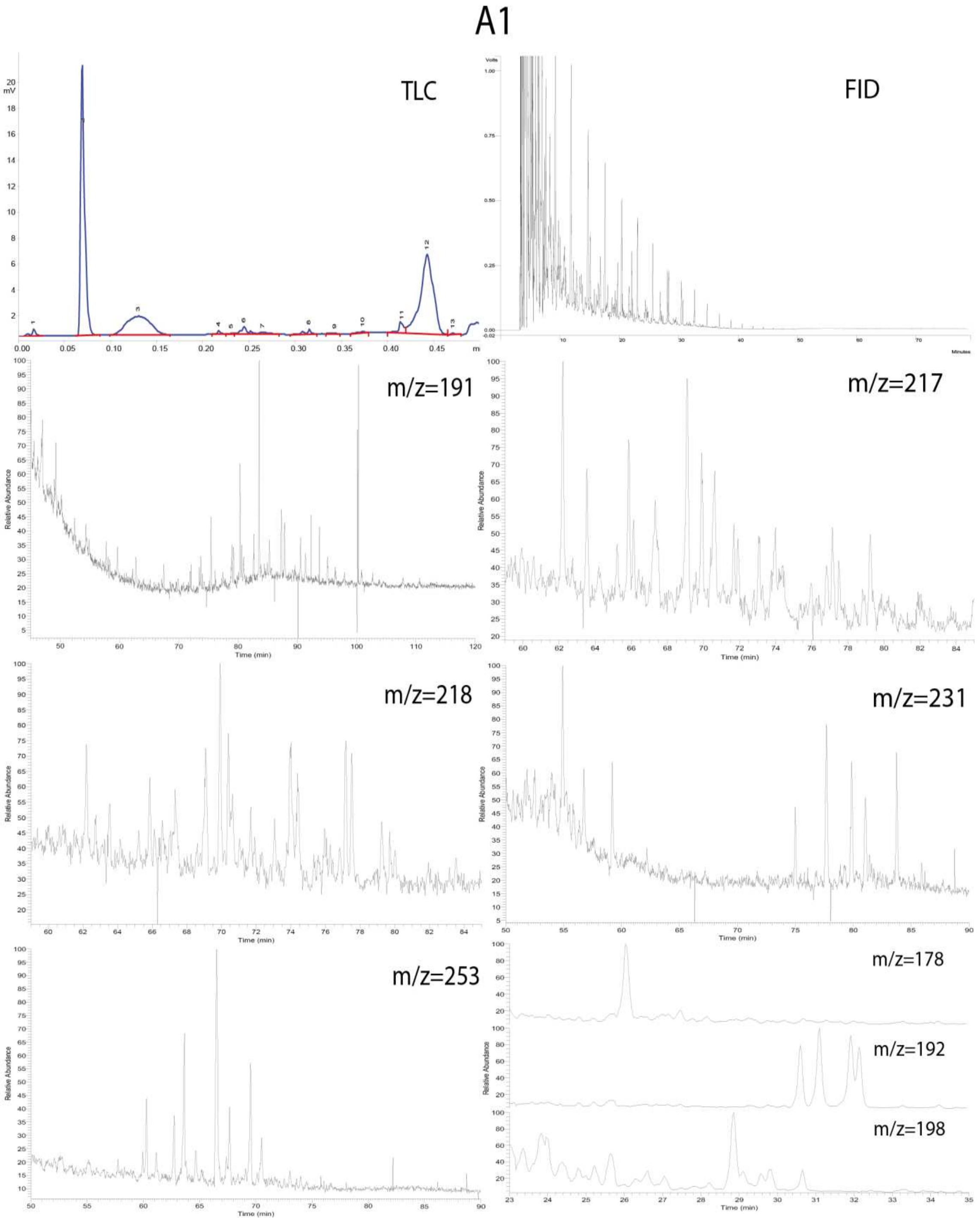

**Figure 6.14: Downscaled TLC-FID, GC-FID and GC-MS chromatograms for A1.**

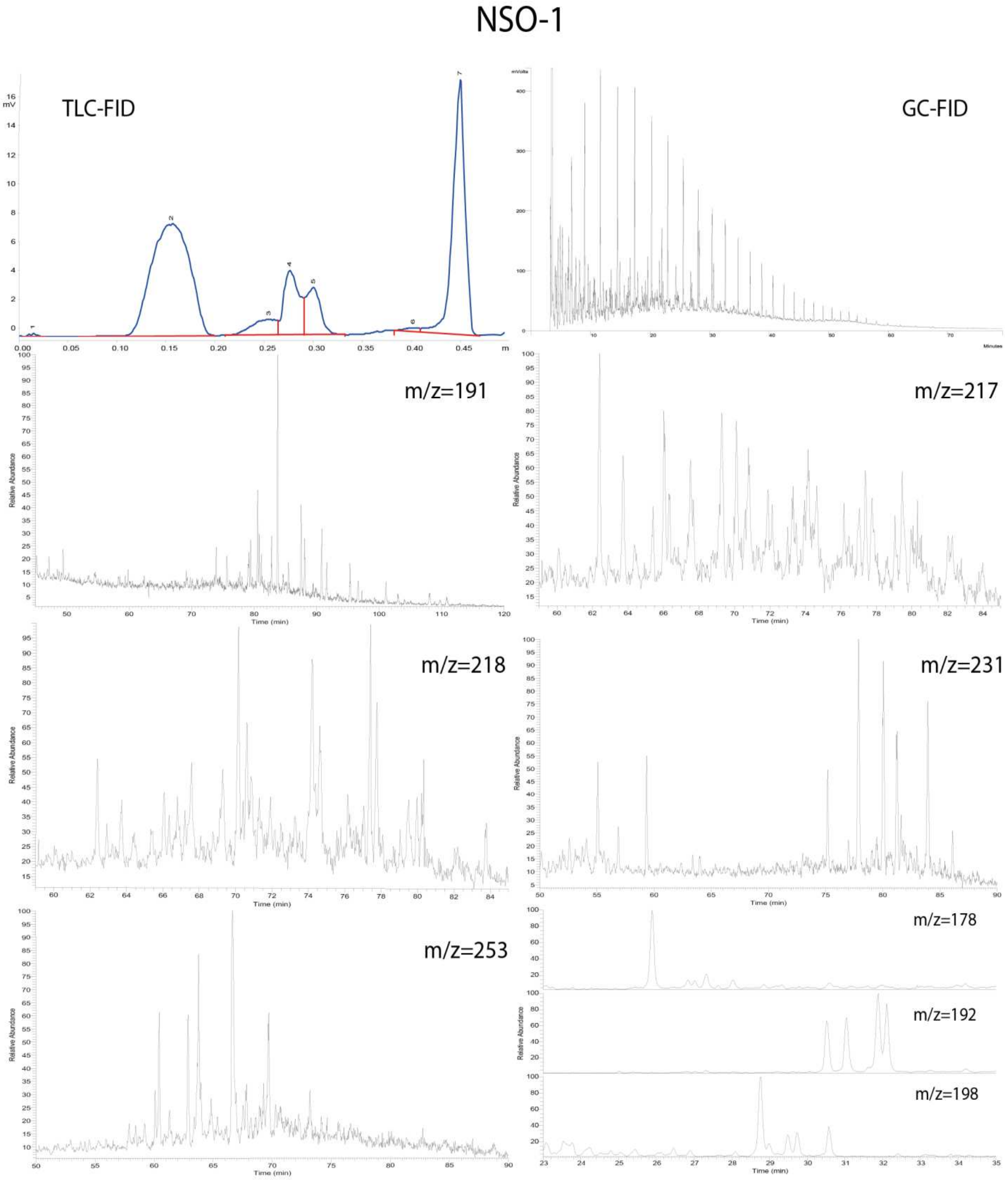

**Figure 6.15: Downscaled TLC-FID, GC-FID and GC-MS chromatograms for NSO-1.**

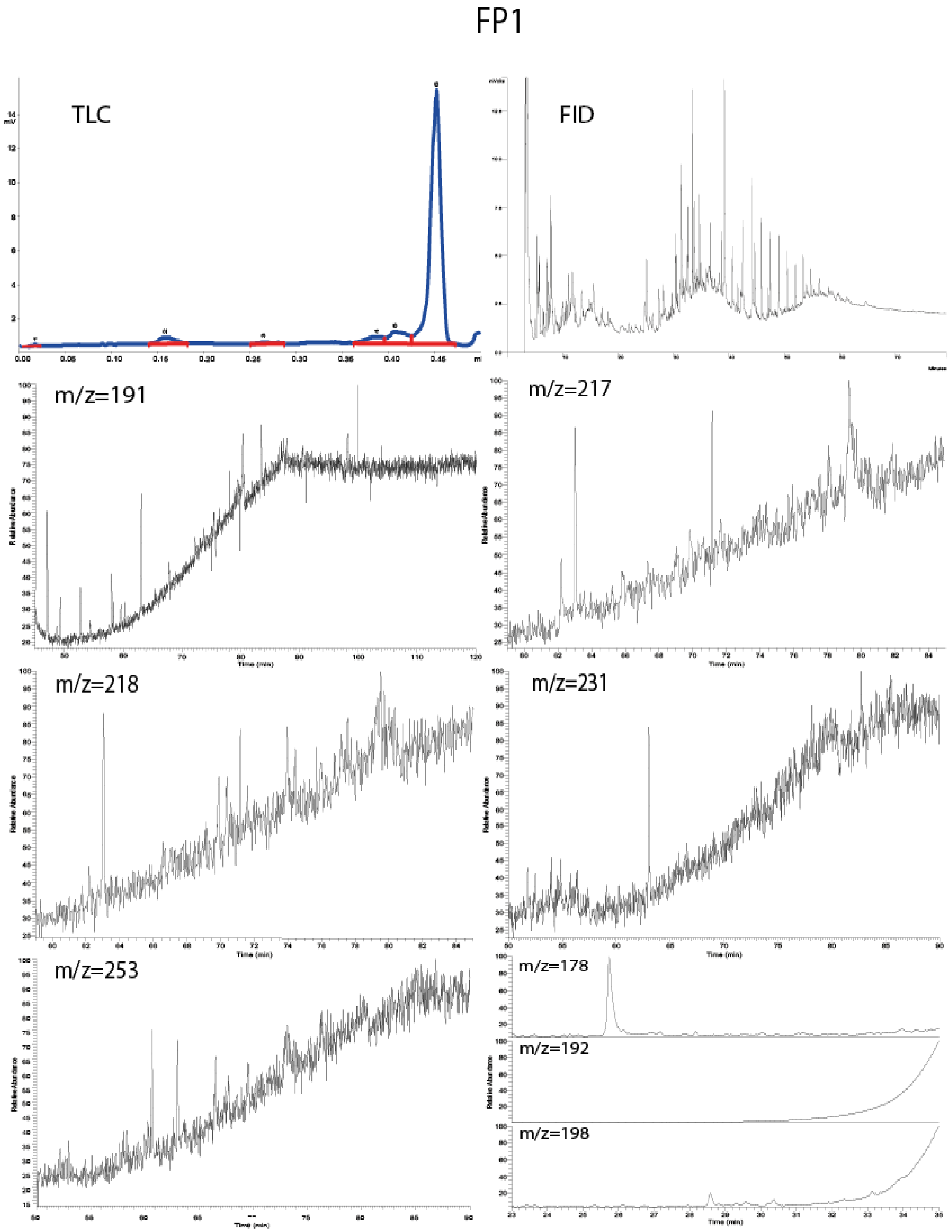

**Figure 6.16: Downscaled TLC-FID, GC-FID and GC-MS chromatograms for FP1.**

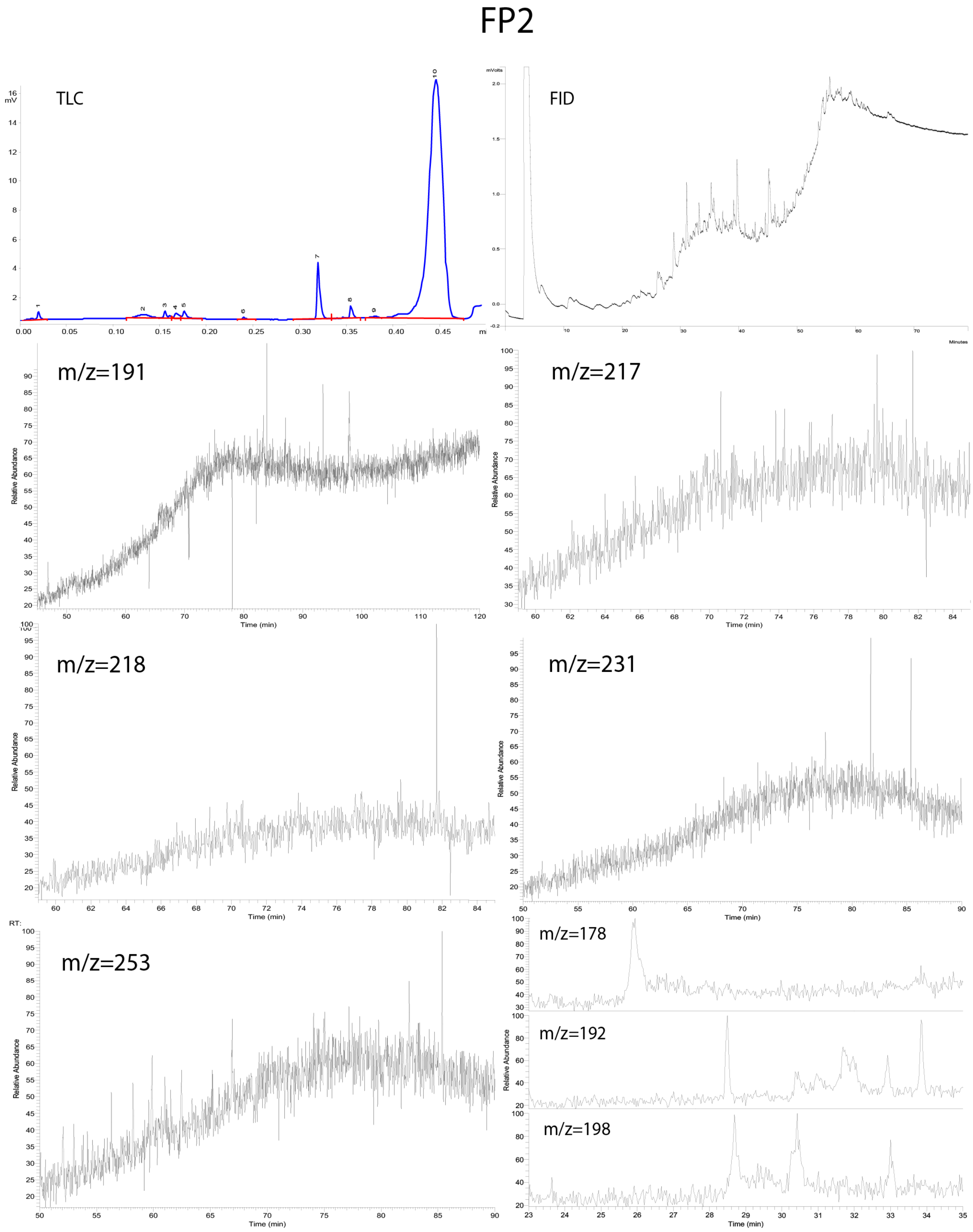

**Figure 6.17: Downscaled TLC-FID, GC-FID and GC-MS chromatograms for FP2.**

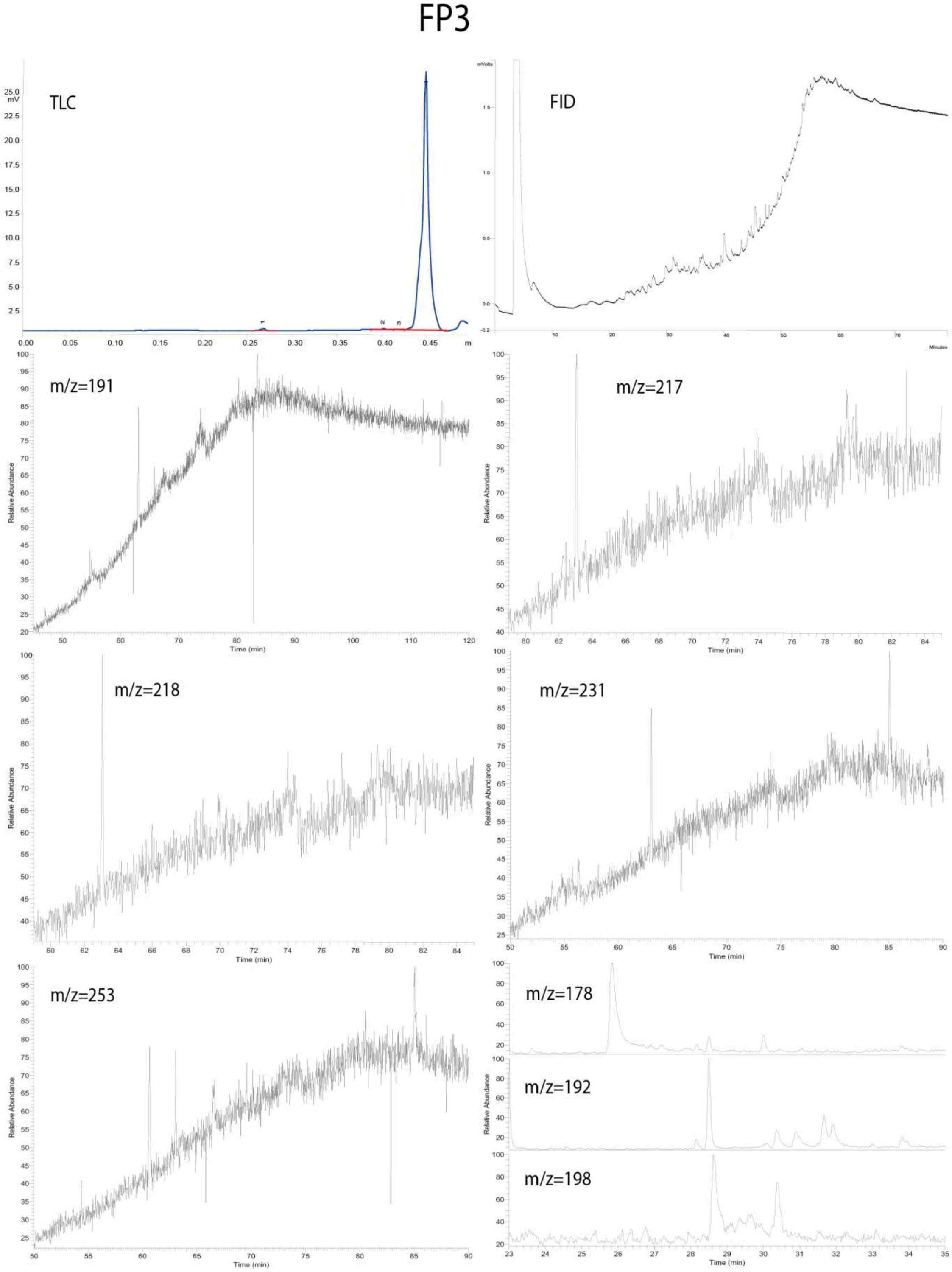

**Figure 6.18: Downscaled TLC-FID, GC-FID and GC-MS chromatograms for FP3.**

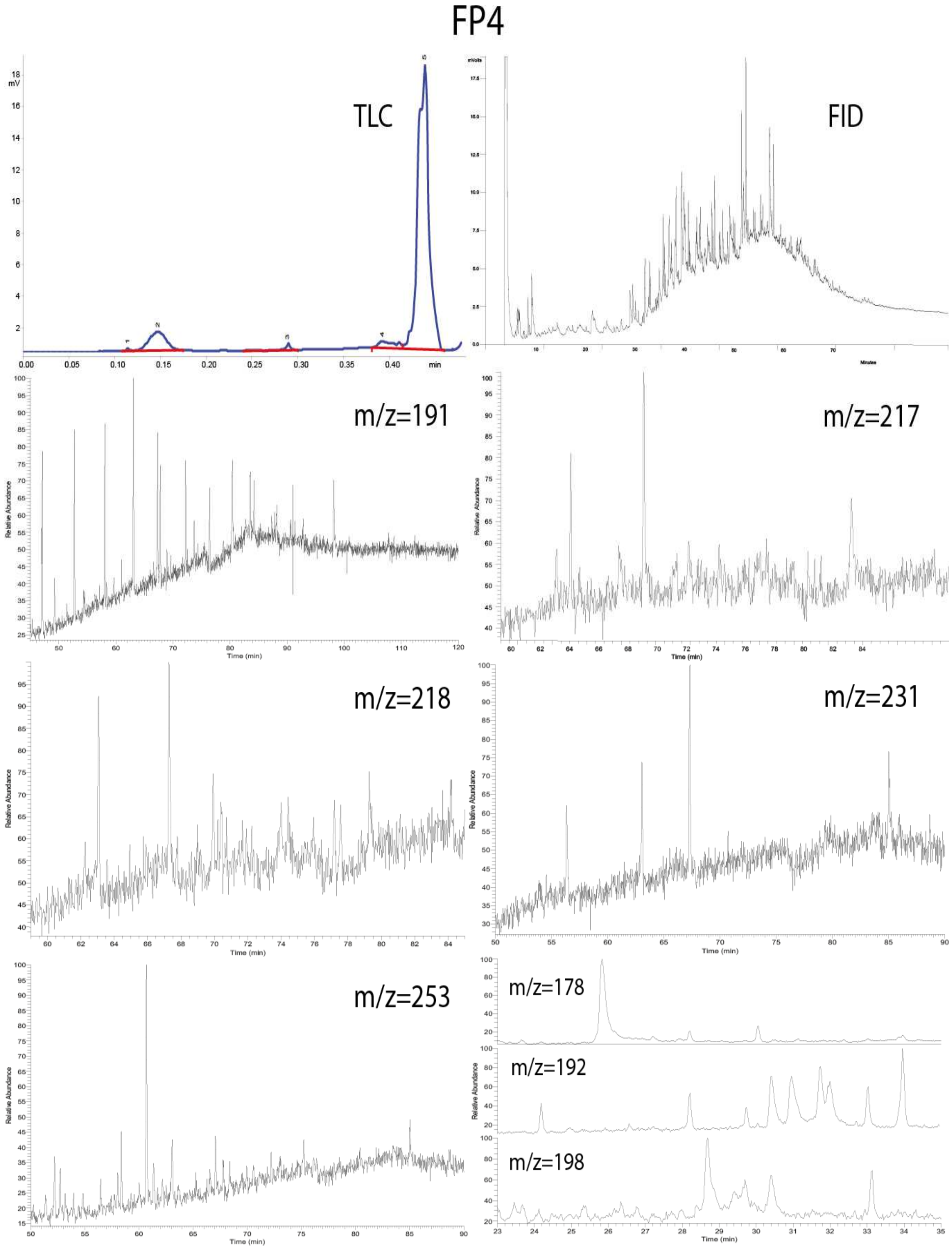

**Figure 6.19: Downscaled TLC-FID, GC-FID and GC-MS chromatograms for FP4.**

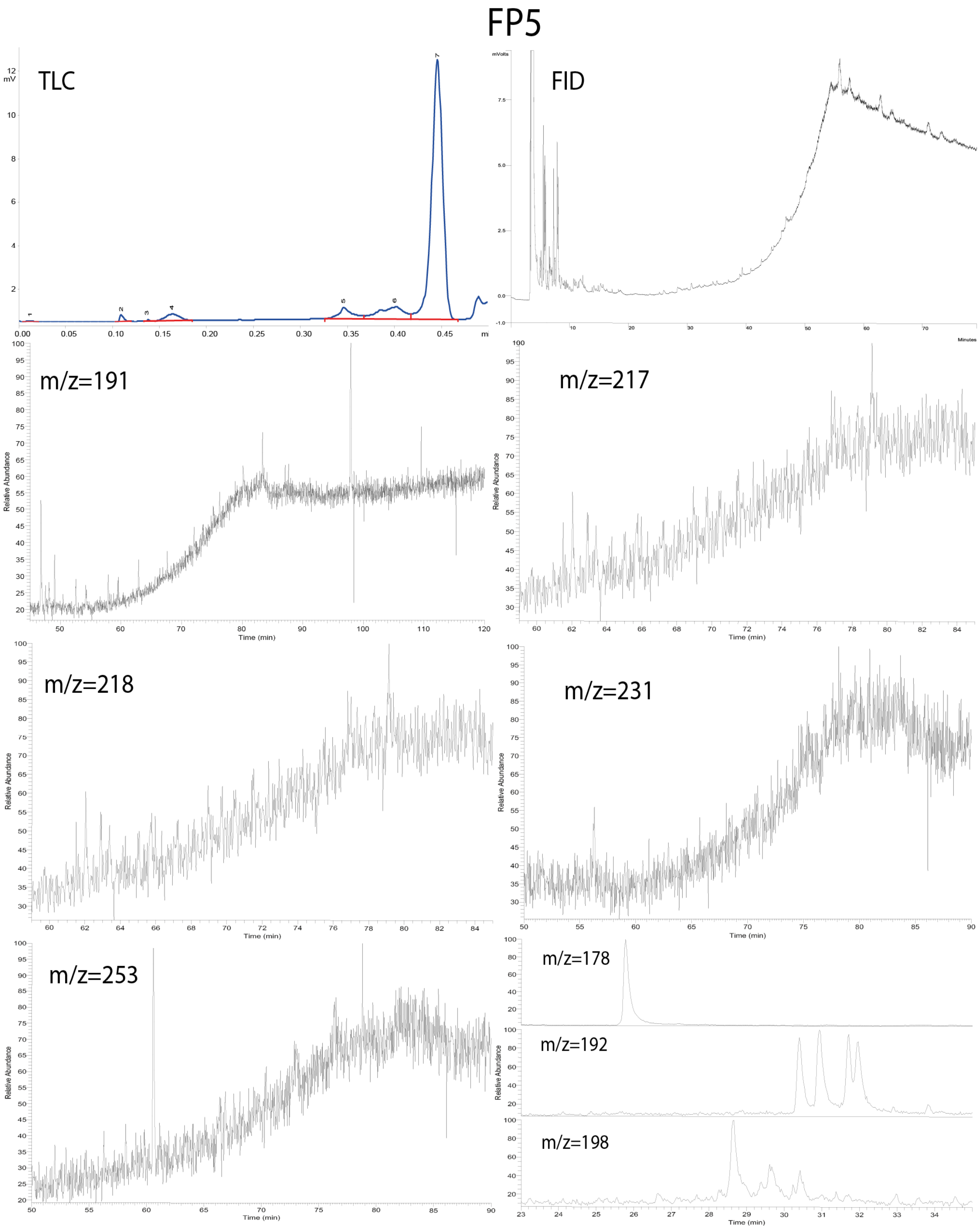

**Figure 6.20: Downscaled TLC-FID, GC-FID and GC-MS chromatograms for FP5.**

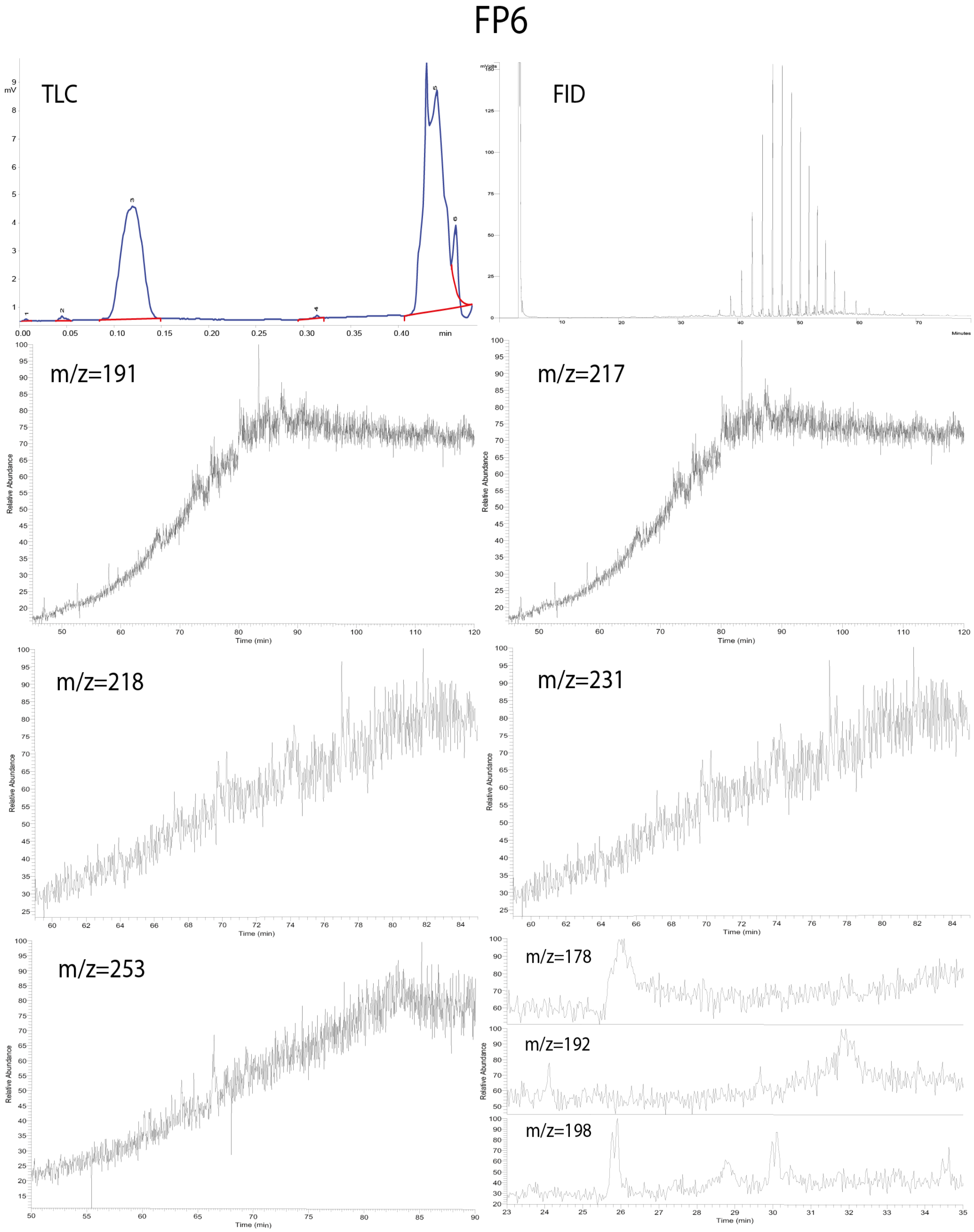

**Figure 6.21: Downscaled TLC-FID, GC-FID and GC-MS chromatograms for FP6.**

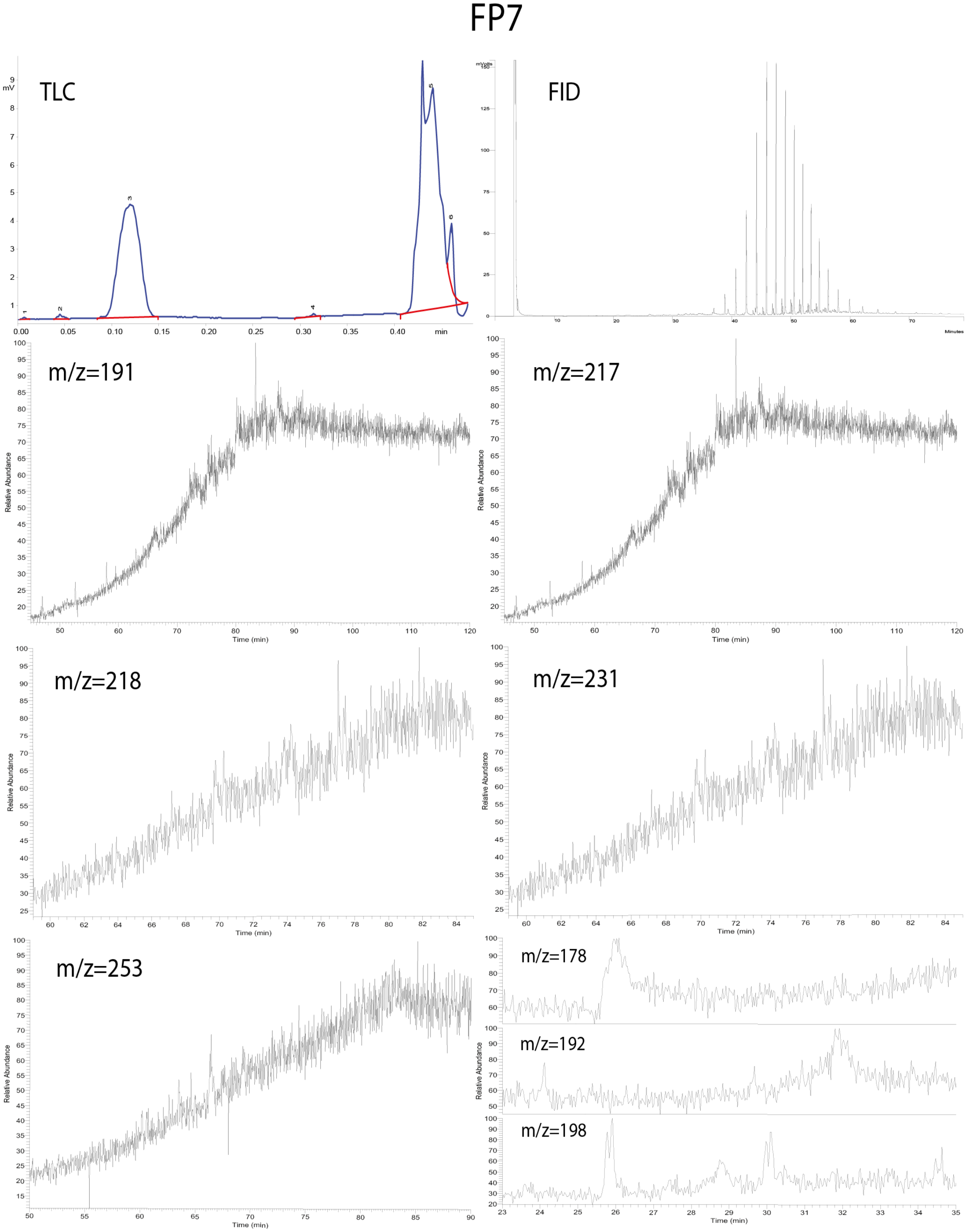

**Figure 6.22: Downscaled TLC-FID, GC-FID and GC-MS chromatograms for FP7.**

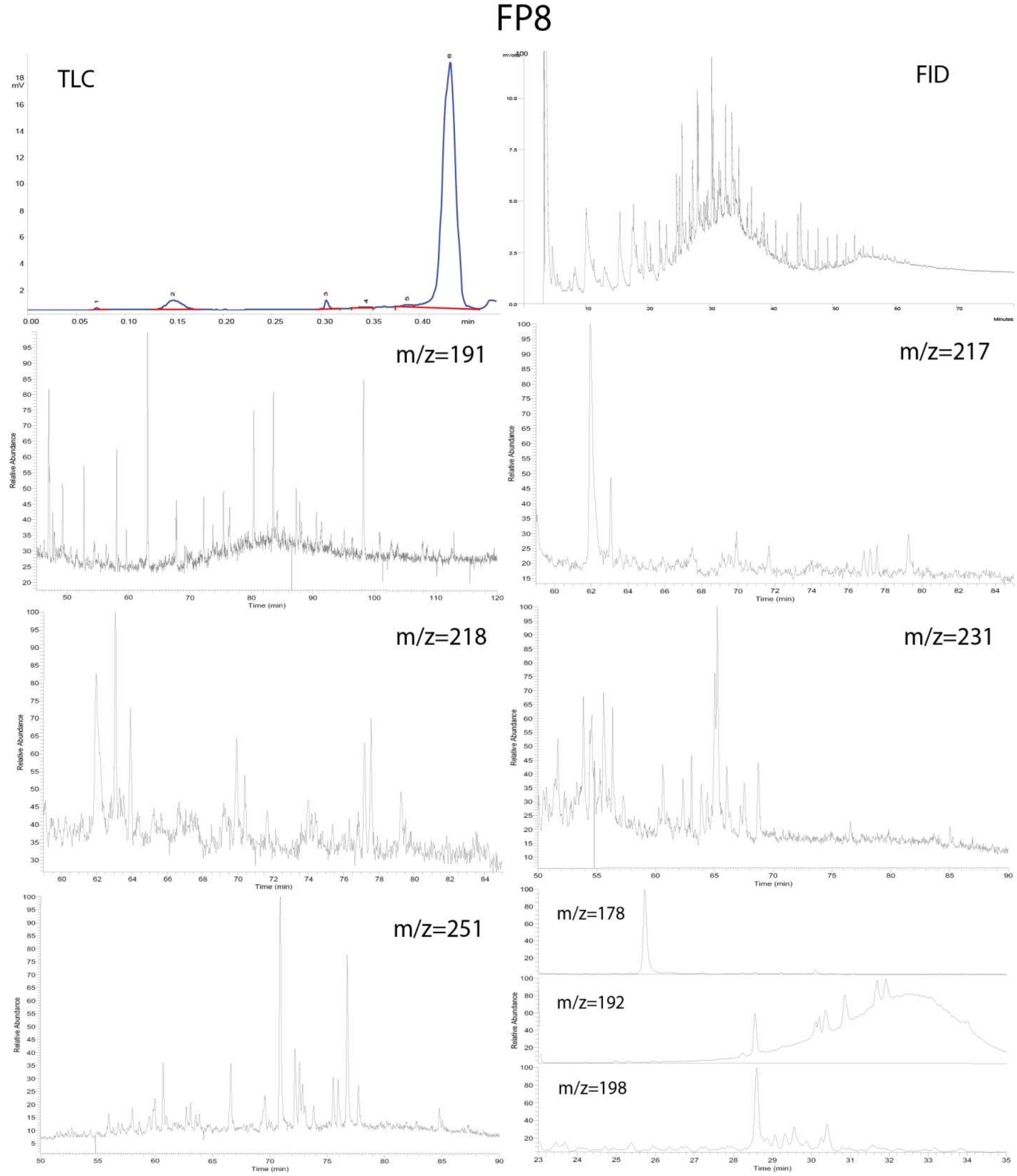

**Figure 6.23: Downscaled TLC-FID, GC-FID and GC-MS chromatograms for FP8.**

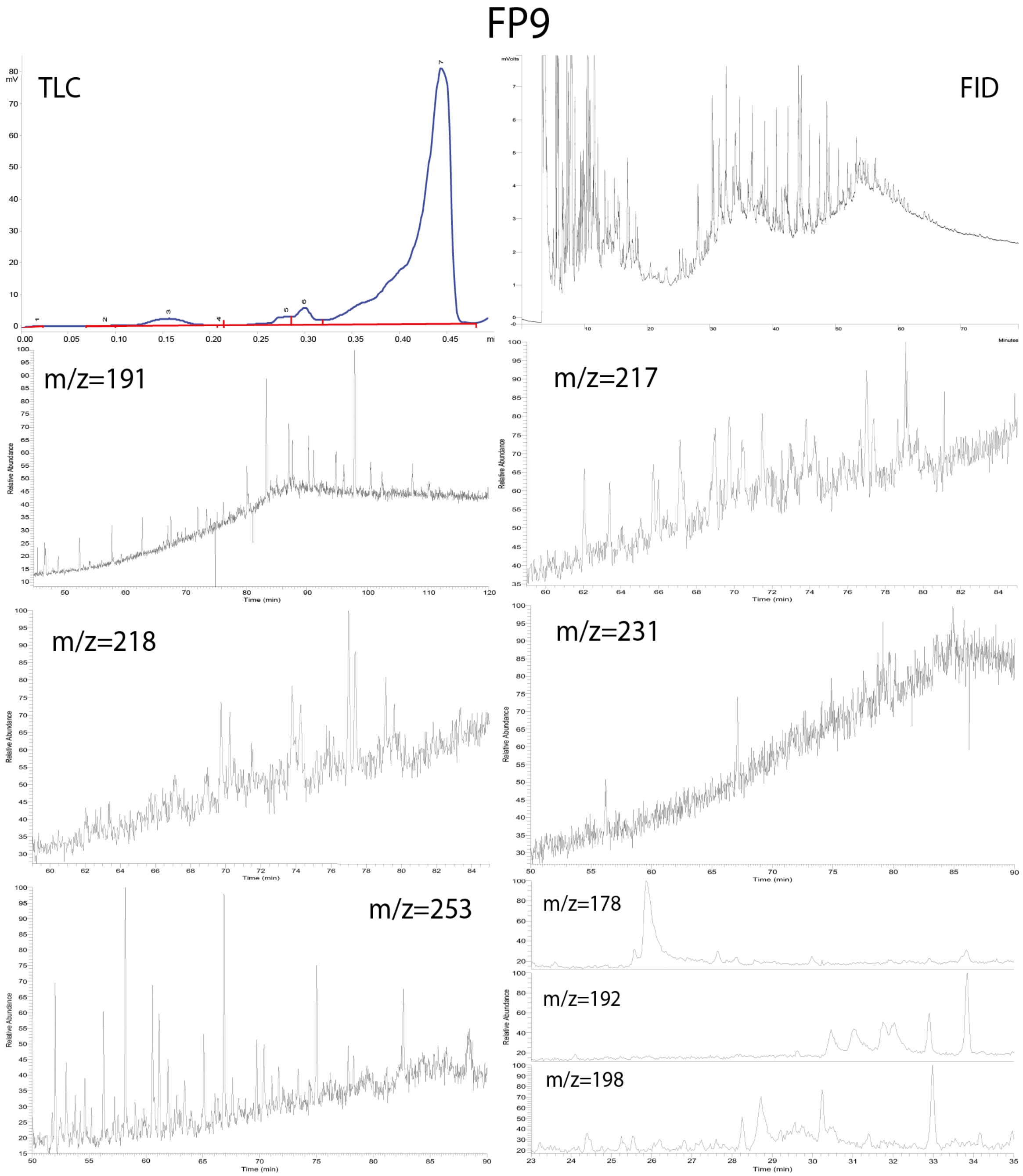

**Figure 6.24: Downscaled TLC-FID, GC-FID and GC-MS chromatograms for FP9.**

FP10

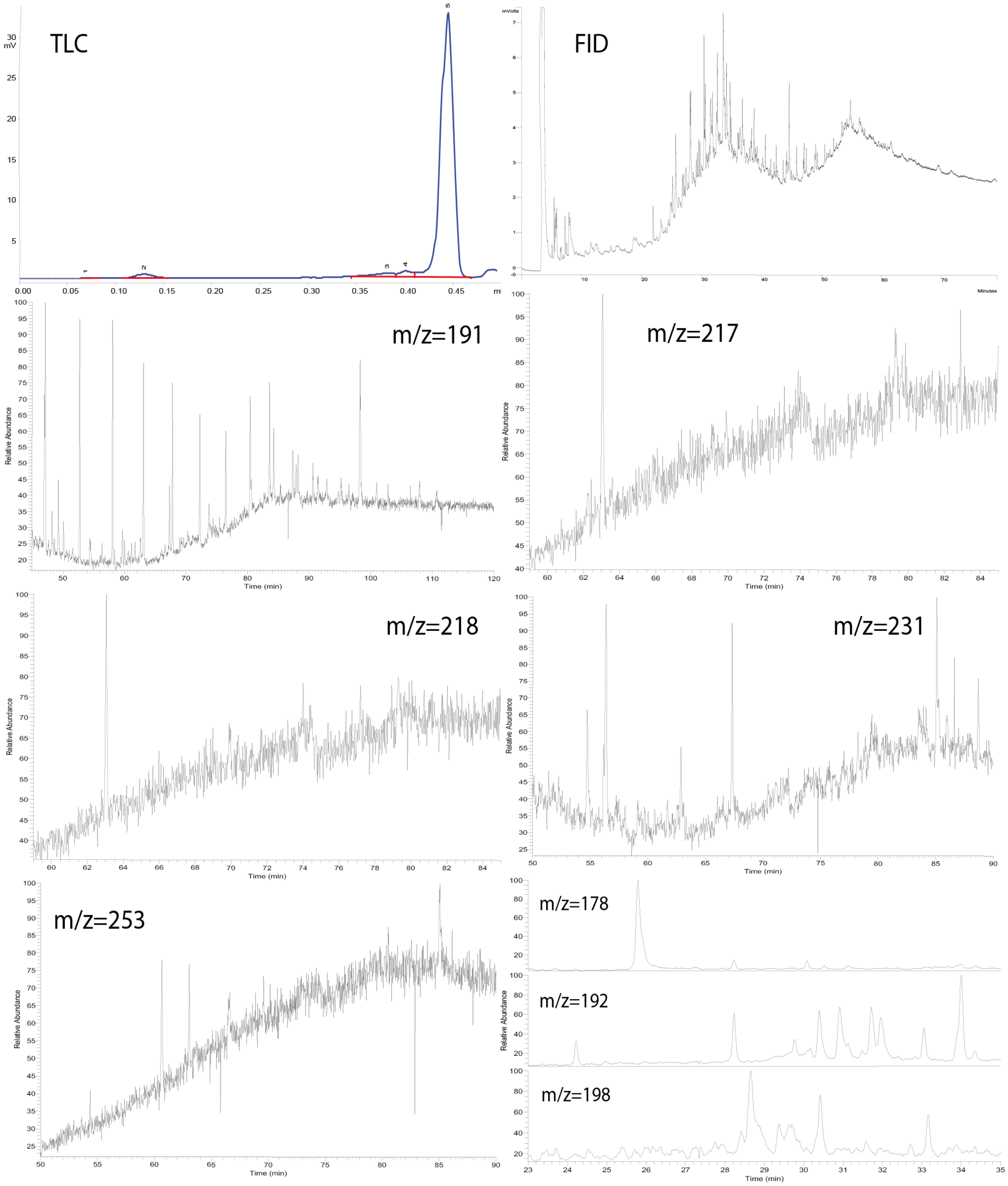

**Figure 6.25: Downscaled TLC-FID, GC-FID and GC-MS chromatograms for FP10.**

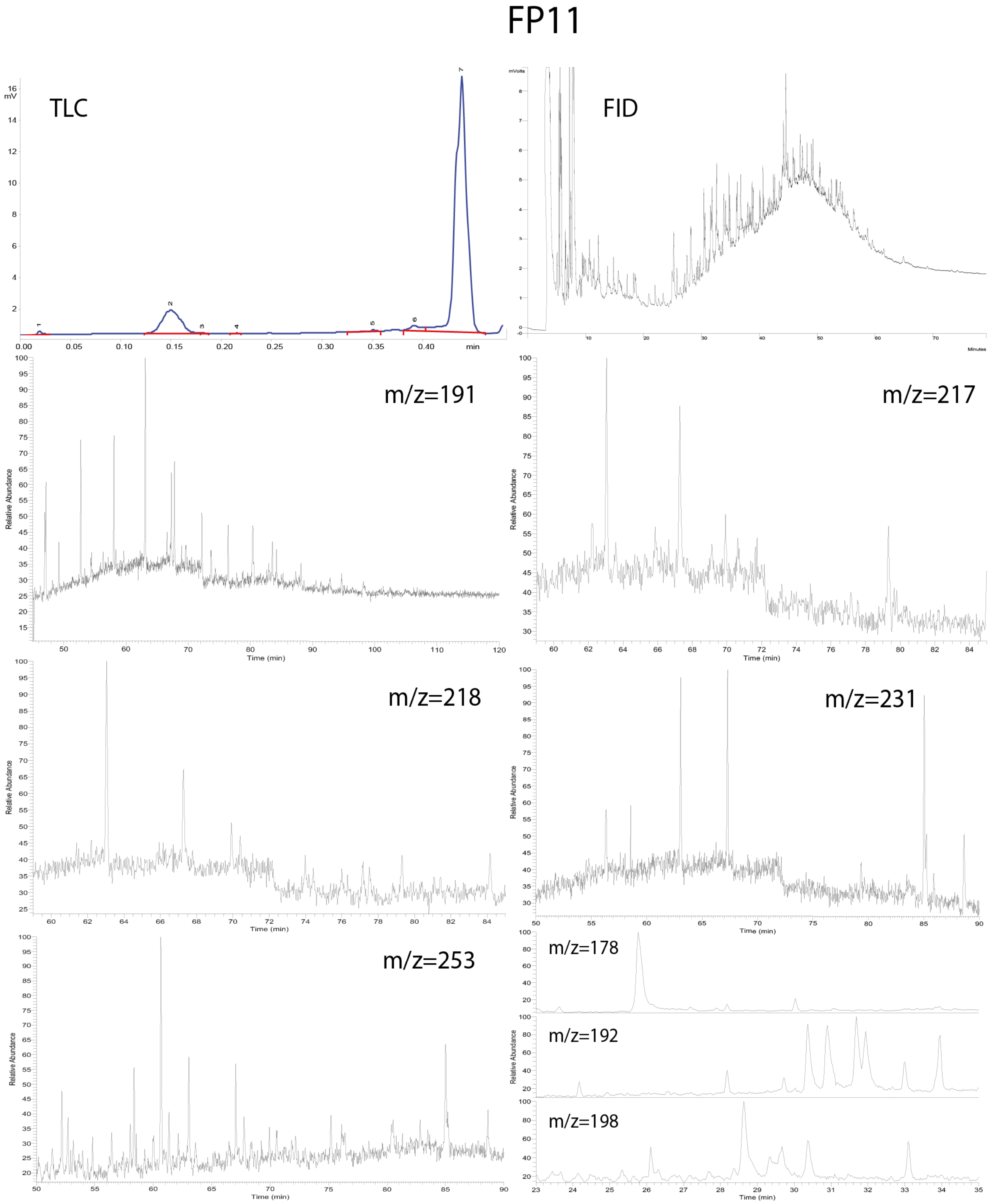

**Figure 6.26: Downscaled TLC-FID, GC-FID and GC-MS chromatograms for FP11.**

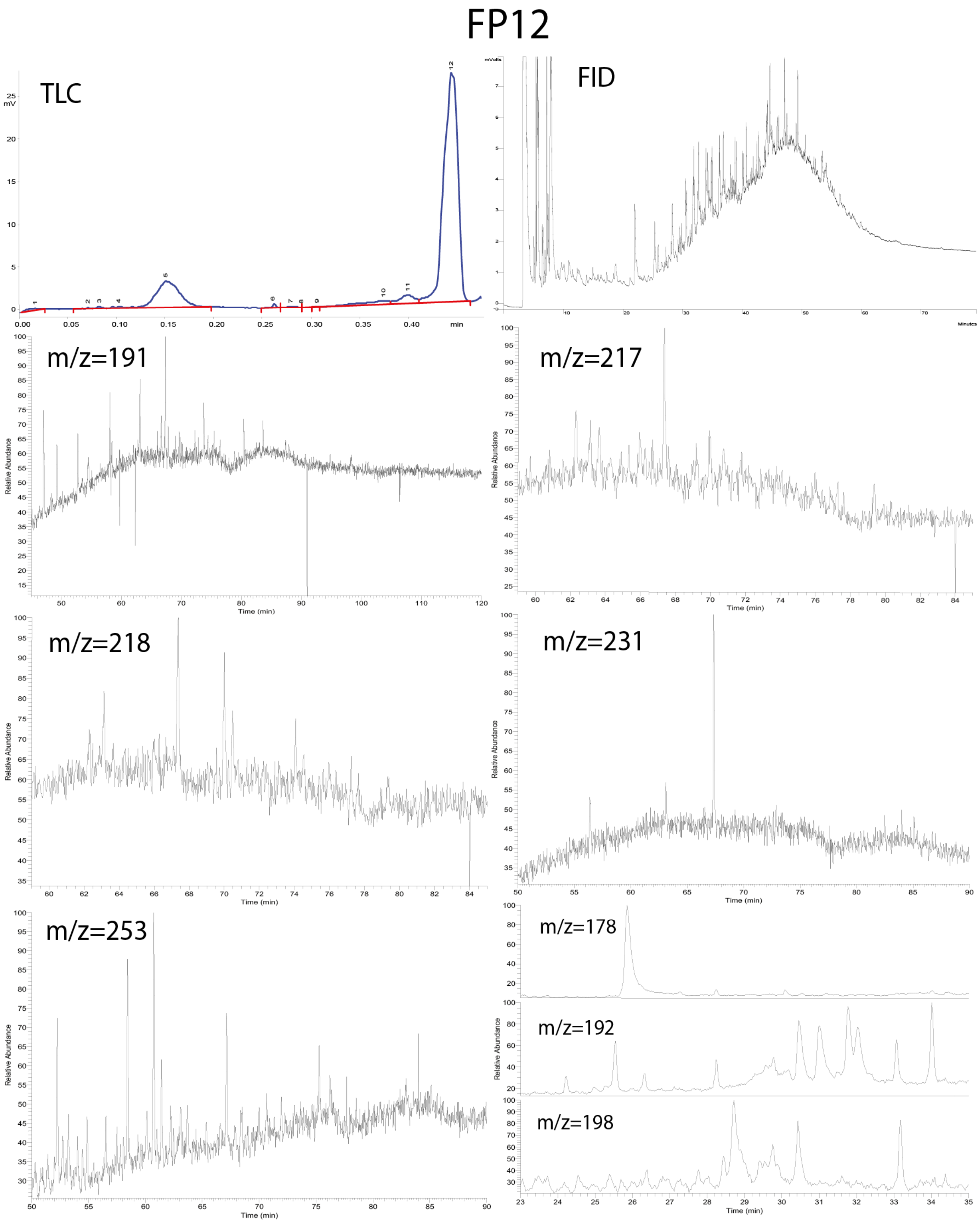

**Figure 6.27: Downscaled TLC-FID, GC-FID and GC-MS chromatograms for FP12.**

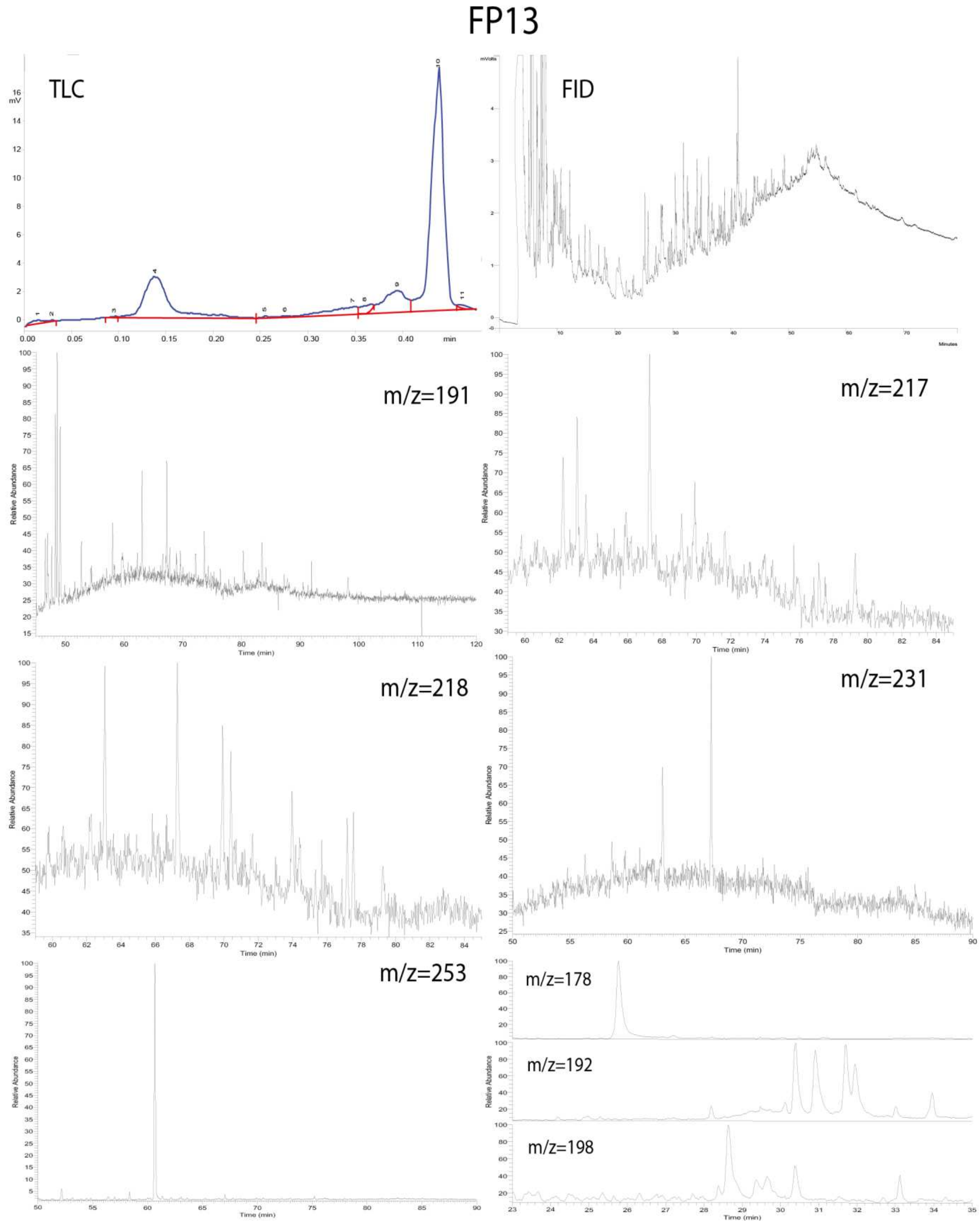

**Figure 6.28: Downscaled TLC-FID, GC-FID and GC-MS chromatograms for FP13.**

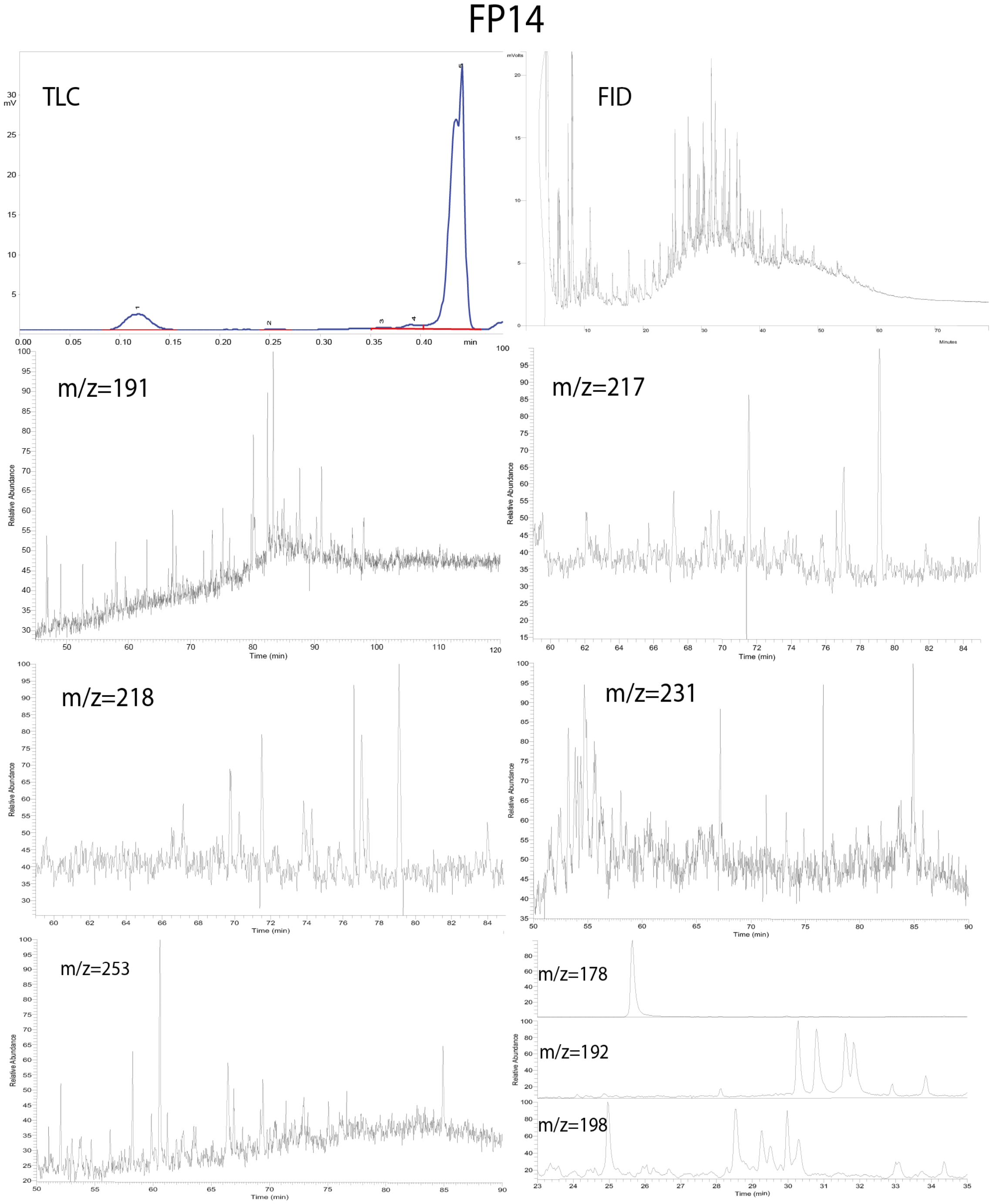

**Figure 6.29: Downscaled TLC-FID, GC-FID and GC-MS chromatograms for FP14.**

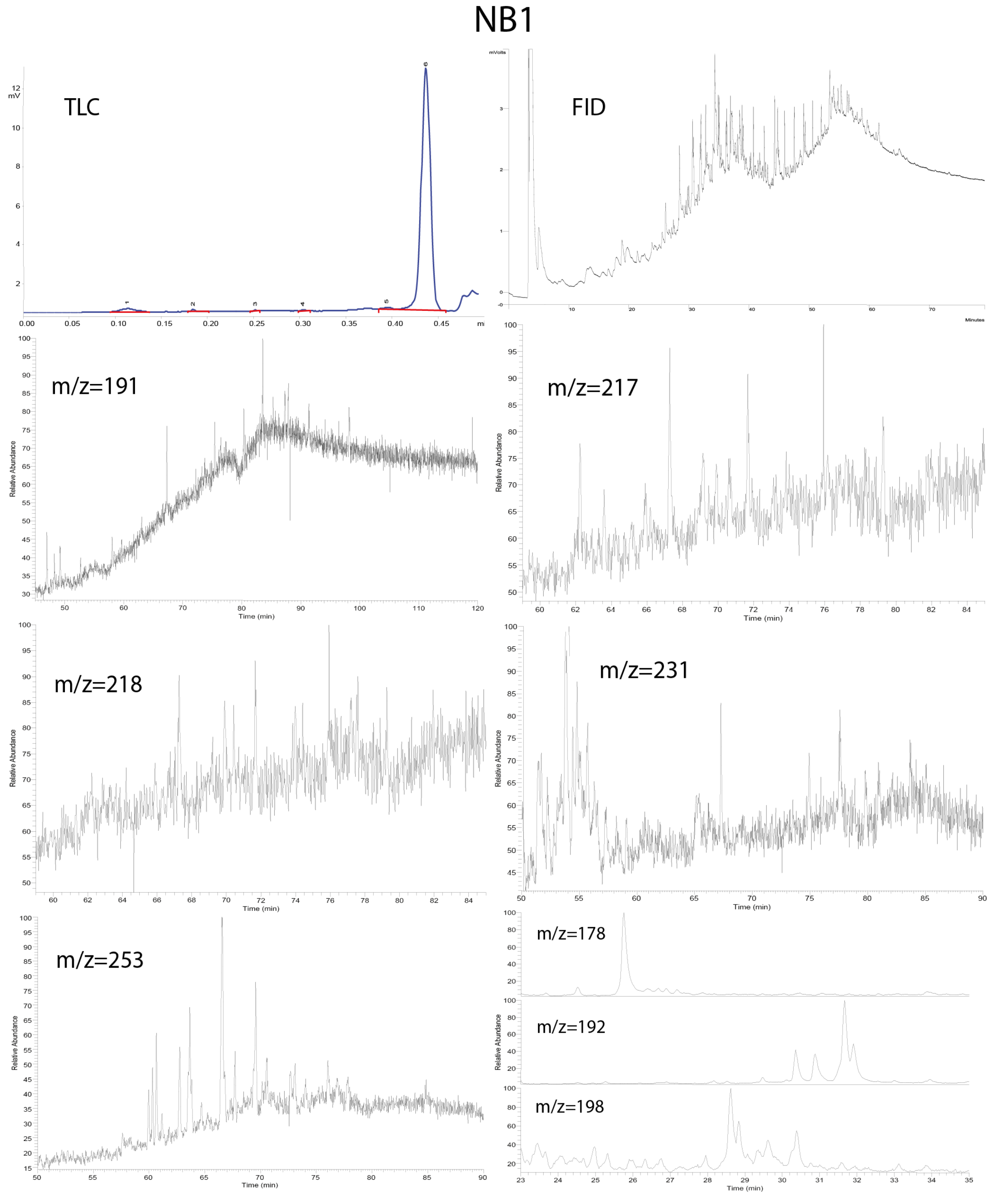

**Figure 6.30: Downscaled TLC-FID, GC-FID and GC-MS chromatograms for NB1.**

# 7. Discussion

The results presented in chapter 6, which are based on the analytical methods described in chapter 4, are discussed in this chapter. The discussion focuses mainly on maturity and organic facies assessments. Biodegradation and migration will also be examined. The main focus is the LH (LH1) sample and the comparison with bitumen from the FP and NB from the same geological era, and similar depositional environment. Moreover, discrepancies and similarities between the given oil/condensate samples from the area are also discussed. The origin of the inferred source rock, migration pathway/timing and number of filling events are key subjects in this respect. It is important to note that the sample set used in this thesis is relatively small, hence it is associated with some uncertainties. Also the subjective evaluation of the samples may contribute to wrong interpretations.

To place the samples into a wider regional and geochemical context, 14 samples from Lerch et al. (2016b) were added to some of the cross plots. These samples will be used in the maturity, organic facies and Oil/condensate families and mixing of sources discussion. The parameters for the respective wells are added in Apendix D.

The added wells are as follows:

**Table 7.1: List of Well name, Sample ID, Depth of the sample, Sample type, Field name, Area and Age. The samples are taken from (Lerch et al., 2016b). [1]O: Oil; C: Condensate; [2]BP = Bjarmland Platform; LH = Loppa High HB = Hammerfest Basin; MNFC = Måsøy Nysleppen Fault Complex FP = Finnmark Platform; NB = Nordkapp Basin: Carb = Carboniferous; P = Permian; T = Triassic; J = Jurassic; C = Cretaceous**

| Well | Sample ID | Depth MD (m) | Type[1] | Field Name | Area[2] | Age[3] |
|---|---|---|---|---|---|---|
| **7120/1-2** | B | 1879-1896 | O | | LH | Early C. |
| **7120/2-2 RFT** | D | 2501 | O | | LH | Early C. |
| **7121/7-1** | P | 1867-1872 | C | Albatross | HB | Middle J. |
| **7122/7-3** | T | 1148 | O | Goliat | HB | Early J. |
| **7122/7-3** | T1 | 1195 | O | Goliat | HB | Late T. |
| **7122/7-3** | T2 | 1812 | O | Goliat | HB | T. |
| **7122/7-3** | T3 | 1874 | O | Goliat | HB | Middle T. |
| **7123/4-1 A** | V | 2165 | O | Tornerose | HB | Late T.-Early J. |
| **7123/4-1 A** | V1 | 2542 | O | Tornerose | HB | Late T.-Early J. |
| **7124/3-1 RFT-3B** | W | 1298 | O | | MNFC | Early J. |
| **7128/4-1 DST 2** | Z1 | 1577-1586 | O | | FP | Late P. |
| **7220/6-1 MDT** | Å | 1184 | O | | LH | Late Carb.-Early P. |
| **7222/11-1 T2** | Æ | 2114 | O | Caurus | BP | Middle T. |
| **7228/7-1 A MDT-1** | AB | 2091 | O | | NB | Late T. |

The chapter is divided into the following sections:

7.1 Gross sample evaluation based on the Iatroscan TLC-FID

- 7.1.1 Gross sample evaluation based on the Iatroscan TLC-FID of the core extracts from the Finnmark Platform and the Nordkapp Basin
- 7.1.2 Oil/Condensate evaluation based on the Iatroscan TLC-FID

7.2 Medium range maturity parameters

- 7.2.1 Qualitative approach to the n-alkane distribution of the GC-FID chromatogram

7.3 Maturity of the oils, condensates and core extracts

- 7.3.1 Maturity estimation based on the biomarkers
- 7.3.2 Maturity assessment based on medium ranged aromatic maturity parameters
- 7.3.3 Summary of the maturity parameters

7.4 Organic facies

- 7.4.1 Organic facies Tables
- 7.4.2 Summary of organic facies

7.5 Biodegradation

- 7.5.1 Biodegradation based on temperatures at present day
- 7.5.2 In-situ temperature for oils and condensates

7.6 Source rock correlation to oils/condensates, oil to oil correlation and mixing of sources

- 7.6.1 The LH samples
- 7.6.2 The JC samples
- 7.6.3 The Heilo prospect (H1) sample
- 7.6.4 The S sample
- 7.6.5 The Alke structure (A1) sample
- 7.6.6 The FP and NB samples

7.7 Migration pathways

## 7.1 Gross sample evaluation based on the Iatroscan TLC-FID

### 7.1.1 Gross sample evaluation based on the Iatroscan TLC-FID of the core extracts from the Finnmark Platform and the Nordkapp Basin

The Finnmark Platform has a dipping trend towards north, due to several phases of upliftment, with the latest event during Tertiary (Larssen et al., 2002). The southern parts of the Finnmark Platform have been heavily subaerial eroded and late Paleozoic sediments can be found at shallow depths, covered by Quaternary deposits. Moreover, the formation of salt diapirs in the Nordkapp Basin resulted in an uplift of late Paleozoic sediments (Bugge et al., 2002). The shallow core samples from Finnmark Platform originates from the Upper Paleozoic (Carboniferous and Permian) and are found in the same formation as the Alta discovery in the Gohta petroleum system.

The idea was to compare the core samples with the Alta discovery as they have much of the same depositional environment. From Figure 7.1 it is evident that the oil sample from Loppa High has a completely different composition than the extracted bitumen samples, since the extracted cores contain almost exclusively polar components. Heavy degradation of saturated hydrocarbons (especially the light hydrocarbons), including removal of n-alkanes, is generally a result of biodegradation (Tissot and Welte, 1984), and possibly some of the aromatic fraction (Deroo et al., 1974). Impoverishment of the most soluble cycloalkanes and aromatic hydrocarbons with one or two rings can also occur as a result of water washing. Moreover, contact with oxygen can lead to degradation of lower molecular weight compounds of the cycloalkanes, aromatic HC and thiophenic fractions (Deroo et al., 1974). The shallow core samples existed close to the sea-floor surface and might have been exposed to both air and also oxygenated water. Consequently, the cores with their organic contents have most likely been severally biodegraded, water washed and oxidized. Hence, the usefulness of the core extracts as an analog for the Gotha petroleum system has diminished. The high amount of polar compounds can also reflect low maturation, as hydrocarbon generation has not yet started. This could be a contributing cause, but most likely not the only one due to the samples being heavily dominated by polar compounds.

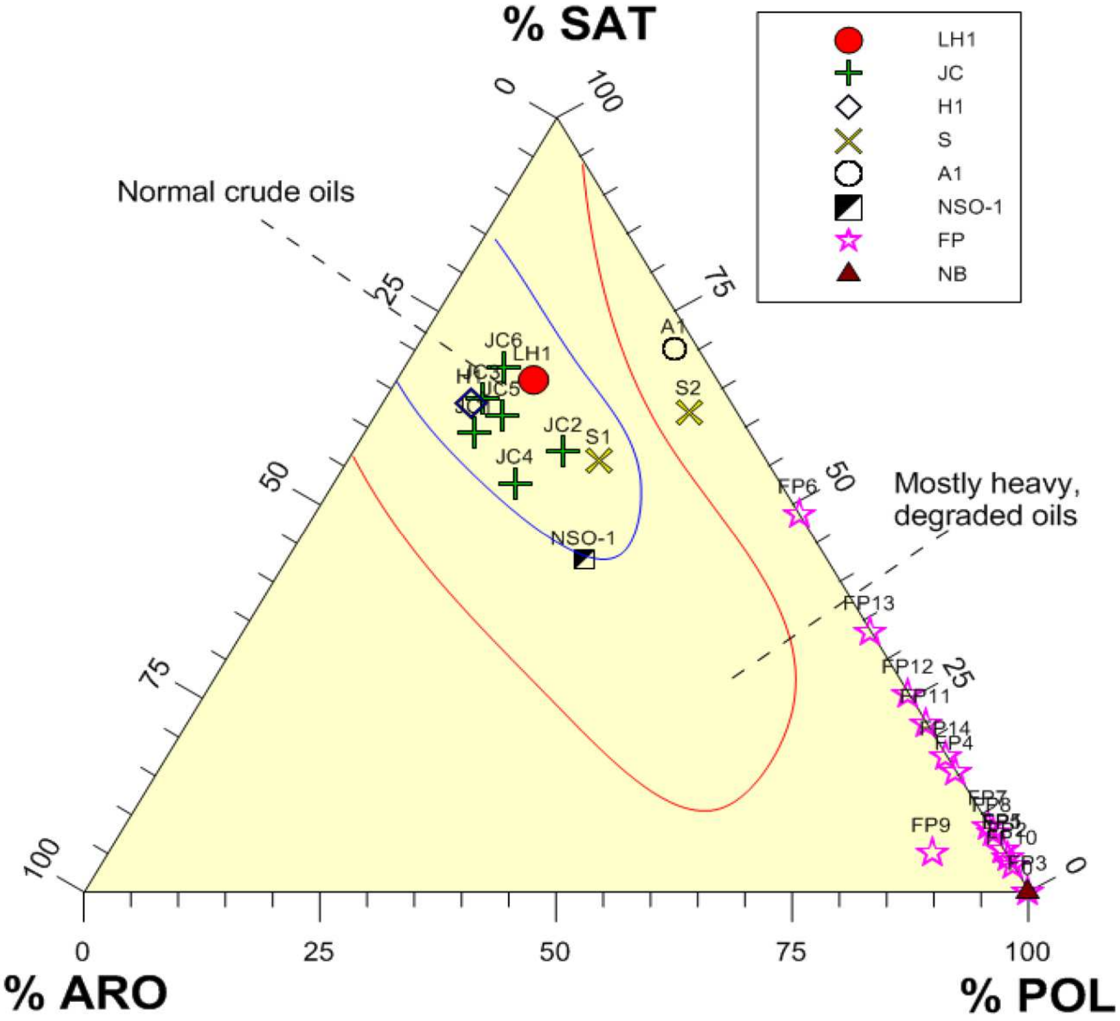

**Figure 7.1: The ternary diagram illustrates the main compounds of the petroleum and bitumen samples. SAT=saturated hydrocarbons, POL=Polar compounds and ARO=Aromatic hydrocarbons. The zones of normal crude oils and heavy degraded oils are based on Tissot and Welte (1984). All of the oils from the sample set plot within the Normal crude oils area, while condensates and core samples plot outside both of the categories.**

Even though the extracts contain a relative high amount of asphaltenes/resins, the polar amount of extracts compared to the amount of rock crushed (mg extract/g rock) are stunningly low, none of the samples exceed 0.003 mg extract/g rock, whilst the aromatics and saturates are even lower. Higher quantities of bitumen extract were expected/ for some of the more consolidated samples, e.g. FP12 and FP14. The only sample showing some remnants of aromatic compounds is FP9. Some of the solvent extracts had a light yellow color while most of the solvent extracts had a waterish color, indicating low bitumen content (Figure 7.2). The reason for the low bitumen content can also be due to low porosity/permeability and bad communication between pores.

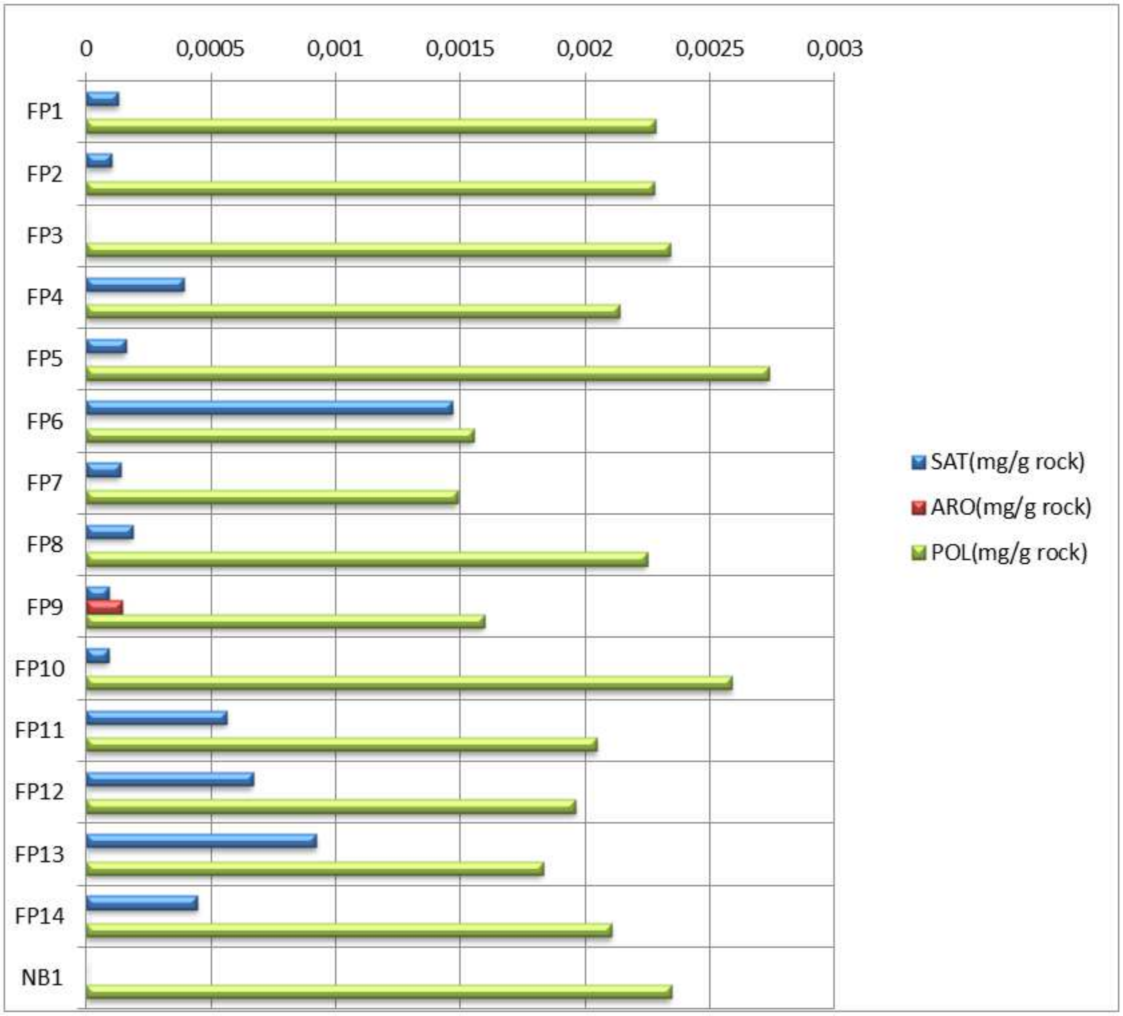

**Figure 7.2: The amount of mg extract/g rock are shown for the SAT (Saturated), ARO (Aromatic) and POL(Polar) compounds. The amount is extremely low for all the samples; FP9 is the only sample with ARO hydrocarbons.**

### 7.1.2 Oil/Condensate evaluation based on the Iatroscan

As seen from Figure 7.1 the LH sample plots well within the normal crude oil window, together with all the Johan Castberg samples and H1 (Figure 7.1). The S1 and the NSO samples fall into the degraded oil area, while S2 and A1 have much lower aromatic hydrocarbon content than the others (Figure 7.1). The S/A ratio for sample JC1 is lower than the two underlying samples in well 7220/5-1. This is the contrary of what would be expected as saturated fractions (light hydrocarbons) tend to migrate to the top of a reservoir. The Skrugard structure is divided into three segments by erosion features, separating the structure into 3 gas-oil contacts (Lindberg et al., 2013). This might influence the vertical variation of the S/A ratio, as the communication between the structures is reduced. The LH1 sample has a relatively high S/A ratio compared to the other oil samples, and this can indicate a higher maturity. It is important to mention that according to Clayton and Bostick (1986) the S/A ratio will increase and later drop at maturities higher than 1.0 %Ro. This means that a sample in the early oil window can have the same S/A ratio as a mature one originating from the same source. Peters and Moldowan (1993) also expressed that low S/A ratios can be correlated with a carbonate facies.

The S2 and A1 samples are both condensates with S/A ratios of 12.61154 and 29.1952 respectively. As mentioned in chapter 5, the S/A ratio can provide some information about maturity, due to the fact that thermal maturation tends to increase the light hydrocarbon fraction ($<C_{15}$). The extreme ratios of sample S2 and A1 seem too high to be caused by maturity alone, and a gas prone source rock or phase fractioning may be possible causes as mentioned in chapter 5.1.1. This will be discussed further in the following sections.

It is important to note that the S/A ratio is only a tentative maturity indicator, and more reliable maturity estimations are done with the biomarker data.

Figure 7.3 puts the samples in order from least to most mature. As mentioned above, the condensate ratios seem too high to be solely influenced by maturity.

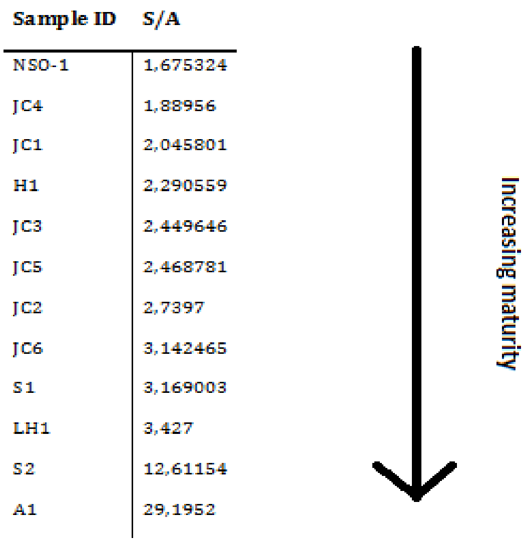

| Sample ID | S/A |
|---|---|
| NSO-1 | 1,675324 |
| JC4 | 1,88956 |
| JC1 | 2,045801 |
| H1 | 2,290559 |
| JC3 | 2,449646 |
| JC5 | 2,468781 |
| JC2 | 2,7397 |
| JC6 | 3,142465 |
| S1 | 3,169003 |
| LH1 | 3,427 |
| S2 | 12,61154 |
| A1 | 29,1952 |

Increasing maturity

**Figure 7.3: Maturity assessment based on the S/A ratio. Higher ratio means higher maturity.**

## 7.2 Medium range maturity parameters

### 7.2.1 Qualitative approach to the n-alkane distribution of the GC-FID chromatogram

The n-alkane distribution shown in the GC-FID chromatograms will change with thermal maturation. The n-alkane composition is also affected by, source input, biodegradation, migration pathway and distance, phase fractioning, evaporation and water washing (Peters et al., 2005). Low maturity terrestrial samples tend to have bimodal n-alkane distributions (Abay, 2010), the bimodality vanishes with the thermal maturation, although, mixing of petroleum with different n-alkane distribution can lead to a bimodal distribution (D.A. Karlsen, 2016, personal communication). Another cause of bimodality can be the kerogen composition of the source rock. A source rock with a blend or mix of kerogen types can produce two n-alkane patterns with differing signatures. Consequently, when these patterns are combined in a chromatogram, the n-alkane pattern of the “blend” may become altered.

**LH1**

The LH1 sample indicates a bimodal signature. This might be a result of several filling events. From Figure 6.5 and appendix B one can see that the lighter hydrocarbons are preserved and the dominating pattern seems to be quite close to a marine shape (Tissot and Welte, 1984), with a convex shape and with the intensity increasing towards the lighter hydrocarbon side of the distribution. However, the method used can only distinguish saturated hydrocarbons down to ~C9-C8. The baseline of the LH1 chromatogram is not elevated (Figure 6.4), and as explained by e.g. Wenger et al. (2001) the lack UCM is an indication of low or non biodegraded oils/condensates.

**JC**

The JC1-3 and JC6 samples show some similar n-alkane trends (Figure 6.5, Figure 6.6, Figure 6.7, Figure 6.10 and appendix B). The baselines are moderately elevated and the light hydrocarbon fraction abundance is low. This indicates slight to moderate biodegradation (Wenger et al., 2001). Another biodegradation indicator is related to the Pr and Ph peaks which show a higher intensity compared to their respective n-alkanes (n-C17 and n-C18), and this phenomenon is explained in Section 5.1.1. These 4 samples are the only oil and condensates which shows this level of biodegradation. This correlates well with the estimated reservoir temperatures at which these samples were gathered, which suggest good conditions for biodegradation (see Figure 7.19). The fourth sample from JC demonstrates a complete specter of saturated hydrocarbons (see Figure 6.8) and the baseline is only slightly elevated, suggesting no or a much lower level of biodegradation than the former mentioned JC samples. Accordingly, the sample from JC5 seems to be placed somewhere in between the JC5 sample and the other samples from the JC field (see Figure 6.9).

**H1**

The H1 sample shows a clearl bimodal distribution, and this strongly indicates two or more infilling events. One of the events seems to be dominated by light hydrocarbons, and the first charge is possibly the heavier fraction (see Figure 6.11). The heavy hydrocarbon part is likely to be biodegraded due to the low content of light hydrocarbons and the observable UCM.

**S**

The S1 sample shows a similar n-alkane distribution as the H1 sample with a light hydrocarbon fraction with a marine n-alkane envelope and a heavier, possible biodegraded one (see Figure 6.12). Compared to this, the S2 sample displays a totally different saturated hydrocarbon pattern. This latter distribution is expected for a condensate. The lightest hydrocarbon part seems to be either evaporated or biodegraded (see Figure 6.13).

**A1**

The A1 condensate has preserved the lightest hydrocarbons part and shows a typical marine distribution (see Figure 6.14). The heavier hydrocarbons (C25+) are not visible on the chromatogram in this print out.

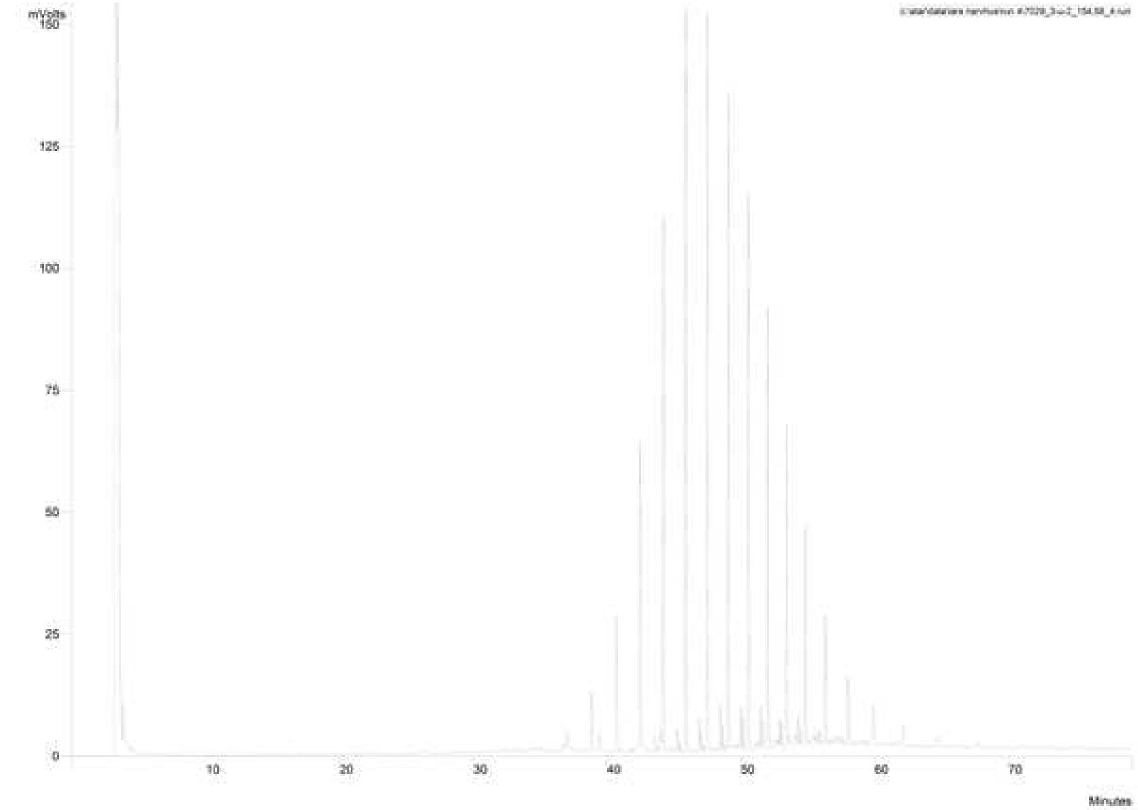

**Figure 7.4: Sample FP6 has much higher mVolt intensity compared to the other samples, and very far out into the chromatogram i.e. peaking at c 50 min. This is believed to be contamination.**

### FP and NB1

The core samples from the Finnmark Platform and Norkapp Basin show a general trend of low n-alkane and isoprenoids abundance (see Figure 6.16-6.30). Most of the samples show large UCM humps e.g. FP10 and NB1 (see Figure 6.25 and 6.30). Some of the samples e.g. FP3 and FP5 show little to no remnants of saturated hydrocarbons and isoprenoids (see Figure 6.19 and 6.21). The complete core sample collection seems to share the same characteristics reflecting severe biodegradation.

FP6 shows a vastly different n-alkane distribution compared to its core relatives, and the peak distribution is different and also the intensities are much higher. Several re-runs of the GC-FID analysis of the respective sample were performed, with the same disappointing results. This leads to the possibility of the sample representing contamination, possibly during the drilling of the core. Quantitative parameters based on the GC-FID chromatogram will be discuss further in the organic facies section.

## 7.3 Maturity of the oils, condensates and core extracts

### 7.3.1 Maturity estimation based on the biomarkers

The biomarkers used in this section are based on the GC-MS, and the m/z ratios used were 191, 217, 218, 231 and 253. The decrease of biomarker abundance indicates increasing maturity (Mackenzie et al., 1985). However, phase fractioning can also remove or separate biomarkers (Karlsen and Skeie, 2006).

The maturity parameters are not independent of facies and diagenetic effects. Maturity assessment based on the heavy (C25+) biomarkers can produce conflicting estimation compared to the medium ranged (C13-C18) maturity parameters (Karlsen et al., 2004).

Most of the parameters used are listed in Figure 5.15, which also shows the variation of the parameters relative to the oil window. Since the samples used in this thesis being mainly are oils and condensates, some of the parameters were excluded e.g. 22S/(22S+22R) of hopanes (Mackenzie et al., 1980), due to the fact that several ratios equilibrate at the start of the oil window (about 0.6%$R_0$).

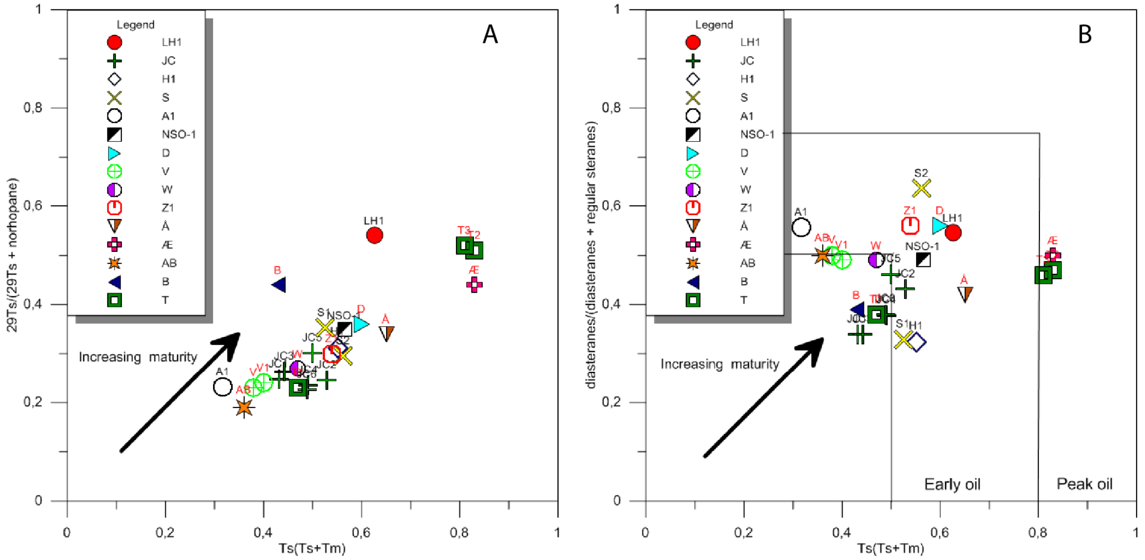

**Figure 7.5: The Figures illustrate the maturity of the samples based on saturated biomarkers. Figure 7.5A is a Table of Ts/(Ts+Tm) (Seifert and Moldowan, 1978) versus 29Ts/(29Ts+norhopane) (Peters and Moldowan, 1991). Figure 7.5B Tables Ts/(Ts+Tm) (Seifert and Moldowan, 1978) versus diasterane/(diasterane + regular steranes) (Seifert and Moldowan, 1978). The ratios of the oils and condensates produced from the laboratory work in this thesis are plotted with black labels and their respective names. The sample parameters taken from Lerch et al. (2016b) are plotted in red with their respective sample names.**

The Ts(Ts + Tm), 29Ts(29Ts +norhopane) and diahopane/(diahopane + normoretane) involve rearrange hopanes into their non-rearranged counterparts. 18a-neohopane (TS and 29Ts) skeletons are not found within organism and are most likely formed in the sediments (Farrimond et al., 1998). Farrimond et al. (1998) also suggest that the conversion does not occur during thermal degradation, rather due to source input or/and during diagenesis. This suggests that the relative abundance of hopanes and non-rearranged counterparts are not solely influenced by maturation, and may vary due to source input and digenetic effects (Rullkötter and Marzi, 1988, Farrimond and Telnæs, 1996). Although 29Ts/(29Ts +norhopane) is not solely affected by maturity, it is viewed as one of the most robust maturity parameters, and the molecules are sufficiently similar in molecular weight for them not to be influenced by phase fractionation during migration (Karlsen and Skeie, 2006). Determining maturity based on single parameters is always difficult, and the reason why several parameters are used for this purpose.

By examining Figure 7.5A it shows that most of the samples plot in a cluster at a surplisingly early stage in the thermal maturity window. Based on this data, he A1 condensate (7120/12-2 DST 2) is estimated to have the lowest maturity, which is somewhat contradicting of what one would expect. Furthermore, the outliers of Figure 7.5A are the two Loppa High samples LH1 (7120/2-1 DST 4) and B (7120/1-2) along with sample Æ (7222/11-1 T2) and two of the Goliat samples T2 and T3 (7122/7-3), and all of these samples express the highest maturity of the sample set. However, as one can observe in Figure 7.5A the do not express high maturity based on the same parameter , LH1 and Å due to elevated 29Ts/(29Ts+norhopane) and Æ, T2 and T3 as a result of elevated Ts/(Ts+Tm). A closer investigation shows that the 17α (H), 21β (H)-30-norehopane (normoretane) peak for the LH1 sample is relatively lower than the other samples. As mention this ratio can be influenced by other factors than thermal degradation. Subroto et al. (1991) reported carbonate derived oils to contain excessive amounts of the 30-norehopane series. As for the Æ sample the Ts/(Ts+Tm) ratio is higher than for the rest of the sample set. Two causes for this can be a siliclastic source (Peters et al., 2005), or source input from a hypersaline environment (Rullkötter and Marzi, 1988). Sample T2 and T3 seem to express more or less the same maturity as the Æ sample. However, the variations can also be a consequence of higher maturation and more maturity parameters must be examined.

Exchanging the 29Ts/(29Ts+norhopane) with diasteranes/(diasteranes + regular steranes) in Figure 7.5B gives the general impression of higher maturity for the sample set, as most of the samples plot within the early oil window. The two condensates S2 (7129/6-1) and A1 (7120/12-2) respectively have a much higher ratio for diasteranes/(diasteranes + regular steranes) compared to the 29Ts//(29Ts+norhopane). Overestimation of the diasteranes/(diasteranes + regular steranes) tends to occur with a shale source (Mello et al., 1988). This can explain some of the shifts in maturities we see when changing the y-axis from 29Ts/(29Ts+norhopane), see Figure 7.5B. Still, no significant changes can be seen in the relative position of the S1 (7129/6-1) sample, which is an oil, suggesting that the changes in sample S2 and A1 might be due to their nature as a condensate.

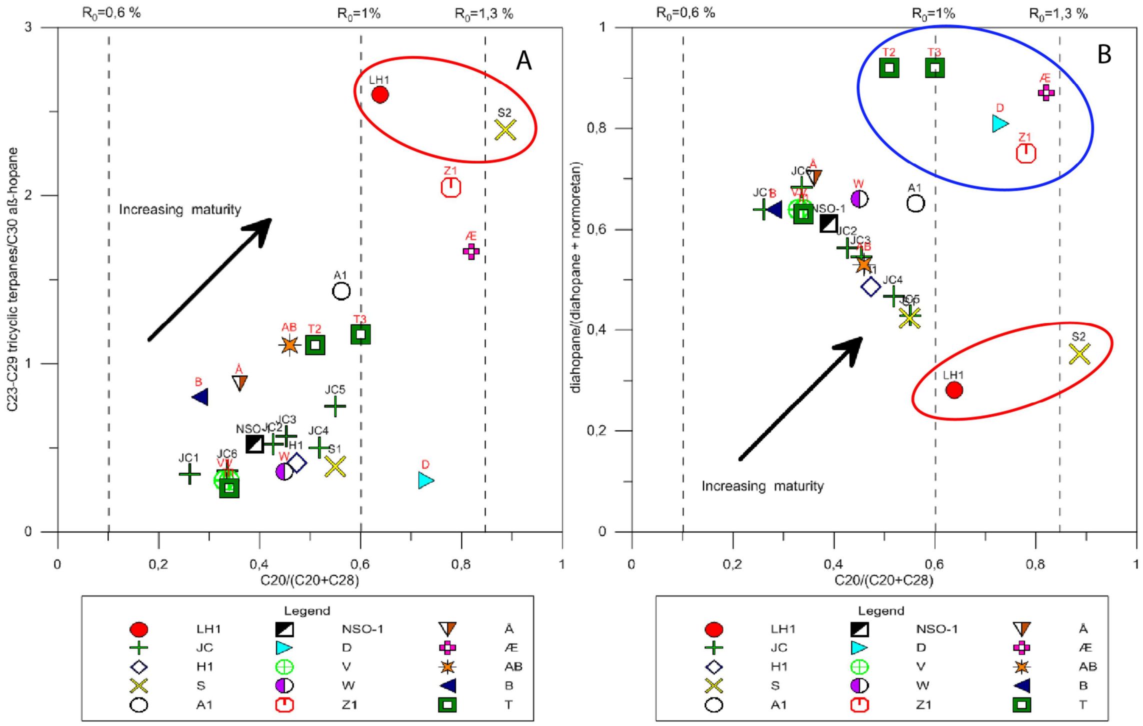

**Figure 7.6: The Figures illustrate the maturity of the samples based on saturated and aromatic biomarkers. Figure 7.6A is a Table of C20/(C20+C28) (Peters et al., 2005) versus C23-C29 tricyclic terpanes/C30 aß-hopane (Mello et al., 1988). Figure 7.6B Tables C20/(C20+C28)(Peters et al., 2005) versus Diahopane/(diahopane + normoretan) (Peters and Moldowan, 1993). The ratios of the oils and condensates produced from the laboratory work in this thesis are plotted with black labels and their respective names (see Table 7.1). The sample parameters taken from Lerch et al. (2016b) are plotted in red with their respective sample names. The extreme values of LH1 and S2 are marked with a red circle in Figure 7.6A. Some of the C23-C29 tricyclic terpanes/C30 aß-hopane ratios show extremely high values. Consequently the y axis on plot 7.6A has to be adjusted, this make the samples with somewhat more "normal" maturity values appear as immature. The LH1 and S2 sample are also delimeted by a red cirlce in Figure 7.6B, sample D, Æ and Z1 are marked with a blue circle.**

Based on Figure 7.6A most of the samples appear to fall within the early-peak oil generation window. Some of the samples analysed in this thesis plot into a higher maturity area, A1, LH1 and S2 respectively. The extreme values of LH1 and S2, and the high value of the A1 sample can be related to phase separation. The lighter fraction of a separated petroleum tends to be enriched in C23-C29 tricyclic terpanes and C20 triaromatic steroids, while the heavier oil phase will be enriched in C30 aß-hopane and C28 triaromatic steroid.

This is due to the higher vapor pressure of C23-C29 and C20 (Karlsen et al., 1995, Karlsen and Skeie, 2006). The separation is likely to happen due to PVT changes during migration (England and Mackenzie, 1989). The LH1 sample is a black oil with relative low viscosity. Moreover, based on the n-alkane distribution from the chromatogram, a lot of waxy hydrocarbon compounds can be identified (see Figure 6.5). Therefore, one could argue that this sample might have two sources, representing both a light and a heavy fraction. Sample Z1 (7128/4-1 DST 2) from the Finnmark Platform, found in Late Permian carbonates is calculated to high maturities (>1%Ro). Along with sample Æ (7222/11-1 T2) from the Bjarmland Platform, and D (7120/2-2 RFT) from the Loppa High, these are also calculated to high maturities (>1%Ro). When changing the Y-axis with diahopane/(diahopane + normoretan) ratio, most of the oils express the same maturity compared to 7.6 (early to peak oil). However, LH1 and S2 display a drastic decrease to lower values and sample D increases greatly (see Figure 7.6A compared to Figure 7.6B). Diahopane is derived from hopanes and rearranged by a clay-mediated catalyst in an oxic- to sub-oxic terrigenous environment (Peters et al., 2005). This coincide with the observations of Volkman et al. (1983) and (Philp and Gilbert, 1986) where diahopane is found in greatest abundance in highly terrigenous oils.

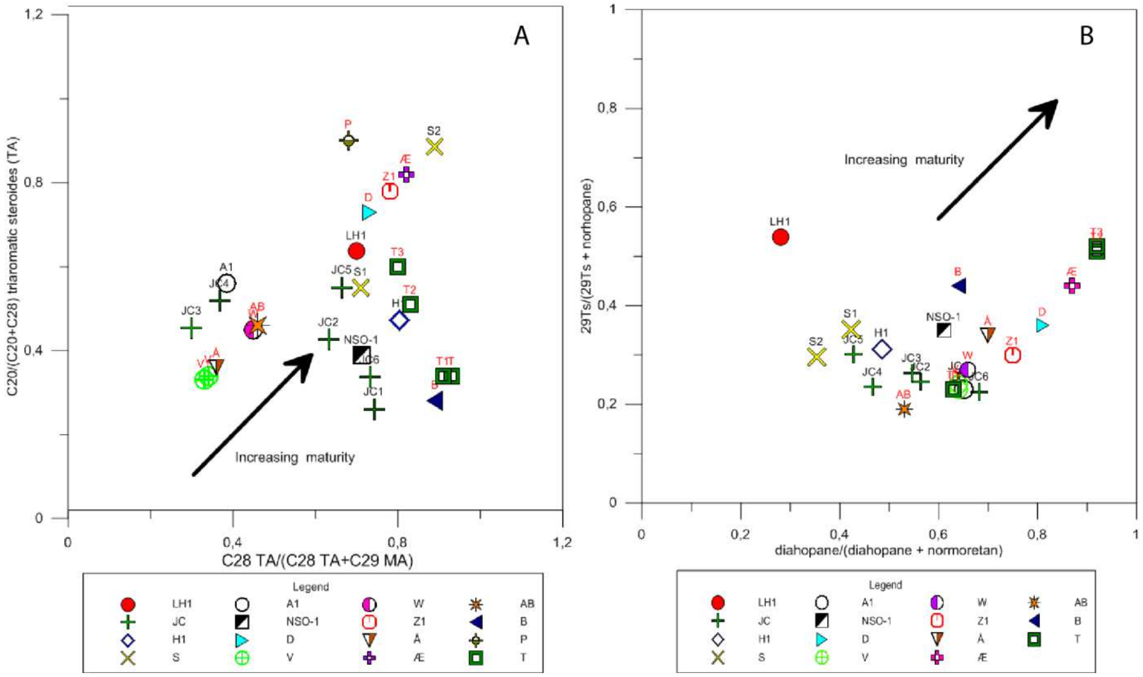

**Figure 7.7: The Figures illustrate the maturity of the samples based on saturated and aromatic biomarkers. Figure 7.7A is a Table of C28 TA/(C28 TA+C28 MA)(Mackenzie et al., 1985) versus C20/(C20+C28) (Peters et al., 2005). Figure 7.7B Tables diahopane/(diahopane + normoretan)(Peters and Moldowan, 1993) versus 29Ts/(29Ts+norhopane). The ratios of the oils and condensates produced from the laboratory work in this thesis are plotted with black labels and their respective names. The sample parameters taken from Lerch et al. (2016b) are plotted in red with their respective sample names.**

High amounts of 17β (H), 21α (H)-30-norehopane (Normoretan) relative to hopanes are associated with an anoxic carbonate or marl environment (Peters et al., 2005). Thus, the variation in maturity from the two plots could reflect variation in depositional environment. The low diahopane/(diahopane + normoretan) ratio for the LH1 sample is somewhat contradicting to the high 29Ts/(29Ts +norhopane) ratios, where the former would suggest a shale source and the latter a carbonate. As mentioned previously, the ratio of 29Ts/(29Ts +norhopane) seems to be quite robust to differences in depositional environment, henceforth a shale source might be a more likely possibility, lowering the impressionable diahopane/(diahopane + normoretan) ratio. Thusly, the high ratio of diahopane/(diahopane + normoretan) of the D sample might indicate a carbonate source.

Mackenzie et al. (1985) reported that oil samples from the same area at the same depth showed variations in the C28 TA/(C28 TA+C28 MA) ratio. This is probably due to differences in organic matter input or lithology effects. Furthermore, Mackenzie et al. (1985) proposed that high ratios often occur in siliceous rocks and low ratios is associated with phosphatic rocks. Curiale and Odermatt (1989) also observed an enrichment of triaromatic steroids in siliceous rocks and a lower abundance in phosphatic/carbonate source. The samples A1, JC3, JC4, V, V1, W and AB seem to be separated from the other samples due to the lower C28 TA/(C28 TA+C28 MA) ratios. Notice that sample P (7121/7-1) which is a condensate and which also expresses high maturity based on the triaromatic steroids ratio (Figure 7.7A). Differences in lithology may be the cause for this separation. Sample D, Z1, Æ, S2, LH1 show high maturity, and this is the general trend for these samples in most of the Tables. As mentioned before, the 29Ts/(29Ts+norhopane) ratio is viewed as one of the most robust parameters for maturity estimations. In Figure 7.7B one can observe big discrepancies between the 29Ts/(29Ts+norhopane) and the diahopane/(diahopane + normoretan) parameters, suggesting that some of the diahopane/(diahopane + normoretan) might be overestimating the maturity for some of the samples, and underestimating for the LH1 sample. Based on Figure 7.7B the Goliat samples T2 and T3 appear to be the most mature of the sample set.

None of the oils and condensates analyzed in this thesis seem to reach the equilibrium threshold, although they are quite close (see Figure 7.8). This indicates that none of the samples have reached peak oil generation. The Johan Castberg samples and also H1 and A1 seem to express the lowest maturity based on this plot (see Figure 7.8). Furthermore, the S samples and LH1 have almost reached equilibrium. All of the samples taken from Lerch et al. (2016b) appear to have reached the equilibrium threshold. It should be noted that both of the parameters are somewhat uncertain, as 20S/(20S+20R) is also influenced by facies, weathering and biodegradation, and ßß/(ßß+aa) can vary due to minerology (Peters and Moldowan, 1993).

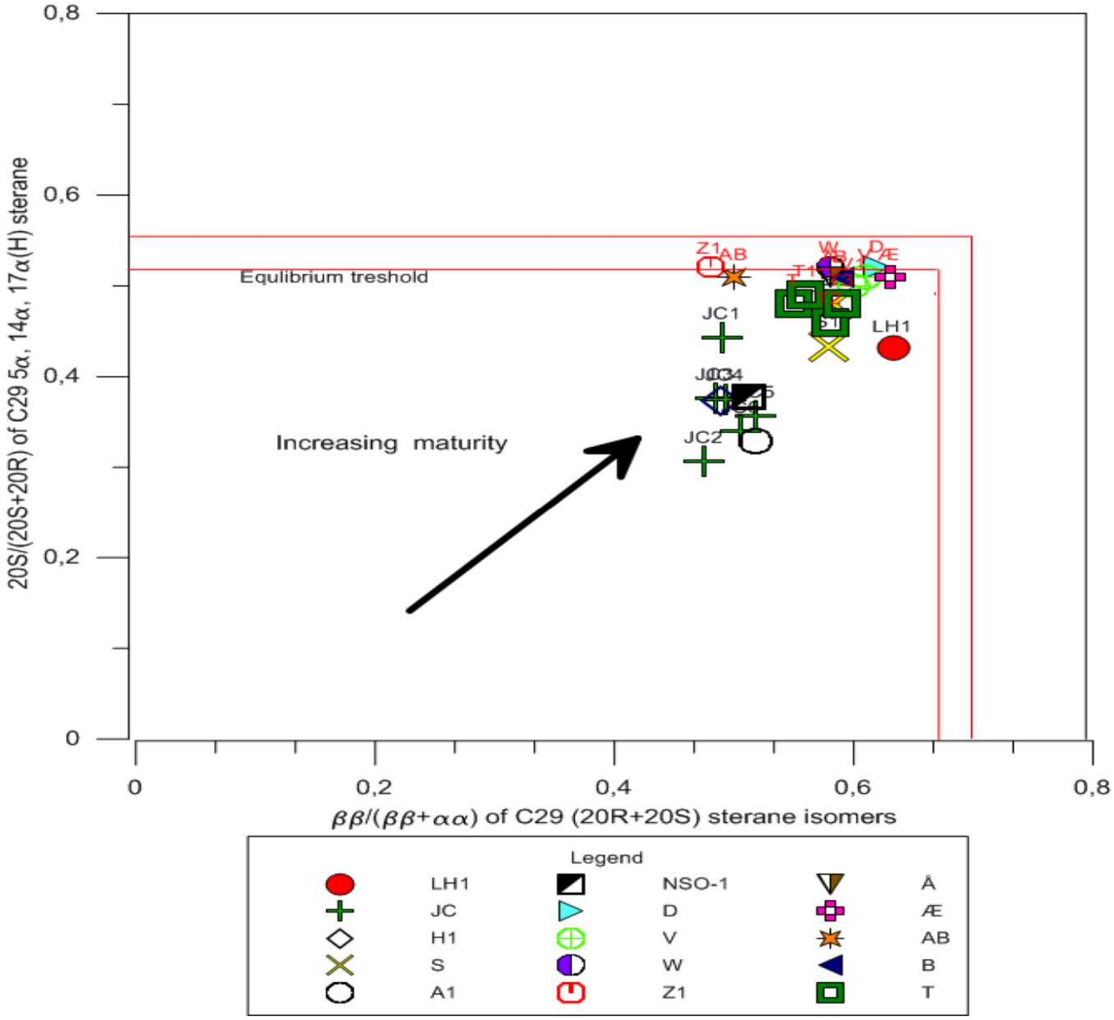

**Figure 7.8: The Figure illustrates the maturity of the samples based on saturated biomarkers. Figure 7.8 is a Table of ßß/(ßß+aa) (Mackenzie et al., 1985) versus 20S/(20S+20R) (Moldowan et al., 1986). The ratios of the oils and condensates produced from the laboratory work in this thesis are plotted with black labels and their respective names. The sample parameters taken from Lerch et al. (2016b) are plotted in red with their respective sample names. The ratios equiiliberate around $0.85R_0$% (peak oil). None of the oil and condensate samples analysed in this thesis seem to have reached the equlibrium treshold, for the 20S/(20S+20R) or ßß/(ßß+aa) ratios. However, all of the samples from Lerch et al. (2016b) seem to have reached equilibrium for 20S/(20S+20R) . The JC samples, A1 sample and H1 sample express the lowest maturtiy. The samples S and LH1 seem both to almost have reached the equilibrium treshold.**

## 7.3.2 Maturity assessment based on medium ranged maturity parameters

The biomarkers used in this section are based on the GC-MS, the m/z ratios used were 178, 192 and 198. From m/z=178 the phenanthrene peak can be identified, from m/z=192 the methylphenanthrene abundance can be identified and for the m/z = 198 chromatogram the methyldibenzothiophenes can be identified.

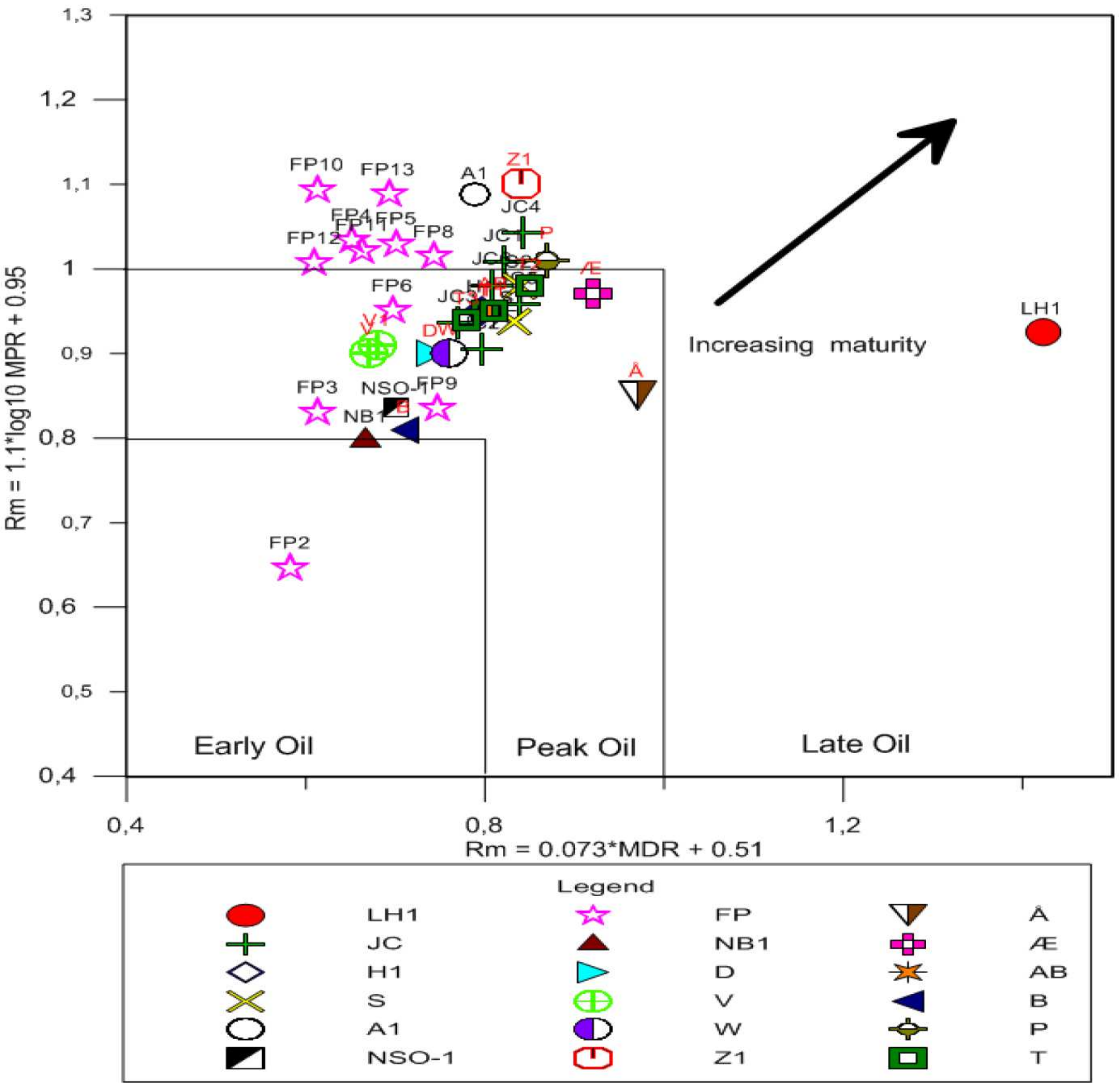

**Figure 7.9: This Figure illustrates the maturity of the samples based on aromatic isomers. The Figure is a Table of Rm = 0.073*MDR + 0.51 (Radke, 1988) versus Rm = 1.1*log10 MPR + 0.95 (Radke, 1988). The ratios of the oils and condensates produced from the laboratory work in this thesis are plotted with black labels and their respective names. The sample parameters taken from Lerch et al. (2016b) are plotted in red with their respective sample names. All samples plot within or close to the "Peak Oil" generation. Sample Å is estimated to the lowest maturtity and A1 to the highest. Most of the sampels plot within the "Peak Oi"l range. A large amount of core samples seems to be within the Late Oil window. The outliers are LH1, Å and FP2.**

The MDR ratio is viewed as a very reliable maturity indicator, relatively independent of variability in the source rock. Nonetheless, Radke (1988) mentions that variabilities related to kerogen II and III have a significant impact on the ratio of immature to mature samples. Oil-prone source rocks at early maturation stages (0.4-0.7%Ro) show MDR ratios <1.0, whereas immature gas source rocks typically elevate the ratio to levels of about 2.5 (Radke et al., 1986). Based on Figure 7.13 and 7.14 the samples from this thesis seem to plot somewhere in between kerogen type II and III, possibly leaning towards kerogen type II. Looking at Figure 7.9 the biggest surprise is possibly the extremely high maturity of the LH1 sample due to the high ratio of MDR, and the relatively high maturity of the Å sample also from the Loppa High situated in the Formations from the same geological era (Late Carboniferous-Early Permian). By examining the GS-MS chromatogram m/z=198 in Figure 6.5 and appendix C of the LH1 sample, it is evident the high ratio is due to an extremely low MDBT 1 peak. As mentioned above this can be a consequence of different sources or simply high maturity. Radke et al. (1986) stated: MDBT 1 for type II kerogen showed a relative concentration decrease above 0.55%Ro, consequently increasing the MDR ratio. Furthermore, a relative decrease in the MDBT 1-isomer for type III kerogen was observed above 0.8%Ro. The same results is also reported by (Radke et al., 1982a). This may indicate a type II source rock for the LH1 and Å sample since the degradation of MDBT 1 is extensive. However, one could argue for the contrary, as the starting ratio for this parameter in kerogen type II is lower than type II for immature oils.

The origin and type of the source rock will be further discussed in the chapter on organic facies. The core samples from the Finnmark Platform and Nordkapp Basin seem to have a lower MDR ratio compared to the MPR. As previously mentioned the S/N ratio for these samples was low, consequently the maturity estimation is somewhat uncertain. Most of the core samples seem to plot within the late oil window, with a few exceptions plotting at lower maturities (see Figure 7.9). Sample Æ, Z1 and A1 express a higher maturity than the rest of the sample set (late Oil). This is in agreement with the previous estimated maturities. The Z1 sample from the FP seems to have the same grade of thermal maturity as most of the FP cores (see Figure 7.9). The samples are taken from the same depositional environment and geological time (Late Carb-Permian). The general trend is that, based on the MDR ratio for the FP samples and NB1 sample, the core samples display low maturity (see Figure 7.9). The reason for this is somewhat unclear, however, it is stated by Bao and Zhu (2009) that MPR ratio decreases with increasing level of biodegradation and this could certainly be a factor to consider.

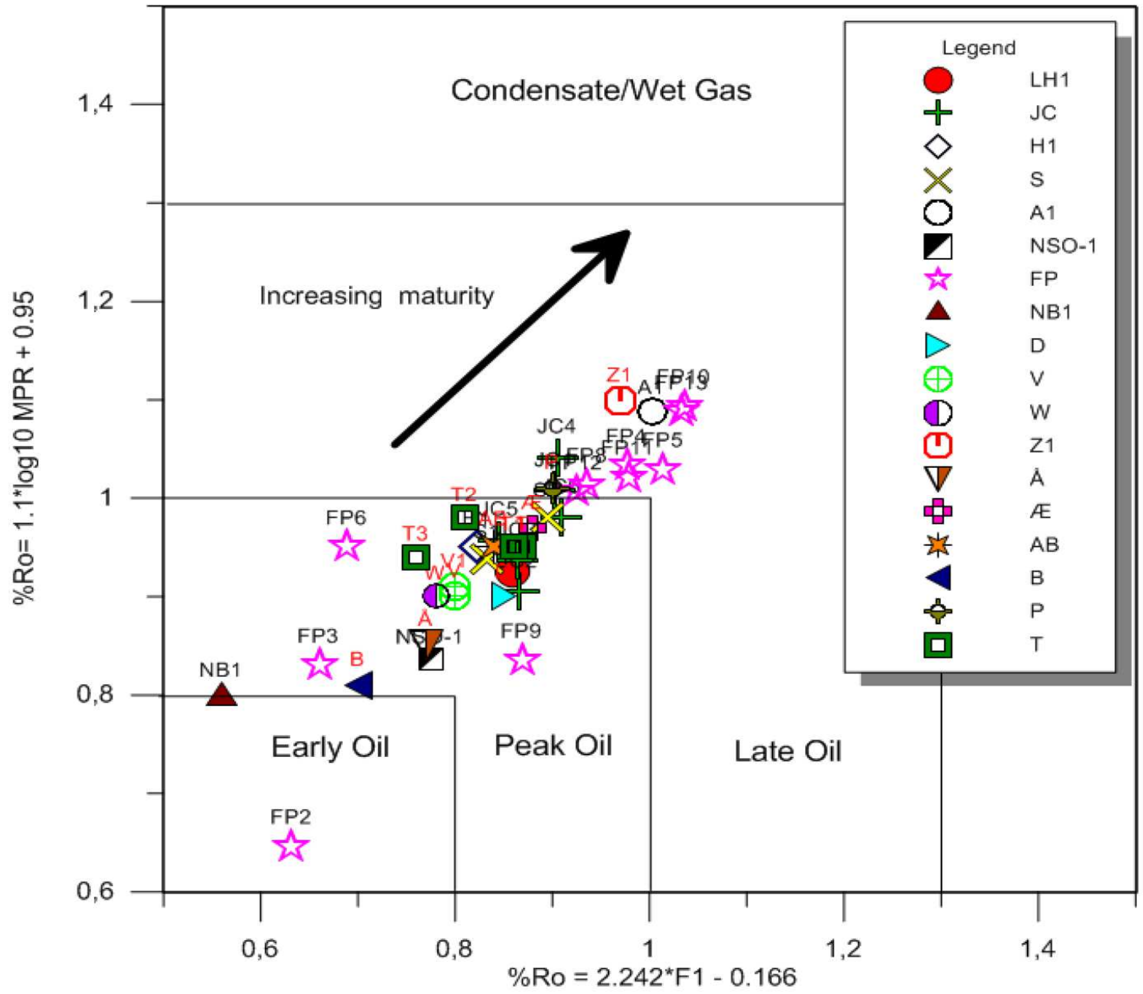

**Figure 7.10: The Figure illustrates the maturity of the samples based on aromatic isomers. The Figure is a Table of %Ro = 2.242*F1 - 0.166 (Kvalheim et al., 1987) versus Rm = 1.1*log10 MPR + 0.95 (Radke, 1988). The ratios of the oils and condensates produced from the laboratory work in this thesis are plotted with black labels and their respective names. The sample parameters taken from Lerch et al. (2016b) are plotted in red with their respective sample names. All samples plot are within or close to the "Peak Oil" generation. A linear trend between the two paramters can be observed. Note that the Å and LH1 samples show a much lower maturity without the MDR vitrinite calculation.**

As observed from Figure 7.10 Z1 and A1 express the highest maturity in Figure 7.10. The plot expresses a linear trend for the samples starting in the middle of the peak oil generation continuing into the late oil window. Note that the Å and LH1 sample show a much lower maturity without the MDR vitrinite calculation. Some of the core samples show immature and scattering values (see Figure 7.10). This is believed to be a cause of low bitumen content resulting in low S/N ratios resulting in uncertain values, rather than actual low maturity .

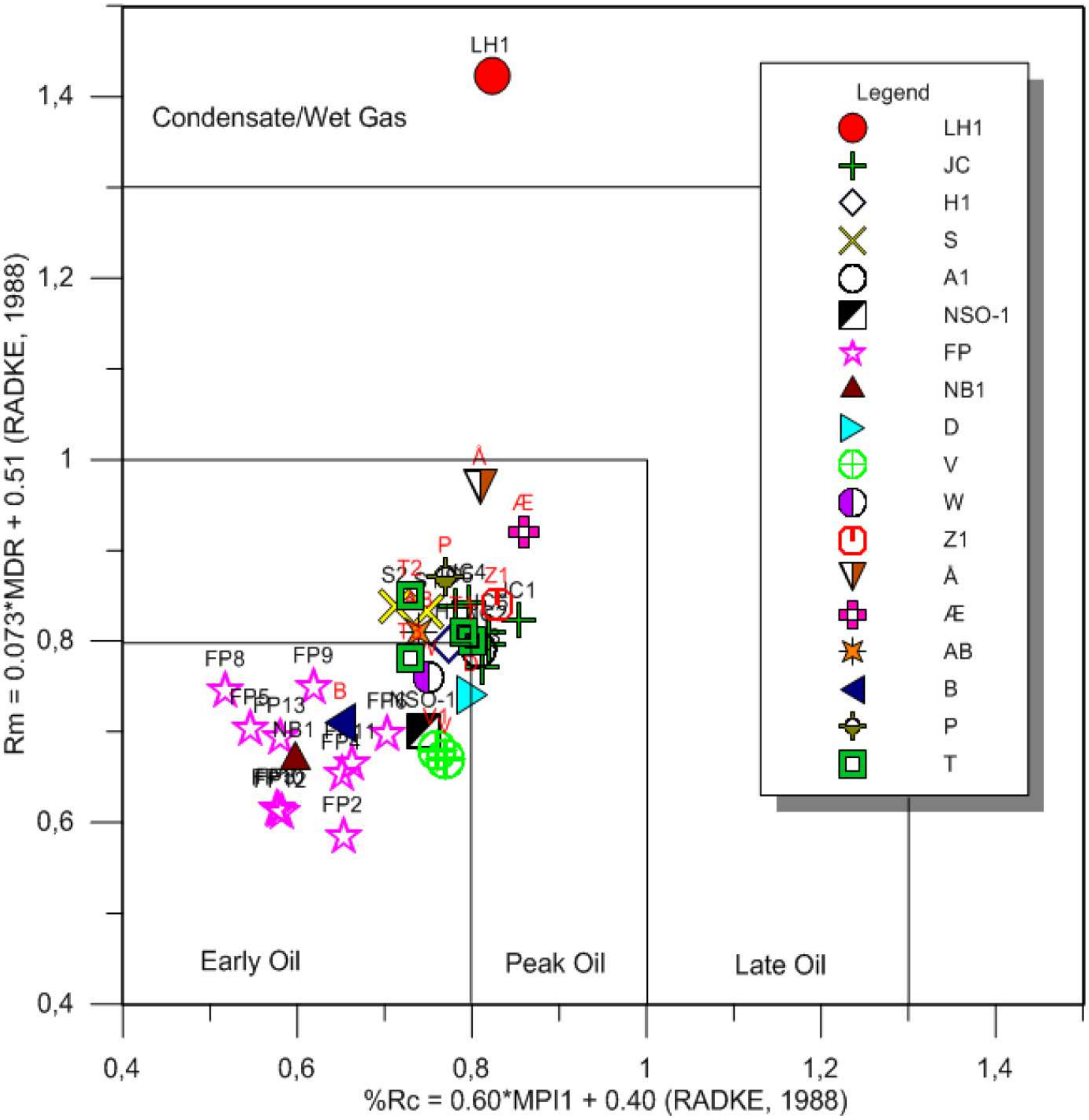

**Figure 7.11: The Figures illustrate the maturity of the samples based on saturated biomarkers. The Figure is a Table of %Rc = 0.60*MPI1 + 0.40 (Radke, 1988) versus %Ro = 2.242*F1 - 0.40 (Kvalheim et al., 1987). The ratios of the oils and condensates produced from the laboratory work in this thesis are plotted with black labels and their respective names. The sample parameters taken from Lerch et al. (2016b) are plotted in red with their respective sample names. All samples plot within or close to the Peak Oil production.**

Contrary to the MPR and MPDF, MPI1 also uses the phenanthrene (in the denumerator) relative abundance to calculate the vitrinite reflectivity. Albeit generally showing perfect correlation with optical vitrinite in coals, its use in oils and condensates has shown variable results (Karlsen et al., 1995). This molecule has one carbon number lower mass as compared to methylphenanthrene, and may for this reason be over represented in condensates (Karlsen et al., 1995). Consequently, one can observe a shift in the general maturity towards lower maturtites for condensates. Most of the oils and condensates now plot at the transition zone between “Early Oil” and “Peak Oil” (see Figure 7.11). The core samples seem to be skewed towards lower maturities, and plot within the “Early Oil” window (see Figure 7.11). The difference in competing stabilities between the α and β position of the methyl phenanthrene along with the more stable phenanthrene (more thoroughly explained in 5.3.6), may be the cause for this. Kvalheim et al. (1987) expressed concern about the MPI1 ratio, due to the use of molecular groups of negatively correlating variables; this would result in a non-linear ratio. Increasing redox potential of a source rock can enrich the phenanthrene concentration relative to the methylphenanthrene. This occurs due to secondary oxidation processed by metal bearing solutions in the rock (Püttmann et al., 1989). Another contributing factor to lower the relative phenanthrene abundance is microbial degradation (Budzinski et al., 2000, Peters et al., 2005). Moreover, depressed levels of phenanthrene can be related to highly reducing facies, caused by radical or ionic demethylation reactions (Szczerba and Rospondek, 2010). Consequently, the shift observed when introducing the MPI1 ratio can likely be related to reducing conditions in the depositonal environment. Further validation of this statement can be found in Figure 7.13 where most of the plots are leaning towards an reducing enviornment.

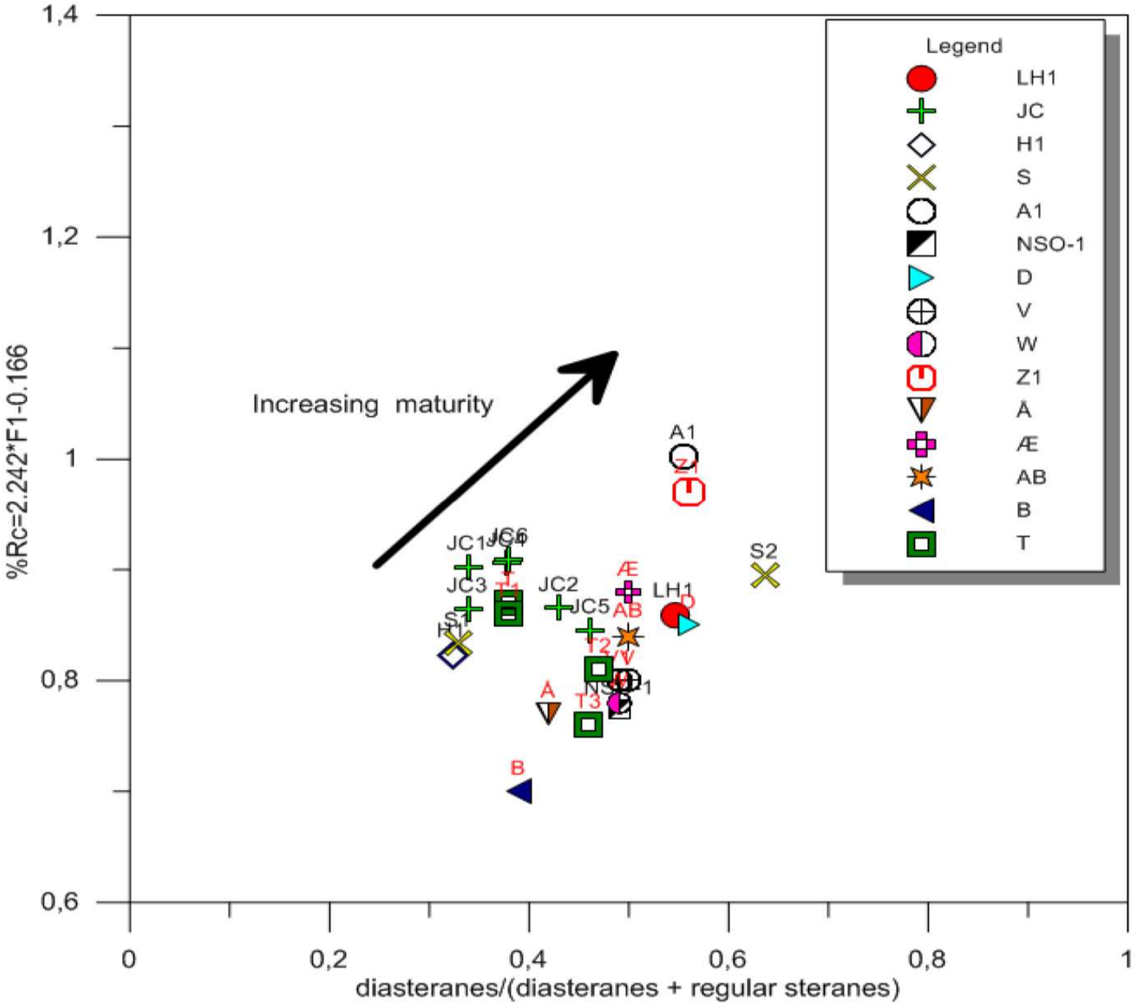

**Figure 7.12: The Figures illustrate the maturity of the samples based on saturated biomarkers. Figure 7.12 is a Table of diasterane/(diasterane + regular steranes)(Seifert and Moldowan, 1978) versus %Ro = 2.242*F1 - 0.40 (Kvalheim et al., 1987). The ratios of the oils and condensates produced from the laboratory work in this Thesis are plotted with black labels and their respective names. The sample parameters taken from Lerch et al. (2016b) are plotted in red with their respective sample names. All samples plot within or close to the Peak Oil production. Sample Å is estimated to be of the lowest maturtity and A1 to represent the highest.**

The two parameters plotted on the x and y axes seem to correlate quite well in terms of maturation (7.12). This gives some leverage to rule out the over- and underestimation affecting the diasterane/(diasterane + regular steranes) ratio due to lithology variations. The two condensates (A1 and S2) express a higher maturity along with sample Z1. The Loppa High sample B and Å indicates in this diagram, a surprisingly low maturity.

### 7.3.3 Summary of the maturity parameters

An attempt to summarize the maturities of the oils, condensates and core samples are proven difficult as there are a lot of variations for each sample deploying different parameters. Moreover, the biomarker maturity parameters and the medium range maturity parameters seem to express conflicting maturities for the oils and condensates. Table 7.2 summarizes the most probable maturities for the oils, condensates and bitumens analyzed in this thesis.

**Table 7.2: In the Table it is attempted to determine the most probable maturity window based on the biomarkers and the medium ranged parameters. The samples are arranged from lowest to highest maturities left to right. A quite significant variation can be seen in the estimated maturity based on the biomarkers compared to the medium range parameters for the oils and condensates. Where the biomarker parameters express lower maturity than the medium range maturity parameters.**

**Maturity Rank of the Source Rocks**

| Number | 1 | 2 | 3 | 4 | 5 | 6 | 7 | 8 | 9 | 10 | 11 | 12 |
|---|---|---|---|---|---|---|---|---|---|---|---|---|
| Maturity Window | - | - | - | - | - | - | - | - | - | - | - | - |
| Biomarkers | - | - | - | - | - | - | - | - | - | - | - | - |
| Medium Range par. | FP2 | NB1 | FP3 | FP9 | FP6 | FP12 | FP11 | FP8 | FP5 | FP4 | FP10 | FP13 |
| Maturity Window | Early Oil | | Early - Peak Oil | | | | | | | | Peak Oil | |

**Maturity Rank of the Oils and Condensates**

| Number | 1 | 2 | 3 | 4 | 5 | 6 | 7 | 8 | 9 | 10 | 11 |
|---|---|---|---|---|---|---|---|---|---|---|---|
| Maturity Window | Early Oil | | | | | | Early-Peak Oil | | | Peak Oil | |
| Biomarkers | JC1 | JC3 | JC2 | JC4 | JC5 | JC6 | H1 | A1 | S1 | LH1 | S2 |
| Medium Range Par. | JC3 | JC2 | JC5 | JC6 | H1 | JC1 | JC4 | S1 | S2 | LH1 | A1 |
| Maturity Window | Peak Oil | | | | | | | | | Late Oil | |

## 7.4 Organic Facies

The data produced by the GC-FID and the GC-MS are useful to determine the depositional environment of the studied samples. Parameters from non-biomarkers and biomarkers are used in conjunction to obtain the highest level of significance when determining the depositional environment, source of organic matter and the correlation between samples (Peters and Moldowan, 1993).

## 7.4.1 Organic Facies Tables

From Figure 7.13 most of the samples express intermediate maturity and no to minor biodegradation. The samples that stand out are: Z1, AB and NSO-1. They all seem to express higher maturity, this coincides well in terms with sample Z1 based on the maturity plots.

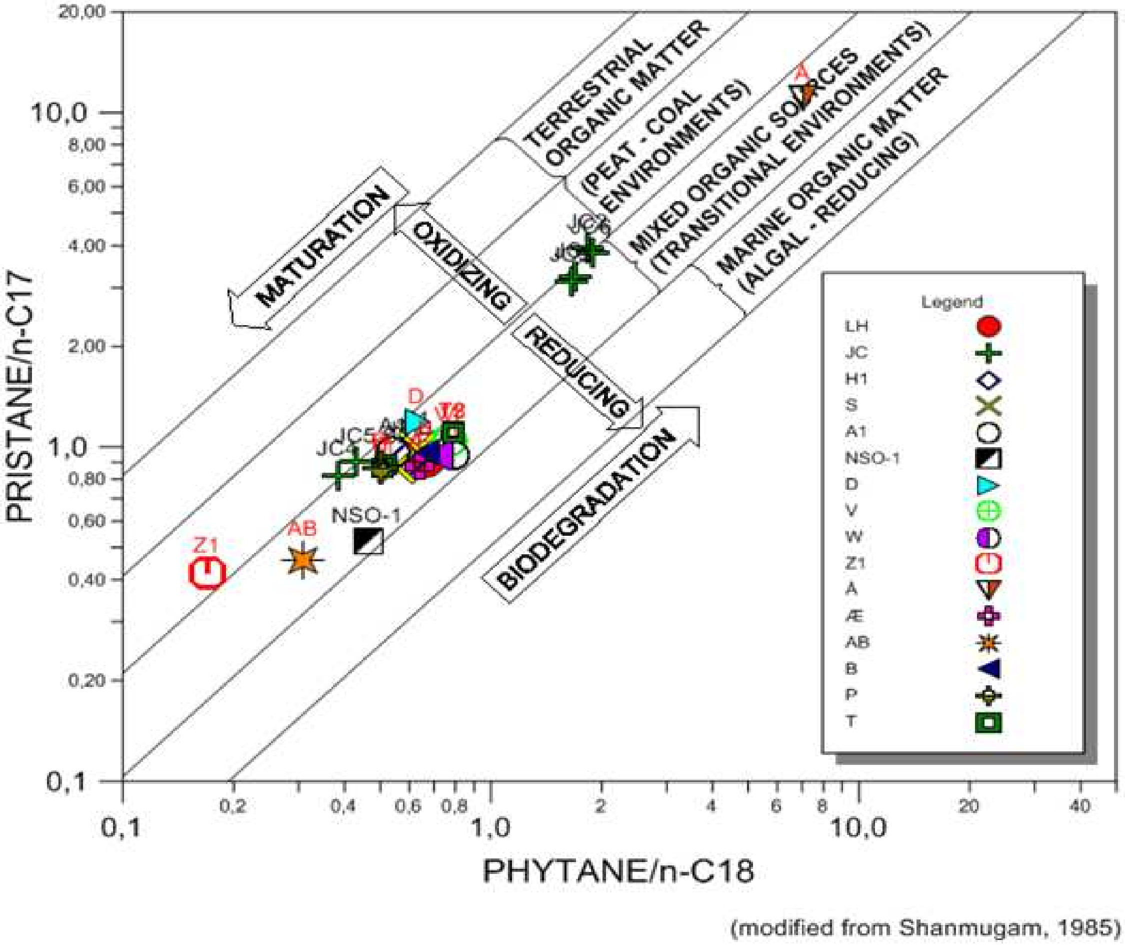

**Figure 7.13: Cross plot illustrating organic facies variation, maturity and biodegradation of the studied samples. The Figure is a Table of Phytane/n-c18 versus Pristane/n-17 (Shanmugam, 1985). Most of the samples are clustered in an area of medium maturity and no minor biodegradation. Within this cluster, samples like the LH1 and W seem to represent the most reducing paleo-depositional environment. Samples like JC4, JC5 and D seem to plot in-between a reducing and oxidizing environment. Furthermore, sample Z1 is the most mature sample, and this fits well with the results based on the maturity parameters in the previous section. The sample also leans towards an oxidizing environment. AB and NSO-1 also reflect a higher maturity. The counter parts are the JC1-3, JC6 and Å sample which all seem to be biodegraded. Sample Å is extremely microbial degraded.**

However, AB and NSO-1 did not express significant high values of maturation based on the previously discussed maturity plots (see Figure 7.13), and the Oseberg sample NSO-1 is generally considered to represent early-/mid-maturity with minor biodegradation (Dahl and Speers, 1985).

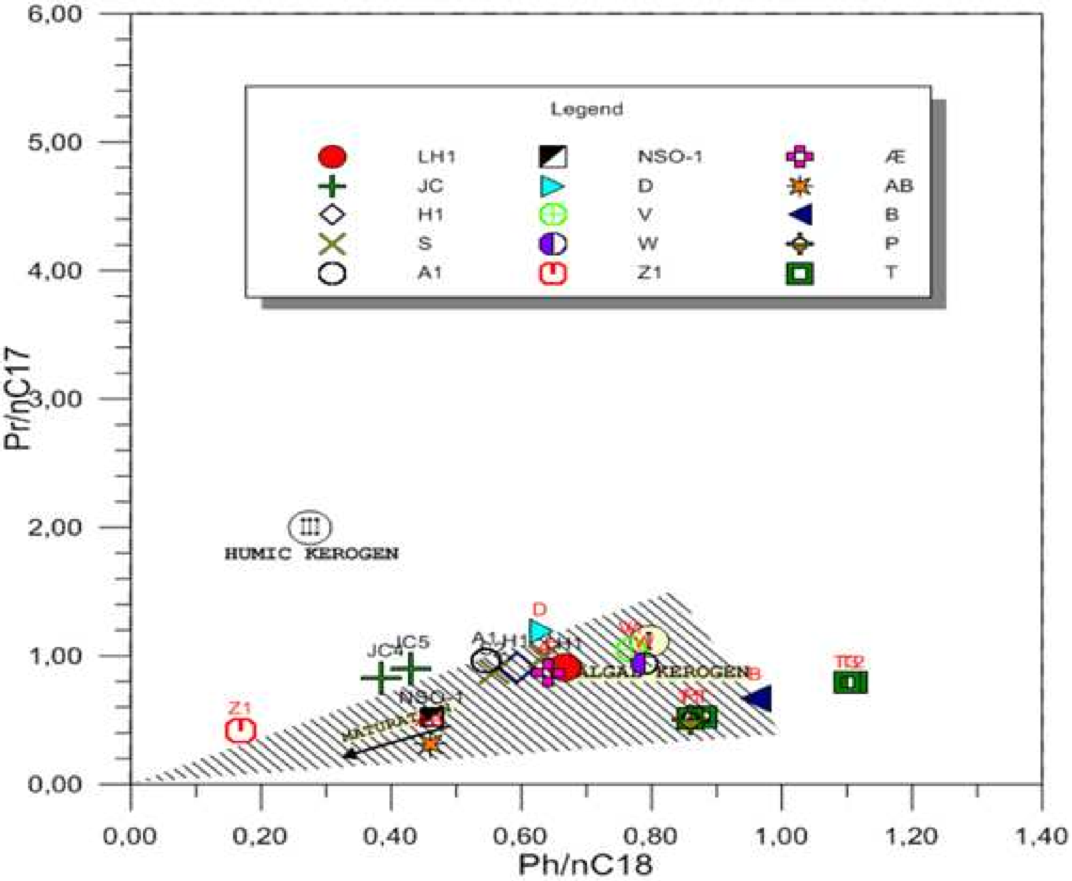

(modified from Connan & Cassou, 1980)

**Figure 7.14: Cross plot illustrating organic facies variation and maturity of the studied samples. The Figure is a Table of Phytane/n-c18 versus Pristane/n-17 (Connan and Cassou, 1980). The Figure expresses in principle the same as 7.13, but the scale of the ratios are not logarithmic but rather linear. Consequently some of the samples are more readily identifiable. The sample plot mainly in the algal kerogen area (type II). Note the two Goliath samples plotting in an area towards biodegradation. JC1-3, JC6 and Å have very high Ph/n-C18 and Pr/n-C17 values and plot out of range, illustrating the weakness of this plot.**

Furthermore, JC1-3 and JC6 indicate biodegradation which coincides well with the qualitative interpretation of the GC-FID chromatogram of the respective samples and the sample depth. Sample Å expresses a severe level of biodegradation (see Figure 7.13). The depth of the aforementioned sample is 1184m, hence biodegradation is expected due to the low temperature and likely access to oxygenated formation water. Still, discovery T and T1 from Goliat are found at depth 1148m and 1195m respectively. Based on Figure 7.13 and 7.14 they show no or little biodegradation. It is possible that the oil represented by these samples arrived so recently that they did not get biodegraded during the last glaciations (cf. Lerch et al., 2016a). Another curiosity is the T and T1 compared to T2 and T3, the former two samples seem to show a lower level of biodegradation and also a higher maturity based on Figure 7.13 and 7.14. This contradicts what the maturity plots expressed and what one would expect based on the depth of the respective samples (see Table 7.1 for depth). Although, the observed variations can be due to slight biodegradation of the T2 and T3 sample, this may also be the case for sample D.

The big majority of the samples plot within the mixed organic sources window (transitional environment), suggesting a mixed source of type II and Type III kerogen in a reducing environment, looking at Figure 7.14 most of the samples are within the kerogen I-II area. Furthermore, sample Z1 seems to originate from a peat or coal environment and the JC samples are in-between the peat/coal window and the transitional environment window. The NSO-1, LH1, B, V and W sample seem to originate from the most anoxic/dysoxic sources.

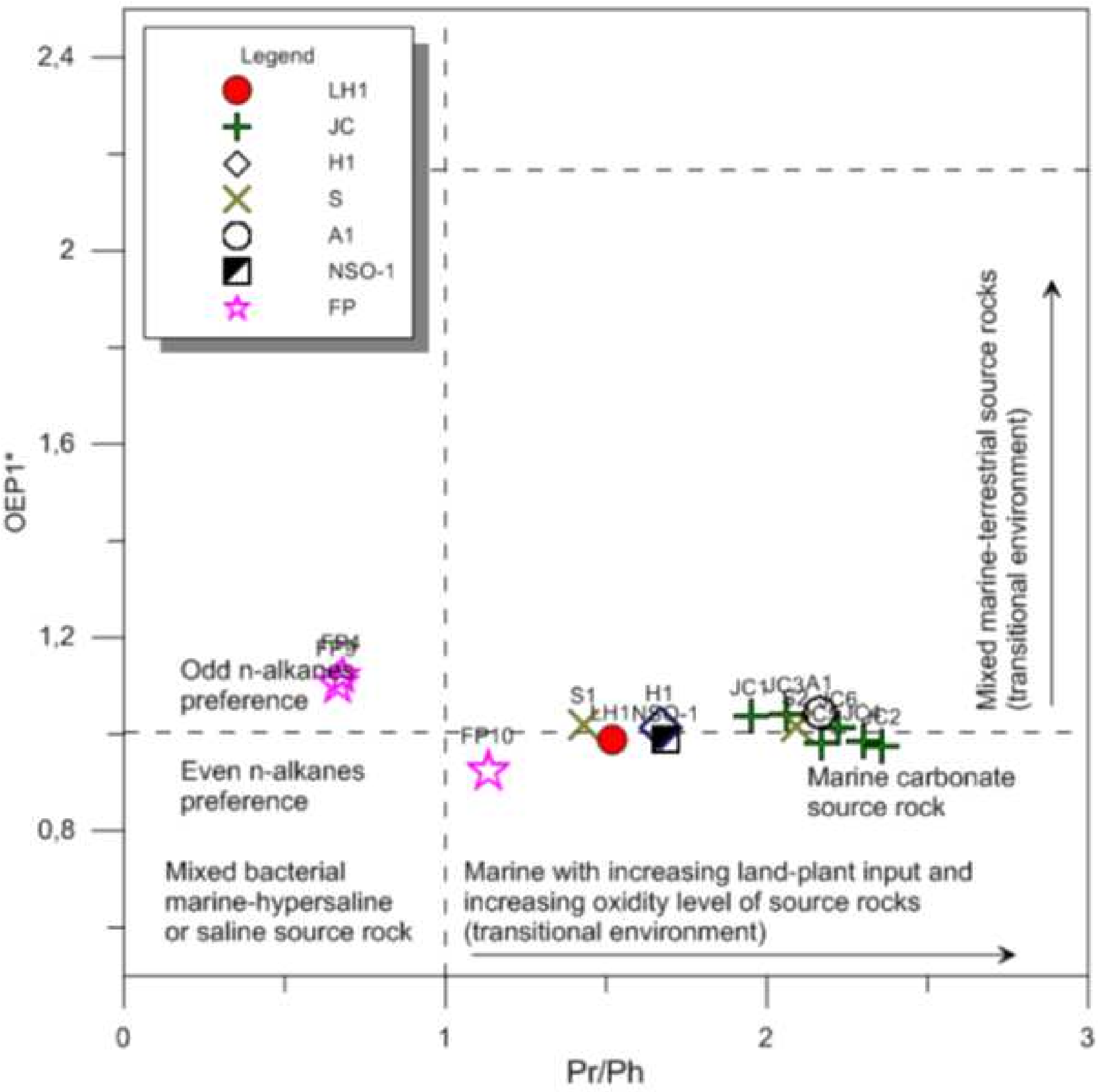

*OEP1: Improved Odd-Even-Predominance = (C21+6C23+C25)/ (4C22+4C24)

**Figure 7.15: Cross plot illustrating organic facies variation, maturity and biodegradation. The Figure is a Table of Phytane/n-C18 versus Pristane/n-C17 (Connan and Cassou, 1980). The majority of the sample set plot close to the unit value for the OEP parameter This is most likely due to the advanced maturity of the samples, i.e. a maturity towards 1%Rc and higher.. The few FP samples showing clear n-alkane distributions were also plotted. However, they seem to vary a lot and are uncertain.**

None of the oils and condensates seem to show any clear proof of lithology variations based. on the OEP values, with higher maturities OEP ratio tending to stabilize at unity and, most of the samples are probably too mature for the use of OEP as an lithology indicator. Based on CPI and OEP2 parameters, sample S2 expresses a clear even dominance which should reflect a carbonate rich source rock.

The core samples do, although this is probably due to poor chromatograms (see Figure 7.15). The LH1, S1, H1 and NSO-1 sample seem to have originated form source rocks with a higher input of algal organic matter (type II kerogen) compared to the rest of the samples, which seem to be more influenced by terrigenous input (type II-III kerogen).

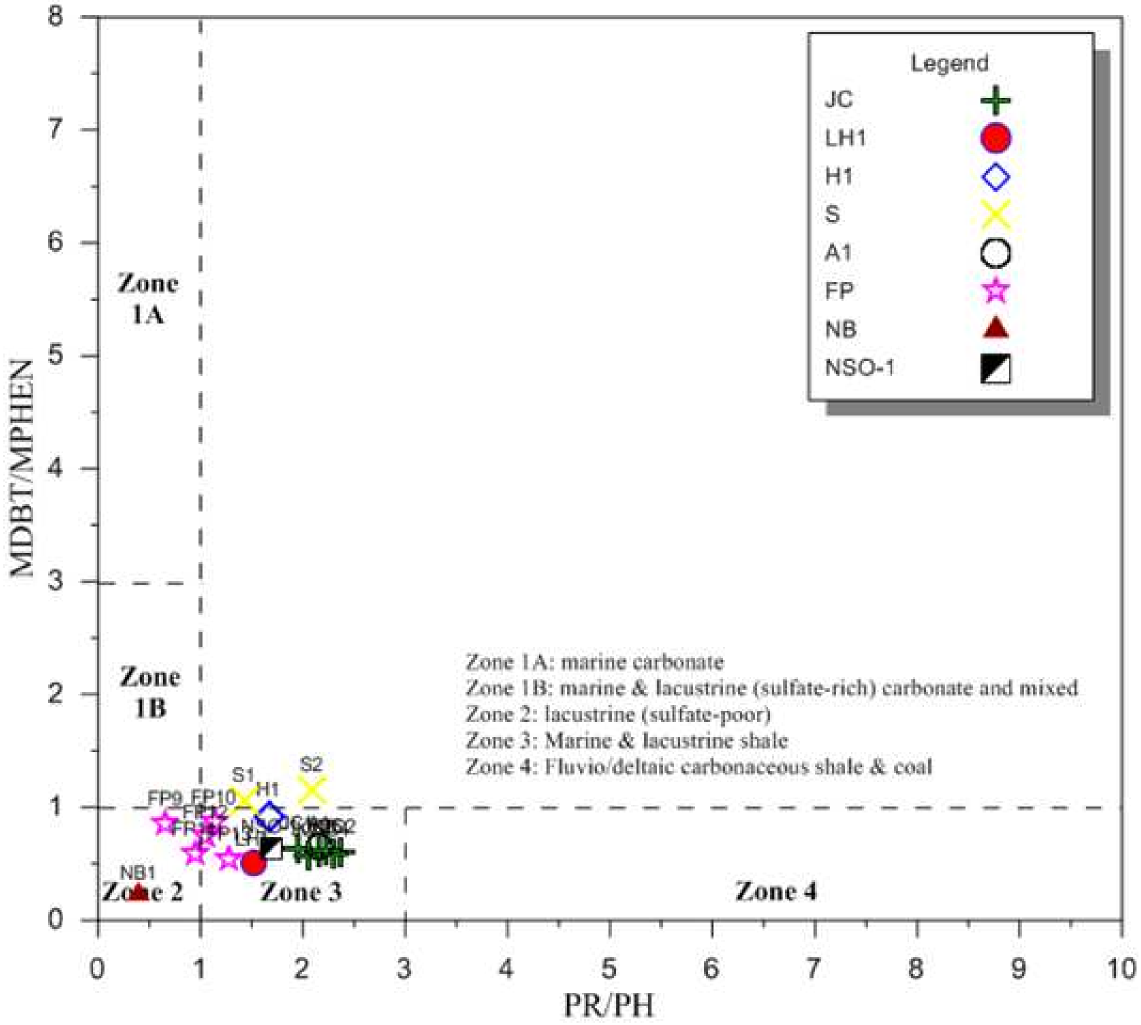

Modified from Hughes et al. (1995)

**Figure 7.16: Cross plot illustrating organic facies variation, maturity and biodegradation. The Figure is a Table of Pr/Ph versus MDBT/MPHEN (Hughes et al., 1995). All the condensates and Oils plot within the marine and lacustrine shale zone (zone 3), with the exception of S1 and S2. The core samples from the FP plot in the transition between zone 2 and zone 3, whereas the NB sample plot in zone 2.**

Figure 7.16 indicates that most of the oil and condensate samples originated from a shale source in a marine (mixed source) and that the input to this paleo-depositional environment was mixed type II and III kerogen.

The Snøhvit oils and condensate do not plot within zone 3 and the high MDBT/MPHEN lean towards a carbonate containing source rock. However, the ratio is close to one. Thus, determining if the lithology is carbonate or shale is difficult, and it is well known that the Hekking Formation is often containing carbonate (Halland et al., 2014). Regardless it is an indication of a sulfate rich source (Radke et al., 2001).

The Pr/Ph ratio appears to be too high for the aforementioned samples to indicate a carbonate source. Samples like H1 and some of the FP samples (FP9 and FP10) also express higher MDBT/MPHEN with calculated ratios right below one. The H1 Pr/Ph ratio is estimated to be too high for a carbonate rock (see Figure 7.15). The Pr/Ph ratios of the FP sample are generally lower, making a carbonate source a more likely scenario. Hughes et al. (1995) also report that the ratio can be lowered by phytane derived from archaebacteria in hypersaline environments and a reducing environment tend to lower the Pr/Ph ratio. The LH1 sample expresses the lowest MDBT/MPHEN ratio of the sample set (apart from the uncertain NB1 sample). This gives a strong indication of a silisiclastic shale source. The JC samples and A1 also express quite low abundances of MDBT compared to MPHEN.

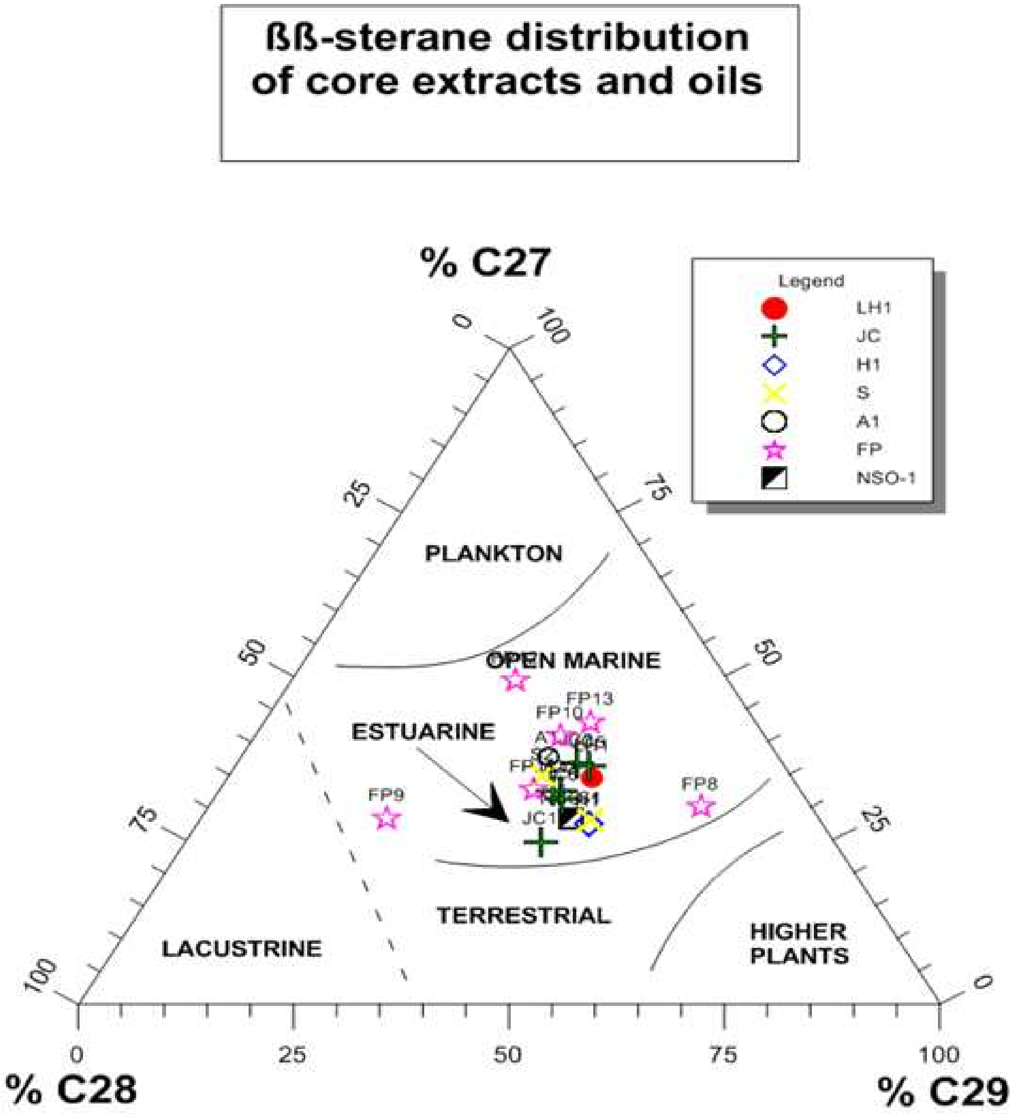

**Figure 7.17: The ternary diagram illustrates variations in depositional environment based on the relative distribution of C27, C28 and C29 steranes (Moldowan et al., 1985). The oils and condensates plot in a cluster within the open marine to estuarine zone, which is quite typical for oils on the NOCS, i.e. environments with Type II and III kerogen deposited in marine settings. Sample LH1, A1, S2, JC3 and JC5 have a higher C27 abundance, and are in-between the estuarine and open marine area. The FP samples added to the plot seem to be scattered somewhat randomly (modified from Shanmugam, 1985)**

The ternary diagram based on the sterane distribution indicates an estuarine depositional environment for the samples (see Figure 7.17). Some of the samples seem to have a higher C27 relative sterane amount and leaning towards an open marine depositional environment, e.g. A1, S2, LH1, JC3 and JC5. Note that generally condensate is relatively enriched in C27 steranes compared to C29, as a result of the carbon number distribution in in the front-end-biased condensates (Karlsen et al., 1995). Nevertheless, high C27 can also be a consequence of phase fractioning, where the lighter fraction will have a higher abundance of C27 sterane (Karlsen et al., 1995). The A1 and S2 condensates are likely influenced by this phenomenon; the variations between the lower C27 sterane abundance in S1 compared to S2 strengthen this proposition. The LH1 sample has also shown characteristics of a lighter oil fraction or condensate fraction with high C20/(C20+C28) and C28 TA/(C28 TA+C29 MA). Consequently the elevated C27 steranes values for the aforementioned sample can be a result of phase separation rather than an open marine environment. Likewise, this proposition cannot be excluded for the JC3 and JC5 sample either.

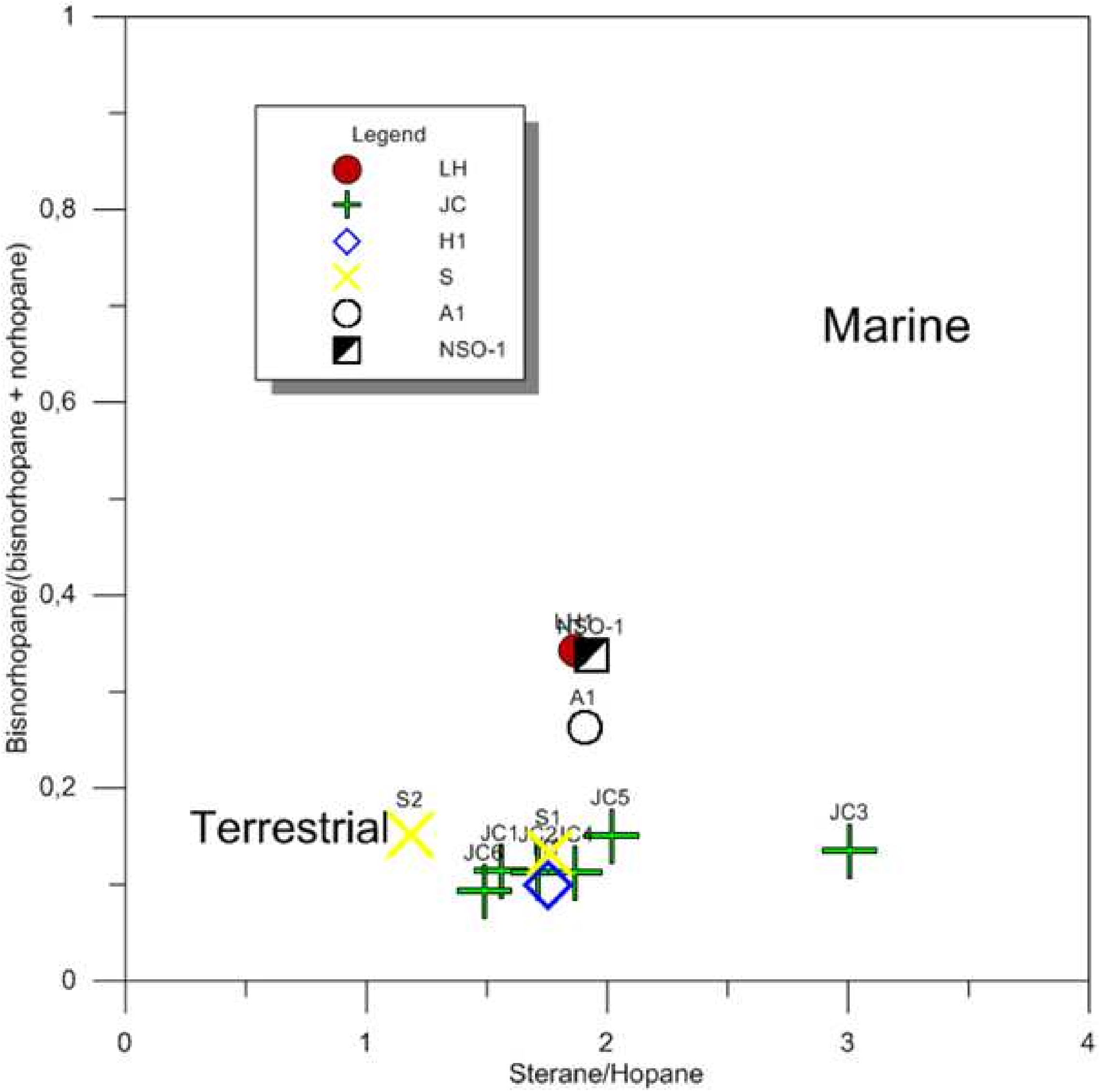

**Figure 7.18: The Figure is a cross plot of Sterane/Hopane (Tissot and Welte, 1984) versus bisnorhopane/(bisnorhopane + norhopane), (Wilhelms and Larter, 1993). The majority of the samples express low bisnorhopane (BNH) abundance, with the exceptions of A1, LH1 and NSO-1, indicating an anoxic marine depositional environment for these three samples. The sterane/hopane ratio is quite similar for most of the samples, with the JC3 as an outlier.**

Based on the BNH content of the samples LH1 and A1 seem to originate from a different source than the rest (Figure 7.18). Higher BNH abundance is reflecting an anoxic marine environment. However, sparse occurrences of BNH do not necessarily exclude anoxia (Peters et al., 2007). The remaining samples are interpreted to be more influenced by a terrigenous environment. BNH will degrade during thermal maturation, thus the variations could also reflect be a result of disparate maturities (Curiale et al., 1985). The sterane/hopane ratio will also vary with lithology, where high ratios are associated with shale and low ratios with carbonate.

### 7.4.2 Summary of organic facies

The sample set analyzed in this thesis express quite similar organic facies parameters. Some distinction can be drawn and are summarized in Table 7.3 of the sample analyzed in this thesis.

**Table 7.3: All of the samples seem to be from an estuarine/marine transitional environment, the Table divides the samples further into three possible groups. [1]The group is first and foremost based on the higher bisnorhopane content (see figure 7.18).**

| **Marine to estuarine, mixed organic sources in a reducing environment (Ker II/III)** | | | |
|---|---|---|---|
| Shale with a higher input of a terrestrial source | | Shale mostly marine input (more anoxic)[1] | Influenced by carbonate |
| FP4 | JC1 | LH1 | S1 |
| FP8 | JC2 | A1 | S2 |
| FP9 | JC3 | | |
| FP10 | JC4 | | |
| FP11 | JC5 | | |
| FP12 | JC6 | | |
| FP13 | H1 | | |

## 7.5 Biodegradation

### 7.5.1 Biodegradation based on temperatures at present day

Bacterial degradation of petroleum is optimal in surface or near-surface temperature, and temperatures exceeding 60-80°C are the upper limit (Peters et al., 2005). The western Barents Sea has general geothermal gradient trend of ~31 °C/km based on the bottom hole temperatures (BHT) of the area and a geothermal gradient of ~35 °C/km based on DST samples by NPD. (2016b). The general geothermal gradient trend seems to fit quite well with the bottom hole temperatures measured in well 7120/2-1 (LH1), 7220/5-1(JC1-JC3), 7220/7-1 (JC4-JC5), 7220/8-1(JC6), 7220/6-1 (S1 and S2). Assuming a temperature at the sea bed at 4°C and the variation in water depth and Kelly Bushing elevation the gradient for well 7120/2-1, 7220/5-1, 7220/7-1 and 7220/6-1 are:

**7120/2-1**: $\frac{97\ ℃-4℃}{2.820\ \text{km}-0.386\text{km}-0.023\text{km}} = 38.57\ ℃/\text{km}$

**7220/5-1:** $\frac{52\ ℃-4℃}{1740.0\ \text{km}-0.388\ \text{km}-0.040\text{km}} = 36.59℃/\text{km}$

**7220/7-1:** $\frac{72\ ℃-4℃}{2229.0\ \text{km}-0.365\ \text{km}-0.040\text{km}} = 37.28℃/\text{km}$

**7220/6-1**: $\frac{46℃-4℃}{1.540\ \text{km}-0.368\text{km}-0.025\text{km}} = 36.62\ ℃/\text{km}$ ,

BHTs for the other wells are not given. The temperatures express slightly higher geothermal gradients than the general trend of the Barents Sea.

### 7.5.2 In-situ temperature for oils and condensates

Based on the present day depth of the samples used in this thesis and the geothermal gradient, all of the samples (excluding H1, since the depth is unknown) from the reservoir strata exceeds optimal temperature for biodegradation (surface temperature or near surface temperature (Peters et al., 2005). However, JC1-JC3 and JC6 seem to be withing semi-optimal temepratures for biodegradation (about 45 ℃). The samples LH1, JC4, JC5 and A1 are estimated to be from reservoirs at about 60 ℃. At temperatuers equal to or above 60 ℃ biodegradation is very unlikly. Even more so, for the S1 and S2 samples where the temperature ranges between 70-80℃, it is important to note that biodegradation cannot be confidently excluded, as it may have occurred in the past at shallower depth, or as bacteria have been reported to live at 250 ℃ (Baross and Deming, 1983). Still, such bacteria are possibly not responsible for degradation of commercial quantities of oil (Peters et al., 2007). However, these temperatures are estimated for present day, and lower temperatures cannot be ruled out in the past. Given the history of the Barents Sea with several phases of subsidence and uplift i.e. tectonism (Gabrielsen et al., 1990), and also eustatic events, different subsurface temperatures are highly likely. Rapid sedimentation or erosion can also alter the geothermal gradient (Bjørlykke, 2015). Based on the temperature estimations for the respective wells, biodegradation discoveries like LH1, JC4 and JC5 could be a likely scenario (see figure 7.19). The reason why there is no clear evidence of biodegradation can be explained the proposition by Wilhelms et al. (2001), where recent uplifted areas which were exposed to high temperatures are sterilized. Subsequently, the system will not contain any microorganisms even though the temperatures are probable for microbial degradation. Moreover, based on the methylphenanthrene and methyldibensothiophene parameters the shallow core samples plot within the early to peak oil window (some samples even suggest the late oil window). Consequently the remnants seem to have been generated and migrated from its source. This strengthens the suggesting of heavy biodegradation of the bitumen contra restriction of petroleum migration into the Formations due to low porosity and bad communication between pores.

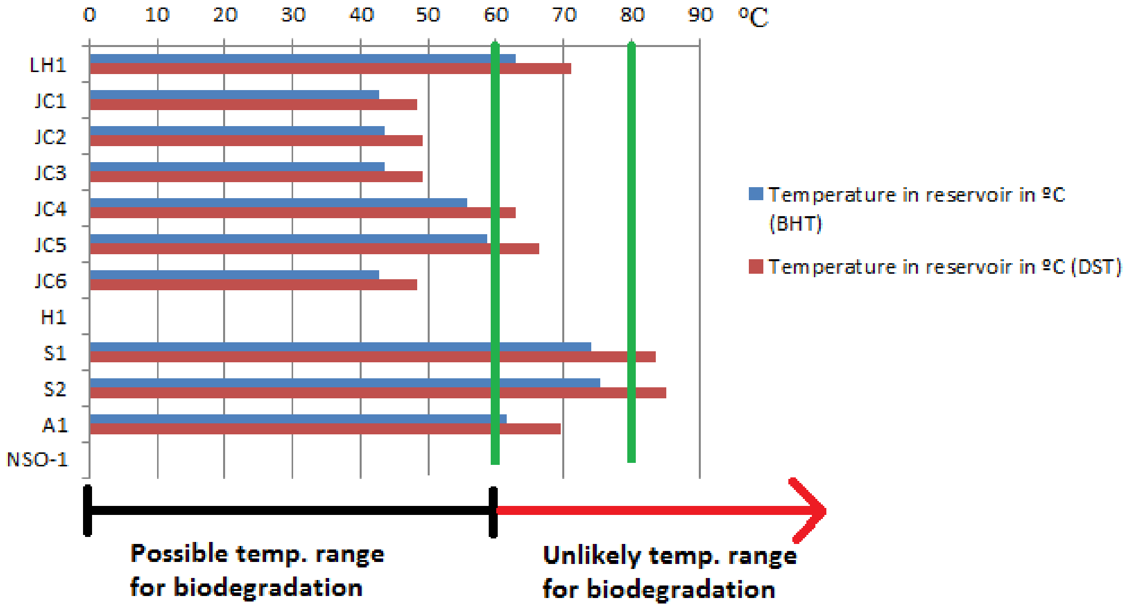

**Figure 7.19: Estimated temperature for the oils and condensates based on the general trend of bottom hole temperatures and drill stem tests taken from (NPD., 2016b). The green lines marks the range were microbial degradation alters (60-80 °C).**

## 7.6 Oil/condensate families and mixing of sources

The existence of multiple source rocks in the Barents Sea (Ohm et al., 2008) and the formation of structural highs and basins, increase the possibility for maturation of several source intervals to expel petroleum and fill reservoirs in the area. Consequently, oil and gas discoveries in the SW Barents Sea are likely to be a mix of several source rocks. Mixed source rocks will naturally express conflicting maturity and organic facies estimations. Ohm et al. (2008) constructed a map suggesting where the Permian, Triassic and Jurassic strata are oil mature, based on $R_0$ from wells in the area, semi-regional maturity trends and depth maps the Figure can be seen in chapter 2. The map suggests that the Permian/Carboniferous source rocks are oil mature ($R_0 \geq 0.6$) around the Loppa High and the southern rim of the Finnmark Platform. In the less uplifted areas around the Loppa High, the Triassic succession is believed to be within the oil prone domain. The Upper Jurassic (Hekkingen Formation) strata together with the Triassic succession (Snadd, Kobbe, Klappmyss, Havert Fms) are believed to be oil mature in the Hammerfest Basin, while the Triassic source rocks are estimated to produce oil on the Bjarmland Platform and in the Nordkapp Basin.

The $C_{24}$ tetracyclic terpanes are likely to be found in greatest quantities in carbonate-evaporitic source rock environments (Connan et al., 1986). On the contrary Philp and Gilbert (1986) suggested that a terrestrial-derived source would contain the highest abundance of $C_{24}$ tetracyclic terpanes. In Figure 7.20 the ratio of tetracyclic terpanes plotted with tricyclic terpanes show linear trends with changing maturities. This diagram was concluded by Lerch et al. (2016b) to be an indicator of pre-Jurassic and Jurassic petroleums.

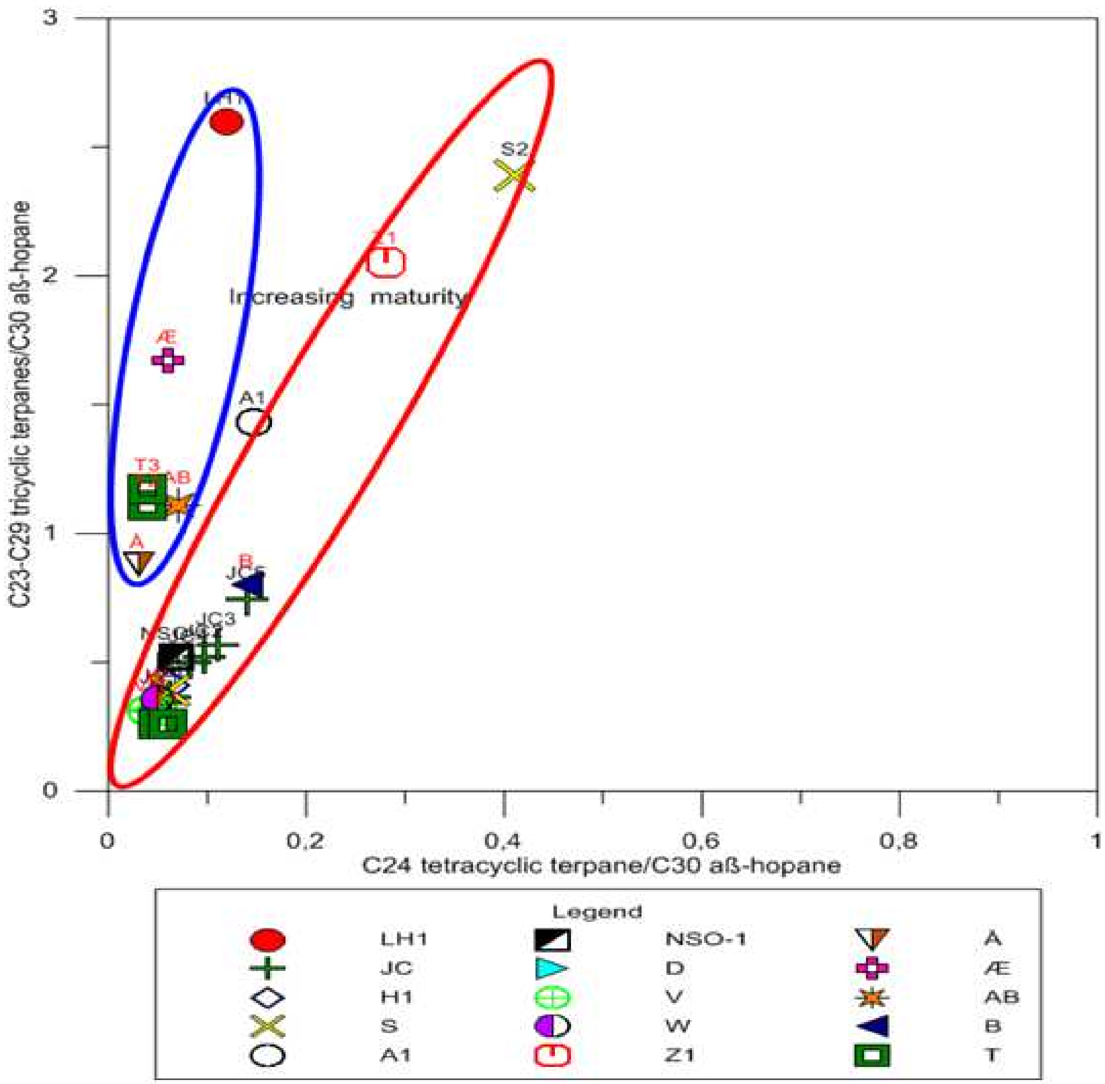

**Figure 7.20: The cross plot is taken from Lerch et al. (2016b), with the addition of samples from this thesis. The Figure is a cross plot of the C24 tetracyclic terpane/C30 aß-hopane (Mello et al., 1988) versus C23-C29 tricyclic terpanes/C30 aß-hopane (Mello et al., 1988). The oils and condensates can be divided into two chatogories based on low and high C24 tetracyclic terpane/C30 aß-hopane ratios, the red ring show a linear correlation for the samples with higher high C24 tetracyclic terpane/C30 aß-hopane ratios when plotted with the tricyclic terpanes over hopanes, the blue circle illustrates the other family with lower C24 tetracyclic terpane/C30 aß-hopane ratios. The two families were interpreted by Lerch et al. (2016b) and Bjorøy et al. (2010) to originate from a Jurassic source (red circle), and a pre-Jurassic source (blue circle) respectively.**

### 7.6.1 The LH samples

The LH1 sample expresses different maturity characteristics compared to the rest of the sample set and based on the MDBT/MPHEN ratio, and the BNH content the sample seems to express a siliclastic source from a marine environment. Figure 7.20 indicates that the LH sample is of pre-Jurassic origin, which is in compliance with what Lerch et al. (2016) found. The ETR ratio of 2.16 further supports a pre-Jurassic origin. However, (Ohm et al., 2008) viewed the ETR ratio of the LH1 sample as too low for a Triassic source and proposed a Paleozoic source. The conflicting maturity and organic facies parameters can be a consequence of mixing, the GC-FID chromatogram of the respective sample also provides a support to a model of a mix of petroleums (see Figure 6.4 and appendix B). The Å discovery expresses the closest similarity to the above mentioned sample based on the maturity parameters (see Figure 7.5B, Figure 7.9), whereas adjacent wells from the Cretaceous express lower maturities (sample B and D from Lerch et al. (2016b)). Moreover, the two samples from the Loppa High plot in the pre-Jurassic zone shown in Figure 7.20, and the B and D samples appear to be Jurassic sourced based on Figure 7.20. The LH1 and the Å sample are found in Formations from the Late Carboniferous-Early Permian and might be from the same Paleozoic source. Lerch et al. (2016a) related the $C_{10+}$ fraction of the LH1 sample to a source of higher maturity than the surrounding wells, and the light hydrocarbon fraction could be of the same origin for the respective wells. Furthermore, the light hydrocarbon fraction filling these discoveries is believed to be live (Lerch et al., 2016a, Ohm et al., 2008). This is further supported by Vadakkepuliyambatta et al. (2013), who reported active fluid flow systems in the Bjørnøya Basin west of the Loppa High.

However, some discrepancies can be discerned between sample LH1 and sample Å, e.g. tricyclic terpanes and diahopane/(diahopane + normoretan). This can be a consequence of biodegradation, and as shown in Figure 7.13 the Å sample is severally biodegraded and the depth of the discovery is 1184m which will result in temperatures allowing for biodegradation. Biodegradation will start to attack biomarkers as tricyclic terpanes before many of the other biomarkers (Wang et al., 2001), and severe biodegradation will degrade diahopane (Peters et al., 2007). Nonetheless, another possible explanation for the maturity variations could be that the Å sample is not sourced by the light hydrocarbon fraction. If that is true the migration path could possibly come from the Hammerfest Basin and won't reach all the way to the Å sample located Bjorøy et al. (2010) suggested the Upper Permian Ørret or Røye Formations to be the most probable Paleozoic sources in the area. The Røye Formation seem to consist mostly of carbonate in the area, as the LH1 sample show no evidence of a carbonate source, it could very likely be the shaly Ørret Formation to be the source. The Formations in which the LH1 and Å are found, are tilting towards the E-NE. The Ørret and Røye Formation can be found at 3km depth in the eastern part of the Loppa High (Halland et al., 2014), which is well within the oil window based on the geothermal gradient of the area. Henceforth, the Paleozoic sources could be filling the discoveries following the same Formations up-dip. The only samples containing hydrocarbon compounds from a Triassic/pre-Trassic source on the Loppa High are found in Late Carboniferous/ Permian/ rocks (based on this sample set), while discoveries in younger Formations do not. This can further support a model in which source and reservoir to be within the same Group or Formation. However, this suggestion requires a migration pathway for the petroleum. Nonetheless, the Æ sample at the Bjarmland Platform close to the boarder of the Loppa High also indicates a pre-Jurassic source (see Figure 7.20). These samples express generally high maturities based on every maturity plot. Lerch et al. (2016) proposed the Æ sample to be generated from a single source, which did not contribute to any of the other discoveries in the area.

### 7.6.2 The JC samples

The JC samples express similar attributes based on the maturity plots and organic facies, with the exception of degraded n-alkanes due to biodegradation of the samples JC1-3 and JC6. The ETR value for the six samples ranges from 0.50-0.83, which is low indicating a Jurassic source. Subsequently the samples plot within the Jurassic sourced family based on Figure 7.20. Liu (2013) suggested that the Snadd Formation to be the source rock filling the JC field. This seems highly unlikely based on biomarker data obtained in this thesis. The oils discovered in the JC field are believed to be sourced by a paleo-oil and a lighter live hydrocarbon fraction (Matapour, 2013). Matapour (2013) suggested the paleo-oil to be biodegraded, furthermore, he suggested that the Spekk Formation was gas-prone to the west of the field and a possible source rock for the lighter fraction. The Spekk Formation is not found in the Barents Sea (NPD., 2016b). However, the equivalent Hekkingen Formation for the Barents Sea is (NPD., 2016b). The biodegradation of the oil fits well with the slightly elevated UCM that all of the Johan Castberg samples express (see Figure 6.5-6.10 and appendix B). Subsequently, the new gas charge seems to be further biodegraded in the shallow samples JC1-3 and JC6, with low n-alkane peaks and elevated Pr and Ph peaks. The question is whether this implies that charging of the shallower discoveries has ended, or is biodegradation occurring at a more rapid pace than fresh infill can keep up? Nevertheless, the same source rock is probable for the two charges, with different maturities of the source rock and the Hekking Formation would be the most likely source. The discoveries are situated in Formations from Middle Jurassic (Stø and Normela Formation) West of the Loppa High platform, on the Bjarmøyrenna Fault complex and the Polheim Sub-Platform. It is interesting to note that these samples found in post-Triassic Formation seem to contain no pre-Jurassic derived oil in the area.

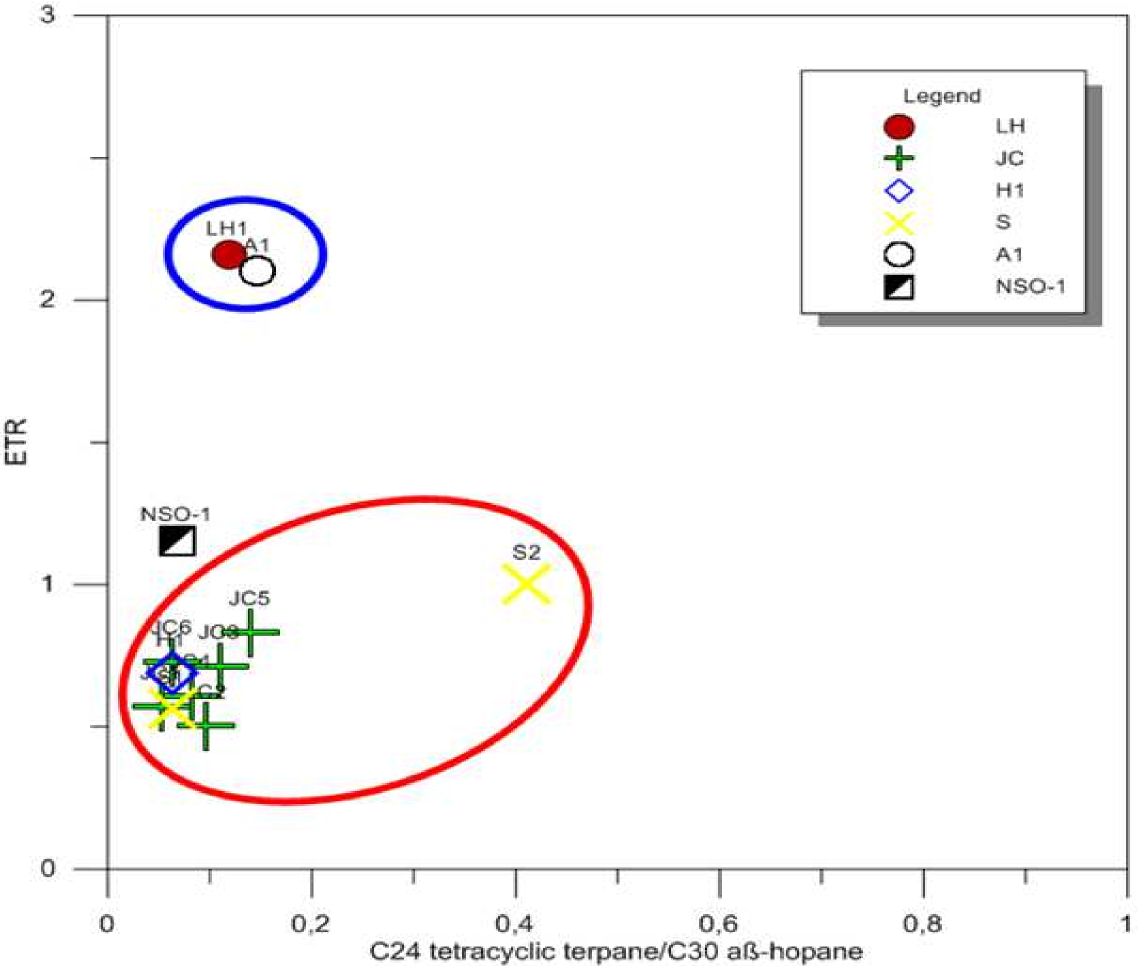

**Figure 7.21: The Figure is a cross plot of the C24 tetracyclic terpane/C30 aß-hopane (Mello et al., 1988) versus ETR (Holba et al., 2001). The group within the red circle is believed to be of Jurassic origin, and the two samples within the blue ring are probably of pre-Jurassic origin.**

### 7.6.3 The Heilo prospect (H1) sample

This sample also expresses a clear indication of mixing based on the n-alkane distribution of a light and heavier petroleum fraction (see Figure 6.11). Moreover, the ETR values and Figure 7.20 indicate a Jurassic source which is in agreement with what Kúld (2009) found based on the 24-norcholestane Ratio (NCR). The odd to even predominance ratios are also above 1 (see Figure 7.15 and Table 6.4), suggesting a shale derived source which is in accordance with the Jurassic Hekkingen Formation.

### 7.6.4 The S samples

The S1 sample shows a clear indication of mixing of two sources based on the GC-FID chromatogram i.e. one light and one heavier fraction (see Figure 6.12). Based on the even-over-odd number between n-$C_{18}$ and n-$C_{24}$, the S1 sample was interpreted to be carbonate-derived (Ohm et al., 2008). Henceforth, Ohm et al. (2008) suggested a Paleozoic source for the heavy hydrocarbon fraction, based on the fact that the most probable carbonate source in the area is of this age. This is contradicting to the results found in this thesis, where the CPI, OEP(1) and OEP(2) are 1.08,1.02 and 1.10 respectively (see Figure 7.15). However, the CPI and OEP ratios calculated in this thesis are based on the heavier fraction of the n-Alkanes (n-$C_{21}$ to n-$C_{30}$), and might explain the discrepancies. The MDBT/MPHEN ratio is also high compared to the rest of the sample set, thus pointing to a carbonate derived source (see Figure 7.16). Furthermore, the ETR values are low for the S1 and S2 samples, 0.56 and 1.00 and the sample plot within the Jurassic sources zone (see Figure 7.20). As mentioned in section 7.4 the Hekkingen Formation do also contain carbonate. The light hydrocarbon fraction is purposed by Lerch et al. (2016a) to be sourced from type II/III kerogen from the Triassic or Jurassic era. The question is why the ETR value is not higher and C24 tetracyclic terpane/C30 aß-hopane ratio less if this is the case? A possible answer could be a contribution of the pre-Jurassic source/sources which might be so low that it doesn’t affect these ratios.

### 7.6.5 The Alke structure (A1) sample

The A1 also expresses low maturities based on saturated and aromatic biomarker parameters compared to the medium ranged, where it plots as one of the most mature in the sample set. Again this could be a cause of mixing petroleums, although the n-alkane distribution shows no clear indication of mixing. Based on Figure 7.20 the sample seems to plot in-between the two main groups. The same was also reported by Bjorøy et al. (2010), and was explained by mixing from two sources, biodegradation, phase differences and higher maturity. Lerch et al. (2016a) proposed a long distance migration of the light hydrocarbon fraction, with a less mature $C_{10+}$ fraction contributing from a local source (Lerch et al., 2016). The Upper Jurassic Hekkingen Formation seems to be a possible source for the mature long distance migrated fraction. The ETR is 2.10 which is the second highest of the sample set, hence questioning the possibility of a Jurassic derived source. However, this could be due to the second source being of pre-Jurassic origin, and might originate from older strata in the Hammerfest Basin.

### 7.6.6 The FP and NB samples

The attempt to determine a source for these samples has proven to be difficult. However, the medium ranged biomarkers imply somewhat lower maturity than what is seen for the oils and condensates. Figure 7.16 suggests a shale source for the Finnmark Platform samples and the Nordkapp Basin sample, leaning towards a lacustrine environment (sulfate poor). The Z1 sample analyzed by Lerch et al. (2016b) taken from Late Permian rocks on the Finnmark Platform are proposed by Van Koeverden et al. (2010) to be sourced from Lower Carboniferous coals in the Tettagras Formation, this is also in agreement with what is shown in Figure 7.13. This could be the source of the core samples in the Finnmark Platform, however the Pr/Ph ratios are likely too low for a coal source, a factor which could point to a co-contribution from shales. The source for the single sample from the Nordkapp Basin is unknown.

## 7.7 Migration pathways

The Middle part of the Hammerfest Basin seems to be heavily dominated by light hydrocarbons, and remnants of paleo oil have been found in many locations (Knutsen et al., 2000). Consequently oil seems to have remigrated out of the system. Cenozoic upliftment are believed to be the main cause for this phenomenon (Ohm et al., 2008, Henriksen et al., 2011b, Lerch et al., 2016a, Karlsen and Skeie, 2006), were oil and possibly gas have remigrated due to expansion of the gas cap se Figure 7.21 (cf. England and Mackenzie, 1989). One or both of the two cases explained in Figure 7.21 are likely to be the process behind the discoveries of oil in the margins of the Hammerfest Basin.

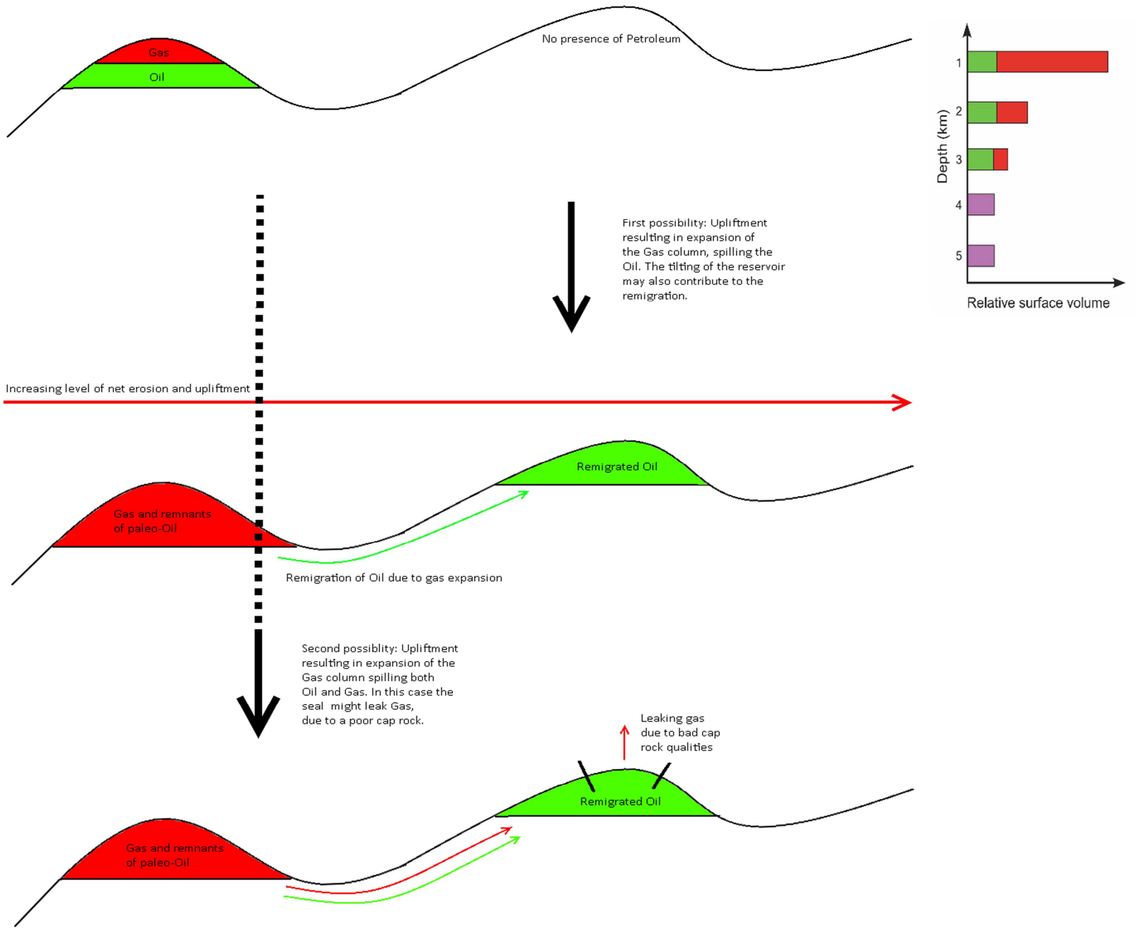
Gas
Oil
No presence of Petroleum
Depth (km)
1
2
3
4
5
Relative surface volume
First possibility: Upliftment resulting in expansion of the Gas column, spilling the Oil. The tilting of the reservoir may also contribute to the remigration.
Increasing level of net erosion and upliftment
Remigrated Oil
Gas and remnants of paleo-Oil
Remigration of Oil due to gas expansion
Second possiblity: Upliftment resulting in expansion of the Gas column spilling both Oil and Gas. In this case the seal might leak Gas, due to a poor cap rock.
Leaking gas due to bad cap rock qualities
Remigrated Oil
Gas and remnants of paleo-Oil

**Figure 7.21: The Figures illustrates two scenarios during upliftment resulting in changes for the PVT, subsequently expanding the gas cap displacing petroleum. The first possibility oil is spilled from the trap and remigrating to the second trap, resulting in an oil filled reservoir. In the second possibility oil and gas will spill from the trap and remigrate, in this scenario the cap rock quality in the second trap is bad. Consequently the trap leaks gas and holds the oil column. This would be a trap II/III type (cf. Sales, 1997). The leaking can be due to faulting or the brittleness of the cap rock. The bar graph is taken from Ohm et al. (2008) modified from England and Mackenzie (1989).**

The Jurassic derived oil seems to originate mainly from the Hammerfest Basin possibly due to upliftment. This assumption is based on the similarities we see in the geochemical parameters. Moreover, the maturity seems to be within the same range suggesting not only the same source, but also hydrocarbons from the same expulsion. The H1 sample could possibly be charged from the Hammerfest Basin and this could be true for both the light and heavier fraction (see Figure 7.22). Moreover, this could also be true for the upper part of the Goliat field and the oil discoveries found in Early Createaceos strata on the Loppa High. Furthermore, the Johan Castberg field seems to express many of the same geochemical features i.e. maturity, organic facies and age estimations, as the oils situated in the margins of the Hammerfest Basin features. Hence, there could be a possibility that the field contains remigrated Jurassic oil from the Hammerfest Basin. However, this is very uncertain and the oil would have to migrate through a heavily faulted area (Ringvassøy-Loppa Fault Complex) of more than 50km, although the fault planes in this area are mostly parallel to the migration pathway. One could also argue that the paleo-oil in the Johan Casberg field seem to be biodegraded, and some of the other oils found in the Hammerfest Basin margins are not. However the shallower discoveries on the Loppa High have shown severe levels of biodegradation (Lerch et al., 2016b) Nonetheless, an equally likely possibility would for the oil to originate from the Bjørnøya Basin, from the same source rock as the Hammerfest basin discoveries (likely Hekkingen Formation). Thus it provides the same geochemical signatures, however the similarities in maturity seem to be very similar, whether this is a coincidence or a connection is hard to determine. Most of the samples also seem to be influenced by a second light hydrocarbon charge, of possibly Jurassic origin, as seen in Figure 7.22. This may originate from the Hammer Fest Basin, and possibly the Bjørnøya Basin.

The oil found in the LH1 sample seems to originate somewhere from the Loppa High where Permian source rocks are mature. The arrows in Figure 7.22 indicate two possible migration pathways. The A1 and the lower parts of the Goliat field seem to have a contribution from a Pre-Jurassic source which could originate from the deeper parts of the Hammerfest Basin. The LH1 sample appears to be influenced by a second lighter hydrocarbon source, whether this is the same source as the other samples are uncertain. Moreover, it is also important to note that the A1 sample is a condensate and might not be of the same origin as the deeper Goliat discoveries, but different pre-Jurassic sources.

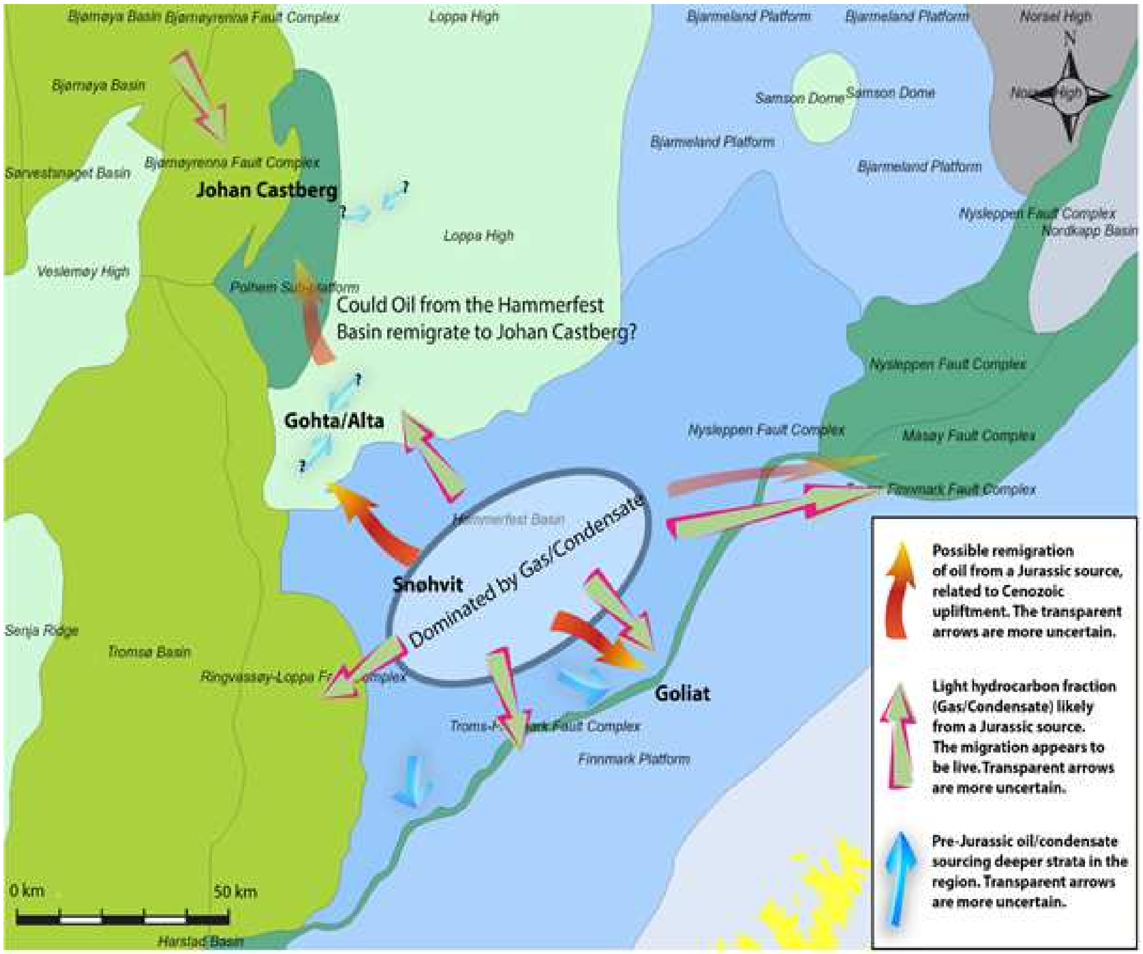
Bjørnøya Basin
Bjørnøyrenna Fault Complex
Loppa High
Bjarmeland Platform
Bjarmeland Platform
Norsel High
N
Bjørnøya Basin
Samson Dome
Samson Dome
Bjarmeland Platform
Sørvestsnaget Basin
Bjørnøyrenna Fault Complex
Bjarmeland Platform
Johan Castberg
?
?
Loppa High
Nysleppen Fault Complex
Nordkapp Basin
Veslemøy High
Polheim Sub-platform
Could Oil from the Hammerfest Basin remigrate to Johan Castberg?
?
Nysleppen Fault Complex
Gohta/Alta
Nysleppen Fault Complex
Måsøy Fault Complex
?
Finnmark Fault Complex
Hammerfest Basin
Snøhvit
Dominated by Gas/Condensate
Senja Ridge
Tromsø Basin
Ringvassøy-Loppa Fault Complex
Goliat
Troms-Finnmark Fault Complex
Finnmark Platform
0 km
50 km
Harstad Basin
Possible remigration of oil from a Jurassic source, related to Cenozoic upliftment. The transparent arrows are more uncertain.
Light hydrocarbon fraction (Gas/Condensate) likely from a Jurassic source. The migration appears to be live. Transparent arrows are more uncertain.
Pre-Jurassic oil/condensate sourcing deeper strata in the region. Transparent arrows are more uncertain.

**Figure 7.22: Tentative map of migration and remigration paths of Jurassic and pre-Jurassic petroleum charges based on the geochemical signatures of the samples analyzed. The transparent arrows are uncertain. All the pre-Jurassic migration pathways are very uncertain. Moreover, which way the charges are coming from is hard to determine, especially on the Loppa High. The underlying map is taken from (NPD., 2016a). Some of the suggested migration pathways is inspired by the article written by Lerch et al. (2016a).**

# 8. Conclusions and future work

## 8.1 Conclusions

Nine oil samples and two condensates have been geochemically analyzed from the SW Barents Sea. In addition 15 shallow core samples from the Finnmark Platform and Norkapp Basin have also been extracted and analyzed. The analytical methods employed have been TLC-FID, GC-FID and GC-MS. The sample set age ranges from Upper Carboniferous to Late Jurassic. The following conclusions can be drawn:

- The range of the maturities for the sample set is between early to the late “Oil window”. Biomarker maturity parameters seem to estimate a lower maturity than the medium range parameters for the oils and condensates.
- Fractionation effects are concluded to alter the estimated maturities for sample S2, A1 and LH1.
- All of the samples are interpreted to be of type II/III kerogen from mixed organic sources in a reducing environment.
- Sample FP4, FP8, FP9, FP10, FP11, FP12, FP13, JC1, JC2, JC3, JC4, JC5, JC6 and H1 have a higher input of marine organic matter. Sample LH1 and A1 have a higher terrigenous input and the Snøhvit samples seem to be influenced by carbonate.
- The sample LH1 from the Loppa High and the condensate from A1 from the southern margin of the Hammerfest Basin are of pre-Jurassic origin. Moreover, the LH1 sample is believed to be Paleozoic sourced, where the Ørret Formation is the most likely succession for the oil to originate from.
- The core samples from the Finnmark Platform are severely biodegraded and water washed. The bitumen seems to have migrated into the Formations pore-space. The comparison with the discovery on the Loppa High cannot be carried out in a satisfying manner due to the poor signal to noise ratio for the extracted cores. However, the bitumen could originate from Lower Carboniferous Tettagras Formation with a secondary influence of a shale source. The Nordkapp Basin sample is also severely biodegraded and water washed. The sample cannot be connected to any source.

- The shallower samples in the Johan Castberg field are biodegraded. The lower discoveries appear biodegraded and later masked by a new hydrocarbon source. This seems to be the case for the LH1 sample as well.
- All of the oils analyzed in this thesis are interpreted to be a mix of sources, one $C_{15-}$ fraction and a heavier $C_{15+}$ fraction. Where the Hekkingen Formation is the source for both fractions, this is the case for all the oils except the LH1 and A1. The Hekking Formation has firstly generated oil and later on when situated deeper, generated a lighter fraction of petroleum in the Hammerfest Basin. The latter is believed to be live.
- Cenozoic upliftment has resulted in remigration of the palaeo-oil in the Hammerfest Basin to basin margins and structural highs. The Johan Castberg oil can be sourced from this remigration or from the Bjørnøya Basin. These two possibilities are also true for the lighter hydrocarbon fraction found in the Johan Castberg field.
- The remigration of oil and the oil discoveries found in the basin margins and structural highs are concluded to be a result of gas column expansion and differences in cap-rock qualities.

## 8.2 Suggestions for future work

The Barents Sea is still a relatively unexplored area in terms of petroleum exploration. Therefore, further geochemical petroleum investigations are needed to gain a better understanding of the area. Due to the limit time writing this thesis (one semester), some suggestions for further work are as follows:

- The addition of more oil and condensate samples from the SW Barents Sea would lead to more confident conclusions.
- The biodegraded bitumen sample proved to give unsatisfying results as a comparison analogue. A possibility would be to analyse cores or petroleum samples from deeper parts of the Finnmark Platform, where the biodegradation is not as severe. The Finnmark Platform is dipping towards the North, consequently Carboniferous-Permian samples can be found deeper.
- The addition of the Gohta discovery in Permian Carbonates from well 7120/1-3 would be of great value to further investigate, in particular related to the interesting Palaeozoic discoveries on the Loppa High

- To further investigate the level of biodegradation it is suggested to evaluate the distribution of naphthalenes. Moreover, if the samples contain 25-norhopanes and seco-hopanes which are created when an oil is exposed to severe biodegradation (Peters et al., 2007).
- Asses the amount of water-soluble aromatic compounds as toluene to indicate long distance migration or water washing for the respective samples. This would be especially interesting for the Johan Castberg Samples and the Måsøy Fault Complex sample.
- Rock-Eval pyrolysis and isotope analysis would also be useful for more confidently concluding maturity and age of the samples.
- Finally, to investigate the light hydrocarbon fraction of the oils and condensate i.e. toluene/n-heptane ratio, heptane/methylcyclohexane ratio and $C_7$ compound ratios to address biodegradation, water washing, and evaporative fractionation.

# References

ABAY, T. B. 2010. *Vertical variation in reservoir core geochemistry: Bitumen samples from a well in the deep and hot Devonian age Embla Oil Field, Offshore Norway.* Master thesis, University of Oslo.

BAO, J. & ZHU, C. 2009. The effects of biodegradation on the compositions of aromatic hydrocarbons and maturity indicators in biodegraded oils from Liaohe Basin. *Science in China Series D: Earth Sciences,* 52**,** 59-68.

BAROSS, J. A. & DEMING, J. W. 1983. Growth of'black smoker' bacteria at temperatures of at least 250° C. *Nature,* 303**,** 423-426.

BEACH, F., PEAKMAN, T., ABBOTT, G., SLEEMAN, R. & MAXWELL, J. 1989. Laboratory thermal alteration of triaromatic steroid hydrocarbons. *Organic geochemistry,* 14**,** 109-111.

BERGLUND, L., AUGUSTSON, J., FÆRSETH, R., GJELBERG, J. & RAMBERG-MOE, H. 1986. The evolution of the Hammerfest Basin. *Habitat of hydrocarbons on the Norwegian continental shelf***,** 319-338.

BHULLAR, A. G., KARLSEN, D. A., BACKER ‐ OWE, K., TRAN, K. L., SKÅLNES, E., BERCHELMANN, H. H. & KITTELSEN, J. E. 2000. Reservoir Characterization By A Combined Micro ‐ Extraction — Micro Thin ‐ Layer Chromatography ( Iatroscan ) Method: A Calibration Study With Examples From The Norwegian North Sea. *Journal of Petroleum Geology,* 23**,** 221-244.

BJORØY, M., HALL, P. B., FERRIDAY, I. L. & MØRK, A. 2010. Triassic source rocks of the Barents Sea and Svalbard. *Search and Discovery article,* 10219**,** 7-10.

BJØRLYKKE, K. 2010. Heat Transport in Sedimentary Basins. Petroleum geoscience : From sedimentary environments to rock physics, Springer Heidelberg, 253–257.

BRAY, E. & EVANS, E. 1961. Distribution of n-paraffins as a clue to recognition of source beds. *Geochimica et Cosmochimica Acta,* 22**,** 2-15.

BUDZINSKI, H., NADALIG, T., RAYMOND, N., MATUZAHROH, N. & GILEWICZ, M. 2000. Evidence of two metabolic pathways for degradation of 2 ‐ methylphenanthrene by Sphingomonas sp. strain (2MPII). *Environmental toxicology and chemistry,* 19**,** 2672-2677.

BUGGE, T., ELVEBAKK, G., FANAVOLL, S., MANGERUD, G., SMELROR, M., WEISS, H. M., GJELBERG, J., KRISTENSEN, S. E. & NILSEN, K. 2002. Shallow stratigraphic drilling applied in hydrocarbon exploration of the Nordkapp Basin, Barents Sea. *Marine and Petroleum Geology,* 19**,** 13-37.

BUGGE, T., MANGERUD, G., ELVEBAKK, G., MØRK, A., NILSSON, I., FANAVOLL, S. & VIGRAN, J. 1995. The Upper Palaeozoic succession on the Finnmark Platform, Barents Sea. *Norsk Geologisk Tidsskrift,* 75**,** 3-30.

CAVANAGH, A. J., DI PRIMIO, R., SCHECK-WENDEROTH, M. & HORSFIELD, B. 2006. Severity and timing of Cenozoic exhumation in the southwestern Barents Sea. *Journal of the Geological Society,* 163**,** 761-774.

CLAYTON, J. & BOSTICK, N. 1986. Temperature effects on kerogen and on molecular and isotopic composition of organic matter in Pierre Shale near an igneous dike. *Organic geochemistry,* 10**,** 135-143.

CONNAN, J., BOUROULLEC, J., DESSORT, D. & ALBRECHT, P. 1986. The microbial input in carbonate-anhydrite facies of a sabkha palaeoenvironment from Guatemala: a molecular approach. *Organic Geochemistry,* 10**,** 29-50.

CONNAN, J. & CASSOU, A. 1980. Properties of gases and petroleum liquids derived from terrestrial kerogen at various maturation levels. *Geochimica et Cosmochimica Acta,* 44**,** 1-23.

CORNFORD, C., MORROW, J., TURRINGTON, A., MILES, J. & BROOKS, J. 1983. Some geological controls on oil composition in the UK North Sea. *Geological Society, London, Special Publications,* 12**,** 175-194.

CORNFORD, C., NEEDHAM, C. & DE WALQUE, L. 1986. Geochemical habitat of North Sea oils and gases. *Habitat of Hydrocarbons on the Norwegian Continental Shelf***,** 39-54.

CURIALE, J. A., CAMERON, D. & DAVIS, D. V. 1985. Biological marker distribution and significance in oils and rocks of the Monterey Formation, California. *Geochimica et Cosmochimica Acta,* 49**,** 271-288.

CURIALE, J. A. & ODERMATT, J. R. 1989. Short-term biomarker variability in the monterey formation, Santa Maria Basin. *Organic Geochemistry,* 14**,** 1-13.

DAHL, B. & SPEERS, G. 1985. Organic geochemistry of the Oseberg Field (I). *Petroleum Geochemistry in Exploration of the Norwegian Shelf.* Springer.

DEROO, G., TISSOT, B., MCCROSSAN, R. & DER, F. 1974. Geochemistry of the heavy oils of Alberta.

DORE., A. G. 1995. Barents Sea Geology, Petroleum Resources and Commercial Potential. *The Arctic Institute of North America,* 48**,** 207-221.

EHRENBERG, S., PICKARD, N., HENRIKSEN, L., SVANA, T., GUTTERIDGE, P. & MACDONALD, D. 2001. A depositional and sequence stratigraphic model for cold-water, spiculitic strata based on the Kapp Starostin Formation (Permian) of Spitsbergen and equivalent deposits from the Barents Sea. *AAPG bulletin,* 85**,** 2061-2088.

EIDVIN, T., GOLL, R. M., GROGAN, P., SMELROR, M. & ULLEBERG, K. 1998. The Pleistocene to Middle Eocene stratigraphy and geological evolution of the western Barents Sea continental margin at well site 7316/5-1 (Bjørnøya West area). *Norsk Geologisk Tidsskrift,* 78**,** 99-124.

ENGLAND, W. & MACKENZIE, A. 1989. Some aspects of the organic geochemistry of petroleum fluids. *Geologische Rundschau,* 78**,** 291-303.

FALEIDE., J. I., GUDLAUGSSON, S. T. & JACQUART, G. 1984. Evolution of the western Barents Sea. *Marine and Petroleum Geology,* 1**,** 123-150.

FARRIMOND, P., TAYLOR, A. & TELNÆS, N. 1998. Biomarker maturity parameters: the role of generation and thermal degradation. *Organic Geochemistry,* 29**,** 1181-1197.

FARRIMOND, P. & TELNÆS, N. 1996. Three series of rearranged hopanes in Toarcian sediments (northern Italy). *Organic Geochemistry,* 25**,** 165-177.

GABRIELSEN, R. H., FÆRSETH, R. B., JENSEN, L. N., KALHEIM, J. E. & RIIS., F. 1990. *Structural Elements of the Norwegian Continental Shelf. Pt. 1. The Barents Sea Region,* Oslo, Norwegian Petroleum Directorate.

GERNIGON, L. & BRÖNNER, M. 2012. Late Palaeozoic architecture and evolution of the southwestern Barents Sea: insights from a new generation of aeromagnetic data. *Journal of the Geological Society,* 169**,** 449-459.

GUDLAUGSSON, S. T., FALEIDE, J. I., JOHANSEN, S. E. & BREIVIK, A. J. 1998. Late Palaeozoic structural development of the South-western Barents Sea. *Marine and Petroleum Geology,* 15**,** 73-102.

HALLAND, E. K., BJØRNESTAD, A., GJELDVIK, I. T., BJØRHEIM, M., MAGNUS, C., MELING, I. M., MUJEZINOVIĆ, J., RIIS, F., SANDE RØD, R., PHAM, V. T. H. & TAPPEL, I. 2014. Geology of the Barents Sea. *CO2 Storage Atlas.* Norwegian Petroleum Directorate.

HENRIKSEN, E., BJØRNSETH, H., HALS, T., HEIDE, T., KIRYUKHINA, T., KLØVJAN, O., LARSSEN, G., RYSETH, A., RØNNING, K. & SOLLID, K. 2011a. Uplift and erosion of the greater Barents Sea: impact on prospectivity and petroleum systems. *Geological Society, London, Memoirs,* 35**,** 271-281.

HENRIKSEN, E., RYSETH, A., LARSSEN, G., HEIDE, T., RØNNING, K., SOLLID, K. & STOUPAKOVA, A. 2011b. Tectonostratigraphy of the greater Barents Sea: implications for petroleum systems. *Geological Society, London, Memoirs,* 35**,** 163-195.

HOLBA, A., ELLIS, L., DZOU, I., HALLAM, A., MASTERSON, W., FRANCU, J. & FINCANNON, A. Extended tricyclic terpanes as age discriminators between Triassic, Early Jurassic and Middle-Late Jurassic oils. 20th International Meeting on Organic Geochemistry, 2001. 464.

HUGHES, W. B., HOLBA, A. G. & DZOU, L. I. 1995. The ratios of dibenzothiophene to phenanthrene and pristane to phytane as indicators of depositional environment and lithology of petroleum source rocks. *Geochimica et Cosmochimica Acta,* 59**,** 3581-3598.

JOHANSEN, S., OSTISTY, B., BIRKELAND, Ø., FEDOROVSKY, Y., MARTIROSJAN, V., CHRISTENSEN, O. B., CHEREDEEV, S., IGNATENKO, E. & MARGULIS, L. 1992. Hydrocarbon potential in the Barents Sea region: play distribution and potential. *Arctic Geology and Petroleum Potential, Norwegian Petroleum Society (NPF), Special Publication,* 2**,** 273-320.

JOHANSEN, S., OSTISTY, B., BIRKELAND, Ø., FEDOROVSKY, Y., MARTIROSJAN, V., CHRISTENSEN, O. B., CHEREDEEV, S., IGNATENKO, E. & MARGULIS, L. 1993. Hydrocarbon potential in the Barents Sea region: play distribution and potential. *Arctic Geology and Petroleum Potential, Norwegian Petroleum Society (NPF), Special Publication,* 2**,** 273-320.

KARLSEN, D., NYLAND, B., FLOOD, B., OHM, S., BREKKE, T., OLSEN, S. & BACKER-OWE, K. 1995. Petroleum geochemistry of the Haltenbanken, Norwegian continental shelf. *Geological Society, London, Special Publications,* 86**,** 203-256.

KARLSEN, D. & SKEIE, J. 2006. Petroleum migration, faults and overpressure, part I: calibrating basin modelling using petroleum in traps—a review. *Journal of Petroleum Geology,* 29**,** 227-256.

KARLSEN, D. A. & LARTER, S. R. 1991. Analysis of petroleum fractions by TLC-FID; applications to petroleum reservoir description. *Organic Geochemistry,* 17**,** 603-617.

KARLSEN, D. A., SKEIE, J. E., BACKER-OWE, K., BJØRLYKKE, K., OLSTAD, R., BERGE, K., CECCHI, M., VIK, E. & SCHAEFER, R. G. 2004. Petroleum migration, faults and overpressure. Part II. Case history: the Haltenbanken Petroleum Province, offshore Norway. *Geological Society, London, Special Publications,* 237**,** 305-372.

KNUTSEN, S.-M., AUGUSTSON, J. H. & HAREMO, P. 2000. Exploring the Norwegian part of the Barents Sea—Norsk Hydro's lessons from nearly 20 years of experience. *Norwegian Petroleum Society Special Publications,* 9**,** 99-112.

KÚLD, I. T. H. 2009. *The age of the source rock and its source facies for the migrated oil in rock samples from Novaya Zemlya.* Master thesis, University of Oslo.

KVALHEIM, O. M., CHRISTY, A. A., TELNÆS, N. & BJØRSETH, A. 1987. Maturity determination of organic matter in coals using the methylphenanthrene distribution. *Geochimica et Cosmochimica Acta,* 51**,** 1883-1888.

LARSSEN, G., ELVEBAKK, G., HENRIKSEN, L., KRISTENSEN, S., NILSSON, I., SAMUELSBERG, T., SVÅNÅ, T., STEMMERIK, L. & WORSLEY, D. 2002. Upper Paleozoic lithostratigraphy of the southern Norwegian Barents Sea: Norwegian Petroleum Directorate Bulletin, v. 9.

LARTER, S. & MILLS, N. 1991. Phase-controlled molecular fractionations in migrating petroleum charges. *Geological Society, London, Special Publications,* 59**,** 137-147.

LERCH, B., KARLSEN, D. A., ABAY, T. B., DUGGAN, D., SELAND, R. & BACKER-OWE, K. 2016a. Regional oil petroleum alteration trends in Barents Sea oils and condensates as a clue to migration regimes and processes. *AAPG Bulletin,* 100**,** 165-190.

LERCH, B., KARLSEN, D. A., MATAPOUR, Z., SELAND, R. & BACKER-OWE, K. 2016b. ORGANIC Geochemistry of Barents Sea Petroleum: Thermal Maturity and Alteration and Mixing Processes In Oils and Condensates. *Journal of Petroleum Geology,* 39**,** 125-148.

LINDBERG, B., ALZENI, F., NORGE, E. & HOLMBOE, J. M. Skrugard–A New Hydrocarbon Province in the Barents Sea. 2013 SEG Annual Meeting, 2013. Society of Exploration Geophysicists.

LIU, Z. 2013. *Petroleum System Analysis in Skrugard Area, SW Barents Sea.* Master Thesis, Norwegian University of Science and Technology.

LUNDSCHIEN, B. A., HØY, T. & MØRK, A. 2014. Triassic hydrocarbon potential in the Northern Barents Sea; integrating Svalbard and stratigraphic core data. *Norwegian Petroleum Directorate Bulletin,* 11**,** 3-20.

MACKENZIE, A., PATIENCE, R., MAXWELL, J., VANDENBROUCKE, M. & DURAND, B. 1980. Molecular parameters of maturation in the Toarcian shales, Paris Basin, France—I. Changes in the configurations of acyclic isoprenoid alkanes, steranes and triterpanes. *Geochimica et Cosmochimica Acta,* 44**,** 1709-1721.

MACKENZIE, A., RULLKOTTER, J., WELTE, D. & MANKIEWICZ, P. 1985. Reconstruction of oil formation and accumulation in North Slope, Alaska, using quantitative gas chromatography-mass spectrometry: source rock evaluation including isotopes and biomarkers. *SG 20: Alaska North Slope Oil-Rock Correlation Study: Analysis of North Slope Crude.* UK: The British Petroleum Co.

MACKENZIE, A. S. 1984. Applications of biological markers in petroleum geochemistry. *Advances in petroleum geochemistry,* 1**,** 1-210.

MATAPOUR, Z. 2013. *The effects of Biodegradation on Barents Sea residual oils, live oils and gases.* Master thesis, University of Oslo.

MELLO, M., TELNAES, N., GAGLIANONE, P., CHICARELLI, M., BRASSELL, S. & MAXWELL, J. 1988. Organic geochemical characterisation of depositional palaeoenvironments of source rocks and oils in Brazilian marginal basins. *Organic geochemistry,* 13**,** 31-45.

MELLO, M. R. 1988. *Geochemical and molecular studies of the depositional environments of source rocks and their derived oils from the Brazilian marginal basins.* Ph.D thesis, University of Bristol.

MOLDOWAN, J. M., FAGO, F. J., CARLSON, R. M., YOUNG, D. C., AN DUVNE, G., CLARDY, J., SCHOELL, M., PILLINGER, C. T. & WATT, D. S. 1991. Rearranged hopanes in sediments and petroleum. *Geochimica et Cosmochimica Acta,* 55**,** 3333-3353.

MOLDOWAN, J. M., SEIFERT, W. K. & GALLEGOS, E. J. 1985. Relationship between petroleum composition and depositional environment of petroleum source rocks. *AAPG bulletin,* 69**,** 1255-1268.

MOLDOWAN, J. M., SUNDARARAMAN, P. & SCHOELL, M. 1986. Sensitivity of biomarker properties to depositional environment and/or source input in the Lower Toarcian of SW-Germany. *Organic Geochemistry,* 10**,** 915-926.

NPD. 2013. *Exploration drilling results* [Online]. The Norwegian Petroleum Directorate. Available: http://www.npd.no/en/news/Exploration-drilling-results/2013/71201-3/ [Accessed 13.03 2016].

NPD. 1988. A lithostratigraphic scheme for the Mesozoic and Cenozoic succession offshore mid- and northern Norway. *(Bulletin 4)***,** 1-65.

NPD. 2014. *Factpages* [Online]. The Norwegian Petroleum Directorate. Available: http://www.npd.no/en/Topics/Geology/Geological-plays/ [Accessed 12.05 2016].

NPD. 2016a. *Fact Maps* [Online]. The Norwegian Petroleum Directorate. Available: http://gis.npd.no/FactMaps/sl_20/?Viewer=FactMaps_20 [Accessed 2.02 2016].

NPD. 2016b. *Well bores* [Online]. The Norwegian Petroleum Directorate. Available: http://factpages.npd.no/factpages/Default.aspx?culture=en&nav1=wellbore [Accessed 16.02 2016].

OHM, S. E., KARLSEN, D. A. & AUSTIN, T. 2008. Geochemically driven exploration models in uplifted areas: Examples from the Norwegian Barents Sea. *AAPG bulletin,* 92**,** 1191-1223.

PEDERSEN, J. 2002. *Atypical oils, unusual condensates and bitumens of the Norwegian Continental Shelf: an organic geochemical study, Cand. Scient.* Thesis in Geology, Department of Geology, University of Oslo.

PEDERSEN, J. H., KARLSEN, D. A., BACKER-OWE, K., LIE, J. E. & BRUNSTAD, H. 2006. The geochemistry of two unusual oils from the Norwegian North Sea; implications for new source rock and play scenario. *Petroleum Geoscience,* 12**,** 85-96.

PETERS, K. & MOLDOWAN, J. 1991. Effects of source, thermal maturity, and biodegradation on the distribution and isomerization of homohopanes in petroleum. *Organic geochemistry,* 17**,** 47-61.

PETERS, K., MOLDOWAN, J. & SUNDARARAMAN, P. 1990. Effects of hydrous pyrolysis on biomarker thermal maturity parameters: Monterey phosphatic and siliceous members. *Organic Geochemistry,* 15**,** 249-265.

PETERS, K. E. & MOLDOWAN, J. M. 1993. The biomarker guide: interpreting molecular fossils in petroleum and ancient sediments.

PETERS, K. E., MOLDOWAN, J. M. & WALTERS, C. C. 2005. *The biomarker guide : 2 : Biomarkers and isotopes in petroleum systems and earth history,* Cambridge, Cambridge University Press.

PETERS, K. E., WALTERS, C. C. & MOLDOWAN, J. M. 2007. *The biomarker guide: Volume 1, Biomarkers and isotopes in the environment and human history*, Cambridge University Press.

PHILP, R. T. & GILBERT, T. 1986. Biomarker distributions in Australian oils predominantly derived from terrigenous source material. *Organic Geochemistry,* 10**,** 73-84.

PÜTTMANN, W., MERZ, C. & SPECZIK, S. 1989. The secondary oxidation of organic material and its influence on Kupferschiefer mineralization of southwest Poland. *Applied Geochemistry,* 4**,** 151-161.

RADKE, M. 1988. Application of aromatic compounds as maturity indicators in source rocks and crude oils. *Marine and Petroleum Geology,* 5**,** 224-236.

RADKE, M., VRIEND, S. & SCHAEFER, R. 2001. Geochemical characterization of lower Toarcian source rocks from NW Germany: Interpretation of aromatic and saturated hydrocarbons in relation to depositional environment and maturation effects. *Journal of petroleum geology,* 24**,** 287-307.

RADKE, M., WELTE, D. & WILLSCH, H. 1986. Maturity parameters based on aromatic hydrocarbons: Influence of the organic matter type. *Organic Geochemistry,* 10**,** 51-63.

RADKE, M., WELTE, D. H. & WILLSCH, H. 1982a. Geochemical study on a well in the Western Canada Basin: relation of the aromatic distribution pattern to maturity of organic matter. *Geochimica et Cosmochimica Acta,* 46**,** 1-10.

RADKE, M., WILLSCH, H., LEYTHAEUSER, D. & TEICHMÜLLER, M. 1982b. Aromatic components of coal: relation of distribution pattern to rank. *Geochimica et Cosmochimica Acta,* 46**,** 1831-1848.

RULLKÖTTER, J. & MARZI, R. 1988. Natural and artificial maturation of biological markers in a Toarcian shale from northern Germany. *Organic Geochemistry,* 13**,** 639-645.

SALES, J. K. 1997. Seal strength vs. trap closure-a fundamental control on the distribution of oil and gas. *Seals, traps, and the petroleum system,* 67**,** 57-83.

SCALAN, E. & SMITH, J. 1970. An improved measure of the odd-even predominance in the normal alkanes of sediment extracts and petroleum. *Geochimica et Cosmochimica Acta,* 34**,** 611-620.

SCOTESE, C. R. 1987. Phanerozoic plate tectonic reconstructions. *Paleoceanographic mapping project, Institute of Geophysics, University of Texas Technical Report,* 90.

SEIFERT, W. K. & MOLDOWAN, J. M. 1978. Applications of steranes, terpanes and monoaromatics to the maturation, migration and source of crude oils. *Geochimica et Cosmochimica Acta,* 42**,** 77-95.

SEIFERT, W. K. & MOLDOWAN, J. M. 1979. The effect of biodegradation on steranes and terpanes in crude oils. *Geochimica et Cosmochimica Acta,* 43**,** 111-126.

SEIFERT, W. K. & MOLDOWAN, J. M. 1980. The effect of thermal stress on source-rock quality as measured by hopane stereochemistry. *Physics and Chemistry of the Earth,* 12**,** 229-237.

SHANMUGAM, G. 1985. Significance of coniferous rain forests and related organic matter in generating commercial quantities of oil, Gippsland Basin, Australia. *AAPG Bulletin,* 69**,** 1241-1254.

SMELROR., M., PETROV., O. V., LARSSEN., B. B. & WERNER., S. 2009. Atlas Geological History ofthe Barents Sea. *Geological Survey of Norway, Trondheim.***,** 1-21.

SUBROTO, E. A., ALEXANDER, R. & KAGI, R. I. 1991. 30-Norhopanes: their occurrence in sediments and crude oils. *Chemical Geology,* 93**,** 179-192.

SUTTON, P. A., LEWIS, C. A. & ROWLAND, S. J. 2005. Isolation of individual hydrocarbons from the unresolved complex hydrocarbon mixture of a biodegraded crude oil using preparative capillary gas chromatography. *Organic Geochemistry,* 36**,** 963-970.

SZCZERBA, M. & ROSPONDEK, M. J. 2010. Controls on distributions of methylphenanthrenes in sedimentary rock extracts: critical evaluation of existing geochemical data from molecular modelling. *Organic Geochemistry,* 41**,** 1297-1311.

TISSOT, B. & CALIFET-DEBYSER, Y. 1971. Origin and Evolution of Hydrocarbons in Early Toarcian Shales, Paris Basin, France. *AAPG Bulletin,* 55**,** 2177-2193.

TISSOT, B. P. & WELTE, D. H. 1984. *Petroleum formation and occurrence,* Berlin, Springer.

VADAKKEPULIYAMBATTA, S., BÜNZ, S., MIENERT, J. & CHAND, S. 2013. Distribution of subsurface fluid-flow systems in the SW Barents Sea. *Marine and Petroleum Geology,* 43**,** 208-221.

VAN GRAAS, G. W. 1990. Biomarker maturity parameters for high maturities: calibration of the working range up to the oil/condensate threshold. *Organic Geochemistry,* 16**,** 1025-1032.

VAN KOEVERDEN, J., KARLSEN, D., SCHWARK, L., CHPITSGLOUZ, A. & BACKER ‐ OWE, K. 2010. Oil ‐ prone lower carboniferous coals in the norwegian Barents Sea: implications for a Palaeozoic petroleum system. *Journal of Petroleum Geology,* 33**,** 155-181.

VIRGAN, J. O., MANGERUD, G., MØRK, A., WORSLEY, D. & HOCHULI, P. A. 2014. *Palynology and geology of the Triassic succession of Svalbard and the Barents Sea,* Norway, Geological Survey of Norway.

VOBES, S. J. 1998. *An organic geochemical study of oils and condensates from the Hammerfest Basin, southern Norwegian Barents Sea:.* Cand. Scient. thesis, University of Oslo.

VOLKMAN, J. K., ALEXANDER, R., KAGI, R. I., NOBLE, R. A. & WOODHOUSE, C. W. 1983. A geochemical reconstruction of oil generation in the Barrow Sub-basin of Western Australia. *Geochimica et Cosmochimica Acta,* 47**,** 2091-2105.

VORREN, T. O., RICHARDSEN, G., KNUTSEN, S.-M. & HENRIKSEN, E. 1991. Cenozoic erosion and sedimentation in the western Barents Sea. *Marine and Petroleum Geology,* 8**,** 317-340.

WANG, Z., FINGAS, M. F., SIGOUIN, L. & OWENS, E. H. Fate and persistence of long-term spilled Metula oil in the marine salt marsh environment: degradation of petroleum biomarkers. International Oil Spill Conference, 2001. American Petroleum Institute, 115-125.

WEISS, H. M., WILHELMS, A., MILLS, N., COTCHMER, J., HALL, P. B., LIND, K. & BREKKE, T. 2000. The Norwegian Industry Guide to Organic Geochemical Analyses. Edition 4**,** 102.

WENGER, L. M., DAVIS, C. L. & ISAKSEN, G. H. Multiple controls on petroleum biodegradation and impact on oil quality. SPE Annual Technical Conference and Exhibition, 2001. Society of Petroleum Engineers.

WILHELMS, A., LARTER, S., HEAD, I., FARRIMOND, P., DI-PRIMIO, R. & ZWACH, C. 2001. Biodegradation of oil in uplifted basins prevented by deep-burial sterilization. *Nature,* 411**,** 1034-1037.

WILHELMS, A. & LARTER, S. R. 1993. Origin of tar mats in petroleum reservoirs. Part I: introduction and case studies. *Marine and Petroleum Geology,* 11**,** 418-441.

WORSLEY, D. 2008. The post ‐ Caledonian development of Svalbard and the western Barents Sea. *Polar Research,* 27**,** 298-317.

ØSTENSEN, M. 2005. *A geochemical assessment of petroleum from underground oil storage caverns in relation to petroleum from natural reservoirs offshore Norway.* Master thesis, University of Oslo.

# Appendix A

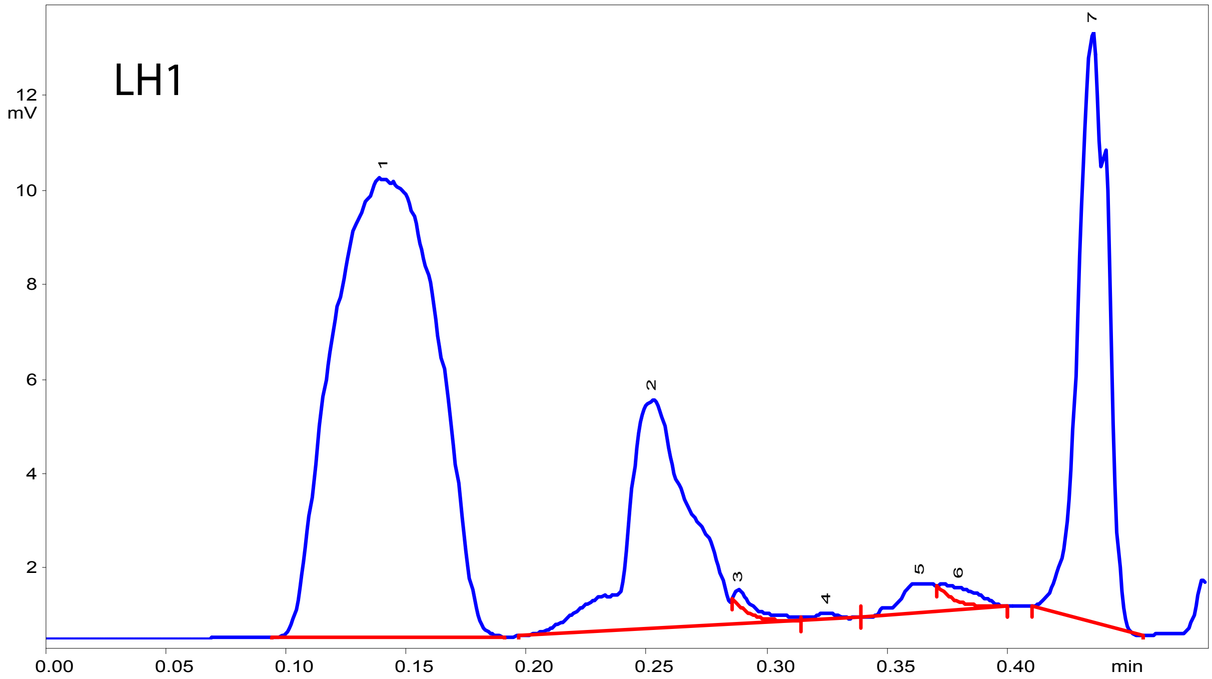
LH1
12
mV
10
8
6
4
2
0.00
0.05
0.10
0.15
0.20
0.25
0.30
0.35
0.40
min
1
2
3
4
5
6
7

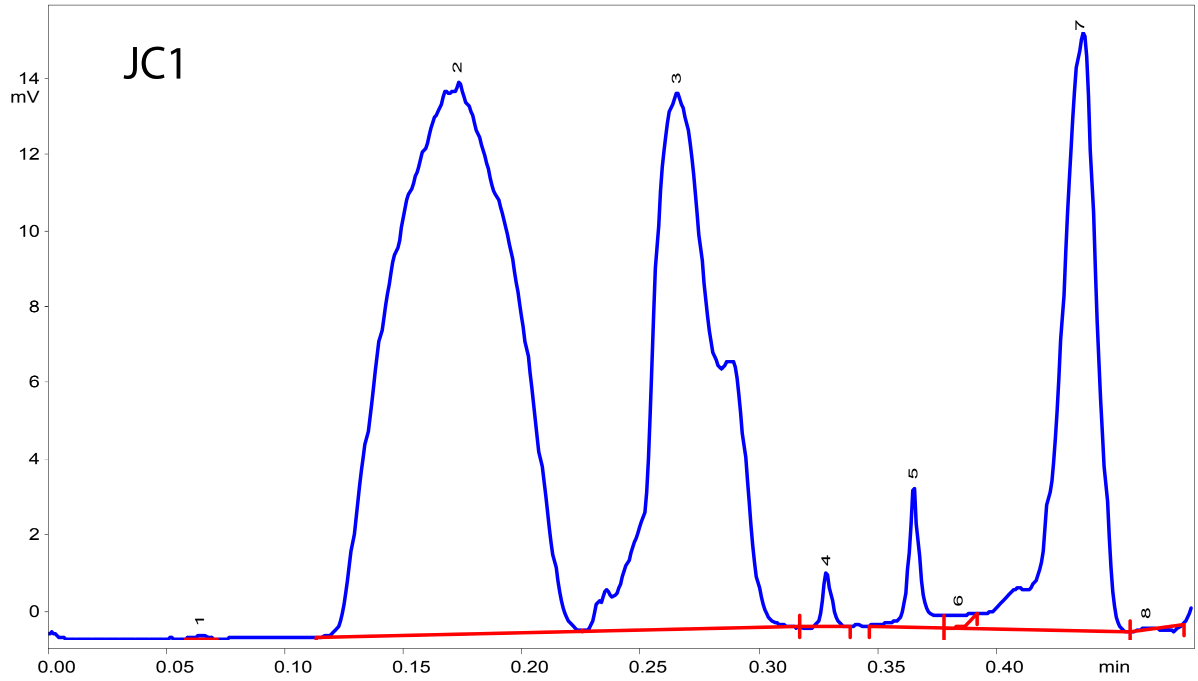
JC1
14
mV
12
10
8
6
4
2
0
0.00
0.05
0.10
0.15
0.20
0.25
0.30
0.35
0.40
min
1
2
3
4
5
6
7
8

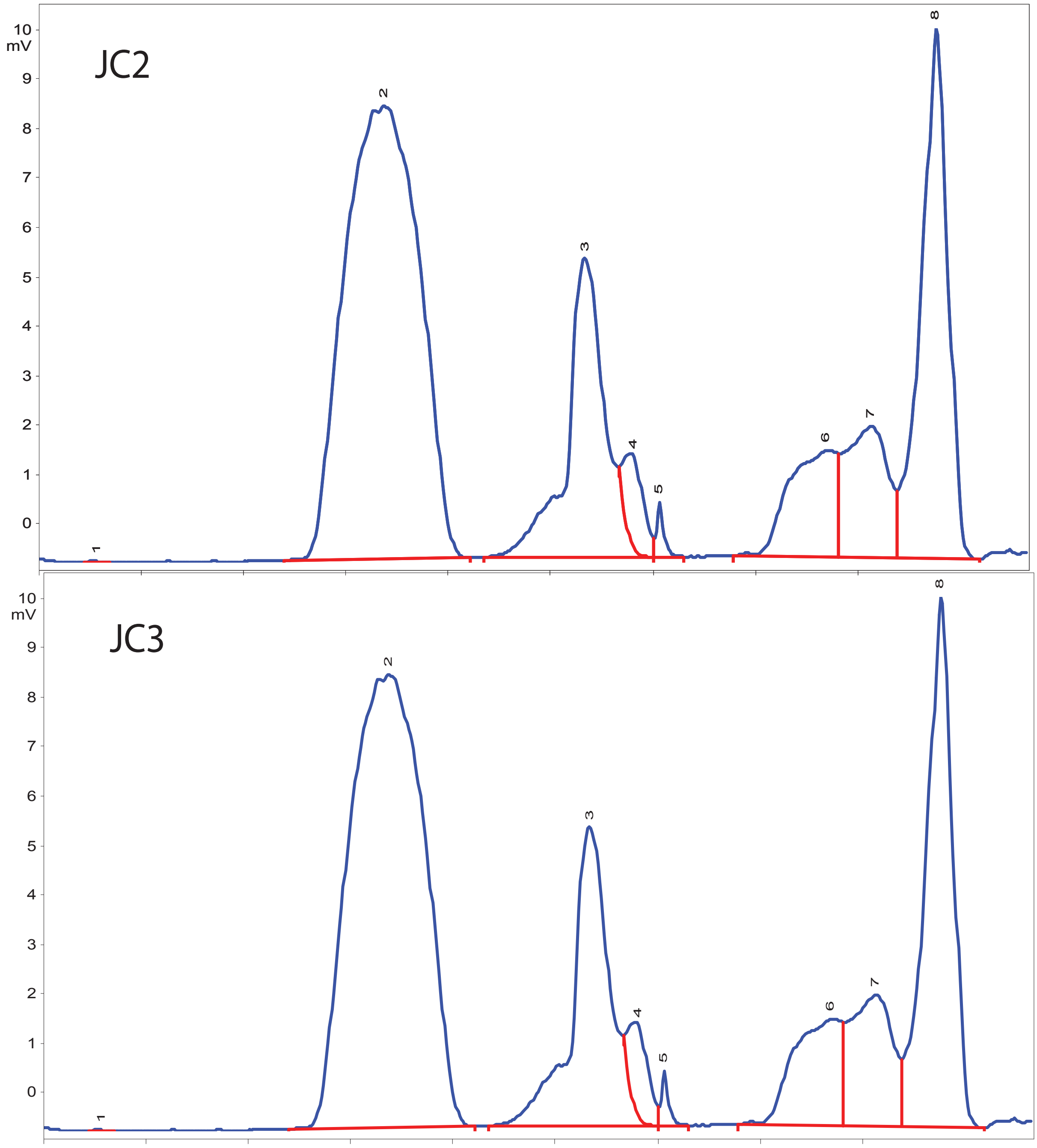
JC2
10
mV
9
8
7
6
5
4
3
2
1
0
1
2
3
4
5
6
7
8
JC3
10
mV
9
8
7
6
5
4
3
2
1
0
1
2
3
4
5
6
7
8

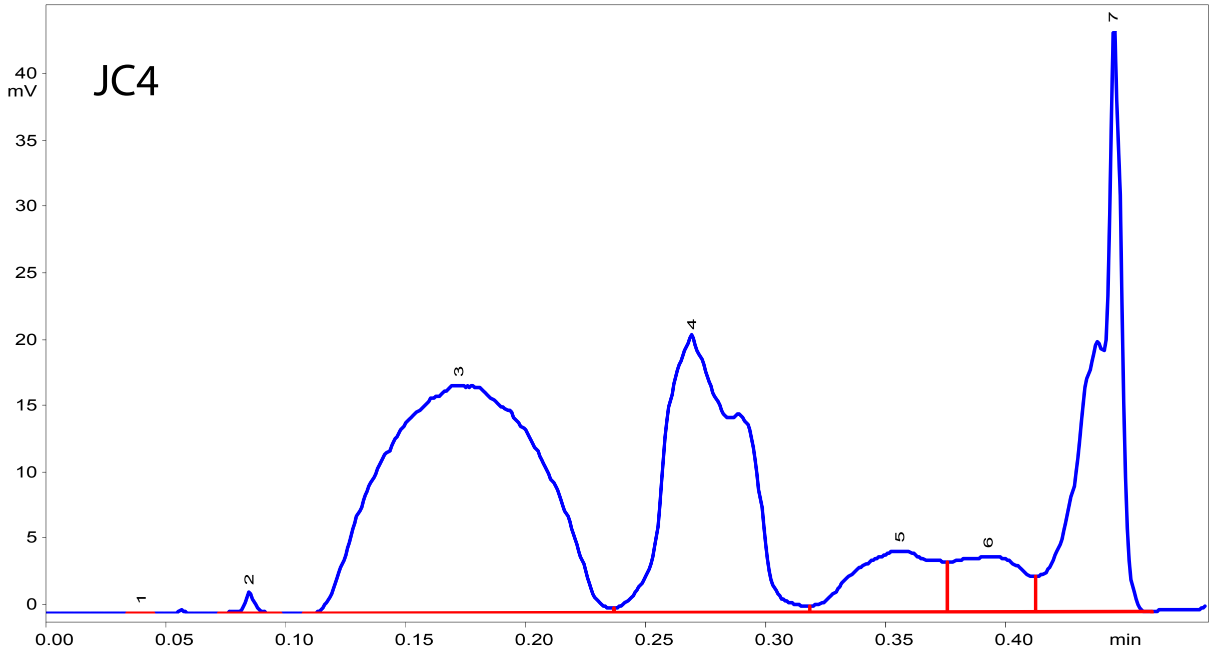
JC4
mV
40
35
30
25
20
15
10
5
0
1
2
3
4
5
6
7
0.00
0.05
0.10
0.15
0.20
0.25
0.30
0.35
0.40
min

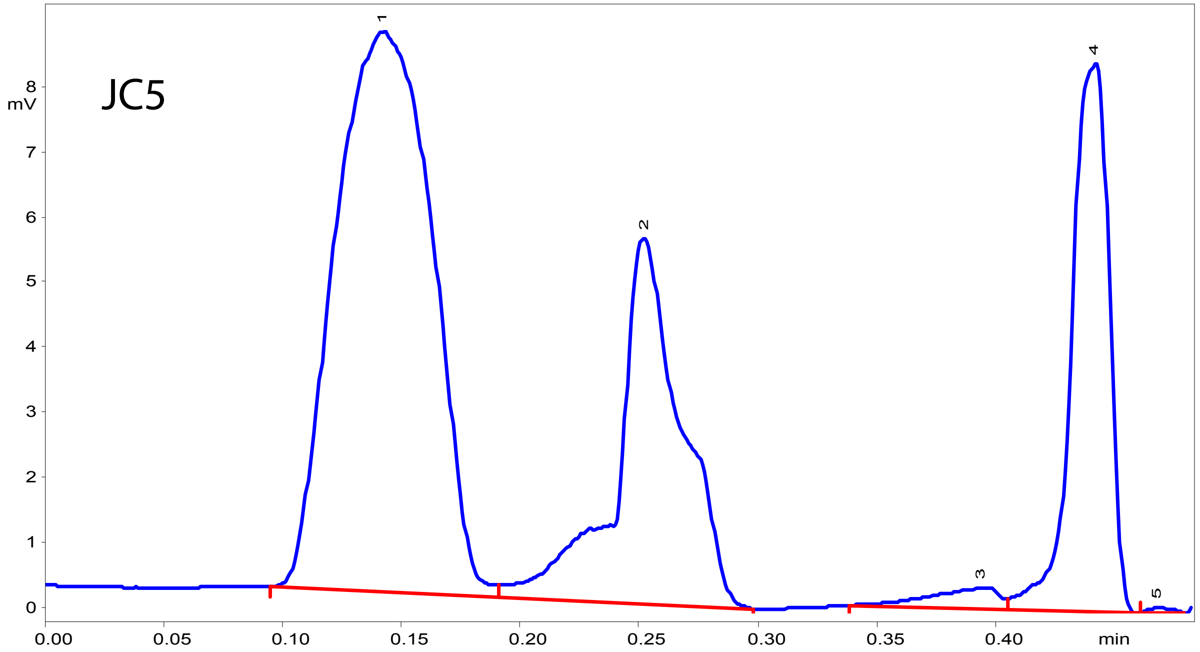
JC5
mV
8
7
6
5
4
3
2
1
0
1
2
3
4
5
0.00
0.05
0.10
0.15
0.20
0.25
0.30
0.35
0.40
min

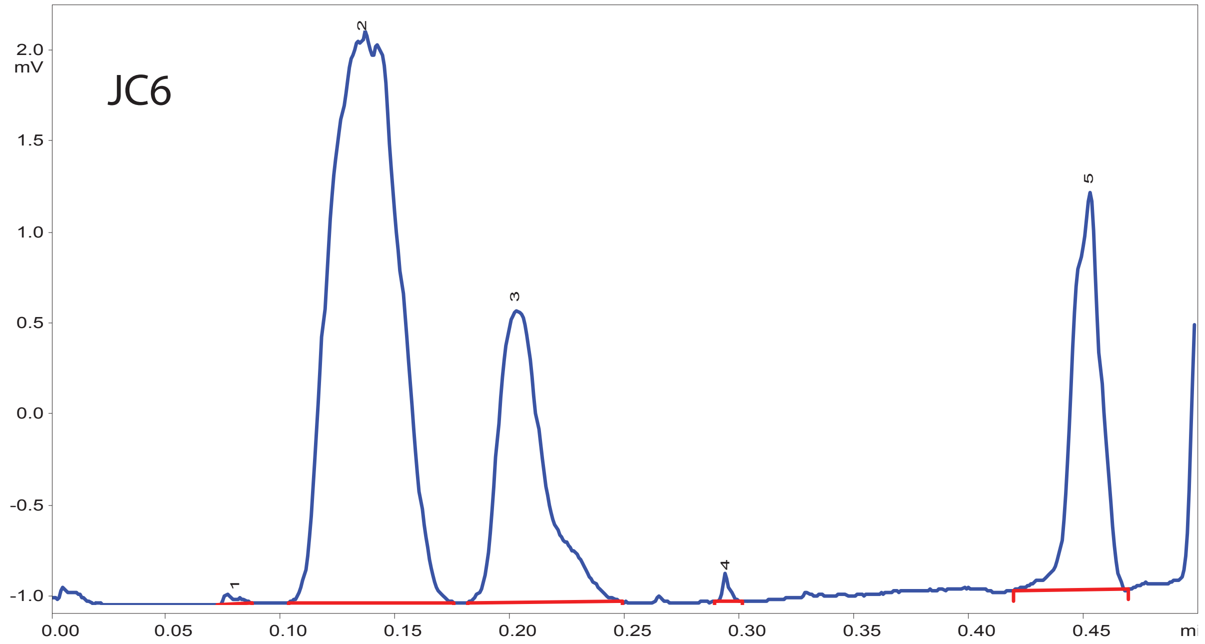
JC6
2.0
mV
1.5
1.0
0.5
0.0
-0.5
-1.0
0.00
0.05
0.10
0.15
0.20
0.25
0.30
0.35
0.40
0.45
mi
1
2
3
4
5

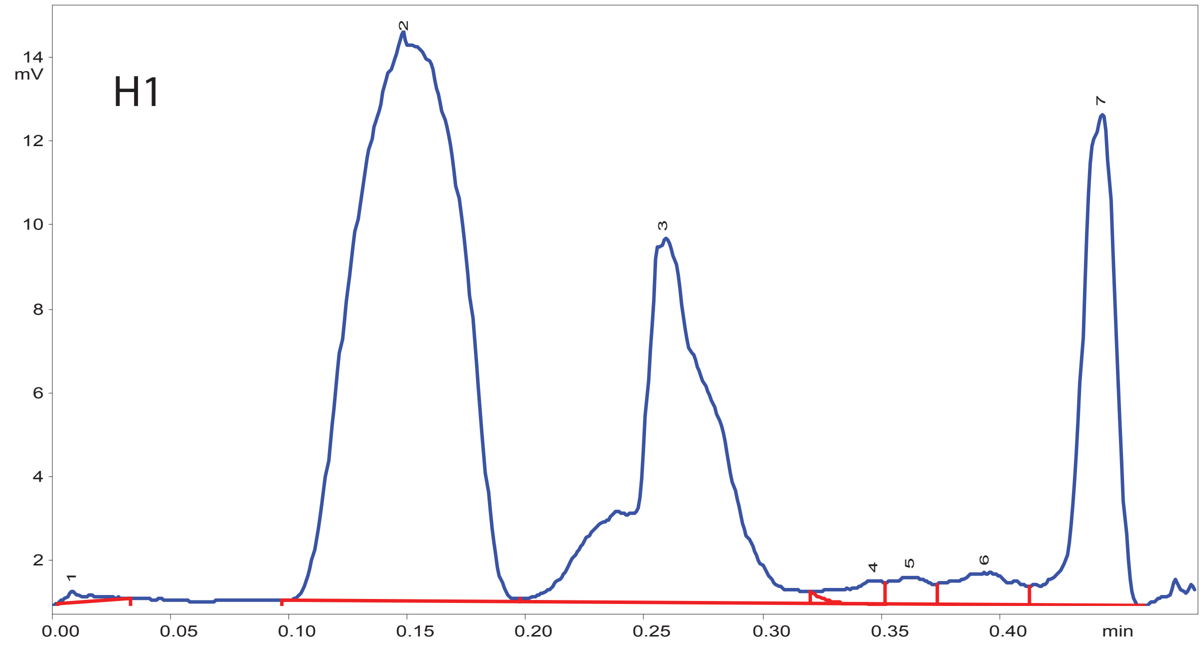
H1
14
mV
12
10
8
6
4
2
0.00
0.05
0.10
0.15
0.20
0.25
0.30
0.35
0.40
min
1
2
3
4
5
6
7

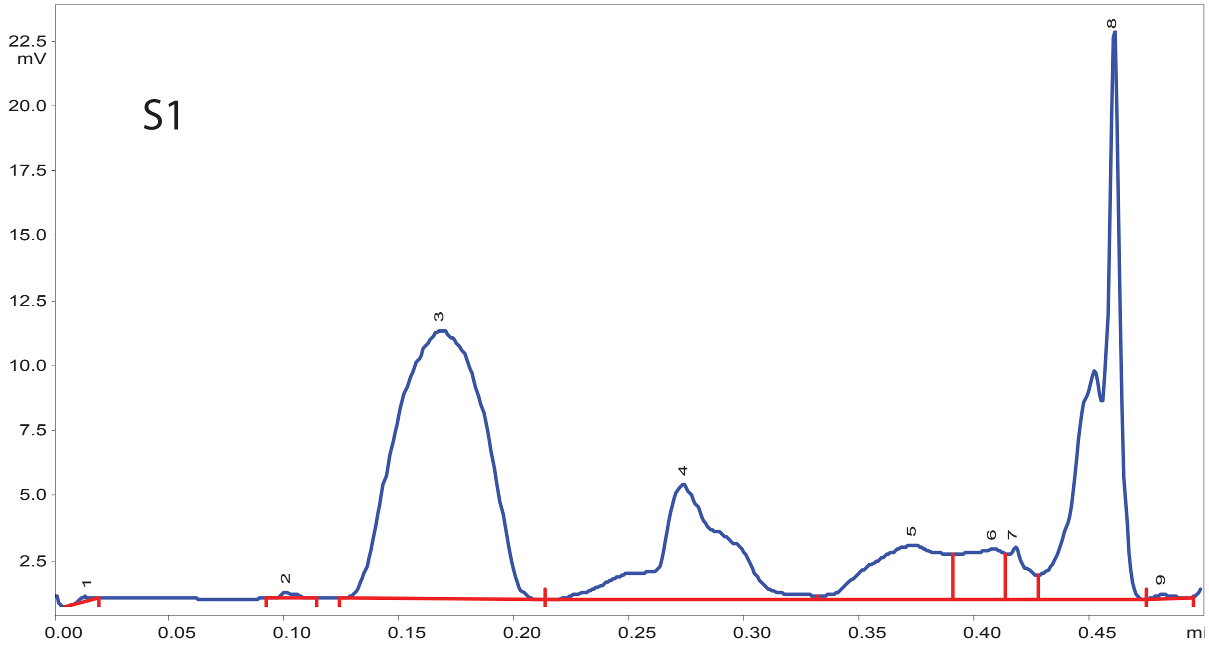
S1
22.5
mV
20.0
17.5
15.0
12.5
10.0
7.5
5.0
2.5
0.00
0.05
0.10
0.15
0.20
0.25
0.30
0.35
0.40
0.45
mi
1
2
3
4
5
6
7
8
9

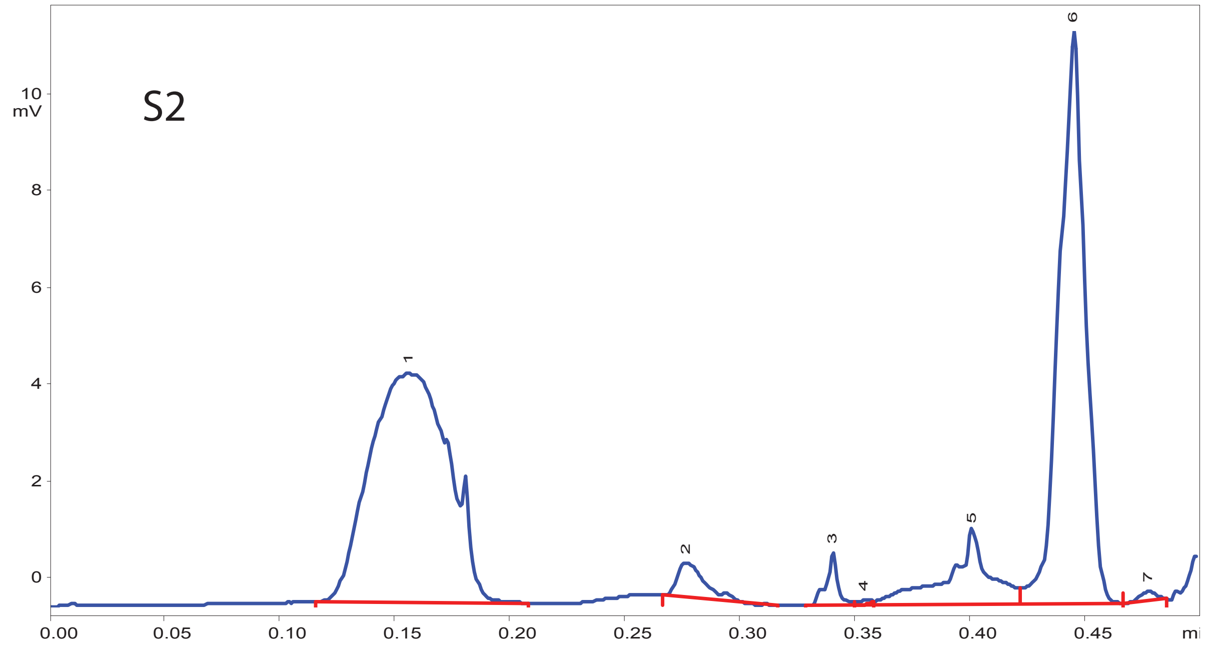
S2
10
mV
8
6
4
2
0
0.00
0.05
0.10
0.15
0.20
0.25
0.30
0.35
0.40
0.45
mi
1
2
3
4
5
6
7

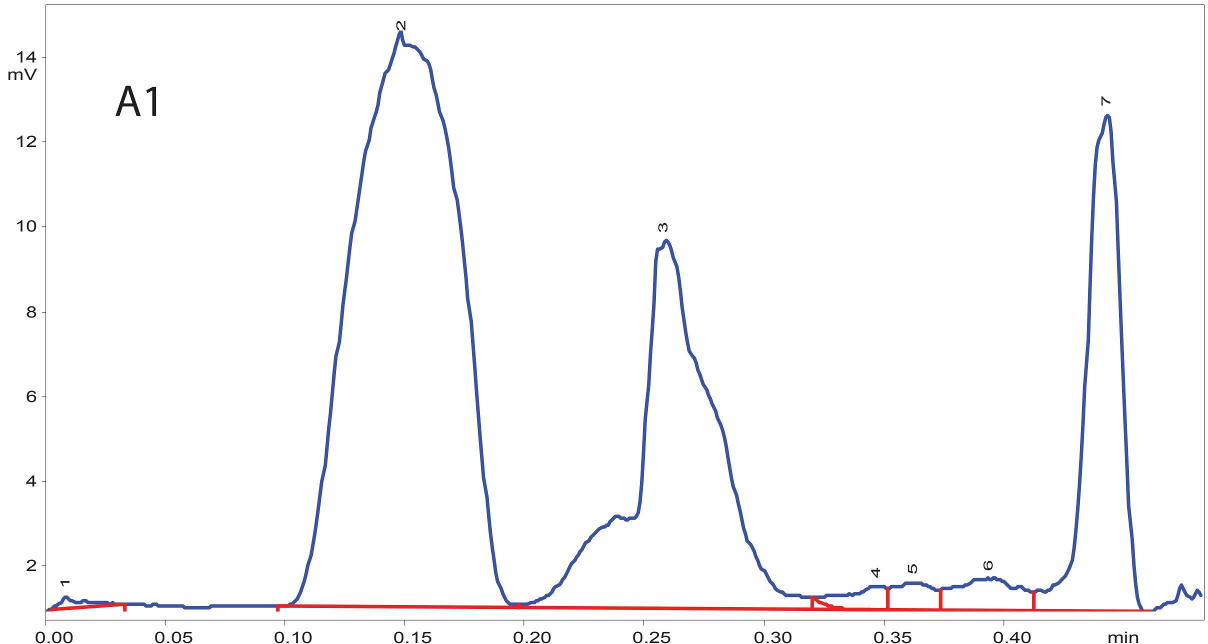
A1
mV
14
12
10
8
6
4
2
1
2
3
4
5
6
7
0.00
0.05
0.10
0.15
0.20
0.25
0.30
0.35
0.40
min

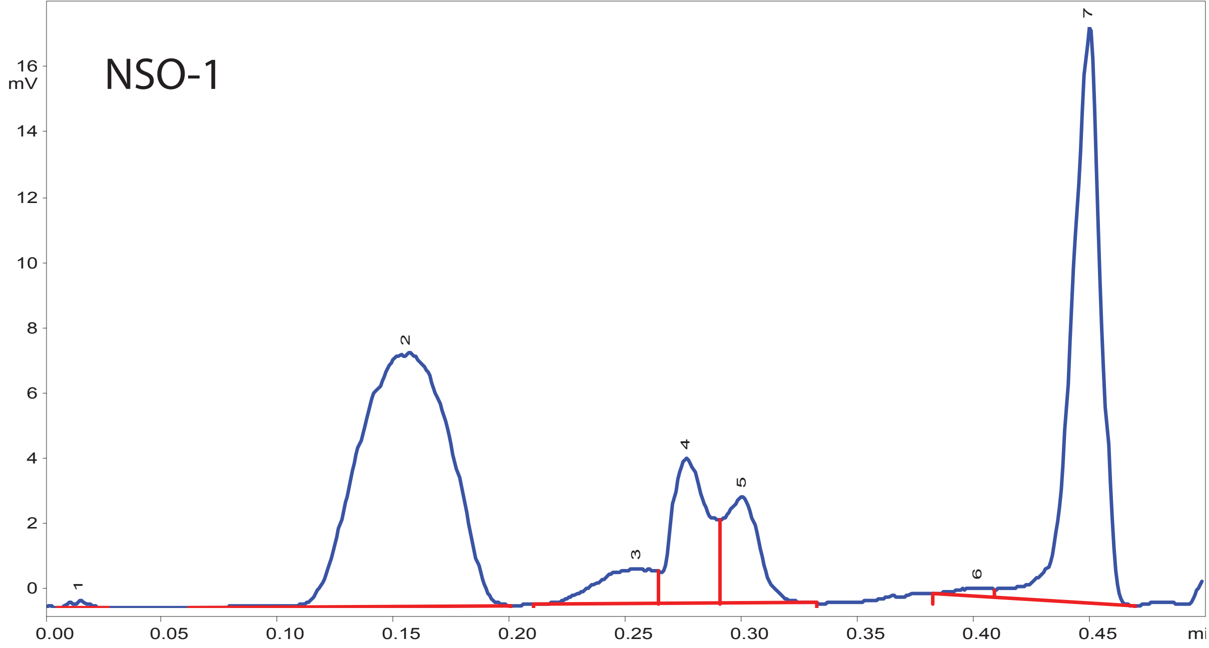
NSO-1
mV
16
14
12
10
8
6
4
2
0
1
2
3
4
5
6
7
0.00
0.05
0.10
0.15
0.20
0.25
0.30
0.35
0.40
0.45
mi

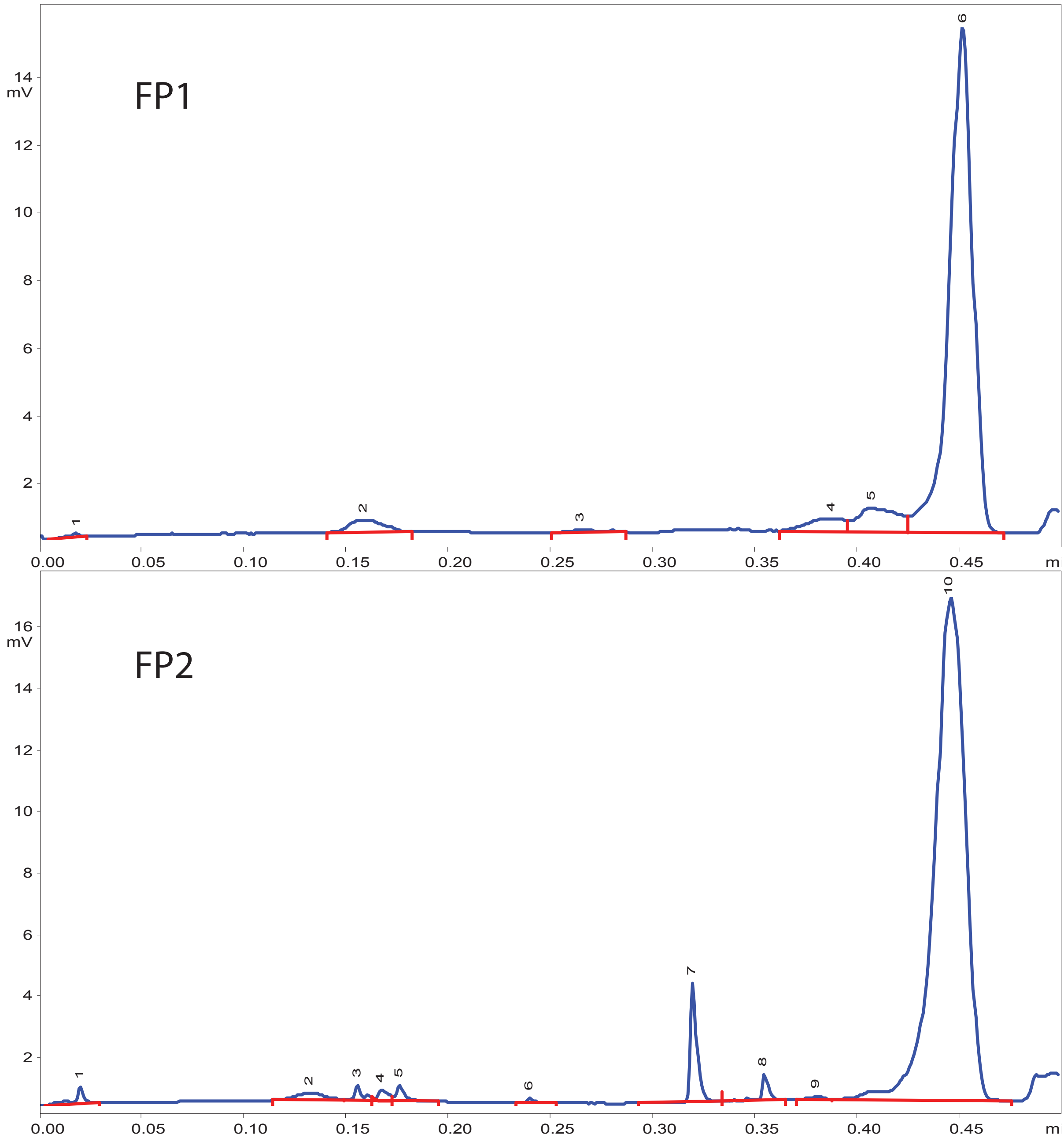
FP1
mV
14
12
10
8
6
4
2
1
2
3
4
5
6
0.00
0.05
0.10
0.15
0.20
0.25
0.30
0.35
0.40
0.45
m
FP2
mV
16
14
12
10
8
6
4
2
1
2
3
4
5
6
7
8
9
10
0.00
0.05
0.10
0.15
0.20
0.25
0.30
0.35
0.40
0.45
m

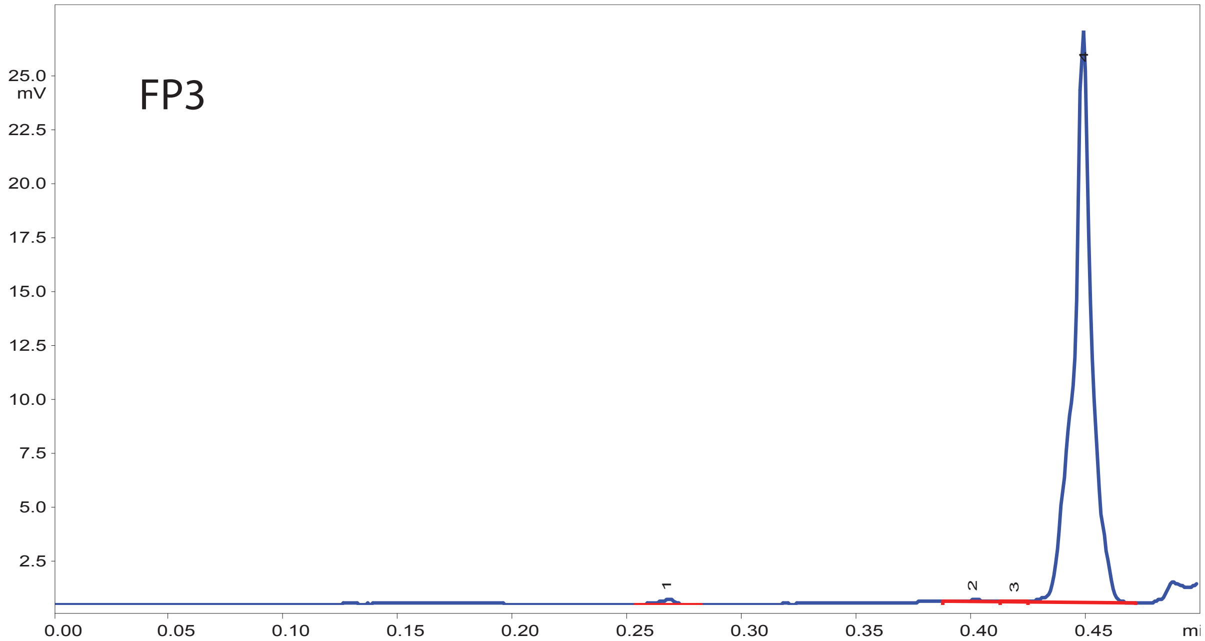
FP3
25.0
mV
22.5
20.0
17.5
15.0
12.5
10.0
7.5
5.0
2.5
0.00
0.05
0.10
0.15
0.20
0.25
0.30
0.35
0.40
0.45
mi
1
2
3
4

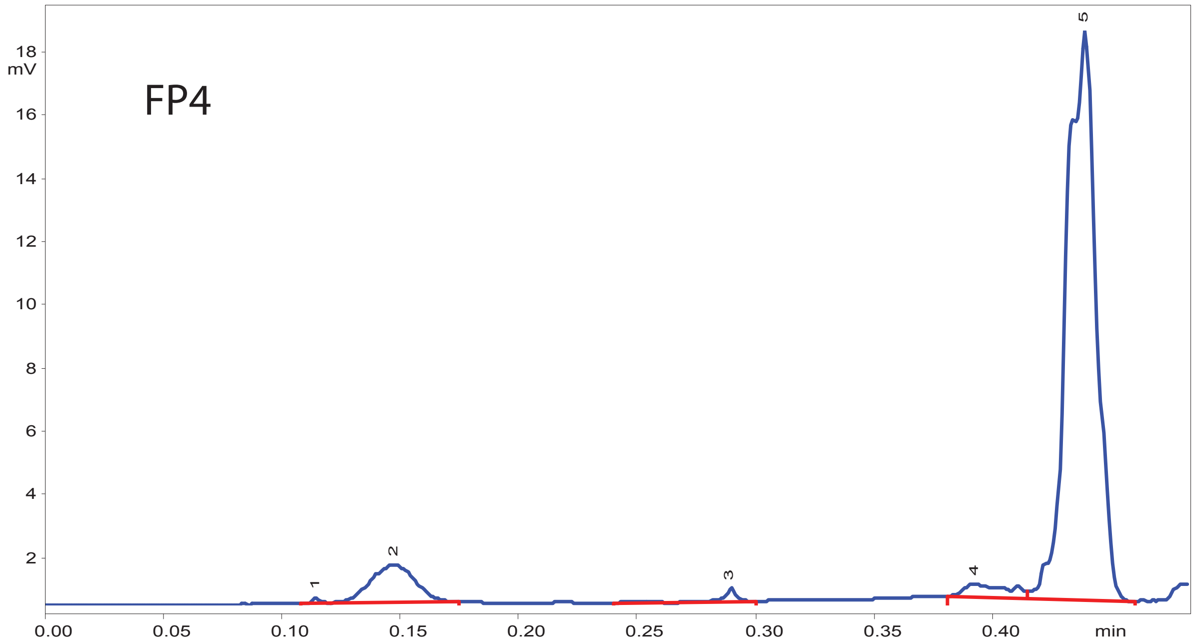
FP4
18
mV
16
14
12
10
8
6
4
2
0.00
0.05
0.10
0.15
0.20
0.25
0.30
0.35
0.40
min
1
2
3
4
5

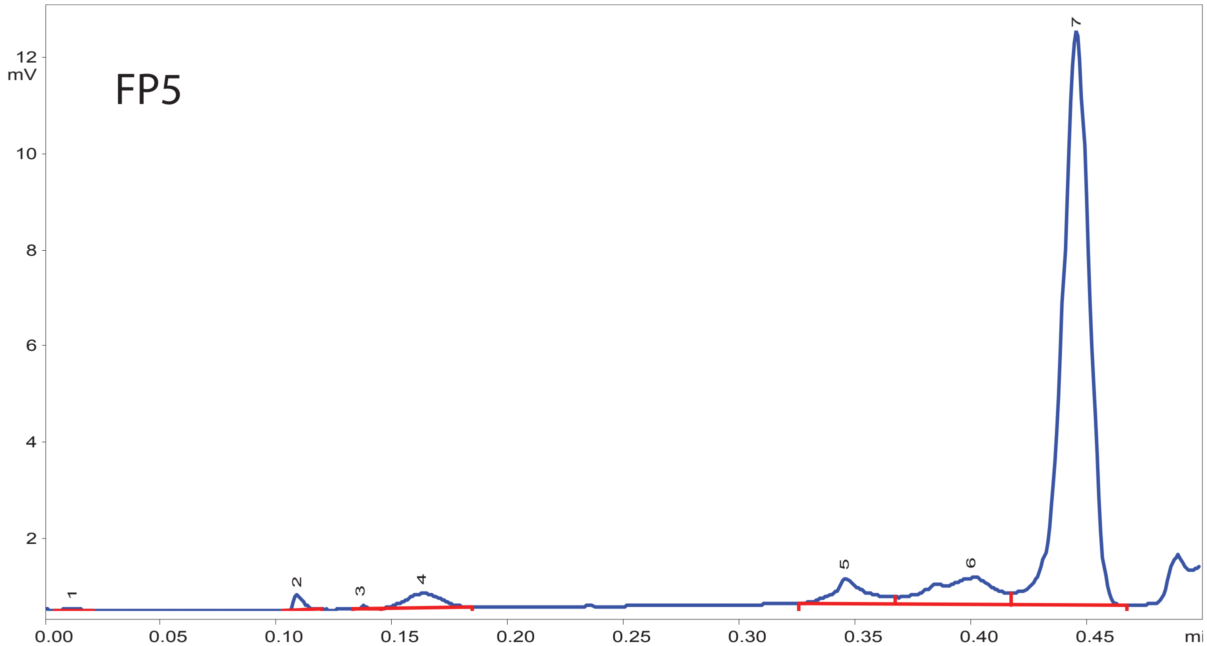
FP5
12
mV
10
8
6
4
2
1
2
3
4
5
6
7
0.00
0.05
0.10
0.15
0.20
0.25
0.30
0.35
0.40
0.45
mi

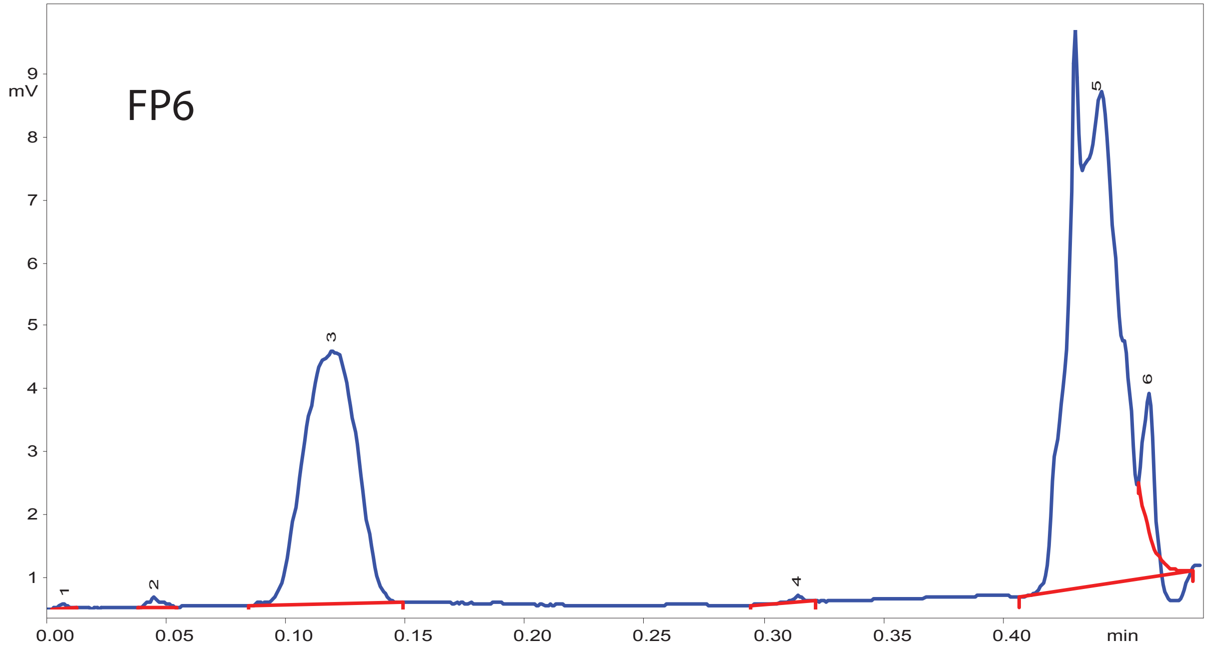
FP6
9
mV
8
7
6
5
4
3
2
1
1
2
3
4
5
6
0.00
0.05
0.10
0.15
0.20
0.25
0.30
0.35
0.40
min

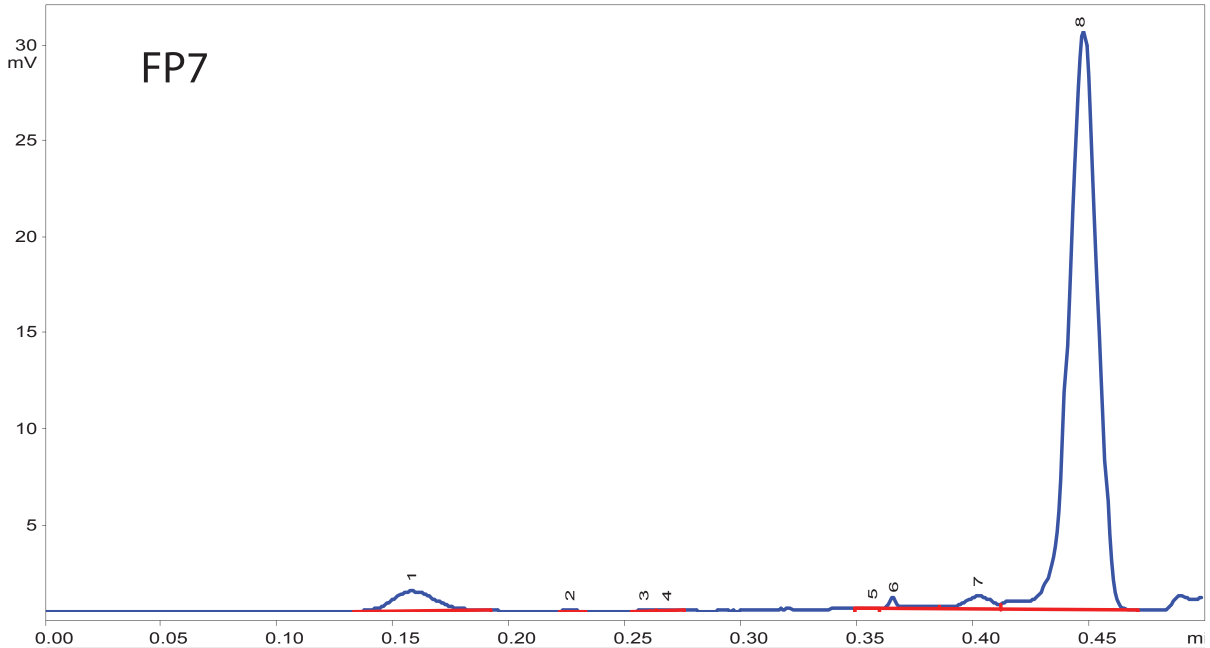
FP7
30
mV
25
20
15
10
5
1
2
3
4
5
6
7
8
0.00
0.05
0.10
0.15
0.20
0.25
0.30
0.35
0.40
0.45
m

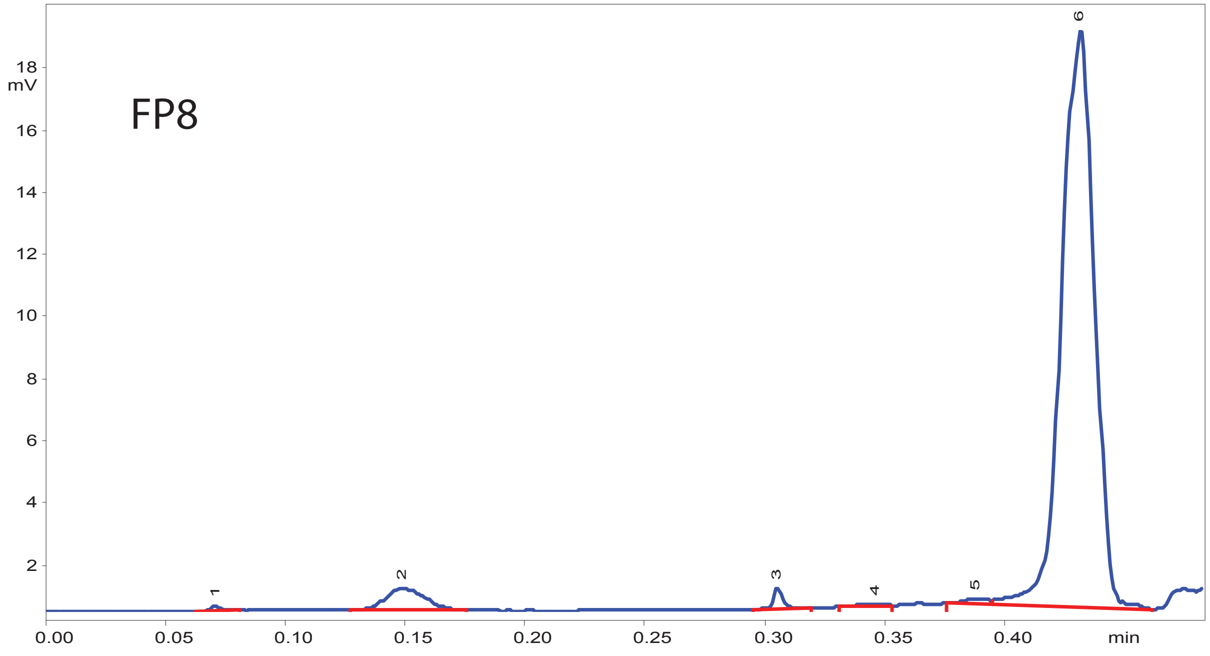
FP8
18
mV
16
14
12
10
8
6
4
2
1
2
3
4
5
6
0.00
0.05
0.10
0.15
0.20
0.25
0.30
0.35
0.40
min

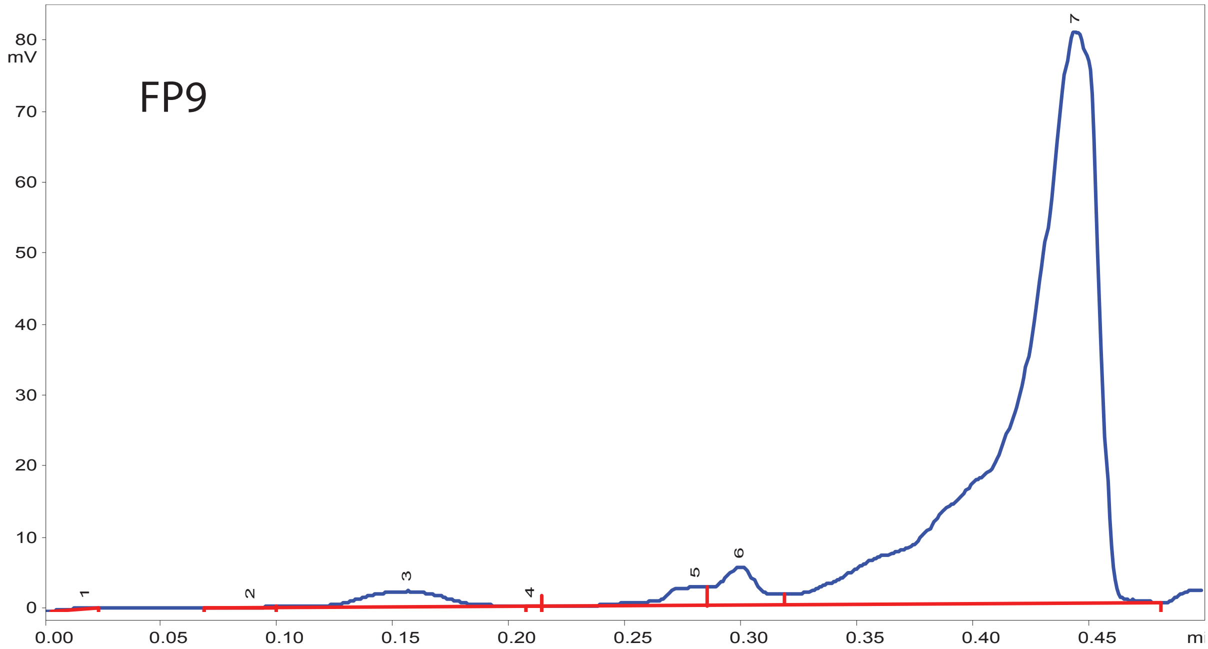
FP9
80
mV
70
60
50
40
30
20
10
0
1
2
3
4
5
6
7
0.00
0.05
0.10
0.15
0.20
0.25
0.30
0.35
0.40
0.45
m

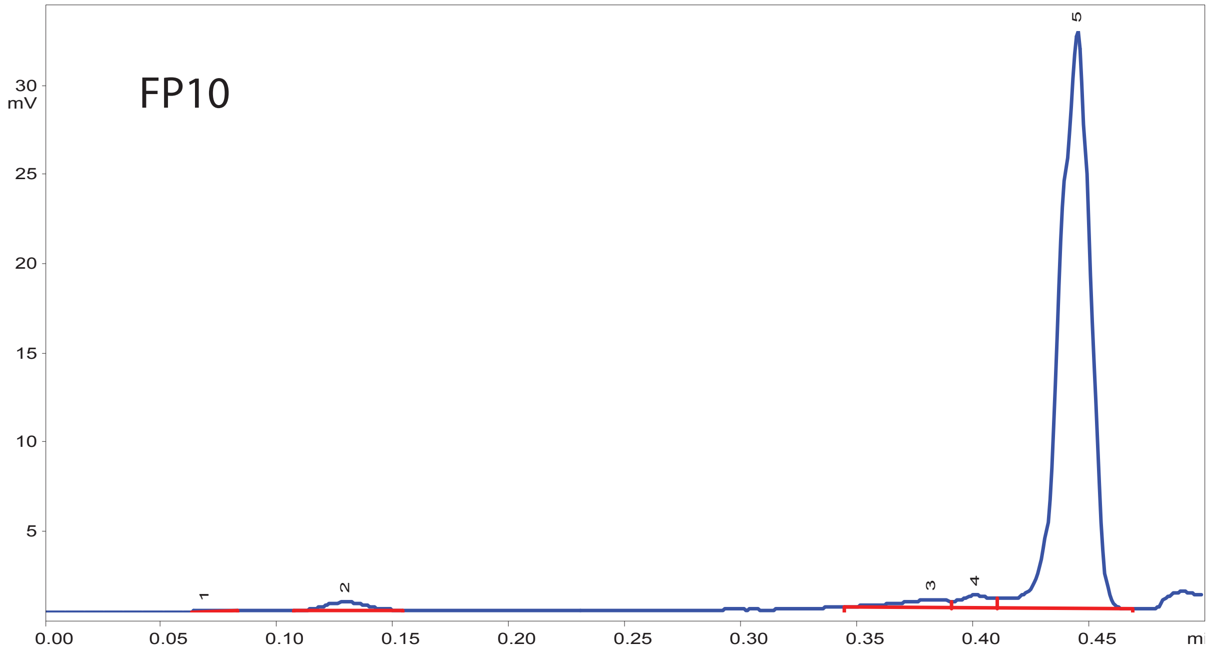
FP10
30
mV
25
20
15
10
5
1
2
3
4
5
0.00
0.05
0.10
0.15
0.20
0.25
0.30
0.35
0.40
0.45
m

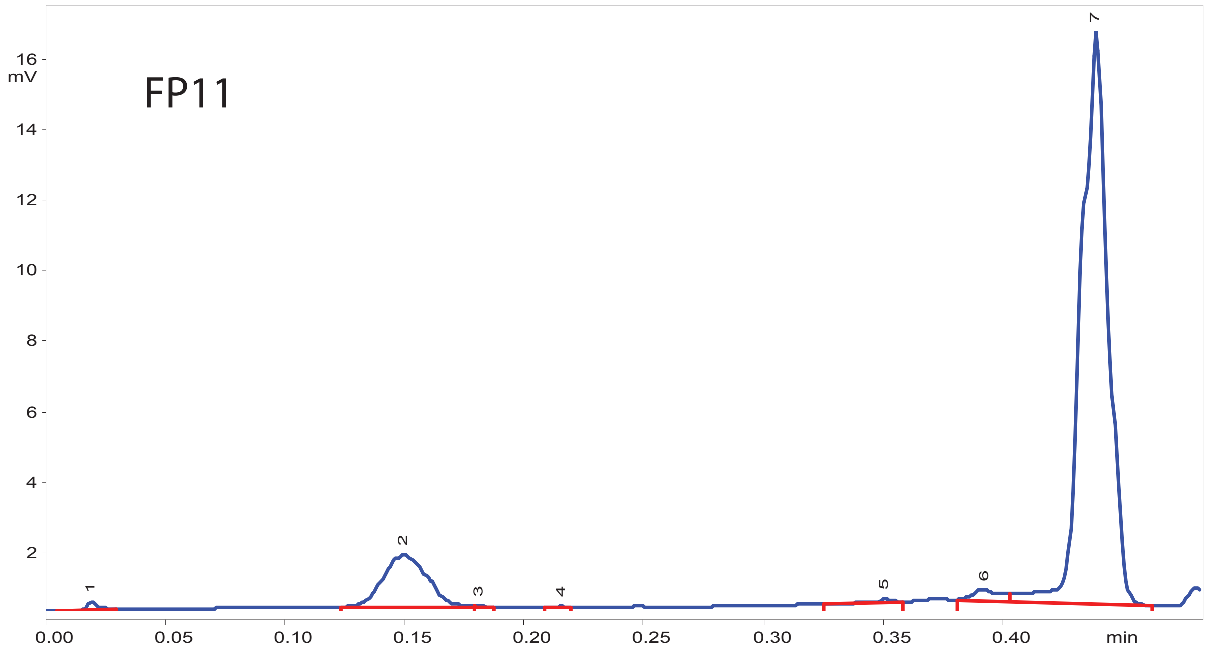
FP11
16
mV
14
12
10
8
6
4
2
1
2
3
4
5
6
7
0.00
0.05
0.10
0.15
0.20
0.25
0.30
0.35
0.40
min

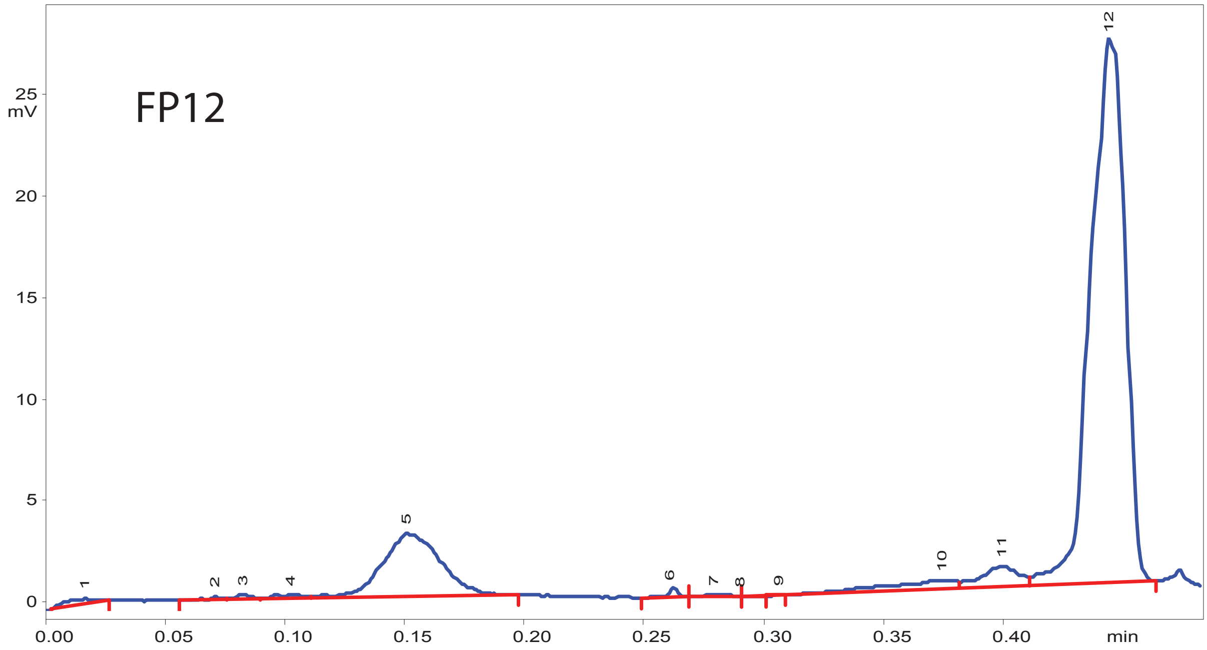
FP12
25
mV
20
15
10
5
0
1
2
3
4
5
6
7
8
9
10
11
12
0.00
0.05
0.10
0.15
0.20
0.25
0.30
0.35
0.40
min

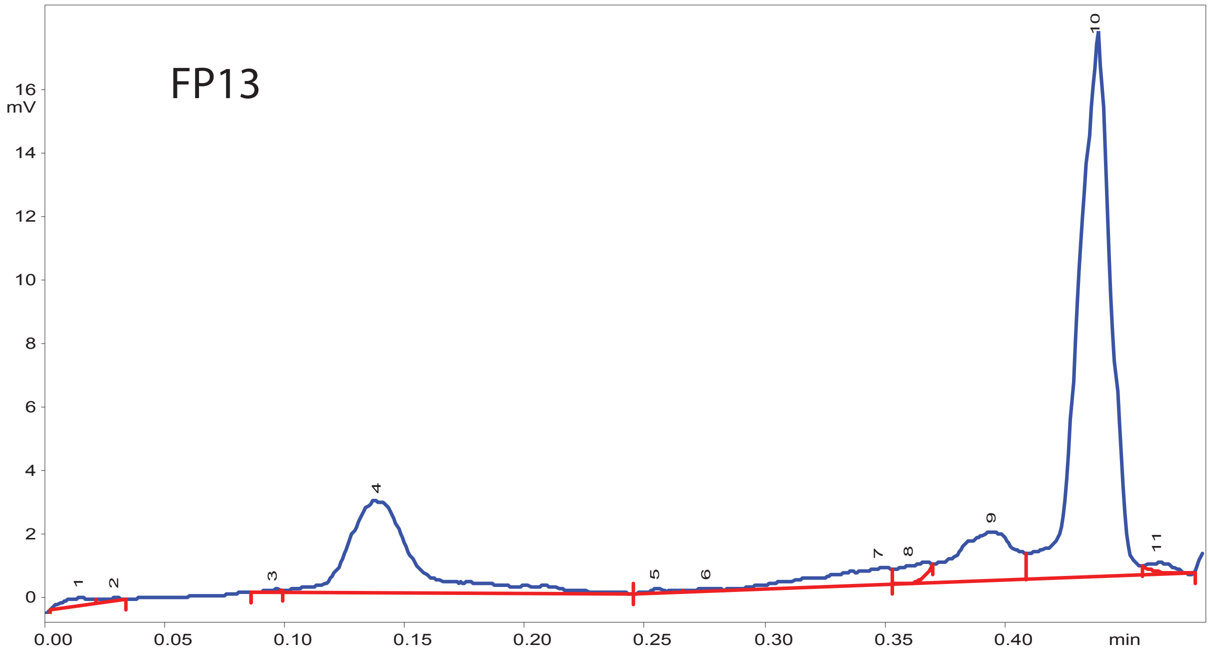
FP13
mV
16
14
12
10
8
6
4
2
0
0.00
0.05
0.10
0.15
0.20
0.25
0.30
0.35
0.40
min
1
2
3
4
5
6
7
8
9
10
11

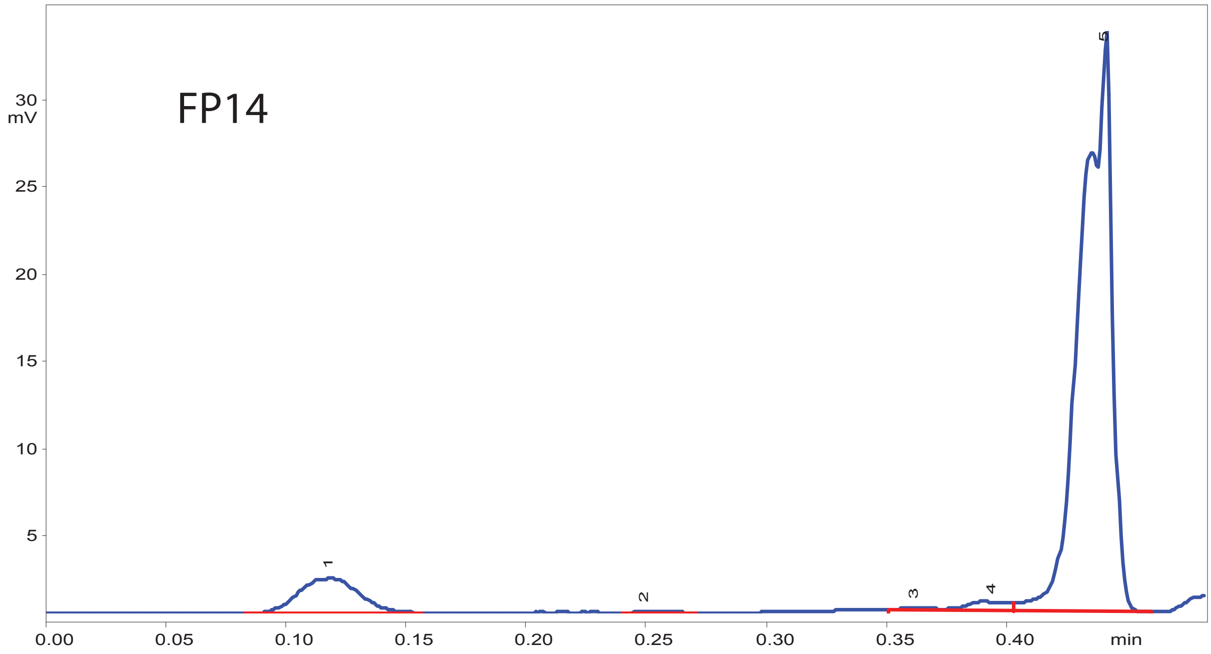
FP14
mV
30
25
20
15
10
5
0.00
0.05
0.10
0.15
0.20
0.25
0.30
0.35
0.40
min
1
2
3
4
5

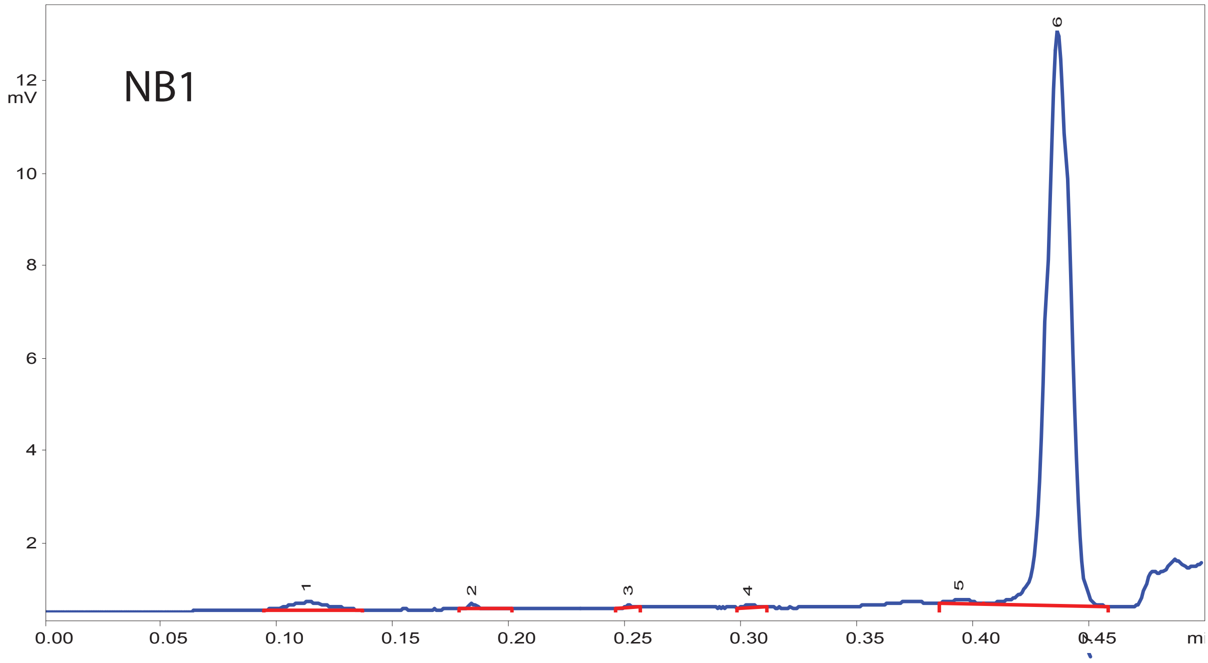
NB1
mV
12
10
8
6
4
2
1
2
3
4
5
6
0.00
0.05
0.10
0.15
0.20
0.25
0.30
0.35
0.40
0.45
m

# Appendix B

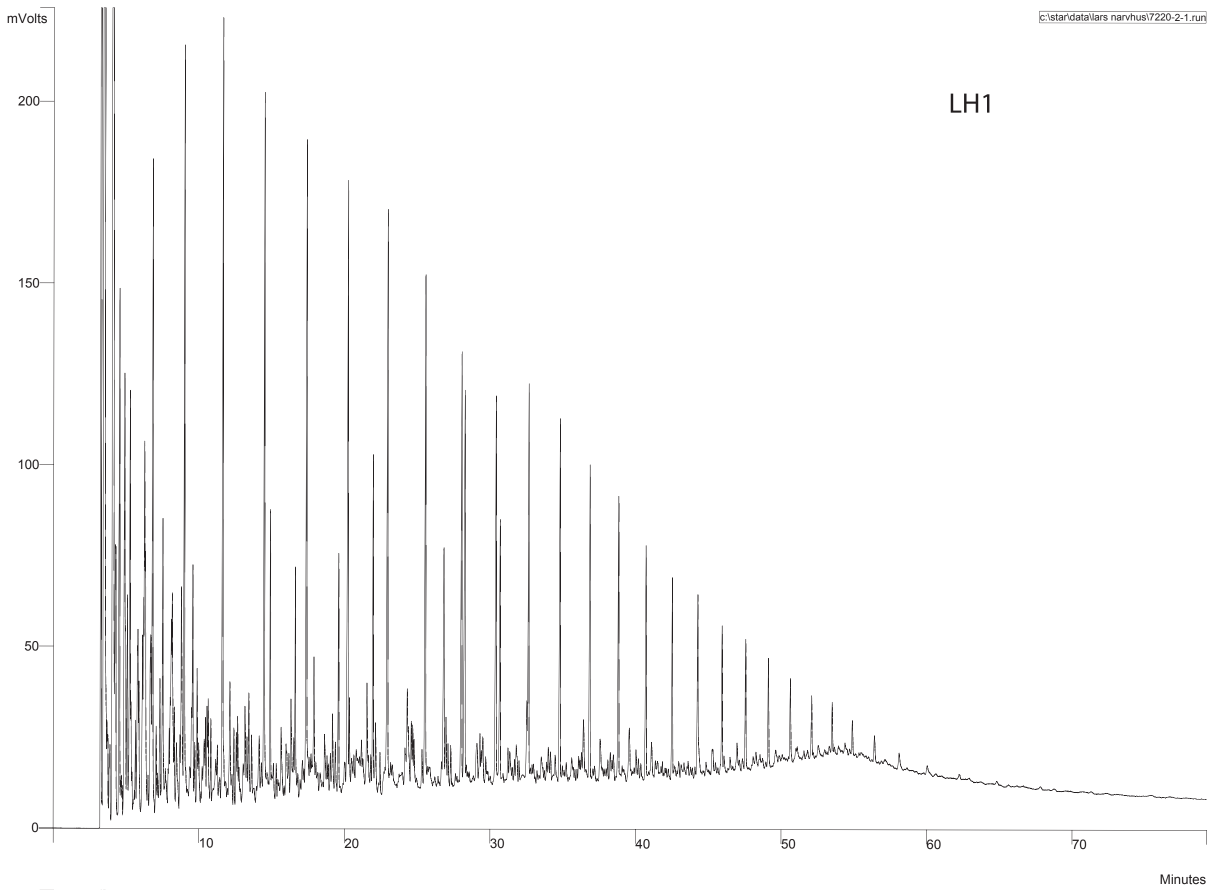
mVolts
c:\star\data\lars narvhus\7220-2-1.run
LH1
200
150
100
50
0
10
20
30
40
50
60
70
Minutes

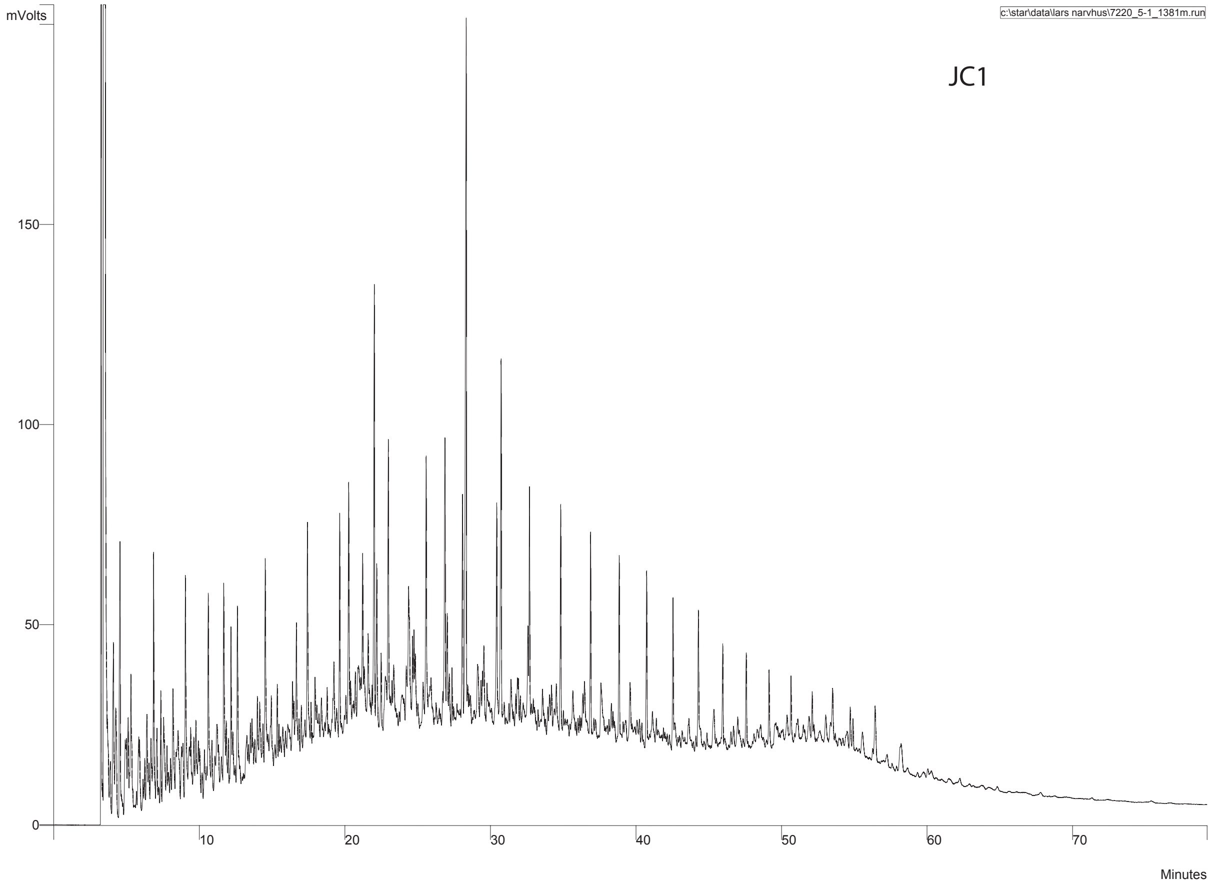
mVolts
c:\star\data\lars narvhus\7220_5-1_1381m.run
JC1
150
100
50
0
10
20
30
40
50
60
70
Minutes

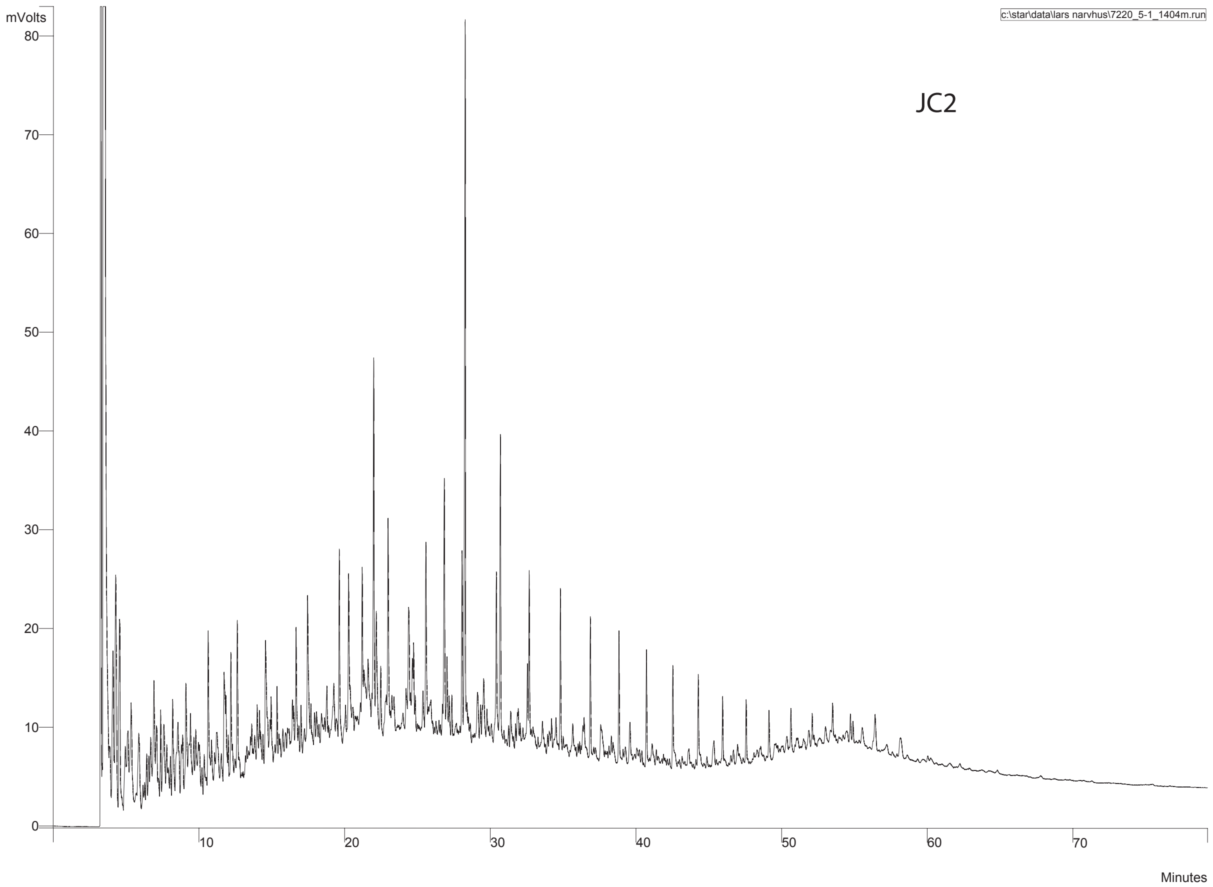
mVolts
80
70
60
50
40
30
20
10
0
c:\star\data\lars narvhus\7220_5-1_1404m.run
JC2
10
20
30
40
50
60
70
Minutes

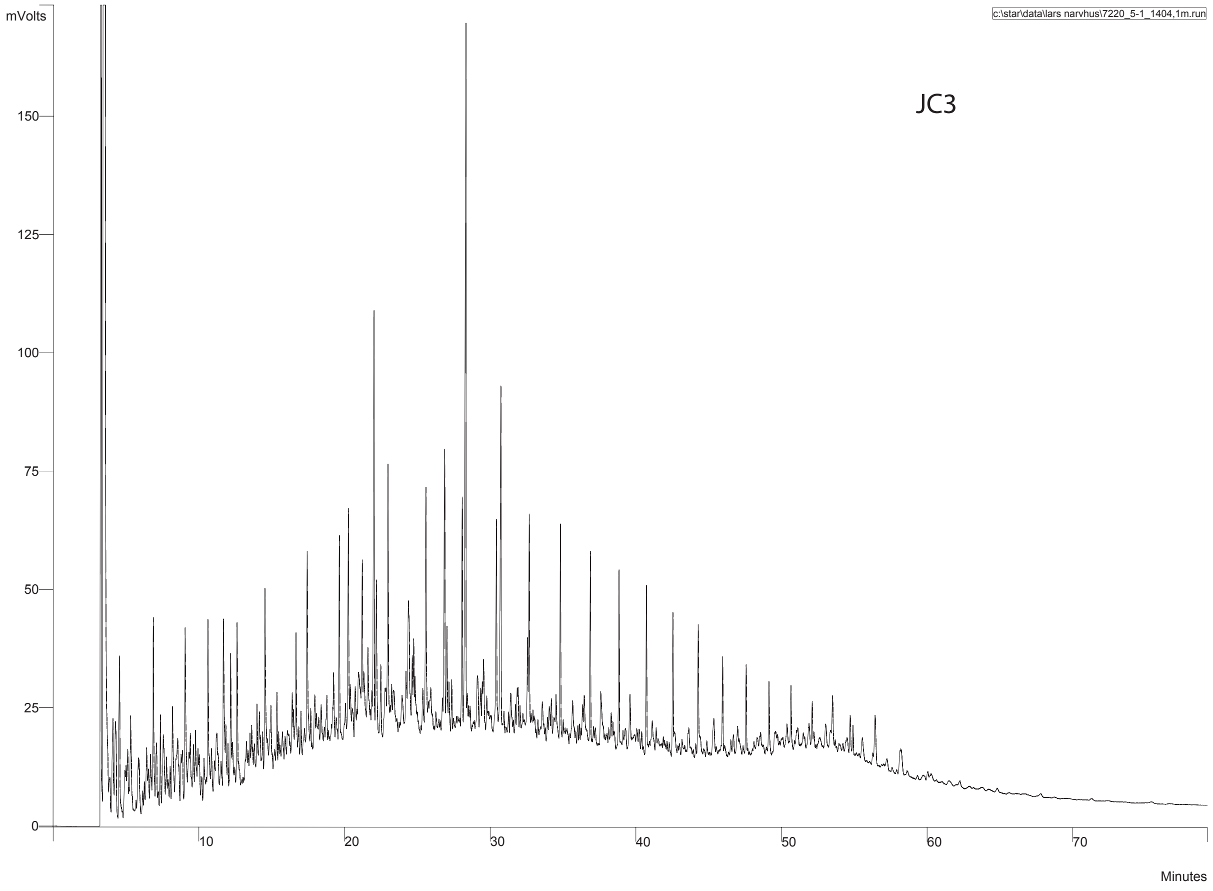
mVolts
150
125
100
75
50
25
0
c:\star\data\lars narvhus\7220_5-1_1404,1m.run
JC3
10
20
30
40
50
60
70
Minutes

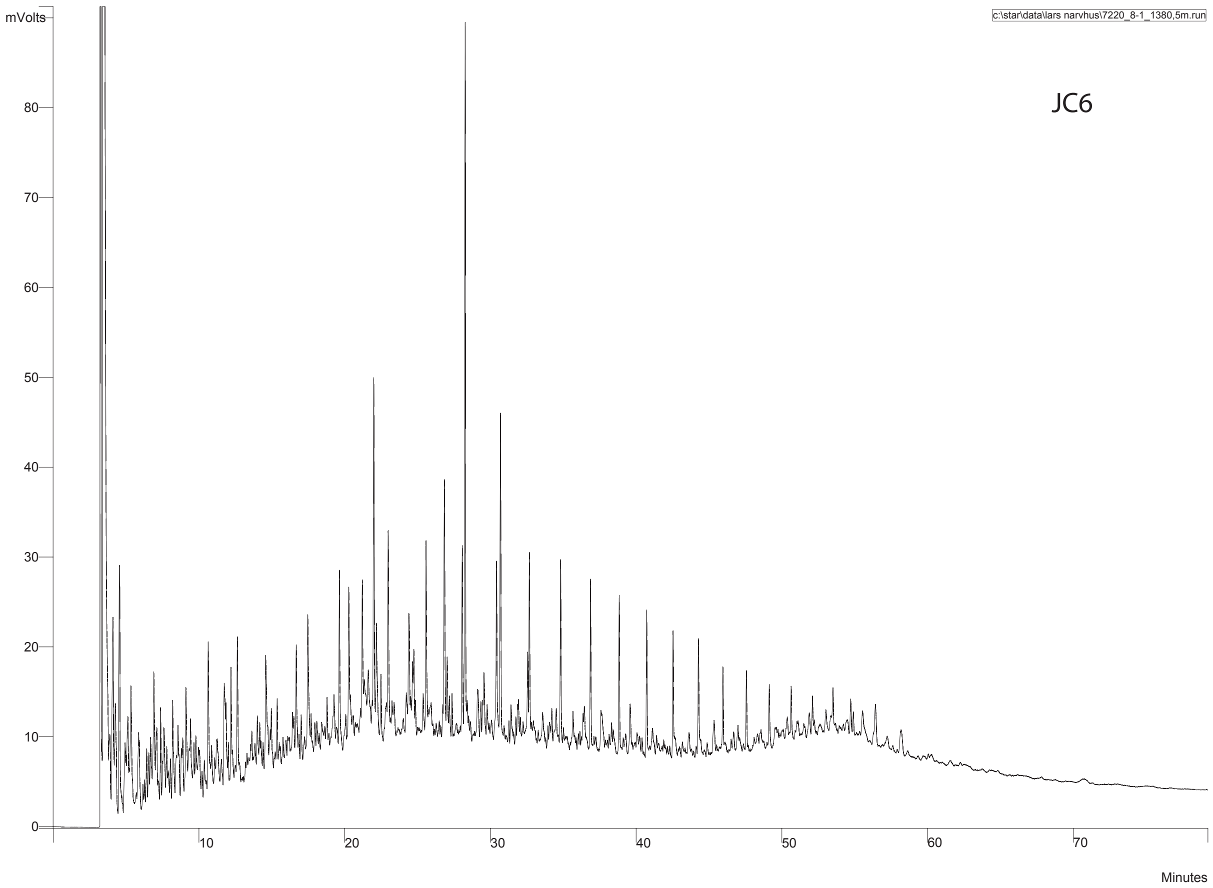
mVolts
80
70
60
50
40
30
20
10
0
10
20
30
40
50
60
70
Minutes
c:\star\data\lars narvhus\7220_8-1_1380,5m.run
JC6

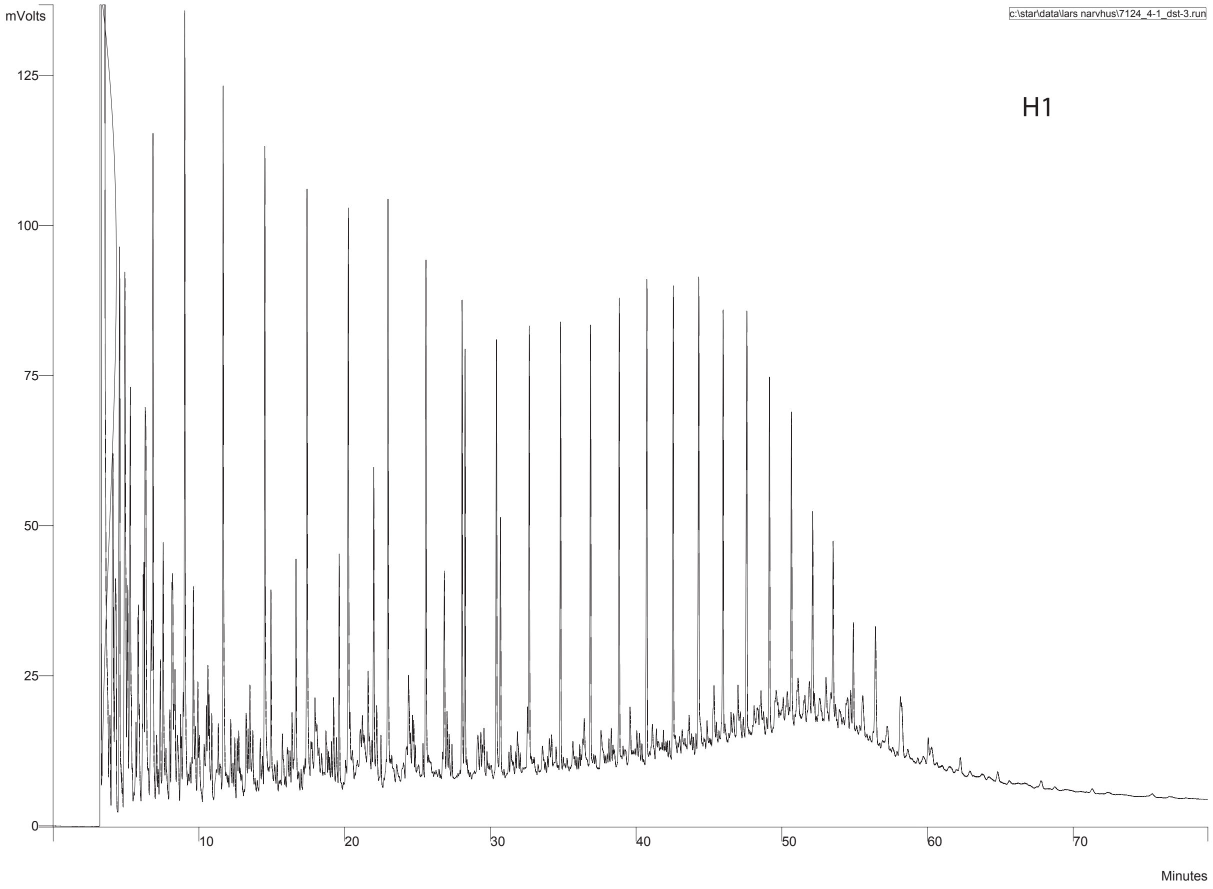
mVolts
125
100
75
50
25
0
10
20
30
40
50
60
70
Minutes
c:\star\data\lars narvhus\7124_4-1_dst-3.run
H1

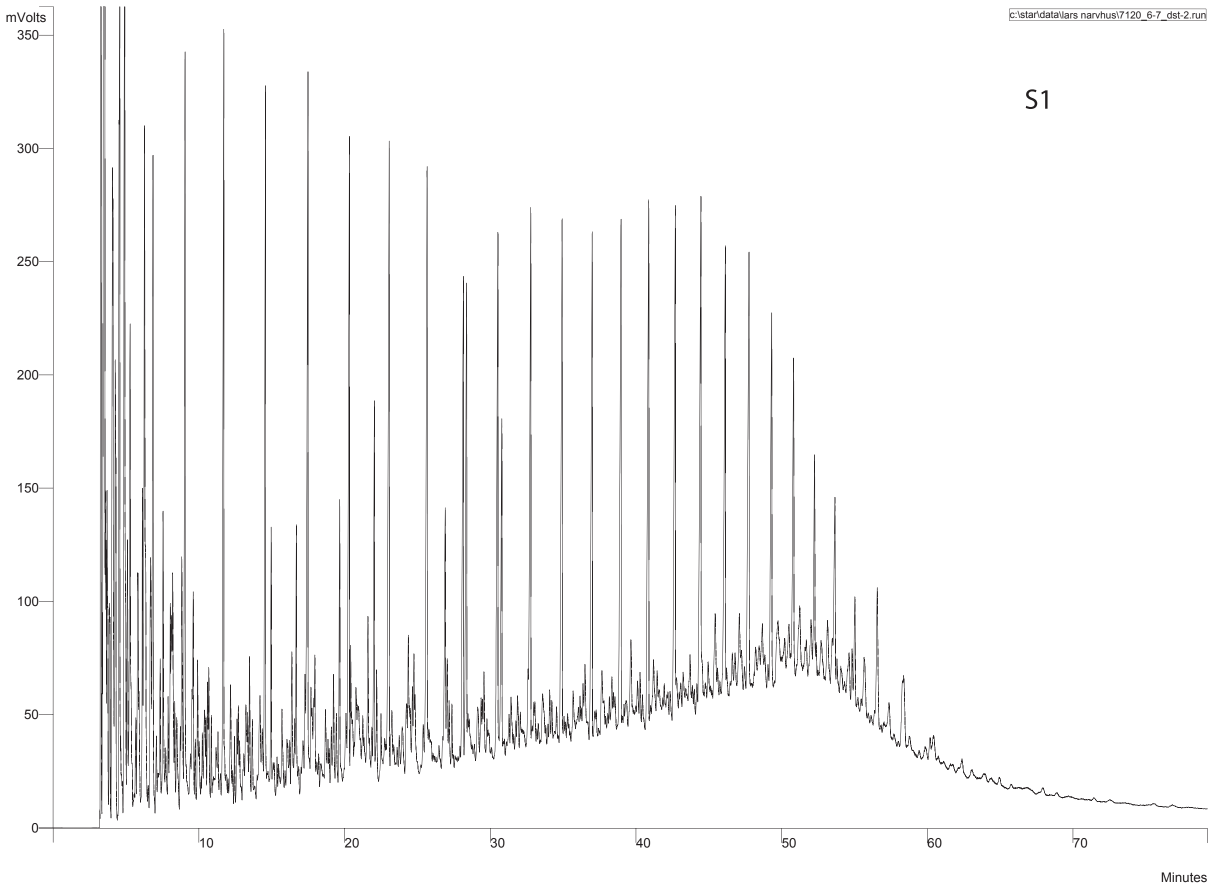
mVolts
350
300
250
200
150
100
50
0
c:\star\data\lars narvhus\7120_6-7_dst-2.run
S1
10
20
30
40
50
60
70
Minutes

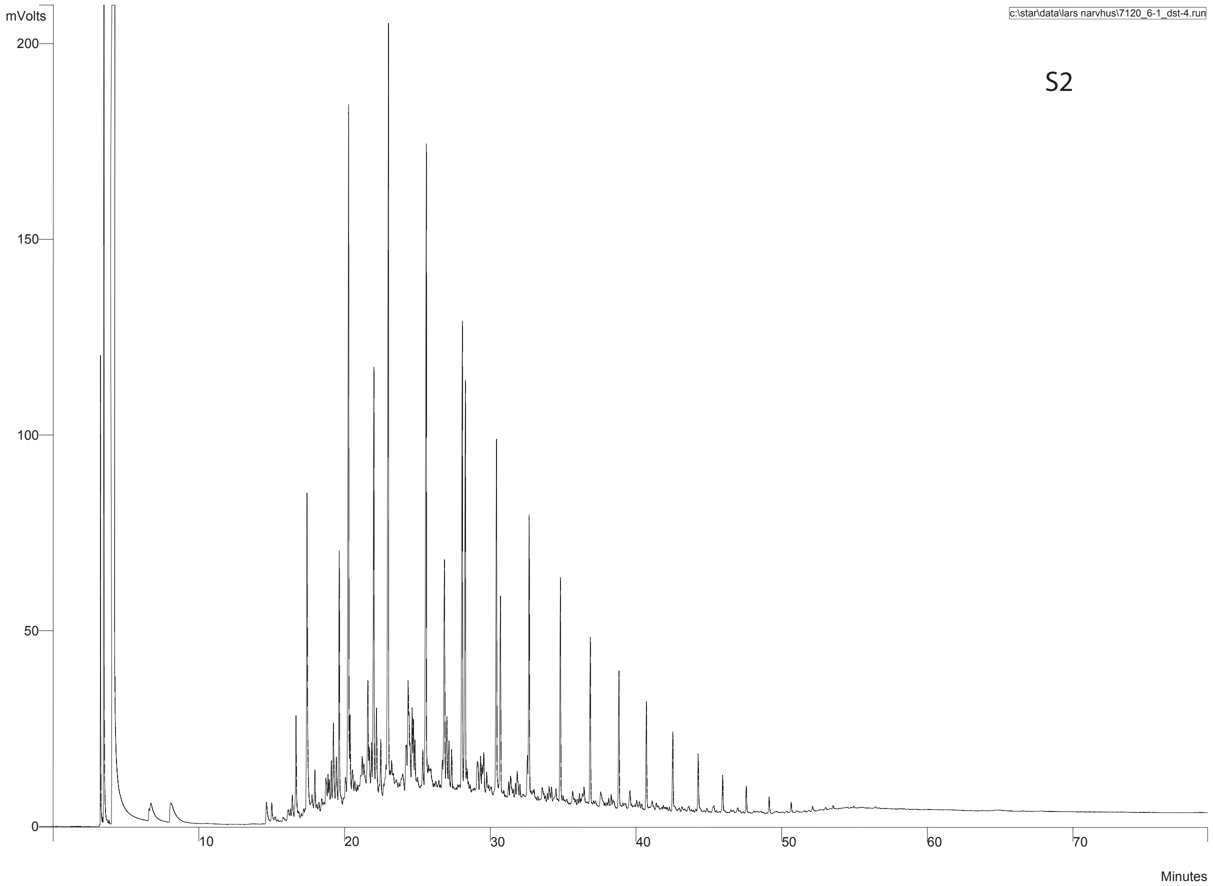
mVolts
200
150
100
50
0
c:\star\data\lars narvhus\7120_6-1_dst-4.run
S2
10
20
30
40
50
60
70
Minutes

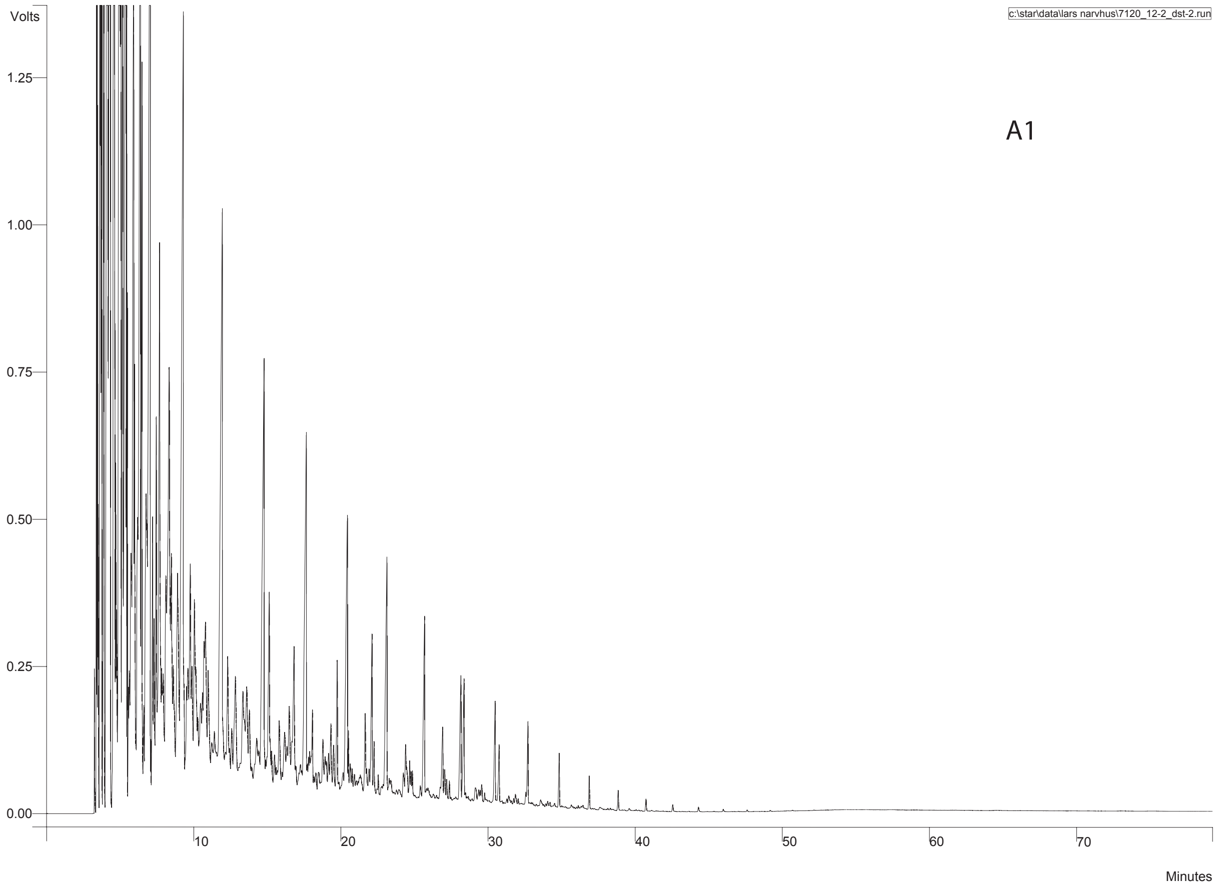
Volts
1.25
1.00
0.75
0.50
0.25
0.00
10
20
30
40
50
60
70
Minutes
c:\star\data\lars narvhus\7120_12-2_dst-2.run
A1

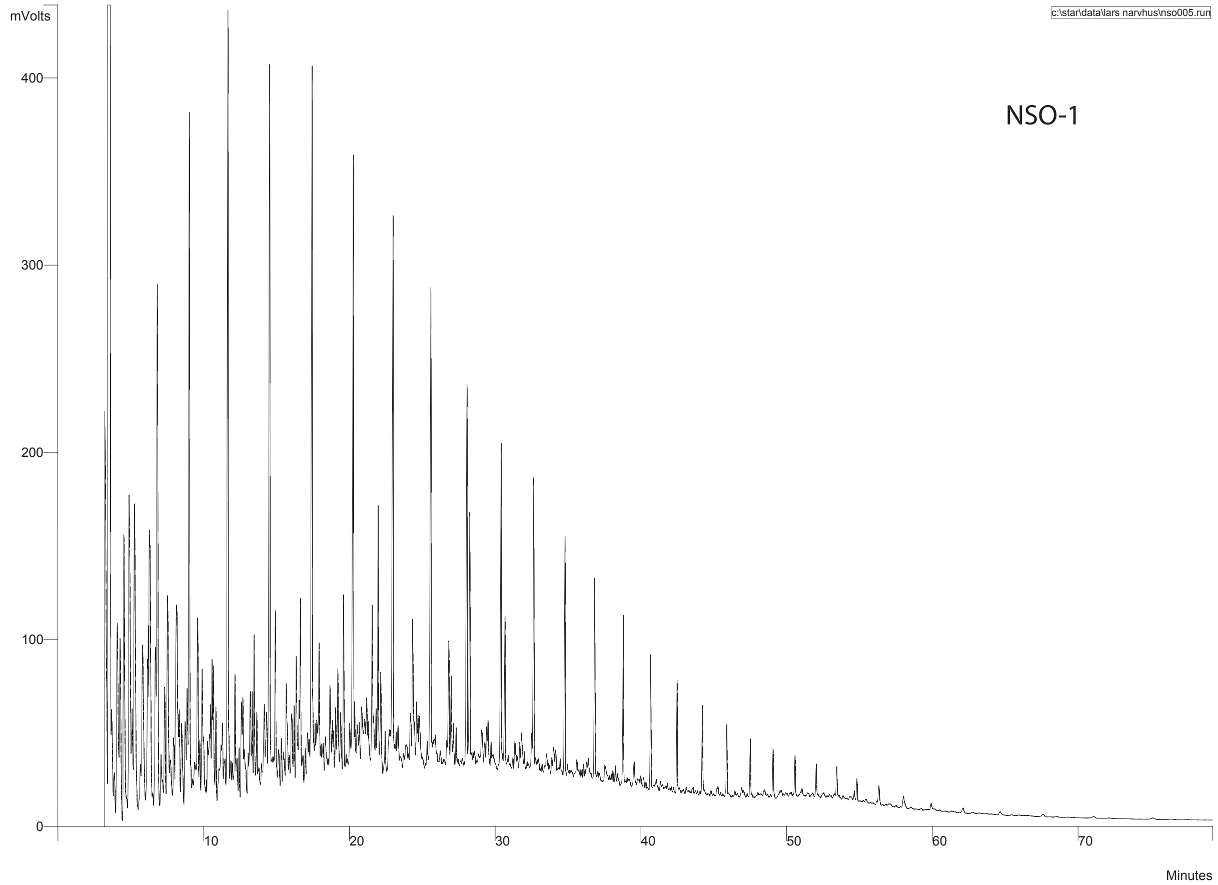
mVolts
400
300
200
100
0
10
20
30
40
50
60
70
Minutes
c:\star\data\lars narvhus\nso005.run
NSO-1

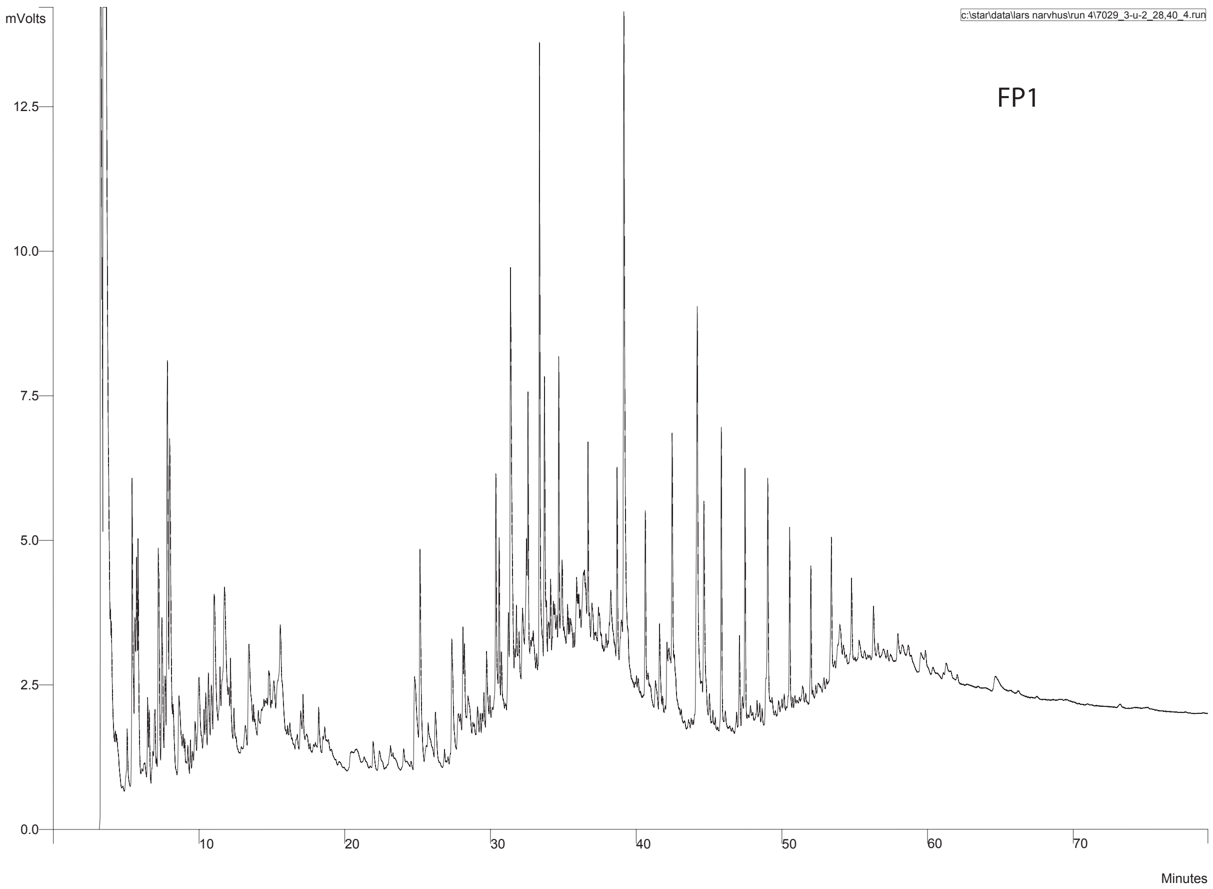
mVolts
12.5
10.0
7.5
5.0
2.5
0.0
10
20
30
40
50
60
70
Minutes
c:\star\data\lars narvhus\run 4\7029_3-u-2_28,40_4.run
FP1

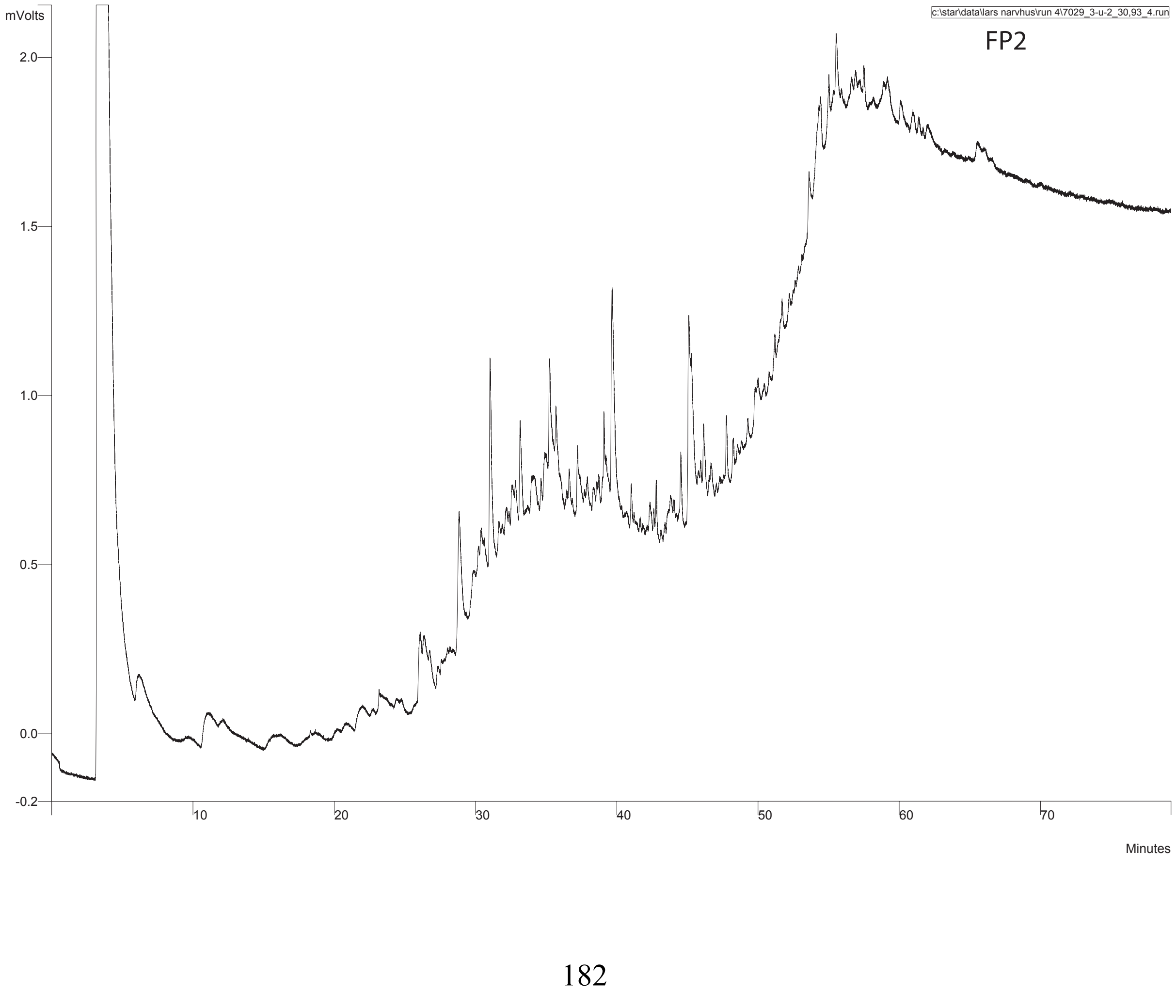
mVolts
2.0
1.5
1.0
0.5
0.0
-0.2
10
20
30
40
50
60
70
Minutes
c:\star\data\lars narvhus\run 4\7029_3-u-2_30,93_4.run
FP2

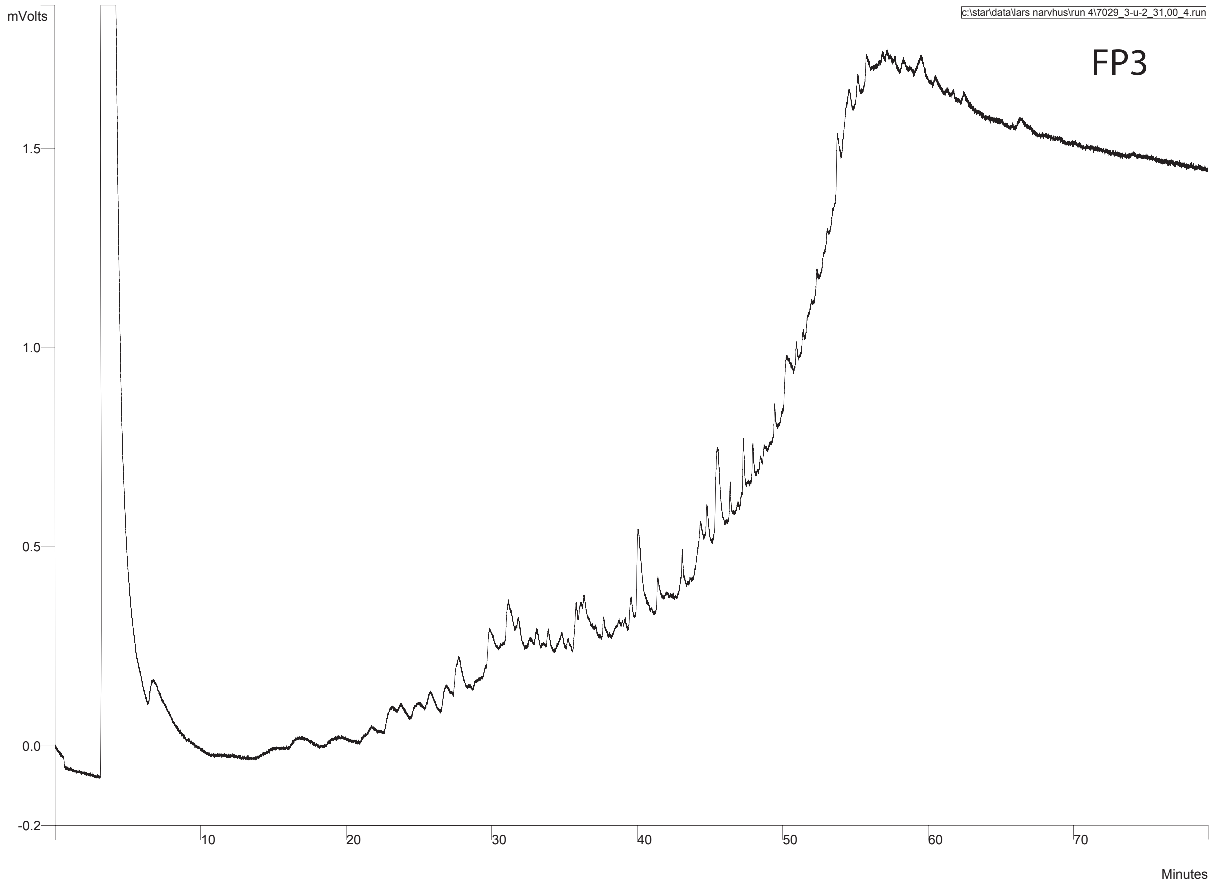
mVolts
c:\star\data\lars narvhus\run 4\7029_3-u-2_31,00_4.run
FP3
1.5
1.0
0.5
0.0
-0.2
10
20
30
40
50
60
70
Minutes

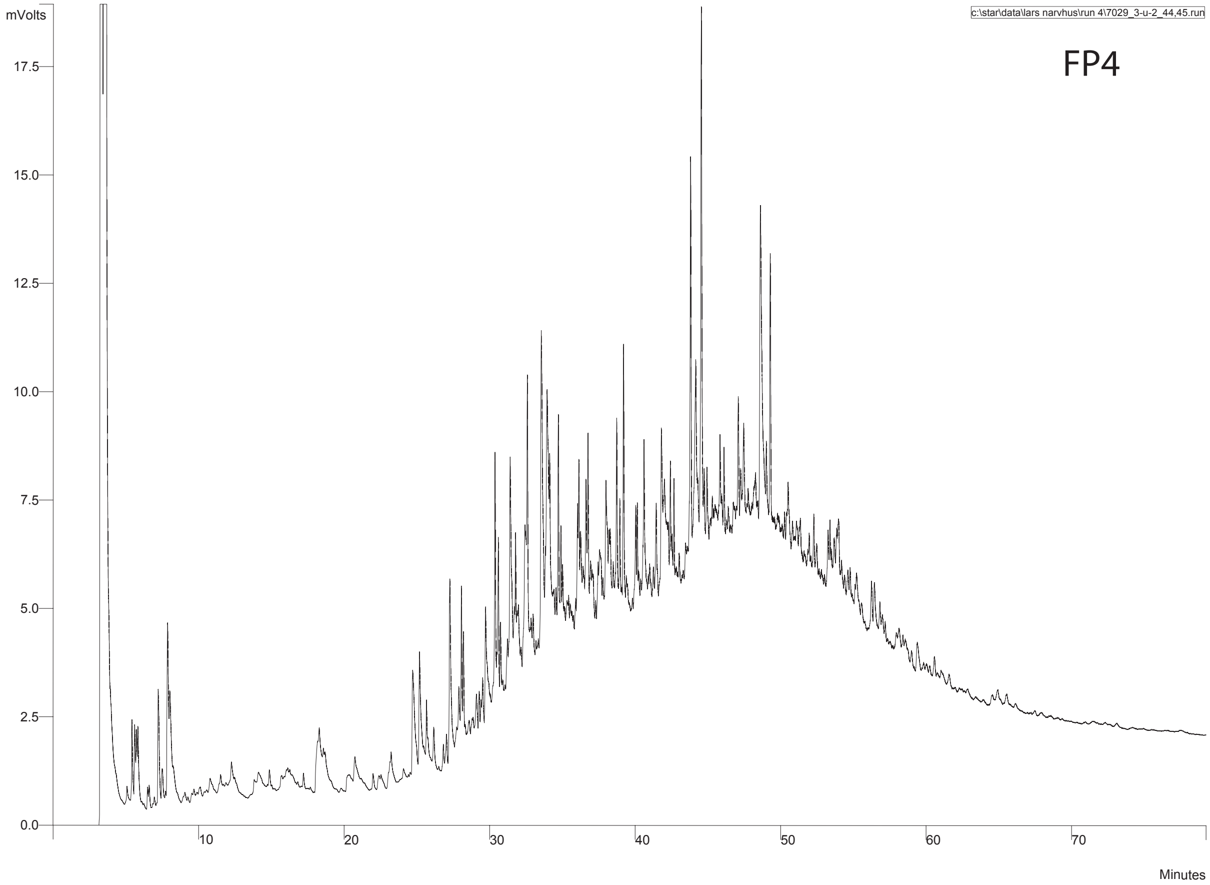
mVolts
c:\star\data\lars narvhus\run 4\7029_3-u-2_44,45.run
FP4
17.5
15.0
12.5
10.0
7.5
5.0
2.5
0.0
10
20
30
40
50
60
70
Minutes

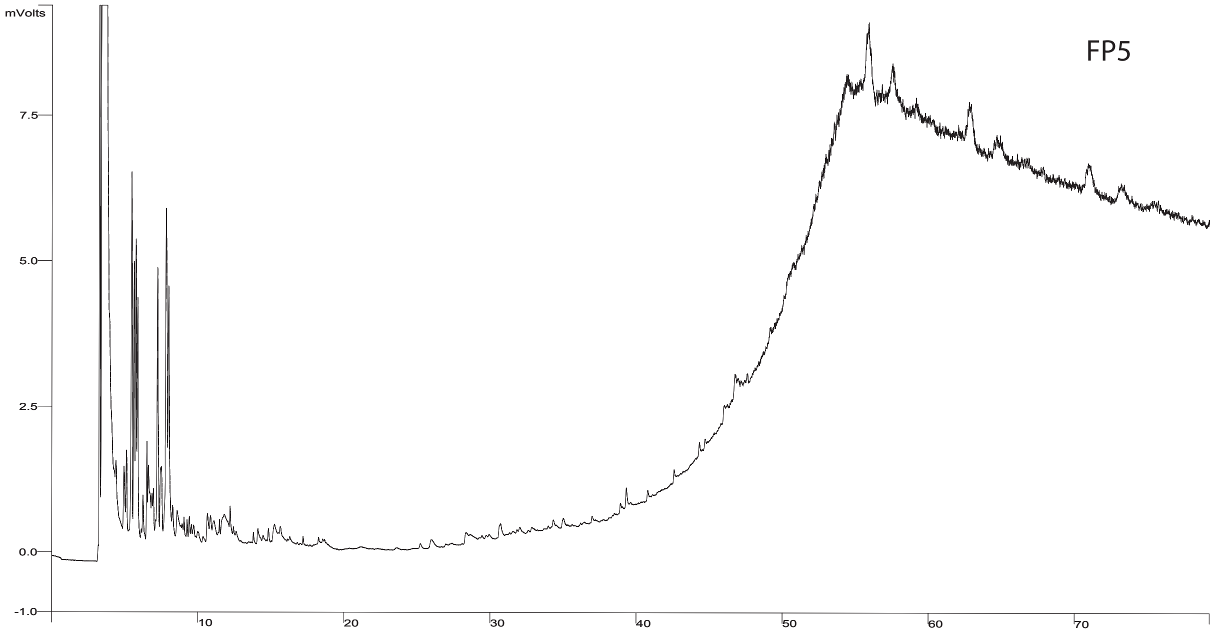
mVolts
7.5
5.0
2.5
0.0
-1.0
10
20
30
40
50
60
70
FP5

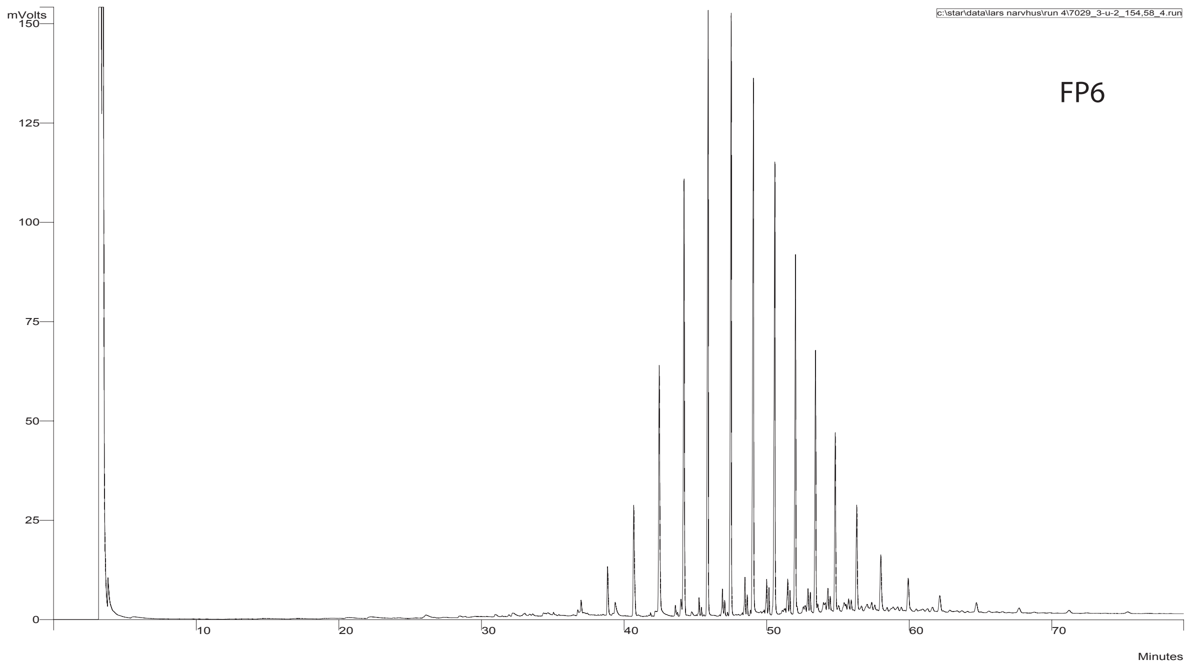
mVolts
150
125
100
75
50
25
0
10
20
30
40
50
60
70
Minutes
c:\star\data\lars narvhus\run 4\7029_3-u-2_154,58_4.run
FP6

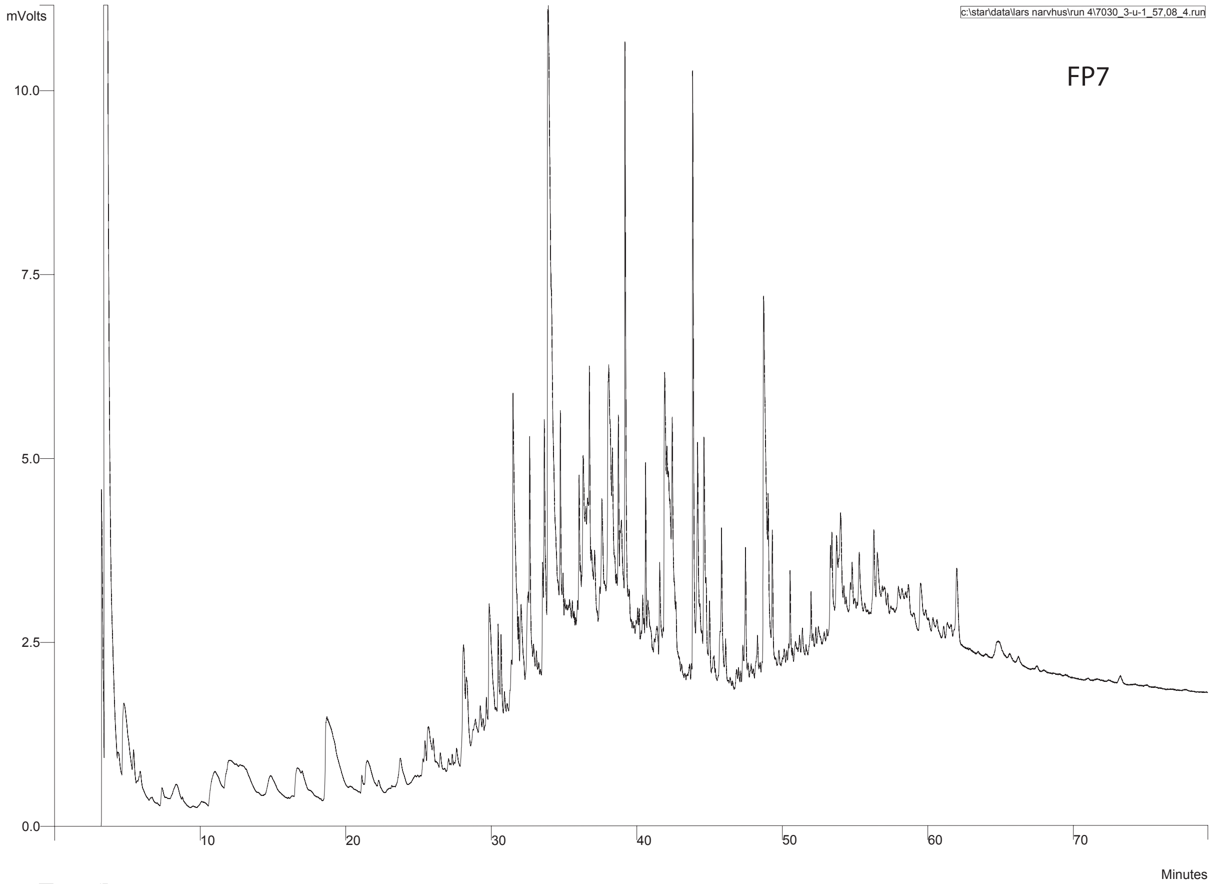
mVolts
10.0
7.5
5.0
2.5
0.0
c:\star\data\lars narvhus\run 4\7030_3-u-1_57,08_4.run
FP7
10
20
30
40
50
60
70
Minutes

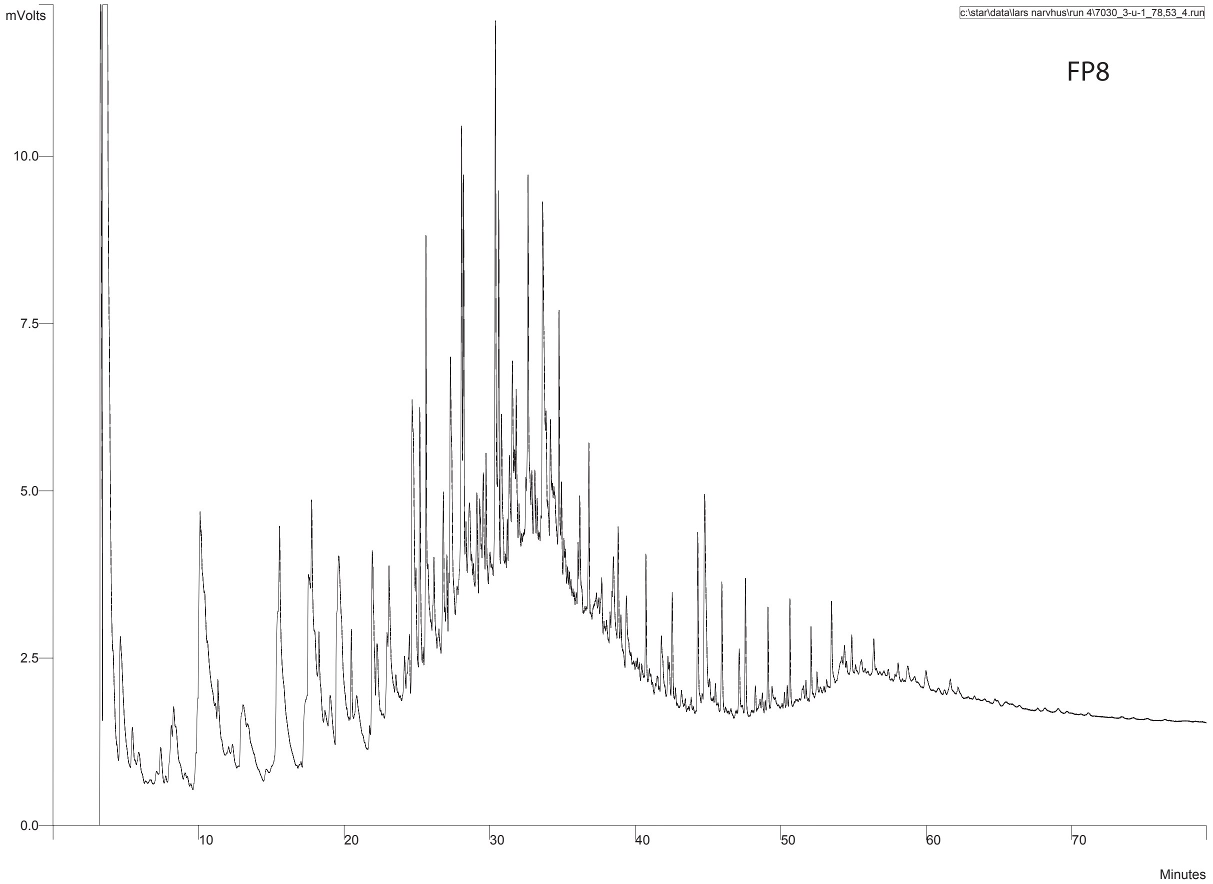
mVolts
10.0
7.5
5.0
2.5
0.0
c:\star\data\lars narvhus\run 4\7030_3-u-1_78,53_4.run
FP8
10
20
30
40
50
60
70
Minutes

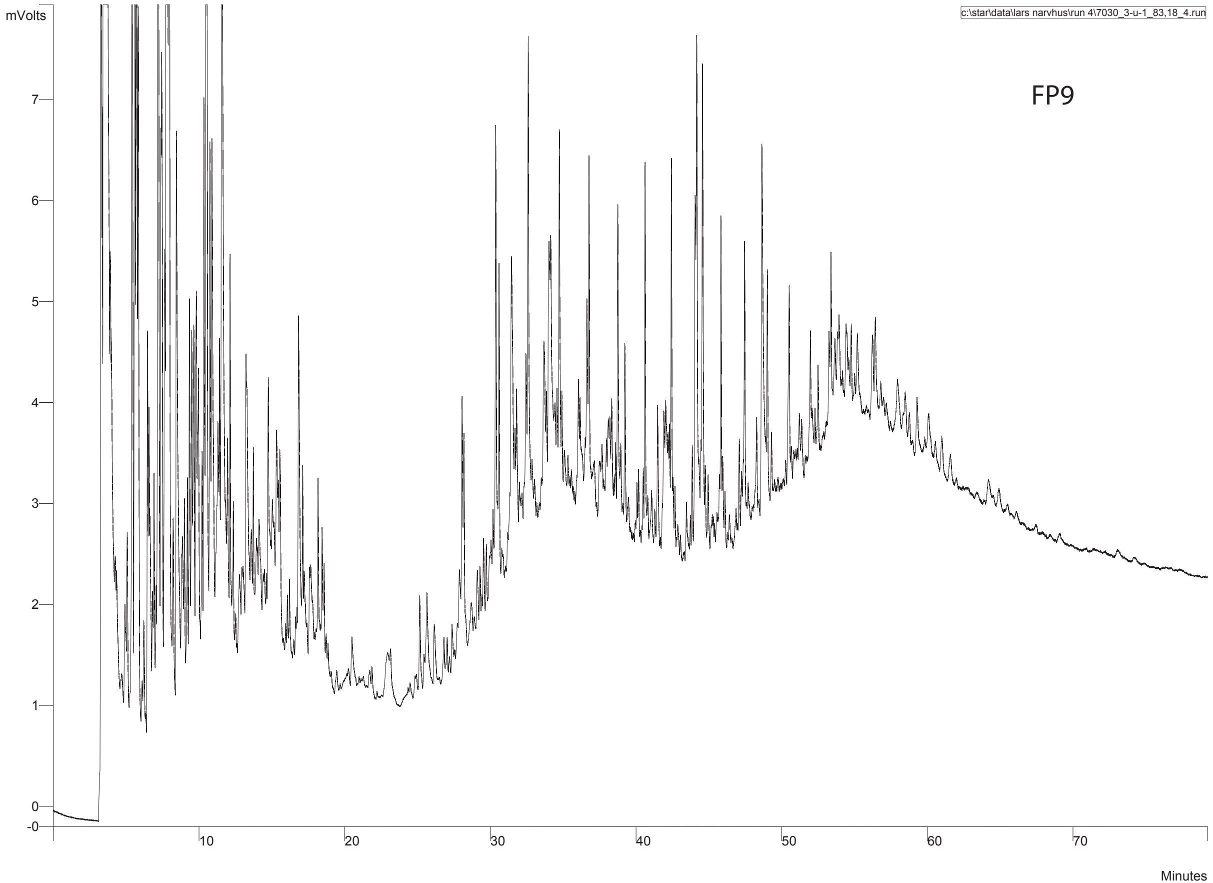
mVolts
c:\star\data\lars narvhus\run 4\7030_3-u-1_83,18_4.run
FP9
7
6
5
4
3
2
1
0
-0
10
20
30
40
50
60
70
Minutes

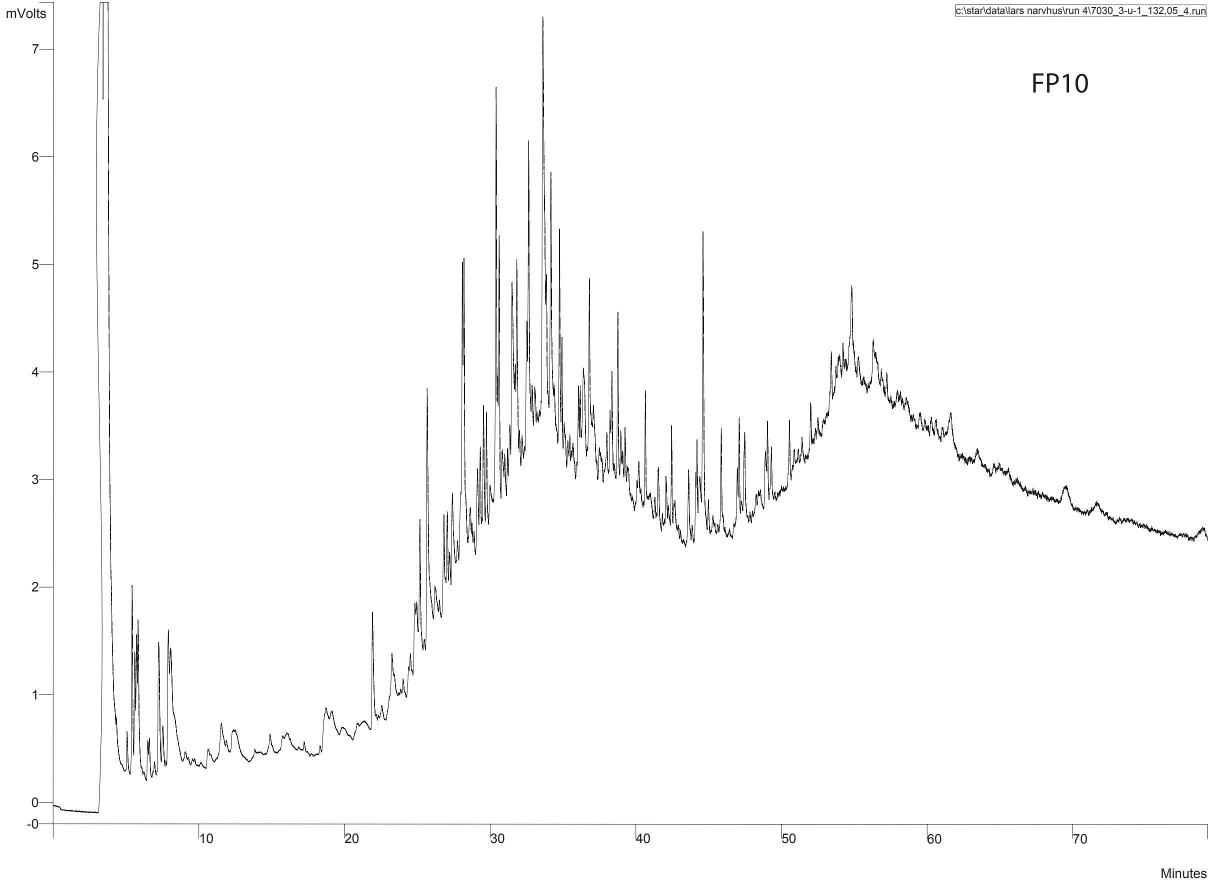
mVolts
c:\star\data\lars narvhus\run 4\7030_3-u-1_132,05_4.run
FP10
7
6
5
4
3
2
1
0
-0
10
20
30
40
50
60
70
Minutes

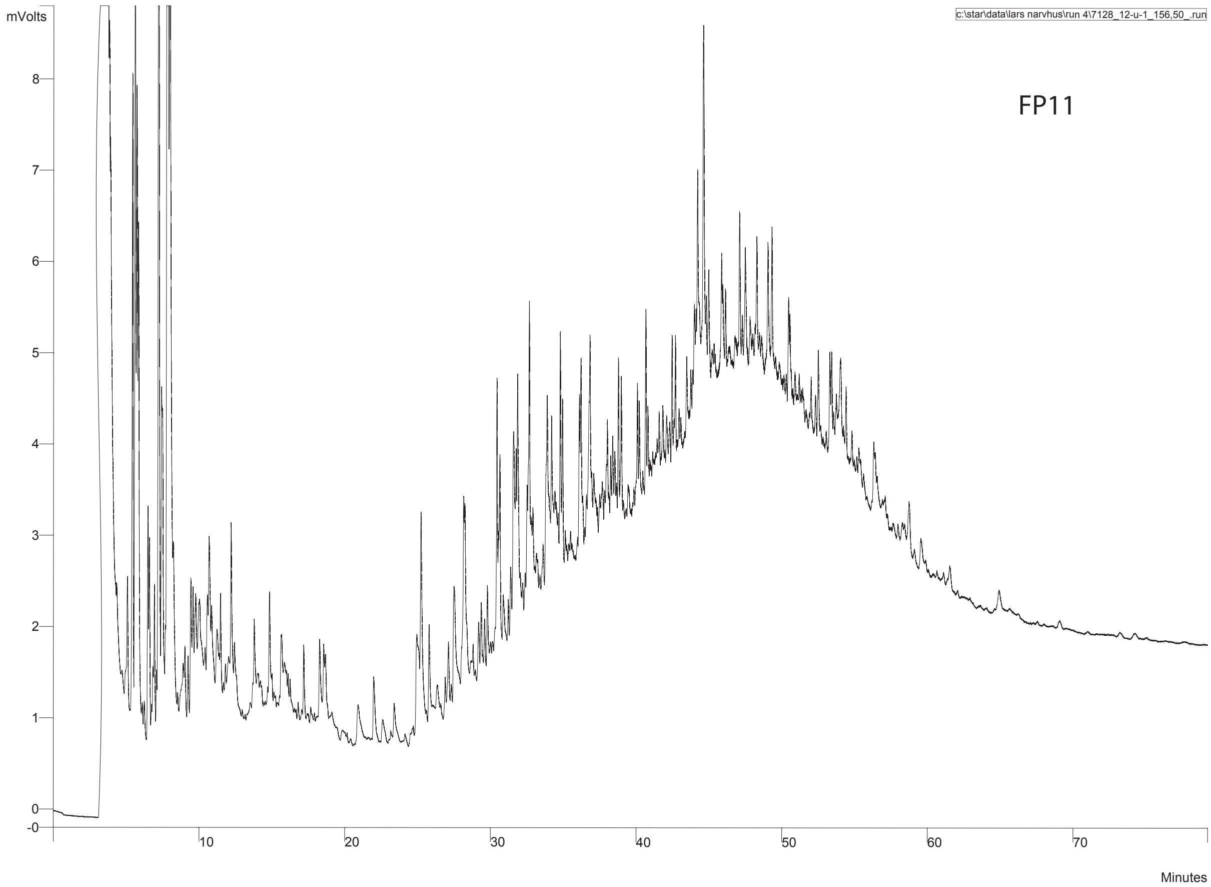
mVolts
8
7
6
5
4
3
2
1
0
-0
10
20
30
40
50
60
70
Minutes
c:\star\data\lars narvhus\run 4\7128_12-u-1_156,50_.run
FP11

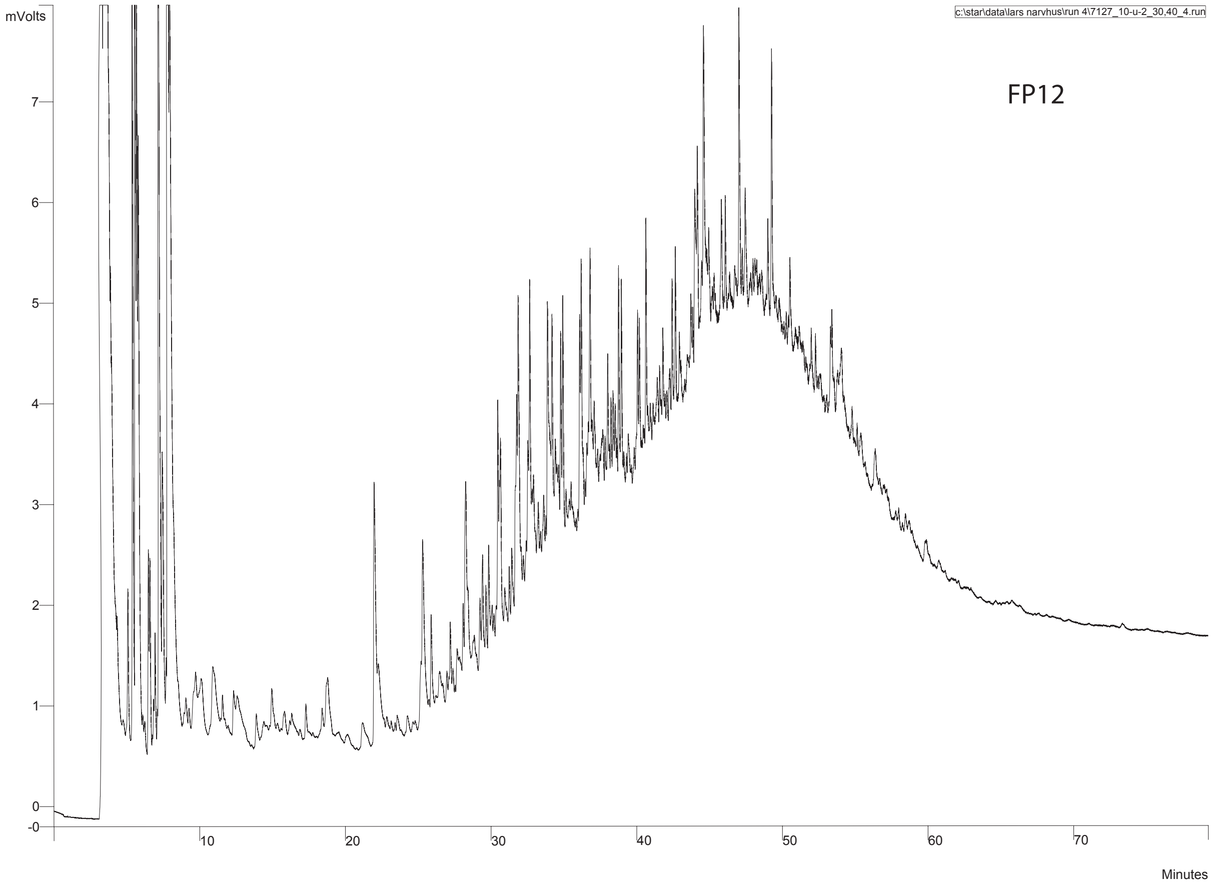
mVolts
7
6
5
4
3
2
1
0
-0
10
20
30
40
50
60
70
Minutes
c:\star\data\lars narvhus\run 4\7127_10-u-2_30,40_4.run
FP12

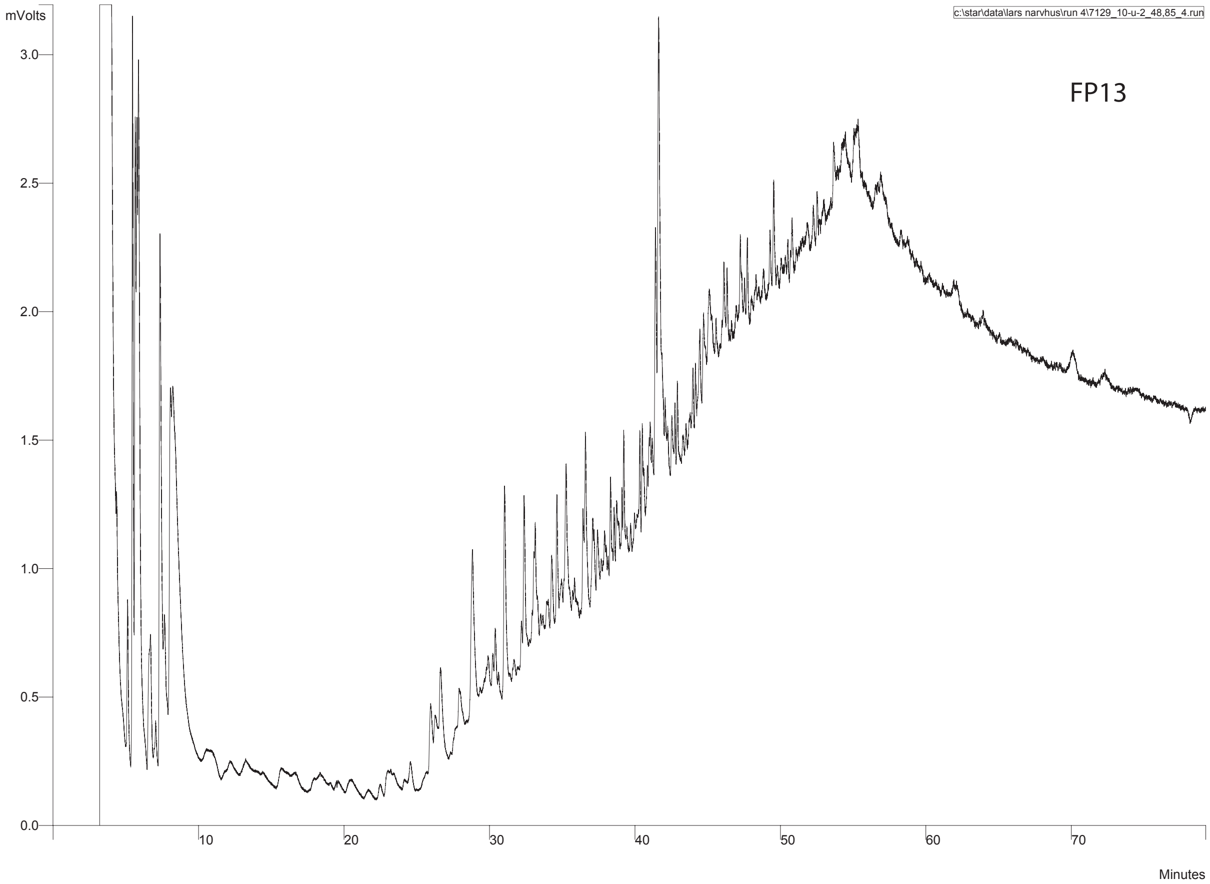
mVolts
3.0
2.5
2.0
1.5
1.0
0.5
0.0
10
20
30
40
50
60
70
Minutes
c:\star\data\lars narvhus\run 4\7129_10-u-2_48,85_4.run
FP13

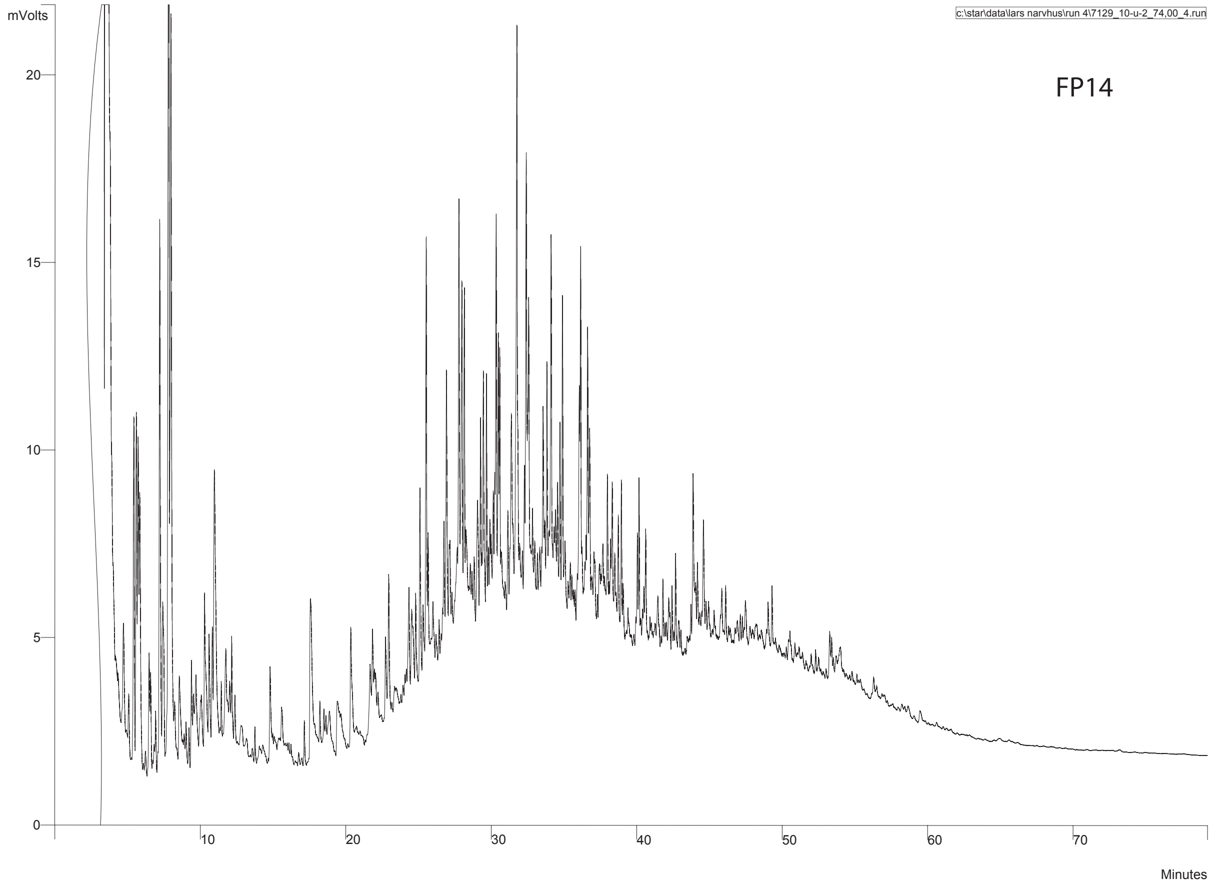
mVolts
20
15
10
5
0
10
20
30
40
50
60
70
Minutes
c:\star\data\lars narvhus\run 4\7129_10-u-2_74,00_4.run
FP14

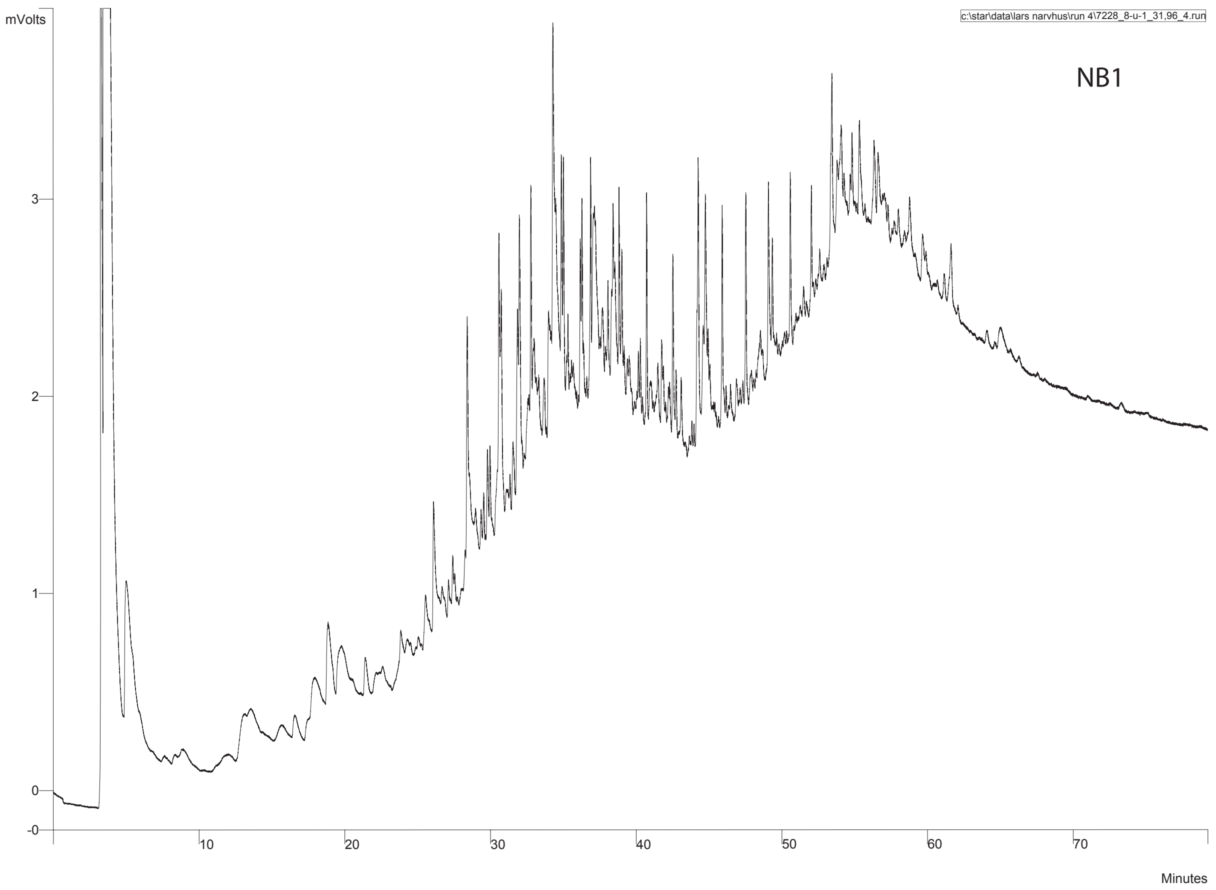
mVolts
3
2
1
0
-0
10
20
30
40
50
60
70
Minutes
c:\star\data\lars narvhus\run 4\7228_8-u-1_31,96_4.run
NB1

# Appendix C

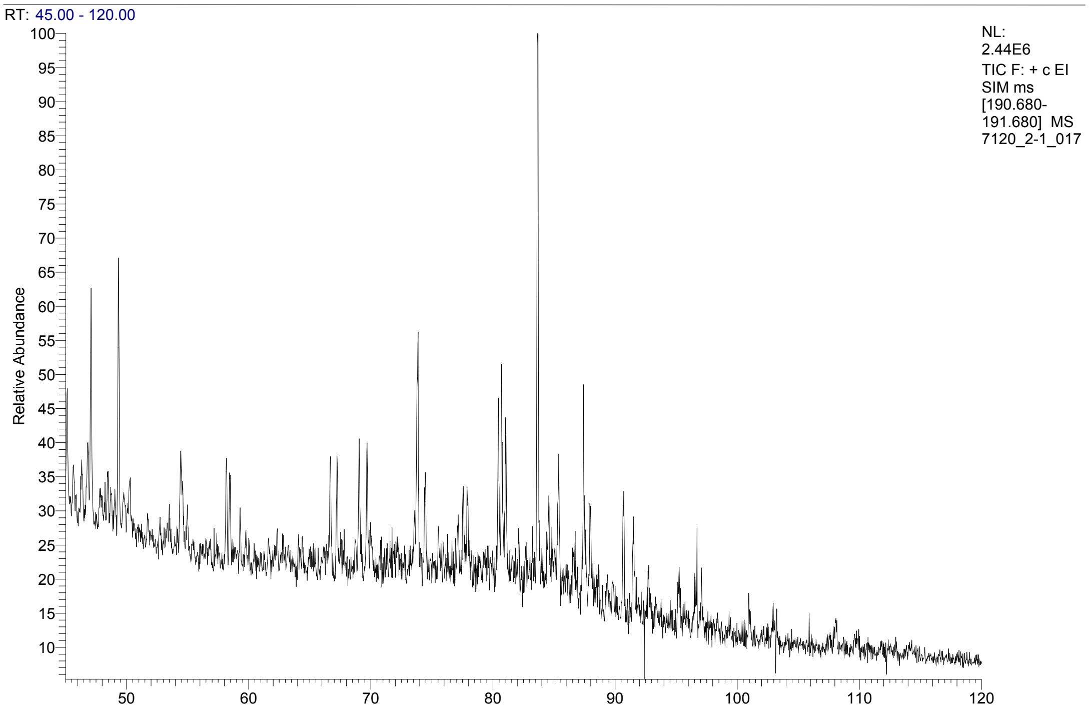
RT: 45.00 - 120.00
NL:
2.44E6
TIC F: + c EI
SIM ms
[190.680-
191.680] MS
7120_2-1_017
Relative Abundance
100
95
90
85
80
75
70
65
60
55
50
45
40
35
30
25
20
15
10
50
60
70
80
90
100
110
120

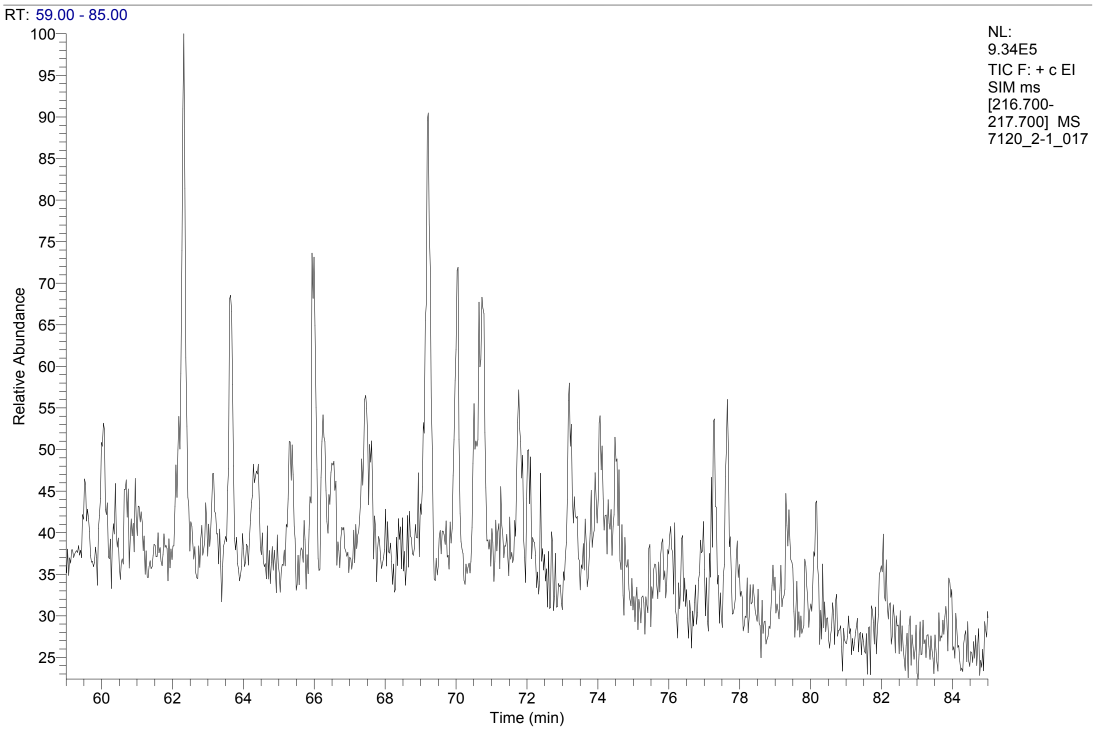
RT: 59.00 - 85.00
NL:
9.34E5
TIC F: + c EI
SIM ms
[216.700-
217.700] MS
7120_2-1_017
Relative Abundance
100
95
90
85
80
75
70
65
60
55
50
45
40
35
30
25
60
62
64
66
68
70
72
74
76
78
80
82
84
Time (min)

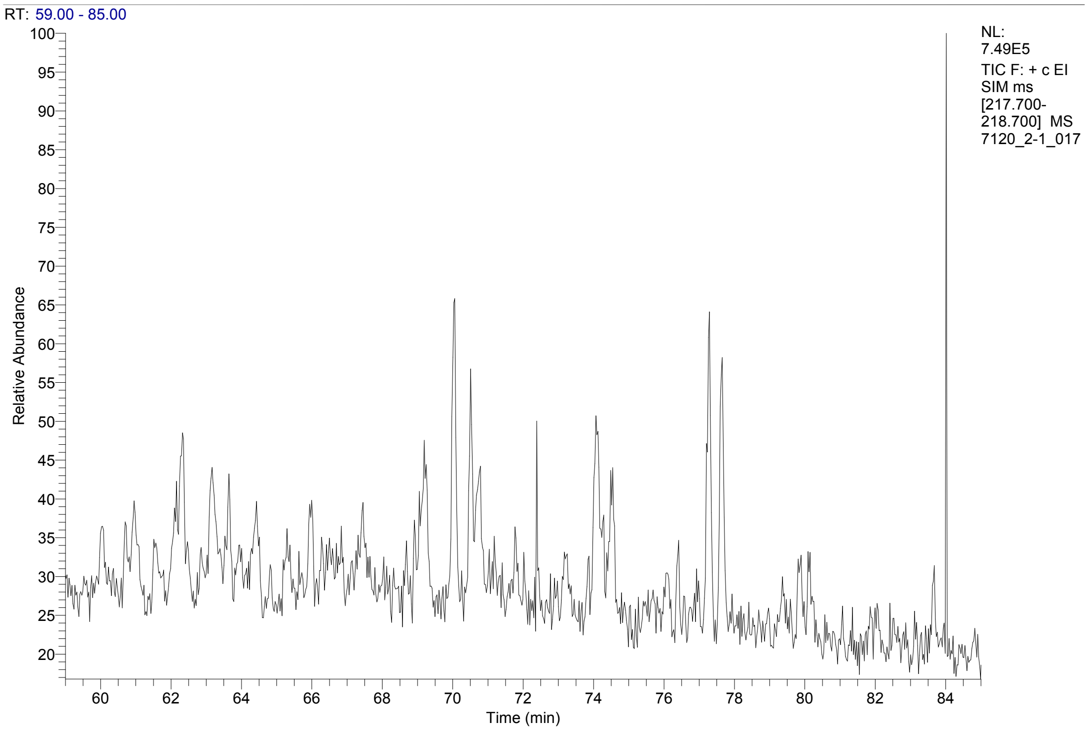
RT: 59.00 - 85.00
Relative Abundance
100
95
90
85
80
75
70
65
60
55
50
45
40
35
30
25
20
60
62
64
66
68
70
72
74
76
78
80
82
84
Time (min)
NL:
7.49E5
TIC F: + c EI
SIM ms
[217.700-
218.700] MS
7120_2-1_017

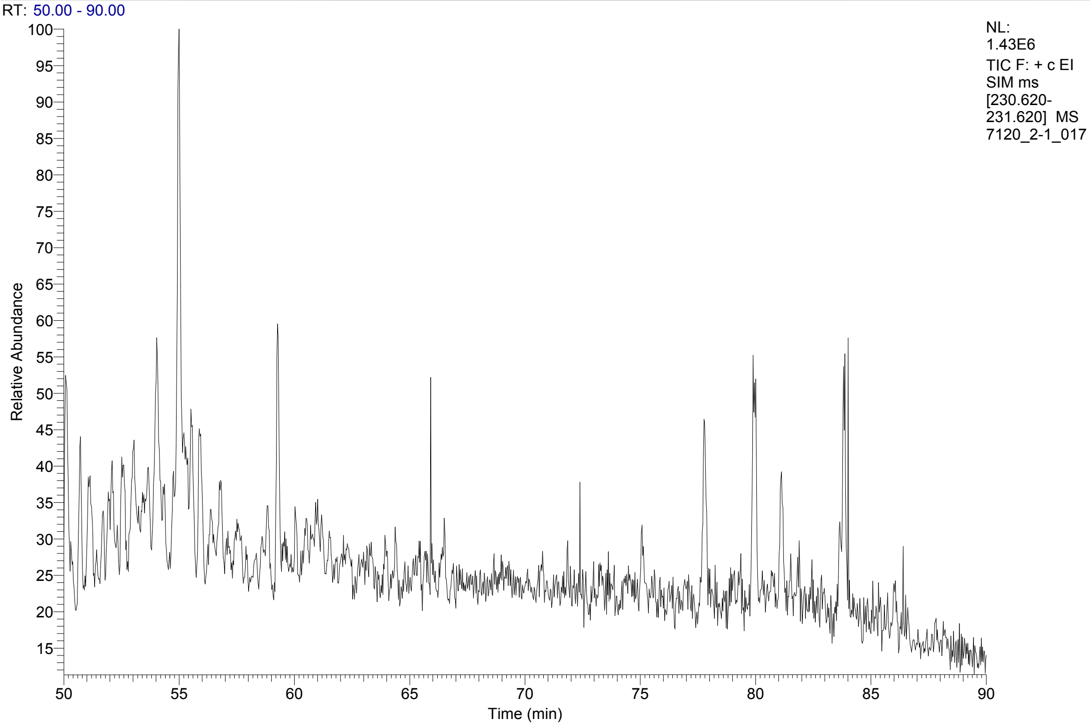
RT: 50.00 - 90.00
Relative Abundance
100
95
90
85
80
75
70
65
60
55
50
45
40
35
30
25
20
15
50
55
60
65
70
75
80
85
90
Time (min)
NL:
1.43E6
TIC F: + c EI
SIM ms
[230.620-
231.620] MS
7120_2-1_017

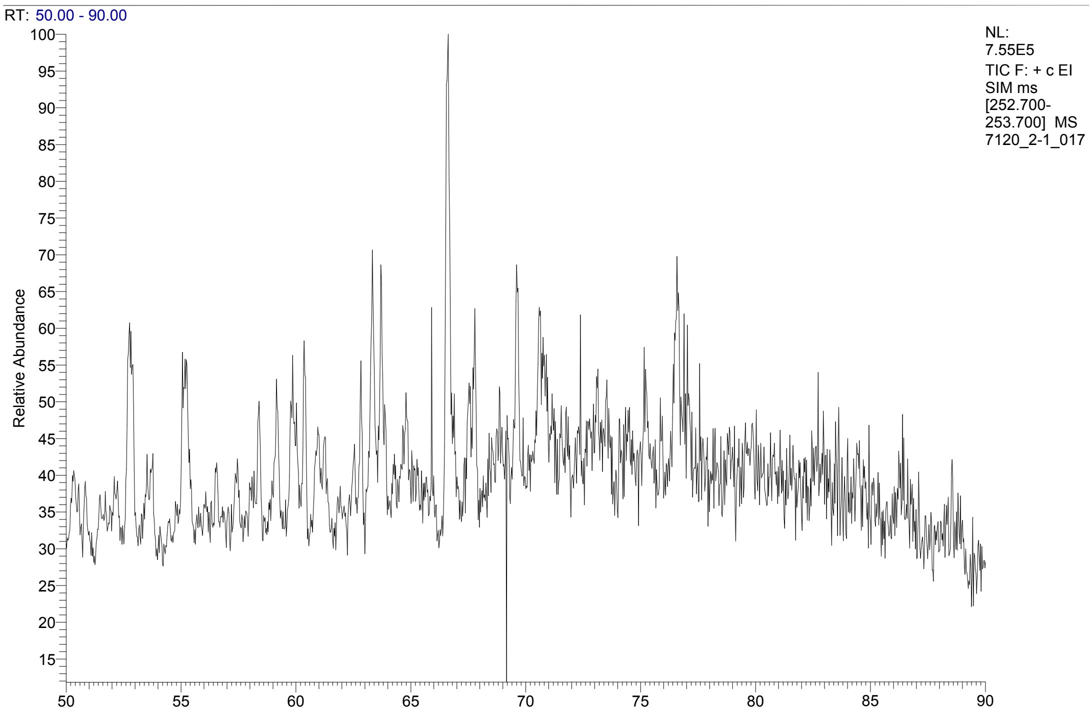
RT: 50.00 - 90.00
Relative Abundance
100
95
90
85
80
75
70
65
60
55
50
45
40
35
30
25
20
15
50
55
60
65
70
75
80
85
90
Time (min)
NL:
7.55E5
TIC F: + c EI
SIM ms
[252.700-
253.700] MS
7120_2-1_017

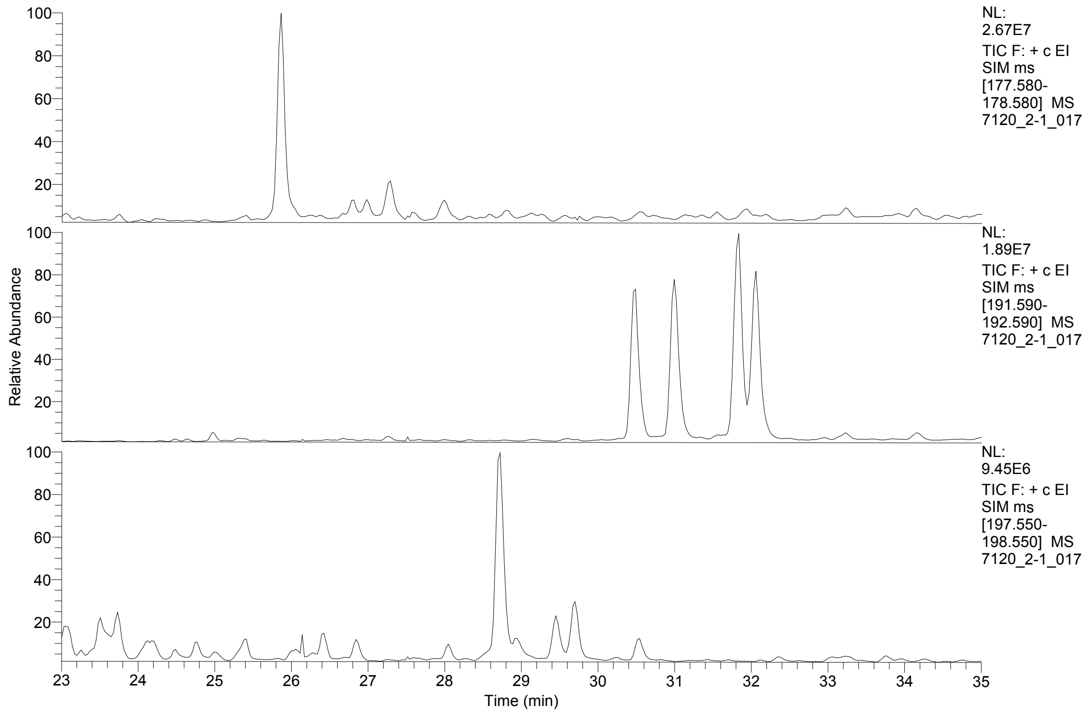
RT: 23.00 - 35.00
Relative Abundance
100
80
60
40
20
NL:
2.67E7
TIC F: + c EI
SIM ms
[177.580-
178.580] MS
7120_2-1_017
100
80
60
40
20
NL:
1.89E7
TIC F: + c EI
SIM ms
[191.590-
192.590] MS
7120_2-1_017
100
80
60
40
20
NL:
9.45E6
TIC F: + c EI
SIM ms
[197.550-
198.550] MS
7120_2-1_017
23
24
25
26
27
28
29
30
31
32
33
34
35
Time (min)

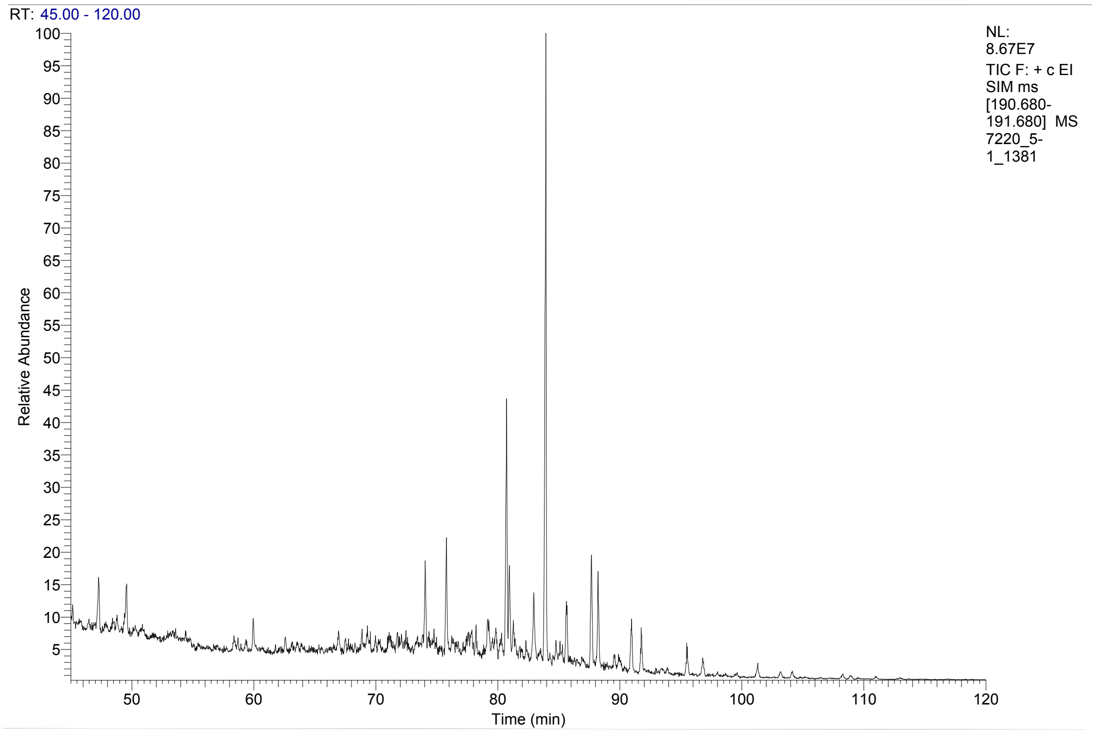
RT: 45.00 - 120.00
NL:
8.67E7
TIC F: + c EI
SIM ms
[190.680-
191.680] MS
7220_5-
1_1381
Relative Abundance
Time (min)
100
95
90
85
80
75
70
65
60
55
50
45
40
35
30
25
20
15
10
5
50
60
70
80
90
100
110
120

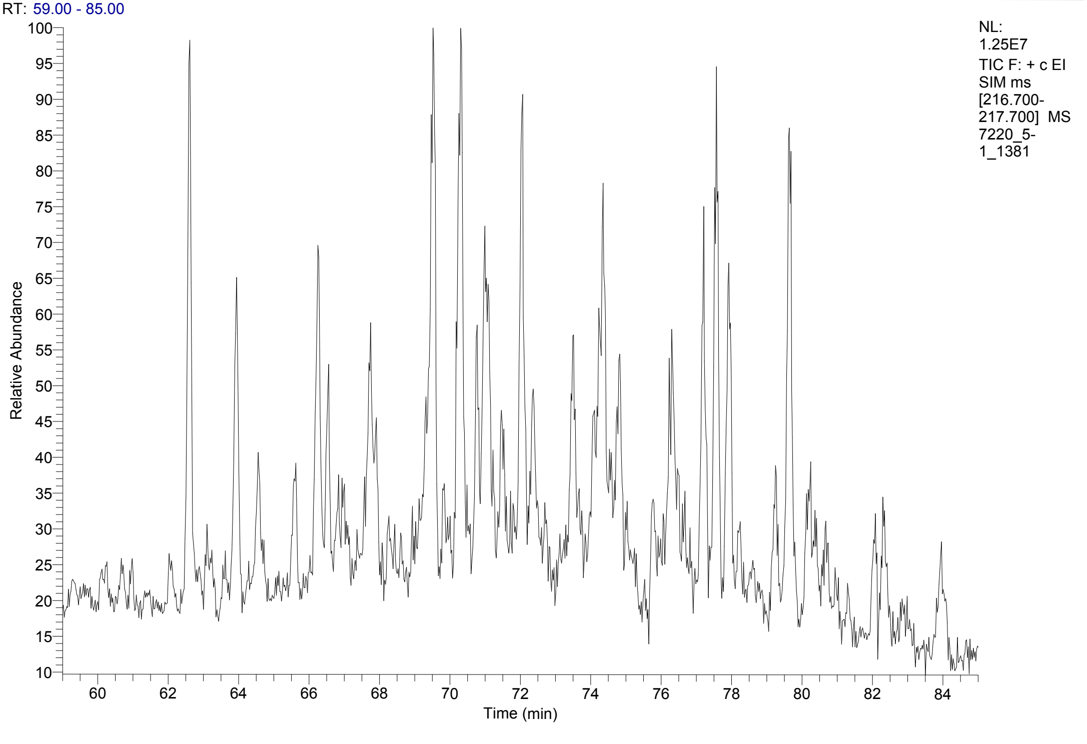
RT: 59.00 - 85.00
NL:
1.25E7
TIC F: + c EI
SIM ms
[216.700-
217.700] MS
7220_5-
1_1381
Relative Abundance
Time (min)
100
95
90
85
80
75
70
65
60
55
50
45
40
35
30
25
20
15
10
60
62
64
66
68
70
72
74
76
78
80
82
84

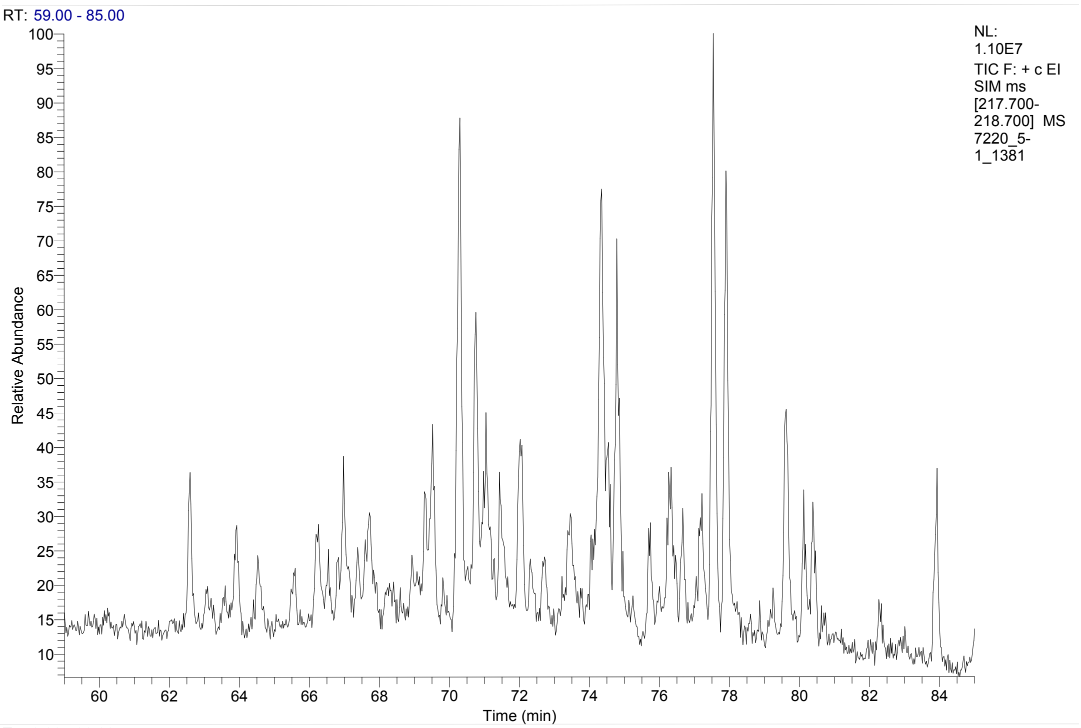
RT: 59.00 - 85.00
NL:
1.10E7
TIC F: + c EI
SIM ms
[217.700-
218.700] MS
7220_5-
1_1381
Relative Abundance
100
95
90
85
80
75
70
65
60
55
50
45
40
35
30
25
20
15
10
60
62
64
66
68
70
72
74
76
78
80
82
84
Time (min)

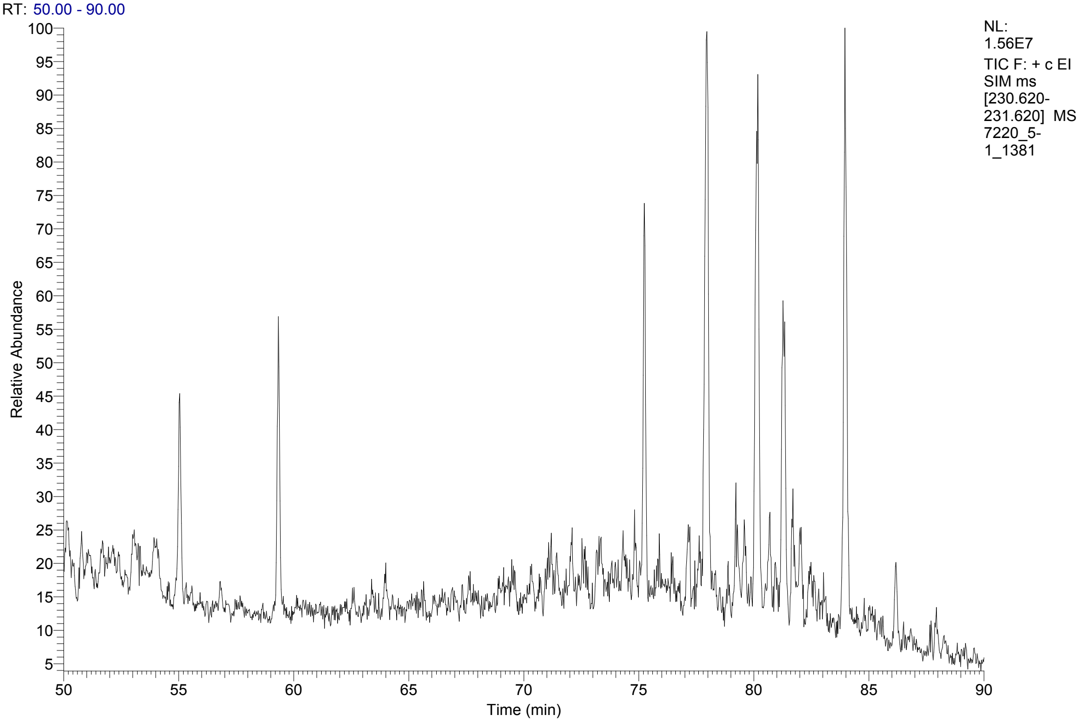
RT: 50.00 - 90.00
NL:
1.56E7
TIC F: + c EI
SIM ms
[230.620-
231.620] MS
7220_5-
1_1381
Relative Abundance
100
95
90
85
80
75
70
65
60
55
50
45
40
35
30
25
20
15
10
5
50
55
60
65
70
75
80
85
90
Time (min)

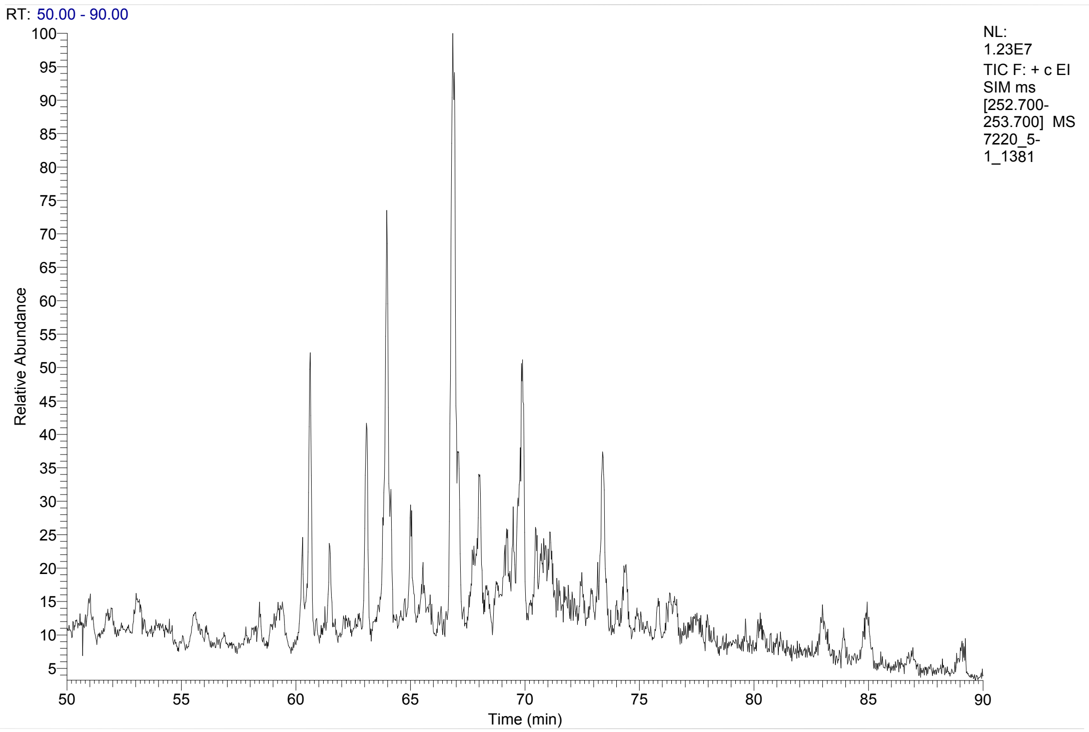
RT: 50.00 - 90.00
NL:
1.23E7
TIC F: + c EI
SIM ms
[252.700-
253.700] MS
7220_5-
1_1381
Relative Abundance
100
95
90
85
80
75
70
65
60
55
50
45
40
35
30
25
20
15
10
5
50
55
60
65
70
75
80
85
90
Time (min)

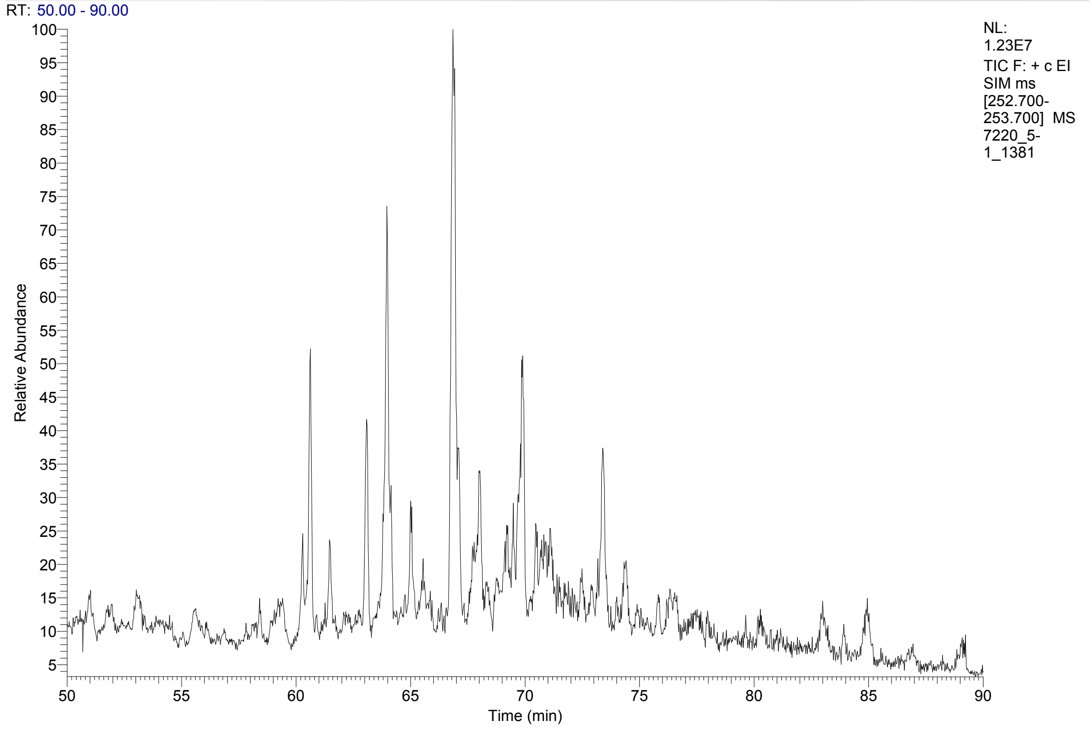
RT: 50.00 - 90.00
NL:
1.23E7
TIC F: + c EI
SIM ms
[252.700-
253.700] MS
7220_5-
1_1381
Relative Abundance
100
95
90
85
80
75
70
65
60
55
50
45
40
35
30
25
20
15
10
5
50
55
60
65
70
75
80
85
90
Time (min)

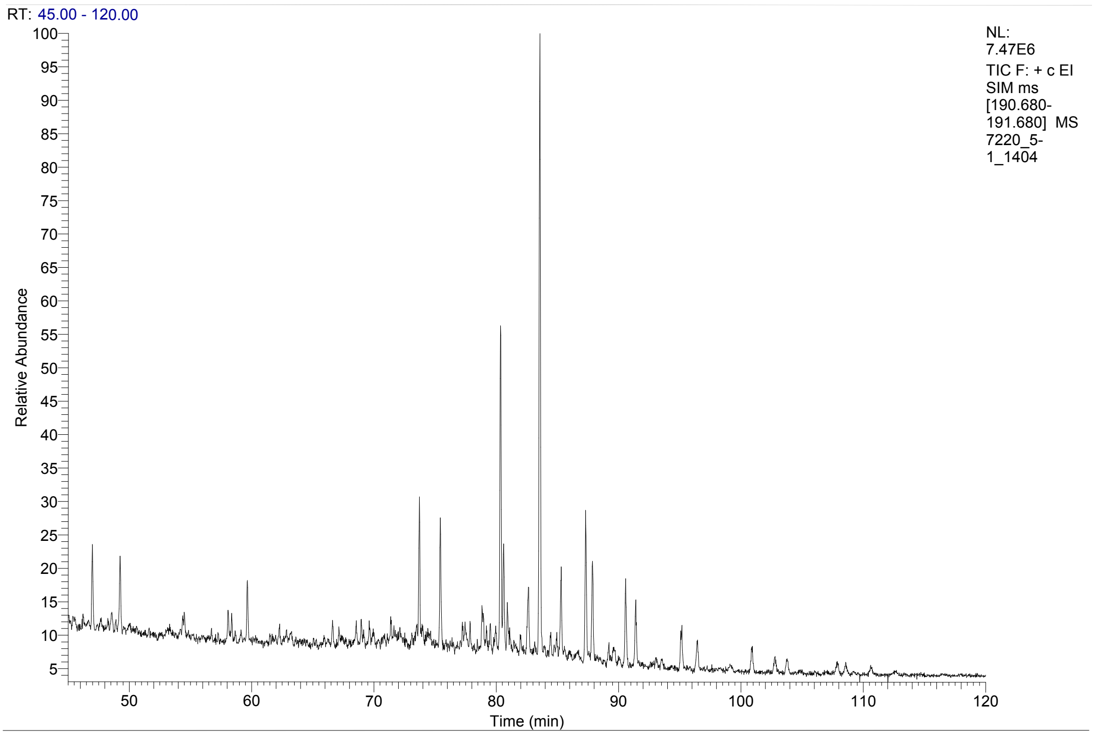
RT: 45.00 - 120.00
NL:
7.47E6
TIC F: + c EI
SIM ms
[190.680-
191.680] MS
7220_5-
1_1404
Relative Abundance
100
95
90
85
80
75
70
65
60
55
50
45
40
35
30
25
20
15
10
5
50
60
70
80
90
100
110
120
Time (min)

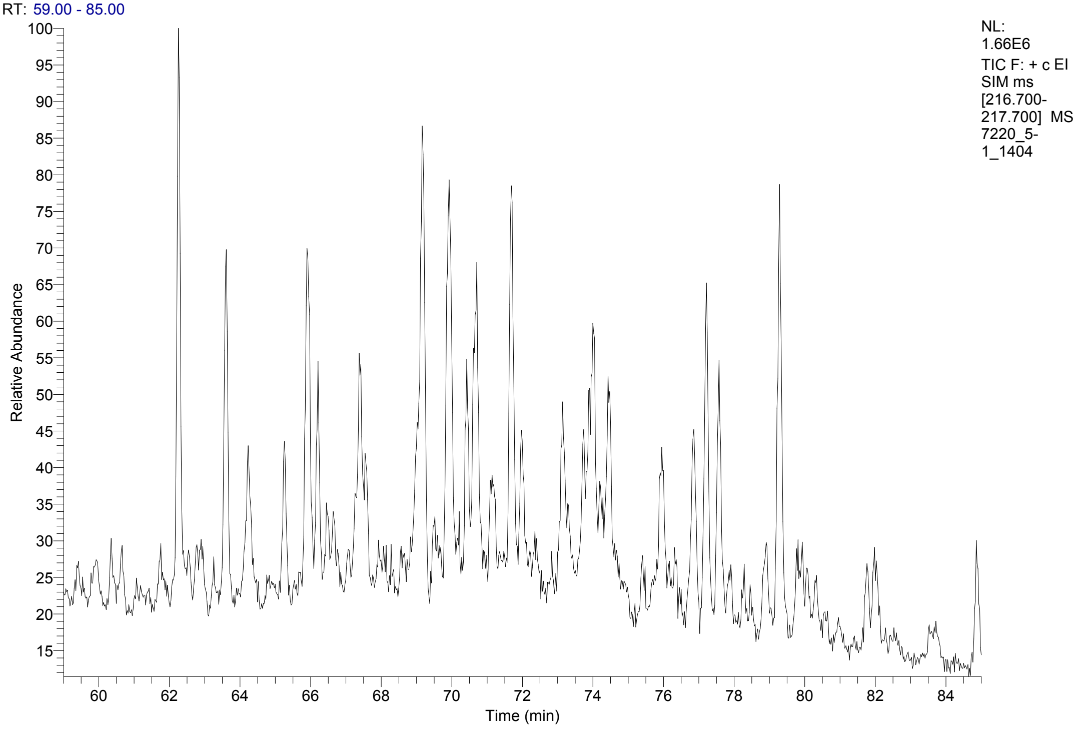
RT: 59.00 - 85.00
NL:
1.66E6
TIC F: + c EI
SIM ms
[216.700-
217.700] MS
7220_5-
1_1404
Relative Abundance
100
95
90
85
80
75
70
65
60
55
50
45
40
35
30
25
20
15
60
62
64
66
68
70
72
74
76
78
80
82
84
Time (min)

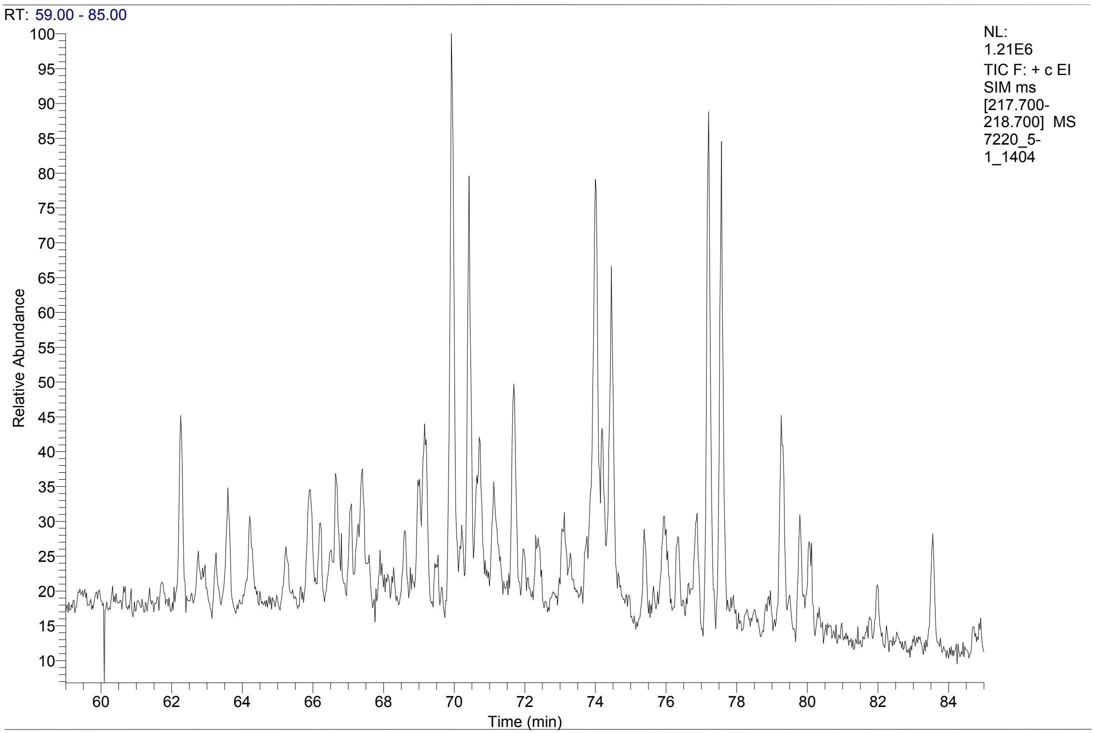
RT: 59.00 - 85.00
NL:
1.21E6
TIC F: + c EI
SIM ms
[217.700-
218.700] MS
7220_5-
1_1404
Relative Abundance
100
95
90
85
80
75
70
65
60
55
50
45
40
35
30
25
20
15
10
60
62
64
66
68
70
72
74
76
78
80
82
84
Time (min)

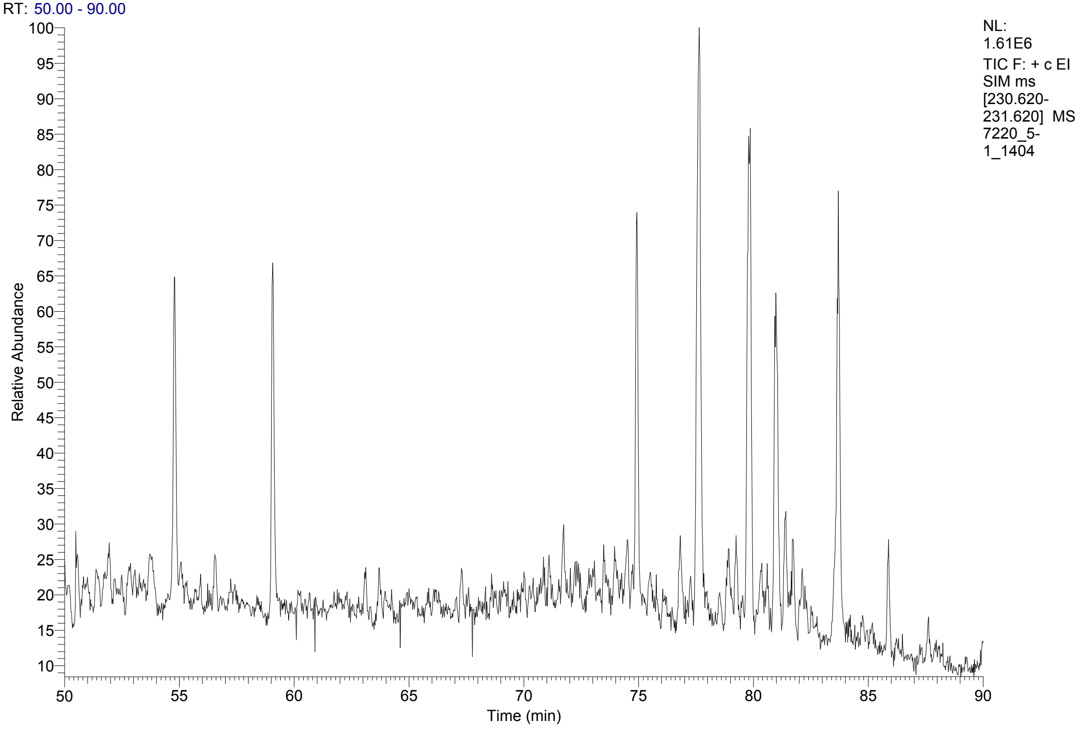
RT: 50.00 - 90.00
NL:
1.61E6
TIC F: + c EI
SIM ms
[230.620-
231.620] MS
7220_5-
1_1404
Relative Abundance
100
95
90
85
80
75
70
65
60
55
50
45
40
35
30
25
20
15
10
50
55
60
65
70
75
80
85
90
Time (min)

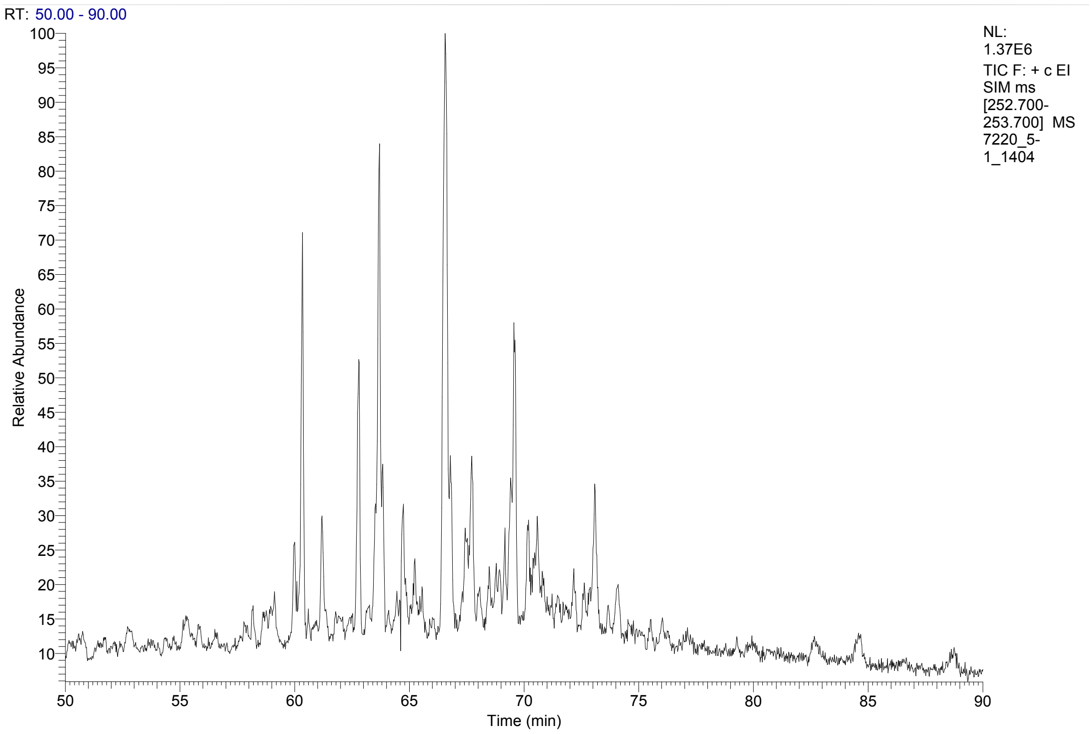
RT: 50.00 - 90.00
Relative Abundance
100
95
90
85
80
75
70
65
60
55
50
45
40
35
30
25
20
15
10
50
55
60
65
70
75
80
85
90
Time (min)
NL:
1.37E6
TIC F: + c EI
SIM ms
[252.700-
253.700] MS
7220_5-
1_1404

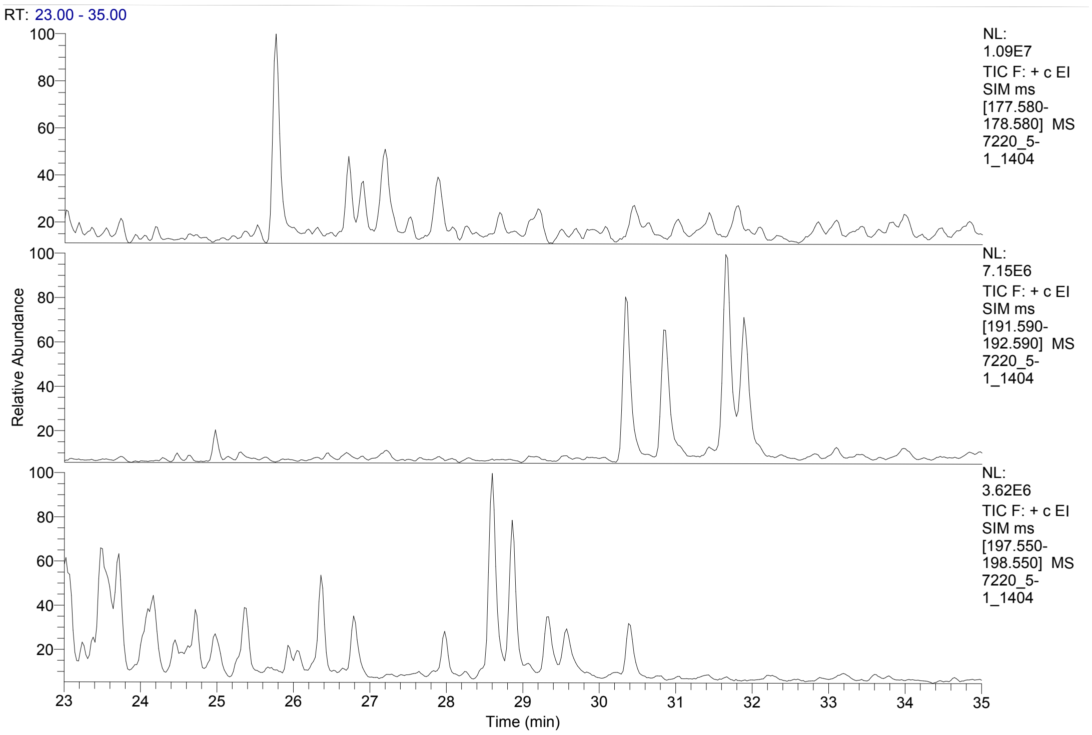
RT: 23.00 - 35.00
Relative Abundance
100
80
60
40
20
NL:
1.09E7
TIC F: + c EI
SIM ms
[177.580-
178.580] MS
7220_5-
1_1404
100
80
60
40
20
NL:
7.15E6
TIC F: + c EI
SIM ms
[191.590-
192.590] MS
7220_5-
1_1404
100
80
60
40
20
NL:
3.62E6
TIC F: + c EI
SIM ms
[197.550-
198.550] MS
7220_5-
1_1404
23
24
25
26
27
28
29
30
31
32
33
34
35
Time (min)

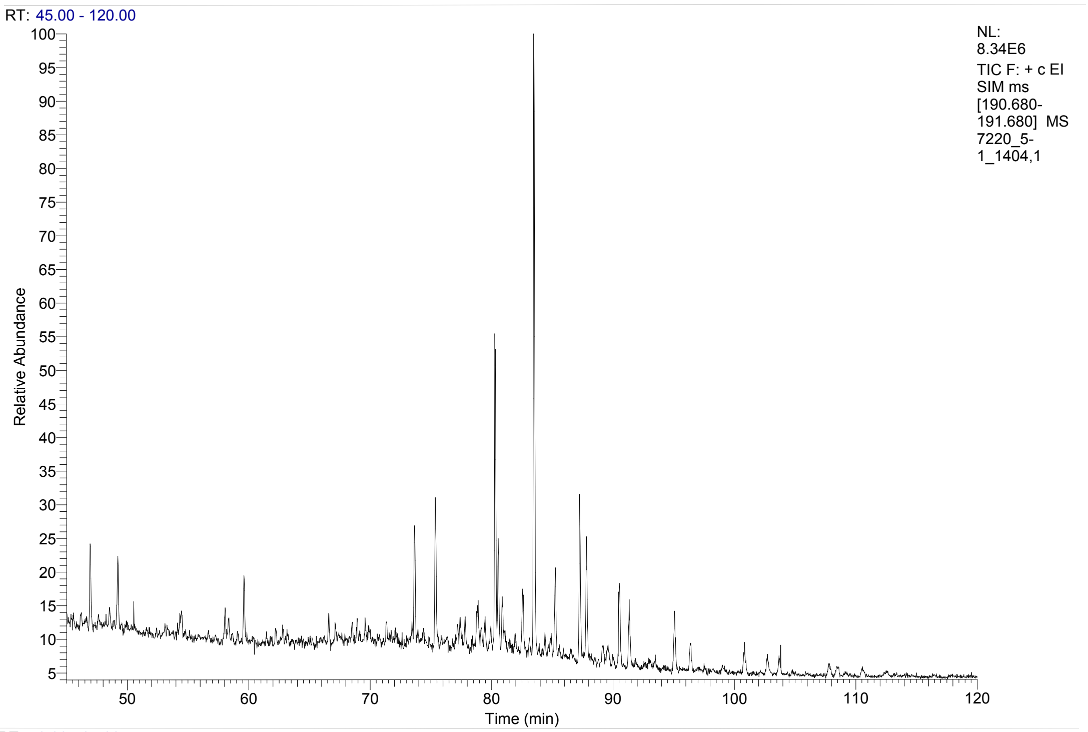
RT: 45.00 - 120.00
NL:
8.34E6
TIC F: + c EI
SIM ms
[190.680-
191.680] MS
7220_5-
1_1404,1
Relative Abundance
100
95
90
85
80
75
70
65
60
55
50
45
40
35
30
25
20
15
10
5
50
60
70
80
90
100
110
120
Time (min)

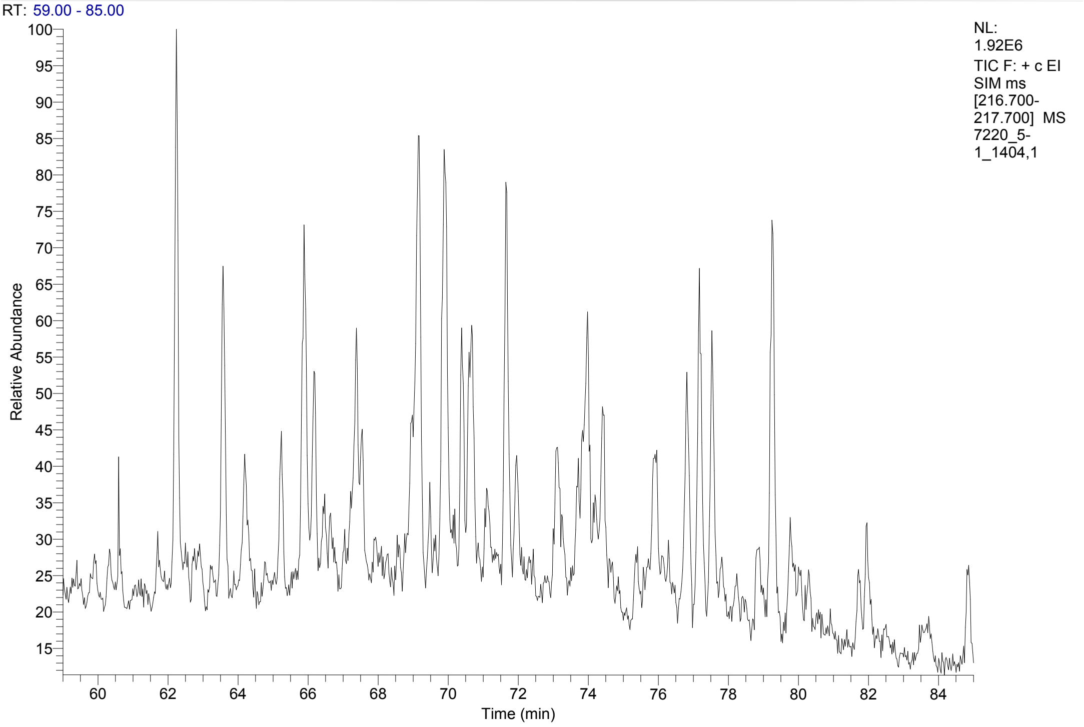
RT: 59.00 - 85.00
NL:
1.92E6
TIC F: + c EI
SIM ms
[216.700-
217.700] MS
7220_5-
1_1404,1
Relative Abundance
100
95
90
85
80
75
70
65
60
55
50
45
40
35
30
25
20
15
60
62
64
66
68
70
72
74
76
78
80
82
84
Time (min)

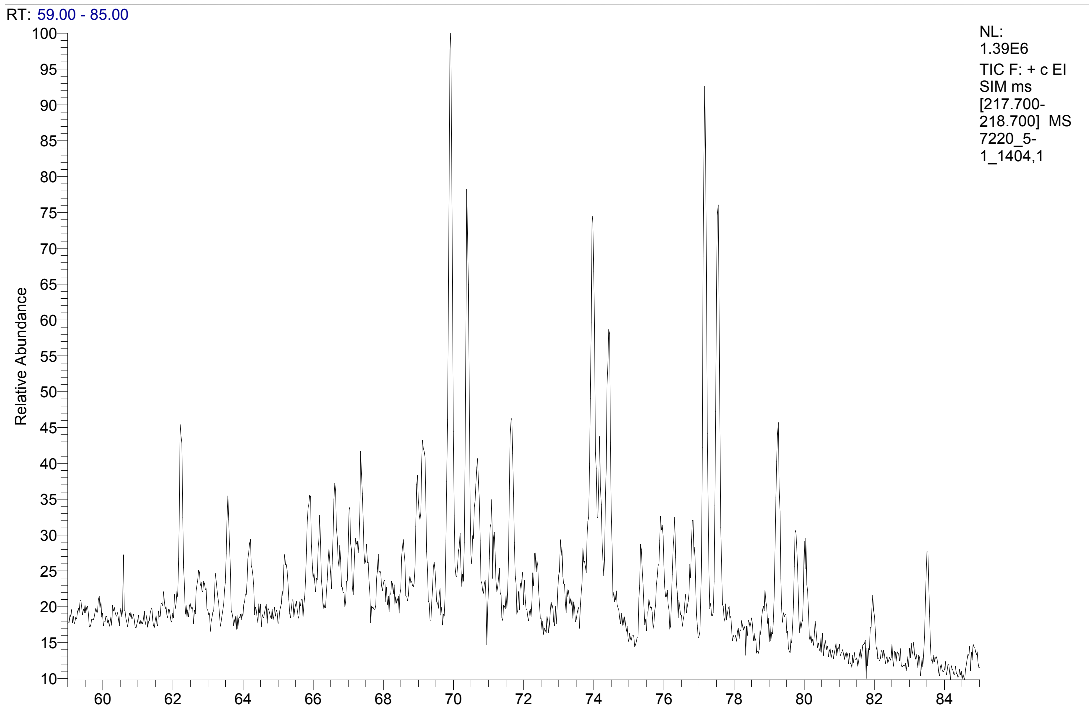
RT: 59.00 - 85.00
NL:
1.39E6
TIC F: + c EI
SIM ms
[217.700-
218.700] MS
7220_5-
1_1404,1
Relative Abundance
100
95
90
85
80
75
70
65
60
55
50
45
40
35
30
25
20
15
10
60
62
64
66
68
70
72
74
76
78
80
82
84
Time (min)

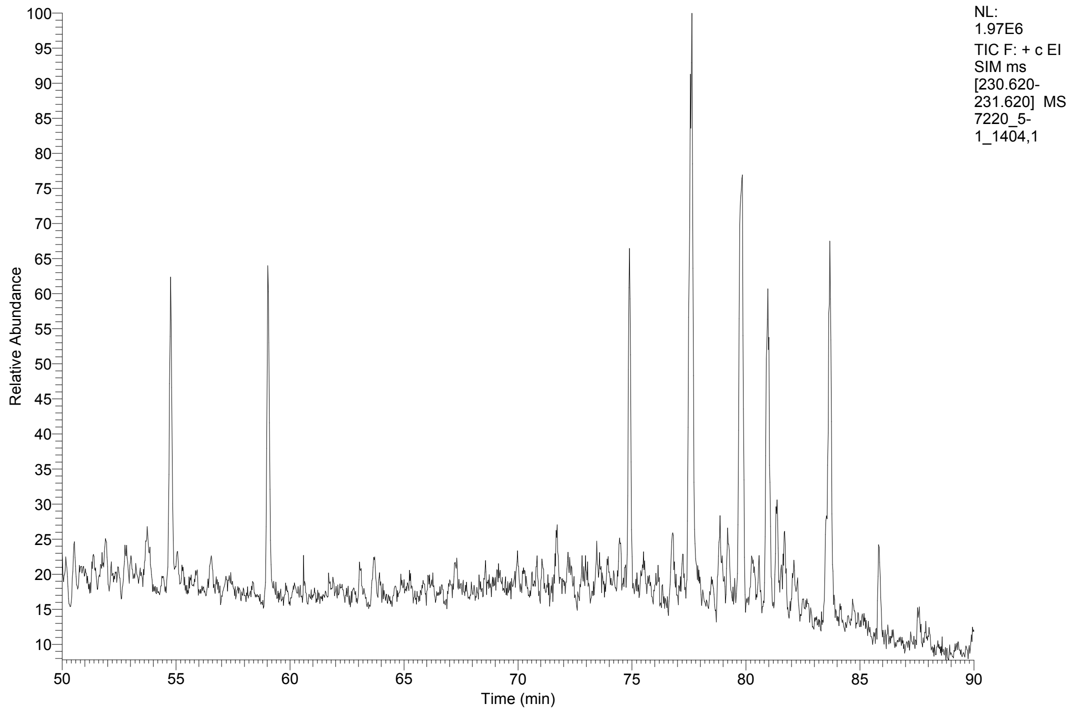
RT: 50.00 - 90.00
NL:
1.97E6
TIC F: + c EI
SIM ms
[230.620-
231.620] MS
7220_5-
1_1404,1
Relative Abundance
100
95
90
85
80
75
70
65
60
55
50
45
40
35
30
25
20
15
10
50
55
60
65
70
75
80
85
90
Time (min)

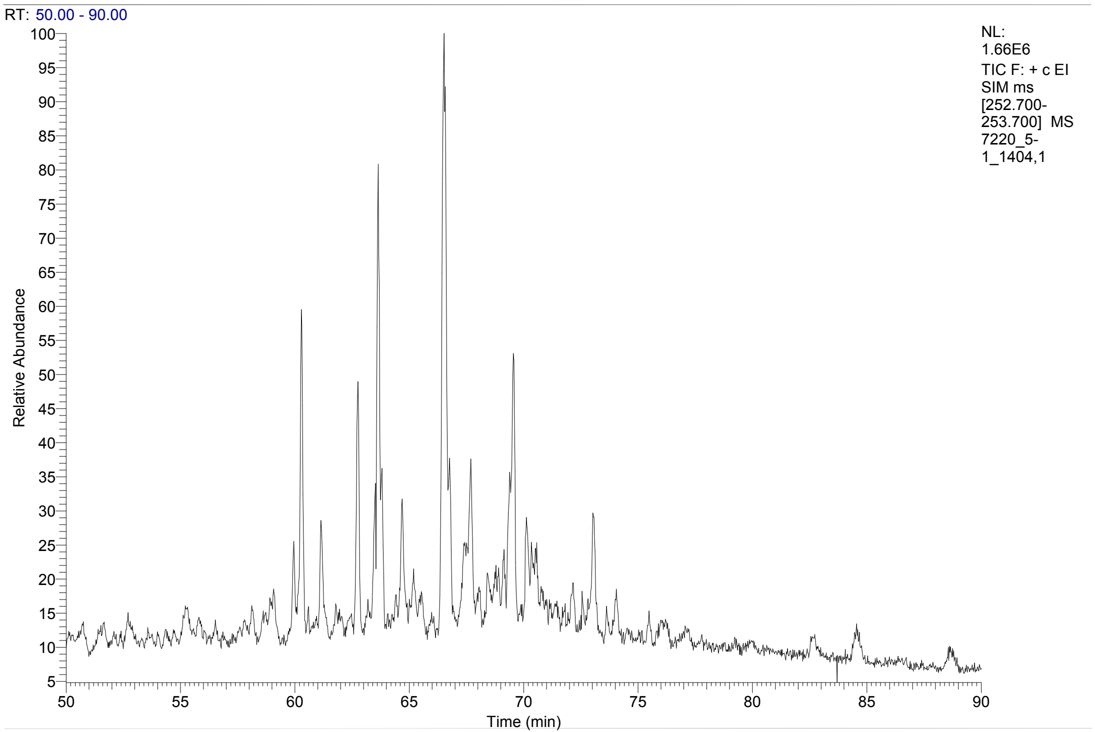
RT: 50.00 - 90.00
NL:
1.66E6
TIC F: + c EI
SIM ms
[252.700-
253.700] MS
7220_5-
1_1404,1
Relative Abundance
100
95
90
85
80
75
70
65
60
55
50
45
40
35
30
25
20
15
10
5
50
55
60
65
70
75
80
85
90
Time (min)

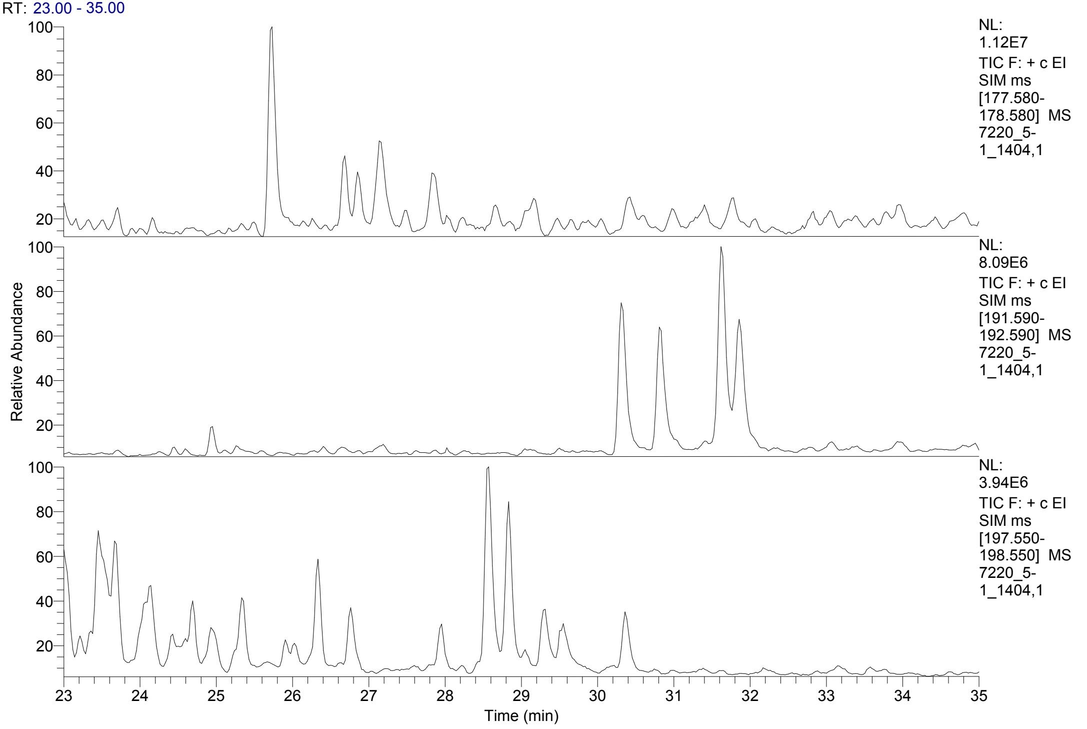
RT: 23.00 - 35.00
NL:
1.12E7
TIC F: + c EI
SIM ms
[177.580-
178.580] MS
7220_5-
1_1404,1
NL:
8.09E6
TIC F: + c EI
SIM ms
[191.590-
192.590] MS
7220_5-
1_1404,1
NL:
3.94E6
TIC F: + c EI
SIM ms
[197.550-
198.550] MS
7220_5-
1_1404,1
Relative Abundance
100
80
60
40
20
23
24
25
26
27
28
29
30
31
32
33
34
35
Time (min)

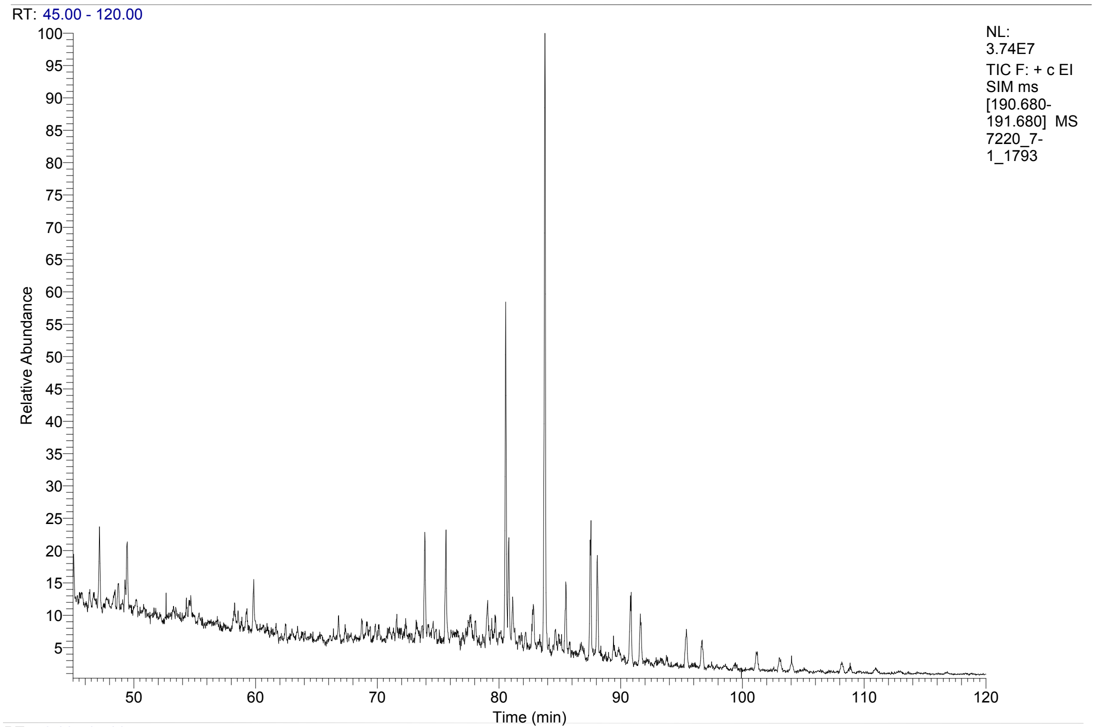
RT: 45.00 - 120.00
NL:
3.74E7
TIC F: + c EI
SIM ms
[190.680-
191.680] MS
7220_7-
1_1793
Relative Abundance
100
95
90
85
80
75
70
65
60
55
50
45
40
35
30
25
20
15
10
5
50
60
70
80
90
100
110
120
Time (min)

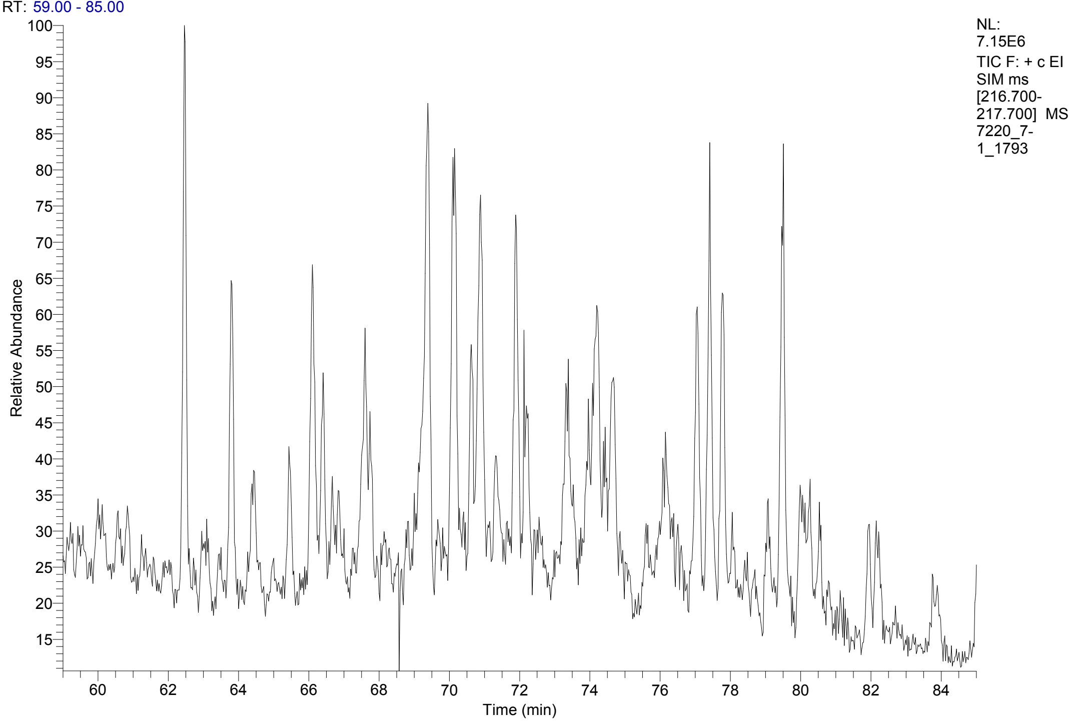
RT: 59.00 - 85.00
NL:
7.15E6
TIC F: + c EI
SIM ms
[216.700-
217.700] MS
7220_7-
1_1793
Relative Abundance
100
95
90
85
80
75
70
65
60
55
50
45
40
35
30
25
20
15
60
62
64
66
68
70
72
74
76
78
80
82
84
Time (min)

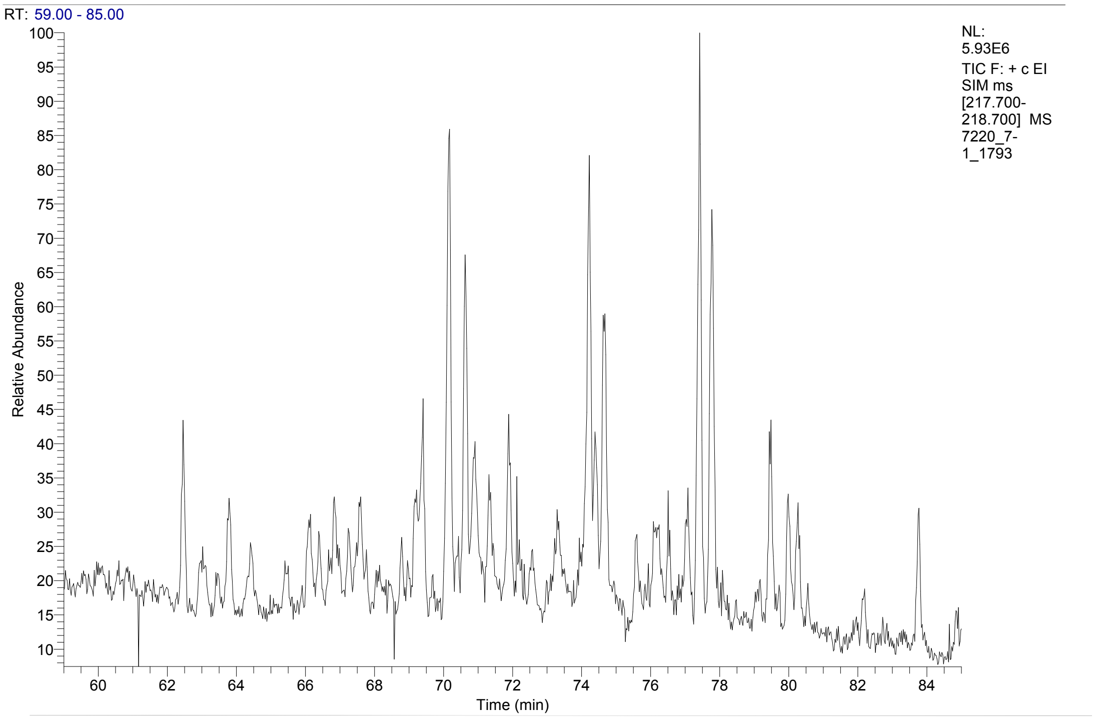
RT: 59.00 - 85.00
NL:
5.93E6
TIC F: + c EI
SIM ms
[217.700-
218.700] MS
7220_7-
1_1793
Relative Abundance
100
95
90
85
80
75
70
65
60
55
50
45
40
35
30
25
20
15
10
60
62
64
66
68
70
72
74
76
78
80
82
84
Time (min)

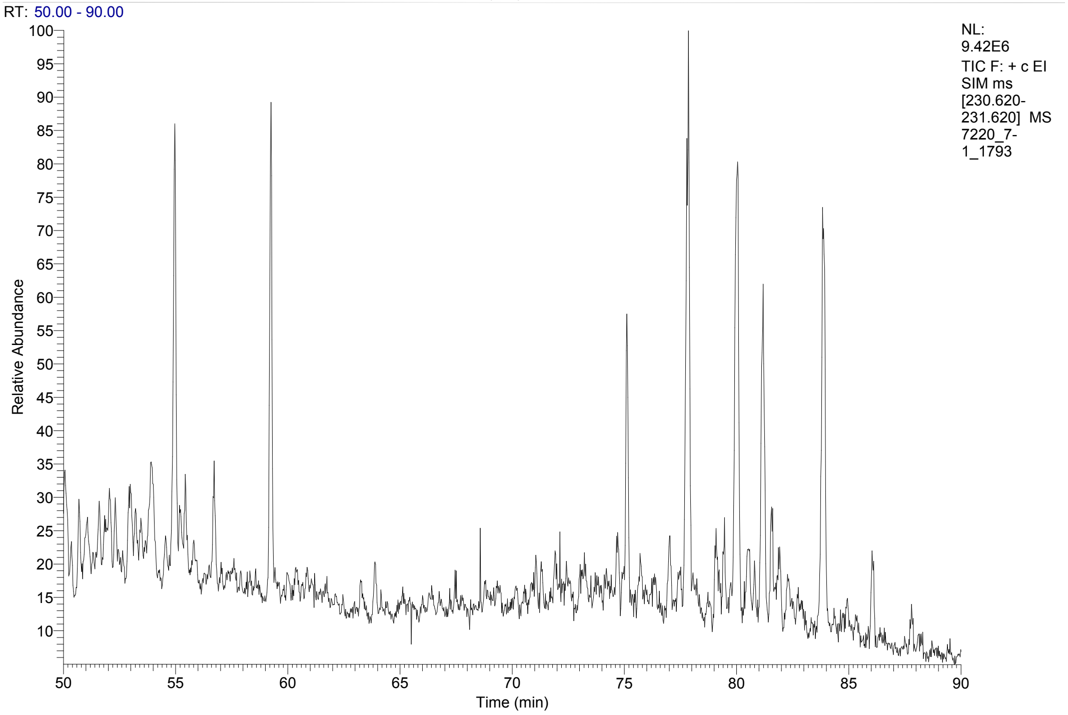
RT: 50.00 - 90.00
NL:
9.42E6
TIC F: + c EI
SIM ms
[230.620-
231.620] MS
7220_7-
1_1793
Relative Abundance
100
95
90
85
80
75
70
65
60
55
50
45
40
35
30
25
20
15
10
50
55
60
65
70
75
80
85
90
Time (min)

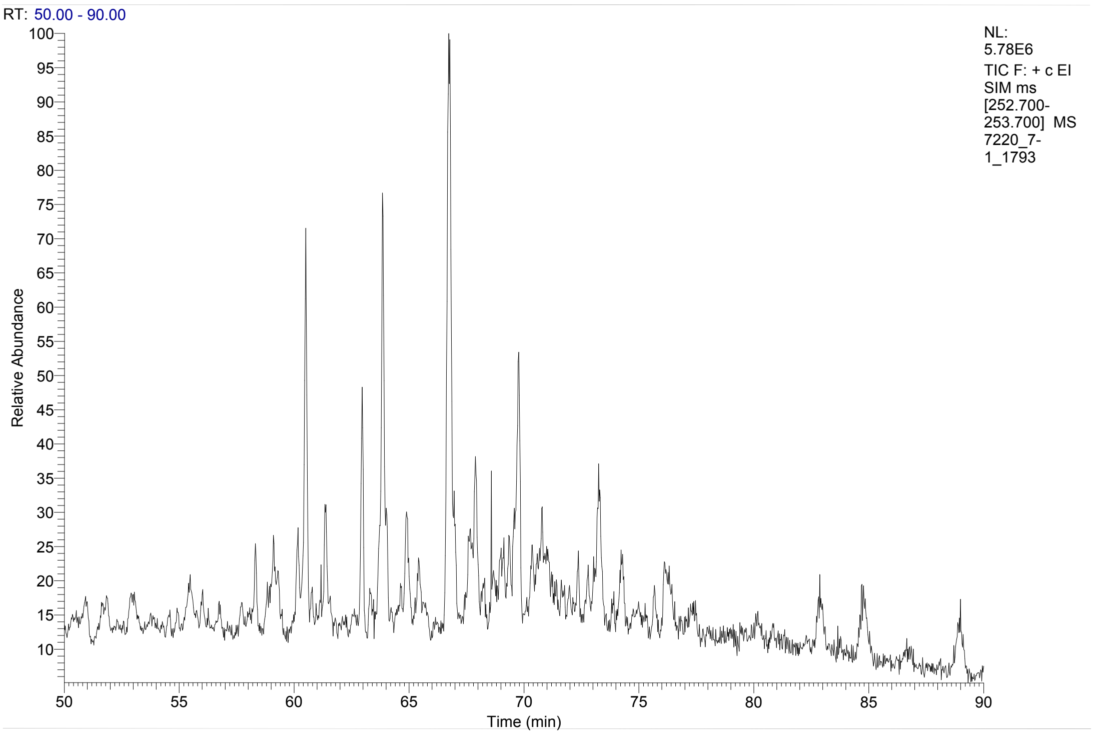
RT: 50.00 - 90.00
NL:
5.78E6
TIC F: + c EI
SIM ms
[252.700-
253.700] MS
7220_7-
1_1793
Relative Abundance
100
95
90
85
80
75
70
65
60
55
50
45
40
35
30
25
20
15
10
50
55
60
65
70
75
80
85
90
Time (min)

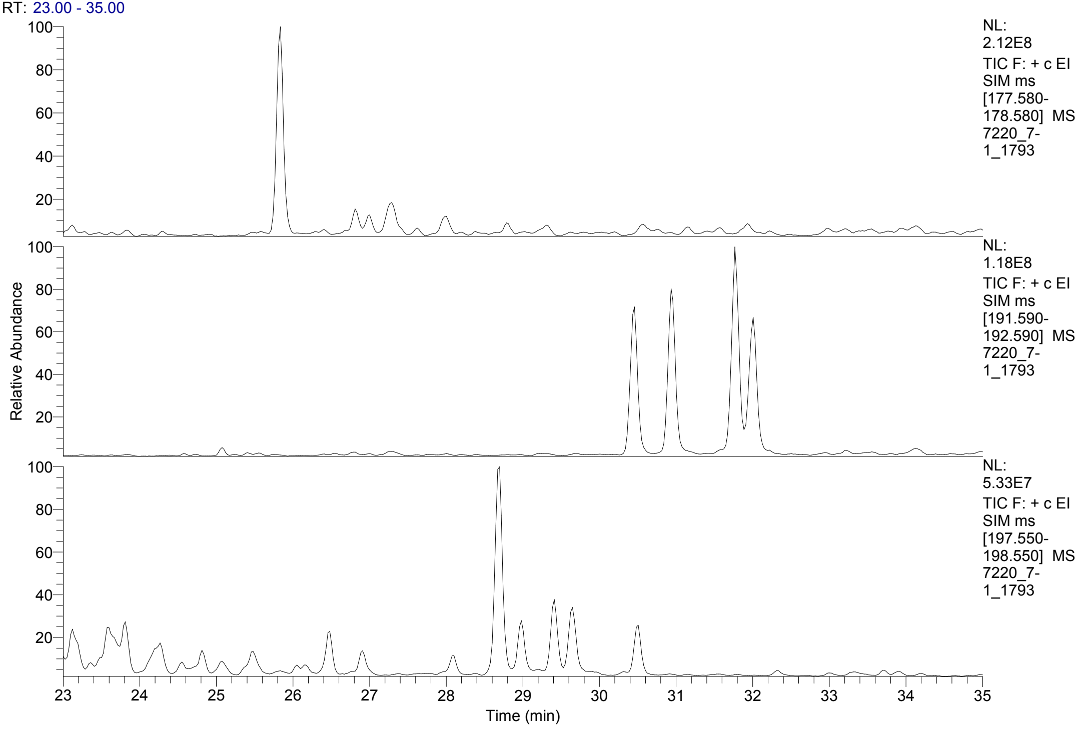
RT: 23.00 - 35.00
NL:
2.12E8
TIC F: + c EI
SIM ms
[177.580-
178.580] MS
7220_7-
1_1793
NL:
1.18E8
TIC F: + c EI
SIM ms
[191.590-
192.590] MS
7220_7-
1_1793
NL:
5.33E7
TIC F: + c EI
SIM ms
[197.550-
198.550] MS
7220_7-
1_1793
Relative Abundance
100
80
60
40
20
23
24
25
26
27
28
29
30
31
32
33
34
35
Time (min)

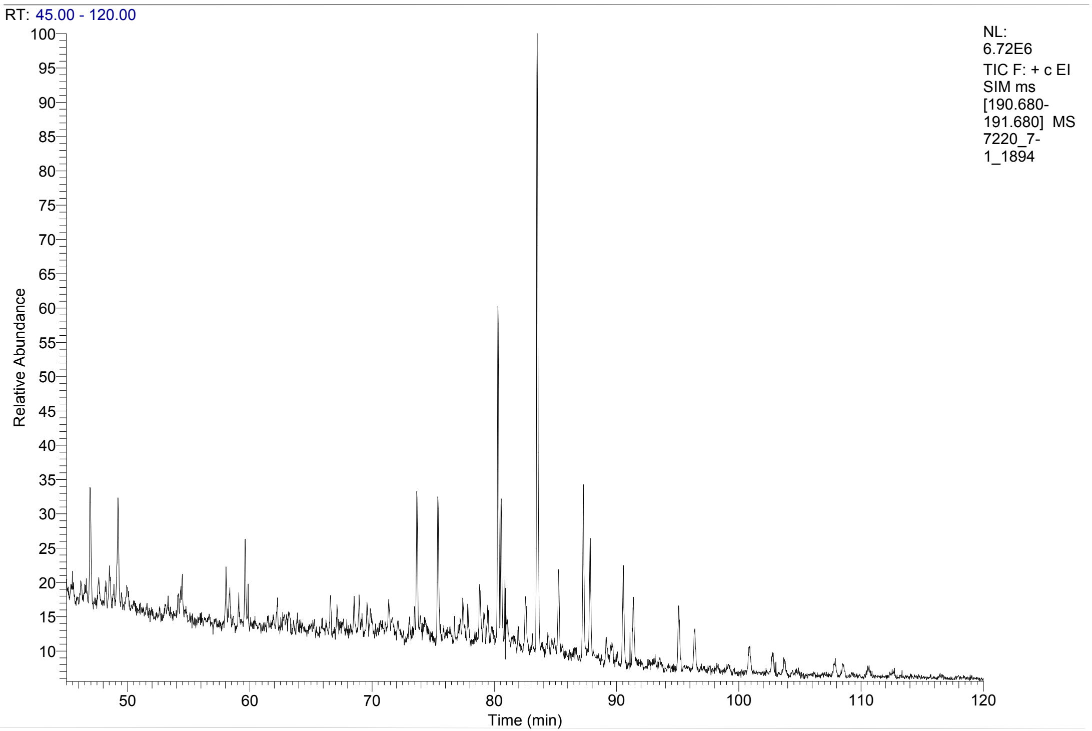
RT: 45.00 - 120.00
NL:
6.72E6
TIC F: + c EI
SIM ms
[190.680-
191.680] MS
7220_7-
1_1894
Relative Abundance
100
95
90
85
80
75
70
65
60
55
50
45
40
35
30
25
20
15
10
50
60
70
80
90
100
110
120
Time (min)

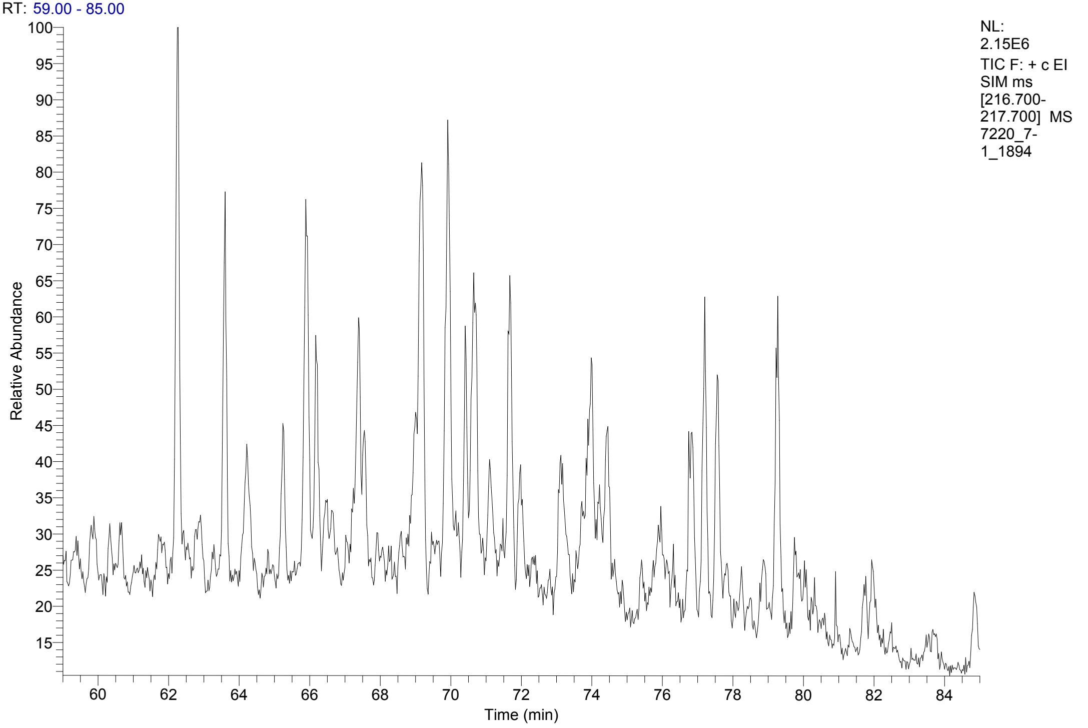
RT: 59.00 - 85.00
NL:
2.15E6
TIC F: + c EI
SIM ms
[216.700-
217.700] MS
7220_7-
1_1894
Relative Abundance
100
95
90
85
80
75
70
65
60
55
50
45
40
35
30
25
20
15
60
62
64
66
68
70
72
74
76
78
80
82
84
Time (min)

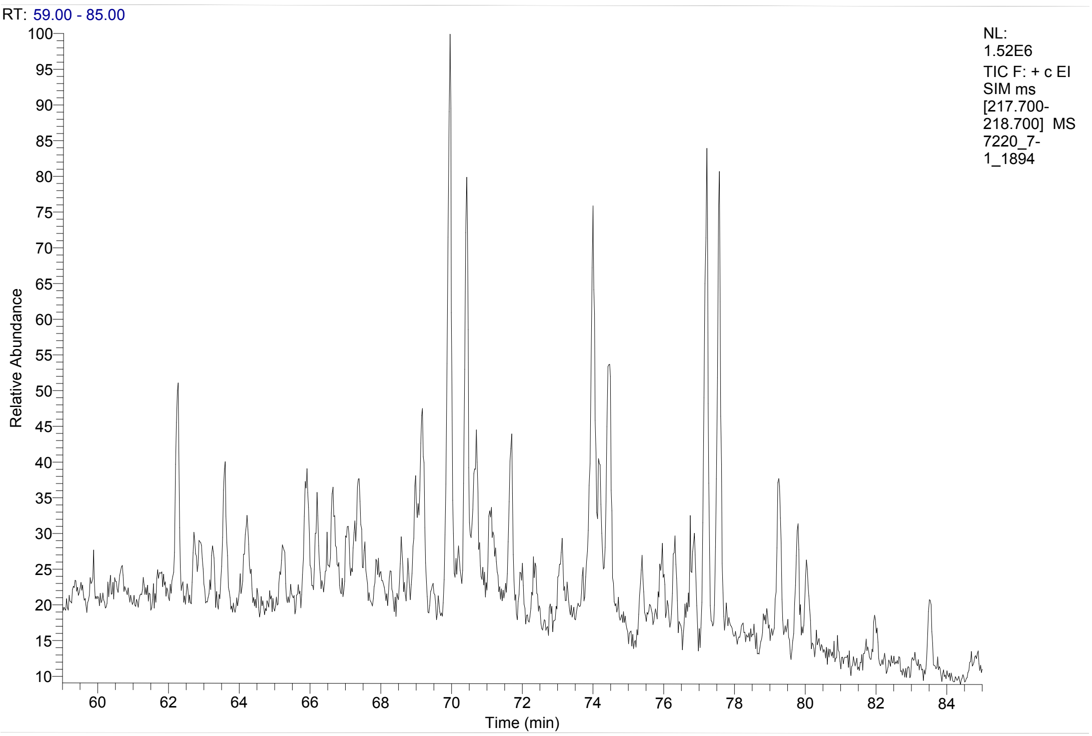
RT: 59.00 - 85.00
NL:
1.52E6
TIC F: + c EI
SIM ms
[217.700-
218.700] MS
7220_7-
1_1894
Relative Abundance
100
95
90
85
80
75
70
65
60
55
50
45
40
35
30
25
20
15
10
60
62
64
66
68
70
72
74
76
78
80
82
84
Time (min)

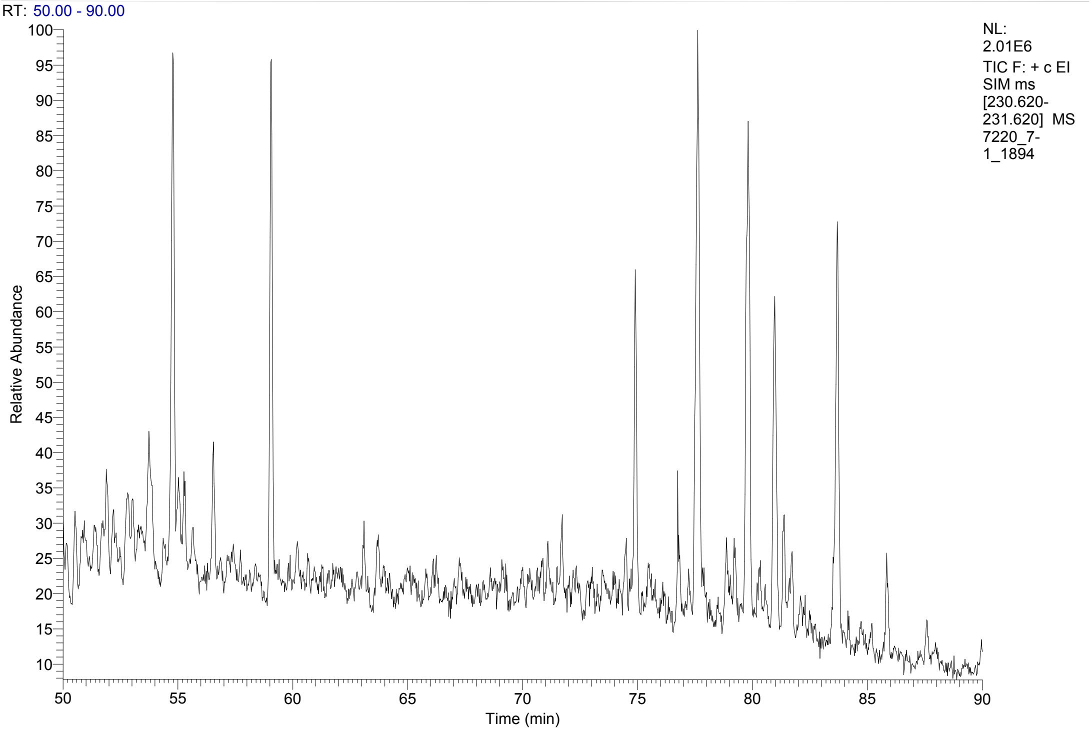
RT: 50.00 - 90.00
NL:
2.01E6
TIC F: + c EI
SIM ms
[230.620-
231.620] MS
7220_7-
1_1894
Relative Abundance
100
95
90
85
80
75
70
65
60
55
50
45
40
35
30
25
20
15
10
50
55
60
65
70
75
80
85
90
Time (min)

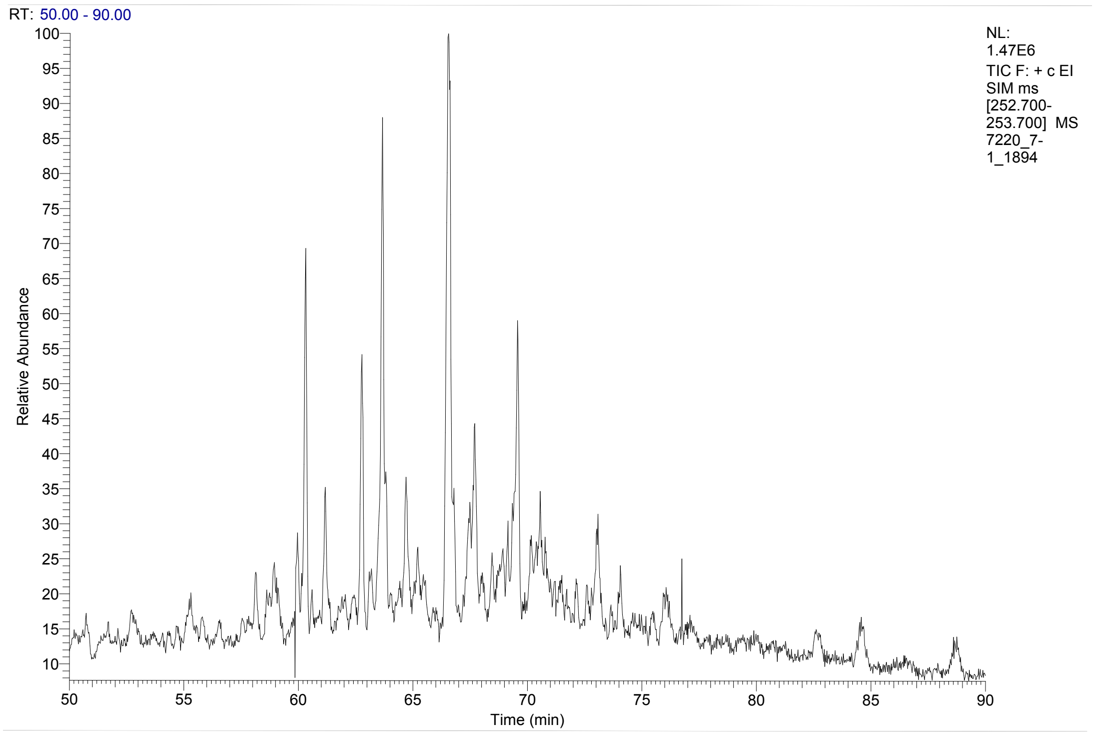
RT: 50.00 - 90.00
NL:
1.47E6
TIC F: + c EI
SIM ms
[252.700-
253.700] MS
7220_7-
1_1894
Relative Abundance
100
95
90
85
80
75
70
65
60
55
50
45
40
35
30
25
20
15
10
50
55
60
65
70
75
80
85
90
Time (min)

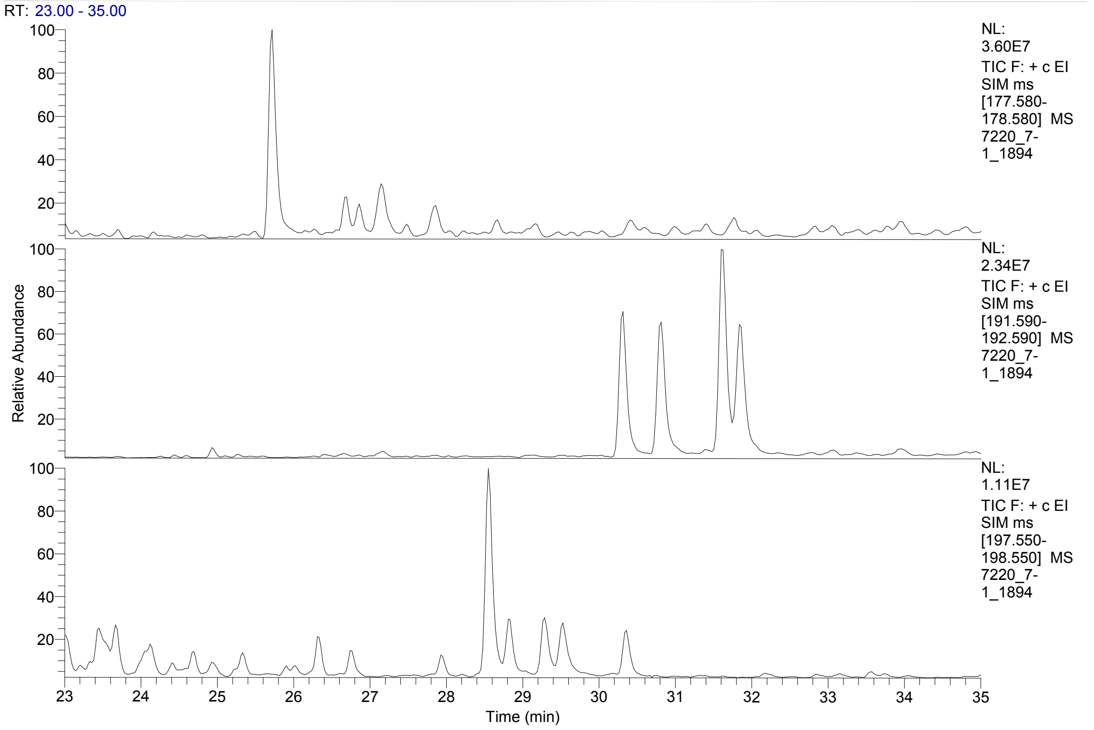
RT: 23.00 - 35.00
NL:
3.60E7
TIC F: + c EI
SIM ms
[177.580-
178.580] MS
7220_7-
1_1894
NL:
2.34E7
TIC F: + c EI
SIM ms
[191.590-
192.590] MS
7220_7-
1_1894
NL:
1.11E7
TIC F: + c EI
SIM ms
[197.550-
198.550] MS
7220_7-
1_1894
Relative Abundance
100
80
60
40
20
23
24
25
26
27
28
29
30
31
32
33
34
35
Time (min)

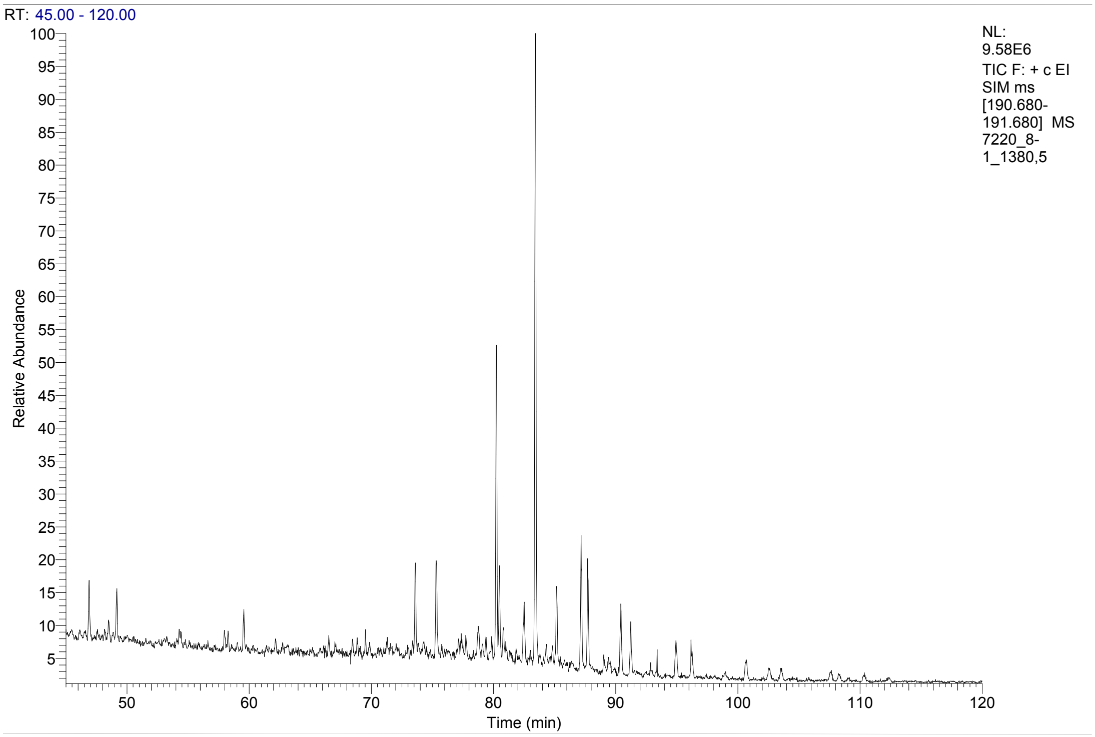
RT: 45.00 - 120.00
NL:
9.58E6
TIC F: + c EI
SIM ms
[190.680-
191.680] MS
7220_8-
1_1380,5
Relative Abundance
100
95
90
85
80
75
70
65
60
55
50
45
40
35
30
25
20
15
10
5
50
60
70
80
90
100
110
120
Time (min)

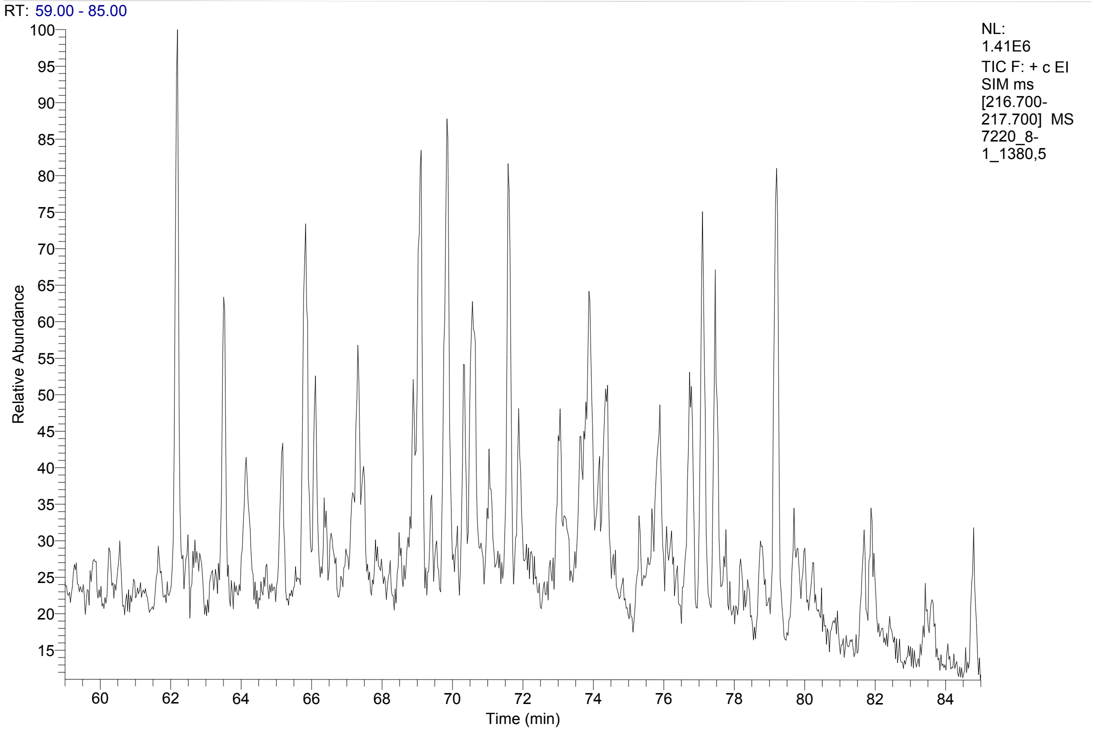
RT: 59.00 - 85.00
NL:
1.41E6
TIC F: + c EI
SIM ms
[216.700-
217.700] MS
7220_8-
1_1380,5
Relative Abundance
100
95
90
85
80
75
70
65
60
55
50
45
40
35
30
25
20
15
60
62
64
66
68
70
72
74
76
78
80
82
84
Time (min)

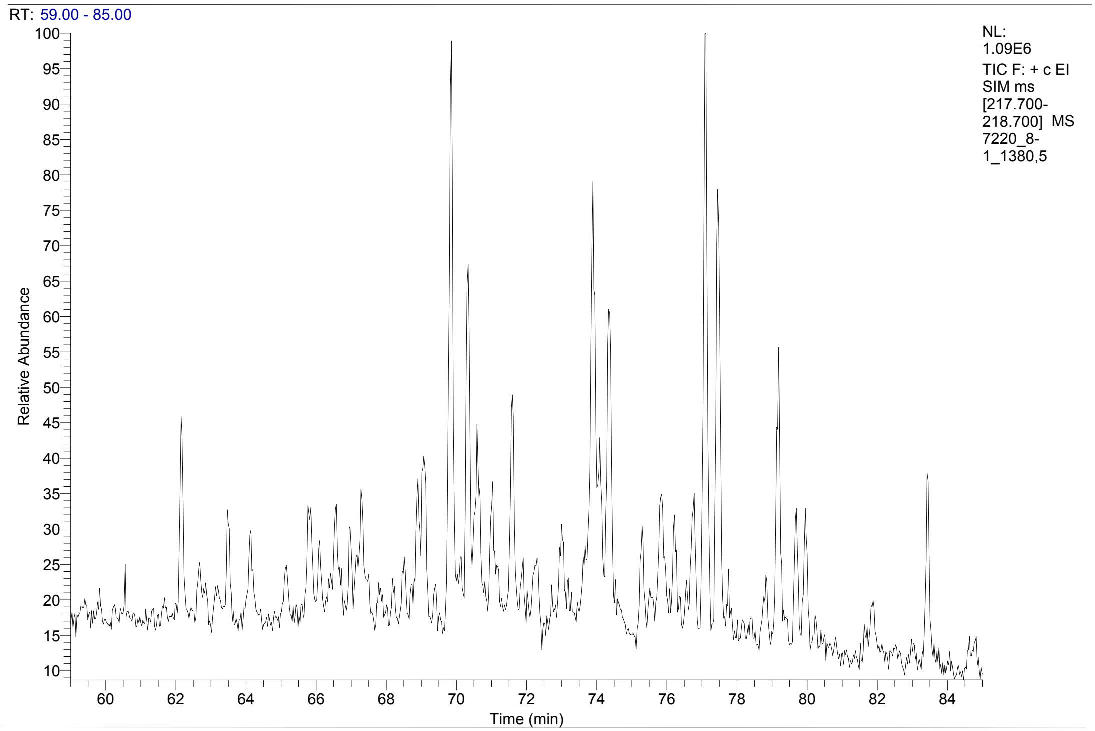
RT: 59.00 - 85.00
NL:
1.09E6
TIC F: + c EI
SIM ms
[217.700-
218.700] MS
7220_8-
1_1380,5
Relative Abundance
100
95
90
85
80
75
70
65
60
55
50
45
40
35
30
25
20
15
10
60
62
64
66
68
70
72
74
76
78
80
82
84
Time (min)

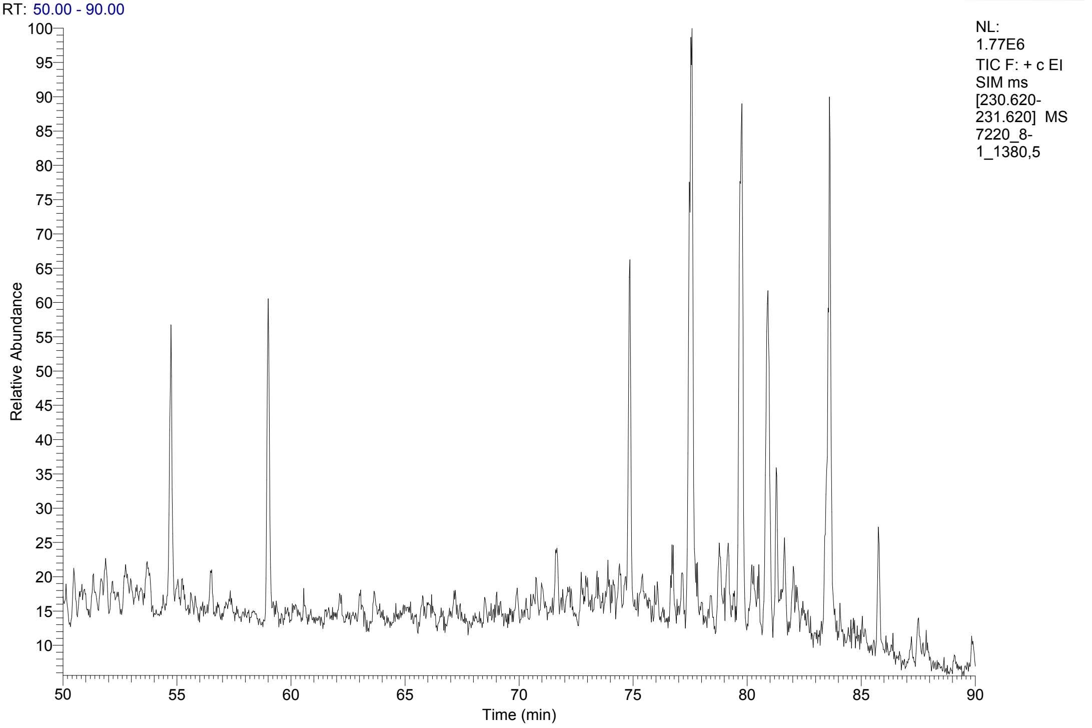
RT: 50.00 - 90.00
NL:
1.77E6
TIC F: + c EI
SIM ms
[230.620-
231.620] MS
7220_8-
1_1380,5
Relative Abundance
100
95
90
85
80
75
70
65
60
55
50
45
40
35
30
25
20
15
10
50
55
60
65
70
75
80
85
90
Time (min)

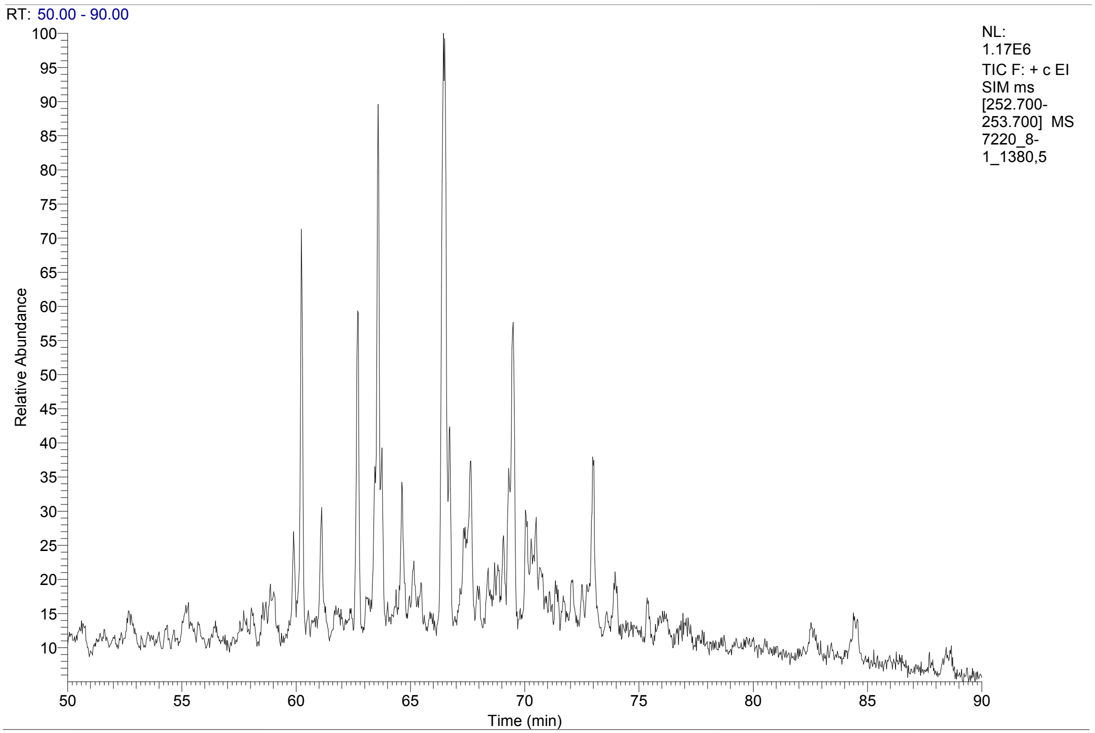
RT: 50.00 - 90.00
NL:
1.17E6
TIC F: + c EI
SIM ms
[252.700-
253.700] MS
7220_8-
1_1380,5
Relative Abundance
10
15
20
25
30
35
40
45
50
55
60
65
70
75
80
85
90
95
100
50
55
60
65
70
75
80
85
90
Time (min)

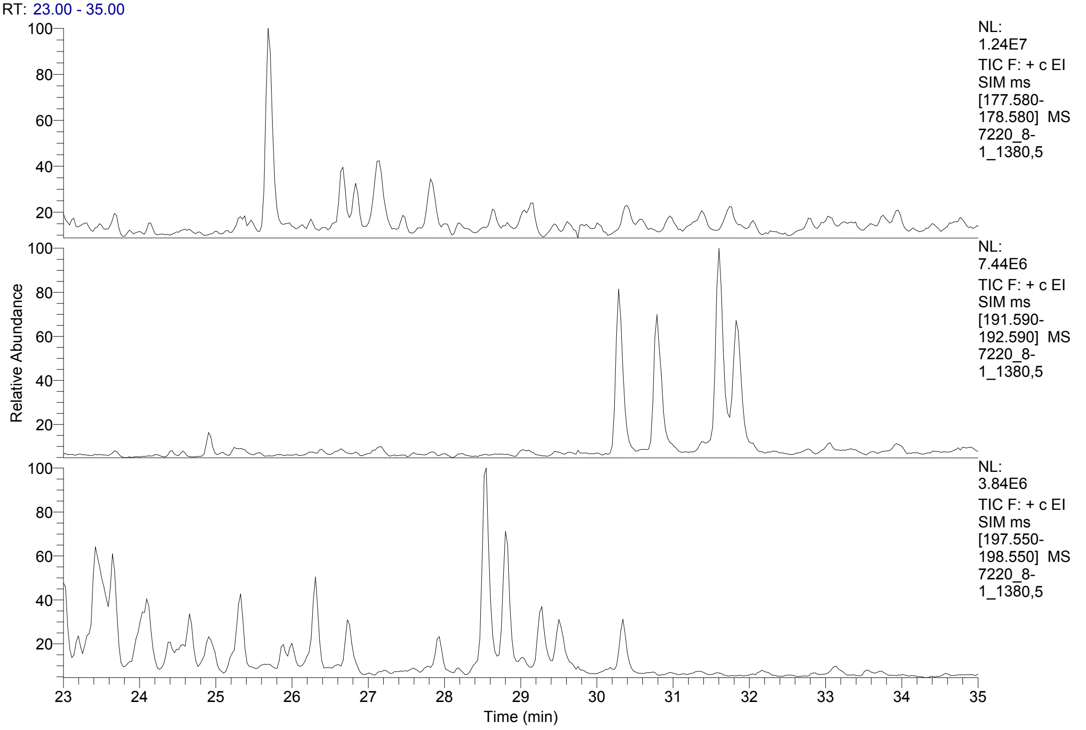
RT: 23.00 - 35.00
NL:
1.24E7
TIC F: + c EI
SIM ms
[177.580-
178.580] MS
7220_8-
1_1380,5
NL:
7.44E6
TIC F: + c EI
SIM ms
[191.590-
192.590] MS
7220_8-
1_1380,5
NL:
3.84E6
TIC F: + c EI
SIM ms
[197.550-
198.550] MS
7220_8-
1_1380,5
Relative Abundance
20
40
60
80
100
23
24
25
26
27
28
29
30
31
32
33
34
35
Time (min)

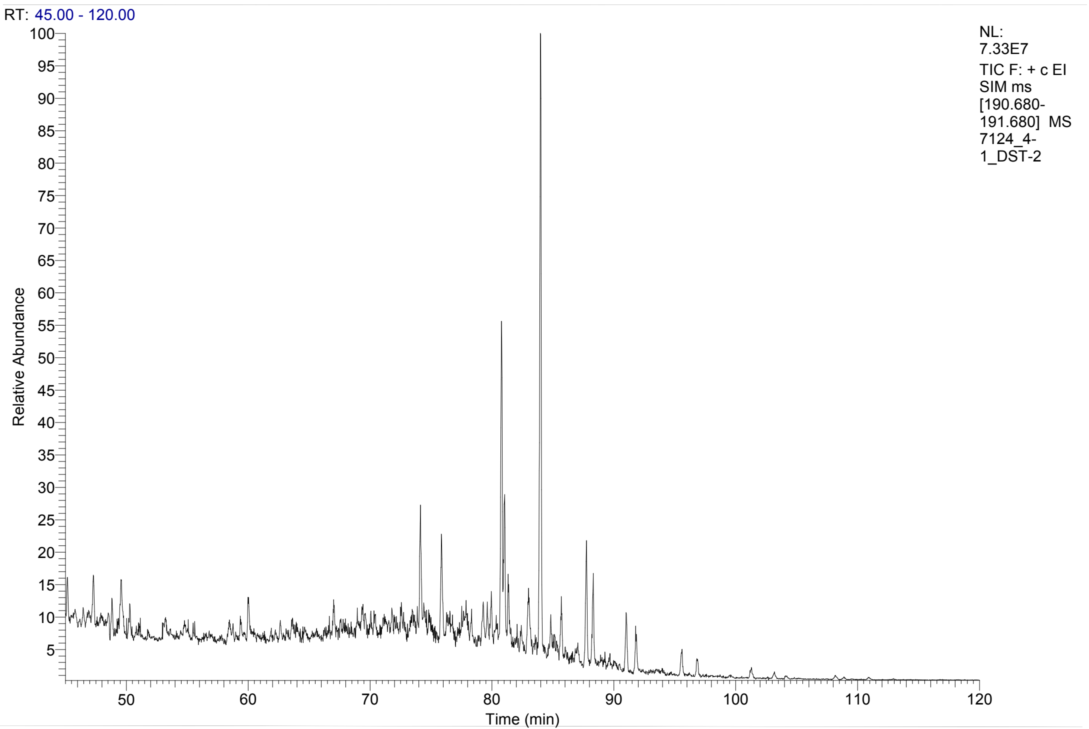
RT: 45.00 - 120.00
NL:
7.33E7
TIC F: + c EI
SIM ms
[190.680-
191.680] MS
7124_4-
1_DST-2
Relative Abundance
100
95
90
85
80
75
70
65
60
55
50
45
40
35
30
25
20
15
10
5
50
60
70
80
90
100
110
120
Time (min)

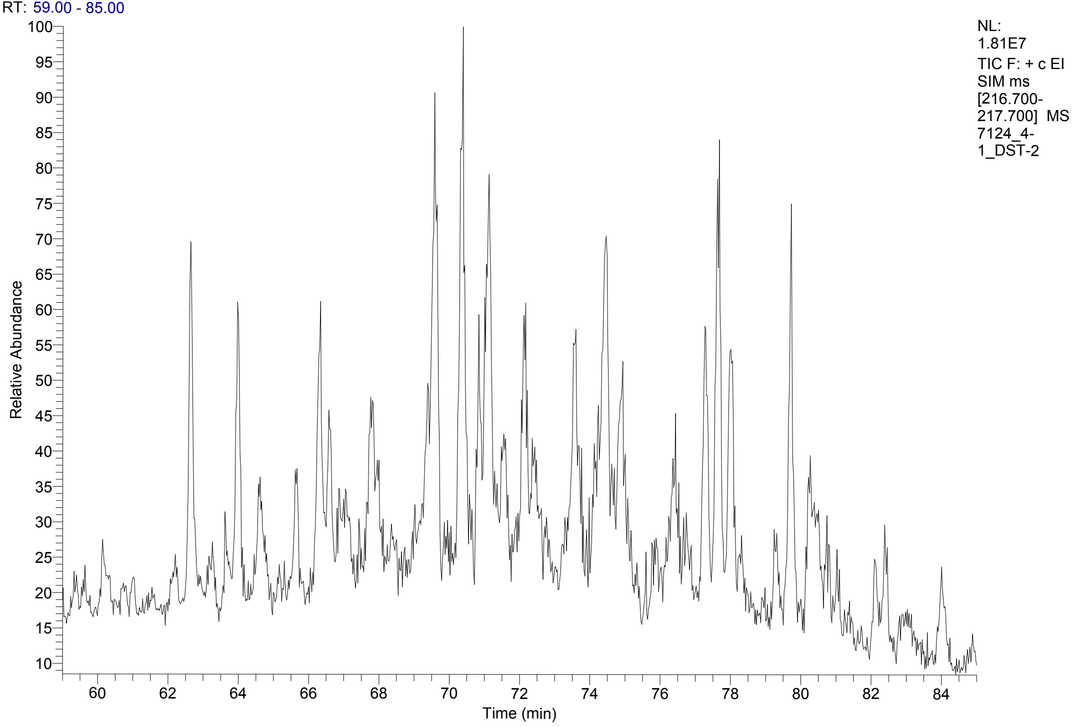
RT: 59.00 - 85.00
NL:
1.81E7
TIC F: + c EI
SIM ms
[216.700-
217.700] MS
7124_4-
1_DST-2
Relative Abundance
100
95
90
85
80
75
70
65
60
55
50
45
40
35
30
25
20
15
10
60
62
64
66
68
70
72
74
76
78
80
82
84
Time (min)

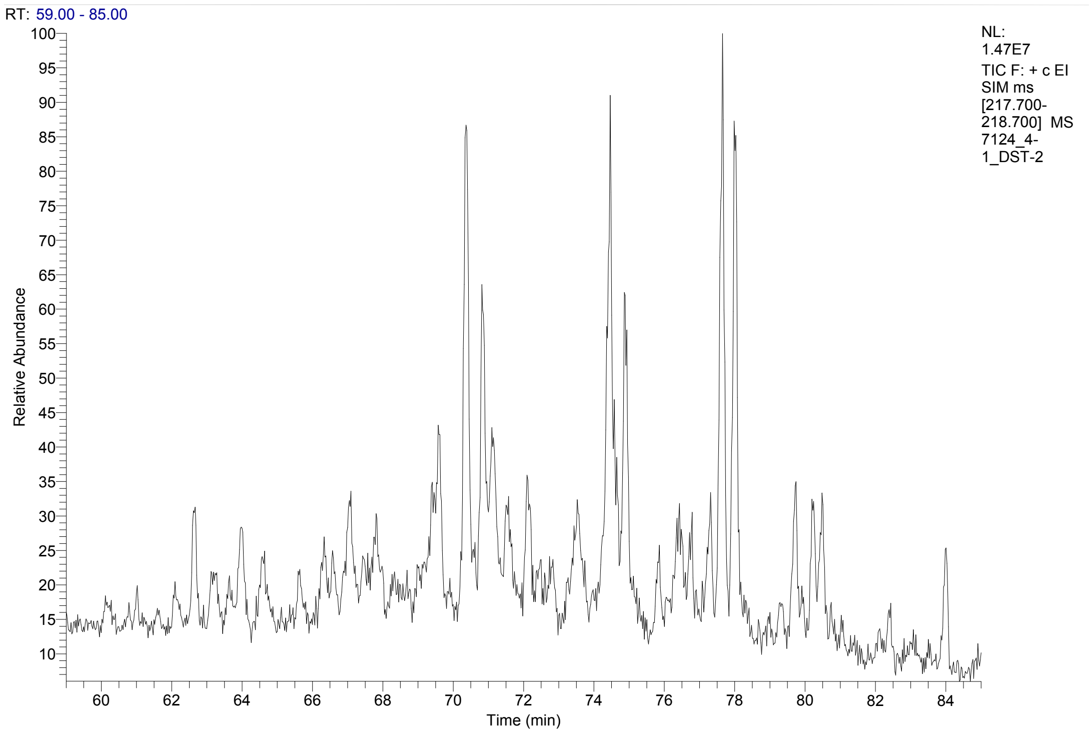
RT: 59.00 - 85.00
NL:
1.47E7
TIC F: + c EI
SIM ms
[217.700-
218.700] MS
7124_4-
1_DST-2
Relative Abundance
Time (min)
100
95
90
85
80
75
70
65
60
55
50
45
40
35
30
25
20
15
10
60
62
64
66
68
70
72
74
76
78
80
82
84

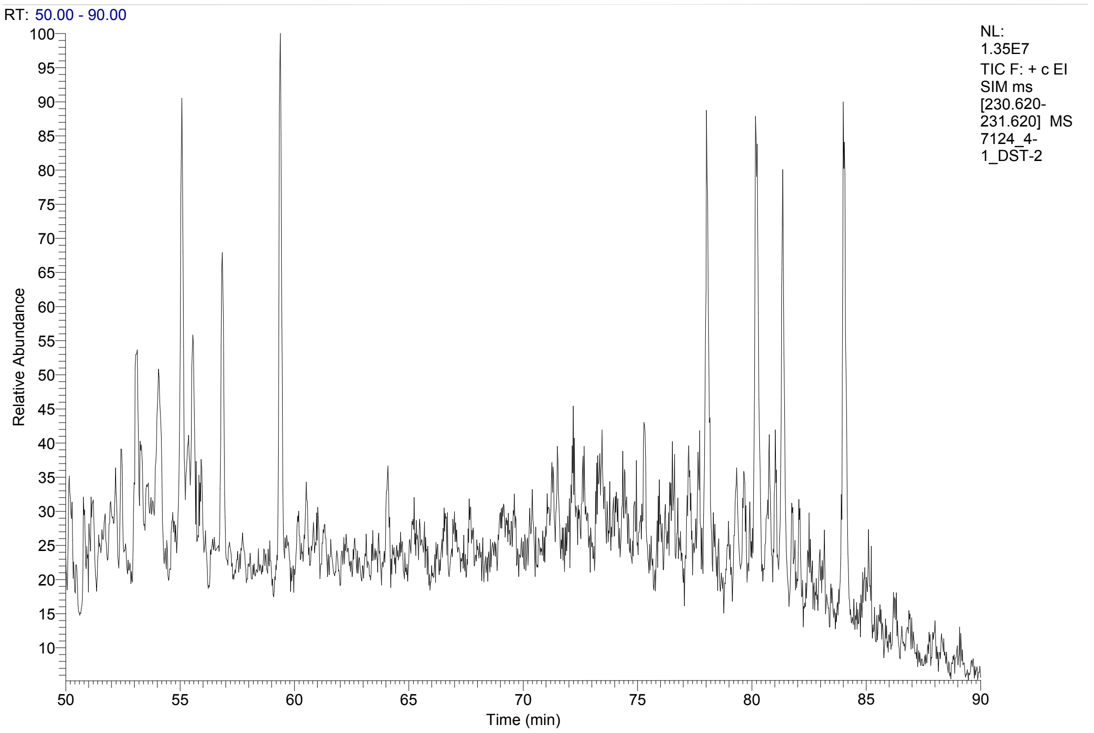
RT: 50.00 - 90.00
NL:
1.35E7
TIC F: + c EI
SIM ms
[230.620-
231.620] MS
7124_4-
1_DST-2
Relative Abundance
Time (min)
100
95
90
85
80
75
70
65
60
55
50
45
40
35
30
25
20
15
10
50
55
60
65
70
75
80
85
90

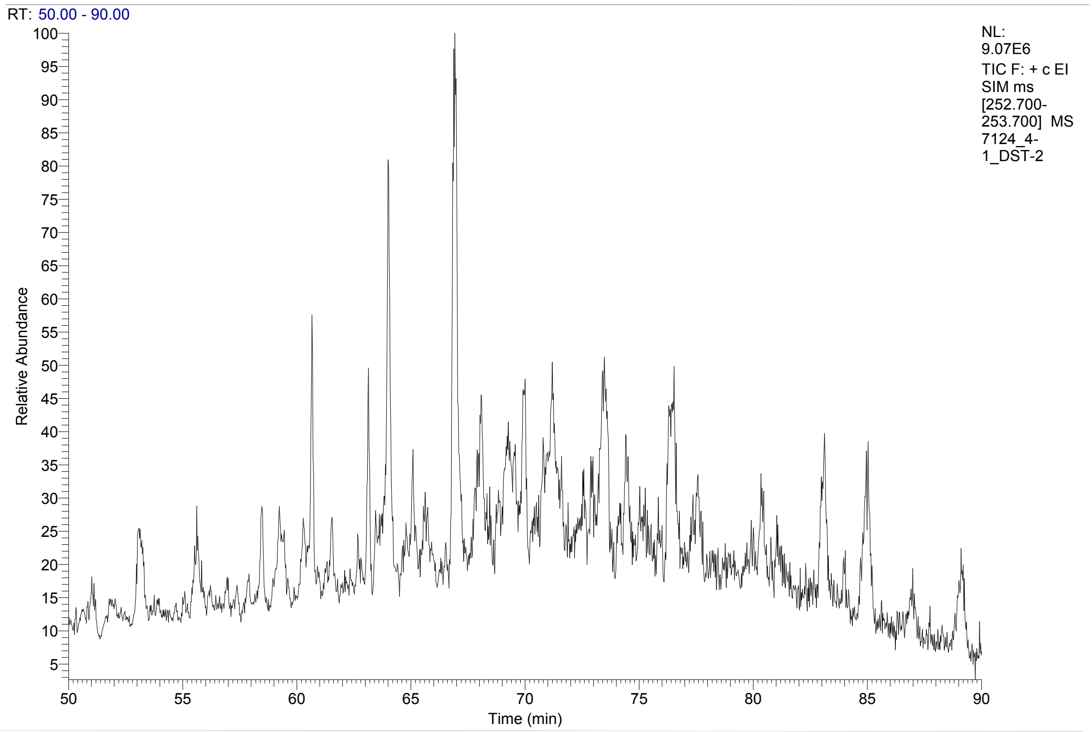
RT: 50.00 - 90.00
NL:
9.07E6
TIC F: + c EI
SIM ms
[252.700-
253.700] MS
7124_4-
1_DST-2
Relative Abundance
100
95
90
85
80
75
70
65
60
55
50
45
40
35
30
25
20
15
10
5
50
55
60
65
70
75
80
85
90
Time (min)

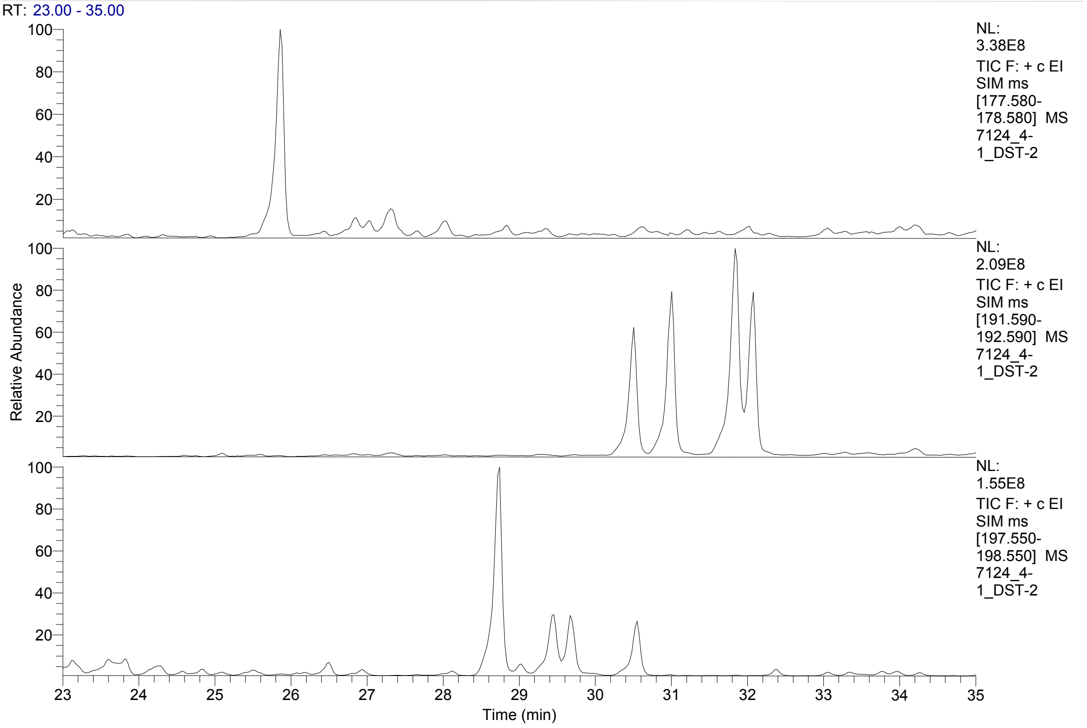
RT: 23.00 - 35.00
NL:
3.38E8
TIC F: + c EI
SIM ms
[177.580-
178.580] MS
7124_4-
1_DST-2
NL:
2.09E8
TIC F: + c EI
SIM ms
[191.590-
192.590] MS
7124_4-
1_DST-2
NL:
1.55E8
TIC F: + c EI
SIM ms
[197.550-
198.550] MS
7124_4-
1_DST-2
Relative Abundance
100
80
60
40
20
23
24
25
26
27
28
29
30
31
32
33
34
35
Time (min)

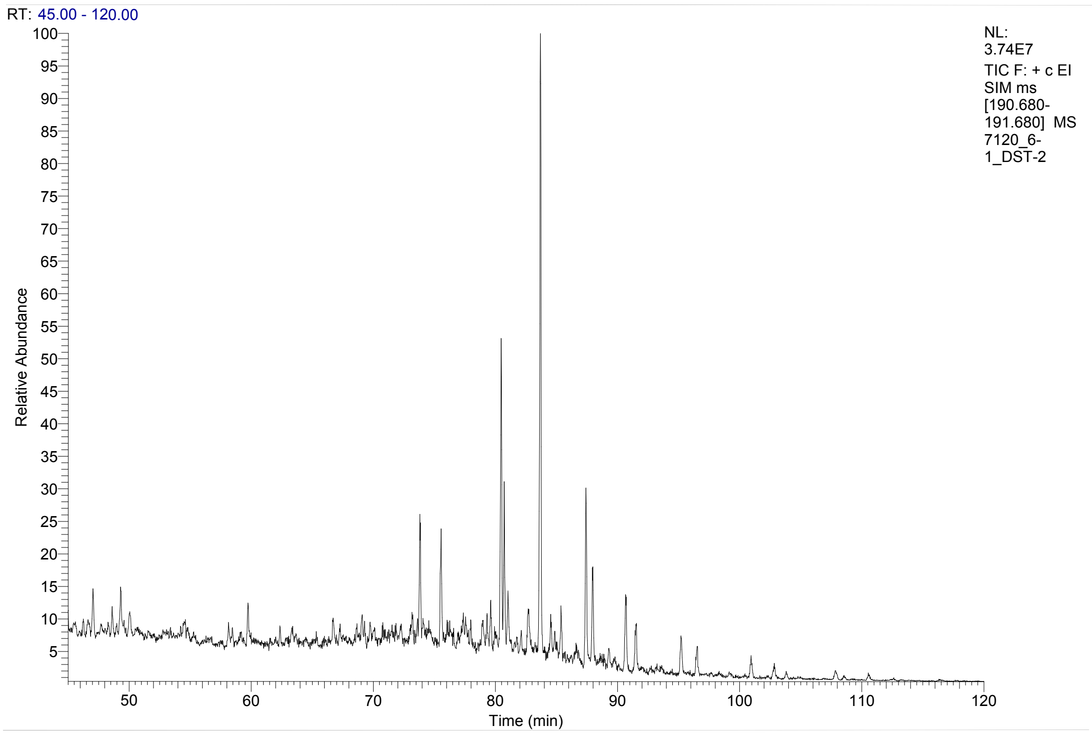
RT: 45.00 - 120.00
NL:
3.74E7
TIC F: + c EI
SIM ms
[190.680-
191.680] MS
7120_6-
1_DST-2
Relative Abundance
100
95
90
85
80
75
70
65
60
55
50
45
40
35
30
25
20
15
10
5
50
60
70
80
90
100
110
120
Time (min)

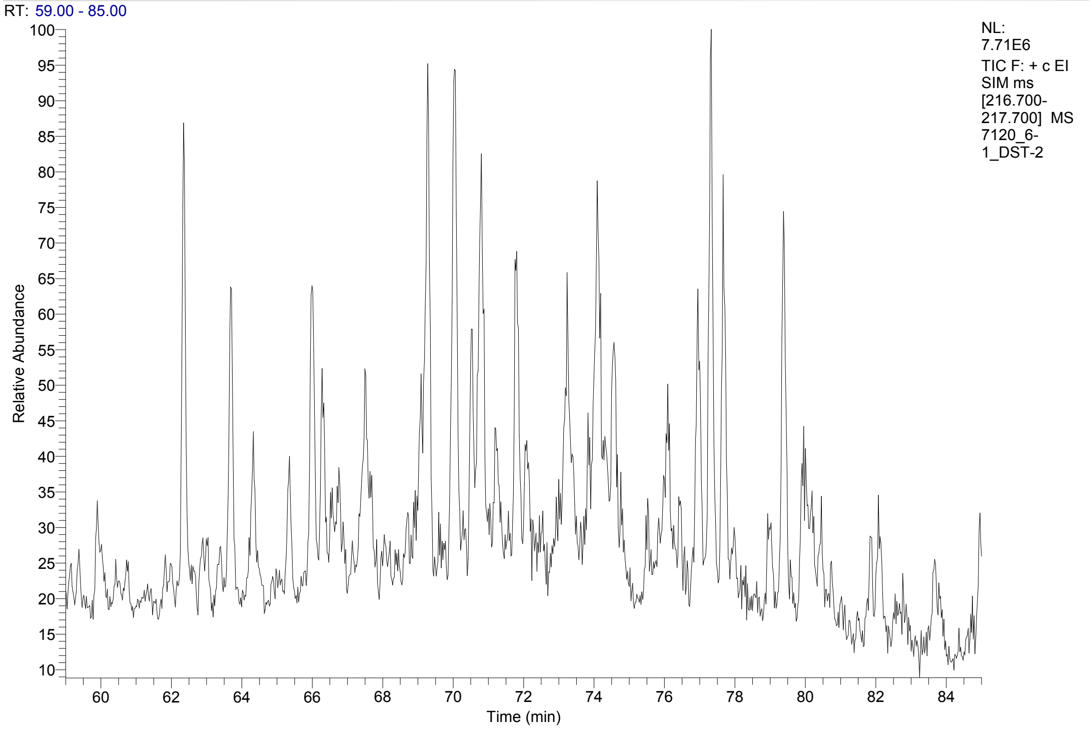
RT: 59.00 - 85.00
NL:
7.71E6
TIC F: + c EI
SIM ms
[216.700-
217.700] MS
7120_6-
1_DST-2
Relative Abundance
100
95
90
85
80
75
70
65
60
55
50
45
40
35
30
25
20
15
10
60
62
64
66
68
70
72
74
76
78
80
82
84
Time (min)

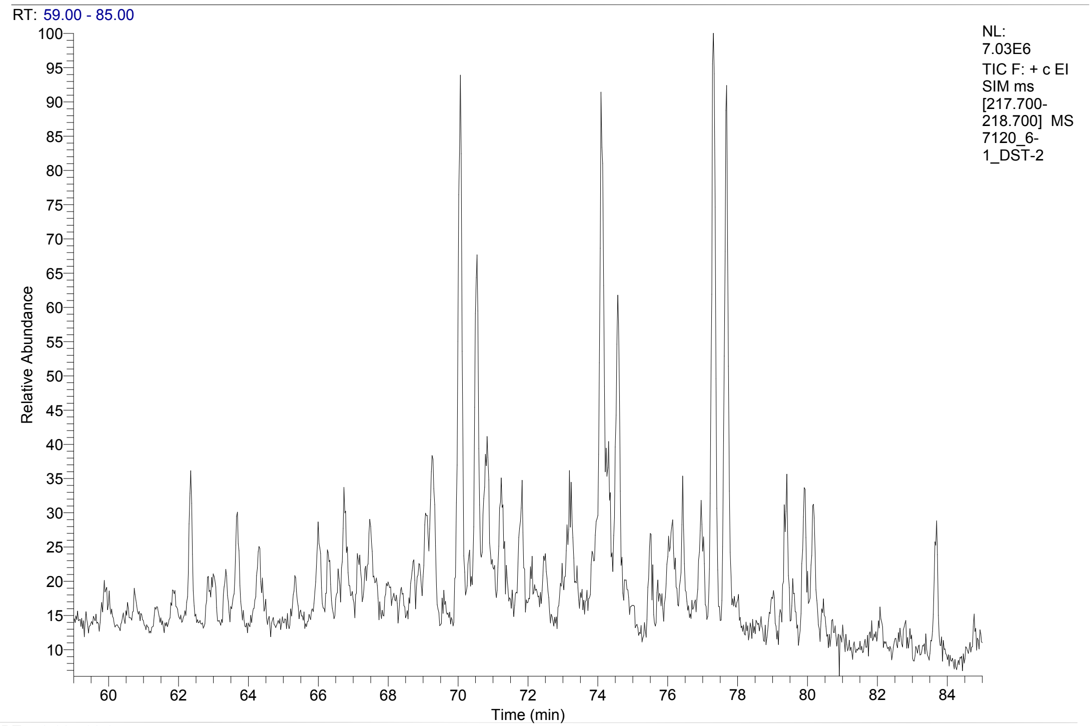
RT: 59.00 - 85.00
NL:
7.03E6
TIC F: + c EI
SIM ms
[217.700-
218.700] MS
7120_6-
1_DST-2
Relative Abundance
100
95
90
85
80
75
70
65
60
55
50
45
40
35
30
25
20
15
10
60
62
64
66
68
70
72
74
76
78
80
82
84
Time (min)

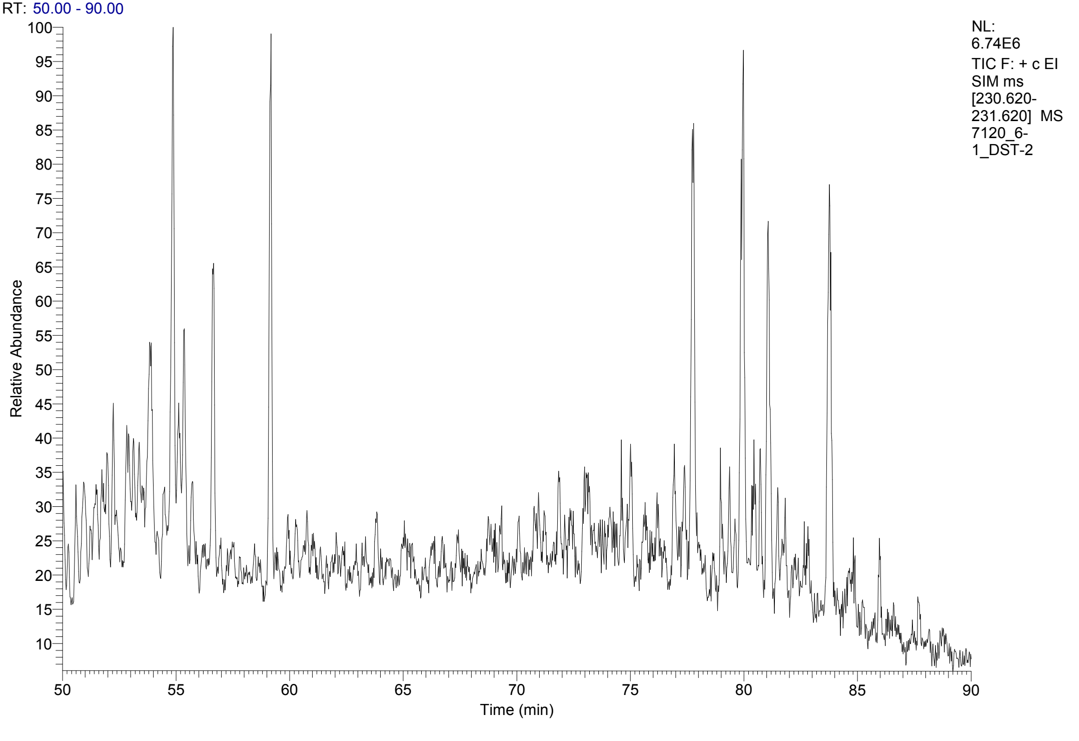
RT: 50.00 - 90.00
NL:
6.74E6
TIC F: + c EI
SIM ms
[230.620-
231.620] MS
7120_6-
1_DST-2
Relative Abundance
100
95
90
85
80
75
70
65
60
55
50
45
40
35
30
25
20
15
10
50
55
60
65
70
75
80
85
90
Time (min)

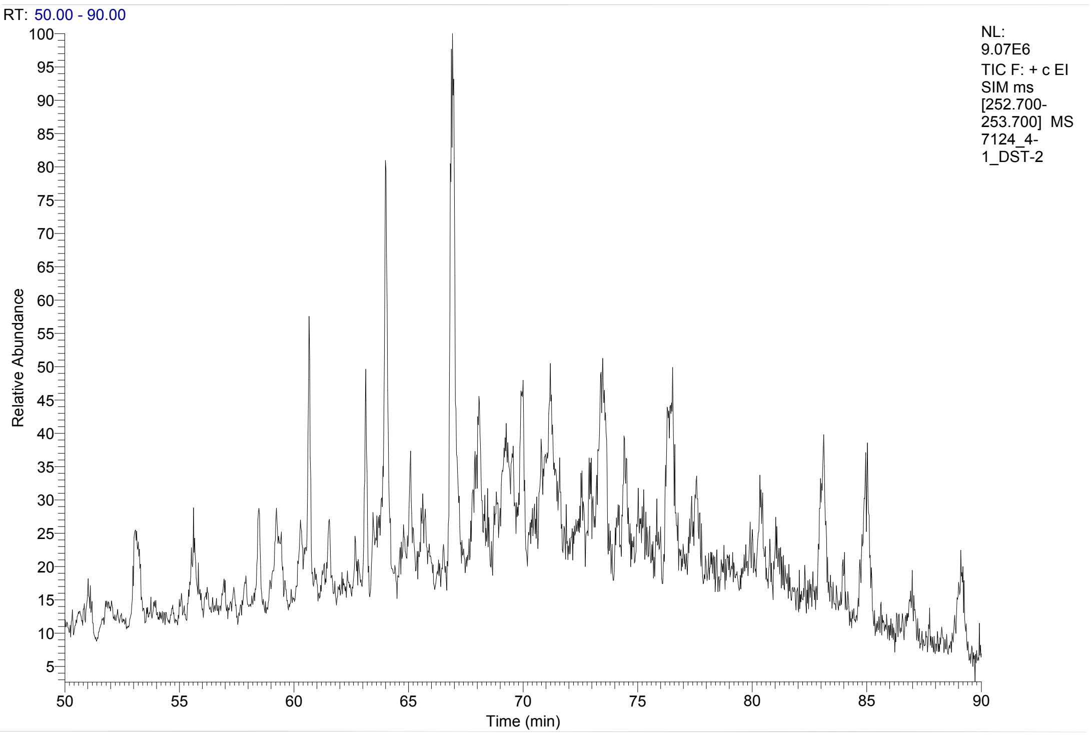
RT: 50.00 - 90.00
NL:
9.07E6
TIC F: + c EI
SIM ms
[252.700-
253.700] MS
7124_4-
1_DST-2
Relative Abundance
Time (min)
100
95
90
85
80
75
70
65
60
55
50
45
40
35
30
25
20
15
10
5
50
55
60
65
70
75
80
85
90

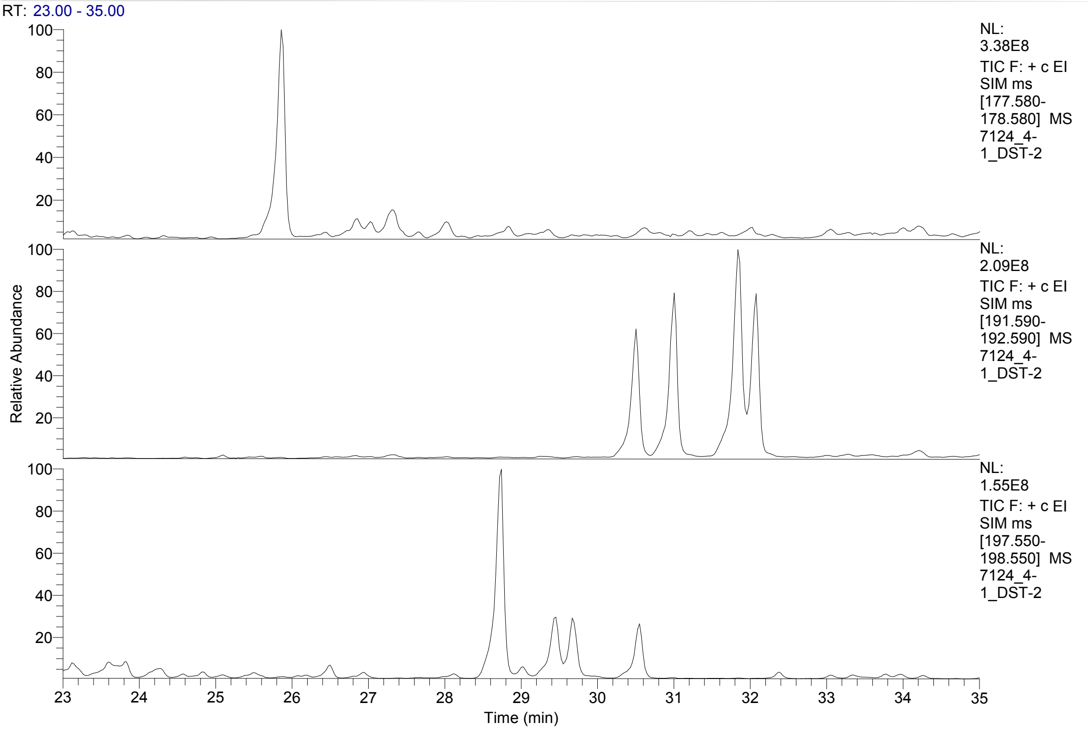
RT: 23.00 - 35.00
NL:
3.38E8
TIC F: + c EI
SIM ms
[177.580-
178.580] MS
7124_4-
1_DST-2
NL:
2.09E8
TIC F: + c EI
SIM ms
[191.590-
192.590] MS
7124_4-
1_DST-2
NL:
1.55E8
TIC F: + c EI
SIM ms
[197.550-
198.550] MS
7124_4-
1_DST-2
Relative Abundance
Time (min)
100
80
60
40
20
23
24
25
26
27
28
29
30
31
32
33
34
35

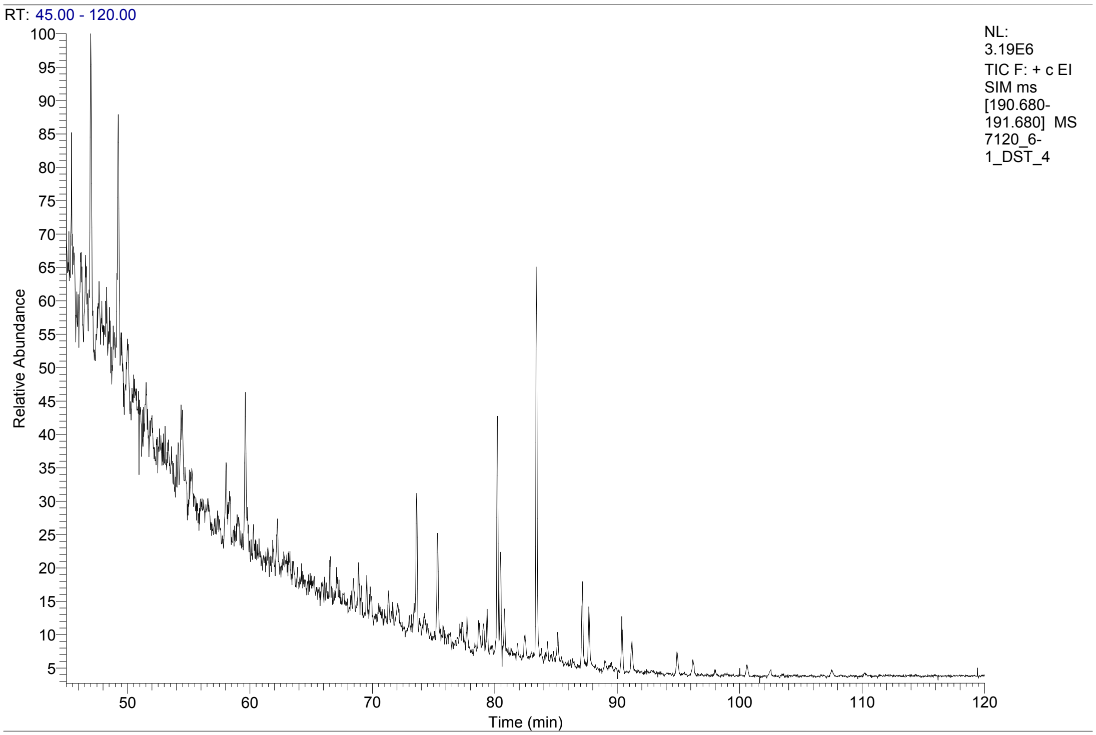
RT: 45.00 - 120.00
NL:
3.19E6
TIC F: + c EI
SIM ms
[190.680-
191.680] MS
7120_6-
1_DST_4
Relative Abundance
100
95
90
85
80
75
70
65
60
55
50
45
40
35
30
25
20
15
10
5
50
60
70
80
90
100
110
120
Time (min)

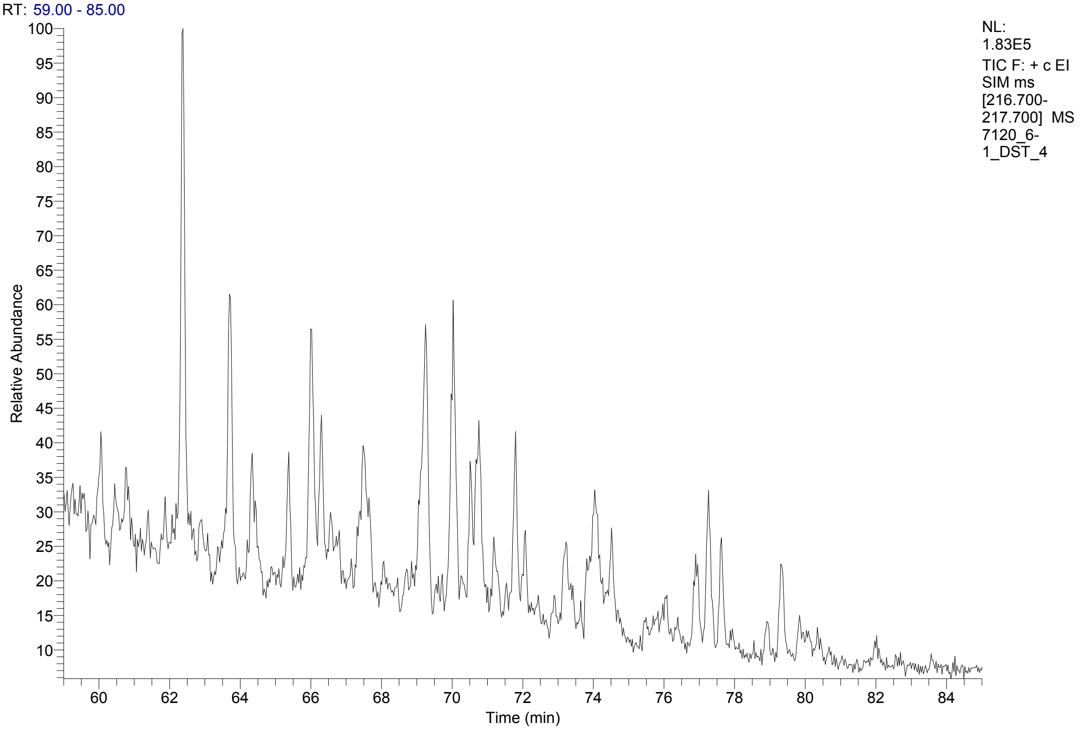
RT: 59.00 - 85.00
NL:
1.83E5
TIC F: + c EI
SIM ms
[216.700-
217.700] MS
7120_6-
1_DST_4
Relative Abundance
100
95
90
85
80
75
70
65
60
55
50
45
40
35
30
25
20
15
10
60
62
64
66
68
70
72
74
76
78
80
82
84
Time (min)

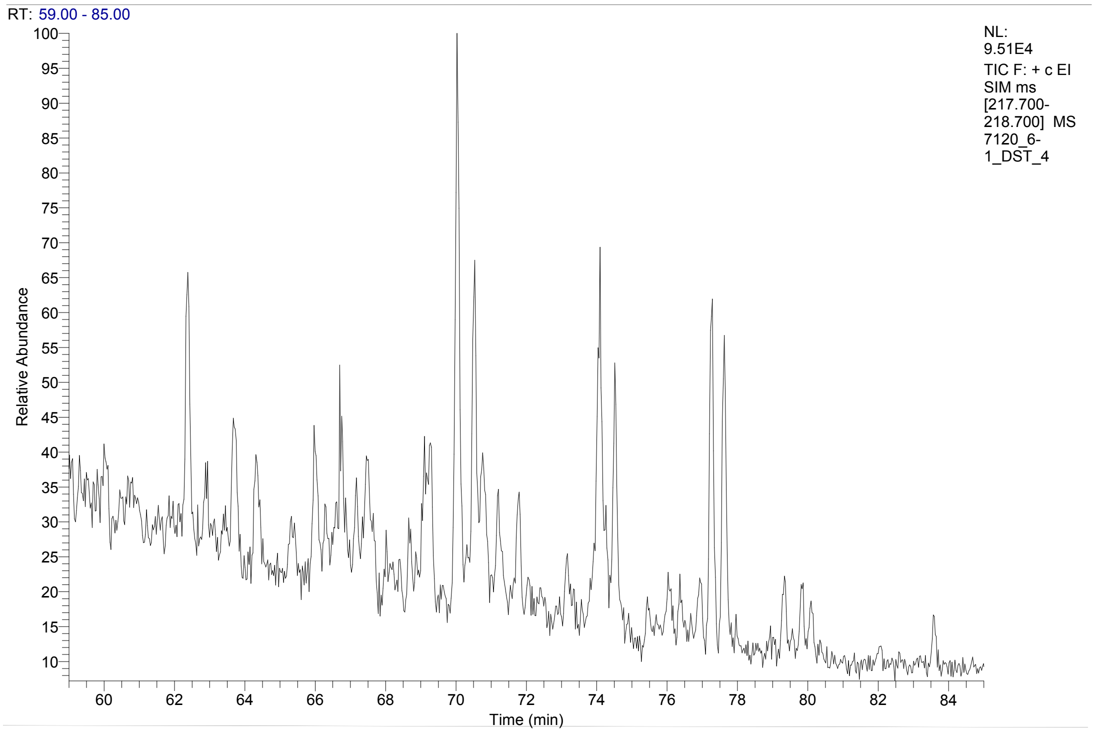
RT: 59.00 - 85.00
NL:
9.51E4
TIC F: + c EI
SIM ms
[217.700-
218.700] MS
7120_6-
1_DST_4
Relative Abundance
100
95
90
85
80
75
70
65
60
55
50
45
40
35
30
25
20
15
10
60
62
64
66
68
70
72
74
76
78
80
82
84
Time (min)

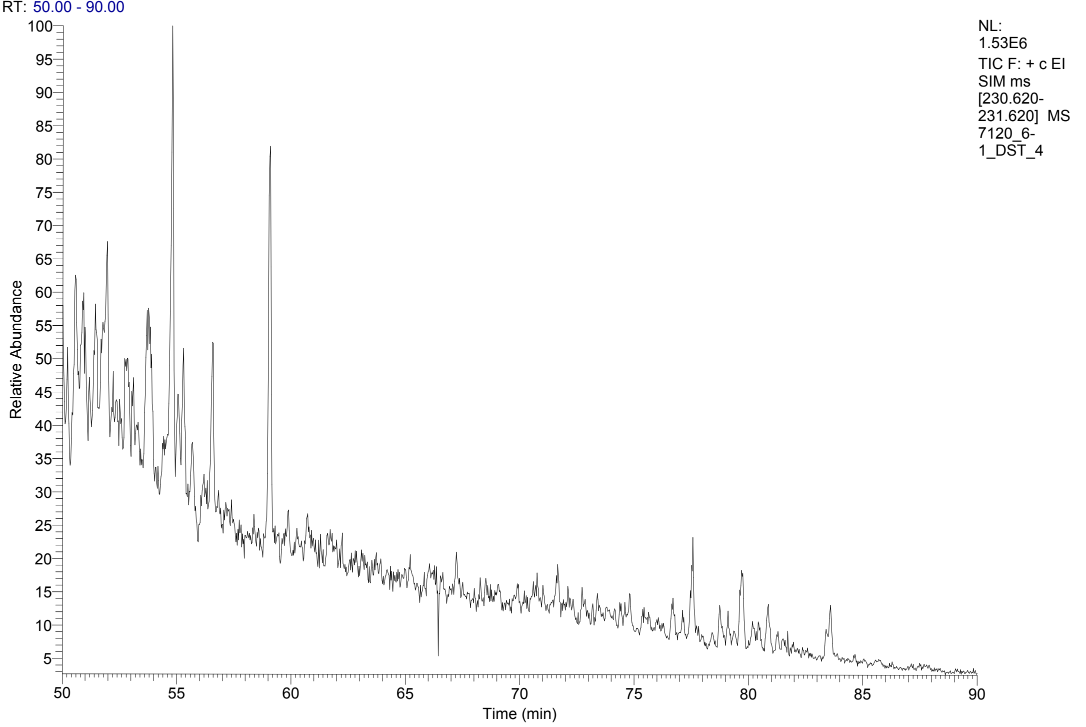
RT: 50.00 - 90.00
NL:
1.53E6
TIC F: + c EI
SIM ms
[230.620-
231.620] MS
7120_6-
1_DST_4
Relative Abundance
100
95
90
85
80
75
70
65
60
55
50
45
40
35
30
25
20
15
10
5
50
55
60
65
70
75
80
85
90
Time (min)

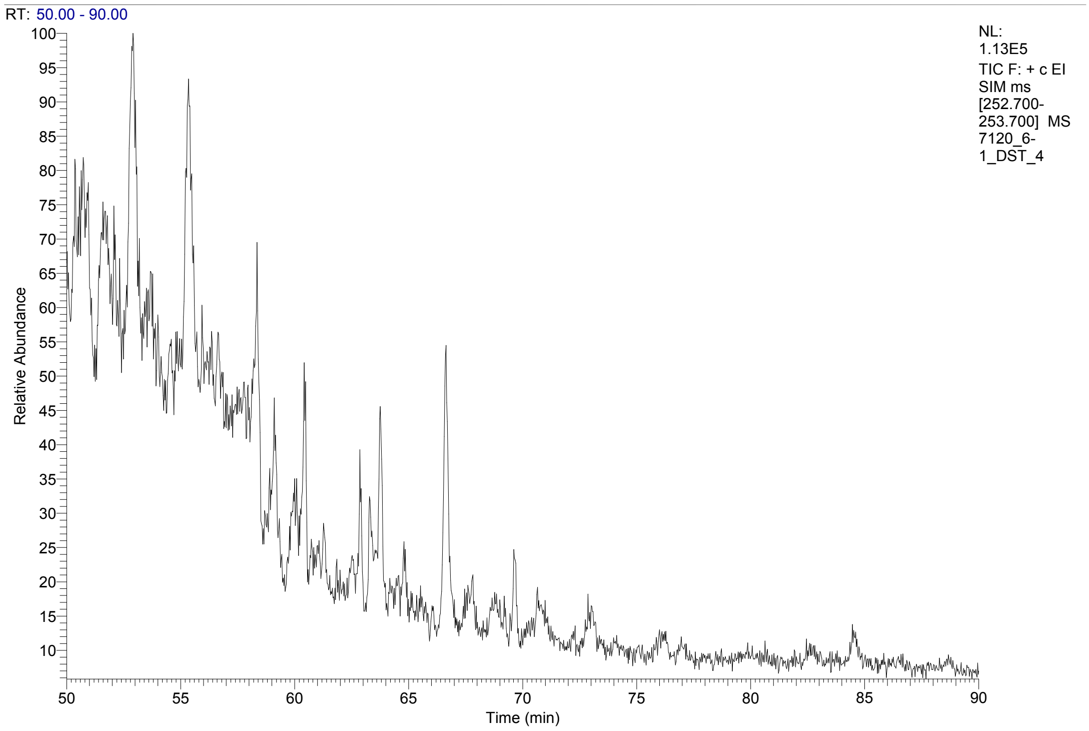
RT: 50.00 - 90.00
NL:
1.13E5
TIC F: + c EI
SIM ms
[252.700-
253.700] MS
7120_6-
1_DST_4
Relative Abundance
Time (min)
100
95
90
85
80
75
70
65
60
55
50
45
40
35
30
25
20
15
10
50
55
60
65
70
75
80
85
90

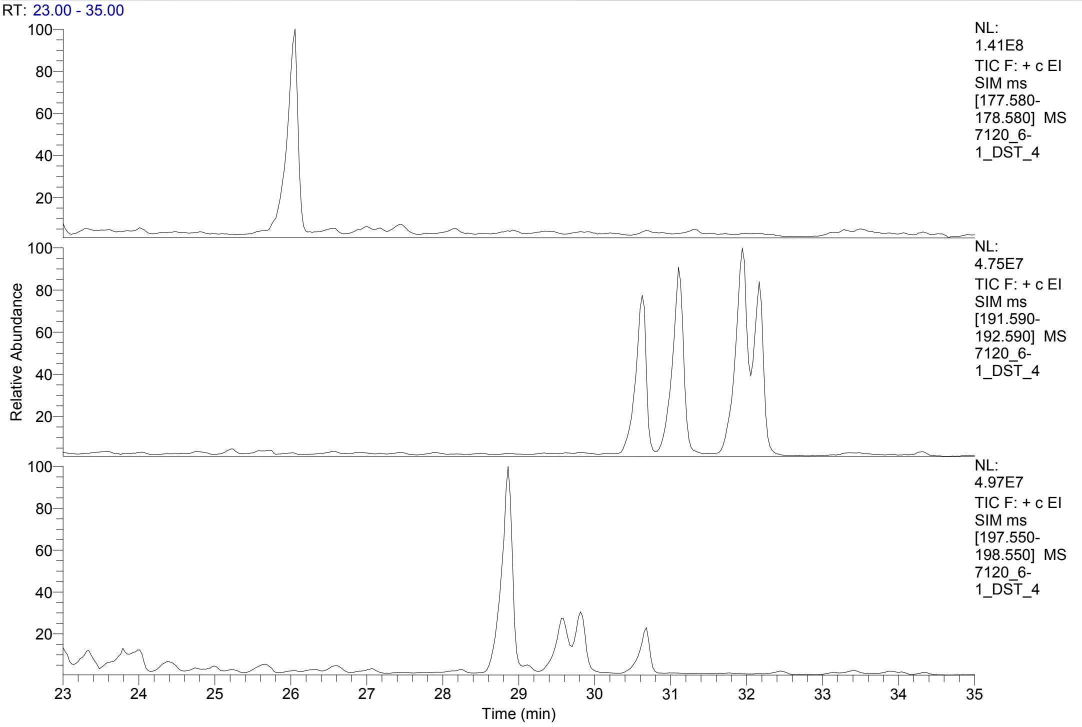
RT: 23.00 - 35.00
NL:
1.41E8
TIC F: + c EI
SIM ms
[177.580-
178.580] MS
7120_6-
1_DST_4
NL:
4.75E7
TIC F: + c EI
SIM ms
[191.590-
192.590] MS
7120_6-
1_DST_4
NL:
4.97E7
TIC F: + c EI
SIM ms
[197.550-
198.550] MS
7120_6-
1_DST_4
Relative Abundance
Time (min)
100
80
60
40
20
23
24
25
26
27
28
29
30
31
32
33
34
35

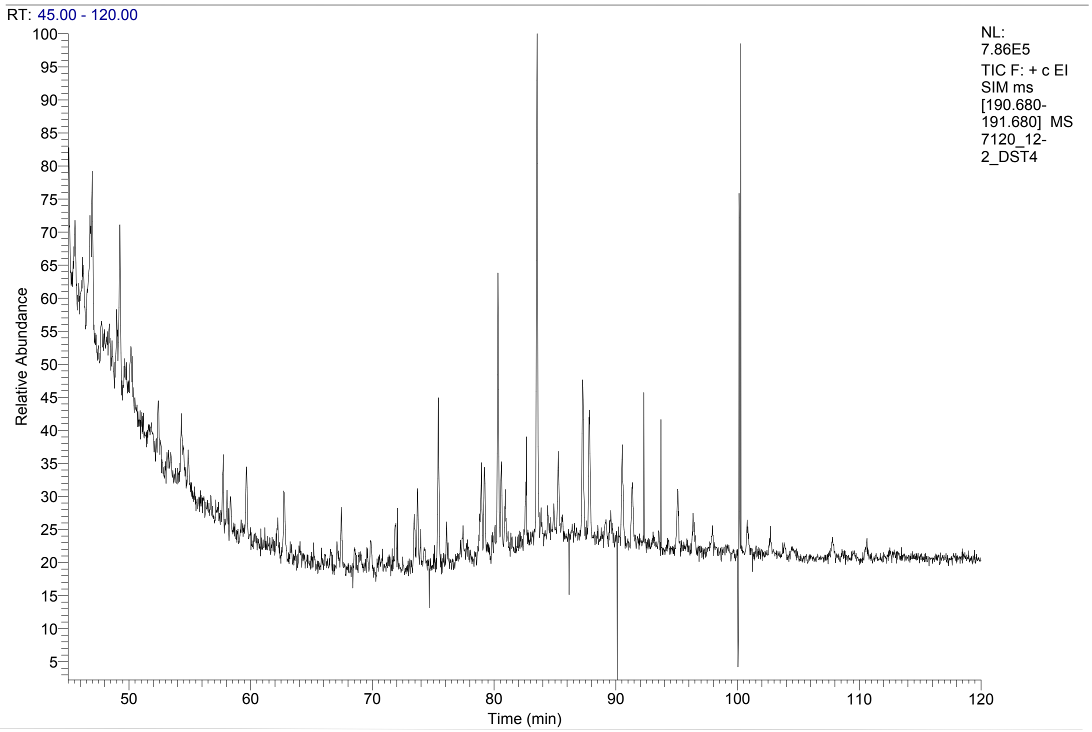
RT: 45.00 - 120.00
NL:
7.86E5
TIC F: + c EI
SIM ms
[190.680-
191.680] MS
7120_12-
2_DST4
Relative Abundance
100
95
90
85
80
75
70
65
60
55
50
45
40
35
30
25
20
15
10
5
50
60
70
80
90
100
110
120
Time (min)

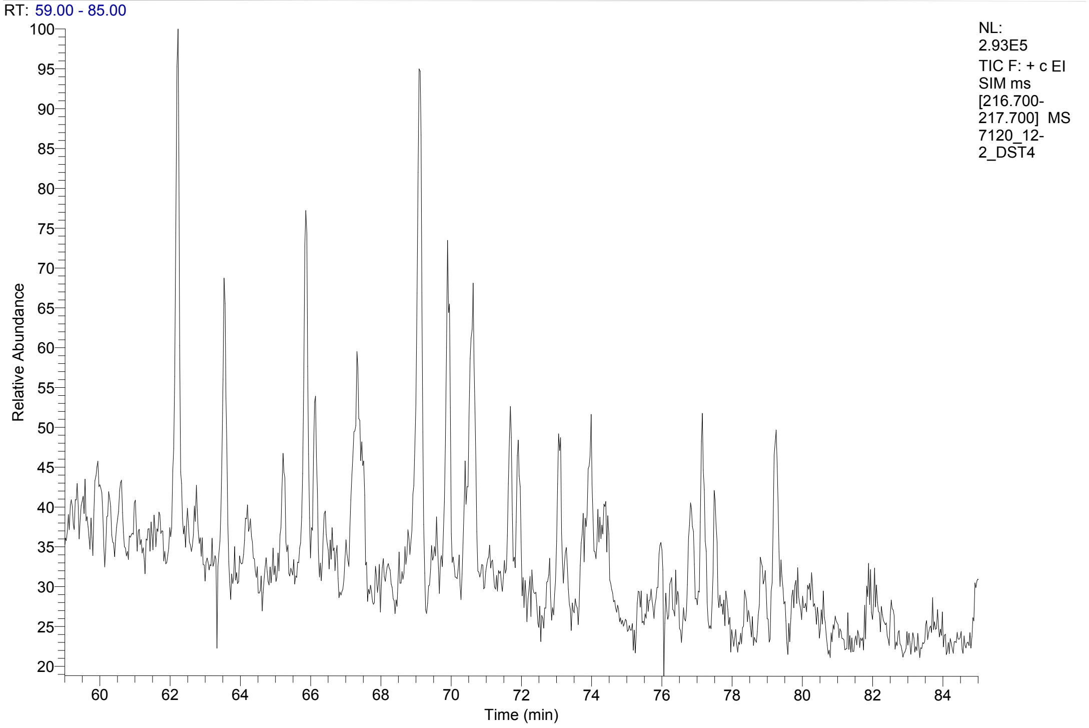
RT: 59.00 - 85.00
NL:
2.93E5
TIC F: + c EI
SIM ms
[216.700-
217.700] MS
7120_12-
2_DST4
Relative Abundance
100
95
90
85
80
75
70
65
60
55
50
45
40
35
30
25
20
60
62
64
66
68
70
72
74
76
78
80
82
84
Time (min)

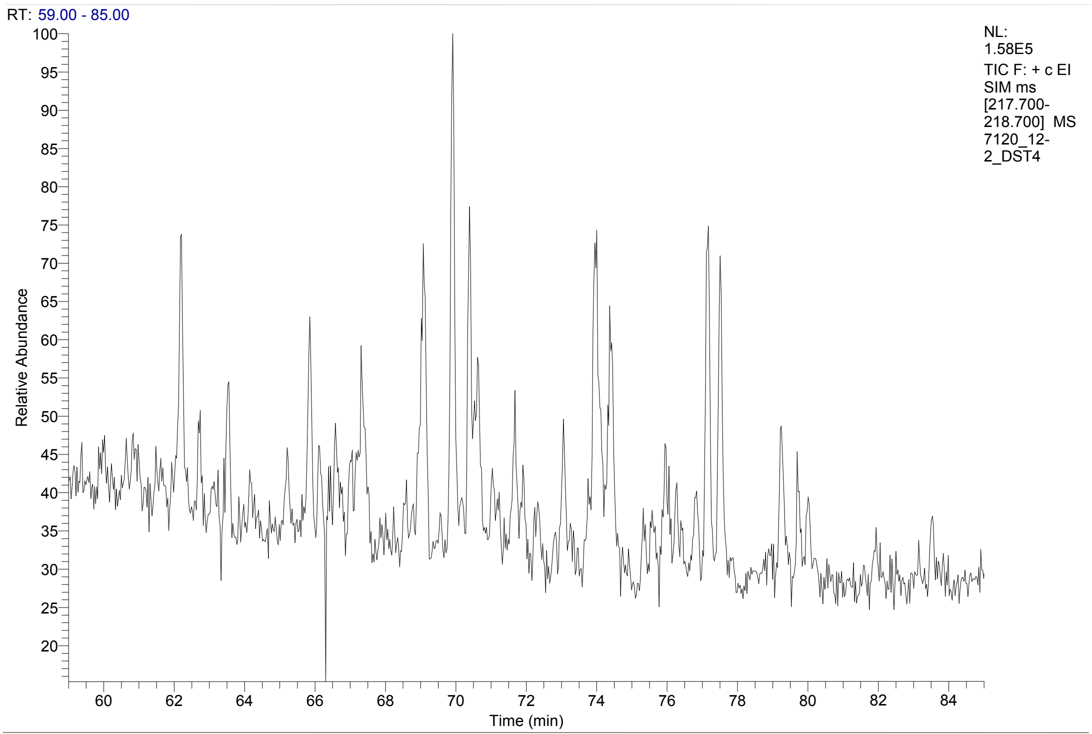
RT: 59.00 - 85.00
NL:
1.58E5
TIC F: + c EI
SIM ms
[217.700-
218.700] MS
7120_12-
2_DST4
Relative Abundance
100
95
90
85
80
75
70
65
60
55
50
45
40
35
30
25
20
60
62
64
66
68
70
72
74
76
78
80
82
84
Time (min)

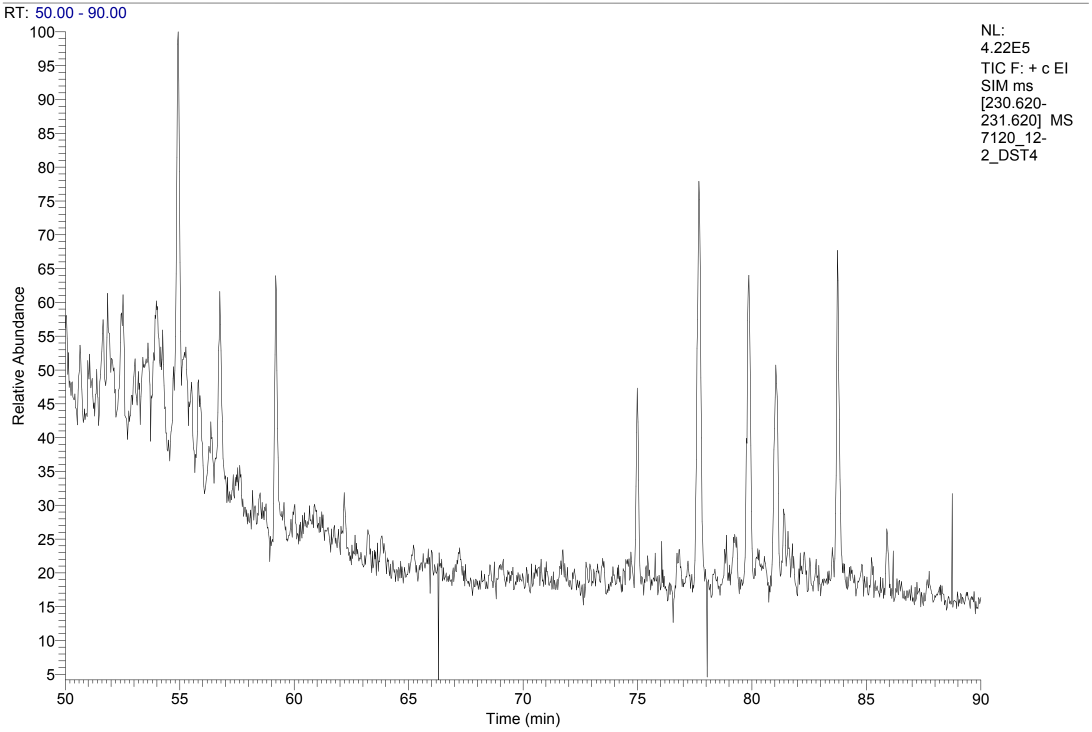
RT: 50.00 - 90.00
NL:
4.22E5
TIC F: + c EI
SIM ms
[230.620-
231.620] MS
7120_12-
2_DST4
Relative Abundance
100
95
90
85
80
75
70
65
60
55
50
45
40
35
30
25
20
15
10
5
50
55
60
65
70
75
80
85
90
Time (min)

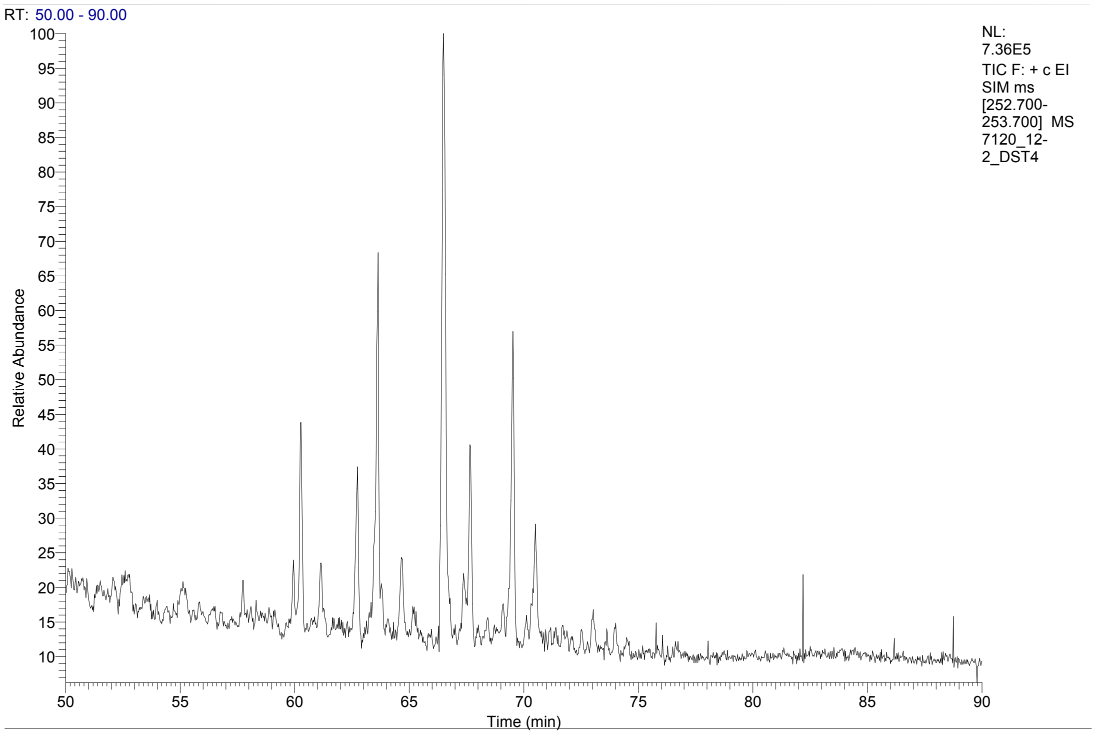
RT: 50.00 - 90.00
Relative Abundance
100
95
90
85
80
75
70
65
60
55
50
45
40
35
30
25
20
15
10
50
55
60
65
70
75
80
85
90
Time (min)
NL:
7.36E5
TIC F: + c EI
SIM ms
[252.700-
253.700] MS
7120_12-
2_DST4

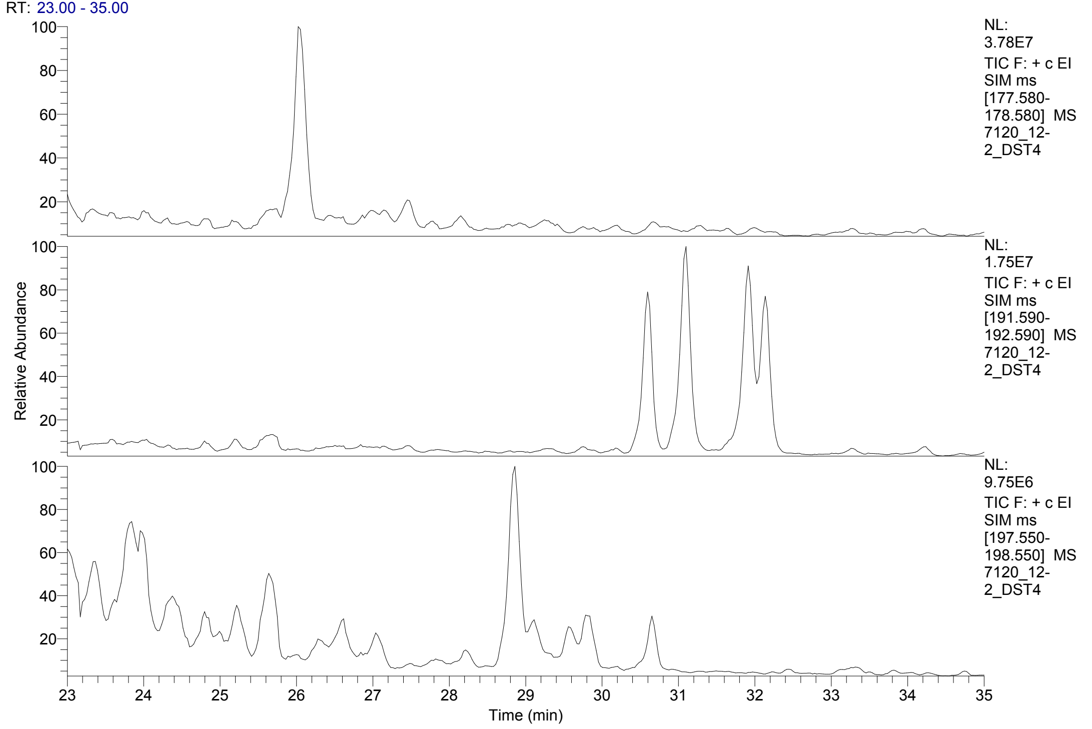
RT: 23.00 - 35.00
Relative Abundance
100
80
60
40
20
NL:
3.78E7
TIC F: + c EI
SIM ms
[177.580-
178.580] MS
7120_12-
2_DST4
NL:
1.75E7
TIC F: + c EI
SIM ms
[191.590-
192.590] MS
7120_12-
2_DST4
NL:
9.75E6
TIC F: + c EI
SIM ms
[197.550-
198.550] MS
7120_12-
2_DST4
23
24
25
26
27
28
29
30
31
32
33
34
35
Time (min)

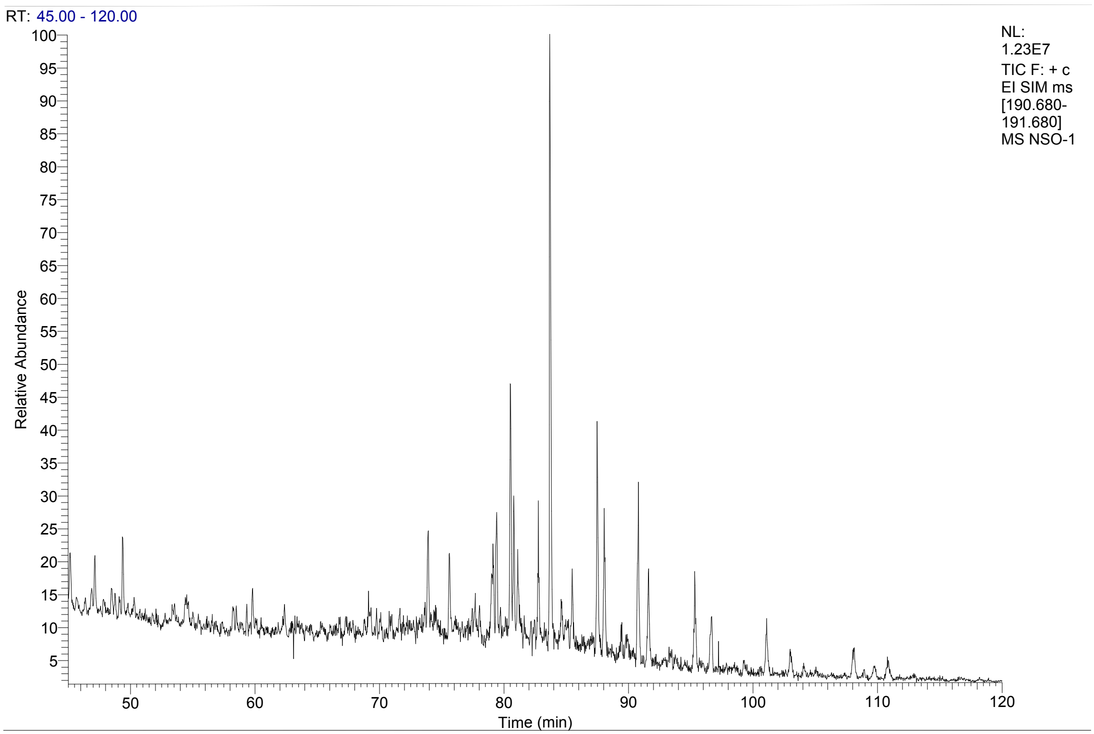
RT: 45.00 - 120.00
NL:
1.23E7
TIC F: + c
EI SIM ms
[190.680-
191.680]
MS NSO-1
Relative Abundance
100
95
90
85
80
75
70
65
60
55
50
45
40
35
30
25
20
15
10
5
50
60
70
80
90
100
110
120
Time (min)

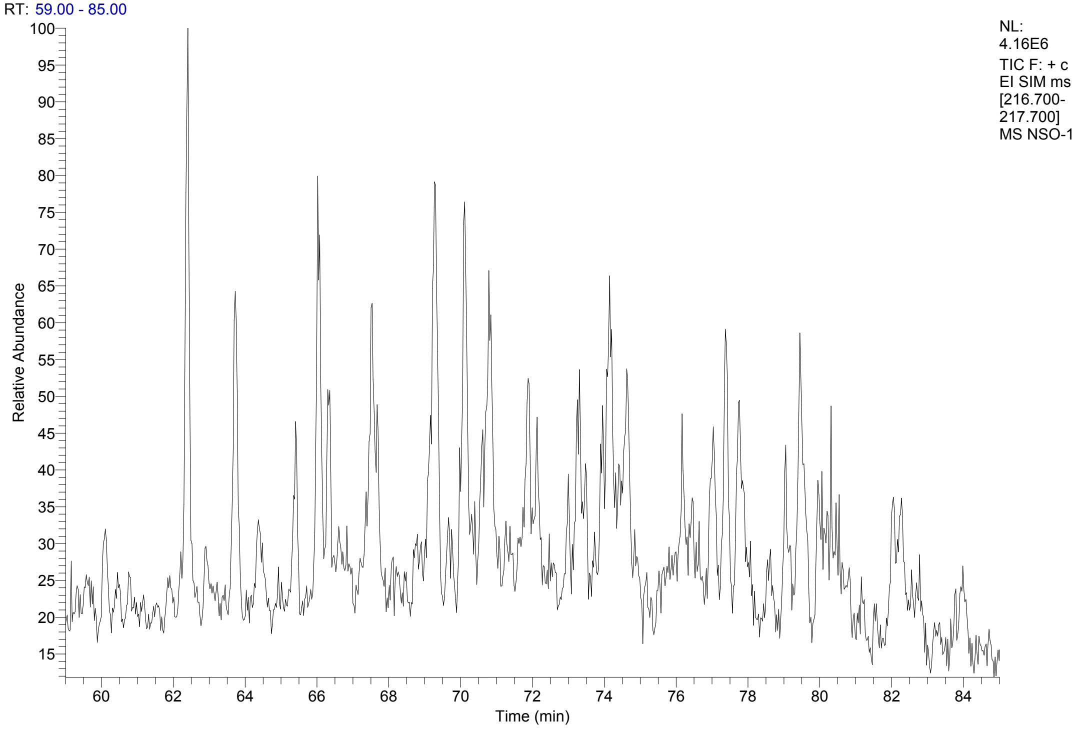
RT: 59.00 - 85.00
NL:
4.16E6
TIC F: + c
EI SIM ms
[216.700-
217.700]
MS NSO-1
Relative Abundance
100
95
90
85
80
75
70
65
60
55
50
45
40
35
30
25
20
15
60
62
64
66
68
70
72
74
76
78
80
82
84
Time (min)

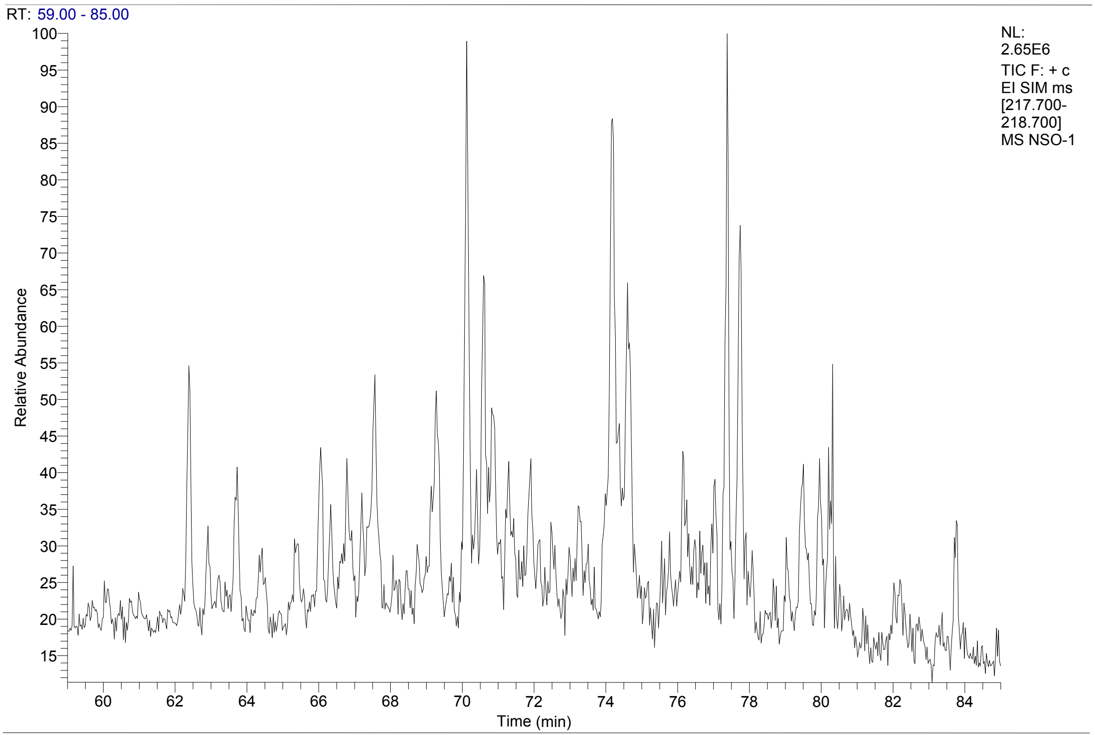
RT: 59.00 - 85.00
NL:
2.65E6
TIC F: + c
EI SIM ms
[217.700-
218.700]
MS NSO-1
Relative Abundance
100
95
90
85
80
75
70
65
60
55
50
45
40
35
30
25
20
15
60
62
64
66
68
70
72
74
76
78
80
82
84
Time (min)

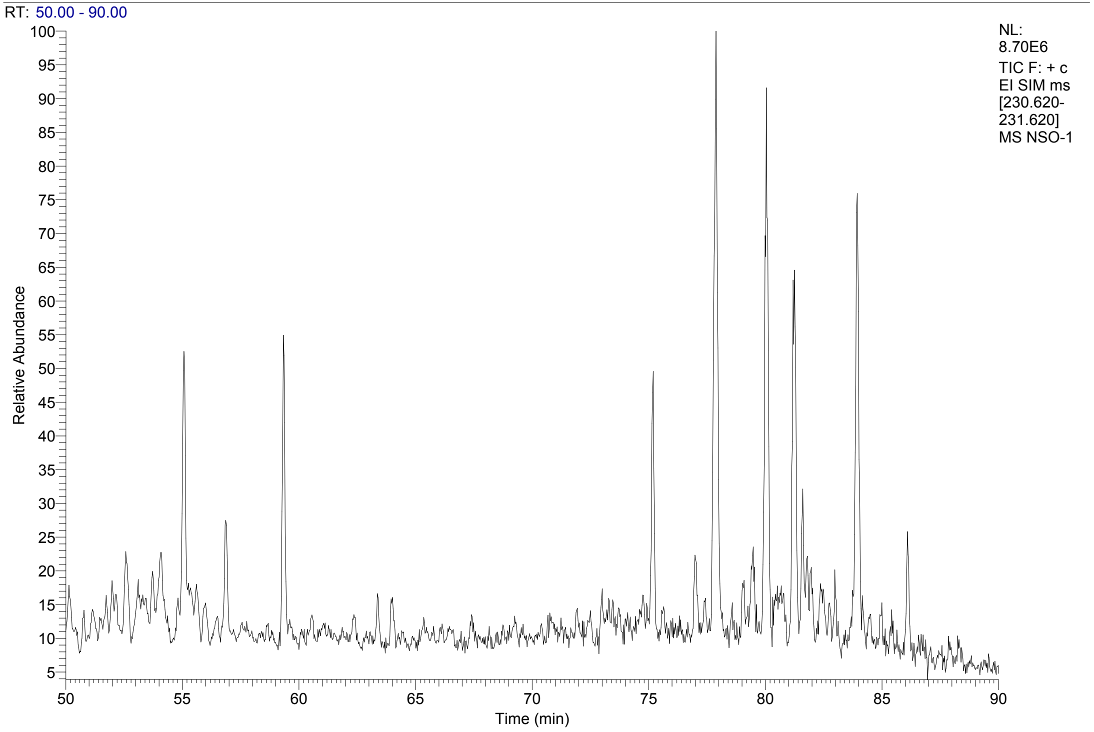
RT: 50.00 - 90.00
NL:
8.70E6
TIC F: + c
EI SIM ms
[230.620-
231.620]
MS NSO-1
Relative Abundance
100
95
90
85
80
75
70
65
60
55
50
45
40
35
30
25
20
15
10
5
50
55
60
65
70
75
80
85
90
Time (min)

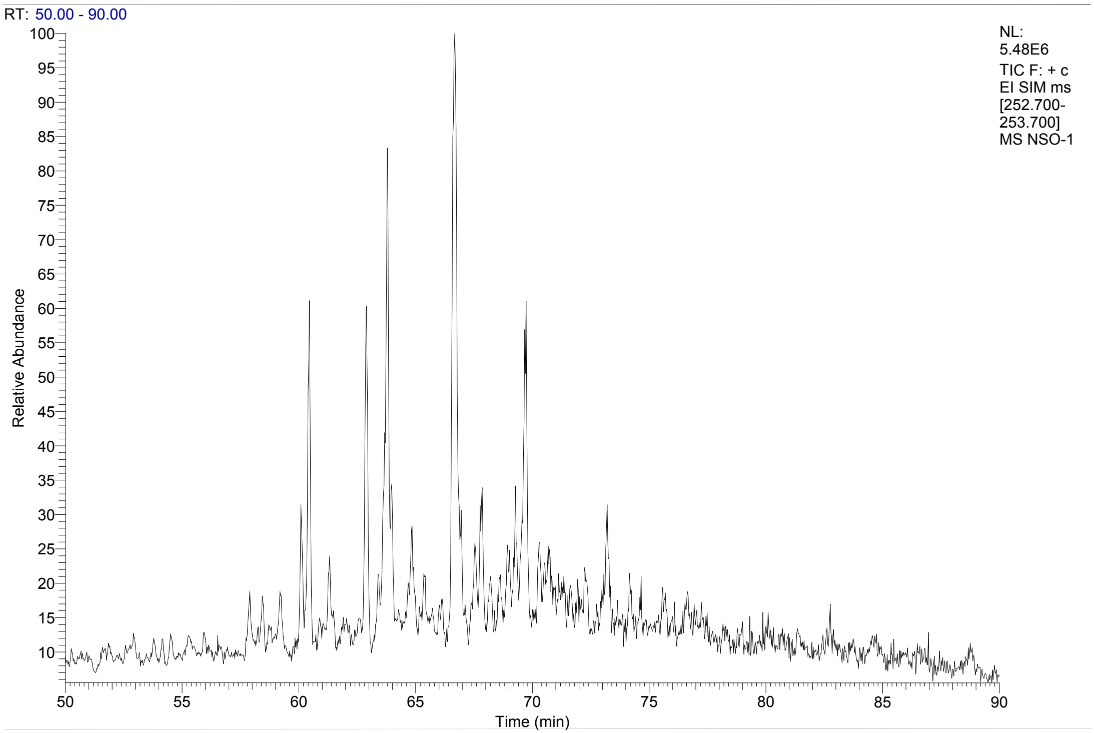
RT: 50.00 - 90.00
Relative Abundance
100
95
90
85
80
75
70
65
60
55
50
45
40
35
30
25
20
15
10
50
55
60
65
70
75
80
85
90
Time (min)
NL:
5.48E6
TIC F: + c
EI SIM ms
[252.700-
253.700]
MS NSO-1

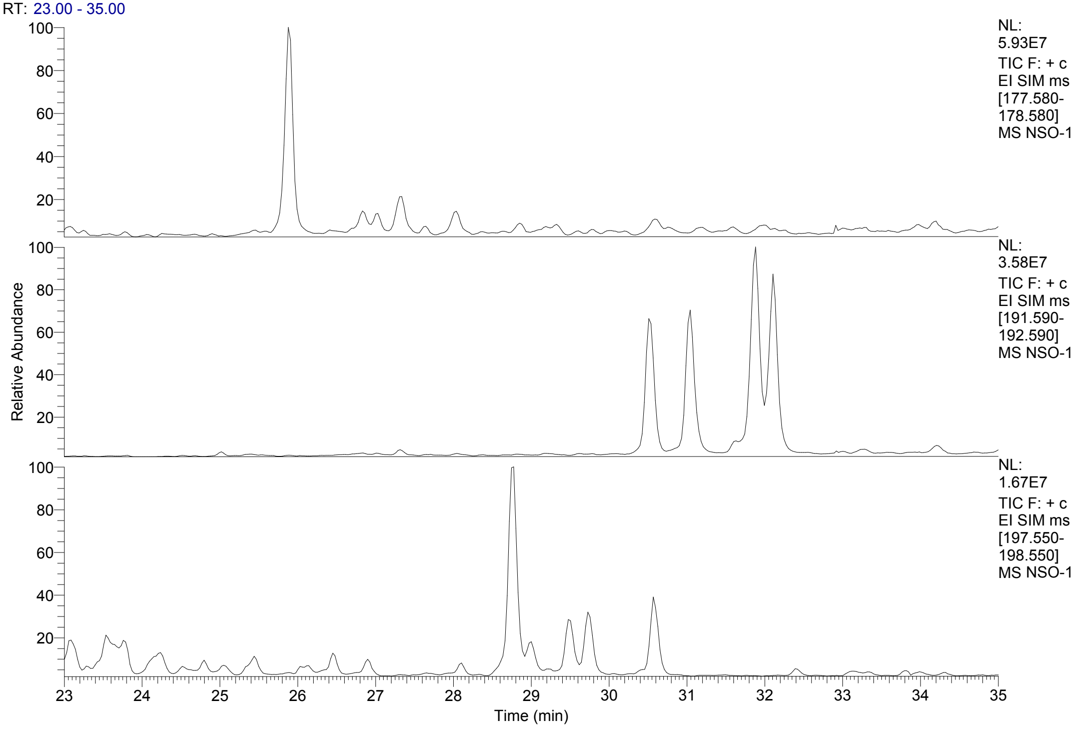
RT: 23.00 - 35.00
Relative Abundance
100
80
60
40
20
NL:
5.93E7
TIC F: + c
EI SIM ms
[177.580-
178.580]
MS NSO-1
NL:
3.58E7
TIC F: + c
EI SIM ms
[191.590-
192.590]
MS NSO-1
NL:
1.67E7
TIC F: + c
EI SIM ms
[197.550-
198.550]
MS NSO-1
23
24
25
26
27
28
29
30
31
32
33
34
35
Time (min)

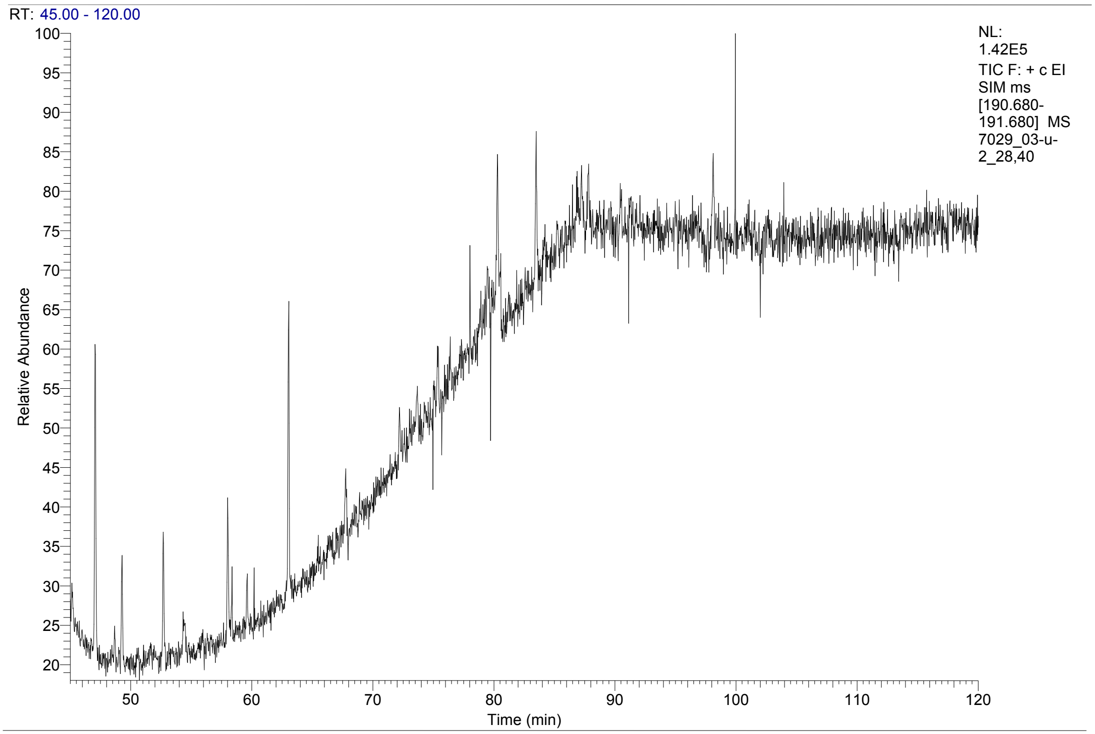
RT: 45.00 - 120.00
NL:
1.42E5
TIC F: + c EI
SIM ms
[190.680-
191.680] MS
7029_03-u-
2_28,40
Relative Abundance
100
95
90
85
80
75
70
65
60
55
50
45
40
35
30
25
20
50
60
70
80
90
100
110
120
Time (min)

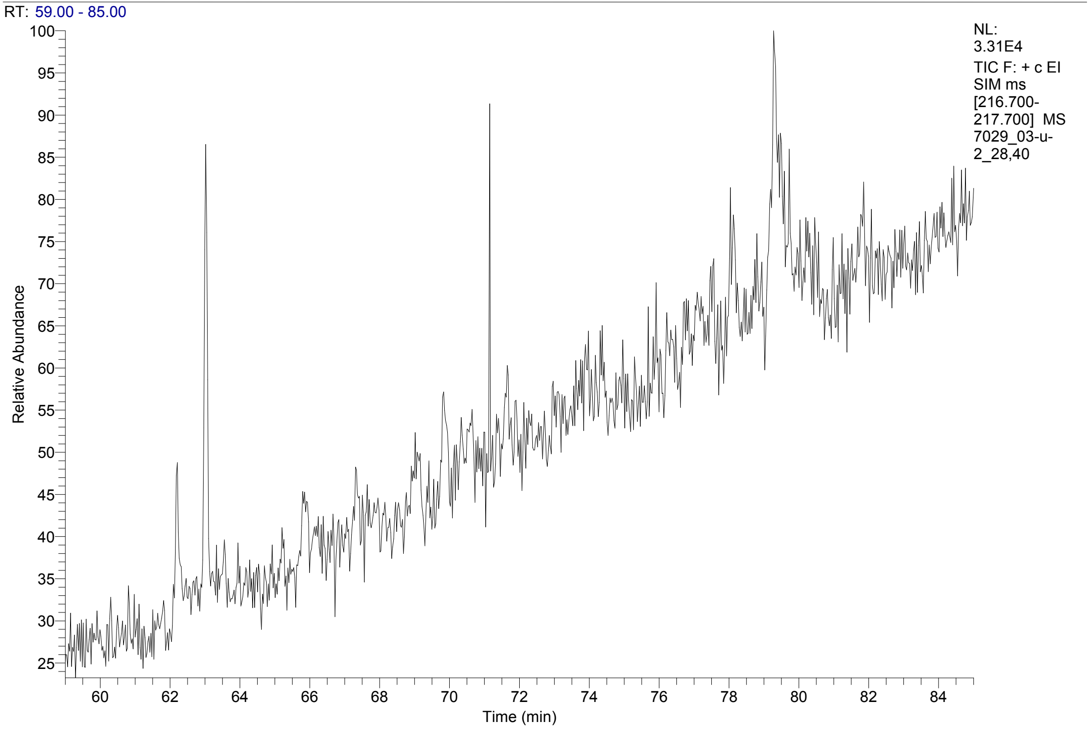
RT: 59.00 - 85.00
NL:
3.31E4
TIC F: + c EI
SIM ms
[216.700-
217.700] MS
7029_03-u-
2_28,40
Relative Abundance
100
95
90
85
80
75
70
65
60
55
50
45
40
35
30
25
60
62
64
66
68
70
72
74
76
78
80
82
84
Time (min)

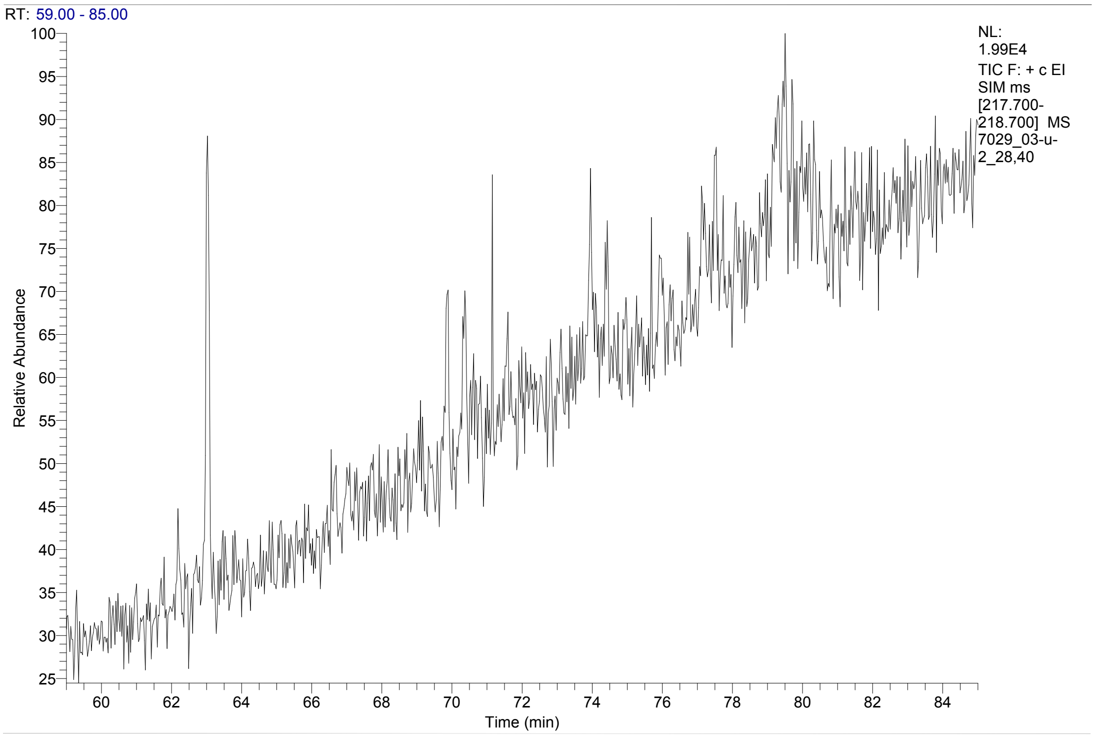
RT: 59.00 - 85.00
NL:
1.99E4
TIC F: + c EI
SIM ms
[217.700-
218.700] MS
7029_03-u-
2_28,40
Relative Abundance
100
95
90
85
80
75
70
65
60
55
50
45
40
35
30
25
60
62
64
66
68
70
72
74
76
78
80
82
84
Time (min)

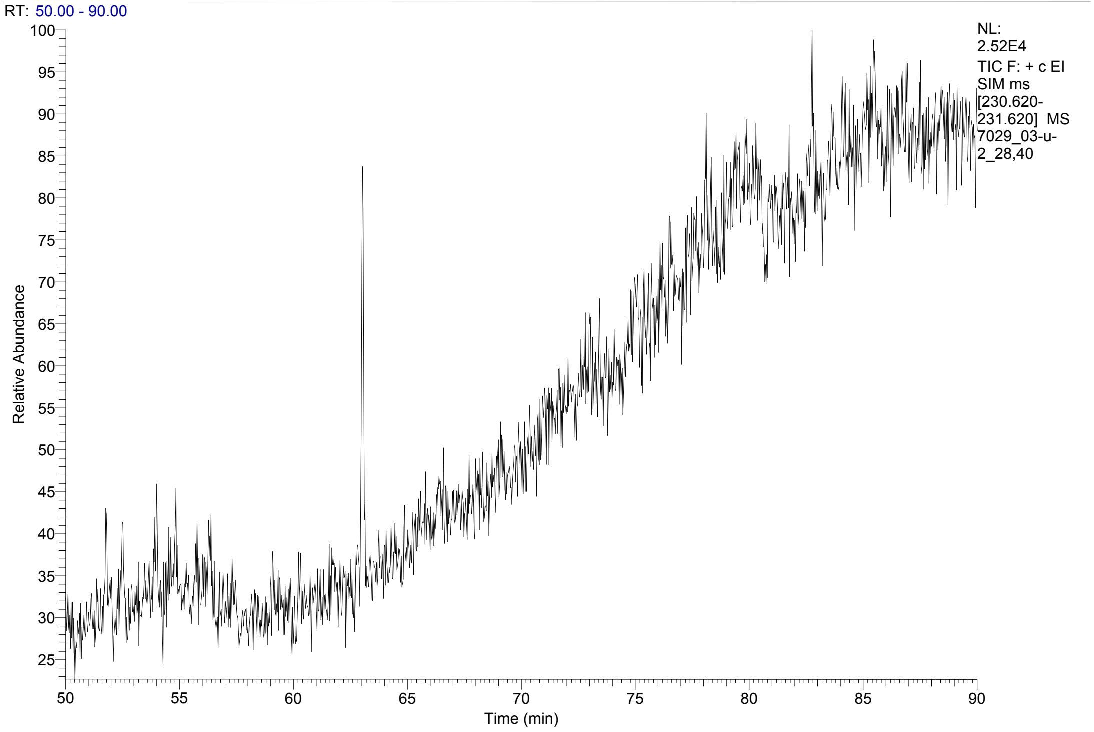
RT: 50.00 - 90.00
NL:
2.52E4
TIC F: + c EI
SIM ms
[230.620-
231.620] MS
7029_03-u-
2_28,40
Relative Abundance
100
95
90
85
80
75
70
65
60
55
50
45
40
35
30
25
50
55
60
65
70
75
80
85
90
Time (min)

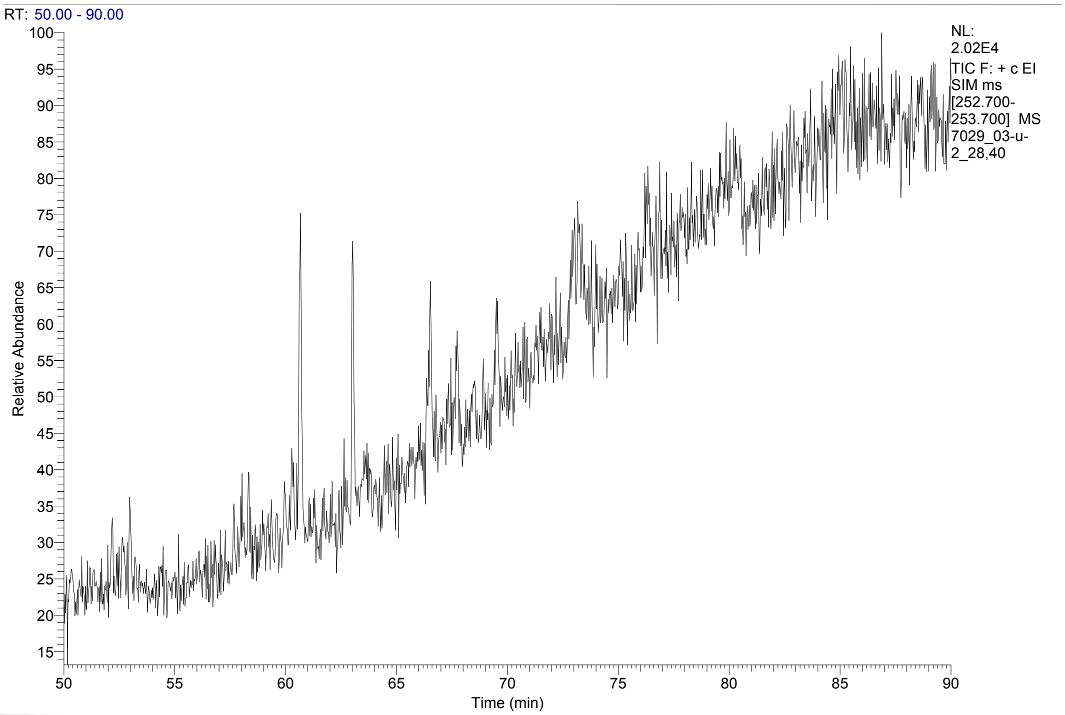
RT: 50.00 - 90.00
NL:
2.02E4
TIC F: + c EI
SIM ms
[252.700-
253.700] MS
7029_03-u-
2_28,40
Relative Abundance
100
95
90
85
80
75
70
65
60
55
50
45
40
35
30
25
20
15
50
55
60
65
70
75
80
85
90
Time (min)

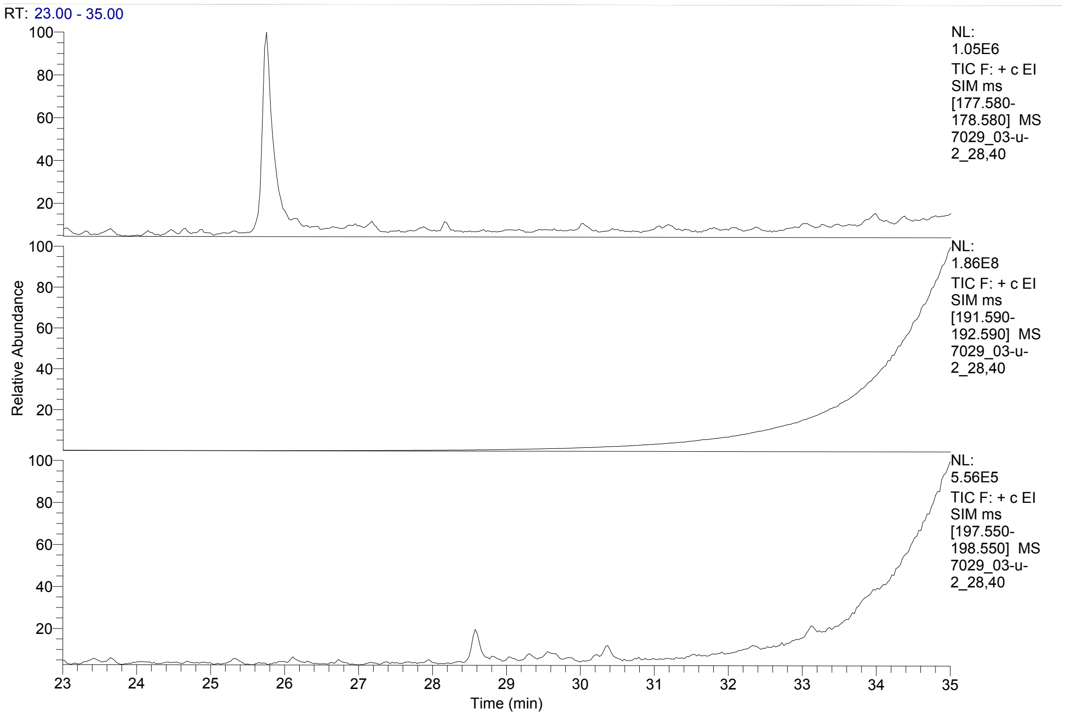
RT: 23.00 - 35.00
NL:
1.05E6
TIC F: + c EI
SIM ms
[177.580-
178.580] MS
7029_03-u-
2_28,40
NL:
1.86E8
TIC F: + c EI
SIM ms
[191.590-
192.590] MS
7029_03-u-
2_28,40
NL:
5.56E5
TIC F: + c EI
SIM ms
[197.550-
198.550] MS
7029_03-u-
2_28,40
Relative Abundance
100
80
60
40
20
23
24
25
26
27
28
29
30
31
32
33
34
35
Time (min)

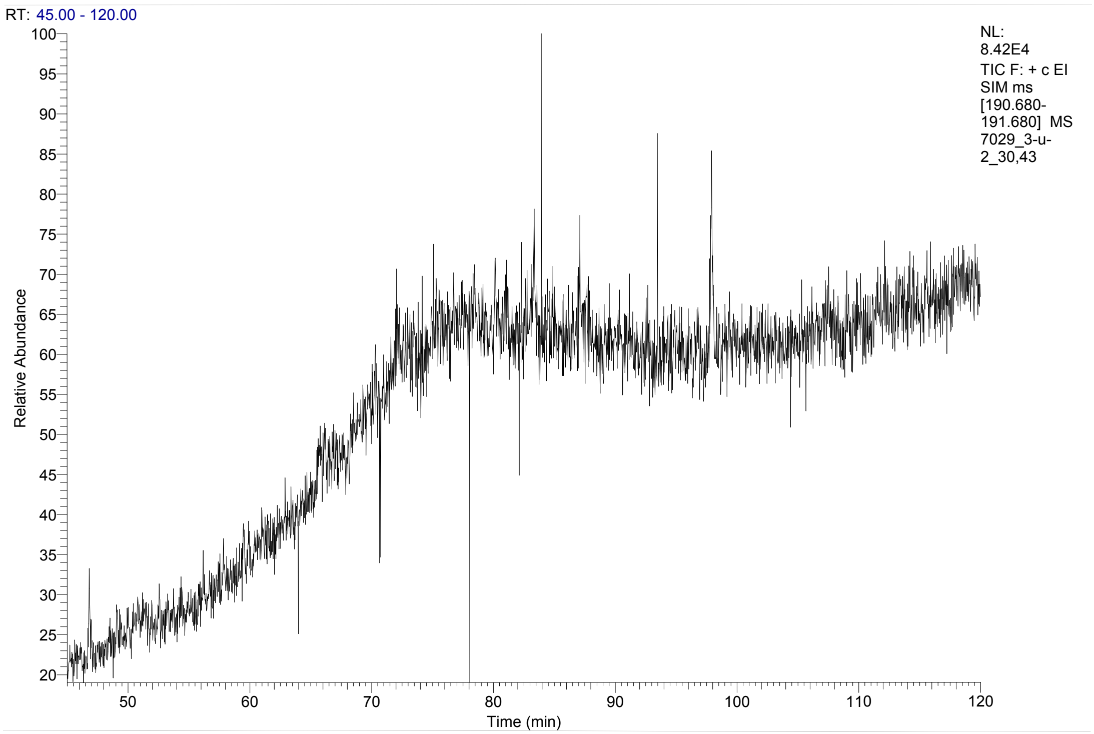
RT: 45.00 - 120.00
NL:
8.42E4
TIC F: + c EI
SIM ms
[190.680-
191.680] MS
7029_3-u-
2_30,43
Relative Abundance
100
95
90
85
80
75
70
65
60
55
50
45
40
35
30
25
20
50
60
70
80
90
100
110
120
Time (min)

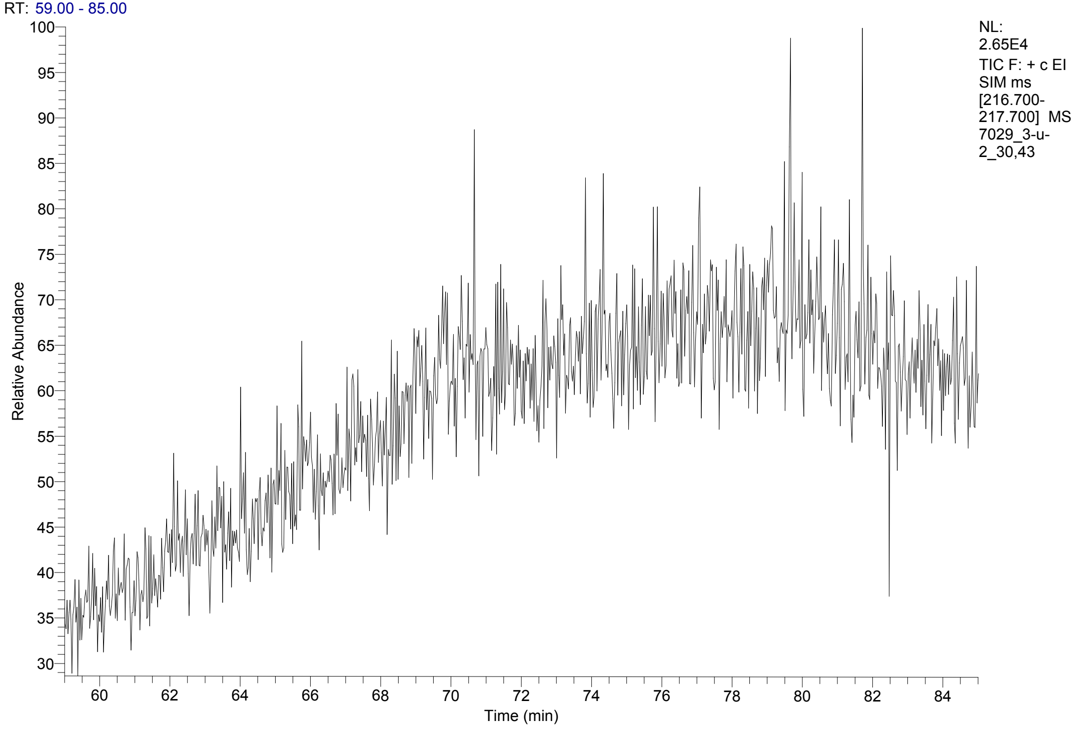
RT: 59.00 - 85.00
NL:
2.65E4
TIC F: + c EI
SIM ms
[216.700-
217.700] MS
7029_3-u-
2_30,43
Relative Abundance
100
95
90
85
80
75
70
65
60
55
50
45
40
35
30
60
62
64
66
68
70
72
74
76
78
80
82
84
Time (min)

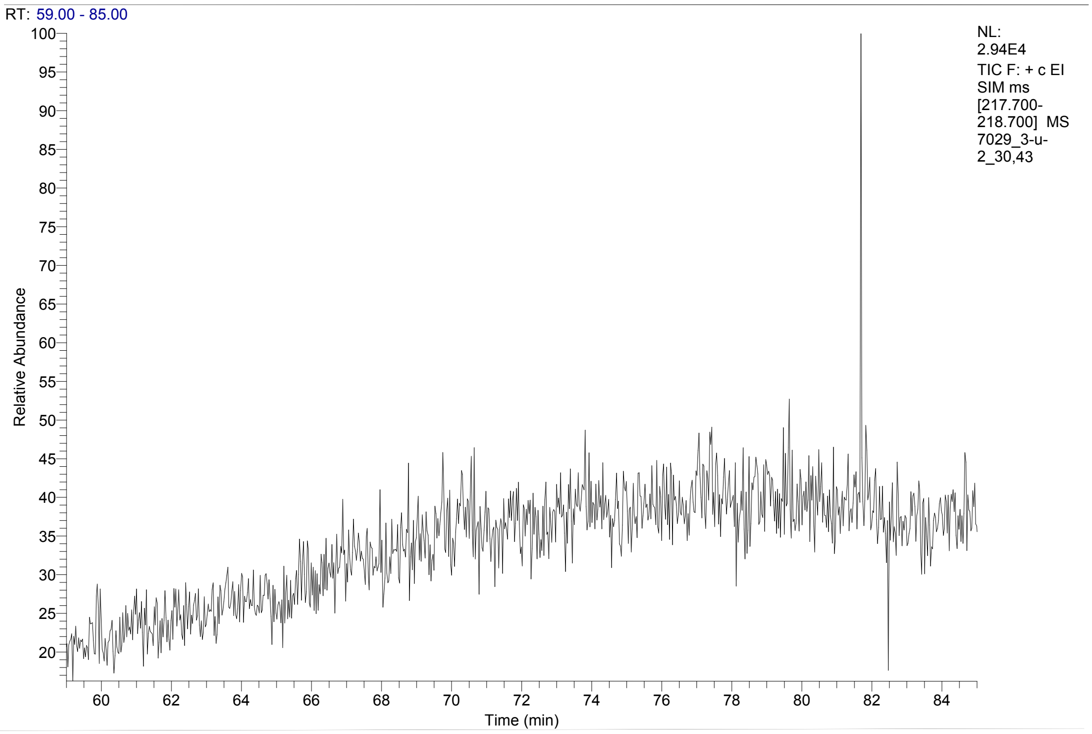
RT: 59.00 - 85.00
Relative Abundance
100
95
90
85
80
75
70
65
60
55
50
45
40
35
30
25
20
60
62
64
66
68
70
72
74
76
78
80
82
84
Time (min)
NL:
2.94E4
TIC F: + c EI
SIM ms
[217.700-
218.700] MS
7029_3-u-
2_30,43

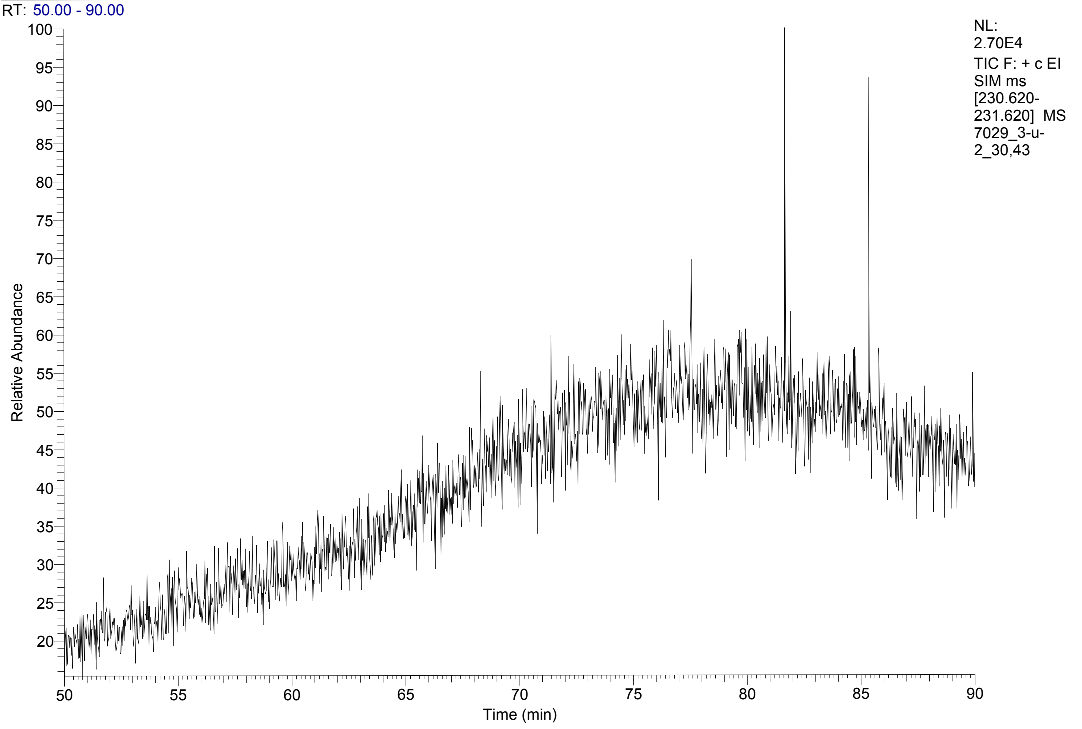
RT: 50.00 - 90.00
Relative Abundance
100
95
90
85
80
75
70
65
60
55
50
45
40
35
30
25
20
50
55
60
65
70
75
80
85
90
Time (min)
NL:
2.70E4
TIC F: + c EI
SIM ms
[230.620-
231.620] MS
7029_3-u-
2_30,43

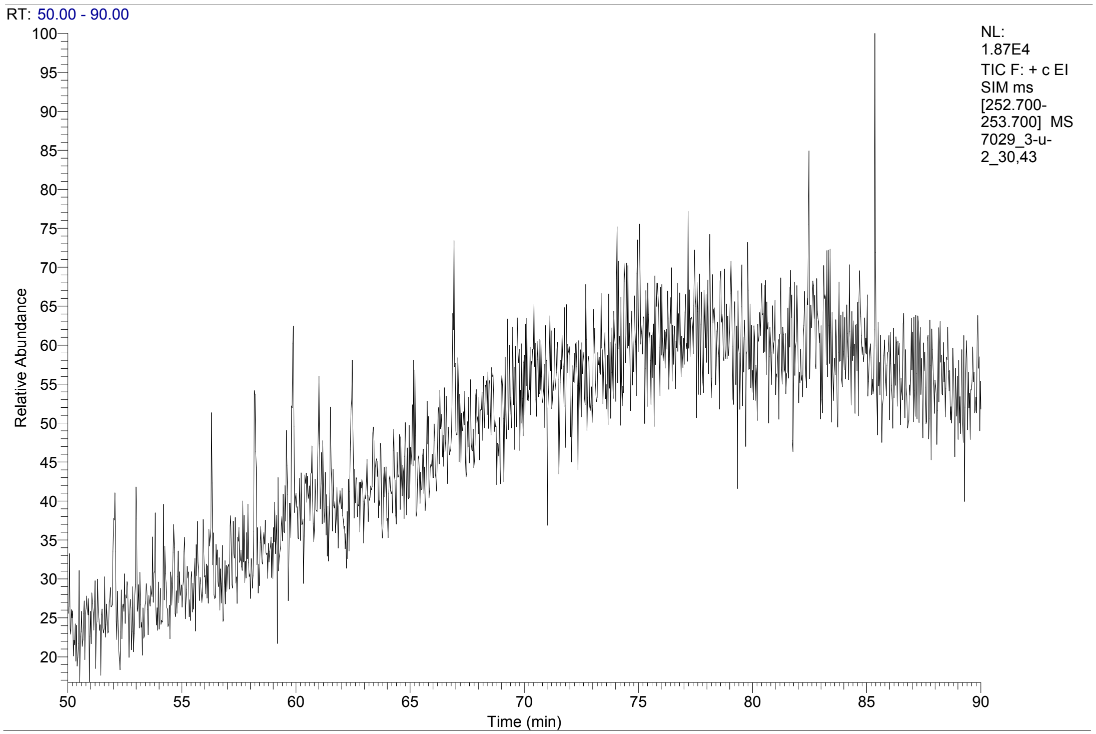
RT: 50.00 - 90.00
NL:
1.87E4
TIC F: + c EI
SIM ms
[252.700-
253.700] MS
7029_3-u-
2_30,43
Relative Abundance
100
95
90
85
80
75
70
65
60
55
50
45
40
35
30
25
20
50
55
60
65
70
75
80
85
90
Time (min)

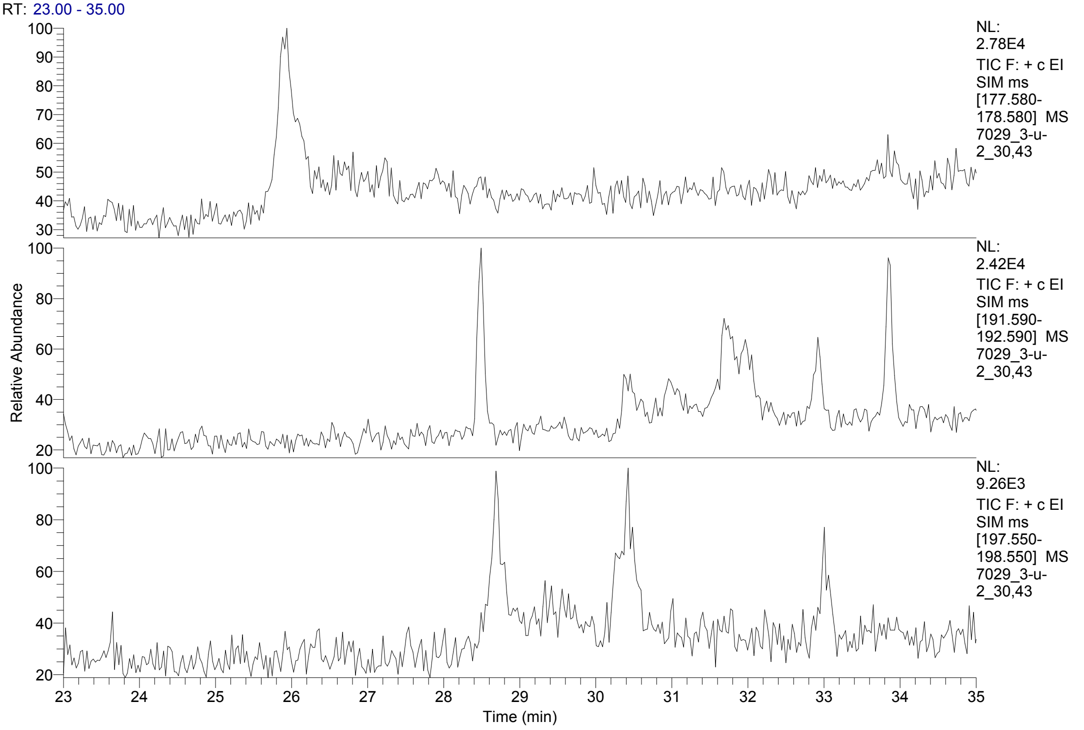
RT: 23.00 - 35.00
NL:
2.78E4
TIC F: + c EI
SIM ms
[177.580-
178.580] MS
7029_3-u-
2_30,43
NL:
2.42E4
TIC F: + c EI
SIM ms
[191.590-
192.590] MS
7029_3-u-
2_30,43
NL:
9.26E3
TIC F: + c EI
SIM ms
[197.550-
198.550] MS
7029_3-u-
2_30,43
Relative Abundance
100
90
80
70
60
50
40
30
100
80
60
40
20
100
80
60
40
20
23
24
25
26
27
28
29
30
31
32
33
34
35
Time (min)

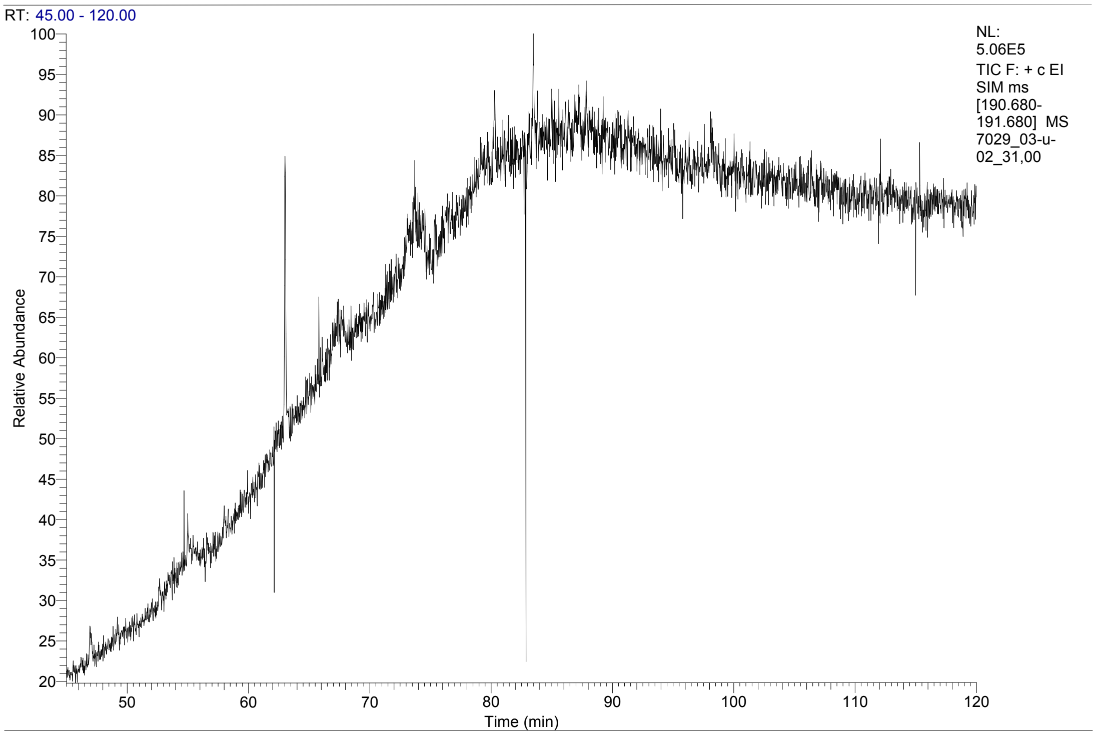
RT: 45.00 - 120.00
NL:
5.06E5
TIC F: + c EI
SIM ms
[190.680-
191.680] MS
7029_03-u-
02_31,00
Relative Abundance
100
95
90
85
80
75
70
65
60
55
50
45
40
35
30
25
20
50
60
70
80
90
100
110
120
Time (min)

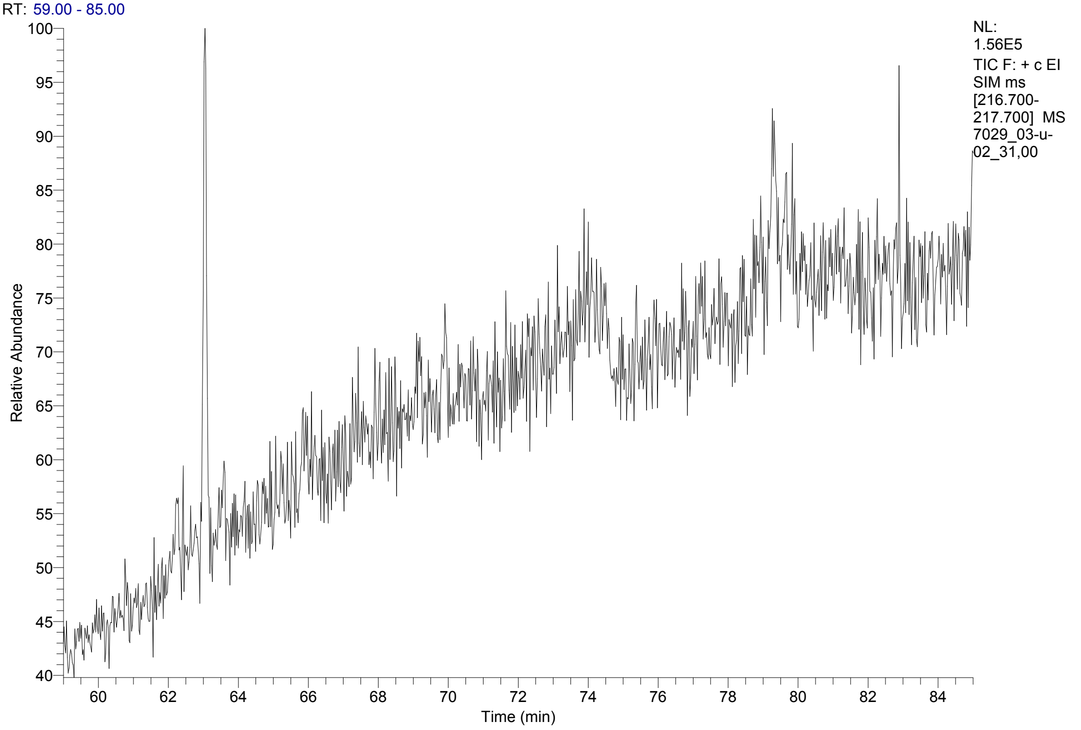
RT: 59.00 - 85.00
NL:
1.56E5
TIC F: + c EI
SIM ms
[216.700-
217.700] MS
7029_03-u-
02_31,00
Relative Abundance
100
95
90
85
80
75
70
65
60
55
50
45
40
60
62
64
66
68
70
72
74
76
78
80
82
84
Time (min)

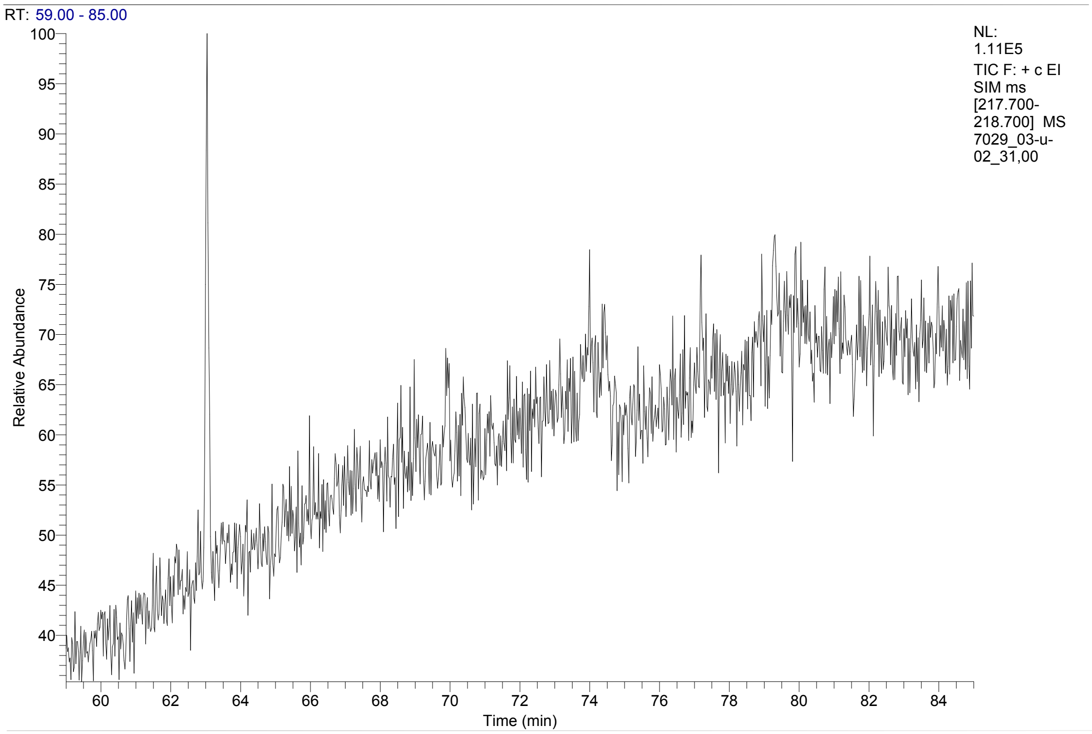
RT: 59.00 - 85.00
NL:
1.11E5
TIC F: + c EI
SIM ms
[217.700-
218.700] MS
7029_03-u-
02_31,00
Relative Abundance
100
95
90
85
80
75
70
65
60
55
50
45
40
60
62
64
66
68
70
72
74
76
78
80
82
84
Time (min)

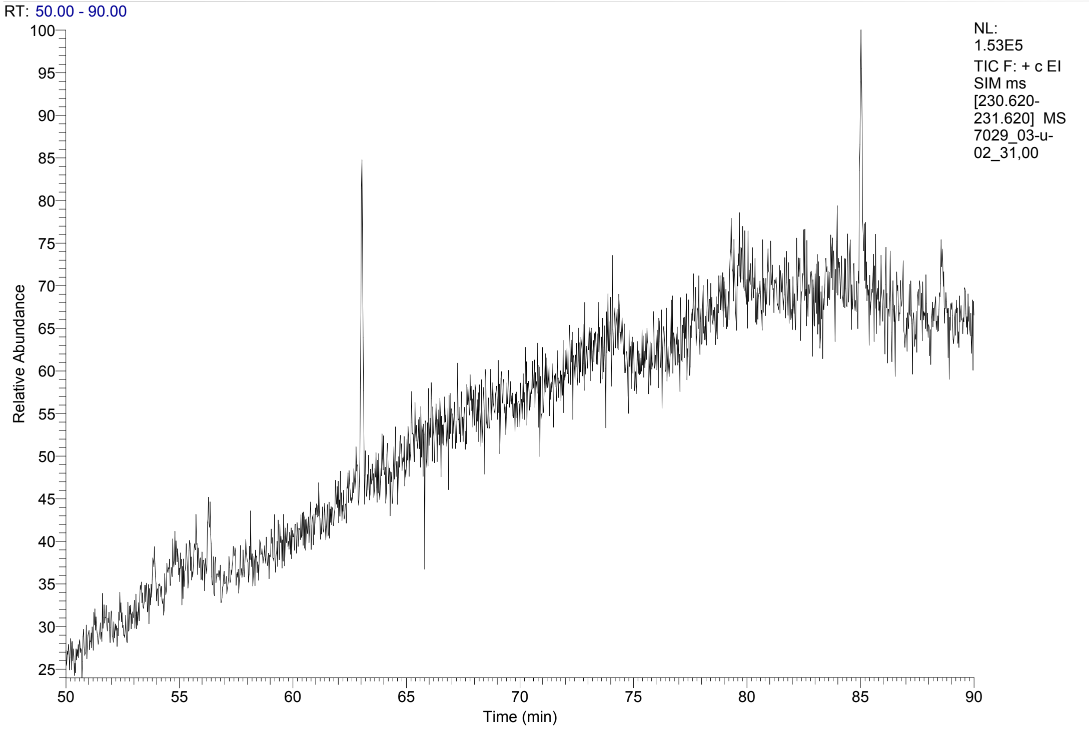
RT: 50.00 - 90.00
NL:
1.53E5
TIC F: + c EI
SIM ms
[230.620-
231.620] MS
7029_03-u-
02_31,00
Relative Abundance
100
95
90
85
80
75
70
65
60
55
50
45
40
35
30
25
50
55
60
65
70
75
80
85
90
Time (min)

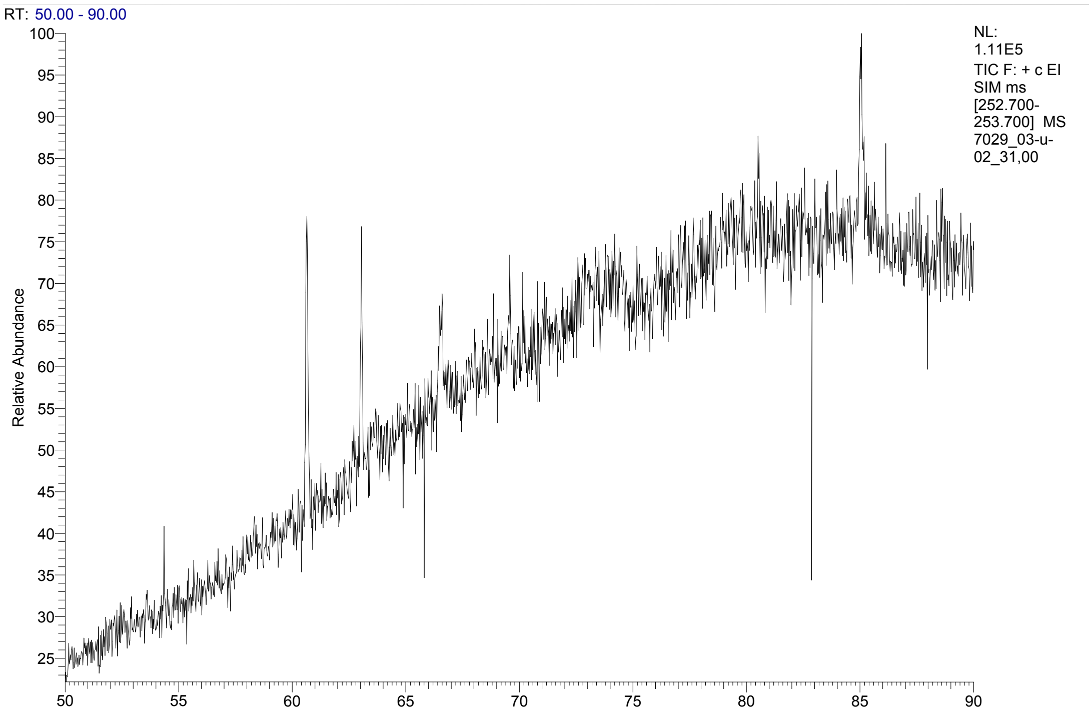
RT: 50.00 - 90.00
Relative Abundance
Time (min)
100
95
90
85
80
75
70
65
60
55
50
45
40
35
30
25
50
55
60
65
70
75
80
85
90
NL:
1.11E5
TIC F: + c EI SIM ms [252.700-253.700] MS 7029_03-u-02_31,00

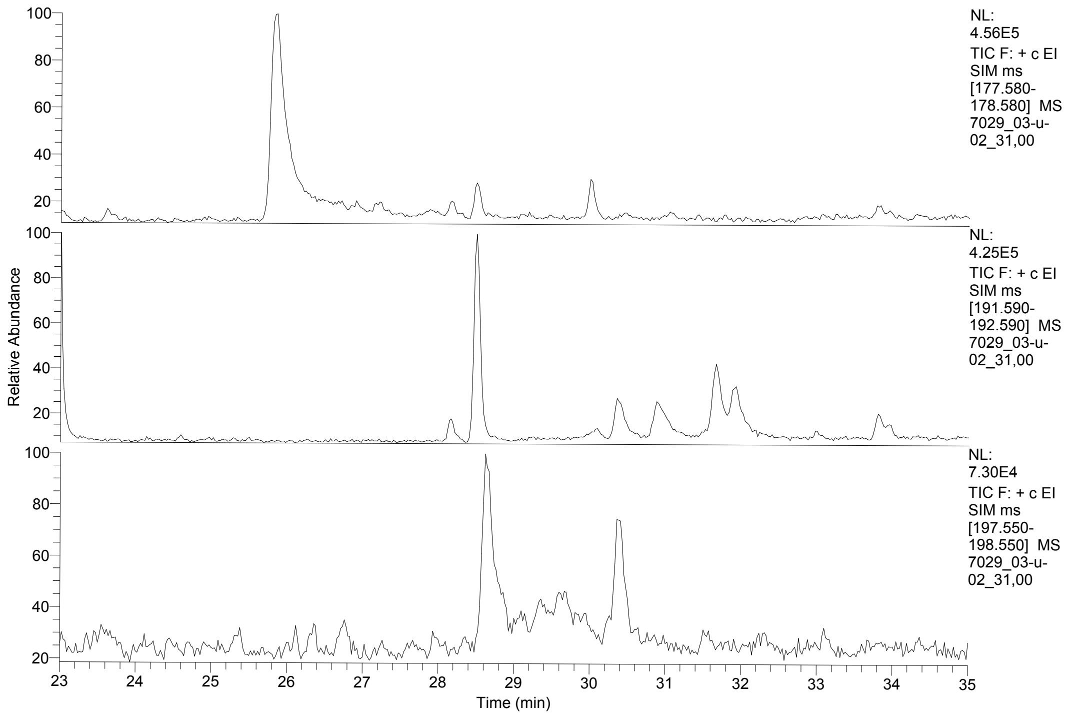
RT: 23.00 - 35.00
Relative Abundance
Time (min)
100
80
60
40
20
23
24
25
26
27
28
29
30
31
32
33
34
35
NL:
4.56E5
TIC F: + c EI SIM ms [177.580-178.580] MS 7029_03-u-02_31,00
NL:
4.25E5
TIC F: + c EI SIM ms [191.590-192.590] MS 7029_03-u-02_31,00
NL:
7.30E4
TIC F: + c EI SIM ms [197.550-198.550] MS 7029_03-u-02_31,00

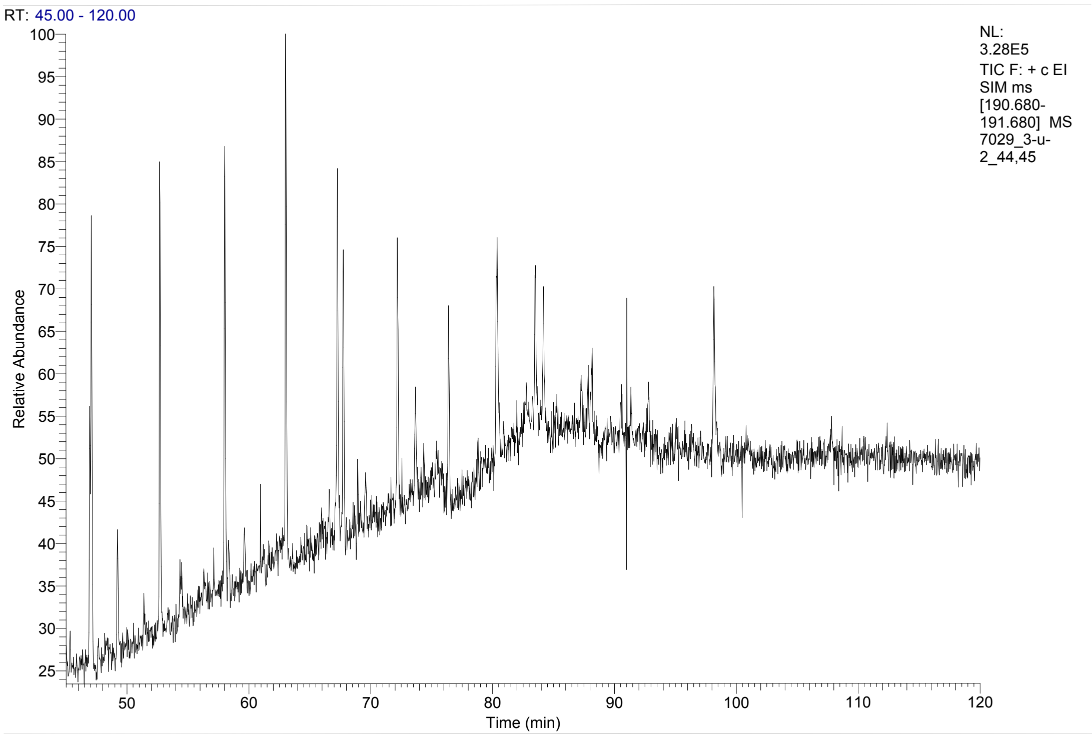
RT: 45.00 - 120.00
NL:
3.28E5
TIC F: + c EI
SIM ms
[190.680-
191.680] MS
7029_3-u-
2_44,45
Relative Abundance
100
95
90
85
80
75
70
65
60
55
50
45
40
35
30
25
50
60
70
80
90
100
110
120
Time (min)

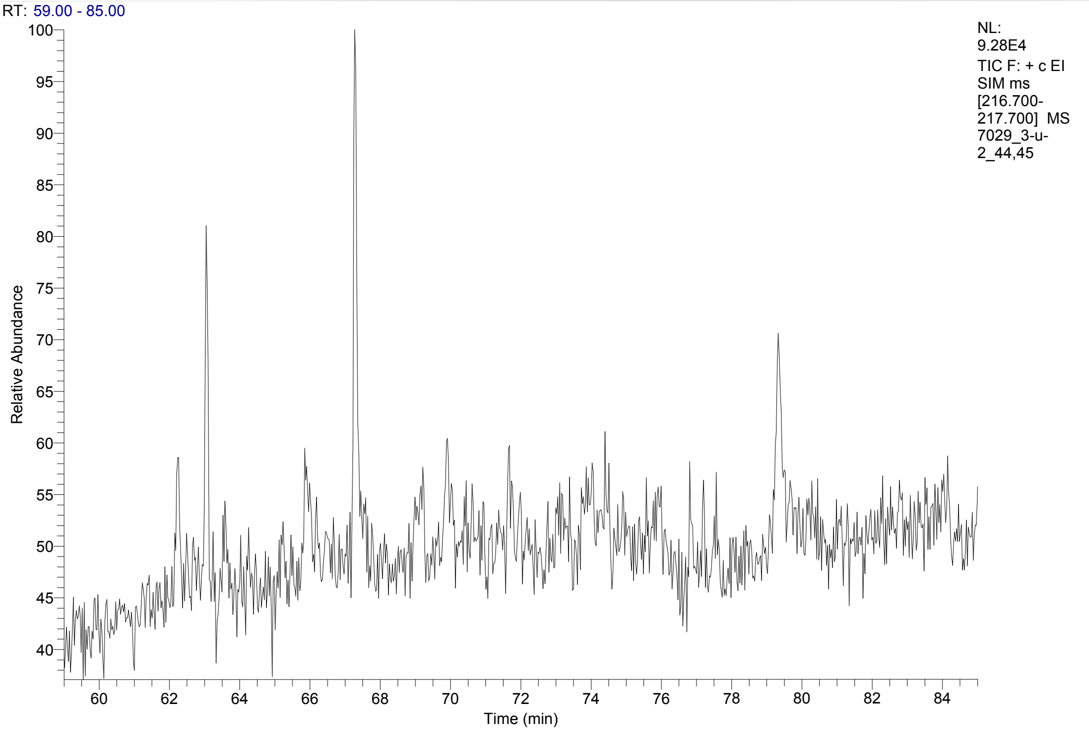
RT: 59.00 - 85.00
NL:
9.28E4
TIC F: + c EI
SIM ms
[216.700-
217.700] MS
7029_3-u-
2_44,45
Relative Abundance
100
95
90
85
80
75
70
65
60
55
50
45
40
60
62
64
66
68
70
72
74
76
78
80
82
84
Time (min)

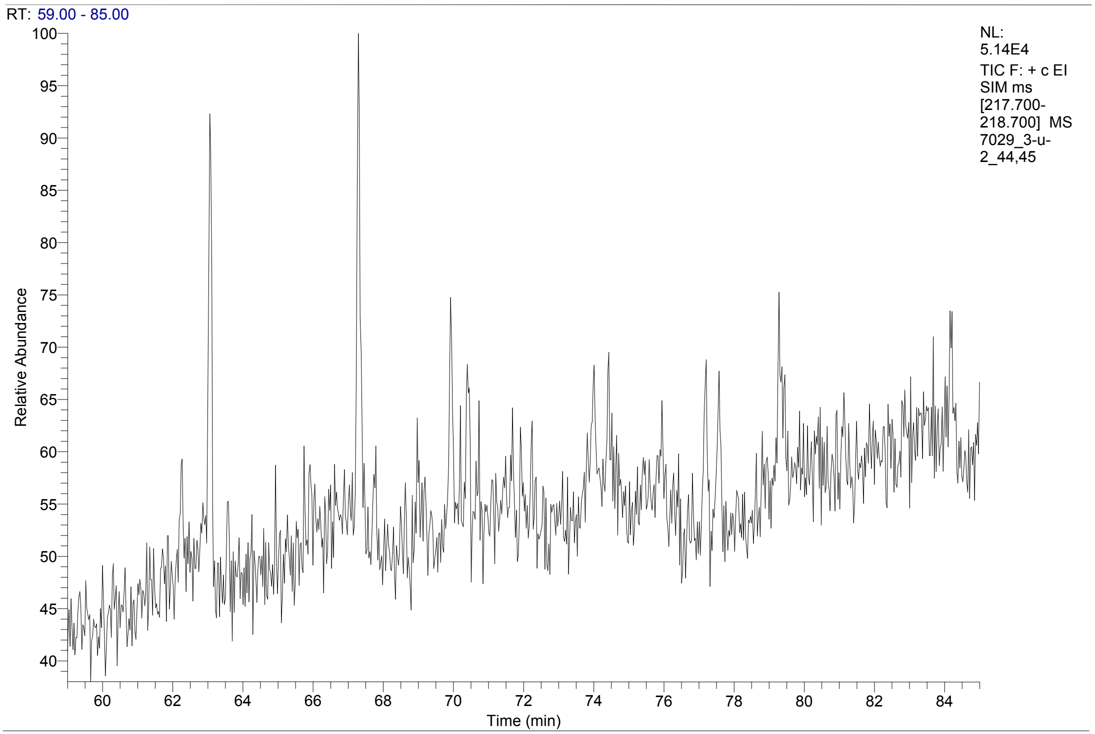
RT: 59.00 - 85.00
NL:
5.14E4
TIC F: + c EI
SIM ms
[217.700-
218.700] MS
7029_3-u-
2_44,45
Relative Abundance
100
95
90
85
80
75
70
65
60
55
50
45
40
60
62
64
66
68
70
72
74
76
78
80
82
84
Time (min)

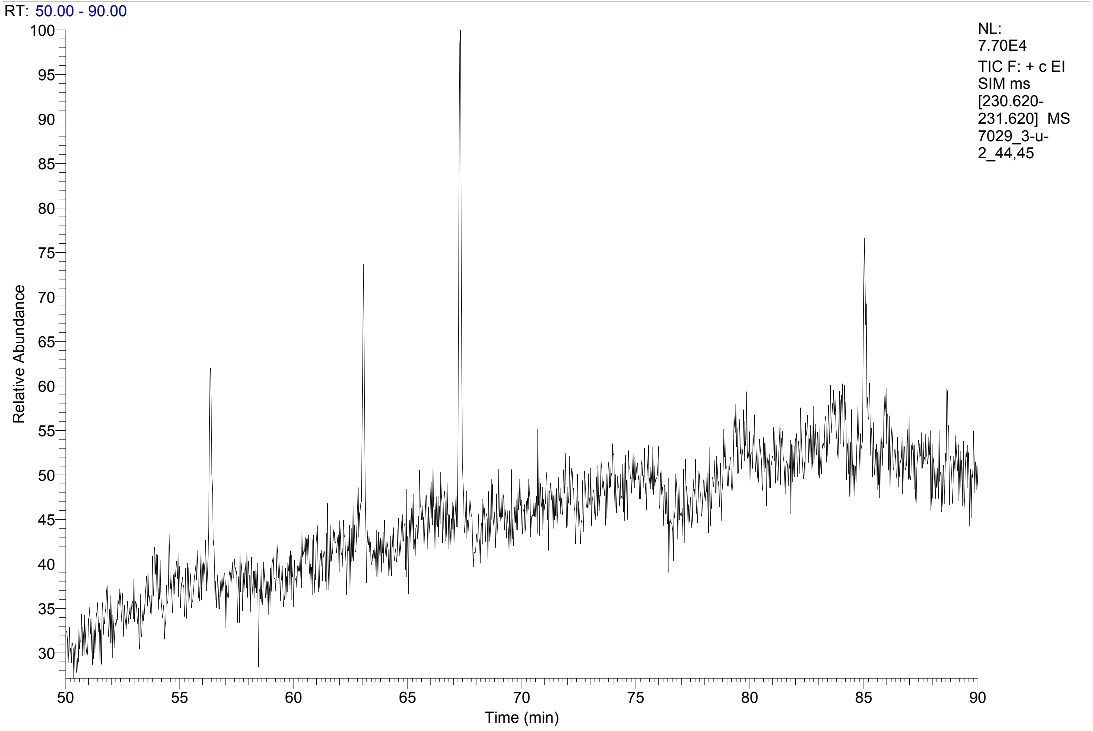
RT: 50.00 - 90.00
NL:
7.70E4
TIC F: + c EI
SIM ms
[230.620-
231.620] MS
7029_3-u-
2_44,45
Relative Abundance
100
95
90
85
80
75
70
65
60
55
50
45
40
35
30
50
55
60
65
70
75
80
85
90
Time (min)

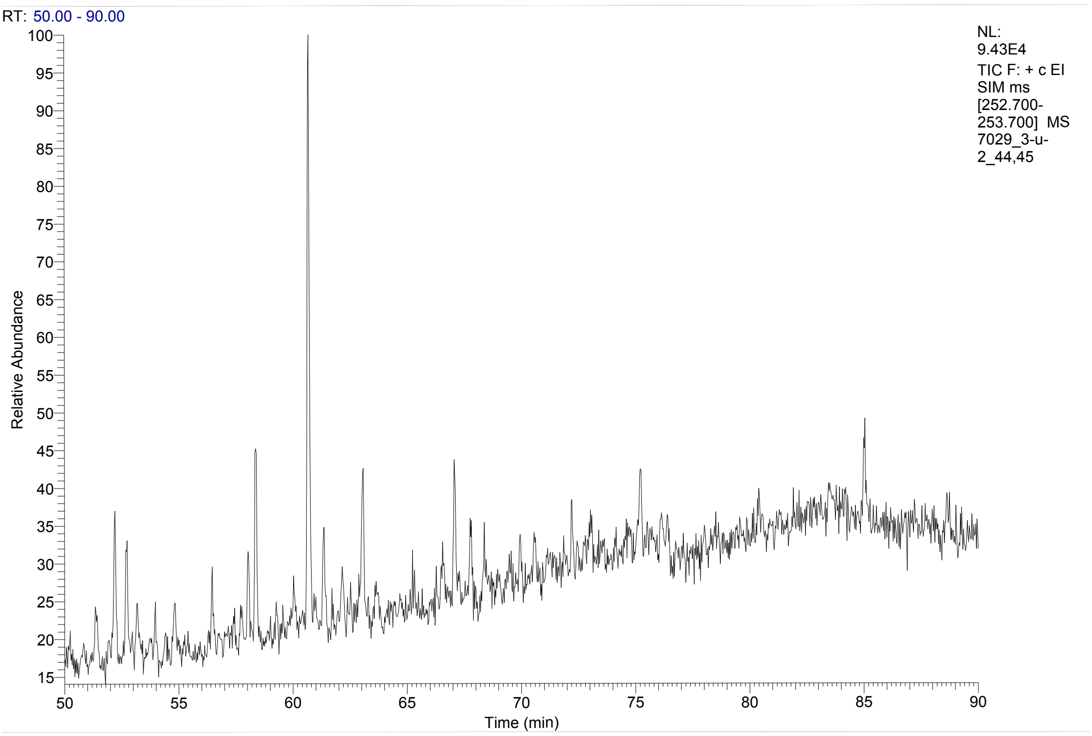
RT: 50.00 - 90.00
NL:
9.43E4
TIC F: + c EI
SIM ms
[252.700-
253.700] MS
7029_3-u-
2_44,45
Relative Abundance
100
95
90
85
80
75
70
65
60
55
50
45
40
35
30
25
20
15
50
55
60
65
70
75
80
85
90
Time (min)

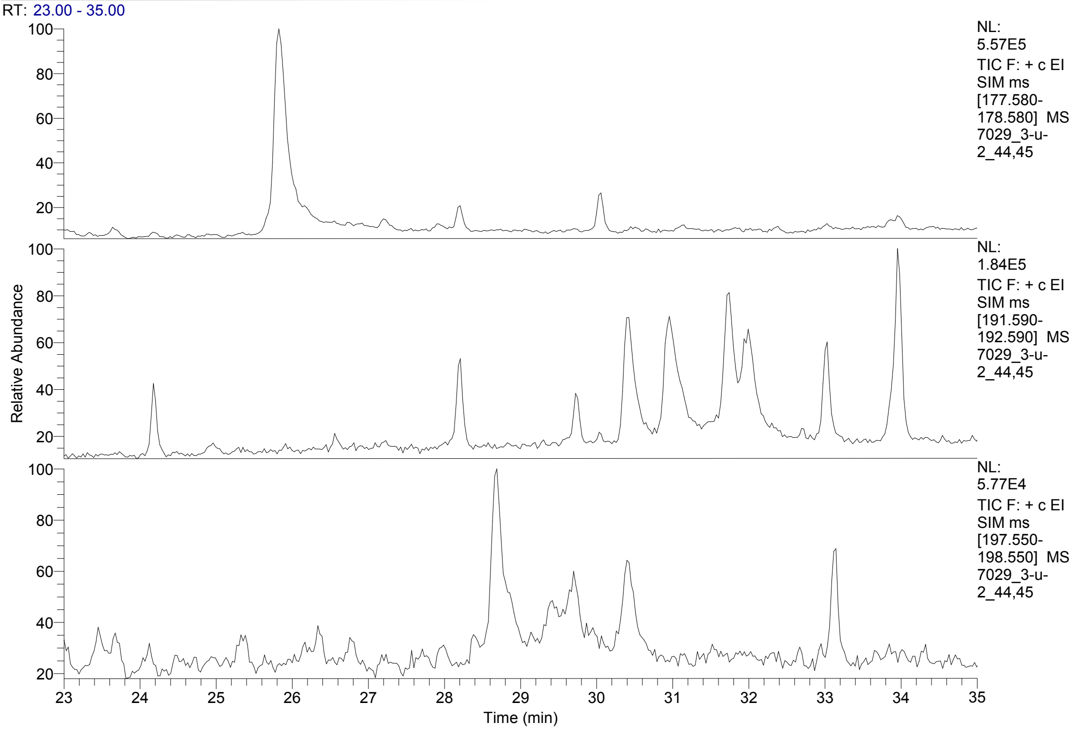
RT: 23.00 - 35.00
NL:
5.57E5
TIC F: + c EI
SIM ms
[177.580-
178.580] MS
7029_3-u-
2_44,45
NL:
1.84E5
TIC F: + c EI
SIM ms
[191.590-
192.590] MS
7029_3-u-
2_44,45
NL:
5.77E4
TIC F: + c EI
SIM ms
[197.550-
198.550] MS
7029_3-u-
2_44,45
Relative Abundance
100
80
60
40
20
23
24
25
26
27
28
29
30
31
32
33
34
35
Time (min)

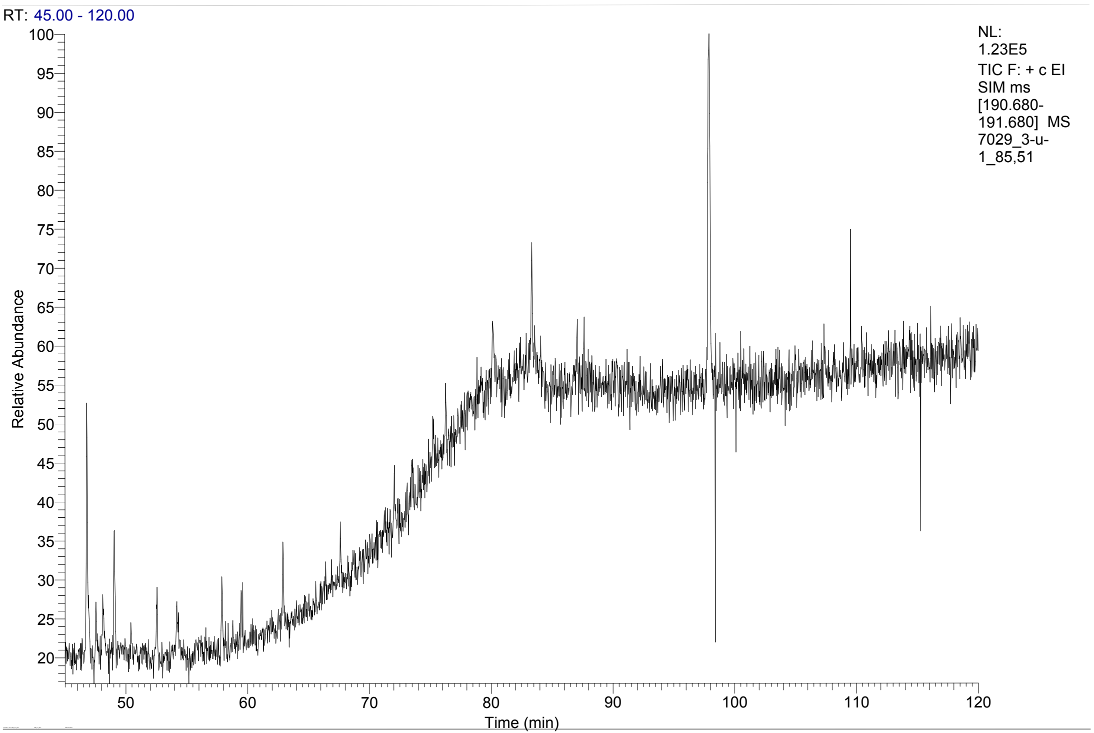
RT: 45.00 - 120.00
NL:
1.23E5
TIC F: + c EI
SIM ms
[190.680-
191.680] MS
7029_3-u-
1_85,51
Relative Abundance
100
95
90
85
80
75
70
65
60
55
50
45
40
35
30
25
20
50
60
70
80
90
100
110
120
Time (min)

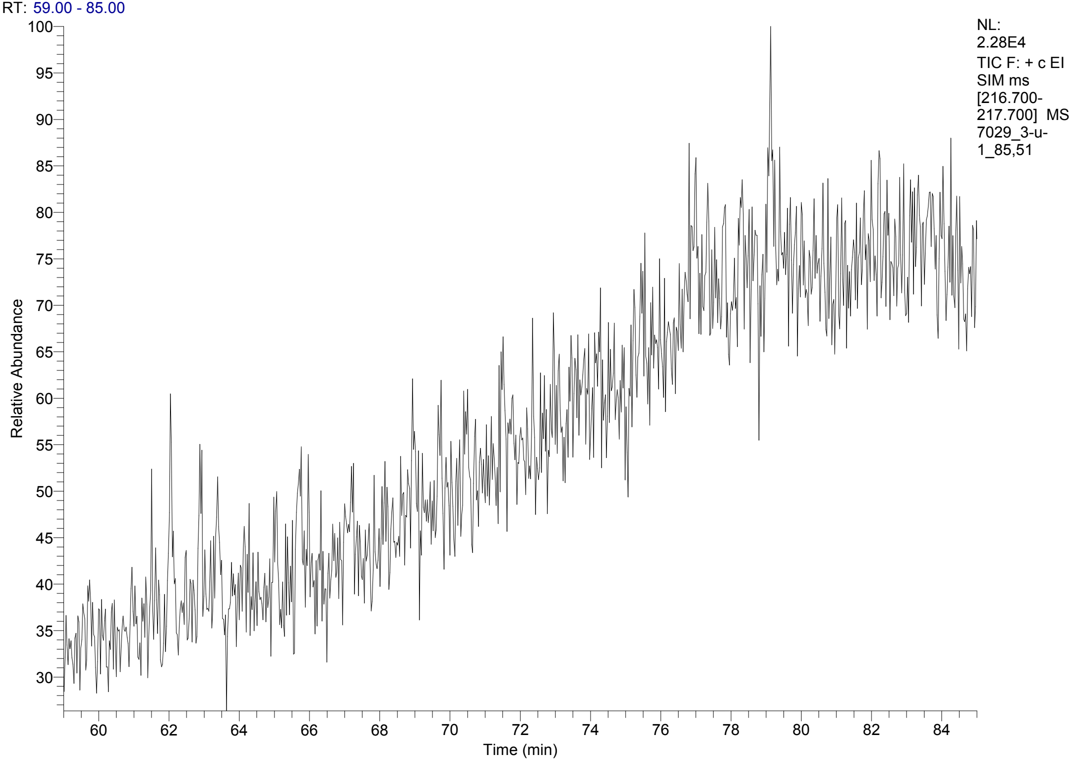
RT: 59.00 - 85.00
NL:
2.28E4
TIC F: + c EI
SIM ms
[216.700-
217.700] MS
7029_3-u-
1_85,51
Relative Abundance
100
95
90
85
80
75
70
65
60
55
50
45
40
35
30
60
62
64
66
68
70
72
74
76
78
80
82
84
Time (min)

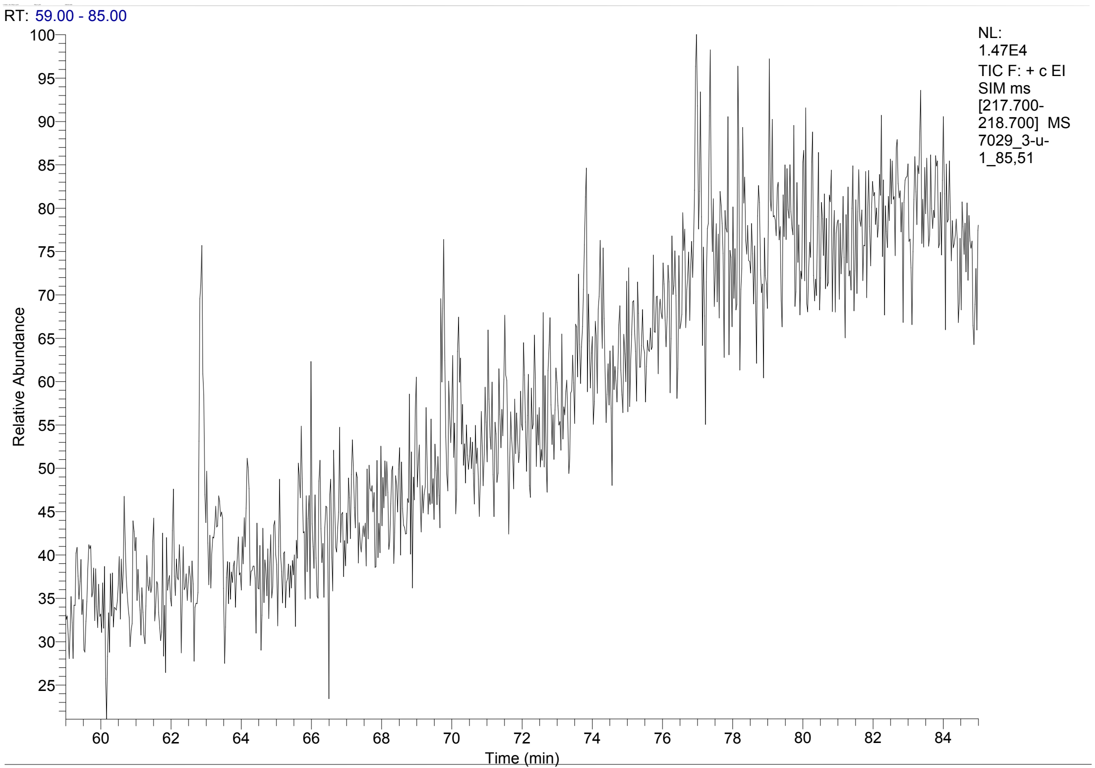
RT: 59.00 - 85.00
NL:
1.47E4
TIC F: + c EI
SIM ms
[217.700-
218.700] MS
7029_3-u-
1_85,51
Relative Abundance
Time (min)
100
95
90
85
80
75
70
65
60
55
50
45
40
35
30
25
60
62
64
66
68
70
72
74
76
78
80
82
84

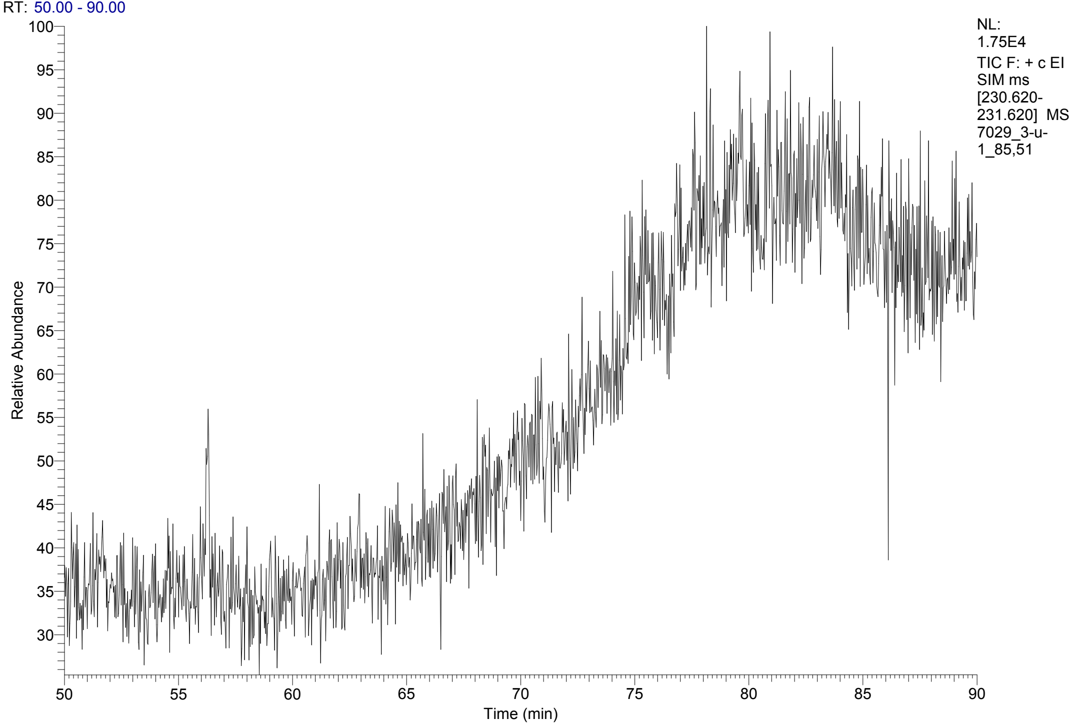
RT: 50.00 - 90.00
NL:
1.75E4
TIC F: + c EI
SIM ms
[230.620-
231.620] MS
7029_3-u-
1_85,51
Relative Abundance
Time (min)
100
95
90
85
80
75
70
65
60
55
50
45
40
35
30
50
55
60
65
70
75
80
85
90

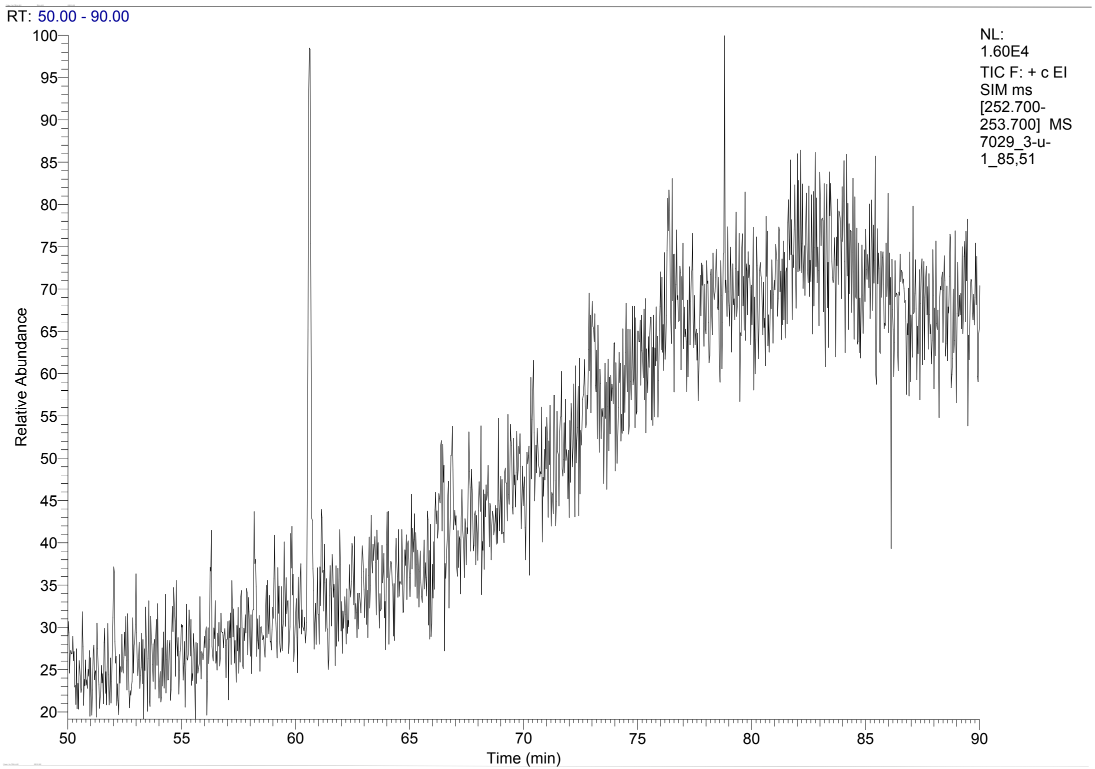
RT: 50.00 - 90.00
NL:
1.60E4
TIC F: + c EI
SIM ms
[252.700-
253.700] MS
7029_3-u-
1_85,51
Relative Abundance
100
95
90
85
80
75
70
65
60
55
50
45
40
35
30
25
20
50
55
60
65
70
75
80
85
90
Time (min)

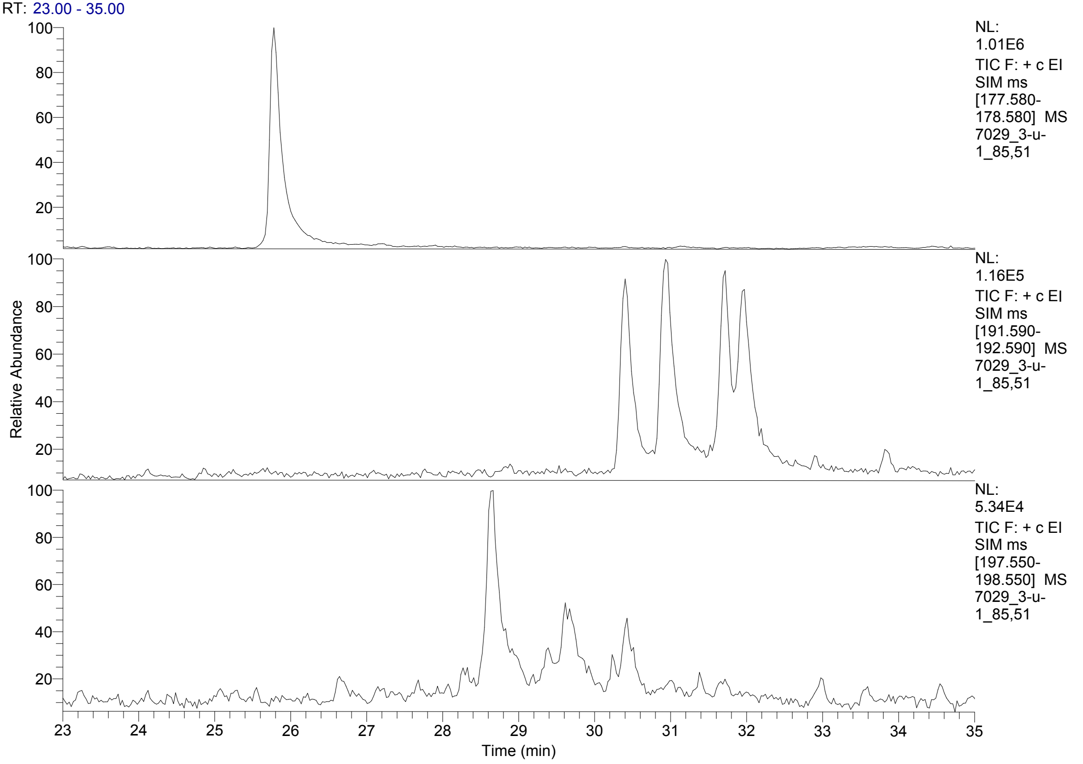
RT: 23.00 - 35.00
NL:
1.01E6
TIC F: + c EI
SIM ms
[177.580-
178.580] MS
7029_3-u-
1_85,51
NL:
1.16E5
TIC F: + c EI
SIM ms
[191.590-
192.590] MS
7029_3-u-
1_85,51
NL:
5.34E4
TIC F: + c EI
SIM ms
[197.550-
198.550] MS
7029_3-u-
1_85,51
Relative Abundance
100
80
60
40
20
23
24
25
26
27
28
29
30
31
32
33
34
35
Time (min)

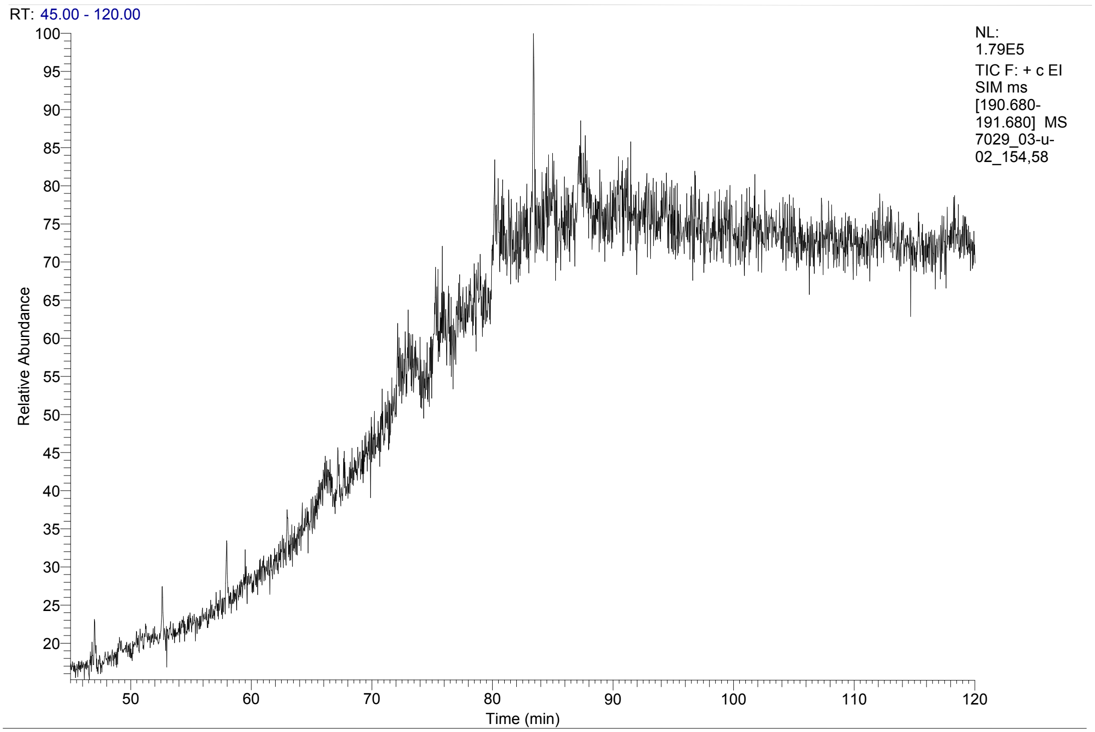
RT: 45.00 - 120.00
NL:
1.79E5
TIC F: + c EI
SIM ms
[190.680-
191.680] MS
7029_03-u-
02_154,58
Relative Abundance
100
95
90
85
80
75
70
65
60
55
50
45
40
35
30
25
20
50
60
70
80
90
100
110
120
Time (min)

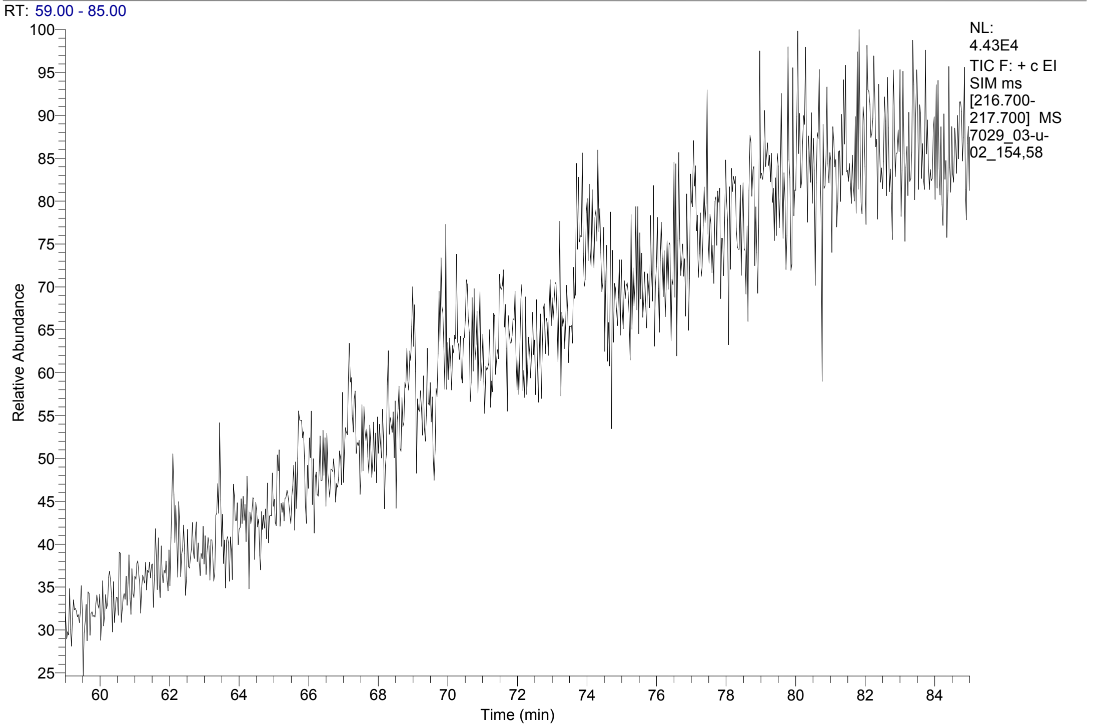
RT: 59.00 - 85.00
NL:
4.43E4
TIC F: + c EI
SIM ms
[216.700-
217.700] MS
7029_03-u-
02_154,58
Relative Abundance
100
95
90
85
80
75
70
65
60
55
50
45
40
35
30
25
60
62
64
66
68
70
72
74
76
78
80
82
84
Time (min)

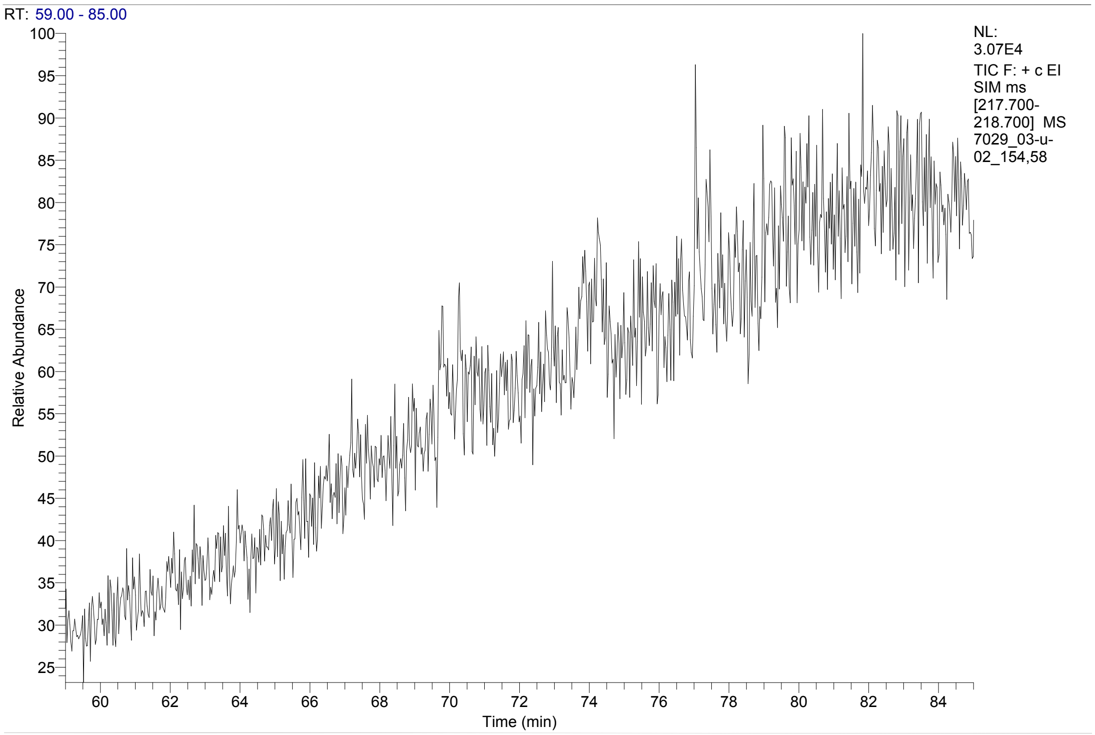
RT: 59.00 - 85.00
NL:
3.07E4
TIC F: + c EI
SIM ms
[217.700-
218.700] MS
7029_03-u-
02_154,58
Relative Abundance
100
95
90
85
80
75
70
65
60
55
50
45
40
35
30
25
60
62
64
66
68
70
72
74
76
78
80
82
84
Time (min)

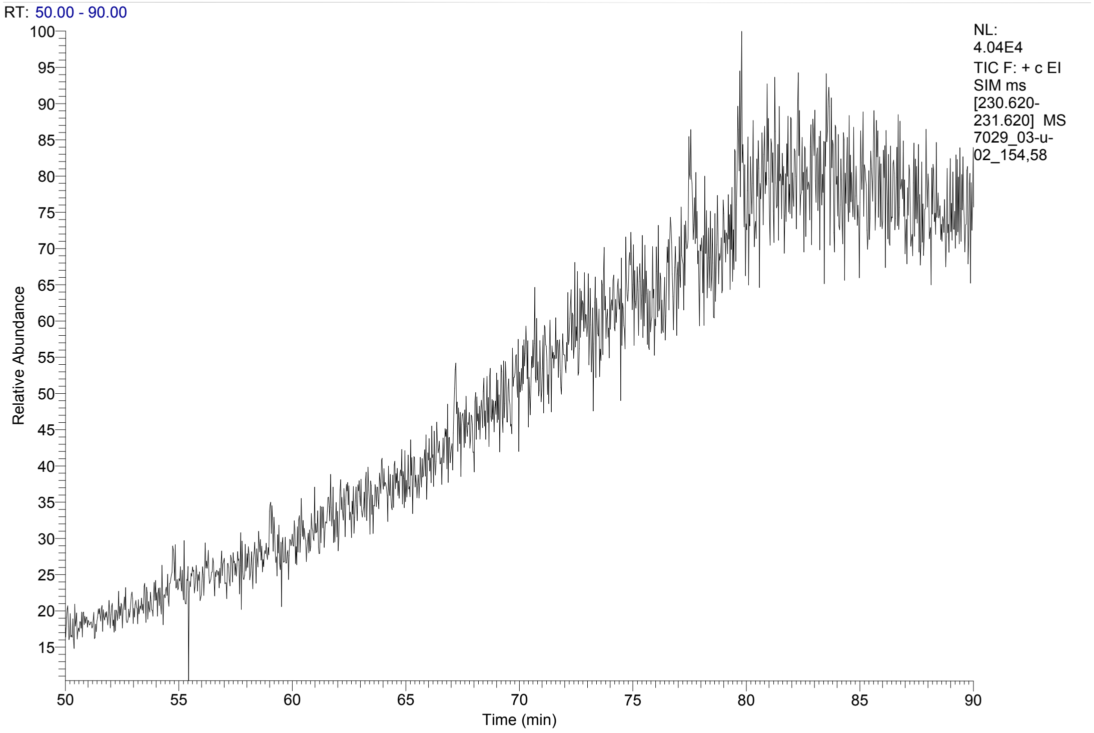
RT: 50.00 - 90.00
NL:
4.04E4
TIC F: + c EI
SIM ms
[230.620-
231.620] MS
7029_03-u-
02_154,58
Relative Abundance
100
95
90
85
80
75
70
65
60
55
50
45
40
35
30
25
20
15
50
55
60
65
70
75
80
85
90
Time (min)

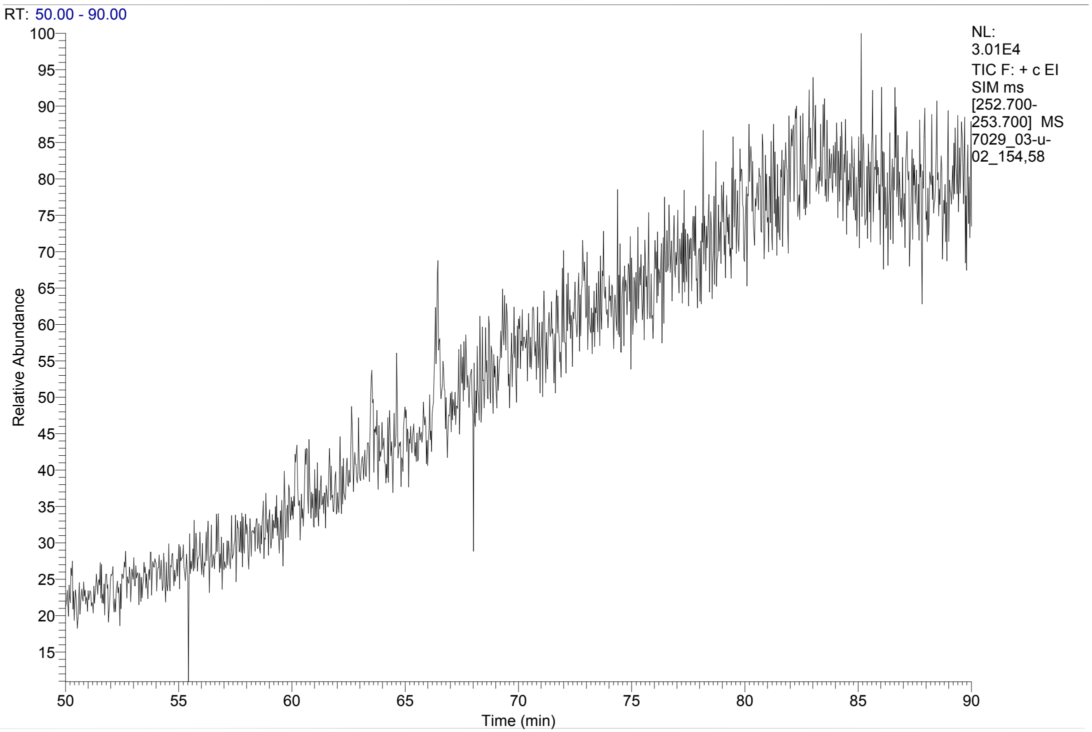
RT: 50.00 - 90.00
NL:
3.01E4
TIC F: + c EI
SIM ms
[252.700-
253.700] MS
7029_03-u-
02_154,58
Relative Abundance
100
95
90
85
80
75
70
65
60
55
50
45
40
35
30
25
20
15
50
55
60
65
70
75
80
85
90
Time (min)

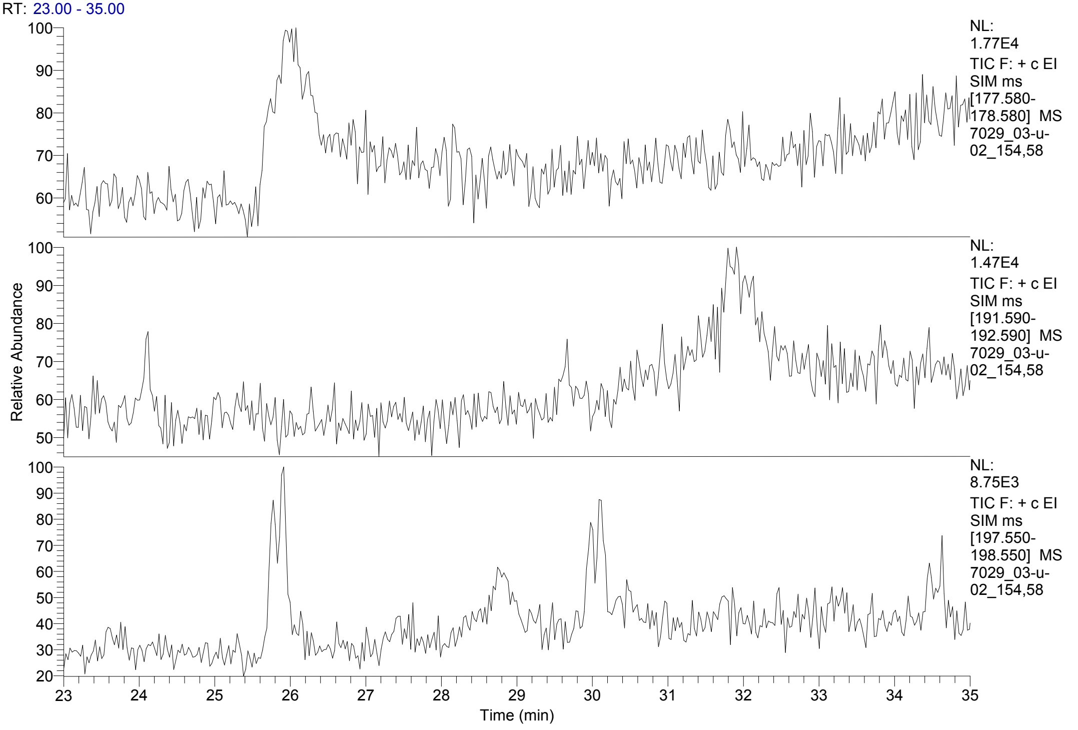
RT: 23.00 - 35.00
NL:
1.77E4
TIC F: + c EI
SIM ms
[177.580-
178.580] MS
7029_03-u-
02_154,58
NL:
1.47E4
TIC F: + c EI
SIM ms
[191.590-
192.590] MS
7029_03-u-
02_154,58
NL:
8.75E3
TIC F: + c EI
SIM ms
[197.550-
198.550] MS
7029_03-u-
02_154,58
Relative Abundance
100
90
80
70
60
50
40
30
20
23
24
25
26
27
28
29
30
31
32
33
34
35
Time (min)

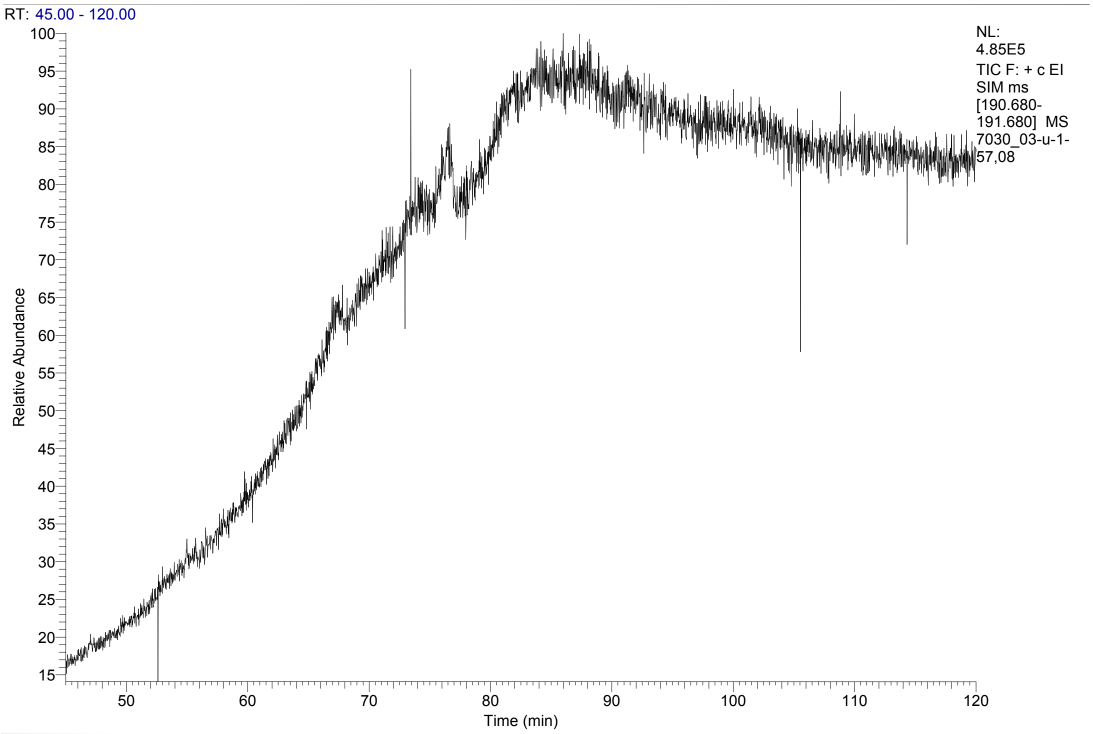
RT: 45.00 - 120.00
NL:
4.85E5
TIC F: + c EI
SIM ms
[190.680-
191.680] MS
7030_03-u-1-
57,08
Relative Abundance
Time (min)
100
95
90
85
80
75
70
65
60
55
50
45
40
35
30
25
20
15
50
60
70
80
90
100
110
120

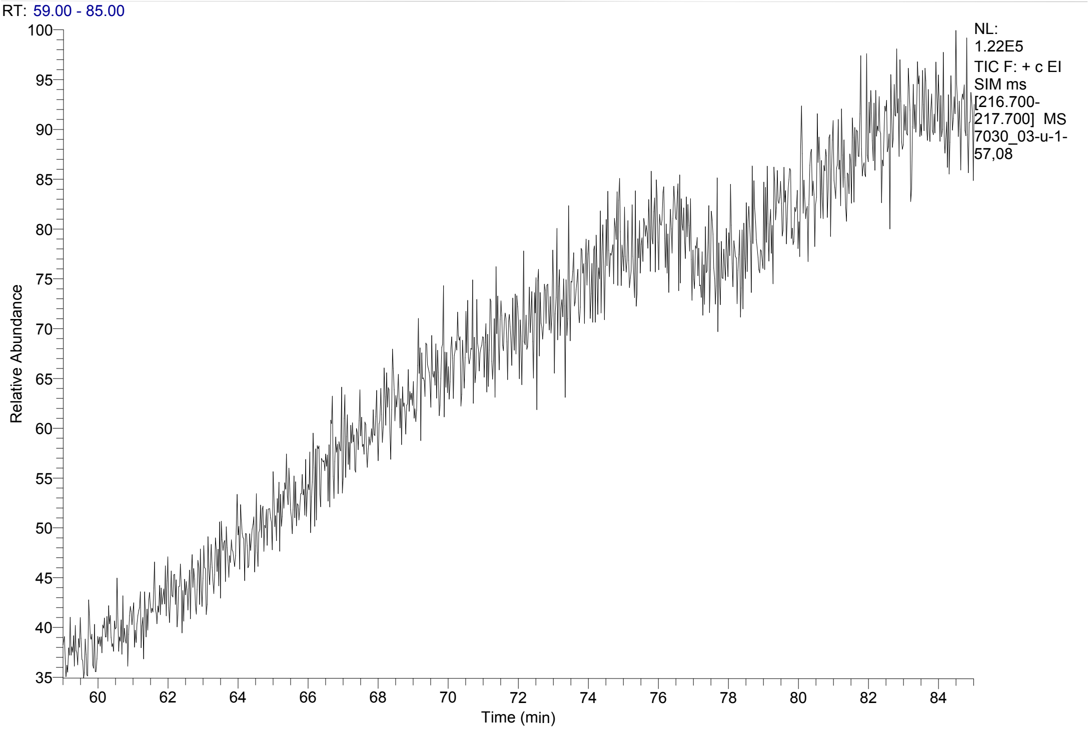
RT: 59.00 - 85.00
NL:
1.22E5
TIC F: + c EI
SIM ms
[216.700-
217.700] MS
7030_03-u-1-
57,08
Relative Abundance
Time (min)
100
95
90
85
80
75
70
65
60
55
50
45
40
35
60
62
64
66
68
70
72
74
76
78
80
82
84

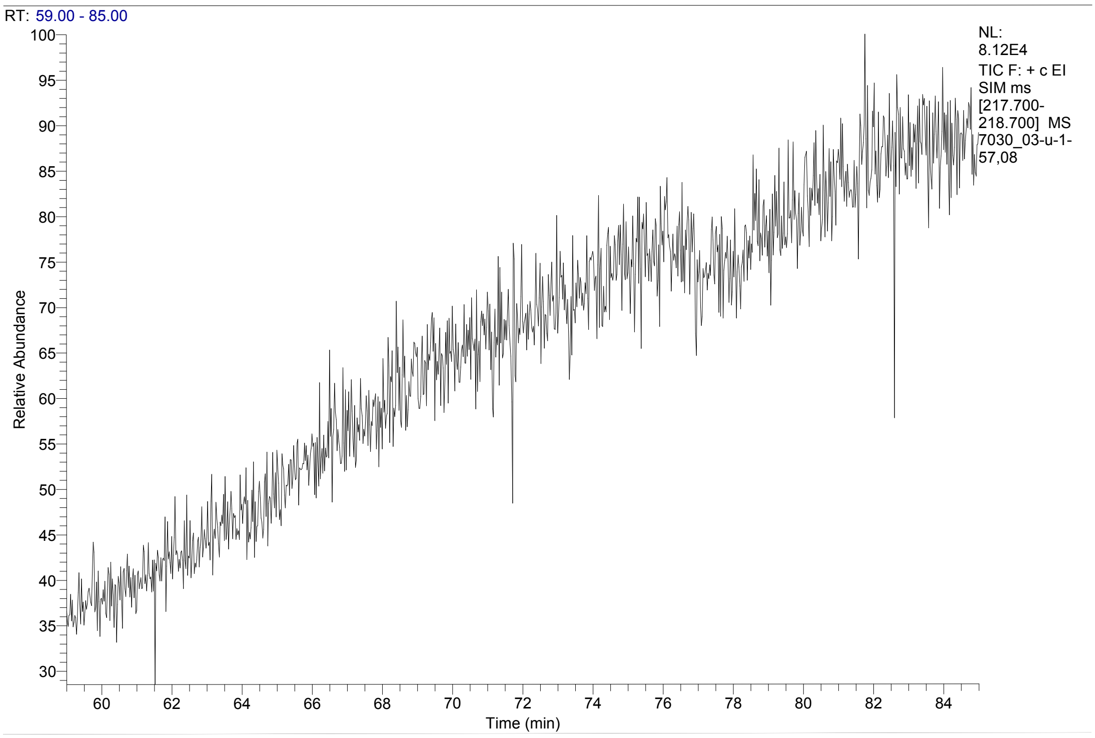
RT: 59.00 - 85.00
NL:
8.12E4
TIC F: + c EI
SIM ms
[217.700-
218.700] MS
7030_03-u-1-
57,08
Relative Abundance
100
95
90
85
80
75
70
65
60
55
50
45
40
35
30
60
62
64
66
68
70
72
74
76
78
80
82
84
Time (min)

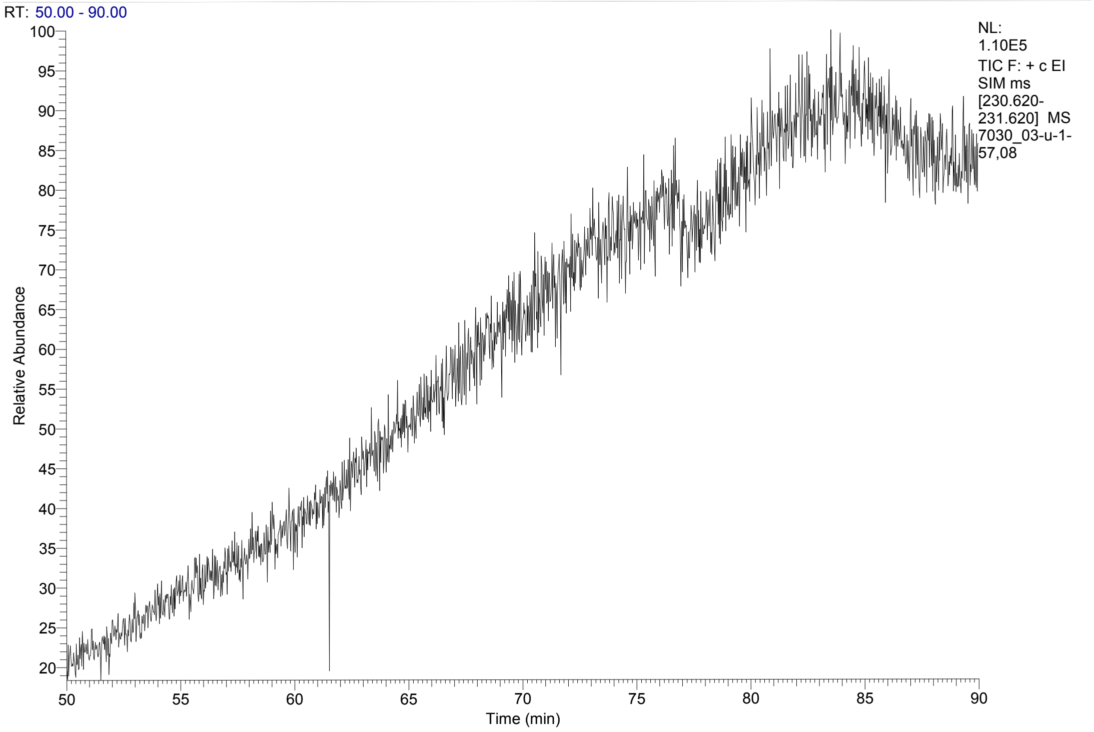
RT: 50.00 - 90.00
NL:
1.10E5
TIC F: + c EI
SIM ms
[230.620-
231.620] MS
7030_03-u-1-
57,08
Relative Abundance
100
95
90
85
80
75
70
65
60
55
50
45
40
35
30
25
20
50
55
60
65
70
75
80
85
90
Time (min)

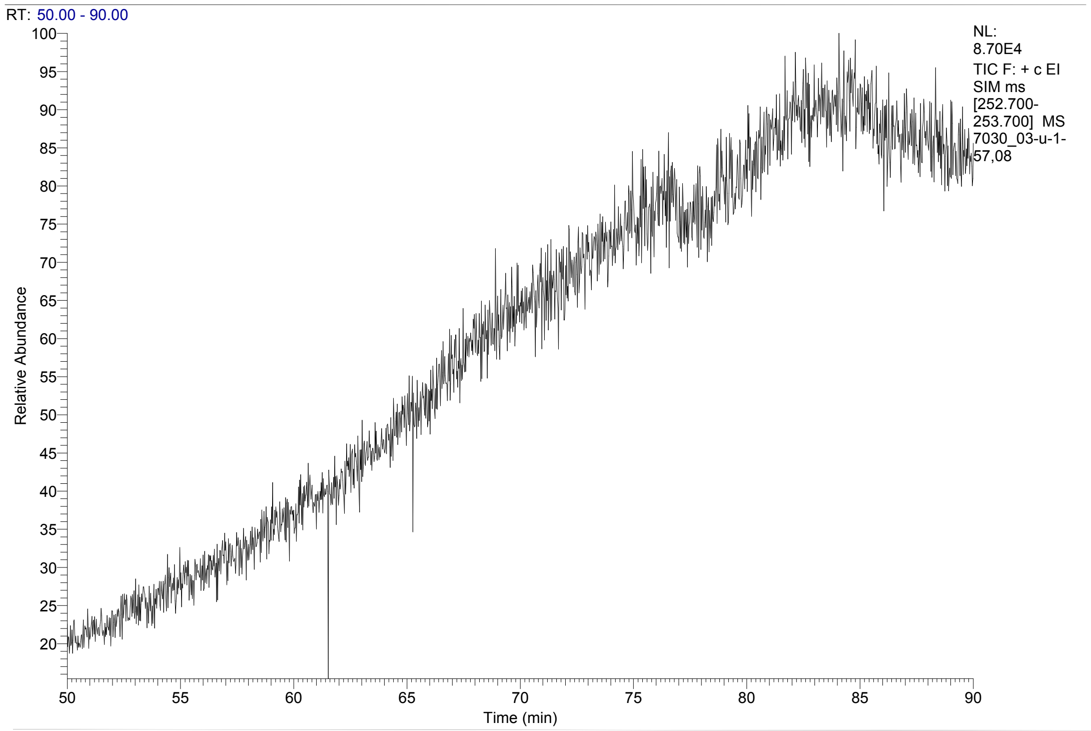
RT: 50.00 - 90.00
Relative Abundance
100
95
90
85
80
75
70
65
60
55
50
45
40
35
30
25
20
Time (min)
50
55
60
65
70
75
80
85
90
NL:
8.70E4
TIC F: + c EI
SIM ms
[252.700-
253.700] MS
7030_03-u-1-
57,08

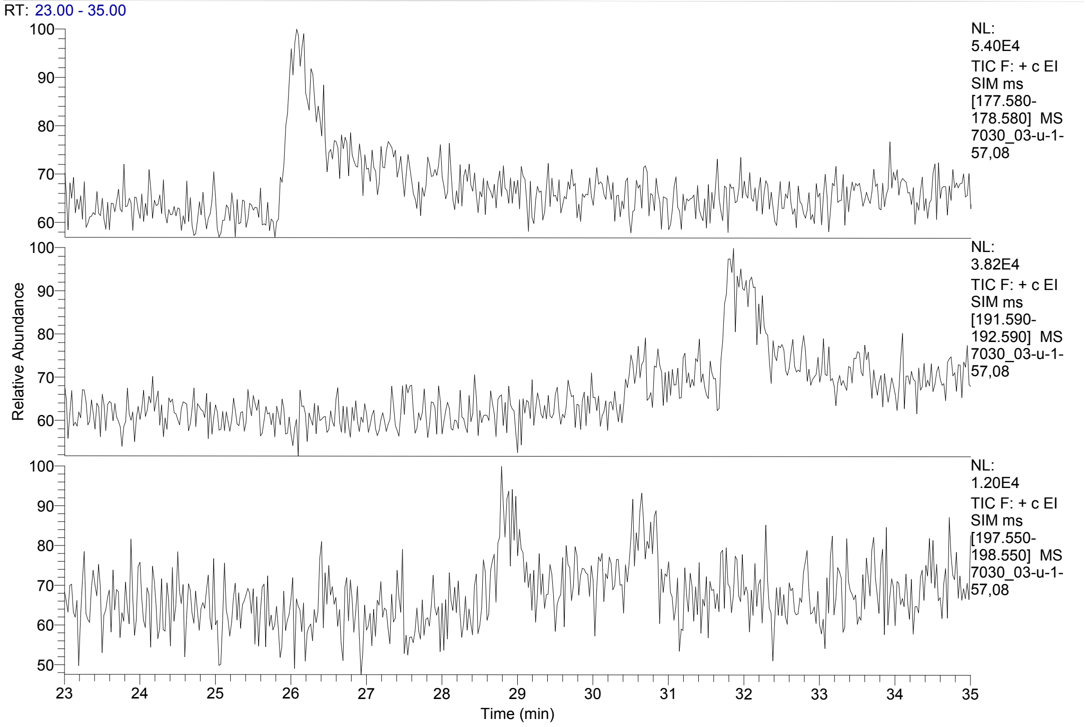
RT: 23.00 - 35.00
Relative Abundance
100
90
80
70
60
50
Time (min)
23
24
25
26
27
28
29
30
31
32
33
34
35
NL:
5.40E4
TIC F: + c EI
SIM ms
[177.580-
178.580] MS
7030_03-u-1-
57,08
NL:
3.82E4
TIC F: + c EI
SIM ms
[191.590-
192.590] MS
7030_03-u-1-
57,08
NL:
1.20E4
TIC F: + c EI
SIM ms
[197.550-
198.550] MS
7030_03-u-1-
57,08

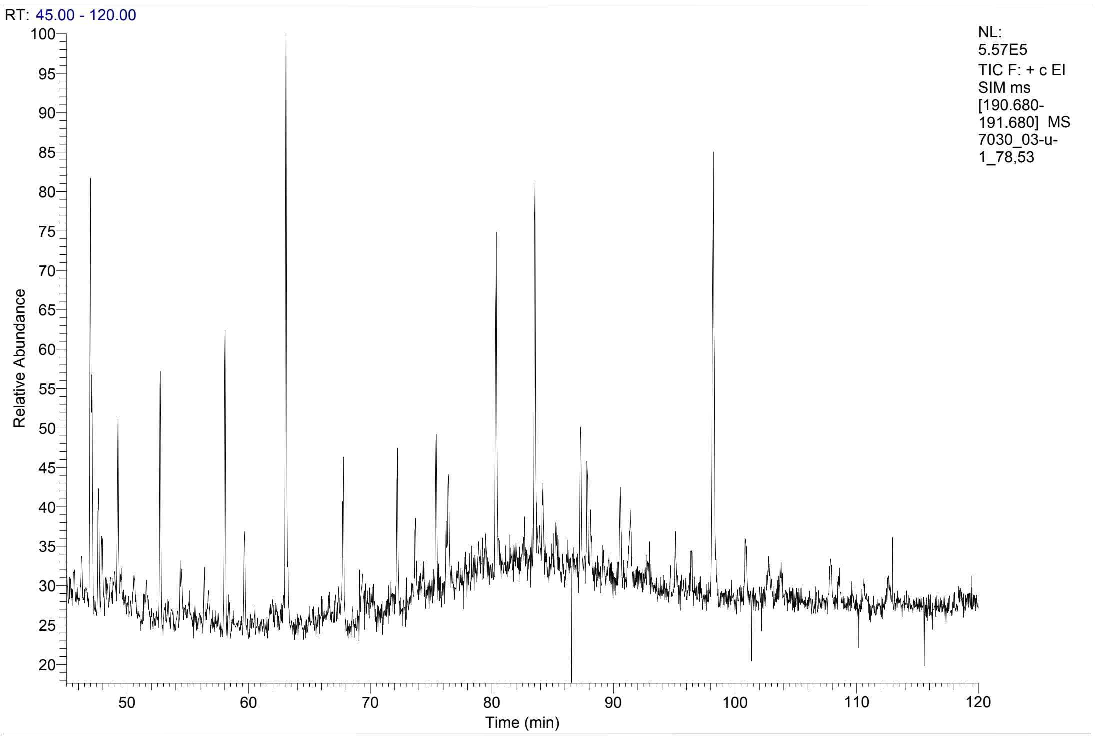
RT: 45.00 - 120.00
NL:
5.57E5
TIC F: + c EI
SIM ms
[190.680-
191.680] MS
7030_03-u-
1_78,53
Relative Abundance
100
95
90
85
80
75
70
65
60
55
50
45
40
35
30
25
20
50
60
70
80
90
100
110
120
Time (min)

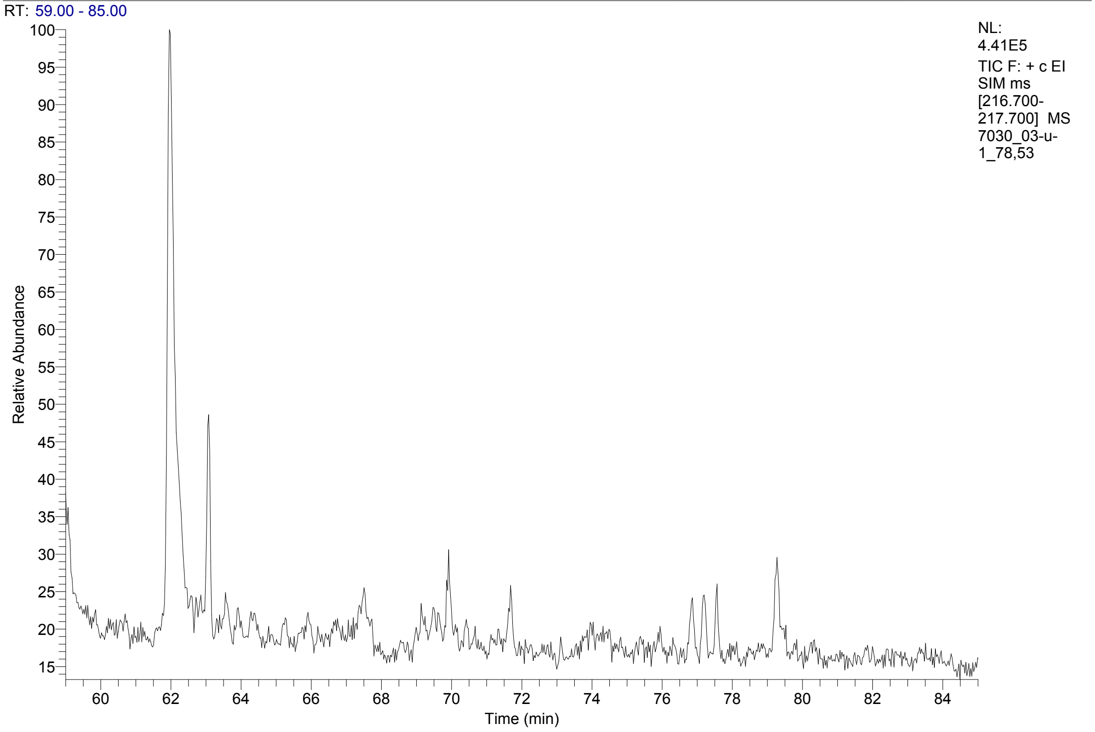
RT: 59.00 - 85.00
NL:
4.41E5
TIC F: + c EI
SIM ms
[216.700-
217.700] MS
7030_03-u-
1_78,53
Relative Abundance
100
95
90
85
80
75
70
65
60
55
50
45
40
35
30
25
20
15
60
62
64
66
68
70
72
74
76
78
80
82
84
Time (min)

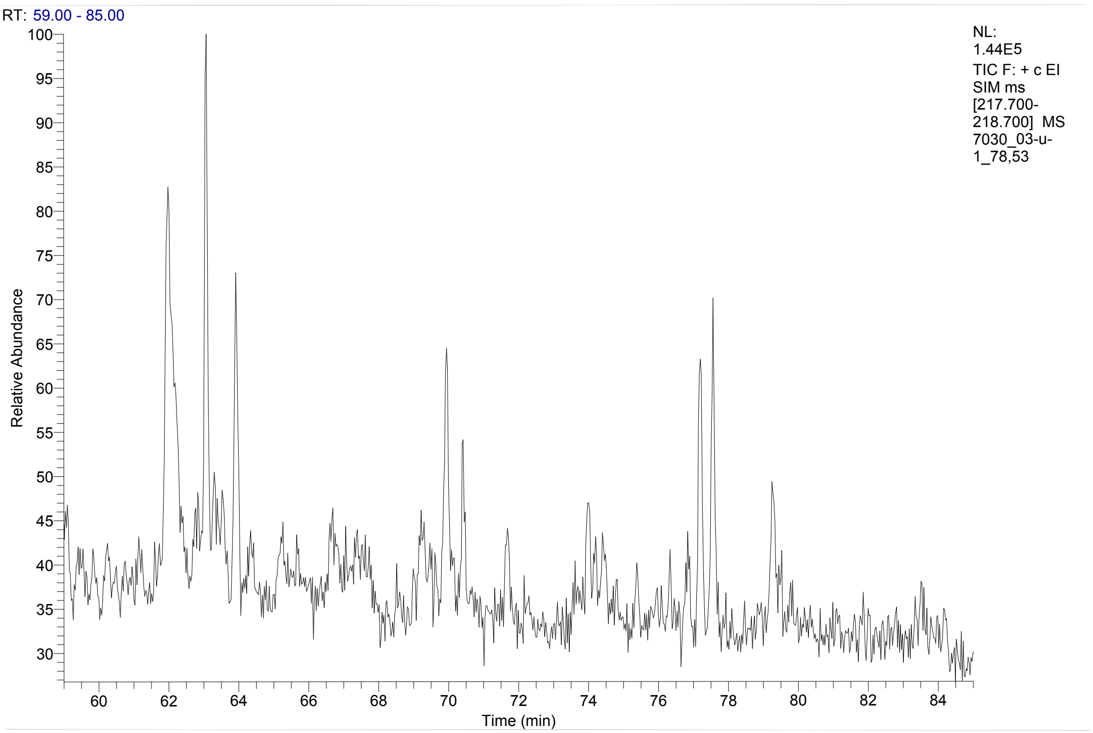
RT: 59.00 - 85.00
NL:
1.44E5
TIC F: + c EI
SIM ms
[217.700-
218.700] MS
7030_03-u-
1_78,53
Relative Abundance
100
95
90
85
80
75
70
65
60
55
50
45
40
35
30
60
62
64
66
68
70
72
74
76
78
80
82
84
Time (min)

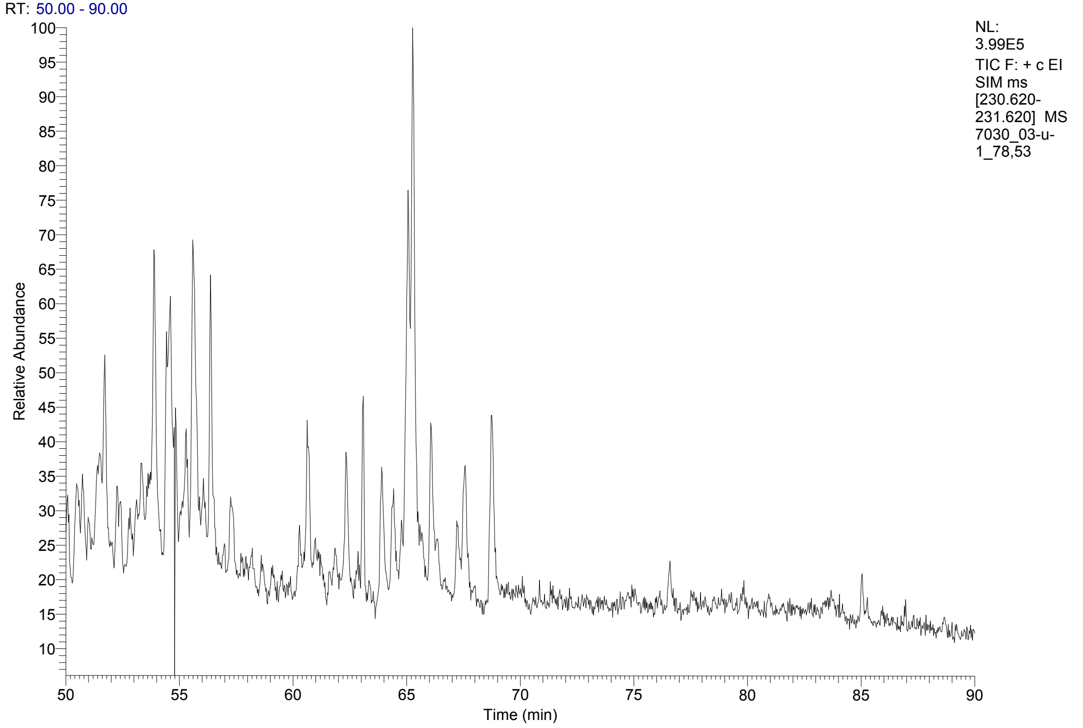
RT: 50.00 - 90.00
NL:
3.99E5
TIC F: + c EI
SIM ms
[230.620-
231.620] MS
7030_03-u-
1_78,53
Relative Abundance
100
95
90
85
80
75
70
65
60
55
50
45
40
35
30
25
20
15
10
50
55
60
65
70
75
80
85
90
Time (min)

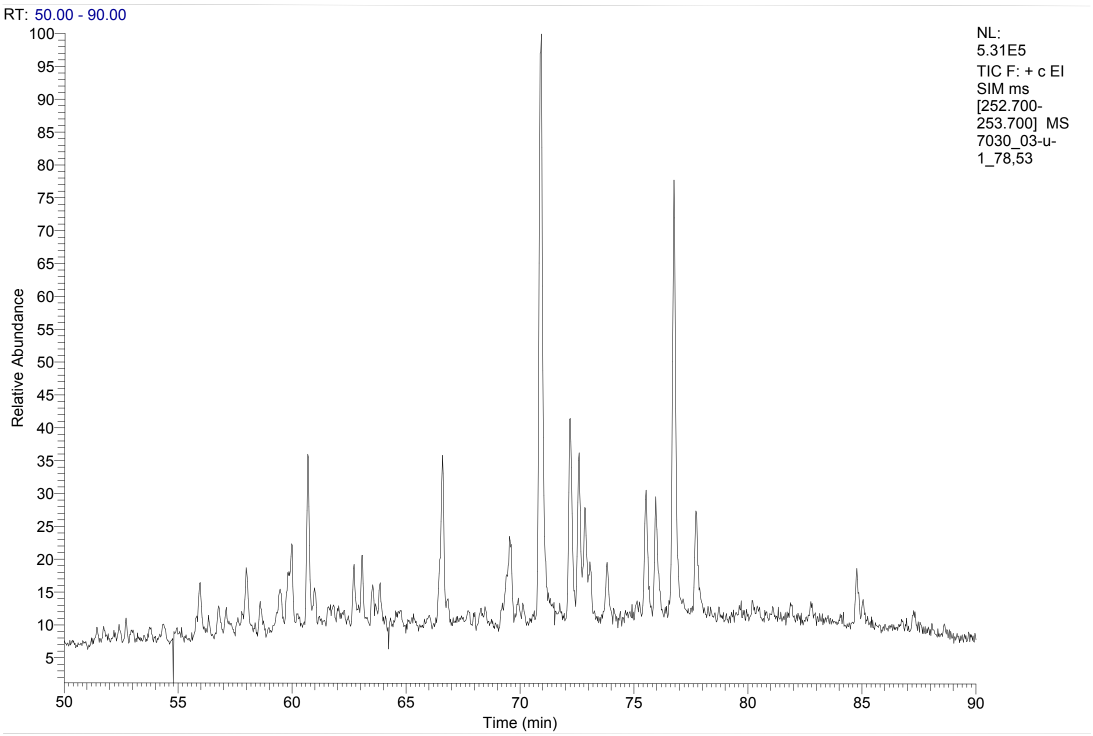
RT: 50.00 - 90.00
Relative Abundance
Time (min)
0
5
10
15
20
25
30
35
40
45
50
55
60
65
70
75
80
85
90
95
100
50
55
60
65
70
75
80
85
90
NL:
5.31E5
TIC F: + c EI
SIM ms
[252.700-
253.700] MS
7030_03-u-
1_78,53

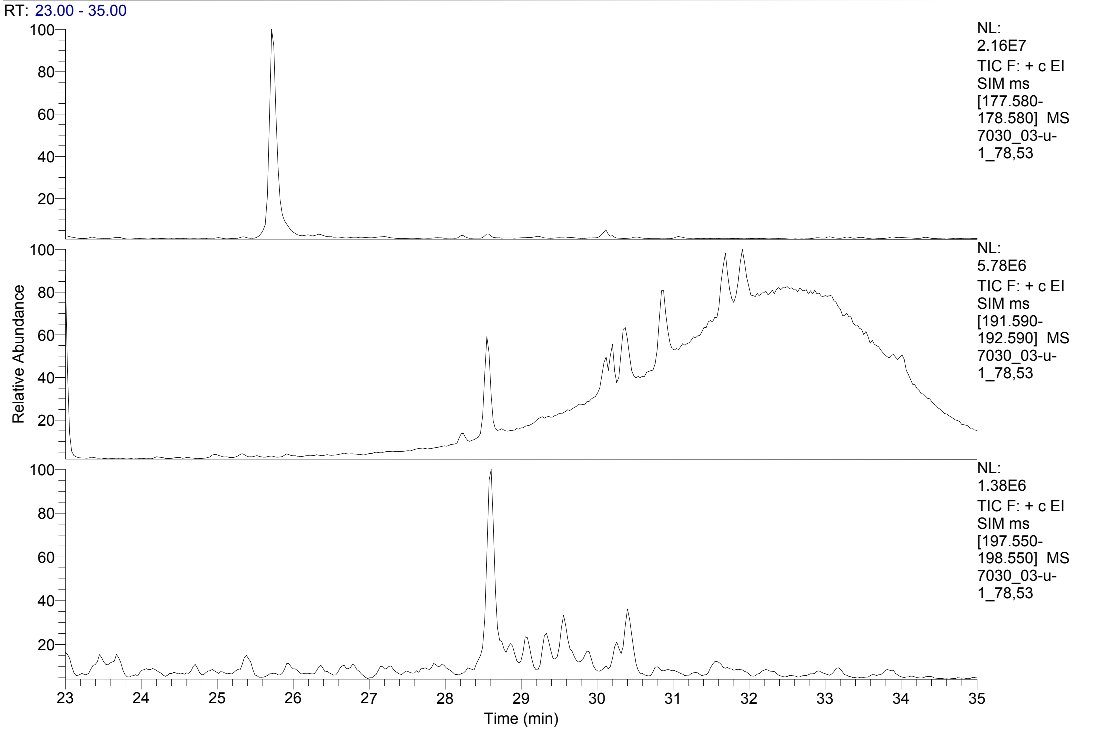
RT: 23.00 - 35.00
Relative Abundance
Time (min)
20
40
60
80
100
23
24
25
26
27
28
29
30
31
32
33
34
35
NL:
2.16E7
TIC F: + c EI
SIM ms
[177.580-
178.580] MS
7030_03-u-
1_78,53
NL:
5.78E6
TIC F: + c EI
SIM ms
[191.590-
192.590] MS
7030_03-u-
1_78,53
NL:
1.38E6
TIC F: + c EI
SIM ms
[197.550-
198.550] MS
7030_03-u-
1_78,53

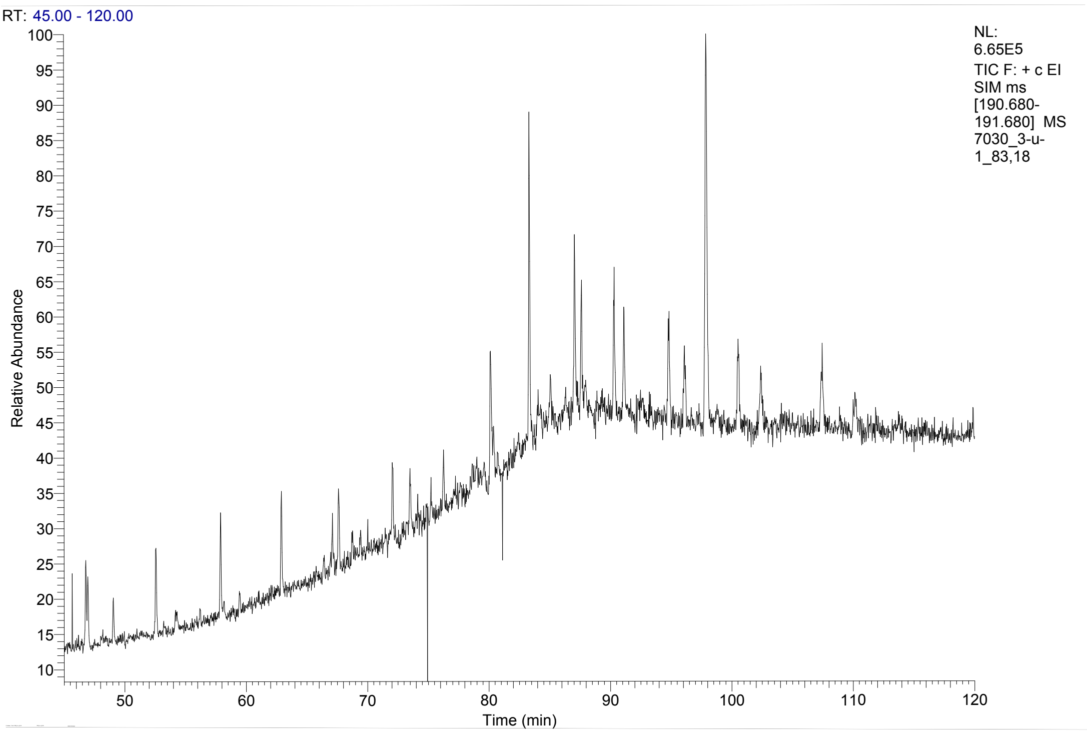
RT: 45.00 - 120.00
NL:
6.65E5
TIC F: + c EI
SIM ms
[190.680-
191.680] MS
7030_3-u-
1_83,18
Relative Abundance
100
95
90
85
80
75
70
65
60
55
50
45
40
35
30
25
20
15
10
50
60
70
80
90
100
110
120
Time (min)

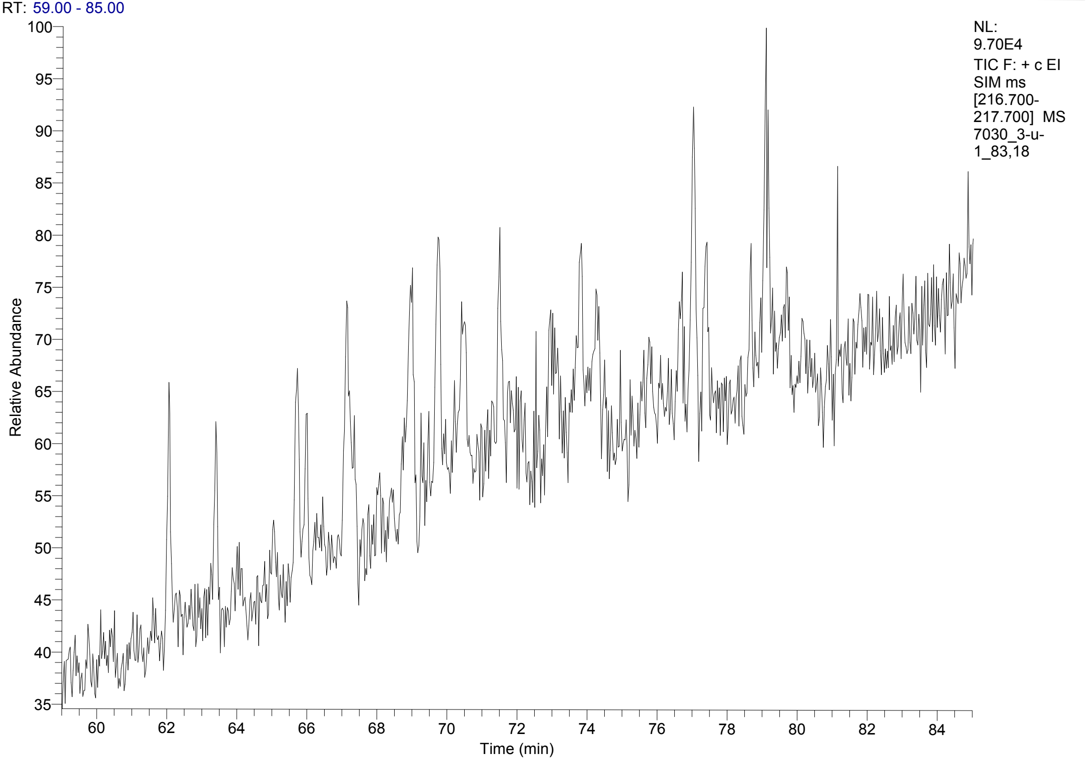
RT: 59.00 - 85.00
NL:
9.70E4
TIC F: + c EI
SIM ms
[216.700-
217.700] MS
7030_3-u-
1_83,18
Relative Abundance
100
95
90
85
80
75
70
65
60
55
50
45
40
35
60
62
64
66
68
70
72
74
76
78
80
82
84
Time (min)

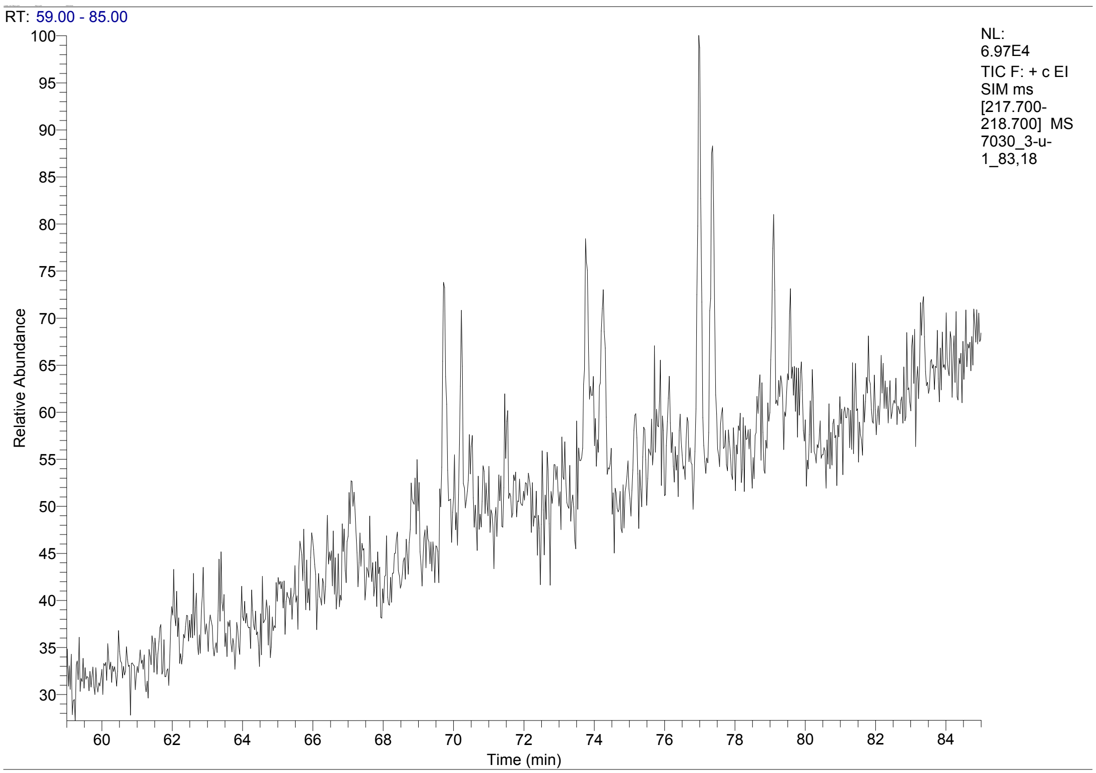
RT: 59.00 - 85.00
NL:
6.97E4
TIC F: + c EI
SIM ms
[217.700-
218.700] MS
7030_3-u-
1_83,18
Relative Abundance
100
95
90
85
80
75
70
65
60
55
50
45
40
35
30
60
62
64
66
68
70
72
74
76
78
80
82
84
Time (min)

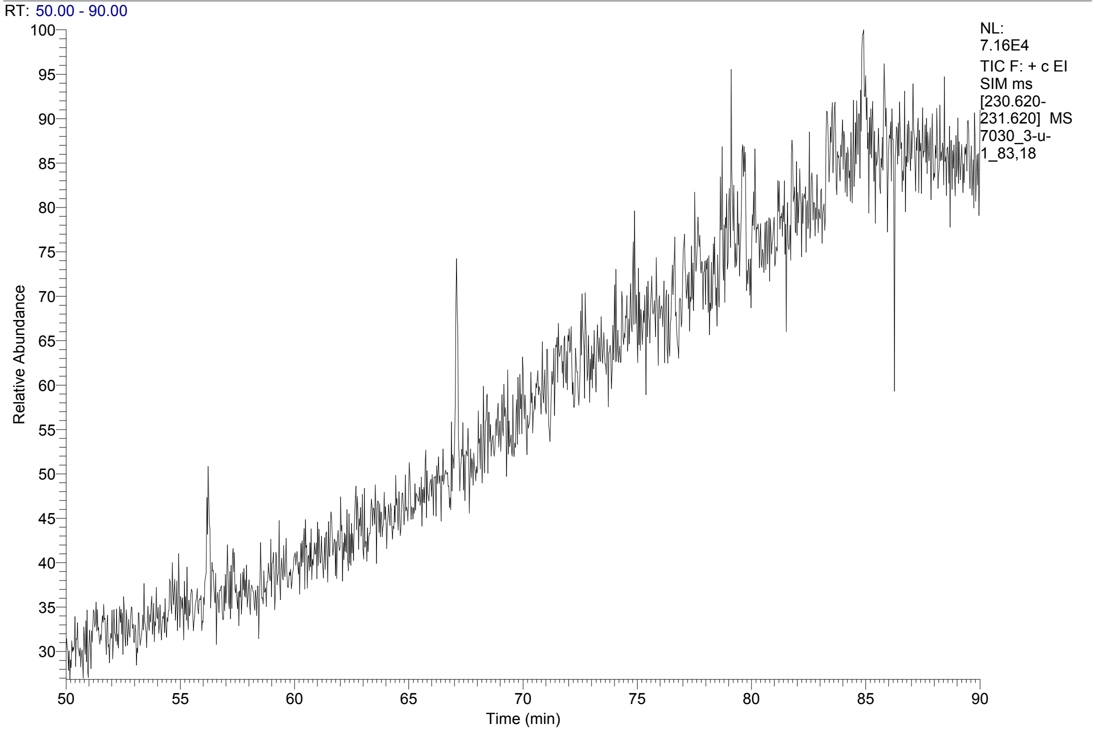
RT: 50.00 - 90.00
NL:
7.16E4
TIC F: + c EI
SIM ms
[230.620-
231.620] MS
7030_3-u-
1_83,18
Relative Abundance
100
95
90
85
80
75
70
65
60
55
50
45
40
35
30
50
55
60
65
70
75
80
85
90
Time (min)

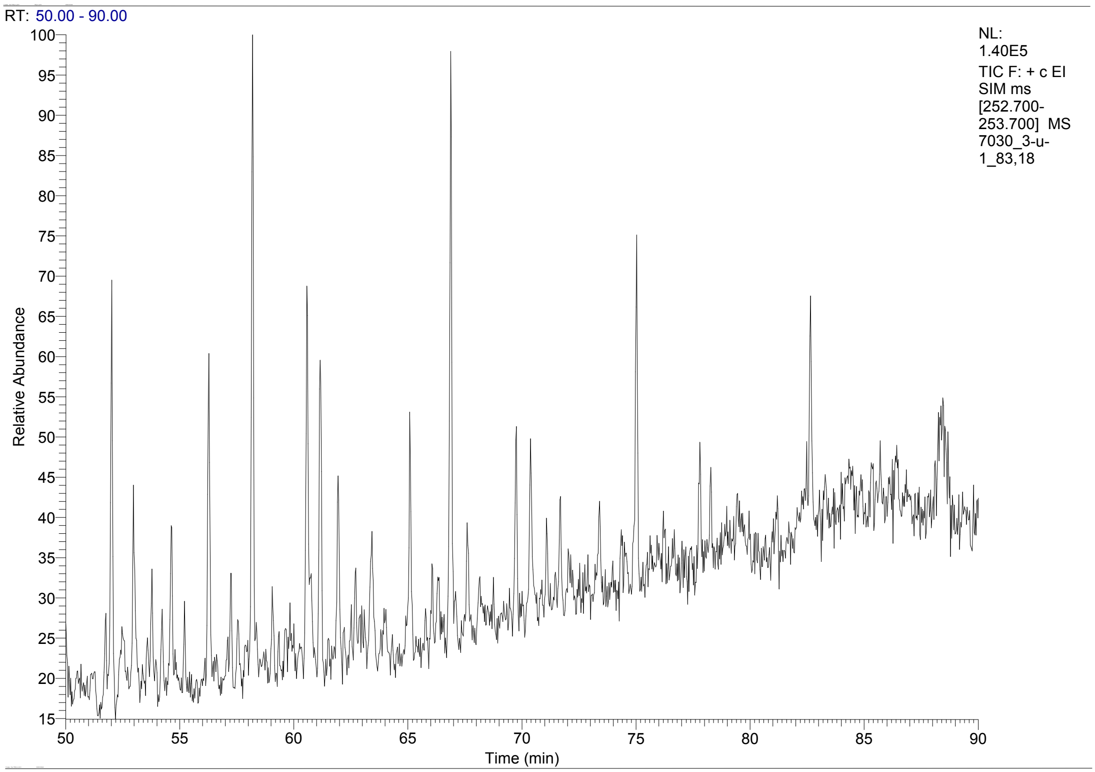
RT: 50.00 - 90.00
NL:
1.40E5
TIC F: + c EI
SIM ms
[252.700-
253.700] MS
7030_3-u-
1_83,18
Relative Abundance
100
95
90
85
80
75
70
65
60
55
50
45
40
35
30
25
20
15
50
55
60
65
70
75
80
85
90
Time (min)

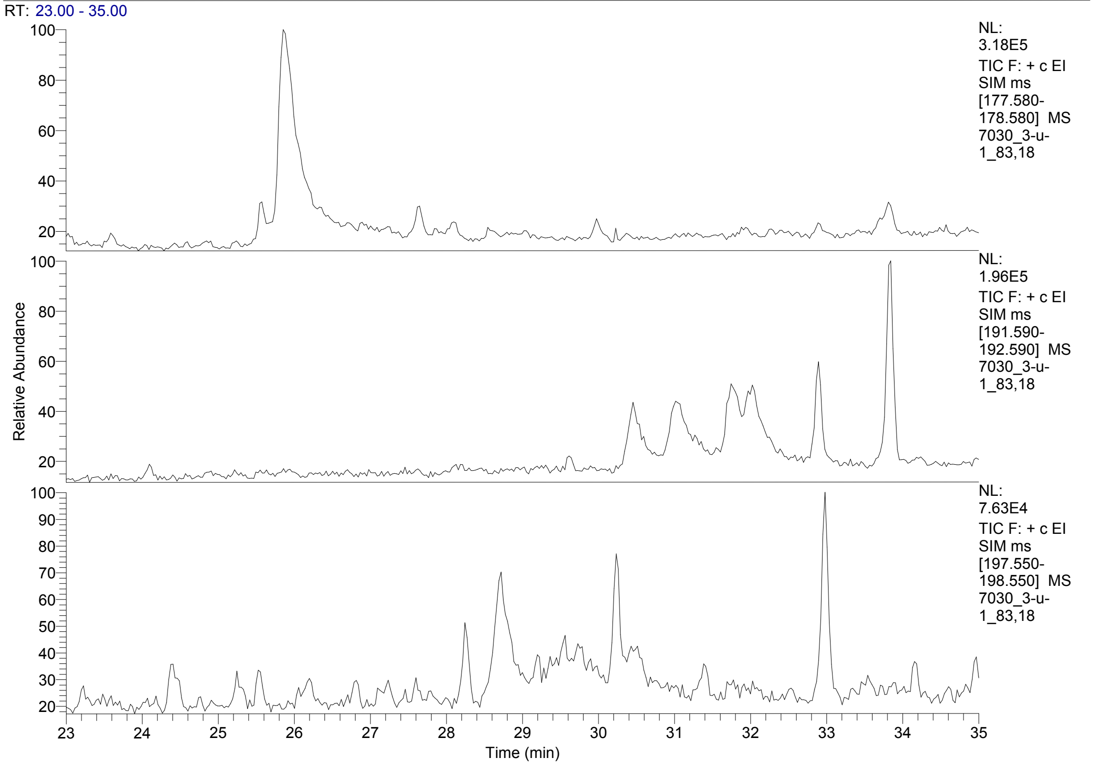
RT: 23.00 - 35.00
NL:
3.18E5
TIC F: + c EI
SIM ms
[177.580-
178.580] MS
7030_3-u-
1_83,18
NL:
1.96E5
TIC F: + c EI
SIM ms
[191.590-
192.590] MS
7030_3-u-
1_83,18
NL:
7.63E4
TIC F: + c EI
SIM ms
[197.550-
198.550] MS
7030_3-u-
1_83,18
Relative Abundance
100
80
60
40
20
100
80
60
40
20
100
90
80
70
60
50
40
30
20
23
24
25
26
27
28
29
30
31
32
33
34
35
Time (min)

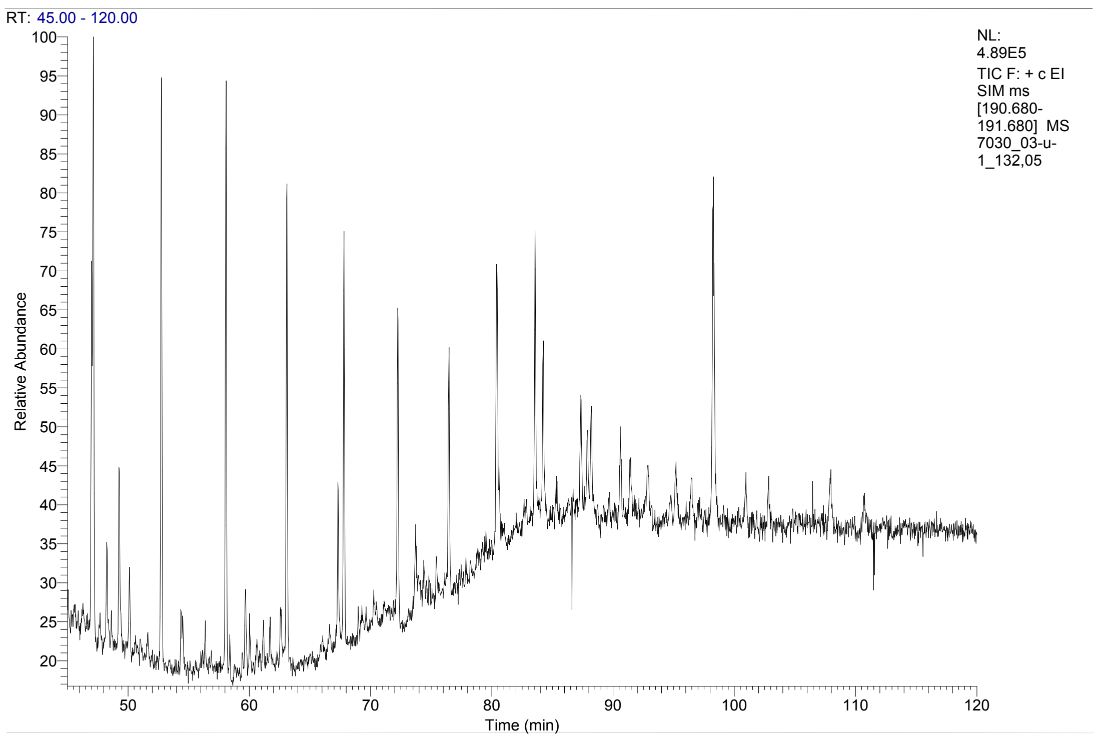
RT: 45.00 - 120.00
NL:
4.89E5
TIC F: + c EI
SIM ms
[190.680-
191.680] MS
7030_03-u-
1_132,05
Relative Abundance
100
95
90
85
80
75
70
65
60
55
50
45
40
35
30
25
20
50
60
70
80
90
100
110
120
Time (min)

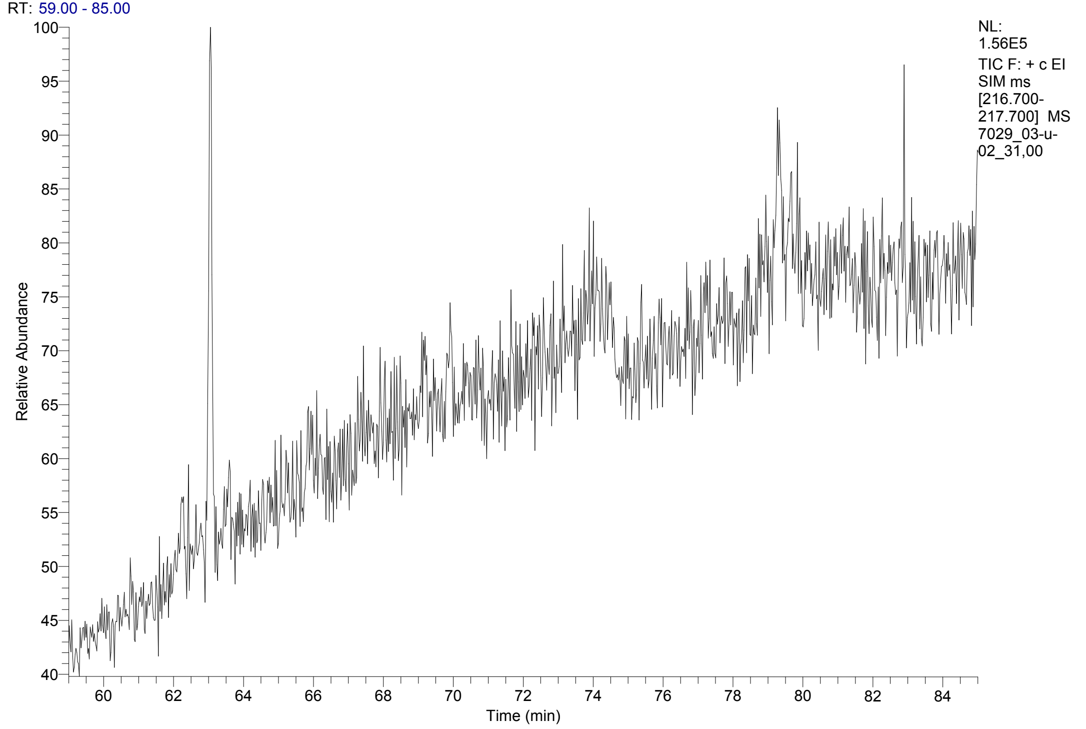
RT: 59.00 - 85.00
NL:
1.56E5
TIC F: + c EI
SIM ms
[216.700-
217.700] MS
7029_03-u-
02_31,00
Relative Abundance
100
95
90
85
80
75
70
65
60
55
50
45
40
60
62
64
66
68
70
72
74
76
78
80
82
84
Time (min)

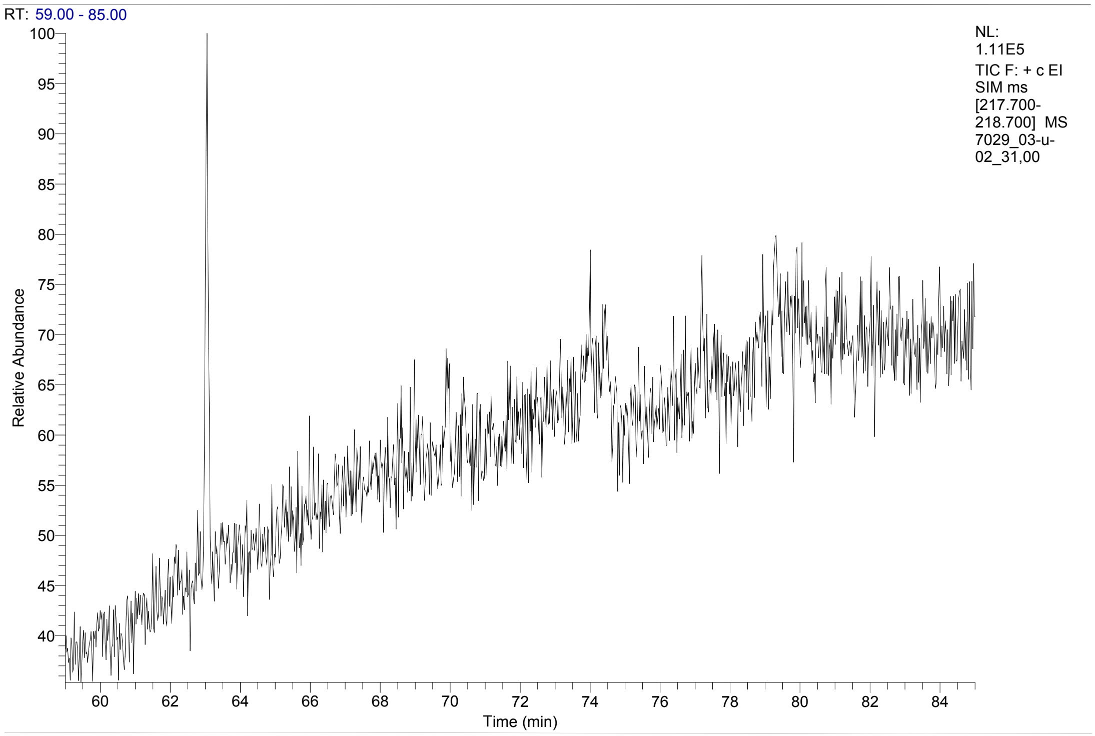
RT: 59.00 - 85.00
NL:
1.11E5
TIC F: + c EI
SIM ms
[217.700-
218.700] MS
7029_03-u-
02_31,00
Relative Abundance
100
95
90
85
80
75
70
65
60
55
50
45
40
60
62
64
66
68
70
72
74
76
78
80
82
84
Time (min)

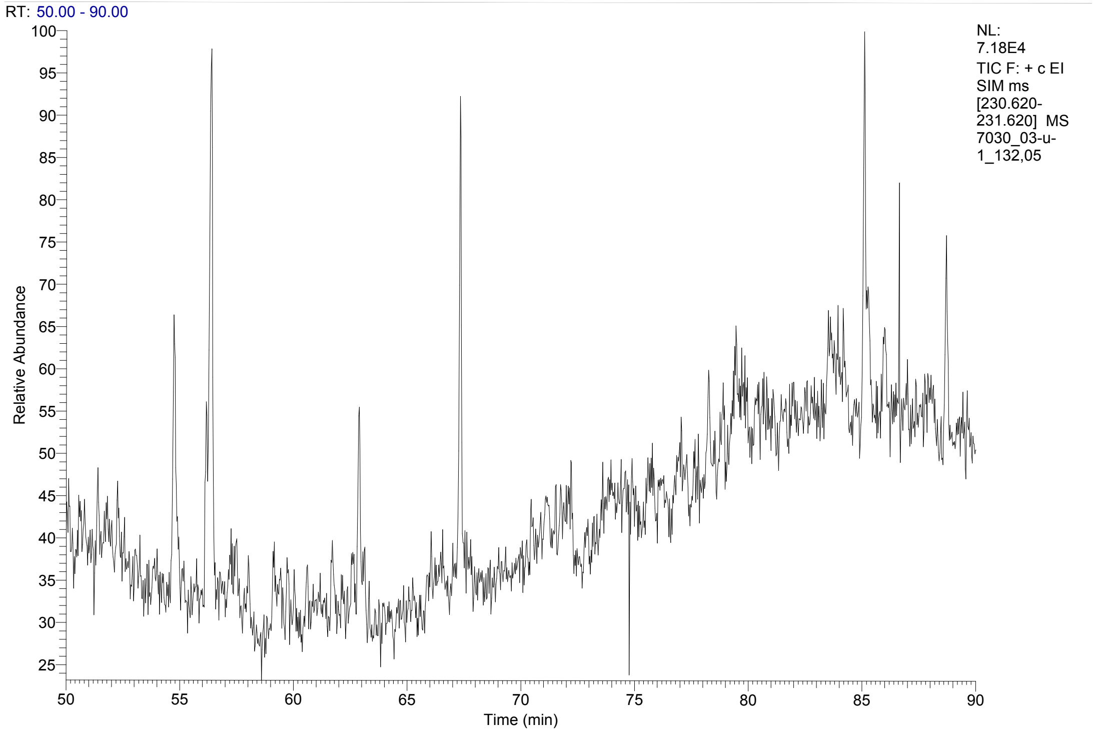
RT: 50.00 - 90.00
NL:
7.18E4
TIC F: + c EI
SIM ms
[230.620-
231.620] MS
7030_03-u-
1_132,05
Relative Abundance
100
95
90
85
80
75
70
65
60
55
50
45
40
35
30
25
50
55
60
65
70
75
80
85
90
Time (min)

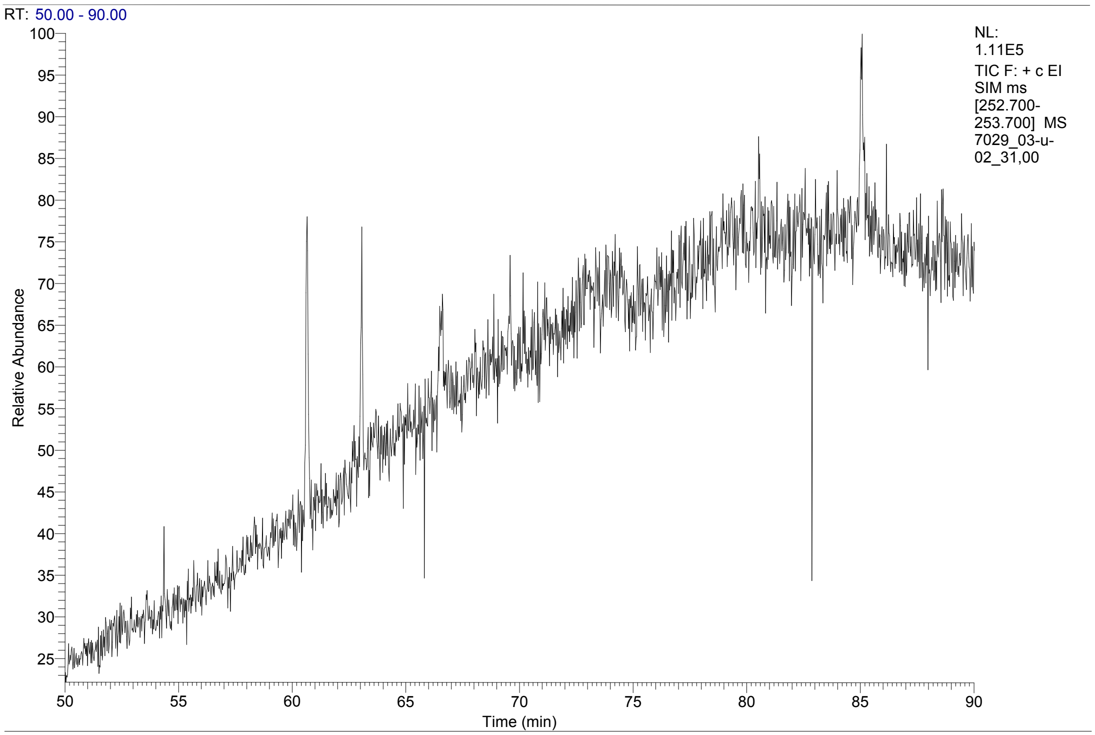
RT: 50.00 - 90.00
NL:
1.11E5
TIC F: + c EI
SIM ms
[252.700-
253.700] MS
7029_03-u-
02_31,00
Relative Abundance
100
95
90
85
80
75
70
65
60
55
50
45
40
35
30
25
50
55
60
65
70
75
80
85
90
Time (min)

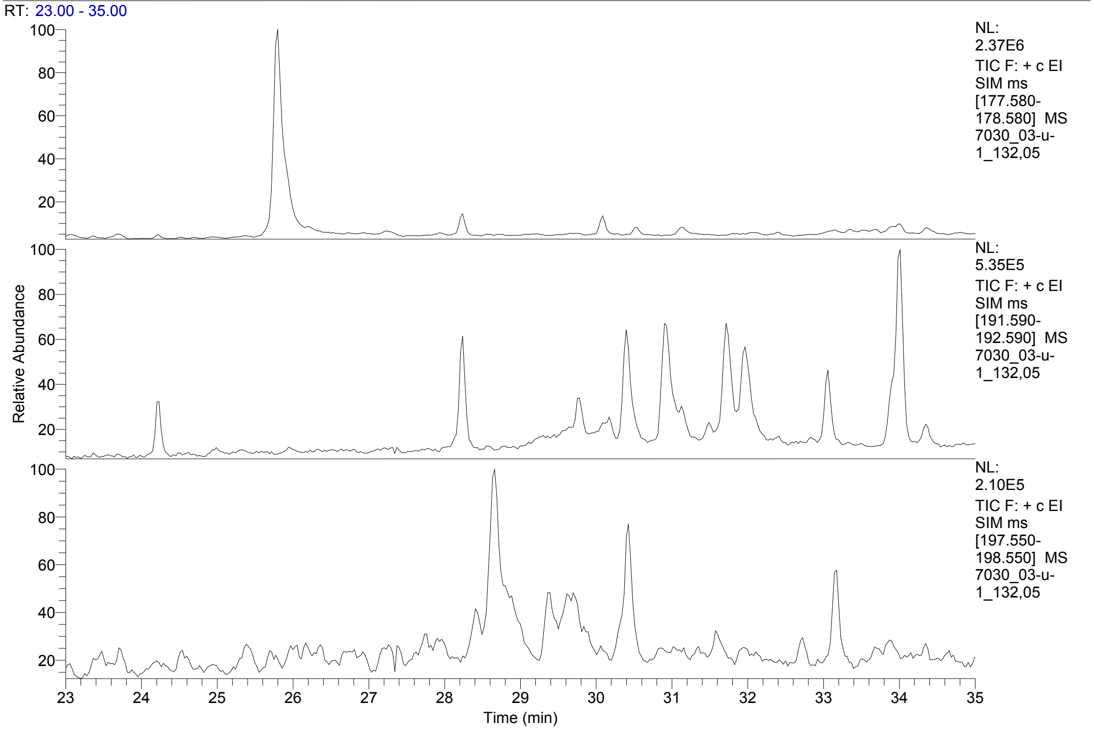
RT: 23.00 - 35.00
NL:
2.37E6
TIC F: + c EI
SIM ms
[177.580-
178.580] MS
7030_03-u-
1_132,05
NL:
5.35E5
TIC F: + c EI
SIM ms
[191.590-
192.590] MS
7030_03-u-
1_132,05
NL:
2.10E5
TIC F: + c EI
SIM ms
[197.550-
198.550] MS
7030_03-u-
1_132,05
Relative Abundance
100
80
60
40
20
23
24
25
26
27
28
29
30
31
32
33
34
35
Time (min)

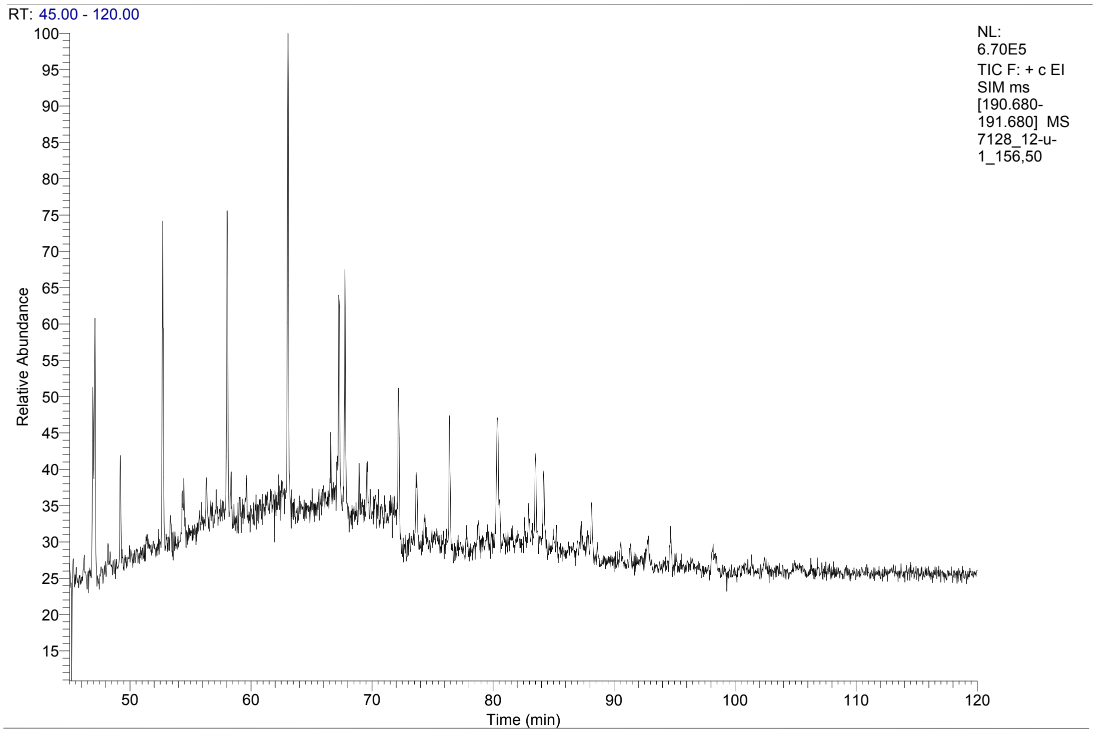
RT: 45.00 - 120.00
NL:
6.70E5
TIC F: + c EI
SIM ms
[190.680-
191.680] MS
7128_12-u-
1_156,50
Relative Abundance
100
95
90
85
80
75
70
65
60
55
50
45
40
35
30
25
20
15
50
60
70
80
90
100
110
120
Time (min)

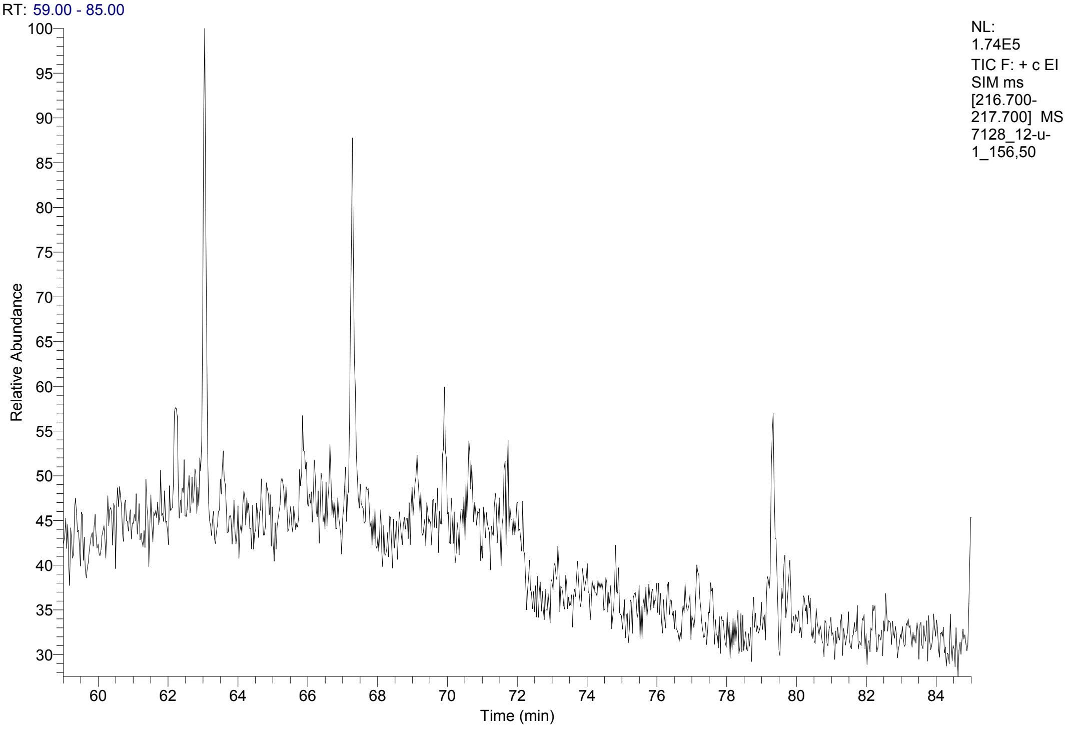
RT: 59.00 - 85.00
NL:
1.74E5
TIC F: + c EI
SIM ms
[216.700-
217.700] MS
7128_12-u-
1_156,50
Relative Abundance
100
95
90
85
80
75
70
65
60
55
50
45
40
35
30
60
62
64
66
68
70
72
74
76
78
80
82
84
Time (min)

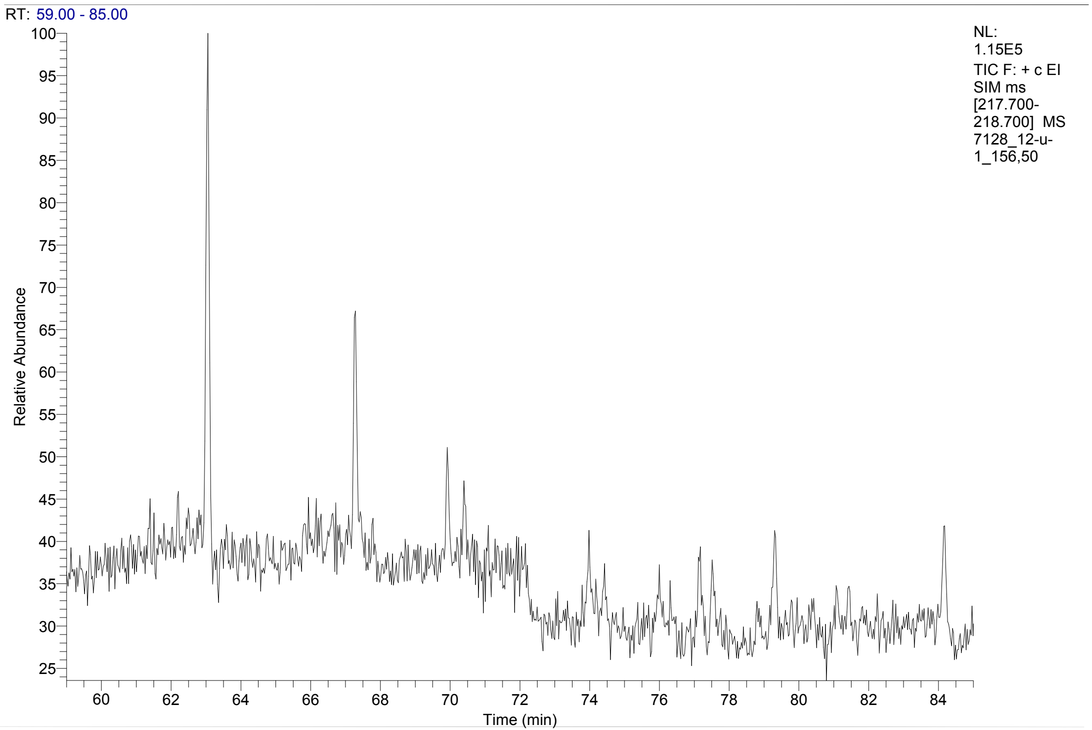
RT: 59.00 - 85.00
NL:
1.15E5
TIC F: + c EI
SIM ms
[217.700-
218.700] MS
7128_12-u-
1_156,50
Relative Abundance
100
95
90
85
80
75
70
65
60
55
50
45
40
35
30
25
60
62
64
66
68
70
72
74
76
78
80
82
84
Time (min)

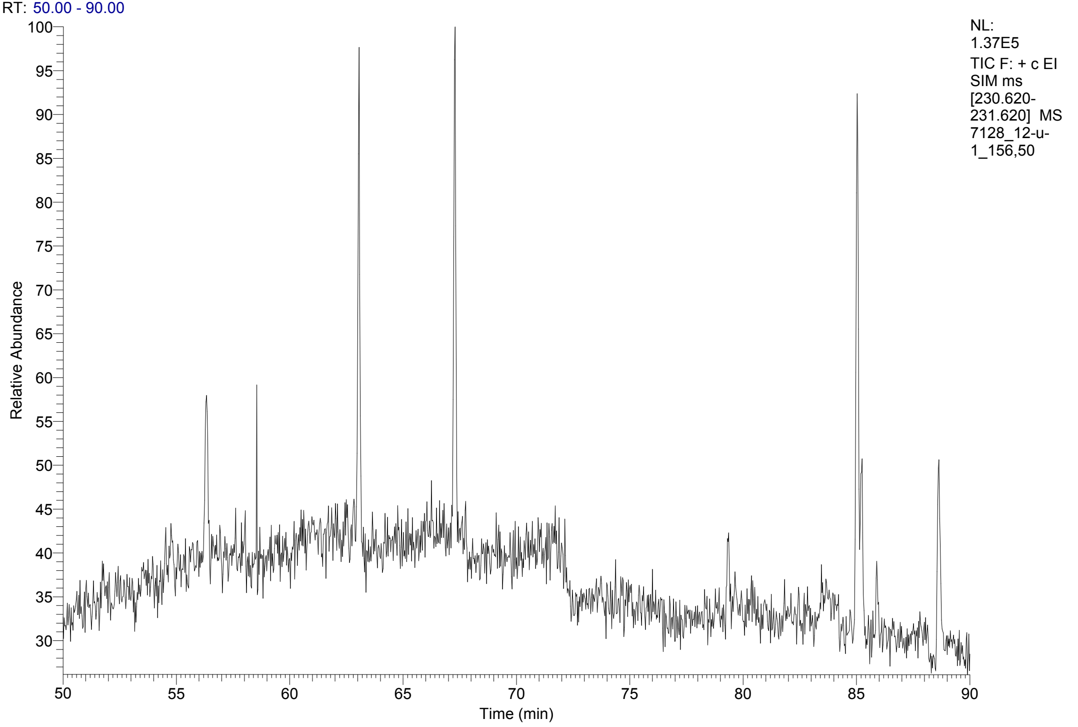
RT: 50.00 - 90.00
NL:
1.37E5
TIC F: + c EI
SIM ms
[230.620-
231.620] MS
7128_12-u-
1_156,50
Relative Abundance
100
95
90
85
80
75
70
65
60
55
50
45
40
35
30
50
55
60
65
70
75
80
85
90
Time (min)

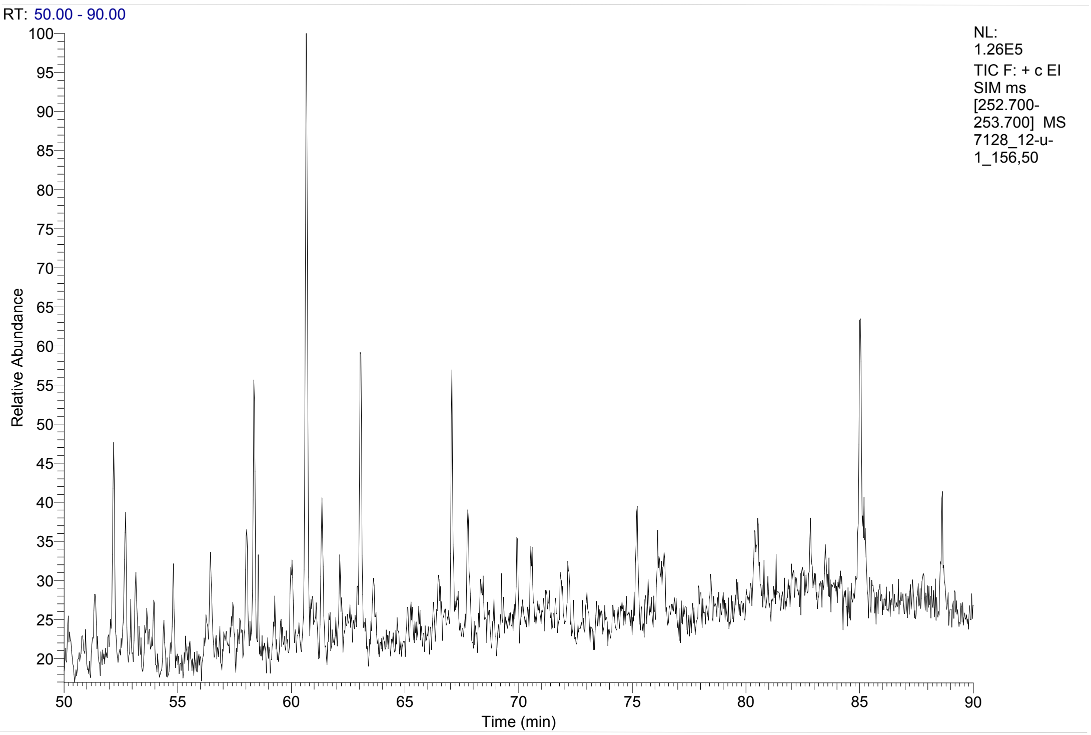
RT: 50.00 - 90.00
NL:
1.26E5
TIC F: + c EI
SIM ms
[252.700-
253.700] MS
7128_12-u-
1_156,50
Relative Abundance
100
95
90
85
80
75
70
65
60
55
50
45
40
35
30
25
20
50
55
60
65
70
75
80
85
90
Time (min)

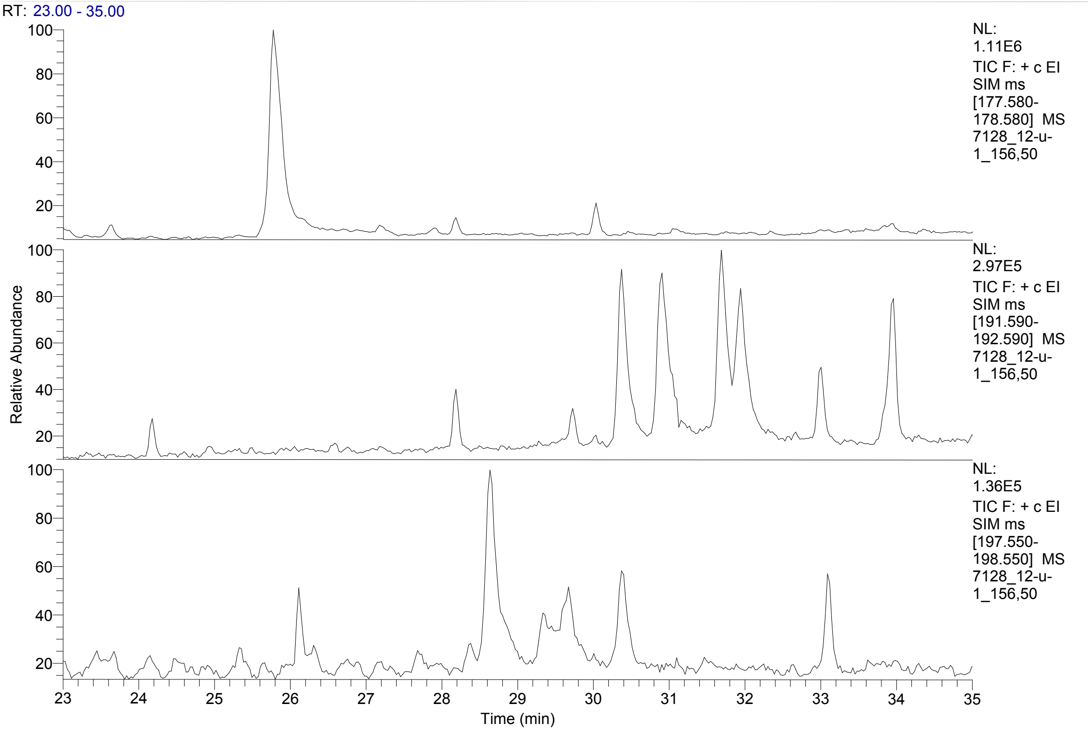
RT: 23.00 - 35.00
NL:
1.11E6
TIC F: + c EI
SIM ms
[177.580-
178.580] MS
7128_12-u-
1_156,50
NL:
2.97E5
TIC F: + c EI
SIM ms
[191.590-
192.590] MS
7128_12-u-
1_156,50
NL:
1.36E5
TIC F: + c EI
SIM ms
[197.550-
198.550] MS
7128_12-u-
1_156,50
Relative Abundance
100
80
60
40
20
23
24
25
26
27
28
29
30
31
32
33
34
35
Time (min)

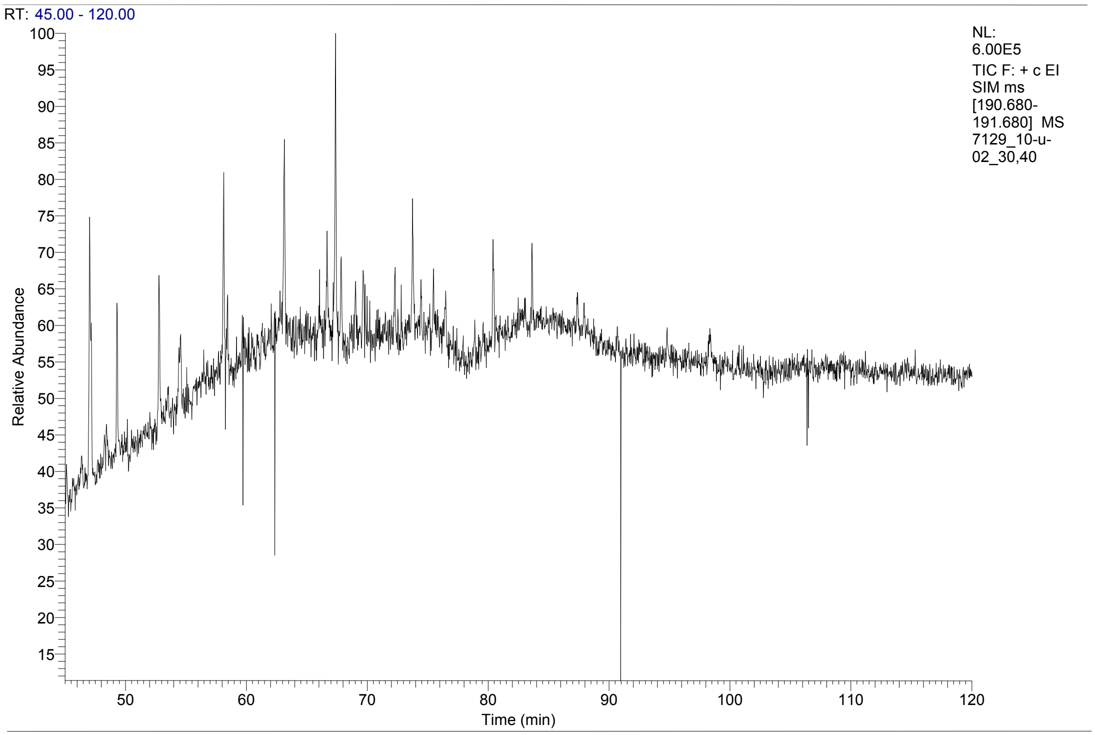
RT: 45.00 - 120.00
NL:
6.00E5
TIC F: + c EI
SIM ms
[190.680-
191.680] MS
7129_10-u-
02_30,40
Relative Abundance
100
95
90
85
80
75
70
65
60
55
50
45
40
35
30
25
20
15
50
60
70
80
90
100
110
120
Time (min)

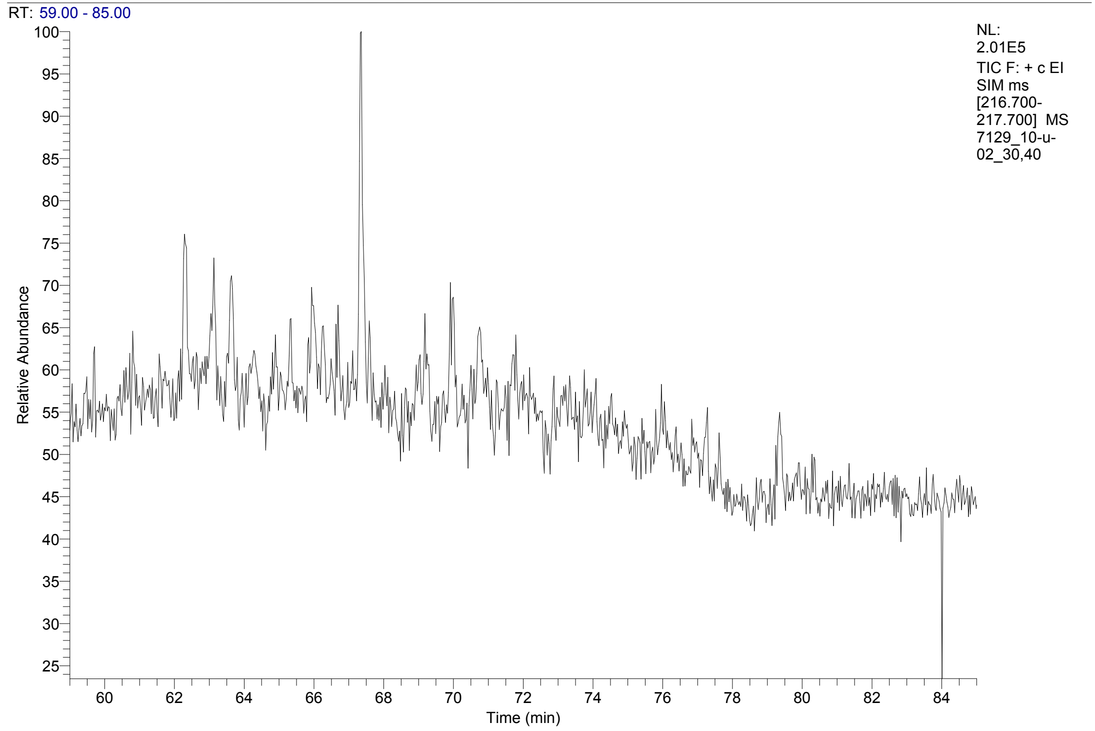
RT: 59.00 - 85.00
NL:
2.01E5
TIC F: + c EI
SIM ms
[216.700-
217.700] MS
7129_10-u-
02_30,40
Relative Abundance
100
95
90
85
80
75
70
65
60
55
50
45
40
35
30
25
60
62
64
66
68
70
72
74
76
78
80
82
84
Time (min)

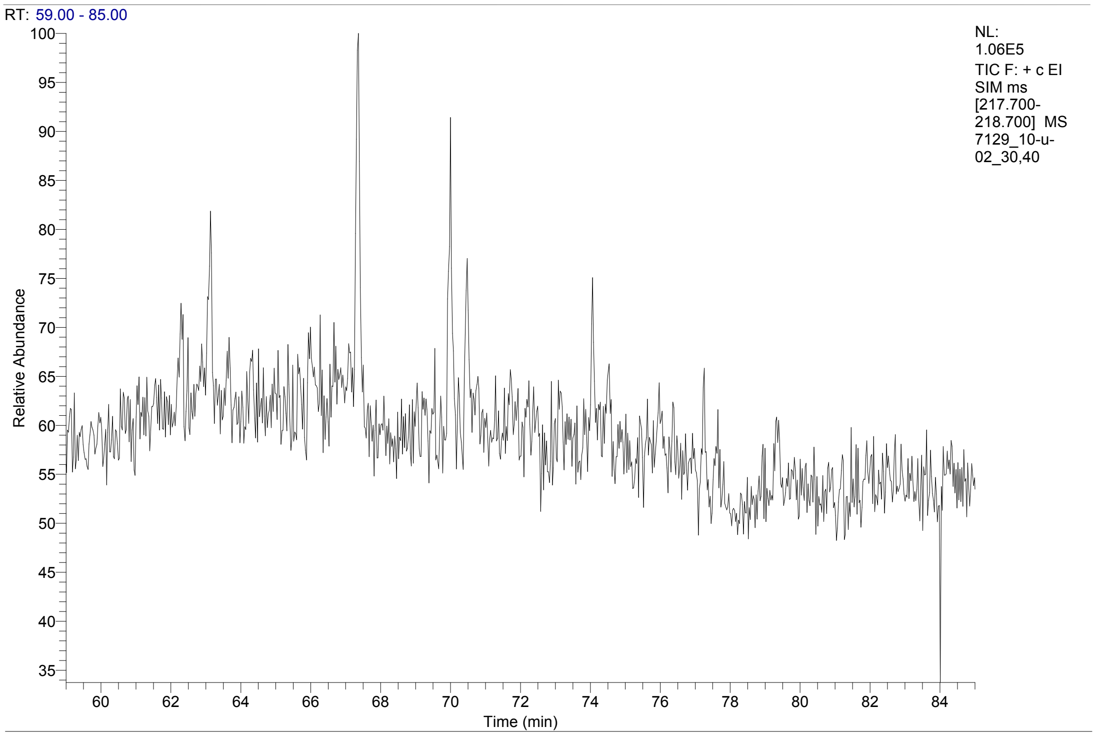
RT: 59.00 - 85.00
NL:
1.06E5
TIC F: + c EI
SIM ms
[217.700-
218.700] MS
7129_10-u-
02_30,40
Relative Abundance
100
95
90
85
80
75
70
65
60
55
50
45
40
35
60
62
64
66
68
70
72
74
76
78
80
82
84
Time (min)

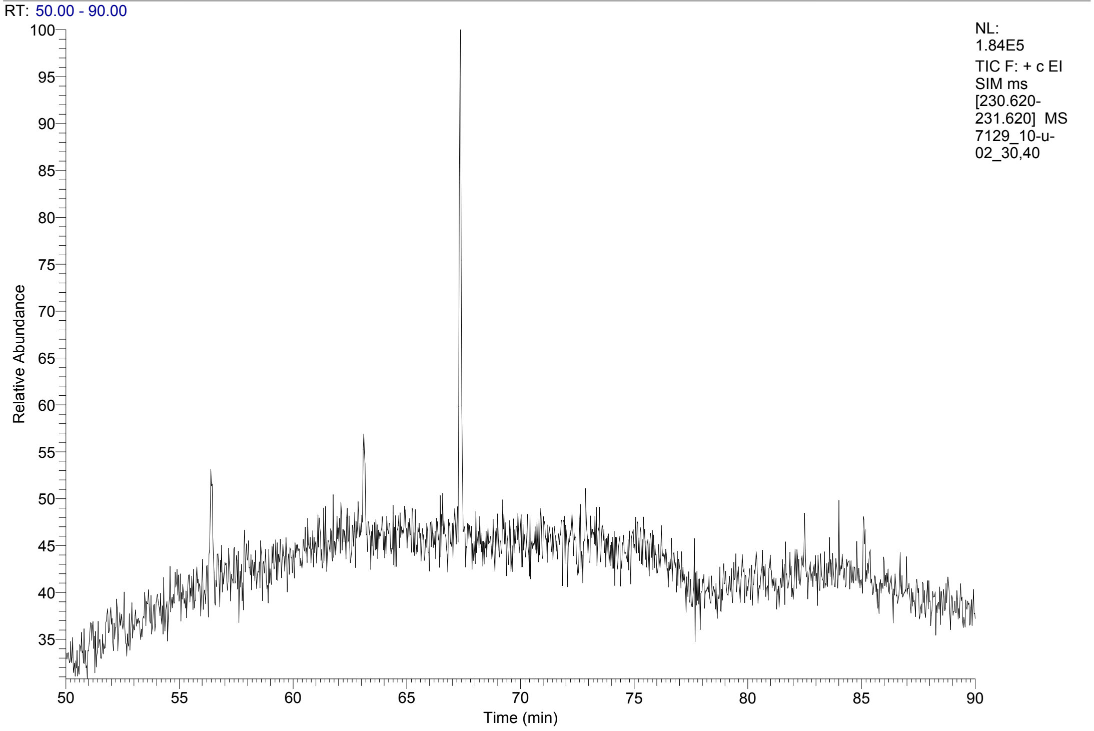
RT: 50.00 - 90.00
NL:
1.84E5
TIC F: + c EI
SIM ms
[230.620-
231.620] MS
7129_10-u-
02_30,40
Relative Abundance
100
95
90
85
80
75
70
65
60
55
50
45
40
35
50
55
60
65
70
75
80
85
90
Time (min)

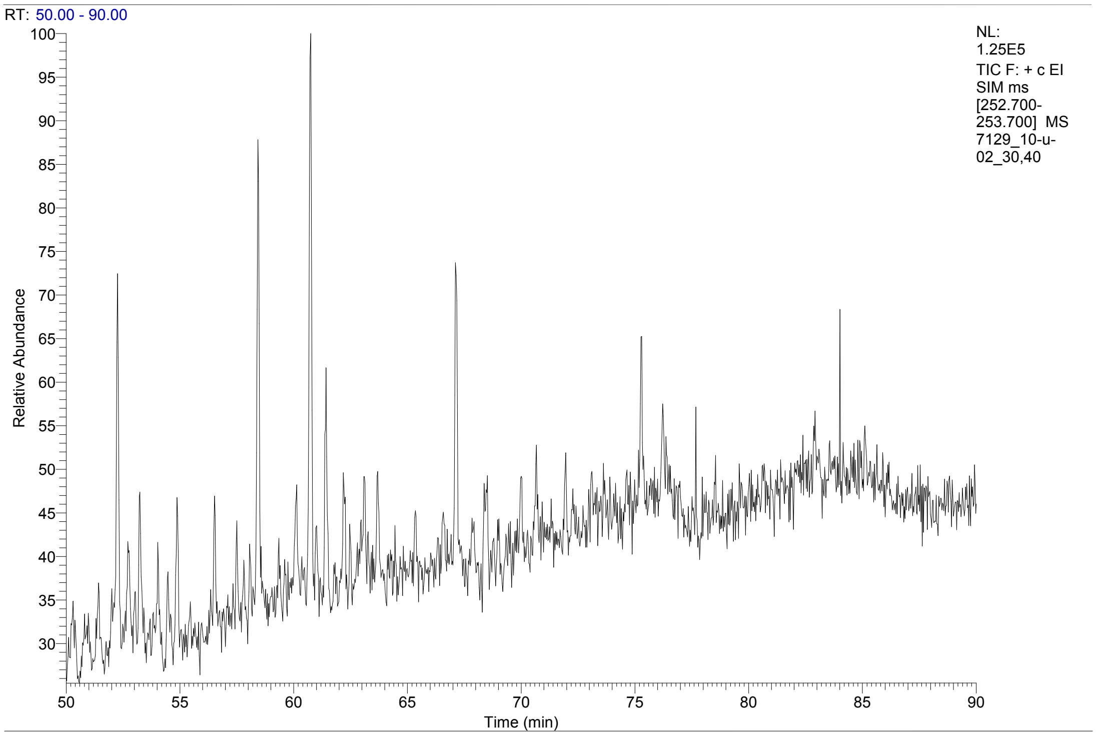
RT: 50.00 - 90.00
Relative Abundance
100
95
90
85
80
75
70
65
60
55
50
45
40
35
30
50
55
60
65
70
75
80
85
90
Time (min)
NL:
1.25E5
TIC F: + c EI
SIM ms
[252.700-
253.700] MS
7129_10-u-
02_30,40

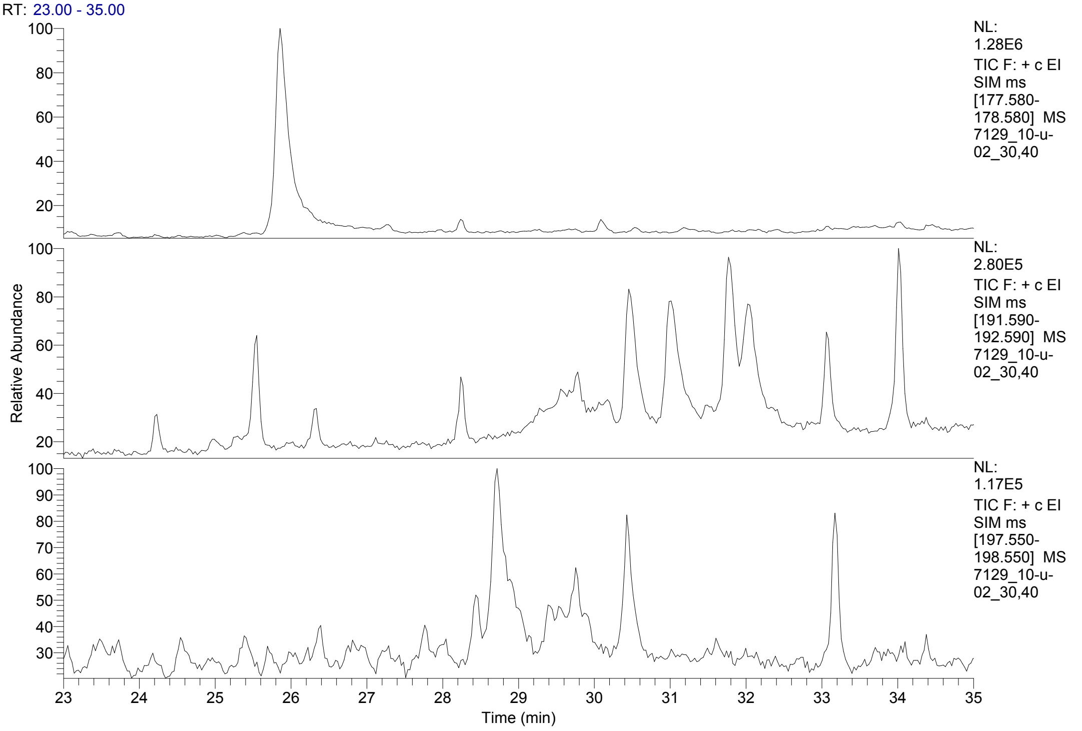
RT: 23.00 - 35.00
Relative Abundance
100
80
60
40
20
NL:
1.28E6
TIC F: + c EI
SIM ms
[177.580-
178.580] MS
7129_10-u-
02_30,40
100
80
60
40
20
NL:
2.80E5
TIC F: + c EI
SIM ms
[191.590-
192.590] MS
7129_10-u-
02_30,40
100
90
80
70
60
50
40
30
NL:
1.17E5
TIC F: + c EI
SIM ms
[197.550-
198.550] MS
7129_10-u-
02_30,40
23
24
25
26
27
28
29
30
31
32
33
34
35
Time (min)

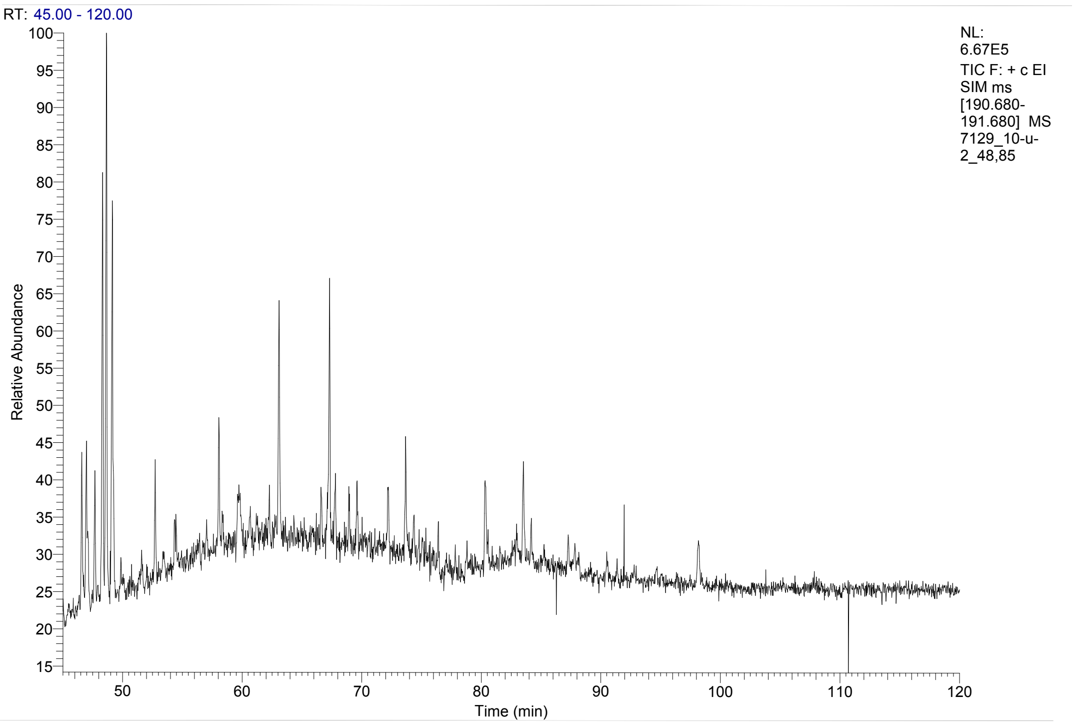
RT: 45.00 - 120.00
NL:
6.67E5
TIC F: + c EI
SIM ms
[190.680-
191.680] MS
7129_10-u-
2_48,85
Relative Abundance
100
95
90
85
80
75
70
65
60
55
50
45
40
35
30
25
20
15
50
60
70
80
90
100
110
120
Time (min)

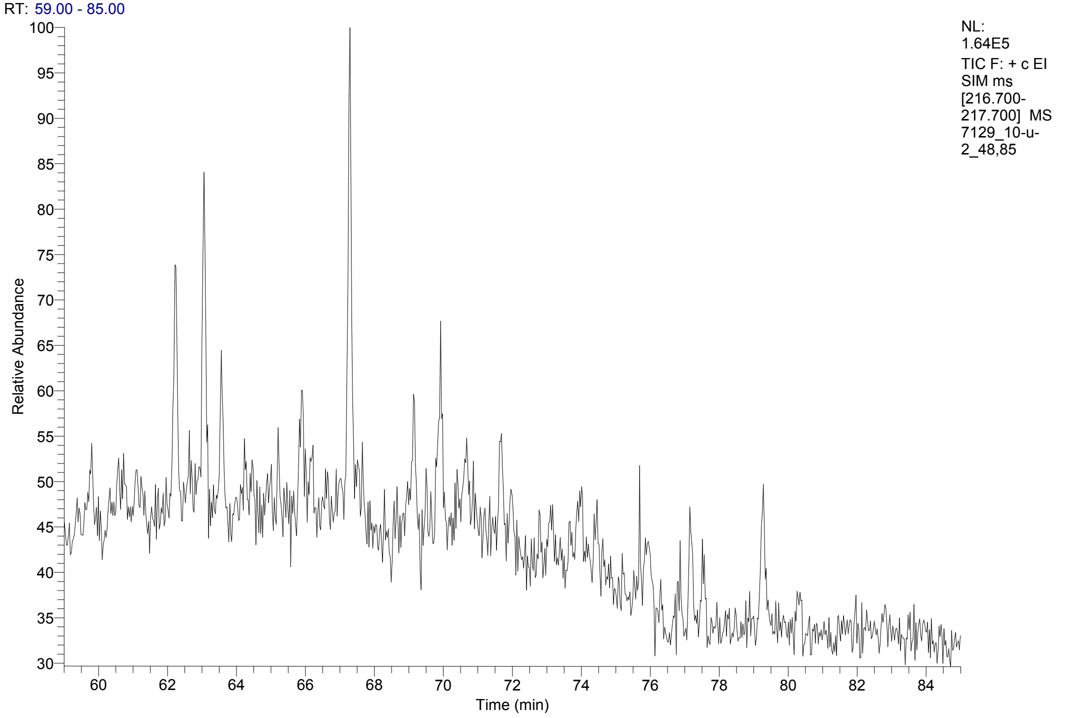
RT: 59.00 - 85.00
NL:
1.64E5
TIC F: + c EI
SIM ms
[216.700-
217.700] MS
7129_10-u-
2_48,85
Relative Abundance
100
95
90
85
80
75
70
65
60
55
50
45
40
35
30
60
62
64
66
68
70
72
74
76
78
80
82
84
Time (min)

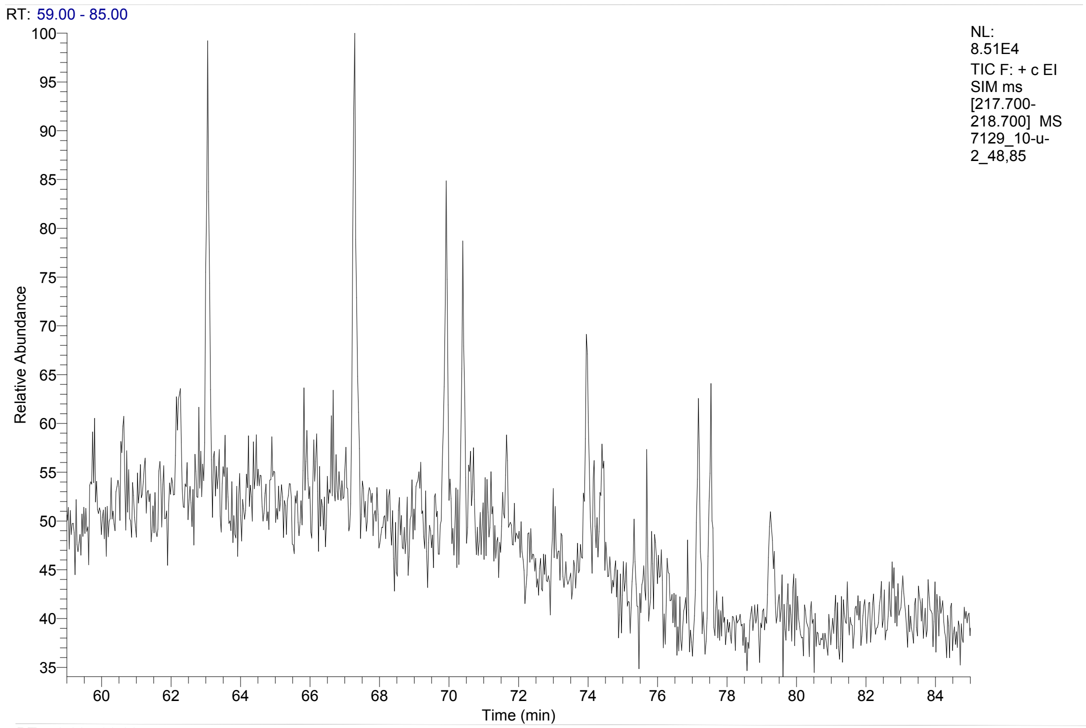
RT: 59.00 - 85.00
NL:
8.51E4
TIC F: + c EI
SIM ms
[217.700-
218.700] MS
7129_10-u-
2_48,85
Relative Abundance
100
95
90
85
80
75
70
65
60
55
50
45
40
35
60
62
64
66
68
70
72
74
76
78
80
82
84
Time (min)

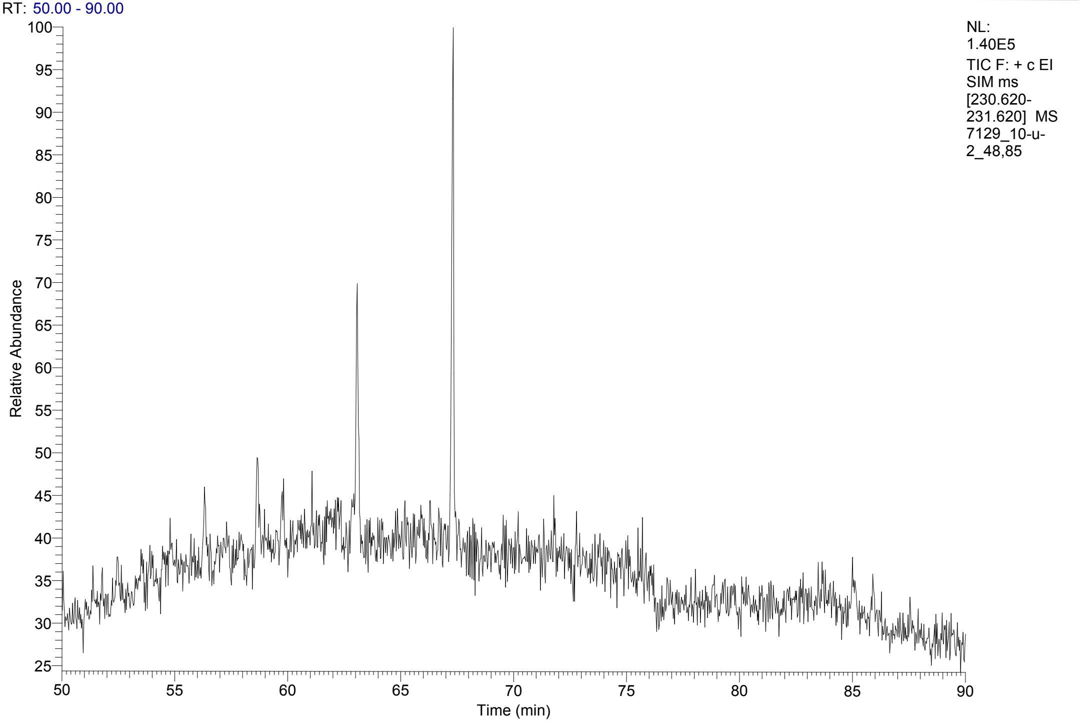
RT: 50.00 - 90.00
NL:
1.40E5
TIC F: + c EI
SIM ms
[230.620-
231.620] MS
7129_10-u-
2_48,85
Relative Abundance
100
95
90
85
80
75
70
65
60
55
50
45
40
35
30
25
50
55
60
65
70
75
80
85
90
Time (min)

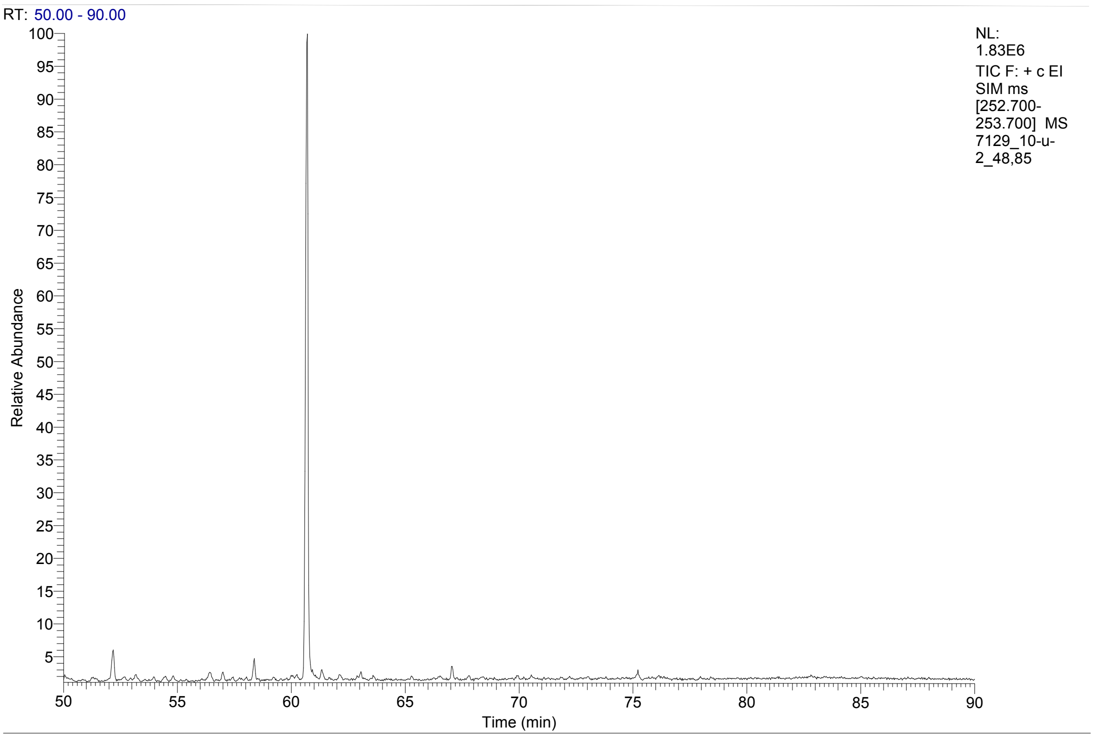
RT: 50.00 - 90.00
NL:
1.83E6
TIC F: + c EI
SIM ms
[252.700-
253.700] MS
7129_10-u-
2_48,85
Relative Abundance
Time (min)
100
95
90
85
80
75
70
65
60
55
50
45
40
35
30
25
20
15
10
5
50
55
60
65
70
75
80
85
90

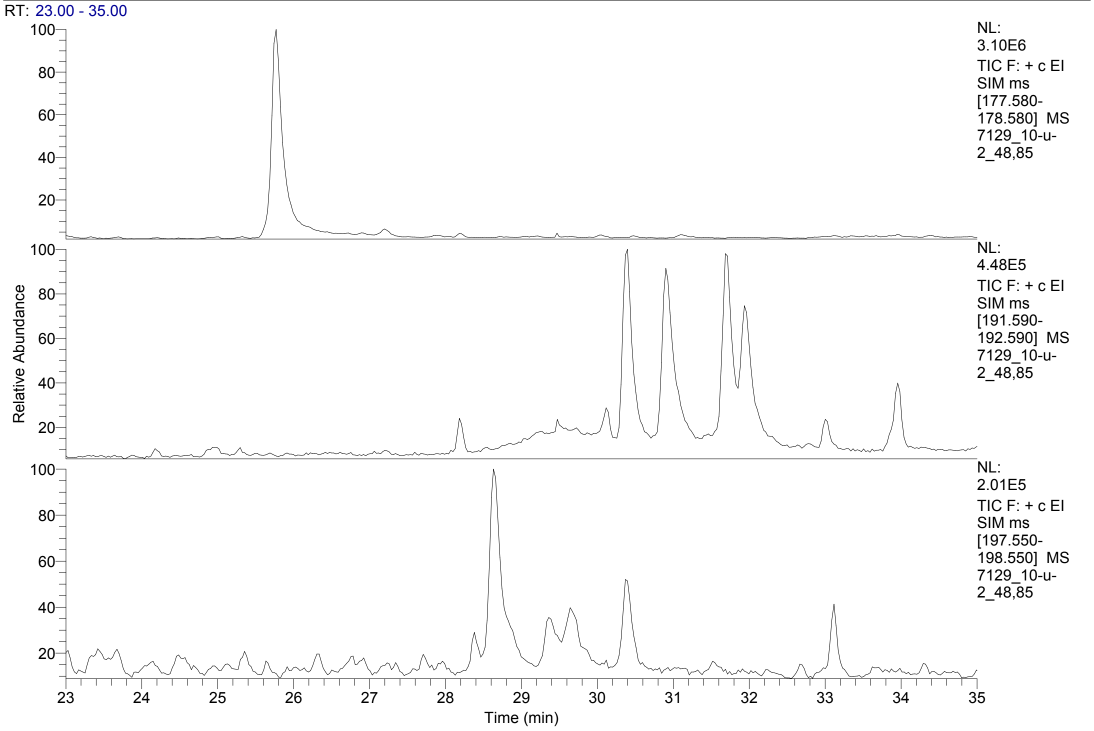
RT: 23.00 - 35.00
NL:
3.10E6
TIC F: + c EI
SIM ms
[177.580-
178.580] MS
7129_10-u-
2_48,85
NL:
4.48E5
TIC F: + c EI
SIM ms
[191.590-
192.590] MS
7129_10-u-
2_48,85
NL:
2.01E5
TIC F: + c EI
SIM ms
[197.550-
198.550] MS
7129_10-u-
2_48,85
Relative Abundance
Time (min)
100
80
60
40
20
23
24
25
26
27
28
29
30
31
32
33
34
35

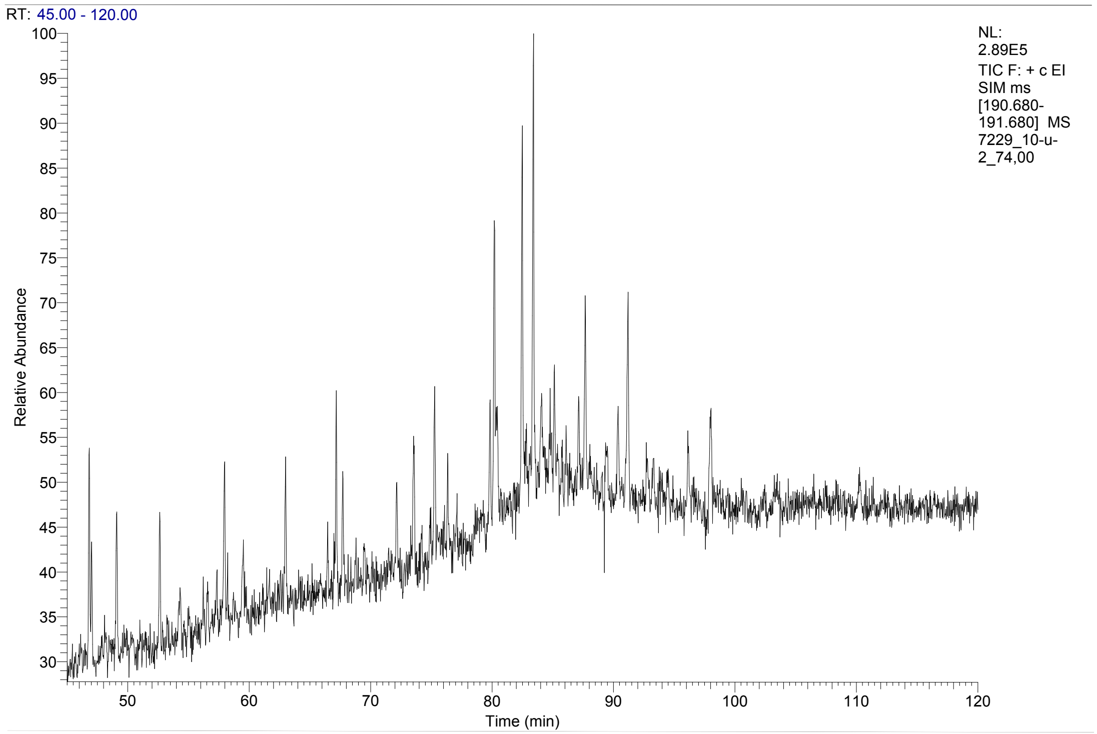
RT: 45.00 - 120.00
NL:
2.89E5
TIC F: + c EI
SIM ms
[190.680-
191.680] MS
7229_10-u-
2_74,00
Relative Abundance
100
95
90
85
80
75
70
65
60
55
50
45
40
35
30
50
60
70
80
90
100
110
120
Time (min)

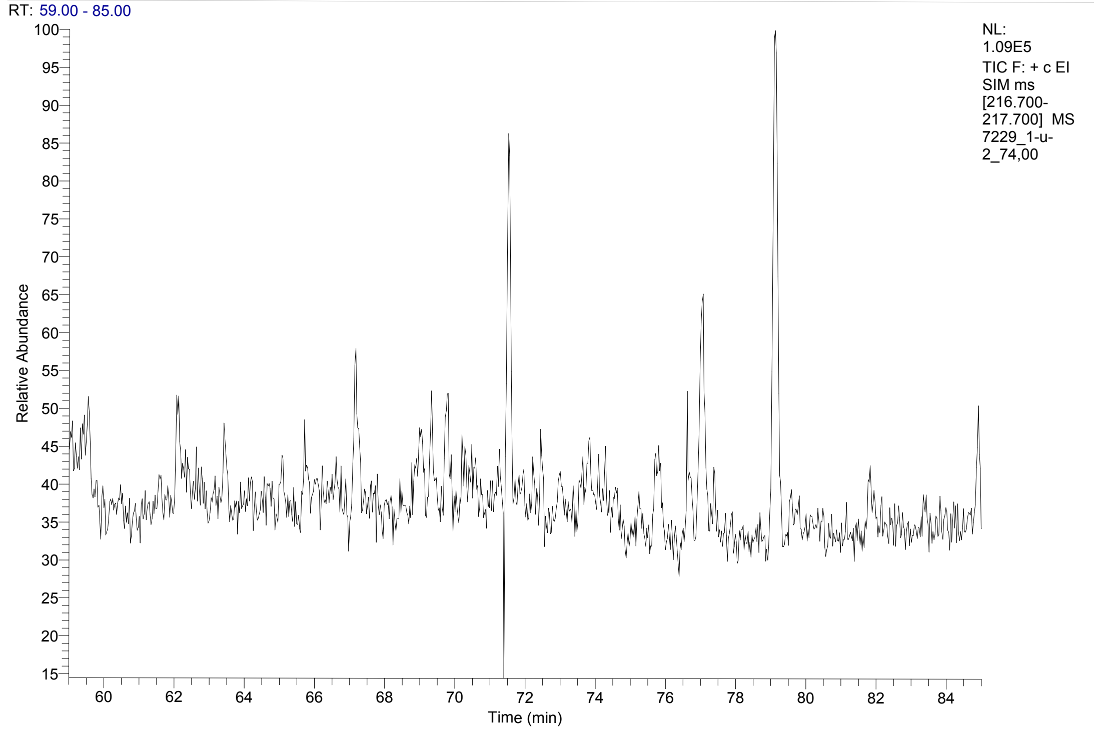
RT: 59.00 - 85.00
NL:
1.09E5
TIC F: + c EI
SIM ms
[216.700-
217.700] MS
7229_1-u-
2_74,00
Relative Abundance
100
95
90
85
80
75
70
65
60
55
50
45
40
35
30
25
20
15
60
62
64
66
68
70
72
74
76
78
80
82
84
Time (min)

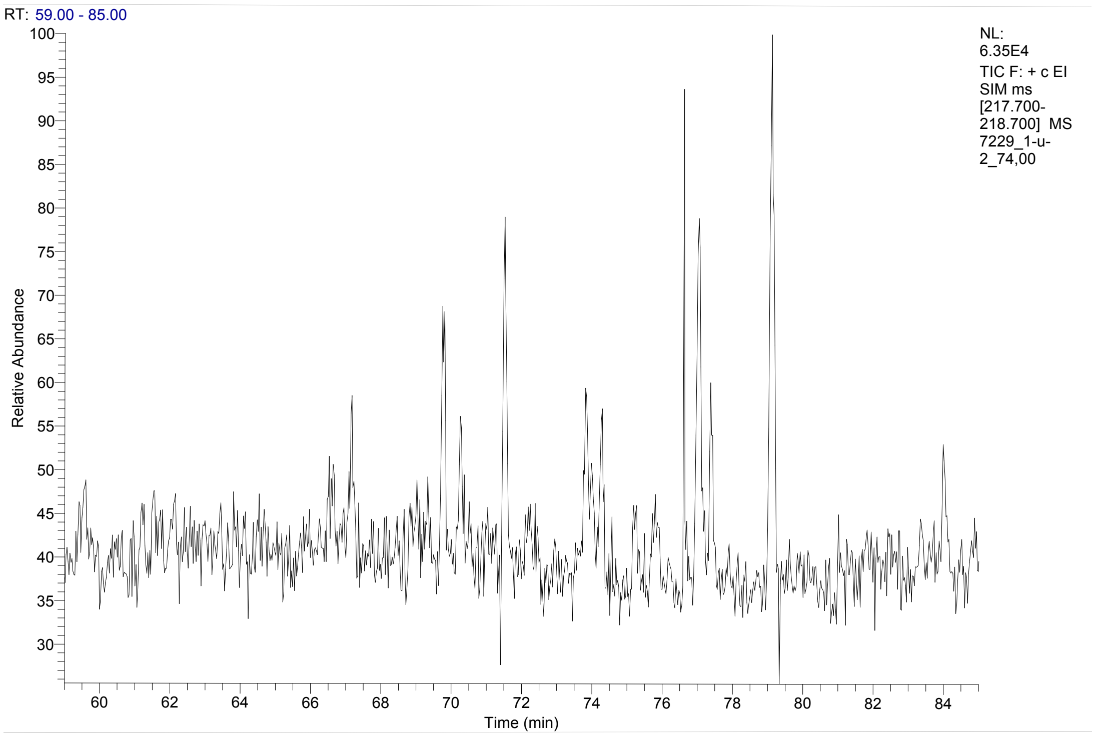
RT: 59.00 - 85.00
NL:
6.35E4
TIC F: + c EI
SIM ms
[217.700-
218.700] MS
7229_1-u-
2_74,00
Relative Abundance
100
95
90
85
80
75
70
65
60
55
50
45
40
35
30
60
62
64
66
68
70
72
74
76
78
80
82
84
Time (min)

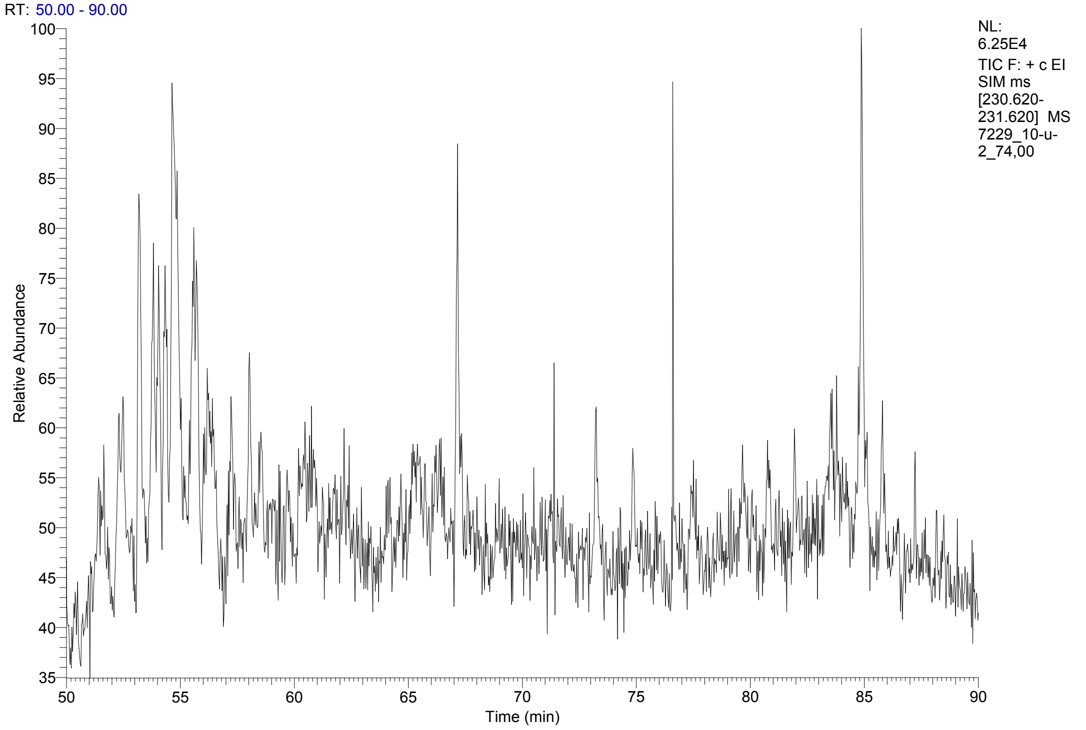
RT: 50.00 - 90.00
NL:
6.25E4
TIC F: + c EI
SIM ms
[230.620-
231.620] MS
7229_10-u-
2_74,00
Relative Abundance
100
95
90
85
80
75
70
65
60
55
50
45
40
35
50
55
60
65
70
75
80
85
90
Time (min)

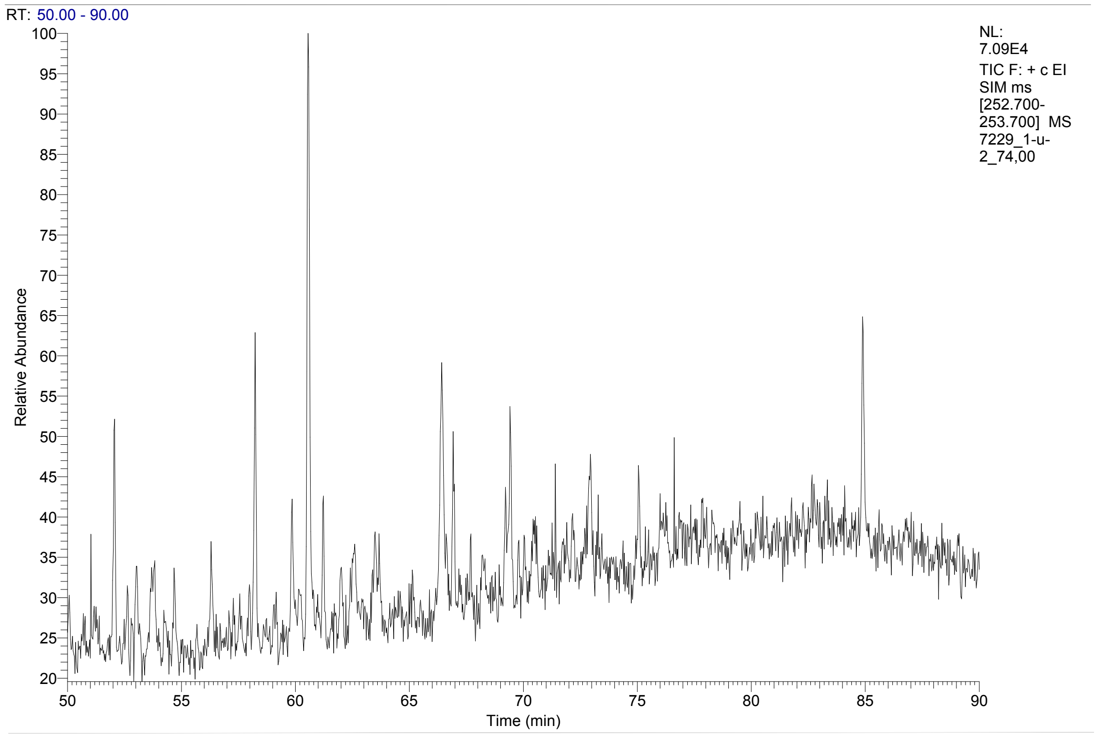
RT: 50.00 - 90.00
NL:
7.09E4
TIC F: + c EI
SIM ms
[252.700-
253.700] MS
7229_1-u-
2_74,00
Relative Abundance
100
95
90
85
80
75
70
65
60
55
50
45
40
35
30
25
20
50
55
60
65
70
75
80
85
90
Time (min)

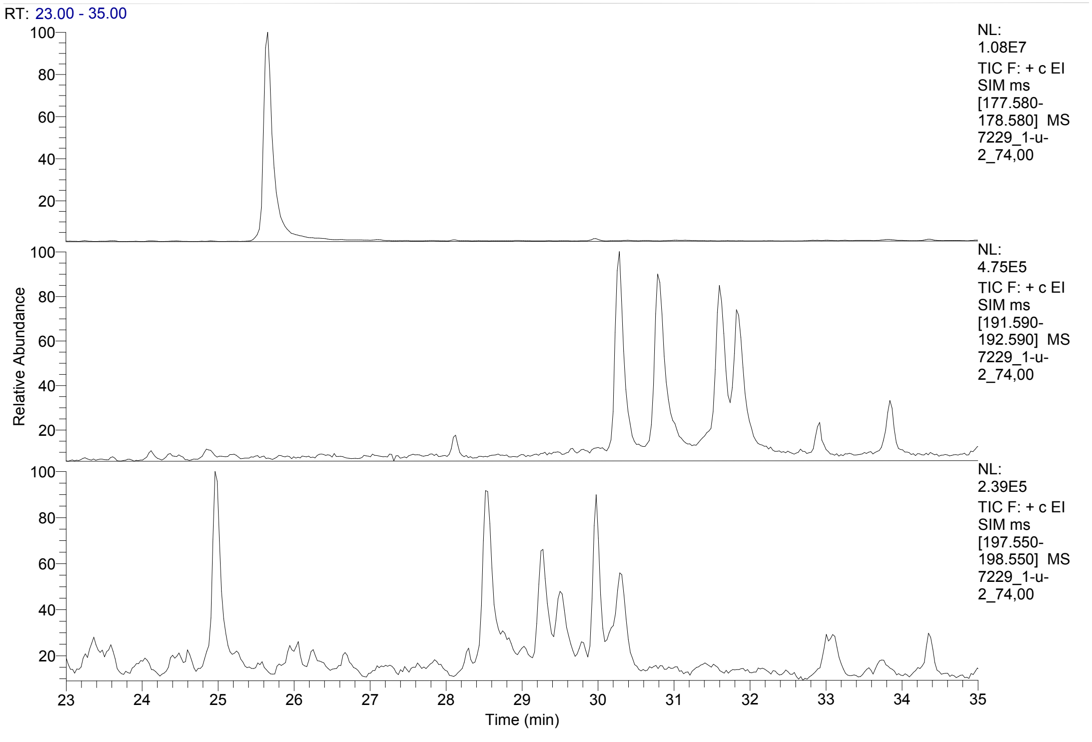
RT: 23.00 - 35.00
NL:
1.08E7
TIC F: + c EI
SIM ms
[177.580-
178.580] MS
7229_1-u-
2_74,00
NL:
4.75E5
TIC F: + c EI
SIM ms
[191.590-
192.590] MS
7229_1-u-
2_74,00
NL:
2.39E5
TIC F: + c EI
SIM ms
[197.550-
198.550] MS
7229_1-u-
2_74,00
Relative Abundance
100
80
60
40
20
23
24
25
26
27
28
29
30
31
32
33
34
35
Time (min)

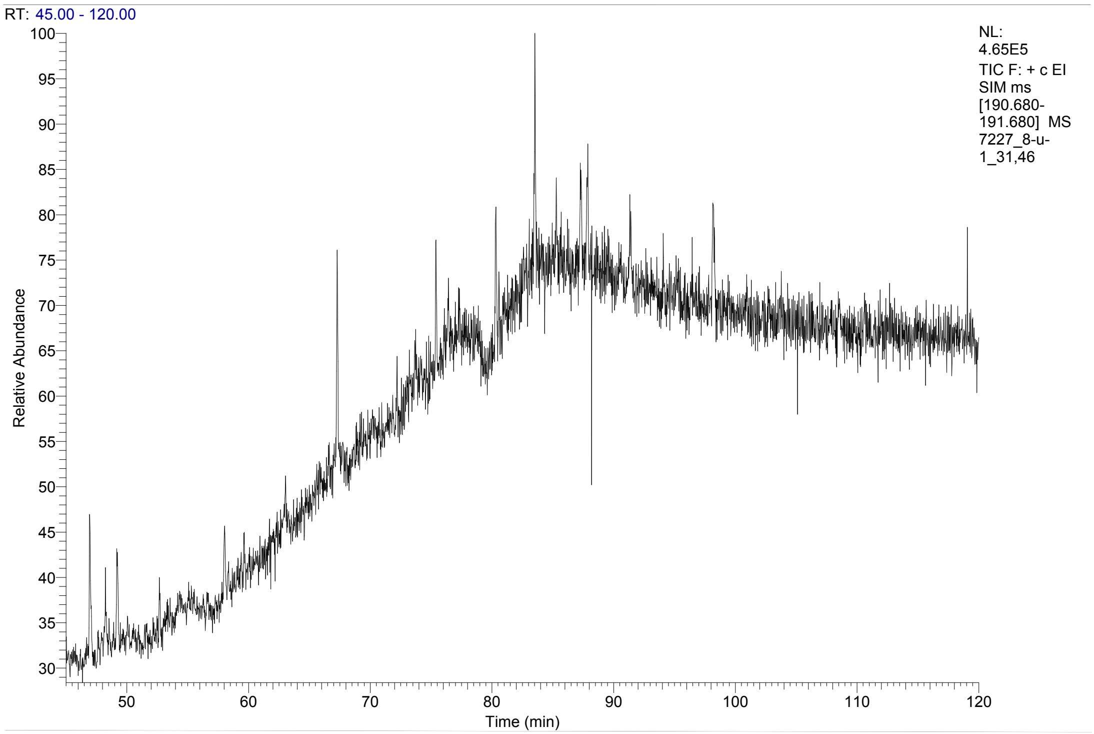
RT: 45.00 - 120.00
NL:
4.65E5
TIC F: + c EI
SIM ms
[190.680-
191.680] MS
7227_8-u-
1_31,46
Relative Abundance
100
95
90
85
80
75
70
65
60
55
50
45
40
35
30
50
60
70
80
90
100
110
120
Time (min)

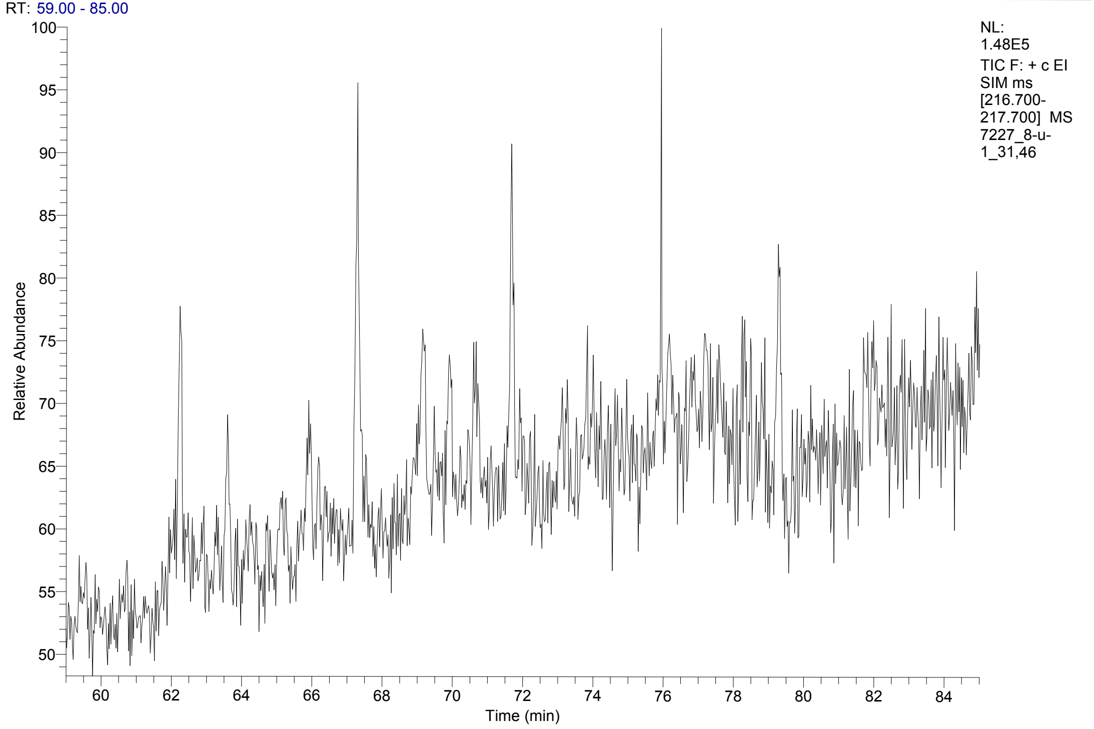
RT: 59.00 - 85.00
NL:
1.48E5
TIC F: + c EI
SIM ms
[216.700-
217.700] MS
7227_8-u-
1_31,46
Relative Abundance
100
95
90
85
80
75
70
65
60
55
50
60
62
64
66
68
70
72
74
76
78
80
82
84
Time (min)

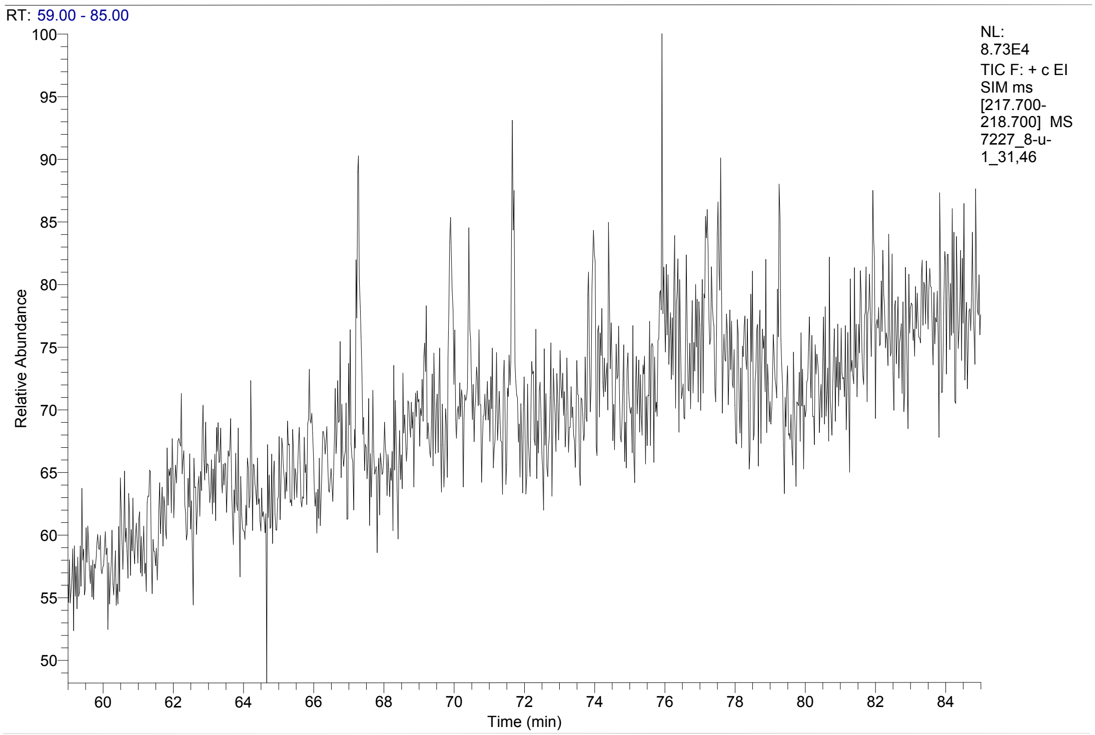
RT: 59.00 - 85.00
NL:
8.73E4
TIC F: + c EI
SIM ms
[217.700-
218.700] MS
7227_8-u-
1_31,46
Relative Abundance
100
95
90
85
80
75
70
65
60
55
50
60
62
64
66
68
70
72
74
76
78
80
82
84
Time (min)

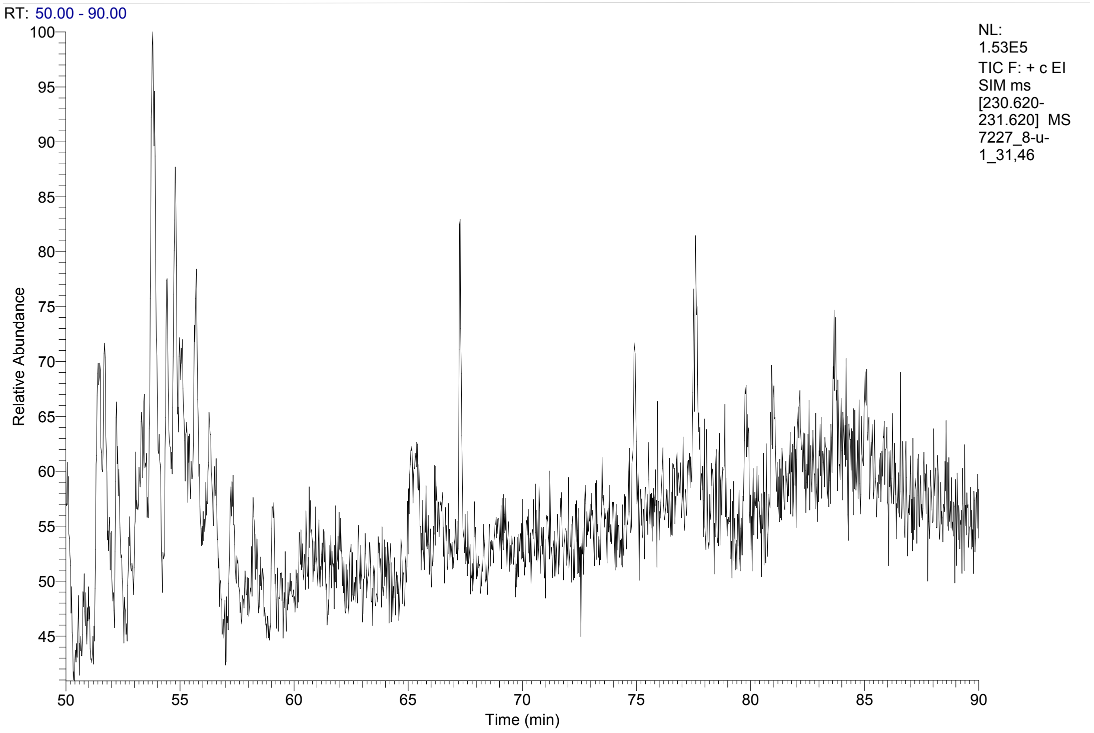
RT: 50.00 - 90.00
NL:
1.53E5
TIC F: + c EI
SIM ms
[230.620-
231.620] MS
7227_8-u-
1_31,46
Relative Abundance
100
95
90
85
80
75
70
65
60
55
50
45
50
55
60
65
70
75
80
85
90
Time (min)

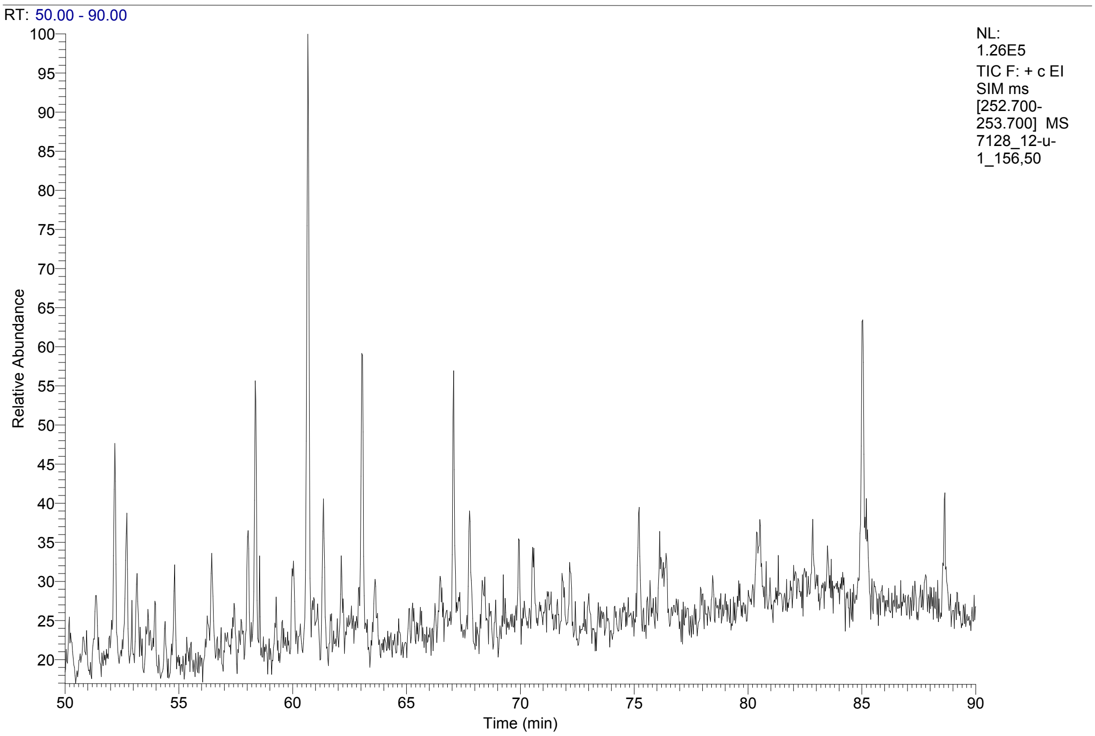
RT: 50.00 - 90.00
NL:
1.26E5
TIC F: + c EI
SIM ms
[252.700-
253.700] MS
7128_12-u-
1_156,50
Relative Abundance
100
95
90
85
80
75
70
65
60
55
50
45
40
35
30
25
20
50
55
60
65
70
75
80
85
90
Time (min)

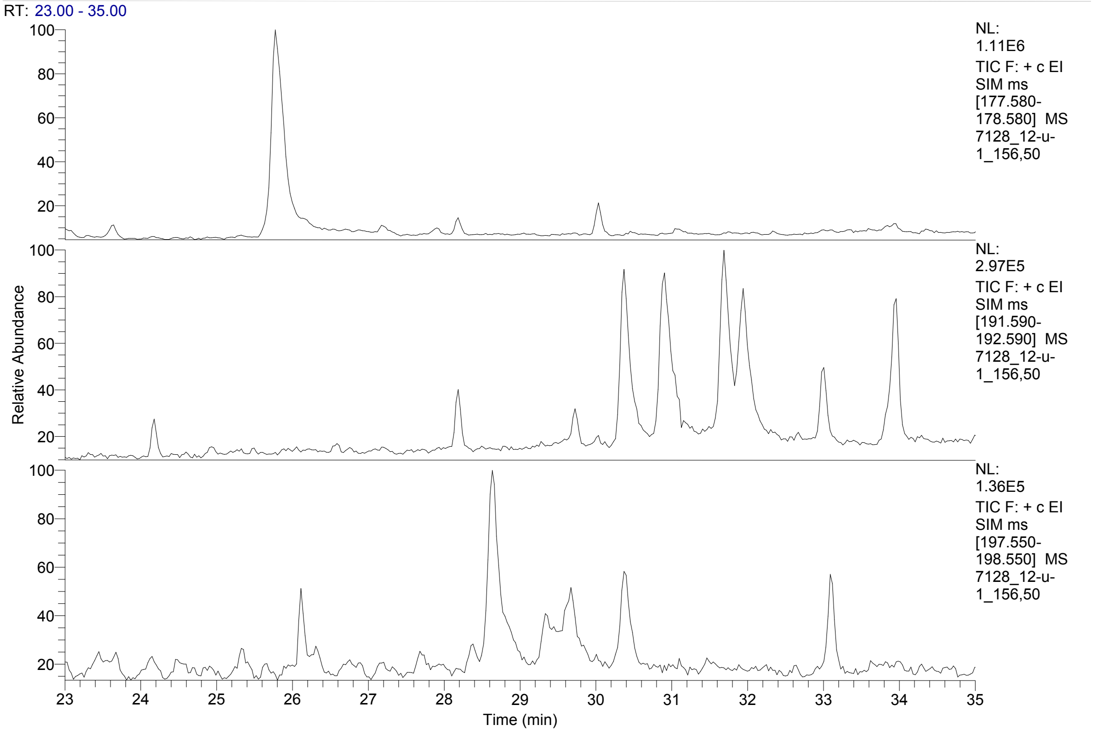
RT: 23.00 - 35.00
NL:
1.11E6
TIC F: + c EI
SIM ms
[177.580-
178.580] MS
7128_12-u-
1_156,50
NL:
2.97E5
TIC F: + c EI
SIM ms
[191.590-
192.590] MS
7128_12-u-
1_156,50
NL:
1.36E5
TIC F: + c EI
SIM ms
[197.550-
198.550] MS
7128_12-u-
1_156,50
Relative Abundance
100
80
60
40
20
23
24
25
26
27
28
29
30
31
32
33
34
35
Time (min)

# Appendix D

Table D1: Parameter 1 -27, Pr/n -C17 and Ph/n-C18. The parameters are taken from (Lerch et al., 2016)

| Sample Name | 1 | 2 | 3 | 4 | 5 | 6 | 7 | 8 | 9 | 10 | 11 | 12 | 13 | 14 | 15 |
|---|---|---|---|---|---|---|---|---|---|---|---|---|---|---|---|
| D | 0.6 | 0.81 | 0.6 | - | 0.36 | - | 0.31 | 0.05 | - | 0.62 | 0.52 | 0.56 | - | - | - |
| V | 0.38 | 0.64 | 0.59 | - | 0.23 | - | 0.31 | 0.05 | - | 0.61 | 0.51 | 0.5 | - | - | - |
| V1 | 0.4 | 0.64 | 0.6 | - | 0.24 | - | 0.31 | 0.04 | - | 0.6 | 0.5 | 0.49 | - | - | - |
| W | 0.47 | 0.66 | 0.6 | - | 0.27 | - | 0.36 | 0.05 | - | 0.58 | 0.52 | 0.49 | - | - | - |
| Z1 | 0.54 | 0.75 | 0.59 | - | 0.3 | - | 2.05 | 0.28 | - | 0.48 | 0.52 | 0.56 | - | - | - |
| Å | 0.65 | 0.7 | 0.54 | - | 0.34 | - | 0.88 | 0.03 | - | 0.58 | 0.51 | 0.42 | - | - | - |
| Æ | 0.83 | 0.87 | 0.57 | - | 0.44 | - | 1.67 | 0.06 | - | 0.63 | 0.51 | 0.5 | - | - | - |
| AB | 0.36 | 0.53 | 0.59 | - | 0.19 | - | 1.11 | 0.07 | - | 0.5 | 0.51 | 0.5 | - | - | - |
| B | 0.43 | 0.64 | 0.56 | - | 0.44 | - | 0.8 | 0.14 | - | 0.59 | 0.51 | 0.39 | - | - | - |
| P | 0.57 | - | 0.51 | - | 0.39 | - | 3.1 | 0.47 | - | - | - | - | - | - | - |
| T | 0.47 | 0.63 | 0.58 | - | 0.23 | - | 0.26 | 0.05 | - | 0.55 | 0.48 | 0.38 | - | - | - |
| T1 | 0.47 | 0.63 | 0.58 | - | 0.23 | - | 0.26 | 0.06 | - | 0.56 | 0.49 | 0.38 | - | - | - |
| T2 | 0.83 | 0.92 | 0.57 | - | 0.51 | - | 1.11 | 0.04 | - | 0.58 | 0.46 | 0.47 | - | - | - |
| T3 | 0.81 | 0.92 | 0.57 | - | 0.52 | - | 1.17 | 0.04 | - | 0.59 | 0.48 | 0.46 | - | - | - |

| Sample Name | 16 | 17 | 18 | 19 | 20 | 21 | 22 | 23 | 24 | 25 | 26 | 27 | Pr/n-C17 | Ph/n-C18 |
|---|---|---|---|---|---|---|---|---|---|---|---|---|---|---|
| D | 0.73 | 0.73 | 0.91 | 0.67 | 0.45 | 3.15 | 0.9 | 0.8 | 0.85 | 0.74 | - | - | 1.19 | 0.63 |
| V | 0.34 | 0.34 | 0.91 | 0.61 | 0.43 | 2.24 | 0.9 | 0.77 | 0.8 | 0.67 | - | - | 1.04 | 0.77 |
| V1 | 0.33 | 0.33 | 0.93 | 0.6 | 0.43 | 2.29 | 0.91 | 0.76 | 0.8 | 0.68 | - | - | 1.04 | 0.77 |
| W | 0.45 | 0.45 | 0.9 | 0.58 | 0.42 | 3.36 | 0.9 | 0.75 | 0.78 | 0.76 | - | - | 0.94 | 0.79 |
| Z1 | 0.78 | 0.78 | 1.38 | 0.72 | 0.51 | 4.54 | 1.1 | 0.83 | 0.97 | 0.84 | - | - | 0.42 | 0.17 |
| Å | 0.36 | 0.36 | 0.82 | 0.68 | 0.42 | 6.29 | 0.85 | 0.81 | 0.77 | 0.97 | - | - | 11.06 | 7.06 |
| Æ | 0.82 | 0.82 | 1.04 | 0.77 | 0.47 | 5.56 | 0.97 | 0.86 | 0.88 | 0.92 | - | - | 0.87 | 0.64 |
| AB | 0.46 | 0.46 | 1 | 0.57 | 0.45 | 4.14 | 0.95 | 0.74 | 0.84 | 0.81 | - | - | 0.46 | 0.31 |
| B | 0.28 | 0.89 | 0.74 | 0.41 | 0.39 | 2.76 | 0.81 | 0.65 | 0.7 | 0.71 | - | - | 0.96 | 0.67 |
| P | 0.9 | 0.68 | 1.13 | 0.62 | 0.47 | 4.98 | 1.01 | 0.77 | 0.9 | 0.87 | - | - | 0.86 | 0.5 |
| T | 0.34 | 0.93 | 1 | 0.66 | 0.46 | 3.93 | 0.95 | 0.8 | 0.87 | 0.8 | - | - | 0.88 | 0.52 |
| T1 | 0.34 | 0.91 | 1 | 0.65 | 0.46 | 4.12 | 0.95 | 0.79 | 0.86 | 0.81 | - | - | 0.86 | 0.51 |
| T2 | 0.51 | 0.83 | 1.06 | 0.55 | 0.43 | 4.62 | 0.98 | 0.73 | 0.81 | 0.85 | - | - | 1.11 | 0.79 |
| T3 | 0.6 | 0.8 | 0.99 | 0.55 | 0.41 | 3.69 | 0.94 | 0.73 | 0.76 | 0.78 | - | - | 1.1 | 0.79 |